

ACTA PHYSICA

ACADEMIAE SCIENTIARUM
HUNGARICAE

ADIUVANTIBUS

Z. GYULAI, L. JÁNOSSY, I. KOVÁCS, K. NOVOBÁTZKY

REDIGIT

P. GOMBÁS

TOMUS XVIII

FASCICULUS I



AKADÉMIAI KIADÓ, BUDAPEST
1964

ACTA PHYS. HUNG.

ACTA PHYSICA

A MAGYAR TUDOMÁNYOS AKADÉMIA FIZIKAI KÖZLEMÉNYEI

SZERKESZTŐSÉG ÉS KIADÓHIVATAL: BUDAPEST V., ALKOTMÁNY UTCA 21.

Az *Acta Physica* német, angol, francia és orosz nyelven közöl értekezéseket a fizika tárgyköréből.

Az *Acta Physica* változó terjedelmű füzetekben jelenik meg: több füzet alkot egy kötetet. A közlésre szánt kéziratok a következő címre küldendők:

Acta Physica, Budapest 502, Postafiók 24.

Ugyanerre a címre küldendő minden szerkesztőségi és kiadóhivatali levelezés.

Az *Acta Physica* előfizetési ára kötetenként belföldre 80 forint, különálló 110 forint.

Megrendelhető a belföld számára az Akadémiai Kiadónál (Budapest V., Alkotmány utca 21. Bankszámla 05-915-111-46), a különálló számára pedig a „Kultúra” Könyv- és Hírlap Külkereskedelmi Vállalatnál (Budapest I., Fő u. 32. Bankszámla 43-790-057-181 sz.), vagy annak különálló képviseleteinél és bizományosainál.

Die *Acta Physica* veröffentlichen Abhandlungen aus dem Bereich der Physik in deutscher, englischer, französischer und russischer Sprache.

Die *Acta Physica* erscheinen in Heften wechselnden Umfangs. Mehrere Hefte bilden einen Band.

Die zur Veröffentlichung bestimmten Manuskripte sind an folgende Adresse zu richten:

Acta Physica, Budapest 502, Postafiók 24.

An die gleiche Anschrift ist auch jede für die Redaktion und den Verlag bestimmte Korrespondenz zu senden.

Abonnementspreis pro Band: 110 Forint. Bestellbar bei dem Buch- und Zeitungs-Aussenhandels-Unternehmen »Kultúra« (Budapest I., Fő u. 32. Bankkonto Nr. 43-790-057-181) oder bei seinen Auslandsvertretungen und Kommissionären.

ACTA PHYSICA

ACADEMIAE SCIENTIARUM
HUNGARICAE

ADIUVANTIBUS

Z. GYULAI, L. JÁNOSSY, I. KOVÁCS, K. NOVOBÁTZKY

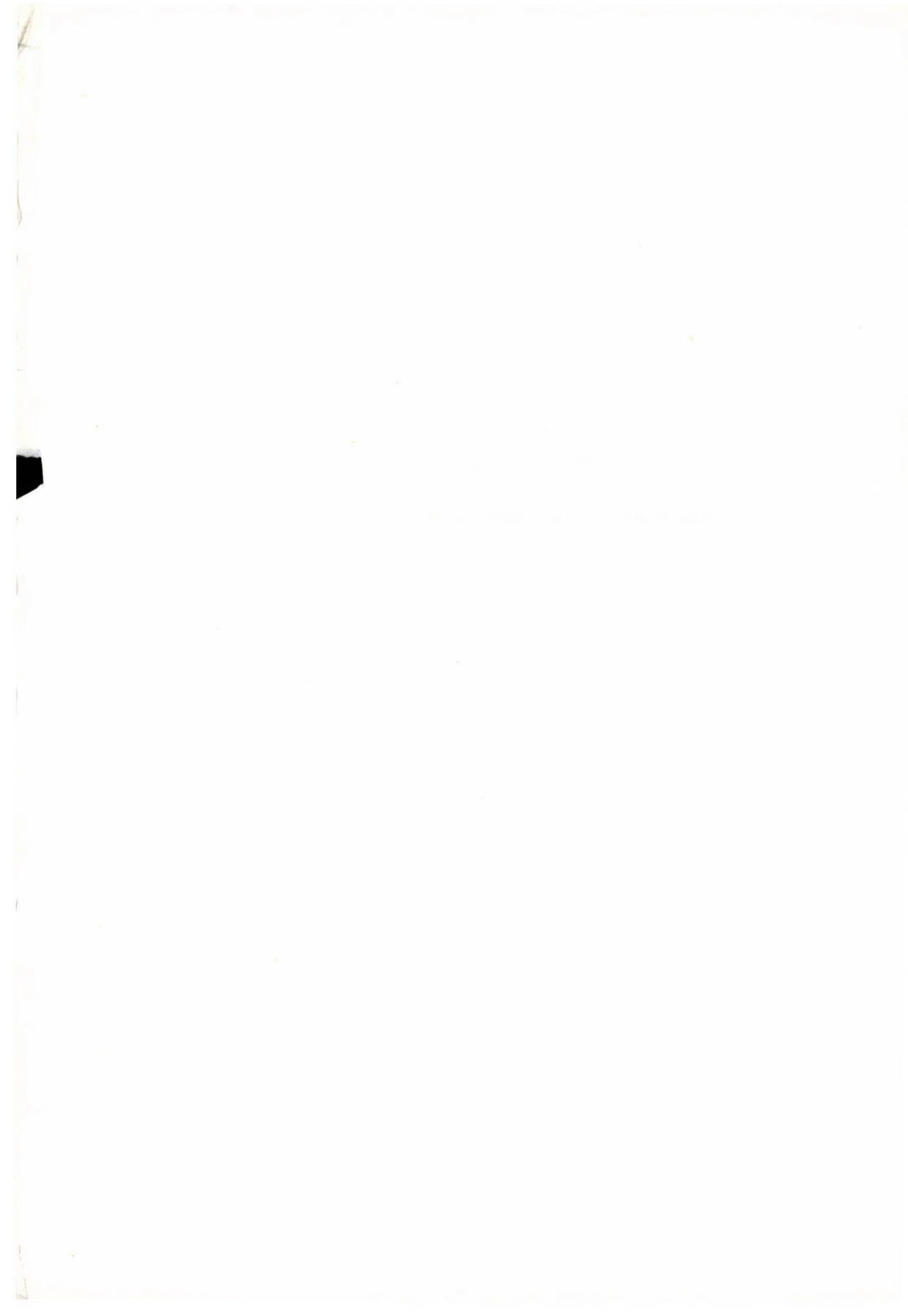
REDIGIT
P. GOMBÁS

TOMUS XVIII



AKADÉMIAI KIADÓ, BUDAPEST
1965

ACTA PHYS. HUNG.



ERRATUM

Zur Rezension des Werkes »Zur Physik und Chemie der Kristallphosphore«
Herausgegeben von Dr. Ing. Henry Ortmann

Acta Phys. Hung. **18**, 151, 1965.

Von

PÁL KOVÁCS

Zeile 16 (Punkt c) in der linken Spalte soll richtig heißen: Lumineszenz der II—VI—Verbindungen;

In Zeile 29 soll III—VI durch II—VI ersetzt werden.

Zeilen 14—22 in der rechten Spalte sollen lauten:

Das Organisationskomitee hatte es sich zum Ziel gesetzt, Forscher von den verschiedensten Arbeitsplätzen einzuladen, um auf diese Weise in den Vorträgen und nachfolgenden Diskussionen einen möglichst breiten Überblick über den Stand dieses interessanten Gebietes der Festkörperphysik zu erhalten, und die Perspektiven der weiteren Forschung zur Diskussion zu stellen.



ACTA PHYSICA

Tomus XVIII

INDEX

<i>J. Bitó: On the Anodic Side Oscillations of Low Pressure DC Gas Discharges.</i> — Й. Бито:			
Об анодных колебаниях газовых разрядов постоянного тока низкого давления			1
<i>Elisabeth Kovács-Csetényi: Electrical Resistivity Change in Cold-Worked Tungsten Wires During Recovery and Recrystallization.</i> — Е. Ковач-Четени:			
Изменение сопротивления вольфрамовых проволок, разработанных в холодном состоянии, в процессах обновления и рекристаллизации			11
<i>S. Datta Majumdar: Wave Equations in Momentum Space.</i> — Ш. Датта Маюмдар:			
Волновые уравнения в пространстве импульсов			19
<i>G. Lakatos and J. Bitó: Some Parameters of the Moving Striations.</i> — Г. Лакатос и			
Й. Бито: О некоторых параметрах подвижного слоеобразования			27
<i>A. Kónya: Quantum Numbers and Energy Levels in the Thomas-Fermi Atom.</i> — А. Конья:			
Квантовые числа и энергетические уровни в атоме Томаса—Ферми			39
<i>Maria Farkas-Jahnke: Graphical Method for the Construction of the Patterson Function of One-Dimensional Structure Models.</i> — М. Фаркаш-Янке:			
Графический метод для определения функции Паттерсона одномерной структурой модели			55
<i>G. Bozóki, E. Fenyves, É. Gombosi and E. Nagy: Inelastic Two-Prong $\pi^- - p$ Interactions at 17,2 GeV in Emulsion.</i> — Г. Бозоки, Э. Фельвеш, Э. Гомбоши и Э. Надь:			
Двухлучевые неупругие взаимодействия в эмульсии при энергии 17,2 Гев.			61
<i>T. Vertse and D. Berényi: Transmission Curve of the S²⁵ Continuous Beta-Radiation in Air</i>			67
<i>G. Pócsik: Restrictions on the Vertex Functions</i>			73
<i>G. Marx and J. Németh: Pressure in a Relativistically Degenerated Fermion Gas with Scalar Interaction</i>			77
<i>L. Bozóky: G. Hertz, Lehrbuch der Kernphysik, Band III. (Recensio)</i>			83
<i>I. Abonyi: R. Jancel—Th. Kahan, Électrodynamique des Plasmas (Recensio)</i>			84
<i>J. Antal: K. J. Binns and P. J. Lawrenson, Analysis and Computation of Electric and Magnetic Field Problems (Recensio)</i>			84
<i>M. Szilágyi: Periodic Focusing of Dense Electron Beams with Thin Lenses.</i> — М. Силайи:			
Периодическая фокусировка интенсивных электронных пучков тонкими линзами			87
<i>I. Kovács and R. Tőrős: The Intensity Distribution of the Triplet Bands of the CO Molecule.</i> — И. Ковач и Р. Тэреш:			
Распределение интенсивности в триплетной связи молекулы CO			101
<i>I. Kovács: The Rotational Structure of the d³A State of the CO Molecule.</i> — И. Ковач:			
Ротационная структура состояния d ³ A молекулы CO			107
<i>P. Gadó: X-Ray Powder Diffraction Study of the WO₃ ⇌ W₂₀O₅₈ Shear Transformation.</i> — П. Гадо:			
Изучение преобразования сдвига WO ₃ ⇌ W ₂₀ O ₅₈ рентгеновыми лучами порошко-дифракционным методом			111
<i>I. Montvay: On the Convergence of the Peratization Method.</i> — И. Монтваи:			
О сходимости ператизационного метода			119

<i>A. Kónya</i> : Theoretical Interpretation of Some Properties of the Periodic System by the Thomas—Fermi Model. — <i>А. Конья</i> : Теоретическая интерпретация некоторых свойств периодической системы элементов моделью Томаса—Ферми	129
<i>T. Tietz</i> : Electron Scattering by Atoms and the Existence of Negative Ions.....	141
<i>J. I. Horváth</i> : Contribution to the Problem of the Entropy Increase of Quantum Mechanical Many-Body Systems	145
<i>F. Dési</i> : D. R. Bates, Theoretical Interpretation of Upper Atmosphere Emissions (Recensio) 149	
<i>I. Kovács</i> : L. Láng, Absorption Spectra in the Ultraviolet and Visible Region. (Recensio) 150	
<i>P. Kovács</i> : H. Ortmann, Zur Physik und Chemie der Kristallphosphore (Recensio)....	151
<i>E. Nagy</i> : F. Sauter, Festkörperprobleme I. (Recensio).....	152
З. Фюзэши: М. А. Сапожков, Защита трактов радио и проводной телефонной связи от помех и шумов (Recensio)	153
З. Фюзэши: М. А. Сапожков, Речевой сигнал в кибернетике и связи (Recensio) ..	154
<i>F. Bokovszky</i> : Elementary Calculations of the Madelung Constants of Some Cubic Lattices. — <i>Ф. Буковски</i> : Вычисление постоянной Маделунга элементарным путем для нескольких кубических решеток	157
<i>J. Ladik</i> : Some Developments in the Semiempirical Theories of Molecular Crystals. I. The Hückel Approximation. — <i>Я. Ладик</i> : О полуэмпирических теориях молекулярных кристаллов I. Приближение Гюкеля	173
<i>J. Ladik</i> : Some Developments in the Semiempirical Theories of Molecular Crystals. II. The Pariser-Parr-Pople Approximation. — <i>Я. Ладик</i> : О полуэмпирических теориях молекулярных кристаллов II. Приближение Паризера—Парра—Попла	185
<i>Gy. Farkas, L. Jánossy, Zs. Náray and P. Varga</i> : Intensity Correlation of Coherent Light Beams. — <i>Дь. Фаркаш, Л. Яноши, Ж. Нарай и П. Варга</i> : Корреляция интенсивности когерентных световых лучей	199
<i>F. Beleznay, G. Biczó and J. Ladik</i> : Theoretical Estimation of the Conductivity of DNA. — <i>Ф. Белезнаи, Г. Бицо и Я. Ладик</i> : Теоретическое определение электрической проводимости DNA	213
<i>J. Németh</i> : A Superconductive Model with Two Kinetic Energies. — <i>Й. Нэмэт</i> : Модель сверхпроводимости с двумя значениями кинетической энергии	221
<i>W. Reichel</i> : Zur Theorie und Praxis der Berechnung der Übertragungsfunktion optischer Systeme. — <i>В. Рейхель</i> : О теории и практике определения передаточной функции оптических систем	233
<i>E. Lendvay</i> : Monocrystals of Mn-Phthalate. — <i>Э. Лендвай</i> : Монокристаллы фталата-Mn	257
<i>P. K. Biswas</i> : Hilbert Transform and the Differential Equations of Hamilton's Canonical Form	263
<i>F. Illés and D. Berényi</i> : Magnetic Characteristic Curve for a Special Permanent-Magnet Beta-Ray Spectrograph Set of Two Units.....	265
<i>J. Antal</i> : Milton Kerker, Electromagnetic Scattering (Recensio).....	269
<i>Z. Gyulai</i> : J. Thewlis, Encyclopaedic Dictionary of Physics Vol. 6. (Recensio).....	270
<i>T. Szondy</i> : R. K. Wangsness, Introduction to Theoretical Physics (Recensio).....	271
<i>Gy. Fáy</i> : Notes on the Quantum-mechanical Discussion of the Gibbs Paradox.— <i>Д. Фай</i> : Замечания к квантовомеханическому рассмотрению парадокса Гиббса ..	273
<i>L. Kohlmann and T. Vörös</i> : New Alpha-Decay Barrier Penetrabilities with Igo Potential: Even- and Odd-Mass Nuclei. — <i>Л. Колмманн и Т. Вереш</i> : Новая проходимость через потенциальный барьер с потенциалом Иго при α -распаде: четные и нечетные ядра	285
<i>J. Bacsó, J. Csikai and A. Pázsit</i> : Investigation of Mo ⁹² (<i>n</i> , 2 <i>n</i>) Mo ^{91,91m} Reaction. — <i>Й. Бачо, Й. Чикаи и А. Пажсит</i> : Исследование реакции Mo ⁹² (<i>n</i> , 2 <i>n</i>) Mo ^{91, 91m} the	295
Г. Нергеш, М. Ш. Силади и Б. Визкеleti: Исследование диффузационного процесса в германии. — <i>G. Nyerges, M. S. Szilágyi and B. Vizkelety</i> : Investigation of the Diffusion Process in Germanium	299

<i>F. Berencz: Die Berechnungen der $1sns^1S$-Zustände des Wasserstoffmoleküls auf Grund der Methode der Molekülbahnen II.</i> — <i>Ф. Беренц:</i> Определение состояния $1sns^1S$ молекулы водорода методом молекулярных орбит II.	307
<i>M. Tisza: Calculation of Nuclear Quadrupole Moments.</i> — <i>M. Тисза:</i> Вычисление ядерного квадрупольного момента	321
<i>M. Силади:</i> Расчет траектории электрона, движущегося между коаксиальными трубами, в присутствии полого пучка. — <i>M. Szilágyi: Calculation of the Trajectory of an Electron Moving between Coaxial Tubes in the Presence of a Hollow Electron Beam</i>	325
<i>M. Силади:</i> Периодическая электростатическая фокусировка ленточных электронных потоков. — <i>M. Szilágyi: Periodic Electrostatic Focusing of Sheet Electron Beams</i>	335
<i>J. Nyiri and A. Sebestyén: The Muon Decay in the Renormalizable Vector Boson Theory.</i> — <i>Ю. Нир и А. Шебештэн:</i> Распад мюона в перенормируемой теории слабых взаимодействий	351
<i>I. Tamassy-Lentei: Extraordinary Orbitals in the United Atom Model.</i> — <i>И. Тамаши-Лентей:</i> Необыкновенные орбиты в соединенной атомной модели	359
<i>C. Bojarski: Über die gegenseitige Beziehung von Konstanten einiger Theorien über Konzentrationsauslösung und Konzentrationspolarisation der Photolumineszenz von Lösungen</i>	367
<i>R. Gáspár: Universal Potential Eigenfunctions and Eigenvalues for the Selenium Atom</i>	371
<i>T. Szondy: A Simple Method for the Calculation of Coulomb and Hybrid Integrals</i>	381
<i>Z. Barát: Tarnóczy Tamás, Akusztika, Fizikai akusztika (Recensio)</i>	385
<i>I. Kovács: R. Ritschl und G. Holdt, Emissionsspektroskopie (Recensio)</i>	386
<i>K. Nagy: G. Ya. Lyubarskii, The Application of Group Theory in Physics (Recensio)</i>	387

ON THE ANODIC SIDE OSCILLATIONS OF LOW PRESSURE DC GAS DISCHARGES

By

J. BITÓ

INDUSTRIAL RESEARCH INSTITUTE FOR TELECOMMUNICATION TECHNIQUE, BUDAPEST

(Presented by G. Szigeti — Received: 10. X. 1963)

The more important results available so far in the literature dealing with the anode oscillations are reviewed and the author's own investigations of the anode oscillations appearing in low-pressure direct current mercury-argon discharges are described. It is found that direct and alternating current heating of the cathode influence the anode oscillations and curves showing the dependence of the amplitude and frequency of the oscillations on the cathode heating current are given. The influence exercised by an external magnetic field on the anode oscillations is also studied.

1. Introduction

The experimental and theoretical investigation of the characteristics of oscillations which appear in the anode space has been undertaken by several authors [1—13].

No unanimous view, however, has been formed so far concerning the explanation of the origin of the anode oscillations. The investigations carried out so far have demonstrated that there are a number of discharge factors that play an important part in the development of the oscillations and that have a strong influence on the characteristics of the oscillations.

Some of the authors [4, 8] trace the development of oscillations back to the periodic fluctuations appearing in the anode fall. Others [11] regard the displacement taking place in the heat equilibrium of the anode as being the cause of these oscillations. The investigations carried out so far [8, 12, 13] have also demonstrated that the surface and shape of the anode have a considerable influence on the oscillations and further that in the case of anodes arranged close to the wall of the discharge tube the disturbing effect of the wall will make itself felt in the characteristics of the oscillation [14]. Also the appearance of the anode spots with their glow balls may exercise an influence on the oscillations of the anode space [15].

In the course of his earlier investigations [13] the present author — after a detailed analysis of the relevant literature — has dealt with the dependence of the characteristics of the anode oscillations on the shape and the dimensions of the anode, on the intensity of the discharge current, as well as on the voltage of the auxiliary electric circuit applied at the anode.

The object of the investigations reported in the present article is to show that there are further factors influencing the oscillations and to analyse the influence of some of them in more detail. In particular the results of investigations of the influence exercised by the cathode heating and the external magnetic field on the anode oscillations will be reported.

2. Method of investigation

The experimental setup employed in the experiments may be seen in Fig. 1. The discharge tube T was fed by the stabilized direct current source SDC, and the current of the discharge limited by the symmetrically arranged ohmic resistances R_1 and R_2 . The discharge current could be read on the instrument I_t and the tube voltage of the discharge on the instrument V_t .

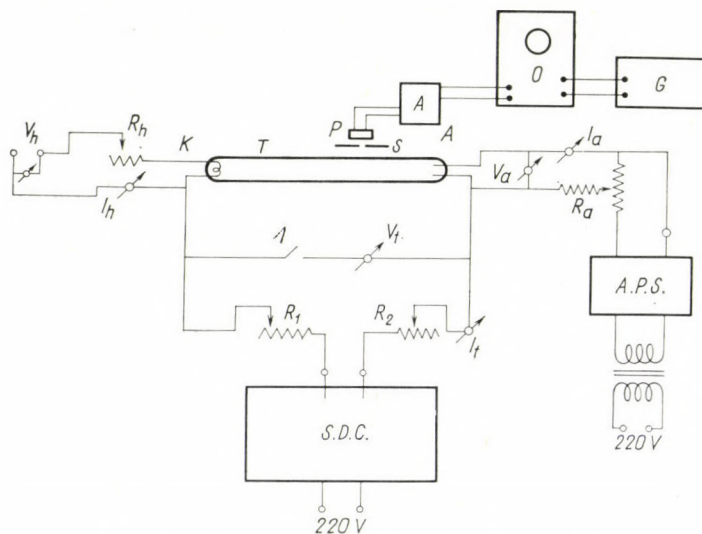


Fig. 1. Circuit diagram of the experimental setup

The current of the heating circuit which was placed next to the cathode K could be adjusted through the variation of the voltage V_h and the resistance R_h respectively. The heating current was measured by the instrument I_h , the heating voltage by the instrument V_h .

At the anode A an auxiliary electric circuit was used which was fed by the stabilized direct current source APS. The current of the circuit was shown by the instrument I_a , the voltage by the instrument V_a .

The measurements were effected partly by using a rotating disc and partly with the help of a photocell. The rotating disc method was applied mainly in the investigation of oscillations of lower frequency. Both with the

photo-cell and the rotating disc method the observations took place directly at the anode.

In the photo-cell measurements the light, the fluctuations of which could be observed at the anode, passed to the photo-cell through a slit which had been appropriately adjusted. The current fluctuations obtained from the photo-cell were amplified by the amplifier A and the signals then passed to the vertical input of the oscilloscope O. The horizontal input obtained oscillations of known frequency of the generator G. The frequency of the anode oscillations was determined by the Lissajoux curve method. The investigations of the oscillations (determination of frequency, amplitude) were limited to investigating the light fluctuations of the anode space, as it appeared from earlier investigations [7, 13], that the frequency of the current oscillations of the anode space is equal and their amplitude proportional to the frequency and amplitude, respectively, of the light fluctuations observed there. This statement was oscilloscopically checked for some value of the discharge current prior to the measurements, under the appropriate experimental conditions.

3. Test conditions

The length of the glass-walled discharge tube was 500 mm, its internal diameter 36 mm, its wall thickness 1 mm.

The cathode of the discharge tube was formed by a wolfram double spiral provided with an oxide coating promoting electron emission. On both sides of the cathode at a distance of 3 mm from the spiral one auxiliary electrode was arranged, each being of a thickness of 0,2 mm, width of 5 mm, length of 14 mm, which had a potential identical with that of the spiral. The anode of the discharge tube was composed of two parts. In the course of the experiments two anode constructions made of nickel were used, which are shown in Fig. 2. In the one case (Fig. 2a) the anode was formed by a cylinder and a disc arranged in it, while in the other a needle was co-axially arranged in the cylinder (Fig. 2b). The tip of the needle pointed in the direction of the positive column. The dimensions and characteristic data of the individual types may be seen in Figs. 2c and 2d, respectively. Both the wall thickness of the nickel cylinder and the thickness of the nickel disc were 0,2 mm. Both anode parts were provided with separate copper terminals.

The discharge tubes passed through the customary vacuum treatment, at the end of which it was filled with argon purified in a FeBa arc and of 3 mmHg pressure, and mercury of some 60 mg weight. In the course of the experiments neither the gas pressure, nor the type of gas has been varied. The adjustment of the gas pressure of the tube was effected to a precision of $\pm 0,05$ mmHg. The pressure of the mercury vapour was determined by the

wall temperature of the discharge tube which depended on the ambient temperature. In the course of the investigations the ambient temperature mounted to $25 \pm 1^\circ\text{C}$.

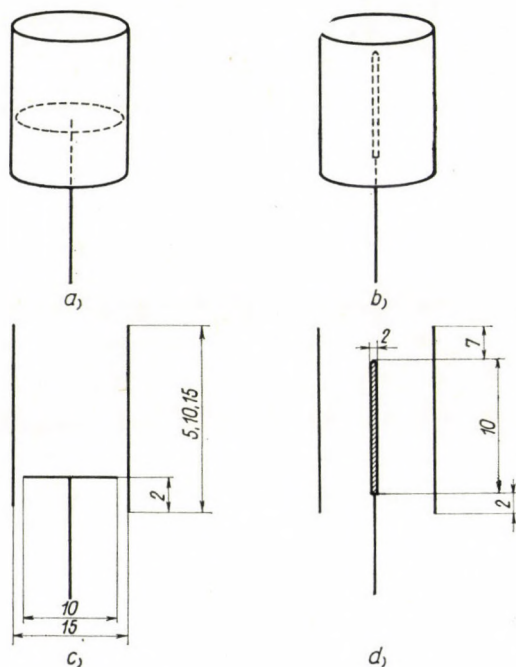


Fig. 2. The nickel anode constructions and their dimensions employed in the tests

Prior to starting the measurements the discharge tube was operated for 30 minutes, under the same conditions as those of the measurement.

The starting of the discharge was effected through the provision of proper cathode heating and the high-frequency pre-ionization of the discharge space.

4. Results

The investigations have been carried out at a discharge current of 100 mA and 400 mA. The voltage-current characteristics typical of the discharge tubes employed in the tests can be seen in Fig. 3. In the region of both the 100 mA and the 400 mA discharge currents the characteristics can be substituted to a good approximation by a straight section of negative slope, hence here there is no distinguished section of the characteristics as would influence the oscillations or bring about further oscillation effects.

SAGGAU [16] has studied the influence of cathode heating on the oscillations of the discharges. In the course of his investigations he has found that

the cathode heating has no influence on the frequency of the oscillations in the case of neon gas of 2 mmHg pressure. From his results it appears that under the investigated discharge conditions the frequency of the oscillations does not depend either on the cathode fall or on the positive anode fall.

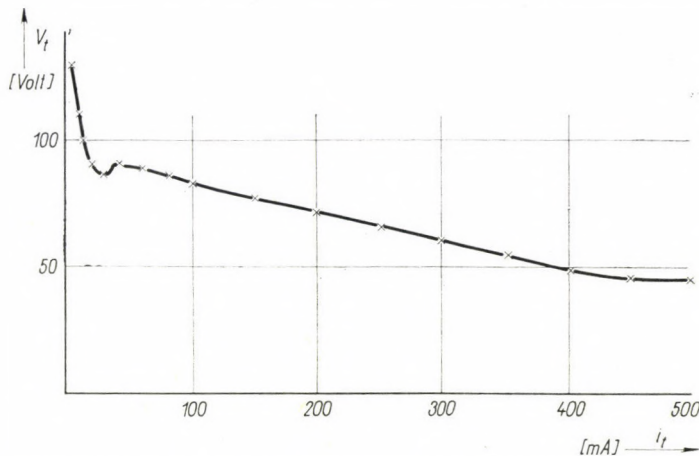


Fig. 3. The tube voltage vs. discharge current characteristics of the discharge tube

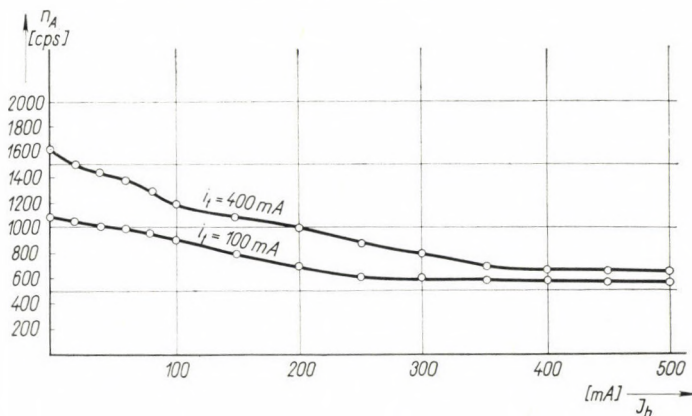


Fig. 4. The dependence in the case of direct current heating of the frequency n_A of anode oscillations on the heating current I_h at a discharge current of 100 mA and 400 mA

His measurements were carried out at a discharge current of 5 mA and the frequency of the observed oscillations was in the 1000 cps frequency range.

Our own investigations also included the determination of the dependence of the oscillation frequency on the cathode heating. The results of the measurements effected under the discharge conditions described above did not agree with the results of SAGGAU [16].

What resulted was that the oscillations of both the positive column and the anode space were influenced by the variation of the cathode heating current. Fig. 4 shows the dependence of the frequency of the oscillations on the intensity of the cathode heating current (direct current heating), at a supply voltage of 400 V in the case of discharge currents of 100 mA and 400 mA. It may be seen that at the given constant discharge current the frequency of the anode oscillations diminishes with the increase of the heating current intensity. The shape of this decreasing curve may be well approximated by reciprocal functions. As it could be expected on the basis of former investigations [13], the growth of the discharge current increased the frequency of the oscillations in this case as well.

Fig. 5 demonstrates the dependence of the oscillation amplitudes on the heating current at a discharge current of 100 mA and a supply voltage of 400 V. The curve *a* was obtained with alternating current heating, while the curve *b* shows the dependence resulting in the case of direct current heating. With the increase of the heating current the amplitude diminishes in both cases. This decrease is considerable particularly in the curve obtained in the case of direct current heating. From Fig. 5 it may also be seen that higher oscillation amplitudes will result with alternating current heating than in the case of direct current heating. Besides, the shape of the oscillations will also be distorted and more harmonic oscillations of the oscillation frequencies will appear, a fact that may be connected with the heating current of 50 cps frequency.

In any case it may be seen from Figs. 4 and 5 that the stability of the anode spaces is considerably affected (at least in the case of the discharge tubes of 500 mm length used and under the discharge conditions described) by the cathode heating, its intensity, and whether it is of a periodic (in this case of 50 cps frequency) or constant character. What may further be seen is that with the increase of the heating current the stability of the anode space will grow both in the case of direct and alternating current, while the amplitude and frequency of the oscillations will diminish.

The results shown in Figs. 4 and 5 have been obtained when the anode construction to be seen in Fig. 2a was employed. When that shown in Fig. 2b was used the frequency and amplitude of the oscillations increased as this could be expected on the basis of the results of [13]. The amplitude and frequency dependence on the heating current is not reproduced here as also in this case these were found to be similar to the dependence obtained in the case of the anode construction shown in Fig. 2a.

The increase of the casing height of the anode cylinder led also in this case to a decrease of only the amplitudes and the number of the harmonic oscillations. The character of the dependence on the heating current remained unchanged.

Summarizing the results it may be seen that under the measuring conditions employed here it is possible to influence not only the characteristics of the oscillations of the positive column but also the oscillations of the anode space from the cathode space through the cathode heating. The results obtained here do not agree with those of SAGGAU [16]. This might possibly be ascribed to the differences between the discharge conditions.

Investigations have also been made concerning the influence exercised by the external magnetic field on the anode oscillations. So far no report has appeared in this connection in the available literature. The effect of the

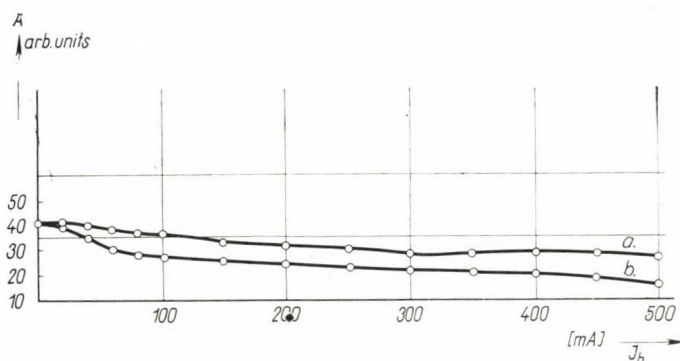


Fig. 5. The dependence of the amplitude A , recorded in arbitrary units, of the anode oscillations on the heating current with direct (b) and alternating current (a) heating

magnetic field upon the positive column and upon the basic processes of the plasma of arc discharge are known [17] but regarding the oscillations of the anode space no investigations have as yet been made.

The conclusions which could be drawn from the present experiments are mostly of a qualitative character. The external magnetic field parallel to the axis of the discharge leads in a known manner [17] to the contraction, perpendicularly to the direction of the field, of the anode glow-space and the shift of the discharge away from the wall. As a consequence, the amplitudes of the oscillations are reduced and the number of harmonic oscillations decrease correspondingly yet the oscillation frequency remains unchanged. Fresh oscillations of any considerable amplitude did not arise up to 20 kcps. Beyond this no investigations have been made. When the discharge current grew, the influence of the magnetic field increased and the amplitudes diminished accordingly. This stabilized the anode space to some extent probably through the reduction of the wall losses.

In certain respects it appears as if the phenomenon observed here may be caused by the same factor [14] as that influencing the oscillations and

mentioned in the introductory section, i.e. the part played by the nearness of the wall. When the wall of the discharge tube is sufficiently near to the axis of the discharge and to the discharge electrode, a significant part of the electrons may reach the wall surface by way of diffusion and thereby near the electrodes for instance in the present case in the space before the anode, the number of ionizations as well as the concentration of the space charges will be reduced. In order to neutralize the electrons accumulating at the wall an ion current will start from the anode space, which will result in further displacements around the anode. If complete neutralization does not result a radial electric field will develop which will strongly influence the value of the anode fall.

The axial magnetic field parallel to the axis of the discharge tube, at the same time, stabilizes also the anode-side end of the positive column. This stabilization has shown itself in the reduction of the oscillation amplitude and the noise level.

When the direction of the magnetic field was perpendicular to the axis of the discharge tube, eddy-like turbulent phenomena, well visible to the naked eye, developed both in the anode space and in the part of the positive column close to the anode. These decayed rapidly, without spreading any further. Here investigations using a photomultiplier have shown that a large number of new frequencies arise while in the centre of the turbulence very high but rapidly decaying amplitudes could be observed.

In the course of previous investigations [13] it was possible, by using the anode construction presented in Fig. 2a, to achieve that one glow light from the discharge should appear also on the tube end side of the anode plate.

This effect could be reproduced also in the present case by using the disc arranged in the cylinder at the anode and leaving the cylinder electrically unconnected. The same could be achieved, however, also through employing a magnetic field, by shifting the external magnetic field of perpendicular direction to the discharge, from the anode-side end of the positive column towards the end of the discharge tube. One may say that the plasma space, originally induced by the magnetic field at the anode-side end of the positive column had become frozen into the magnetic lines of force. Through the displacement of the magnetic field this also was shifted to the end of the tube. The glow light behind the electrodes at the back plate of the anode remained as long as the magnetic field existed there.

Similarly to the influence exerted on the anode oscillations [13] by the electric circuit arranged at the anode, the stabilizing effect (lower amplitudes, lower noise level) of a magnetic field could be observed also in the case of an external magnetic field parallel to the discharge axis. When in addition to the anodic circuit also the magnetic field perpendicular to the discharge axis acted upon the anode space, the turbulent effects described above increased considerably at low currents of the anode circuit I_a .

It will have become clear from the above that also the cathode heating influences the oscillations of both the positive column and the anode space. In the case of direct current cathode heating it was possible to achieve a more stable anode space as against that of the alternating current. A similar stabilizing effect was also found when an external magnetic field was applied parallel to the axis of the discharge.

REFERENCES

1. W. PUPP, Phys. Z., **33**, 844, 1932.
2. W. PUPP, Phys. Z., **34**, 756, 1933.
3. W. PUPP, Phys. Z., **36**, 61, 1935.
4. E. ROHNER, Appl. Sci. Res. Sec. **B5**, 90, 1955.
5. G. SZIGETI and J. BITÓ, Acta Phys. Hung., **II**, 103, 1960.
6. J. BITÓ, Hung. Telecomm. Techn., **II**, 23, 1960.
7. J. BITÓ, Hung. Phys. J., **10**, 303, 1962.
8. E. NÖLLE, Technisch-Wiss. Abh. der Osram Gesellschaft, **7**, 65, 1958.
9. A. V. RUBTSINSKI et al., Radiotechn. i Elektronika **4**, 1311, 1959.
10. K. OGAWA, J. Phys. Soc. Japan, **14**, 1746, 1959.
11. J. D. COBINE, Gaseous Conductors, Dover Publ., 1958.
12. N. A. KAPZOW, Elektrische Vorgänge in Gasen und in Vakuum. Deutscher Verl. der Wiss., Berlin, 1955.
13. J. BITÓ, Acta Phys. Hung., **17**, 283, 1964.
14. S. FLÜGGE, Handbuch der Phys., XXII, 422. Springer Verlag, Berlin, 1956.
15. K. G. EMELEUS, The Conduction of Electricity through Gases, Methuen, 1951.
16. B. SAGGAU, Proc. 4th Int. Conf. on Ioniz. Phenomena in Gases, **II**, 280, 1960.
17. A. GUTHRIE and R. K. WAKERLING, The Characteristics of Electrical Discharges in Magnetic Fields, McGraw-Hill Book Comp. Inc., New York, 1949.

ОБ АНОДНЫХ КОЛЕБАНИЯХ ГАЗОВЫХ РАЗРЯДОВ ПОСТОЯННОГО
ТОКА НИЗКОГО ДАВЛЕНИЯ

Й. БИТО

Р е з и о м е

Автор ознакомляет читателя с важнейшими результатами, относящимися к анодным колебаниям газовых разрядов и встречающимися по настоящий день в литературе. Появляющиеся при газовом разряде анодные колебания исследуются в ртутно-аргонном разряде постоянного тока низкого давления. В работе рассматривается далее, какое влияние оказывает нагревание катода постоянным и переменным токами на анодные колебания. Даётся зависимость амплитуды и частоты колебаний от тока нагревания катода. Исследуется влияние внешнего магнитного поля на анодные колебания.

ELECTRICAL RESISTIVITY CHANGE IN COLD-WORKED TUNGSTEN WIRES DURING RECOVERY AND RECRYSTALLIZATION

By

ELISABETH KOVÁCS-CSETÉNYI*

RESEARCH INSTITUTE FOR TECHNICAL PHYSICS, BUDAPEST

(Presented by T. Millner. — Received 24. X. 1963)

The isochronal annealing of tungsten (with K, Si, Al impurity contents, cold-worked in factory) shows that the electrical resistivity measured in liquid air decreases in stages with increasing temperature. From simultaneous microscopical and isothermal annealing investigations it was found that the first stage, which was observed above 900° K, is due to the rearrangement of the dislocations, while the second and the third stage arise from the primary and secondary recrystallization. The resistivity of the samples, which contain K, Si impurities, decreases continuously, because in this case the secondary recrystallization takes place quickly after the primary recrystallization. The resistivity change in the first stage shows logarithmic kinetics, the activation energy being 110 ± 10 Kal/mol for both samples, which value is an estimate for the activation energy of self-diffusion in tungsten.

Introduction

The recovery and recrystallization in cold-worked tungsten have been investigated by many authors [1—8]. According to SCHULTZ [4] the resistivity of tungsten wire deformed by drawing at room temperature decreases during isochronal annealing in stages. He assumed the first of these observed at about 400° C to be due to vacancy migration, while the processes taking place above 600° C arise from dislocation annihilation. Resistivity change during the secondary recrystallization was obtained only in highly deformed samples.

KOO [5] as well as NEIMARK and SWALIN [6] investigated the resistivity change in the temperature range of 250 — 450° C, and explained the obtained decrease by vacancy annihilation. Their isothermal annealing data, however, showed that in this temperature interval different processes occur.

Increasing of the resistivity has been observed during recrystallization by KLEBER and KOHLSTRUNG [8]. We have shown, however, that this anomalous behaviour arises from the change of the geometrical sizes of the wire, probably caused by a Langmuir cycle during heat treatment.

It is difficult to make a comparison between the available data because the samples investigated by different authors contained different impurities and were deformed by different amounts at different temperatures.

In order to study the recovery and recrystallization in tungsten with different impurity contents its electrical resistivity was measured in liquid air.

* Present address: Research Institute of Non-Ferrous Metals, Budapest, XI. Fehérvári út.

Investigations of the kinetics of the dislocation rearrangement in tungsten are not available in the literature. In the present work this process was investigated also by isothermal annealing. From the measurements we determined the kinetics and obtained an estimate for the activation energy of the process.

Experimental procedure

The specimens were drawn at constantly decreasing temperatures from sinterized tungsten rods forged at 1500° C. The final drawing was done at about 600° C, and after this process the diameter of the wires became 0,3 mm. The differences between the two kinds of samples investigated by us were as follows:

a) before the reduction K, Si (UC) and K, Si, Al (GK) impurities were added to the tungsten oxide, respectively, the total amount of these impurities being about 1% [9];

b) the sinterizing and the annealing of the rods were carried out in somewhat different ways during the forging. A large part of the impurity content has been evaporated during the sinterizing. The drawing process between 4,3 and 0,3 mm diameter and the initial grain size were approximately the same in the case of both samples. The densities of the two kinds of 4,3 mm diameter rods differed (GK 18,8 g/cm³ and UC 19,0 g/cm³), therefore the same drawing process caused different amounts of strain.

The heat treatment of the wires was carried out in vacuum by direct heating in the temperature interval 900—2500° K. Before heating the pressure was 10⁻⁵ mmHg it became about 10⁻³ mmHg at 2500° K because of the warming up of the entire system.

During isochronal annealing the specimens were heated for 15 minutes at each temperature in steps of 100—200° C. Isothermal annealing was made in the temperature interval of 1000—1400° K with annealing times from 5 minutes to 7 hours. The temperature of the specimen was determined on the basis of the data of Langmuir by measuring the heating current. The error incurred in the temperature measurement arises from the following factors:

1. resistivity change of the sample during the heating;
2. change of the geometrical sizes caused by the Langmuir cycle;
3. the cooling effect of the grips is a function of the temperature;
4. the error in the current measurement.

The errors 1—3 can be eliminated by suitable corrections. The accuracy of the temperature measurement at about 1500° K was $\pm 10^\circ$ C.

The resistivity of the specimens was measured after every annealing process in liquid air and in alcohol at room temperature. The change of the temperature in liquid air was eliminated by the use of a tungsten dummy of the same diameter as that of the specimen. The resistivity measurements

were carried out by means of a Diesselhorst compensator. The error in these measurements amounted to 0,2%. In order to eliminate the geometrical sizes of the specimen we used the ratio

$$\frac{r_{80^\circ K}}{r_{293^\circ K}} \approx \frac{\varrho_{80^\circ K}}{\varrho_{293^\circ K}}.$$

Simultaneously with the resistivity measurements microscopical investigations were made after every step of annealing.

Experimental results

Figs. 1a and 1b show the results obtained by isochronal annealing. Before annealing the resistivity of the GK samples is about 5% higher than that of the UK samples. The recovery process takes place in both materials at about $900^\circ K$ and up to $1500^\circ K$ the resistivity varies in the same manner.

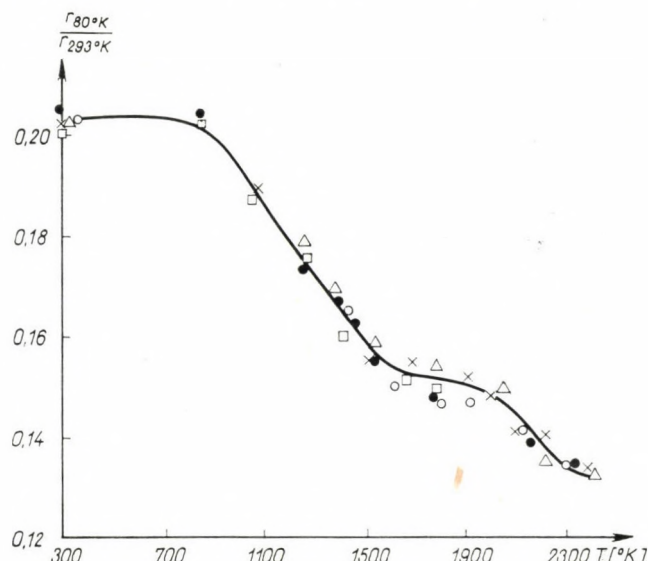


Fig. 1a. Resistivity change in GK wires during isochronal annealing. Annealing time is 15'

In this interval there is no change in the texture of the samples (Fig. 2), further at this stage the resistivity of the drawn wires decreases by more than 20%. In the deformed matrix of the GK wires grains of about 1μ diameter appear, after heating at $1700^\circ K$. This process can be considered as the beginning of the primary recrystallization. The resistivity change up to $1900^\circ K$ is less than 1%. After heating at $2100^\circ K$ large grains with well-defined boundar-

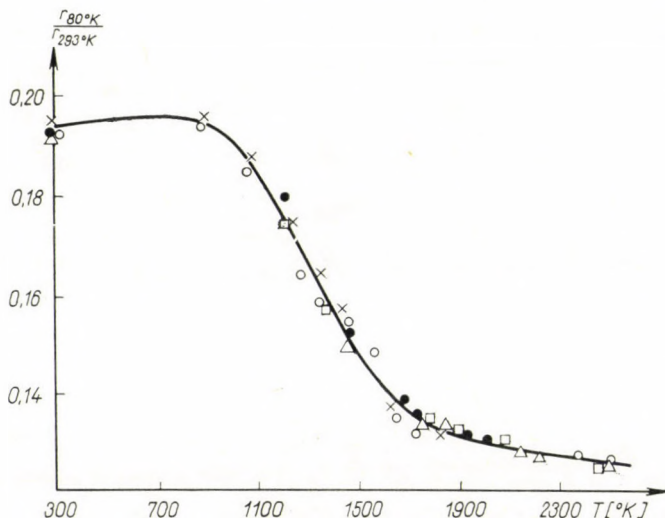


Fig. 1b. Resistivity change in UC wires during isochronal annealing. Annealing time is 15'

ies appear. After 2300° K the whole cross-section is covered by large grains of 10–15 mm length and of 0,1–0,3 mm diameter produced during secondary recrystallization. The resistivity decreases by a further 10% during this process.

According to our resistivity measurements carried out on UC wires, the last two processes are not sharply separated, further, the primary and secondary recrystallization take place at lower temperatures (Fig. 2). When the length of the grains becomes about one millimeter the resistivity gradually tends towards a constant value.

The isothermal recovery process of UC wires treated at different temperatures is shown in Fig. 3.

Discussion

According to the data of THOMPSON [10] the vacancies produced by cold working in b.c.c. metals disappear at temperatures lower than $T_M/5$, where T_M is the temperature of the melting point in °K, which is 730° K in the case of tungsten. Our specimens were worked at higher temperatures, therefore we can assume that the vacancy migration took place during the deformation process.

Our results show that the recovery during isothermal annealing has logarithmic kinetics (Fig. 4):

$$\frac{\Delta \varrho}{\varrho_0} = A - B \log t, \quad (1)$$

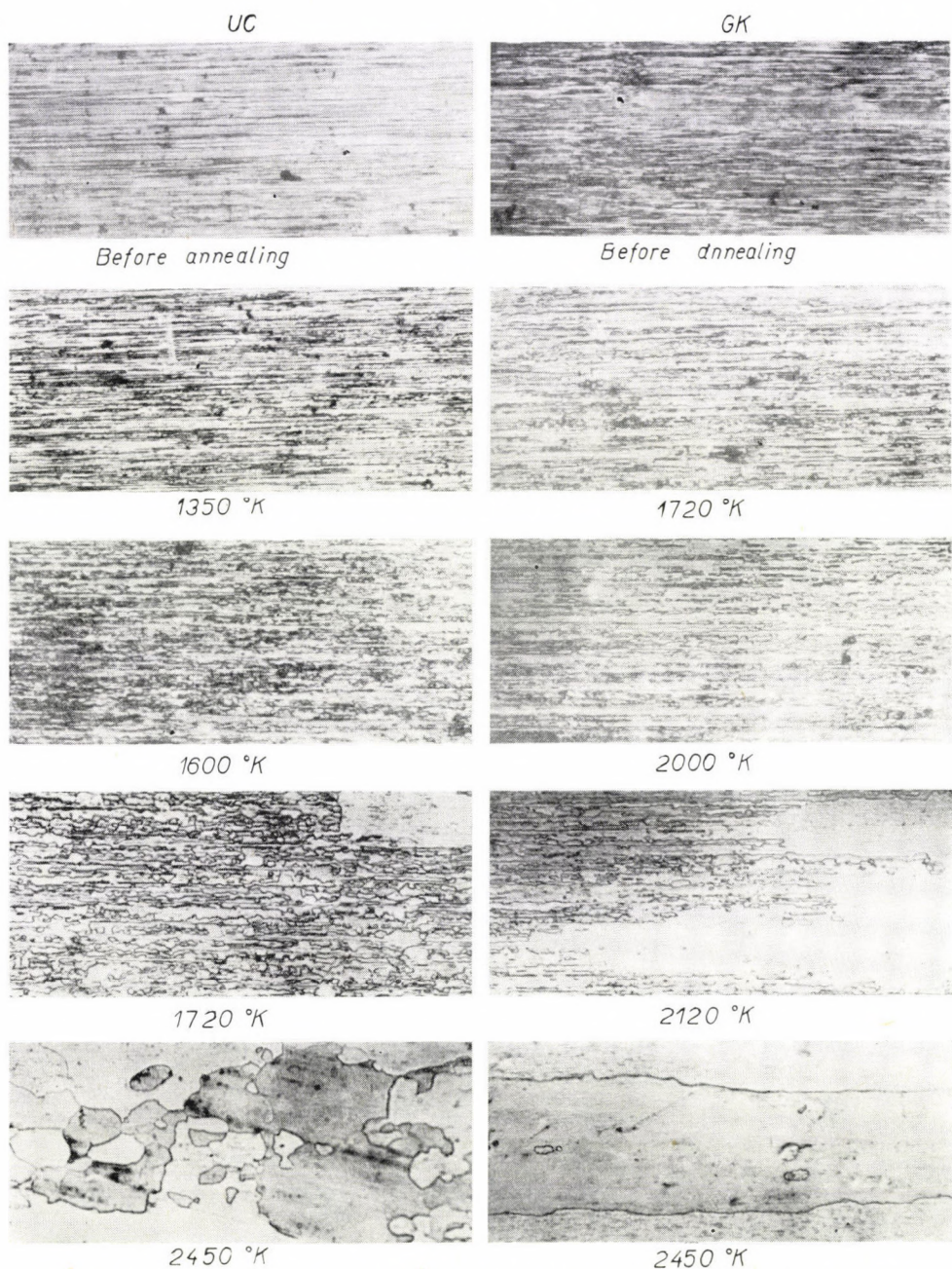


Fig. 2. Micro-photographs made from UC and GK wires at different stages of the heat treatment

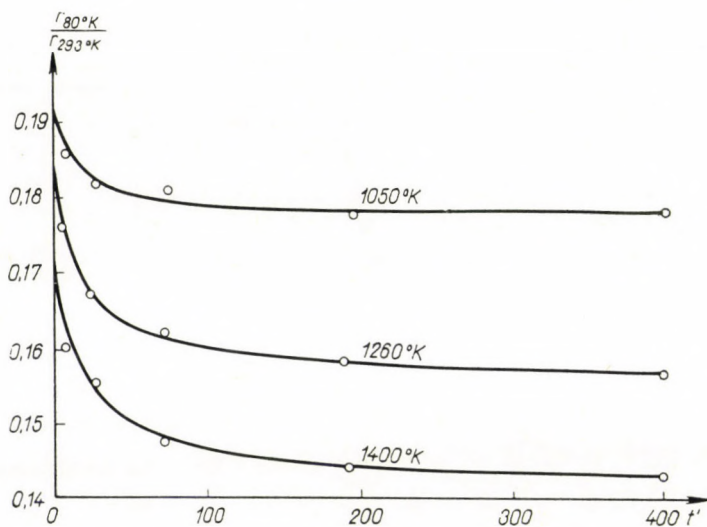
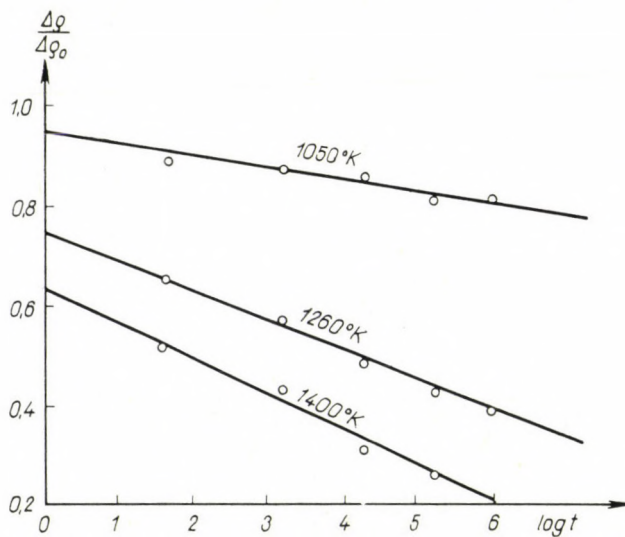


Fig. 3. Resistivity change in UC wires during isothermal annealing

Fig. 4. Resistivity change in UC wires as a function of $\log t$

where $\Delta \rho$ is the extra-resistivity measured in liquid air after time t and $\Delta \rho_0$ is the total resistivity change during heat treatment, and A and B are constants.

Similar kinetics has also been observed during recovery in yield point investigations [11] as well as in the release of the stored energy [12]. In these cases the recovery process took place by dislocation rearrangement and annihilation. It may be assumed therefore that the process is the same in our case.

The rate of such a process is governed by the climb motion of the dislocations, which means that the activation energy is proportional to the measured quantity [13], therefore the rate of the resistivity change may be given in the following form:

$$\frac{d \frac{\Delta \varrho}{\Delta \varrho_0}}{dt} = - k e^{-\frac{E_0 - b \frac{\Delta \varrho}{\Delta \varrho_0}}{RT}}, \quad (2)$$

where E_0 is the activation energy of the self-diffusion, T is the absolute temperature, R is the universal gas constant, and k and b are constants. Eq. (2) can be transformed by integration into (1), therefore E_0 can be determined from the data given by the linear function $\left(\frac{\Delta \varrho}{\Delta \varrho_0} (\log t) \right) 1$. From the present measurements we obtained $E_0 = 110 \pm 10$ Kal/mol. According to VAN LIEMPT [14] the activation energy of self-diffusion in tungsten is about 140 Kal/mol. The migration energy of the vacancy in tungsten was measured by Koo [5] who obtained 39,2 Kal/mol. KRAFTMAKHER and STRELKOV [15] from specific heat measurements obtained an energy of 72,5 Kal/mol for the vacancy formation in tungsten. With the use of these values for the activation energy of the self-diffusion in tungsten we obtain 111,7 Kal/mol. Our result is in good agreement with the mentioned data within the given accuracy for both UC and GK samples.

The resistivity change during secondary recrystallization in tungsten with different impurity contents may be caused by dislocation annihilation, decreasing of the grain boundary surface and impurity segregation. The individual effect of these processes is not well known at present, but further measurements will be made in order to investigate the effect of the single processes.

Summary

The resistivity of highly deformed tungsten was measured in liquid air during annealing. From the measurements, it was found that if the tungsten contains K, Si, Al impurities, the resistivity decreases in stages, while if the impurity contains only K, Si, the resistivity decreases continuously. The resistivity decrease starting above 900° K may probably be ascribed to dislocation rearrangement, the activation energy of this process being 110 ± 10 Kal/mol for both Uc and GK wires. For GK wires a stage of constant resistivity begins at about 1500° K. Simultaneous microscopical investigations show that this stage is due to the primary recrystallization. Another stage was also observed above 2100° K, which arises from the secondary recrystallization.

The continuous decrease of the resistivity in UC wires can be explained by the fact that in these wires the secondary recrystallization takes place very quickly after the primary recrystallization.

Acknowledgement

The author is indebted to Prof. T. MILLNER for suggesting the problem and for valuable discussions.

REFERENCES

1. J. W. PUGH, 3. Plansee Seminar "De Re Metallica", 97, Reutte, Tyrol, 1959.
2. G. L. DAVIS, Metallurgia, **68**, 177, 1958.
3. R. C. KOO and J. LESS, Common Metals, **3**, 412, 1961.
4. H. SCHULTZ, Zs. Naturforschung, **142**, 361, 1959.
5. R. C. KOO, Reactive Metals, p. 265, Interscience Publishers, New York, London, 1958.
6. L. A. NEIMARK and R. A. SWALIN, Trans. AIME, **218**, 82, 1960.
7. W. KÖSTER and W. SCHÜLE, Zs. Metallkunde, **48**, 634, 1957.
8. W. KLEBER and G. KOHLSTUNG, Die Technik, **14**, 281, 1959.
9. T. MILLNER, Acta Techn. Acad. Sci. Hung., **17**, 67, 1957.
10. M. W. THOMPSON, Phil. Mag., **5**, 278, 1960.
11. G. MASING and J. RAFFELSIEPER, Zs. Metallkunde, **41**, 65, 1950.
12. H. U. ASTROM, Acta Met., **3**, 508, 1955.
13. M. B. BEVER, Creep and Recovery, p. 22, Am. Soc. Met., Cleveland, Ohio, 1957.
14. J. A. M. VAN LIEMPT, Rec. Trav. Chim., **64**, 239, 1945.
15. J. A. A. KRAFTMAKER and P. G. STRELKOV, Fiz. Tverd. Tel., **4**, 2271, 1962.

ИЗМЕНЕНИЕ СОПРОТИВЛЕНИЯ ВОЛЬФРАМОВЫХ ПРОВОЛОК, РАЗРАБОТАННЫХ В ХОЛОДНОМ СОСТОЯНИИ, В ПРОЦЕССАХ ОБНОВЛЕНИЯ И РЕКРИСТАЛЛИЗАЦИИ

Е. КОВАЧ-ЧЕТЕНИ

Р е з ю м е

Измерённое в жидкокомpressed воздухе сопротивление вольфрамовой проволоки, изготовленной в заводских условиях холодным методом и содержащей К, Si и Al, при изохронном темперировании изменяется скачками. В соответствии с результатами, полученными съёмками металлического микроскопа и изотермическим темперированием, уменьшения сопротивления обусловливаются: появляющееся выше 900° К — перераспределением дислокаций, начинающийся при 1500° К близко горизонтальный участок — первичной рекристаллизацией, а следующее уменьшение, начинающееся при 2100° К — вторичной рекристаллизацией. Сопротивление проволоки с легирующими элементами К, Si уменьшается монотонно, так как первичная и вторичная рекристаллизации быстро следуют одна за другой. Предшествующий первичной рекристаллизации процесс показывает логарифмическую кинетику, энергия активации 110 ± 10 kcal/mol для обоих видов проволоки. Это можно считать оценкой по отношению самодиффузионной энергии активации вольфрама.

WAVE EQUATIONS IN MOMENTUM SPACE

By

S. DATTA MAJUMDAR

DEPARTMENT OF PHYSICS, UNIVERSITY COLLEGE OF SCIENCE, CALCUTTA, INDIA

(Presented by A. Kónya. — Received 4. XI. 1963)

The behaviour of wave functions in momentum space under rotation is studied in detail and the results are used to reduce the number of independent variables in the integral wave equation for a three-particle system.

1. Introduction

It is known that the number of independent variables in SCHRÖDINGER's equation for N interacting particles can be reduced from $3N$ to $3N - 6$ by making use of the translational and rotational invariance of the problem. The reduction has been carried out explicitly by a number of authors [1–5]. SCHRÖDINGER's equation transforms into an integral equation [6–13] in the momentum space, and from the invariance of this equation under rotation it is evident that a similar reduction should be possible in the momentum space also. But, this problem, unlike its counterpart in the coordinate space, has not attracted much attention, probably because integral equations are believed to be less convenient for physical applications than differential equations. But, if we leave aside the question of solvability of the equations, the reduction of the number of independent variables by itself is a problem of considerable theoretical interest. In this connection mention must be made of the work of M. LÉVY [14] who, by using some theorems of HECKE and ERDÉLYI, succeeded in reducing the integral equation for a single particle in a central field to one involving a single variable. By analogy with the equation in coordinate space this may be called "the radial equation in momentum space". In the relativistic case he gets a pair of linked integral equations which are different but derivable from the four equations previously obtained by RUBINOWICZ [12] by applying the Fourier transformation to DIRAC's equation. The equations are new and cannot be derived from the radial equations in coordinate space by the simple Fourier transformation.

In the present paper we consider a system of three spinless particles interacting through a potential dependent only on their mutual distances, and discuss methods for setting up the radial equations in momentum space

for states of definite symmetry and orbital angular momentum. The case of S states being trivial, only P states are discussed here in some detail. The generalization to an arbitrary number of particles and to arbitrary values of l is straightforward, although the equations may be too complicated to be presented. The procedure in outline is as follows:

After the elimination of the motion of the centre of mass the wave function in momentum space $G(p_1, p_2)$ is described by means of six coordinates, the lengths of the vectors p_1, p_2 , the angle θ between them, and three Euler angles ϕ, χ, λ determining the orientation in the p -space of the triangle formed by p_1 and p_2 . The rotational symmetry of the problem permits $G(p_1, p_2)$ to be expanded in a series of the form (6) which, when substituted in the integral equation, again gives a linear expression in $U_{lm\tau}$ with coefficients involving integrals over f_τ . Equating to zero the coefficient of each $U_{lm\tau}$ in this expression one gets a system of simultaneous integral equations for determining the f_τ . These are the radial equations in momentum space. The equations split up into two independent sets, one involving only odd values of τ , and the other only even values.

Before proceeding to derive the radial equations we must emphasize that the rotation, reflection and permutation symmetries remain unaltered in momentum space. If, for instance, a wave function has the form $\psi(r) = R(r) Y_{lm}(\ell, \varphi)$ in coordinate space, then its Fourier transform will have the form

$$G(p) = \left[i^l p^{-1/2} \int_0^\infty R(r) J_{l+1/2}(pr) r^{3/2} dr \right] \cdot Y_{lm}(\theta', \varphi'), \quad (1)$$

where θ', φ' are the polar and azimuthal angles of the vector p . In fact, the entire theory of angular momentum, as formulated in coordinate space, can be taken over unmodified to the momentum space.

2. The integral equation and the Poincaré—Whittaker coordinates

In the author's work on the problem of three bodies [4] in quantum mechanics (to be referred to as I) the coordinates used by POINCARÉ and WHITTAKER [15] in the classical problem proved to be very helpful in deriving the radial equations and in introducing the symmetries mentioned in the previous section. As pointed out by JACKSON [5] this system of coordinates is superior in many respects to those used by other workers. As we wish to retain the advantages gained, the same coordinates will be used in momentum space with the consequent simplification in the mathematical analysis.

If r_1 and r_2 are the Cartesian coordinates of the particles 1 and 2 relative to the 3rd particle and if, to avoid unnecessary complications, the centre of

gravity of the system is taken to be at rest, then the angular momentum operators take the form (see end of Sec. 157, ref. [15])

$$M_{(r)} = -ir_1 \times \nabla_1 - ir_2 \times \nabla_2. \quad (2)$$

In momentum space these operators become

$$M_{(p)} = -ip_1 \times \frac{\partial}{\partial p_1} - ip_2 \times \frac{\partial}{\partial p_2} \quad (3)$$

and SCHRÖDINGER's equation for the three-particle system with the potential energy $U_1(r_1) + U_2(r_2) + U_{12}(r_{12})$ goes over into the integral equation

$$\begin{aligned} & - (2\pi)^{3/2} \left[\frac{1}{2} \left(\frac{1}{m_1} + \frac{1}{m_3} \right) p_1^2 + \frac{1}{2} \left(\frac{1}{m_2} + \frac{1}{m_3} \right) p_2^2 + \right. \\ & \left. + \frac{1}{m_3} p_1 \cdot p_2 - E \right] G(p_1, p_2) \equiv TG(p_1, p_2) = \\ & = \int [V_1(\varrho) G(p_1 + \varrho, p_2) + V_2(\varrho) G(p_1, p_2 + \varrho) + V_{12}(\varrho) G(p_1 + \varrho, p_2 - \varrho)] d\varrho, \end{aligned} \quad (4)$$

where the V 's are the Fourier transforms of the U 's. We now pass on to the POINCARÉ—WHITTAKER coordinates by the transformations

$$\begin{aligned} p_1^{-1}(p_{1X} + ip_{1Y}) &= \sin \theta_1 e^{i\varphi_1} = e^{i\chi} (\cos \Phi_1 + i \sin \Phi_1 \cos \lambda), \\ p_2^{-1}(p_{2X} + ip_{2Y}) &= \sin \theta_2 e^{i\varphi_2} = e^{i\chi} (\cos \Phi_2 + i \sin \Phi_2 \cos \lambda), \\ p_{1Z}/p_1 &= \cos \theta_1 = \sin \Phi_1 \sin \lambda, \quad p_{2Z}/p_2 = \cos \theta_2 = \sin \Phi_2 \sin \lambda, \\ \Phi &= \Phi_1, \quad \Theta = \Phi_2 - \Phi_1. \end{aligned} \quad (5)$$

The coordinates are interpreted physically as follows: In addition to the axes OX, OY, OZ fixed in momentum space let us take another set of axes Ox, Oy, Oz determined partly by the vectors p_1, p_2 . Then Φ, χ, λ are the Euler angles specifying the relative orientation of the two sets of axes. If OK is perpendicular to the plane ZOz, then $\chi = \langle \text{OK}, \text{OX} \rangle$, $\Phi = \langle \text{OK}, \text{Ox} \rangle$, and $\lambda = \langle \text{OZ}, \text{Oz} \rangle$. The symbol $\langle A, B \rangle$ used here denotes the angle between the vectors A, B . It is easily seen that the vectors p_1 and p_2 both lie in the xy-plane and that p_1 is directed along Ox.

It is to be noted that, while in coordinate space the transformation affects only the kinetic part of the Hamiltonian leaving the potential energy unaltered, in momentum space it does just the opposite thing. The difference is brought to clear relief when one considers the contribution to the kinetic energy arising from the motion of the third particle. While in eq. (5) of I it

gives rise to all the eight terms occurring as the coefficient of $2C$, in eq. (4) of the present paper the full effect is contained in a single term $\frac{1}{m_s} p_1 \cdot p_2$. This is an important difference between the two treatments.

Returning to eq. (3) we find that the components of angular momentum in the new coordinates involve the Euler angles Φ, χ, λ only and have the usual forms given in the literature [16]. It should, therefore, be possible to write the wave function G as a linear combination of the symmetric top functions $U_{lm\tau}(\Phi, \chi, \lambda)$ (see Appendix) with coefficients which are functions of p_1, p_2, Θ . Thus,

$$G(p_1, p_2) = \sum_{\tau} f_{\tau}(p_1, p_2, \Theta) U_{lm\tau}(\Phi, \chi, \lambda). \quad (6)$$

This is the analogue of eq. (1) in the three-particle case. For states of even (or odd) parity the summation extends over even (or odd) values of τ only. The simplification results from the fact that a total reflection at the origin of the p -space is obtained by changing Φ to $\pi + \Phi$ and by keeping the other coordinates unaltered. A symmetric top function, as a consequence, gets multiplied by a factor $e^{i\tau\pi}$. Thus, for P states of odd parity arising, for instance, from component angular momenta $l_1 = 0, l_2 = 1$, the wave function can be written in the form

$$G_{1m}^0 = f_1 U_{1m1} + f_{-1} U_{1m-1}.$$

This will be called Case (ii). For P states of even parity, which can occur only when l_1 and l_2 are equal, we must have

$$G_{1m}^e = f_0 U_{1m0}.$$

This will be called Case (i). The rotational symmetry of the problem, however, makes it unnecessary to carry out the calculation for the $2l + 1$ values of m separately, the functions f_{τ} being the same for all m . We, therefore, put $m = 0$ in the above equations, obtaining

$$G_{10}^0 = f_1 U_{101} + f_{-1} U_{10-1}, \quad G_{10}^e = f_0 U_{100}. \quad (7)$$

The next step is to substitute the expressions (7) into eq. (4). It is expected that after some manipulations one will get on the right-hand side a linear expression in U_{101} and U_{10-1} , in Case (ii), with coefficients involving integrals over f_1 and f_{-1} . The linear independence of the functions U_{101}, U_{10-1} will then give a pair of simultaneous integral equations for determining f_1 and f_{-1} . In Case (i) one should get a single integral equation for f_0 . But, at the very outset a difficulty arises in substituting the series into the integral equation, because the two are expressed in different coordinates. Two courses are open to us, either, to transform eq. (4) to the new coordinates, or, to express the

functions U_{lmr} in Cartesian coordinates. The second alternative is found to be more convenient if use is made of the following analysis.

The components of angular momentum of the system are given by the expressions (2) or (3), which are formally the same as the angular momentum of *two* particles relative to a fixed centre. It is, therefore, possible to write the eigenfunctions of total angular momentum as Clebsch—Gordan series, that is, as series of products of the spherical harmonics $Y_{l_1 m_1}(\ell_1, \varphi_1)$, $Y_{l_2 m_2}(\ell_2, \varphi_2)$. Since the U_{lmr} are also eigenfunctions of the same operators, it follows that a Clebsch—Gordan series χ_{lm} must admit of an expansion of the form $\sum_r g_r(\theta) U_{lmr}$. The expansion for a spherical harmonic, which is the simplest example of such a series, is worked out in the Appendix. For given l and m a Clebsch—Gordan series can, however, originate from component angular momenta in an infinite variety of ways. For series of different origin (that is, arising from different pairs of values of l_1 and l_2) the coefficients $g_r(\theta)$ in the expansion will, of course, be different. Let us now select at random $2l + 1$ series χ_{lm} of different origin. These may be looked upon as $2l + 1$ equations for determining the U_{lmr} in terms of the χ_{lm} . If the equations are solved and the solution is expressed in Cartesian coordinates then the result must be unique, that is, must be independent of the choice of the $2l + 1$ Clebsch—Gordan series. Thus, we are able to express the U_{lmr} in Cartesian coordinates without getting involved in intricate calculations.

3. Reduction of the integral equation

Once the functions U_{lmr} are expressed in Cartesian coordinates it is easy to substitute them into eq. (4) and eliminate the angular variables. In Case (i) some simplification is achieved by taking the wave function in the form $-2ip_1 p_2 \sin \Theta F(p_1, p_2, \langle p_1, p_2 \rangle) U_{100}$ which, by the procedure outlined above, can be written as

$$G(p_1, p_2) = [p_{1+} p_{2-} - c.c.] F. \quad (8)$$

Here, $p_{1+} = p_{1X} + ip_{1Y}$, $p_{2-} = p_{2X} - ip_{2Y}$, $\langle p_1, p_2 \rangle$ is the angle between p_1, p_2 , and *c.c.* means 'the complex conjugate'. For this wave function eq. (4) takes the form

$$\begin{aligned} -2i p_1 p_2 \sin \Theta \cdot T F U_{100} = & \int [V_1(\varrho) F^{(1)} \{(p_{1+} + \varrho_+) p_{2-} - c.c.\} \\ & + V_2(\varrho) F^{(2)} \{p_{1+} (p_{2-} + \varrho_-) - c.c.\} + \\ & + V_{12}(\varrho) F^{(12)} \{(p_{1+} + \varrho_+) (p_{2-} - \varrho_-) - c.c.\}] d\varrho, \end{aligned}$$

where

$$\begin{aligned} F^{(1)} &= F(|p_1 + \varrho|, p_2, \langle p_1 + \varrho, p_2 \rangle), \quad F^{(2)} = F(p_1, |p_2 + \varrho|, \langle p_1, p_2 + \varrho \rangle), \\ F^{(12)} &= (|p_1 + \varrho|, |p_2 - \varrho|, \langle p_1 + \varrho, p_2 - \varrho \rangle). \end{aligned}$$

Since the integration is to be performed with p_1 and p_2 fixed, we can use for the purpose the components of ϱ in the frame Oxyz and write

$$\varrho_R = \varrho_x(xR) + \varrho_y(yR) + \varrho_z(zR),$$

($R = X, Y, Z$, and (xX) etc. are the direction cosines.) This gives

$$\varrho_+ = [\varrho_x(\cos\Phi + i\sin\Phi\cos\lambda) + \varrho_y(-\sin\Phi + i\cos\Phi\cos\lambda) + \varrho_z(-i\sin\lambda)] e^{i\zeta}.$$

The last term in this expression involves $\sin\lambda$ and will cause difficulties unless the corresponding integral over ϱ vanishes. That the integral does indeed vanish can be seen by reflecting the vector ϱ on the p_1p_2 -plane. This leaves $\langle p_1 + \varrho, p_2 \rangle$, $|p_1 + \varrho|$ etc. unchanged but changes ϱ_z into its negative. Thus, the integrand changes sign after the reflection, and the contributions to the integral from the original and the reflected volume elements cancel exactly. The term involving ϱ_z can, therefore, be omitted from the expressions for ϱ_+ , ϱ_- which, after substitution in the integral equation, give rise to an expression containing the factor U_{100} only. The omission of this common factor then leads to the equation

$$\begin{aligned} TF = & \int [V_1(\varrho) F^{(1)} \{1 + p_1^{-1}(\varrho_x - \varrho_y \cot\Theta)\} + \\ & + V_2(\varrho) F^{(2)} \{1 + p_2^{-1}(\varrho_y \operatorname{cosec}\Theta)\} + \\ & + V_{12}(\varrho) F^{(12)} \{1 + p_1^{-1}(\varrho_x - \varrho_y \cot\Theta) - p_2^{-1} \varrho_y \operatorname{cosec}\Theta\}] d\varrho. \end{aligned} \quad (9)$$

This is the radial equation for P states of even parity. It differs from the equation for S states by the additional terms involving ϱ_x and ϱ_y . The symmetry with respect to the indices 1 and 2 can be restored in this equation by writing $-\varrho_x \sin\Theta + \varrho_y \cos\Theta$ as the component of ϱ perpendicular to p_2 .

In Case (ii) it is convenient to take the wave function in the form

$$\sqrt{2}iG(p_1, p_2) = p_1 F_1(U_{101}(\Phi_1) + U_{10-1}(\Phi_1)) + p_2 F_2(U_{101}(\Phi_2) + U_{10-1}(\Phi_2)), \quad (10)$$

which is explicitly symmetrical in the indices 1 and 2 and is, therefore, suitable for introducing the permutation symmetry in the case of two identical particles. The expression simplifies to

$$G(p_1, p_2) = p_1 F_1 \cos\theta_1 + p_2 F_2 \cos\theta_2$$

and the calculation proceeds as in Case (i) with the necessary modifications. As already mentioned, the result will be a pair of simultaneous integral equations for F_1 and F_2 obtained by equating to zero the coefficients of U_{101} and U_{10-1} in the final equation. The derivation is simple and is omitted for brevity.

Appendix

The expression for a spherical harmonic in terms of the symmetric top functions.

Since the coefficient of $U_{lm\tau}$ in the expansion is independent of m , it is sufficient to derive the expression for one particular value of m . For $m = -l$ the function $U_{l-l\tau}$ has the simple form

$$U_{l-l\tau} = \exp.(-il\zeta + i\tau\Phi) \cdot i^l \sqrt{(2l)!} \left[(l-\tau)! (l+\tau)! \right]^{-1/2} \left(\cos \frac{\lambda}{2} \right)^{l-\tau} \left(\sin \frac{\lambda}{2} \right)^{l+\tau}.$$

This value of m is, therefore, likely to simplify the calculation. The spherical harmonics are defined by the formula

$$Y_{lm}(\theta, \varphi) = \left[\frac{(l-m)!}{(l+m)!} \right]^{1/2} e^{im\varphi} (-\sin \theta)^m \left[\frac{d}{d(\cos \theta)} \right]^{l+m} (\cos^2 \theta - 1)^l$$

with $\left[\frac{2l+1}{4\pi} \right]^{1/2} \cdot \frac{1}{2^l l!}$ as the normalization factor. For $m = -l$

$$\begin{aligned} Y_{l-l}(\theta_1, \varphi_1) &= \sqrt{(2l)!} (\sin \theta_1 e^{-i\varphi_1})^l = \sqrt{(2l)!} \left(e^{i\Phi} \sin^2 \frac{\lambda}{2} + e^{-i\Phi} \cos^2 \frac{\lambda}{2} \right)^l e^{-il\zeta} = \\ &= (-i)^l l! \sum_{\tau} \left[(l-\tau)! (l+\tau)! \right]^{1/2} \left[\frac{l-\tau}{2}! \frac{l+\tau}{2}! \right]^{-1} U_{l-l\tau}. \end{aligned}$$

The desired expansion is obtained by replacing $-l$ by m in Y_{l-l} and $U_{l-l\tau}$ in the above equation, and is

$$\begin{aligned} \bar{Y}_{lm}(\theta_1, \varphi_1) &= \left[\frac{2l+1}{4\pi} \right]^{1/2} \frac{(-i)^l}{2^l} \cdot \sum_{\tau} \left[(l-\tau)! (l+\tau)! \right]^{1/2} \times \\ &\quad \times \left[\frac{l-\tau}{2}! \frac{l+\tau}{2}! \right]^{-1} U_{lmt}, \end{aligned} \tag{11}$$

where, the index τ increases from $-l$ in steps of 2, and the bar over Y_{lm} means that the function is normalized. Finally, the replacement of U_{lmt} by $e^{i\tau\Theta} U_{lmt}$ in eq. (11) gives the corresponding expansion for $\bar{Y}_{lm}(\theta_2, \varphi_2)$.

REFERENCES

1. G. BREIT, Phys. Rev., **35**, 569, 1930.
2. J. O. HIRSCHFELDER and E. P. WIGNER, Proc. Nat. Acad. Sci. (USA), **21**, 113, 1935.
3. C. F. CURTISS, J. O. HIRSCHFELDER and F. T. ADLER, J. Chem. Phys., **18**, 1638, 1950.
4. S. D. MAJUMDAR, Z. Physik, **131**, 528, 1952.
5. T. A. S. JACKSON, Proc. Cambridge Phil. Soc., **50**, 298, 1954.
6. O. D. KELLOG, Math. Ann., **86**, 14, 1922.
7. N. SVARTHOLM, The binding energies of lightest atomic nuclei, Thesis, Lund, 1945.
8. R. MCWEENY and C. A. COULSON, Proc. Phys. Soc. A, **62**, 509, 1949.
9. R. MCWEENY, Proc. Phys. Soc. A, **62**, 519, 1949.
10. B. PODOLSKY and L. PAULING, Phys. Rev., **34**, 109, 1929.
11. W. ELSASSER, Z. Physik, **81**, 332, 1933.
12. A. RUBINOWICZ, Phys. Rev., **73**, 1330, 1948.
13. E. T. COPSON, Proc. Roy. Soc. Edinburgh, **61**, 260, 1943.
14. M. LÉVY, Proc. Roy. Soc. A, **204**, 145, 1950.
15. E. T. WHITTAKER, Analytical Dynamics, 4th Edition, Cambridge Univ. Press, pp. 339—346, 1952.
16. S. D. MAJUMDAR, Proc. Phys. Soc., **72**, 635, 1958.

ВОЛНОВЫЕ УРАВНЕНИЯ В ПРОСТРАНСТВЕ ИМПУЛЬСОВ

Ш. ДАТТА МАЮМДАР

Р е з ю м е

Детально изучается поведение волновых функций во вращающемся пространстве импульсов. Результаты использованы для уменьшения числа независимых переменных в интегральном волновом уравнении для трёхчастичной системы.

SOME PARAMETERS OF THE MOVING STRIATIONS

By

G. LAKATOS and J. BITÓ

INDUSTRIAL RESEARCH INSTITUTE FOR TELECOMMUNICATION TECHNIQUE, BUDAPEST

(Presented by G. Szigeti. — Received: 17. XII. 1963)

The authors present their results relating to the development and the properties of moving striations. A brief outline of the measuring method and the test conditions is given. The current dependence of the striation frequency, the temperature dependence of the discharge characteristics, the current dependence of the relative current, light and voltage fluctuation amplitudes were determined at stabilized temperatures of 20, 25 and 40° C with a discharge tube arranged in a water jacket. A relation found empirically and valid in a given current range representing the current dependence of the striation frequency is given. Similarly, another such relation represents the current and pressure dependence of the travelling speed of striations.

1. Introduction

The instability of the positive column of the individual gas and vapour discharges is a fact that has long been known. ABRIA had conducted observations already in 1843 of the oscillation effects appearing in rare gas and mercury vapour discharges and according to the available reference works [1] he was the first to describe the individual characteristics of the striation processes. By now there are many papers available dealing with this subject, which testify the importance the subject has gained.

There is as yet no agreement concerning the origin of the moving striation. The cause of the striation lies according to some authors in the anisotropy of the charge distribution in the cathode space [3, 4] according to others it may be due to the anisotropy on the cathode side [5, 6] or that of the basic processes of the discharge [7, 8]. In the case of a sufficiently high degree of ionization the plasma of the positive column will collect the oscillations appearing in a certain frequency range and conduct and amplify them [2]. According to DONAHUE et al. [9] the moving striation develops as the superposition of two space charge waves with different signs which will move along the axis of the discharge tube in opposite directions. The travelling speed of the negative space charge waves gained along the axis is — in the case of non-electronegative gases and vapours — substantially higher than the corresponding velocity of the positive space charge waves [2].

There are various possibilities for the theoretical description of the moving striation. It is usual to consider the plasma as a dielectric medium of

known charge distribution [10] and to solve the space equations for it by taking into account the corresponding initial and boundary conditions. The waves resulting in this way will not always be of a sinusoidal character [10].

In the theoretical investigations it is usual to start from the BOLTZMANN transport equation and the FOKKER—PLANCK equation making use of the MAXWELL equation and supposing the MAXWELL—BOLTZMANN or FERMI—DIRAC distribution [7].

In the course of their earlier investigations [11, 12] the authors have established that the character (ohmic or inductive) and the size of the limiting resistance placed in the external electric circuit influence the parameters of the striation. For certain currents they could show [11] that the inductive resistance inserted in the limiter circuit influences the frequency of the moving striation, while the variation of the ohmic resistance of the external circuit will change the velocity and wavelength of the striation; with increasing ohmic resistance the travelling speed and wavelength of the striation will diminish.

From the results obtained in earlier investigations [13] the authors have drawn the conclusion that the slope and type (positive or negative tangent) of the discharge characteristics play an important part in the development of the oscillations and the striation. It was possible to show that there is an unambiguous connection — which was discussed by the authors also theoretically [14] — between the observed number of oscillations and the angle formed by the characteristics and the straight line characterizing the limiter resistance.

In the present article the authors report the results of their investigations of the dependence of certain characteristic parameters of the moving striation on current and pressure and discuss the characteristic points of the recorded curves characterizing the individual sections by equations obtained empirically.

2. Test method

In their investigations the authors applied the measuring method introduced by DONAHUE et al. [9] which they [15] described in detail earlier. Accordingly, the investigation of the characteristics of the moving striation was effected by the photocell method: With the help of an oscilloscope it was possible to demonstrate the current fluctuations — which are caused by the light fluctuation characteristic of the striation — of a photocell adjusted to the discharge section to be investigated, the fluctuations being amplified by an amplifying stage. The determination of the frequency of the oscillations was effected by a generator of calibrated frequency, by the help of the Lissajoux method. With this method the spot dependence of the light intensity of the striation developing along the axis of the discharge tube could be

investigated. On the basis of frequency and wavelength measurements also the travelling speed of the striation could be determined.

The discharge was maintained by a stabilized direct current supply source and the ohmic resistances arranged symmetrically with respect to the supply source used for limiting the discharge current. The authors limited their investigations to the striation processes connected with negative space charge waves of fairly high travelling speed.

3. Test conditions

The discharge tube was a glass tube of 1200 mm length, 38 mm external diameter and 1 mm wall thickness. Following vacuum technical treatment the tube was filled with argon gas of different pressures, (1, 2, 3 and 4 mm mercury pressure) and mercury of some 60 mg weight. The vapour pressure of the mercury was determined by the ambient temperature, while the gas pressure could be set to a precision of $\pm 0,05$ mm Hg.

The determination of the pressure dependence of the individual striation parameters was carried through in a discharge tube, in order to prevent possible discrepancies in the results due to differences caused by the use of discharge tubes or electrodes. The variation of the pressure of the discharge tubes could be achieved with the help of the glass extensions [16] arranged at one of the ends of the tube.

In order to maintain the pressure of the mercury vapour at a given constant value the whole discharge tube was arranged in a water jacket, in which a constant flow of water of given velocity was maintained. With the help of an ultra-thermostat the temperature of the water performing thermostation could be set to the required value to an accuracy of $\pm 0,02^\circ$ C.

The tests were started after the discharge tube had operated for 20 minutes during which its performance could be considered to be stationary at the individual temperatures set in advance.

The measurements were carried out at water jacket temperatures of 20, 25 and 40° C. The electrodes soldered in at the two ends of the discharge tube were of identical construction. They were formed by a wolfram double-spiral to which an electron emitting coating had been applied and two auxiliary electrodes arranged at the two sides of the spiral and on a potential identical with that of the spiral. The cathode did not obtain any external heating, it was heated by the discharge only.

4. Results

The dependence of the striation frequency on the discharge current at stabilized external wall temperatures of 20, 25 and 40° C is shown in Fig. 1. The authors gave already earlier [13] the curve representing the current

dependence of the striation at 25°C . There they have pointed out that the frequency separation occurring at currents under 20 mA and presented in the case of a temperature of 25°C arises on account of the different sizes of the external ohmic limiter elements. At another occasion [14] the authors discussed also theoretically the influence exerted by the external parameters

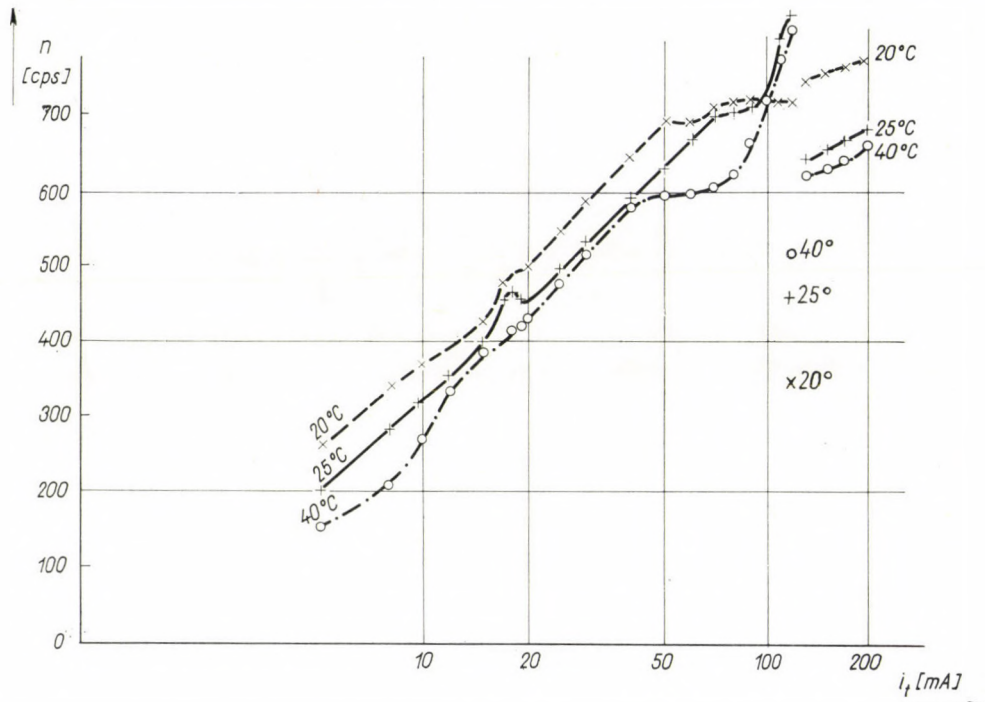


Fig. 1. The dependence of the frequency n of the moving striation on the discharge current i_t at temperatures of 20 , 25 and 40°C

mentioned here upon the moving striation, and the theoretical and experimental results have shown good agreement.

In the present case in order to ensure greater clarity the frequency separation under 20 mA observed earlier is not shown in Fig. 1, only the frequency curve belonging to a feed voltage of 200 V. Similarly to the results obtained previously at 25°C and reported in [13] the measurements carried out at temperatures of 20 and 40°C have also shown that under 20 mA, different frequency curves belong to the ohmic limiter resistances of different sizes. This may be explained on the basis of the results of [13, 14], when the sections of the characteristics under 20 mA are considered. These sections are represented for the various temperatures in Fig. 2.

Above 20 mA the size of the external ohmic limiter resistance has no influence on the frequency of the striation. It may be seen from the curves

of Fig. 1 that the frequency of the striation will grow with increasing discharge current and further that the oscillation frequency will be reduced with the increase of the temperature.

In Fig. 1 the sections of the curve above 20 mA and plotted in a semi-logarithmic scale may be characterized by straight lines up to a certain current

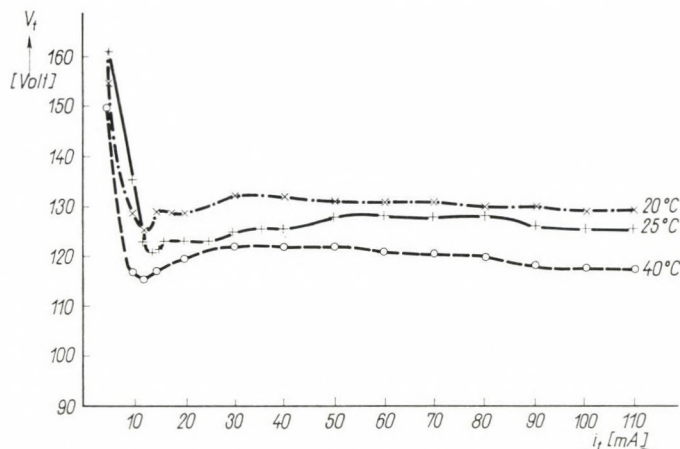


Fig. 2. The dependence of the discharge tube voltage V_t on the current i_t of the discharge tube, at stabilized temperatures of 20, 25 and 40°C

intensity. These may be described by a relatively simple relation which was found empirically:

$$n(i_t) = n_0(T) + C(T) \ln(i_t/i_{t0}), \quad (1)$$

where $n(i_t)$ is the frequency of the striation,

i_t the discharge current,

i_{t0} 20 mA,

$n_0(T)$ the frequency resulting at 20 mA, its value depending on the temperature,

$C(T)$ the constant depending on the temperature (in the investigated current range).

The values of $n_0(T)$ resulting at different temperatures are shown in Table 1.

Table 1

T ($^\circ\text{C}$)	$n_0(T)$ (cps)
20	500
25	450
40	430

The temperature dependence of $C(T)$ in the range $20-40^\circ\text{C}$ may be seen in Fig. 3.

The intervals of validity of the relation (1) are the current ranges extending at 40°C from 20mA to 40mA, at 25°C from 20mA to 70mA and at 20°C from 20mA to 50mA. Inside these current ranges the relation (1) describes unambiguously the current dependence of the frequency of the moving striation. Here the frequency is independent of the variation of the size of the external resistance. This as well as the temperature dependence of the frequency curves may be explained when the type of the characteristics shown in Fig. 2 and the earlier results [13, 14] are remembered.

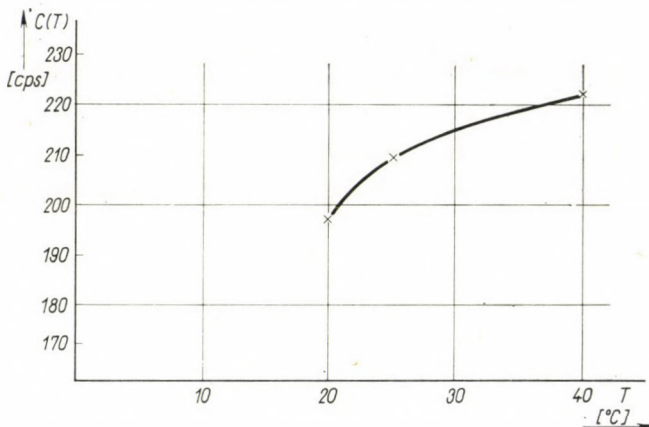


Fig. 3. The dependence of $C(T)$ in relation (1) on the temperature T

In Fig. 1 the characteristics representing the current dependence of the frequency have a characteristic point at 120 mA, where the frequency breaks down. It is remarkable that the breaking points — which appear in the case of all three temperatures at a discharge current of 120 mA — do not lie above each other as is to be expected from the earlier sections of the frequency curves recorded at the different temperatures. In the current section extending to 120 mA, with the exception of a few values, the highest striation frequencies were found for all currents to belong to the curves recorded at 20°C while the lowest ones belonged to the 40°C curves. Against this at 120 mA the highest break-down was found in the 20°C frequency curve. The amount of the frequency-breaks at the investigated temperatures is shown in Table 2. With the increase of the temperature the frequency breakdown will become smaller. This admits of the conclusion, that the cause giving rise to the breakdown is temperature-dependent and that its effect will be reduced with the increase of the temperature. As an internal cause of this kind in the first place the pressure of the mercury vapour may be considered, as the voltage-discharge

Table 2

T ($^{\circ}$ C)	20 $^{\circ}$ C	25 $^{\circ}$ C	40 $^{\circ}$ C
Amount of frequency-breaks (cps)	375	370	285

current characteristics recorded at various temperatures have no distinctive section or point in the break-down current range around 120 mA. Here the characteristics may be replaced by a straight line of small negative slope (Fig. 2).

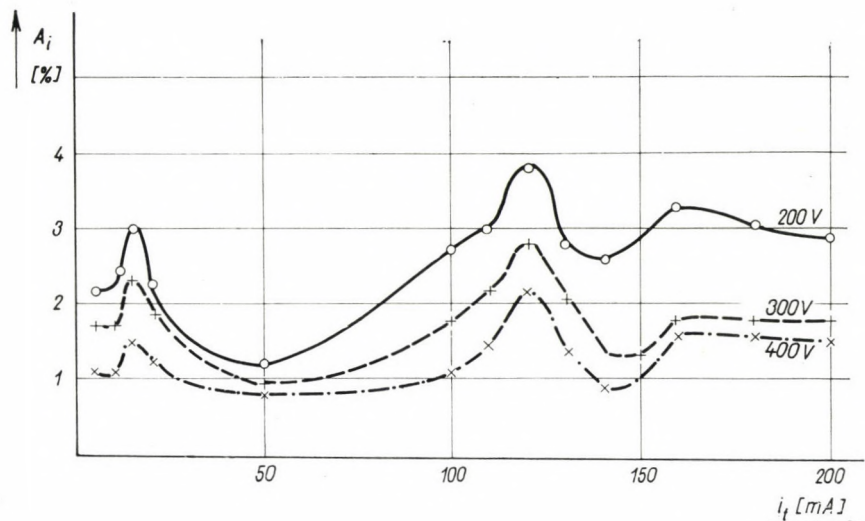


Fig. 4. The dependence of the amplitude A_l of the relative light fluctuations on the discharge current i_l

The pressure of the mercury vapour in the discharge tube will increase with the rise of the temperature and the concentration of the neutral mercury atoms in the discharge space will grow accordingly. The frequency break-down to be seen in Fig. 1 as well as the values given in Table 2 permit of the conclusion that the growing concentration of the mercury atoms will suppress the cause giving rise to the frequency break-down. A deeper interpretation of this phenomenon necessitates above all the measurements to be carried out at higher temperatures. Here we shall merely show the influence of this frequency break-down on the other parameters.

The striation has been accompanied also in the present case by a current fluctuation of the same frequency as that of the light fluctuation and the voltage fluctuation. The dependence of these current fluctuations on the discharge current is shown in Fig. 4. The vertical axis shows the relative current

fluctuation in per cents of the discharge current plotted, while the horizontal axis gives the discharge current in mA. Fig. 4 only shows the curves recorded at 40° C as the curves recorded at all three temperatures are similar to each other, the position of their characteristic points being identical.

The voltage values by which the three curves shown in Fig. 4 are marked refer to the feed voltages corresponding to the external resistances at which

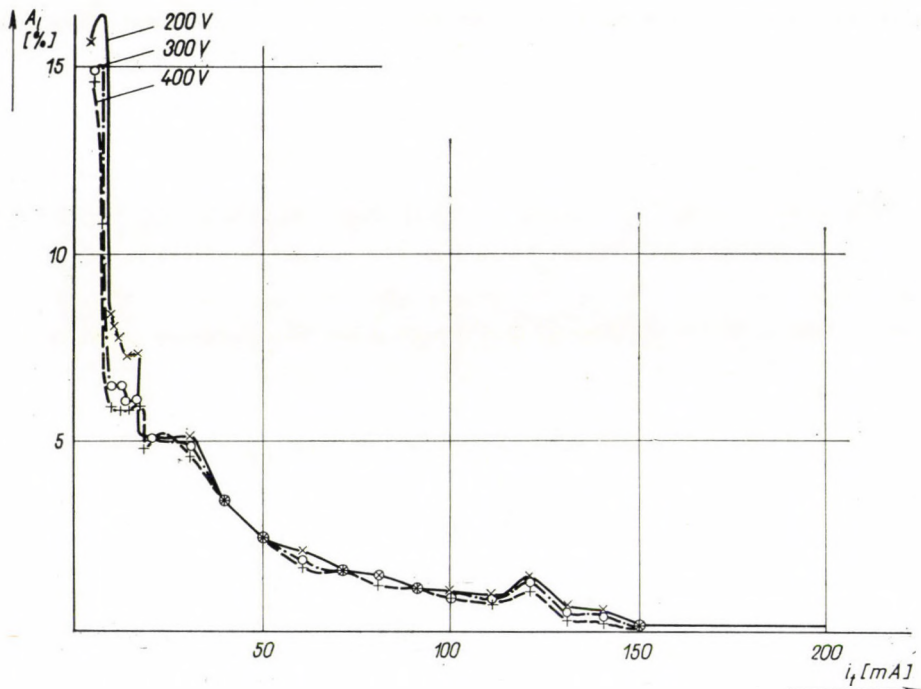


Fig. 5. The dependence of the amplitude A_i of the relative light fluctuations on the discharge current i_t at various supply voltages

the individual curves were obtained. Therefore the size of the external resistance was of influence in this case as well. This external influence — as is shown by Fig. 4 — will assert itself not only in the current range below 20 mA, as this could have been expected on the basis of Fig. 1, but in the whole of the investigated current range.

The curves shown in Fig. 4 have two characteristic maxima, amplitude jumps appearing at 15 mA and at 120 mA. Of these the latter is the larger. The amplitude jump appearing at 15 mA may be interpreted on the basis of the discharge characteristics shown in Fig. 2 using the arguments of [13]. The very high amplitude jump appearing at 120 mA is presumably connected with the frequency breakdown to be observed in Fig. 1 at the very same cur-

rent. The phenomenon possesses — to a certain extent — the character of a resonance. Its fuller explanation may presumably be found through the variation of the concentration of the atoms in the mercury vapour and by investigating the influence on the oscillations of the number of neutral mercury atoms at the given temperature, e.g. by investigating the processes of heat conduction, damping, loss of energy connected with metastable atoms, etc.

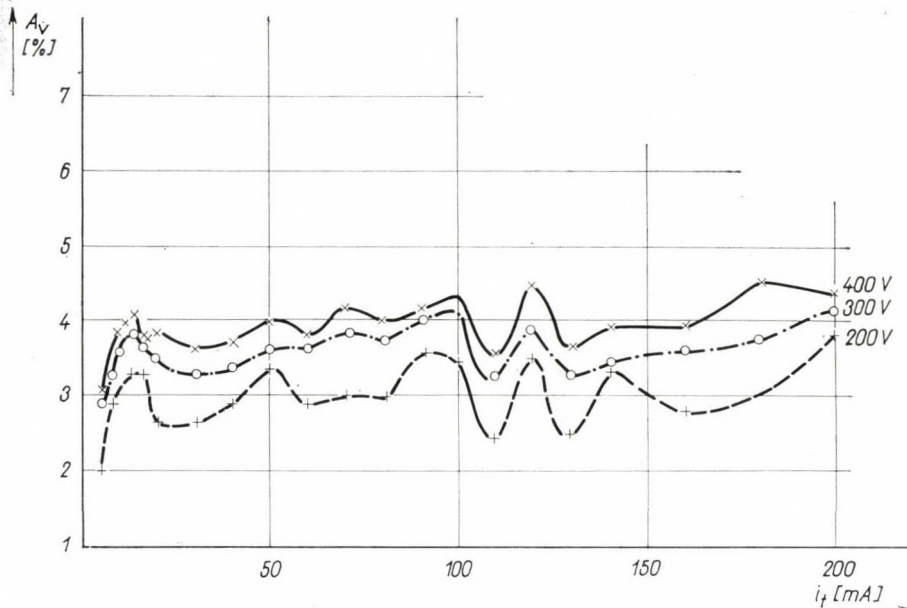


Fig. 6. The dependence of the amplitude A_v of the relative voltage fluctuations on the discharge current i_t at various supply voltages

In Fig. 5 the current dependence of the light fluctuations relative to the overall light emitted by the discharge tube at a temperature of 20°C is reproduced. On the vertical axis the amplitudes of the light fluctuation are given in per cent of the overall light, while the horizontal axis shows the discharge current. The curves were taken at all three temperatures mentioned above. The current dependence of the investigated striation parameter has been influenced also in this case by the size of the external resistance. With the increase of the current intensity the size of the relative light fluctuation diminishes. In the case of low currents it was possible to demonstrate that very high relative light fluctuations occur below 20 mA, this may be connected with the specific features of the characteristics [13] (Fig. 2).

At 120 mA the curves have a distinguished section also in this case. Here, too, a maximum relative light fluctuation appears at the point of the frequency breakdown. Similarly to the case shown in Fig. 4 in Fig. 5 the higher

values belong to the lower supply voltage values. At lower supply voltage values the limiting resistance will be smaller at a given current and also the angle formed by the resistance characteristics and the discharge characteristics will be smaller. Keeping these facts in mind it is presumably possible to interpret also this influence of the external resistance.

The voltage fluctuations in percentages of the discharge tube voltages are shown in Fig. 6 as function of the discharge current.

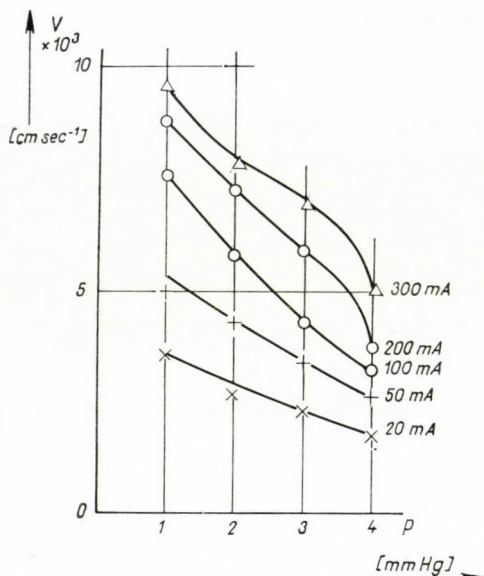


Fig. 7. The dependence of the velocity V of the moving striation on the gas pressure p in the case of argon gas, at various current values

Similarly to the curves representing the current dependence of the striation parameters examined earlier a characteristic section may be found also in this curve at a discharge current of 120 mA. Also the size of the relative amplitudes of the voltage fluctuations is influenced by the resistance of the external electric circuit, as this is evident from Fig. 6. Here, however, there is that difference as against the current and light fluctuation curves shown in Figs. 4 and 5 that the curve that represents the current dependence of the amplitudes of the voltage fluctuations at the lower supply voltage has amplitude values lower than the curve taken at the higher supply voltage. In the cases of the two oscillation parameters examined previously (Figs. 4 and 5) the higher amplitudes belonged to the curve corresponding to the higher supply voltage values.

Earlier [15] the authors reported that the travelling speed of moving striations depend on the pressure of the argon gas employed together with

mercury in the discharge tube. The investigations were carried out at a temperature of 25°C and the argon pressure was varied in the 1–4 mm Hg pressure range. They determined the travelling speed of moving striations in the current range of 20–300 mA. The pressure dependence of the travelling velocity could be represented by a hyperbolic curve reproduced here in Fig. 7.

In the course of the present investigations further computations and measurements have been made of the pressure dependence of the velocity of striations and it was found empirically that in the current range of 20–100 mA it can be expressed by the following relation:

$$v = \frac{c_0}{p \cdot \exp [a_1(i - i_0)] + n_0 \exp [(a_1 - a_3)(i - i_0)]} + a_2(i - i_0) - m_0, \quad (2)$$

where v is the travelling velocity of the moving striation,

p the pressure of the employed argon gas,

i the discharge current.

The values and the dimensions of the constants in the above relation are shown in Table 3. It is evident from the Table that the difference $a_1 - a_3$

Table 3

Constant	Numerical value	Dimension
c_0	$3,275 \cdot 10^5$	cm sec^{-1} mm Hg
m_0	$1,15 \cdot 10^4$	cm sec^{-1}
n_0	$2,10 \cdot 10$	mm Hg
a_1	$2,36 \cdot 10^{-2}$	mA^{-1}
a_2	$1,03 \cdot 10^{-2}$	cm sec^{-1} mA^{-1}
a_3	$2,24 \cdot 10^{-2}$	mA^{-1}
i_0	$2,00 \cdot 10$	mA

in the denominator of the first member of equ. (2) may be taken to good approximation as zero:

$$a_1 - a_3 = 0. \quad (3)$$

With this relation (2) can be written in the simpler form:

$$v = \frac{c_0}{p \cdot \exp [a_1(i - i_0)] + n_0} + a_2(i - i_0) - m_0. \quad (4)$$

This relation is valid for the 20–100 mA current range only. For currents above 100 mA the shape of the curve will differ from that given above. The

reason for this is probably that the output fed in to the tube will grow nearly proportionally with the increase of the current intensity (the tube voltage changing only little meanwhile) and simultaneously with this the temperature difference will increase between the mercury and the water jacket and thus the vapour pressure of the mercury cannot be maintained in a sufficiently stable way.

In order to give physical meaning to the coefficients appearing in equ. (2), (3) and (4) further experiments are required in which for instance the vapour pressure of the mercury should be varied or the vapour pressure of the mercury maintained at a stable value.

REFERENCES

1. J. J. THOMPSON, Phil. Mag., **18**, 441, 1909.
2. J. BITÓ, Hung. Phys. J., **10**, 303, 1962.
3. L. B. LOEB, Phys. Rev., **76**, 255, 1949.
4. E. B. ARMSTRONG and T. R. NEILL, Nature, **160**, 713, 1947.
5. A. A. ZAJCEV, Dokl. Akad. Nauk., **84**, 41, 1952.
6. W. PUPP, Phys. Zs., **34**, 756, 1933.
7. H. S. ROBERTSON, Phys. Rev., **105**, 368, 1957.
8. A. W. M. COOPER, U. S. Naval Postgrad. School, private communication.
9. T. DONAHUE and G. DIEKE, Phys. Rev., **81**, 248, 1951.
10. A. W. TRIVELPIECE and R. W. GOULD, J. Appl. Phys., **30**, 1784, 1959.
11. G. LAKATOS and J. BITÓ, Acta Phys. Hung., **13**, 245, 1961.
12. G. LAKATOS and J. BITÓ, Zs. T. F., **32**, 902, 1962.
13. G. LAKATOS and J. BITÓ, Lecture delivered at the II Electronics Conference, Prague, 1962.
14. G. LAKATOS and J. BITÓ, Lecture delivered at the Plasmaphysical Conference, Balaton-szabadi, 1963. Acta Phys. Hung., **17**, 271, 1964.
15. G. LAKATOS and J. BITÓ, Acta Phys. Hung., **13**, 193, 1961.
16. J. SZABÓ and G. LAKATOS, Hung. patent, No. 146.209.

О НЕКОТОРЫХ ПАРАМЕТРАХ ПОДВИЖНОГО СЛОЕОБРАЗОВАНИЯ

ДЬ. ЛАКАТОШ и Й. БИТО

Р е з и о м е

После обзора важнейших результатов, связанных с появлением и свойствами подвижного слоеобразования, авторами кратко описываются метод измерения и условия исследования. При температурно — стабилизированной разрядной трубке, помещенной в водяном кожухе, для значений температуры 20, 25 и 40° С определяются зависимости частоты слоеобразования от тока; характеристики разряда от температуры; амплитуды колебаний относительного тока, света и напряжения от тока. Зависимость частоты слоеобразования от тока, действительная в определённом интервале тока, выводится экспериментально. Даётся зависимость поступательной скорости слоеобразования от тока и давления, найдённая также экспериментально.

QUANTUM NUMBERS AND ENERGY LEVELS IN THE THOMAS-FERMI ATOM

By

A. KÓNYA

RESEARCH GROUP FOR THEORETICAL PHYSICS, HUNGARIAN ACADEMY OF SCIENCES, BUDAPEST

(Received: 2. IV. 1964)

The electrons of the THOMAS-FERMI atom with equal energy and angular momentum are considered as being in the same quantum states. With the help of the BOHR-SOMMERFELD quantization condition these states are characterized by continuously varying quantities n_r^* and n^* corresponding to the radial and principal quantum numbers of wave mechanics. States with integral n^* and half-integral n_r^* -values correspond to the wave-mechanical one-electron states.

As an application of the method developed the energy and the BOHR-SOMMERFELD orbits corresponding to the occupied quantum-mechanical states of the Ag atom are determined here. The results are in satisfactory agreement with those of wave mechanics.

1. Introduction

The statistical theory of the atom as worked out by THOMAS and FERMI and developed by DIRAC, WEIZSÄCKER and GOMBÁS [1-3] does not contain quantum numbers. Recently ALFRED has pointed out [4] that for the improvement of the THOMAS-FERMI (TF) model and also for its applications to more subtle physical problems it seems necessary to define a total set of quantum numbers and to decompose the total charge density into shells or subshells corresponding to these quantum numbers.

The definition of the quantity corresponding to the azimuthal quantum number and the construction of the l -subshells was first given by FERMI [5]. On this basis KÓNYA has suggested [6] that the quantity corresponding to the magnetic quantum number is the component of the angular momentum of the electron in an arbitrarily fixed direction.

GOMBÁS and his coworkers were the first to aim at a statistical model of the atom with electron shells corresponding to the principal quantum number [3, 7-9]. They used a complex method applying the statistical method separately to every shell with fixed number of electrons and successively determined the charge distribution of the shells by the help of the variational method, minimizing the total energy of the atom.

A method by which to define a total set of quantum numbers n, l, m was given by ALFRED [4]. His method is mathematically exact and the quantum numbers obtained have only integer values. However, the physical mean-

ing of his quantum numbers is not very clear and can be inferred only from the resulting charge distribution in the shells and subshells.

In practice the definition of the principal quantum number and the grouping of the electrons in corresponding shells is of the greatest importance. We deal here with the problem of the principal quantum number in the TF atom starting from well-known physical ideas: the BOHR—SOMMERFELD quantization rule [10, 11] and the connection between the quantum numbers of the old quantum theory and those of wave mechanics, as this was shown by KRAMERS [12] and LANGER [13] with the help of the WENTZEL—KRAMERS—BRILLOUIN (WKB) method [14—16].

As an application of the proposed method allowing comparison of the results with those obtained from wave mechanics we present here a calculation of one-electron energy levels corresponding to the occupied wave mechanical states of the Ag atom.

2. Definition of quantities corresponding to the radial and principal quantum numbers

The principal quantum number has no such obvious, physically evident meaning as e.g. the angular momentum has in respect of the azimuthal quantum number. We, therefore, can define it only by starting from the well-known relation

$$n = n_r + l + 1 = n_r + k, \quad (1)$$

n_r , l and k representing the radial, angular and azimuthal quantum numbers respectively.

In (1) only the meaning of k is known in the statistical theory of the atom. As FERMI has shown [5], the continuously varying quantity corresponding to this quantum number is

$$k^* = \frac{1}{\hbar} M, \quad (2)$$

where M is the absolute value of the angular momentum ($\hbar = h/2\pi$, $h =$ PLANCK's constant).

To attribute a reasonable meaning in the statistical theory also to n_r , we apply the BOHR—SOMMERFELD quantization rule

$$\oint p_r dr = \int_{r_1}^{r_2} p_r dr = 2\pi\hbar n_r. \quad (3)$$

Here p_r denotes the radial component of the momentum along the orbit to be defined presently and r_1 and r_2 are the radii belonging to the extreme points of the orbit.

We now define a BOHR—SOMMERFELD orbit as follows. In the statistical theory of the atom electrons in a volume element dv are treated as totally free. Consequently, we may describe the states of these electrons by their momentum vectors \bar{p} the maximum possible absolute value of which,

$$P(r) = (3\pi^2)^{1/3} \hbar \varrho^{1/3}(r), \quad (4)$$

is the radius of the FERMI sphere in the momentum space [$\varrho(r)$ is the total electronic charge density and r the distance from the nucleus].

An electron with momentum \bar{p} has an energy

$$E = \frac{P^2}{2m} - e_0 V(r) \quad (5)$$

and an angular momentum

$$\bar{M} = \bar{r} \times \bar{p}, \quad (6)$$

where e_0 denotes the elementary charge and $V(r)$ the potential. As is well known, in the TF model

$$e_0 V(r) = \frac{P^2(r)}{2m}. \quad (7)$$

Denoting the radial and azimuthal components of the momentum by p_r and p_{\perp} we obtain from formulas (4)–(7)

$$p_{\perp} = \frac{M}{r}, \quad (8)$$

$$\begin{aligned} p_r &= \pm (P^2 - p_{\perp}^2)^{1/2} = \pm \left[2me_0 V(r) + 2mE - \frac{M^2}{r^2} \right]^{1/2} = \\ &= \pm \left[P^2(r) + 2mE - \frac{M^2}{r^2} \right]. \end{aligned} \quad (9)$$

These formulas give the momentum components of all electrons possessing equal energy and angular momentum. In a volume element dv at a distance r from the nucleus (see Fig. 1) these electrons are those which have a momentum \bar{p} with end point on the curve of intersection between the sphere with radius $P = (2m)^{1/2} [E + e_0 V(r)]^{1/2}$ around the origin of the momentum space and the spherical cylinder with radius $p_{\perp} = M/r$ and with its axis parallel to \bar{r} through the origin of the momentum space.

It follows from (9) that electrons with energy $E < 0$ and angular momentum M can be found only in a spherical shell around the nucleus the limiting

spheres having the respective radii r_1 and r_2 which distances are the roots of the equation

$$P^2(r) + 2mE - \frac{M^2}{r^2} = 0. \quad (10)$$

All electrons move in a central field of force. Classically we can consider them as revolving on the same orbit. Formula (9) gives the radial momentum

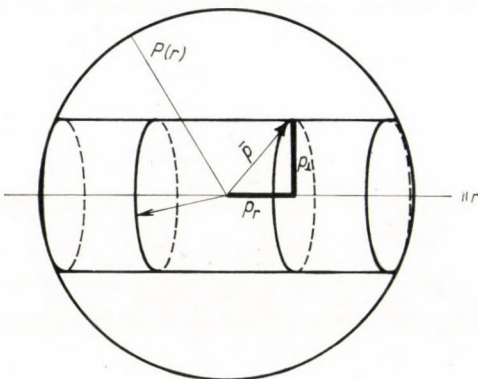


Fig. 1. Momentum vectors in the FERMI sphere belonging to the same energy and angular momentum values

component along one of these possible orbits. Making use of (3) the continuously varying quantity

$$n_r^* = \frac{1}{\pi\hbar} \int_{r_1}^{r_2} \left[2me_0 V(r) + 2mE - \frac{M^2}{r^2} \right]^{1/2} dr, \quad (11)$$

which is the analogue of the discrete radial quantum number of the quantum theory, may be regarded as corresponding to these electrons.

Further, we define with the help of (1), (2) and (11) the quantity

$$n^* = n_r^* + k^*, \quad (12)$$

which also varies continuously and which in the TF theory is the quantity corresponding to the principal quantum number of quantum theory.

In this way electrons of energy E and angular momentum M are correlated with a BOHR-SOMMERFELD orbit characterized by the quantities n_r^* and n^* and perihelion and aphelion r_1 and r_2 , respectively.

Since the angular momenta of the electrons in the TF atom have all possible directions, strictly speaking we do not obtain one orbit only for given E and M -values, but a continuity of orbits characterized by the same data (n_r^*, n^*, r_1, r_2) and lying in different planes which all contain the nucleus of the atom.

For the case $E = 0$ [i.e. for an electron with maximum momentum $P(r)$] our definition (11) is identical with the formula used by GOMBÁS [17] to calculate the number of electrons with given l -values.

3. Formulas and numerical data for the TF atom

We now treat numerically the free, neutral TF atom. For this case the electronic charge density may be written [1]

$$\varrho = \frac{Z}{4\pi\mu^3} \left[\frac{\varphi(x)}{x} \right]^{3/2}, \quad (13)$$

where

$$r = \mu x, \quad \mu = \frac{1}{4} \left(\frac{9\pi^2}{2Z} \right)^{1/3} a_0, \quad (14)$$

$$a_0 = \frac{\hbar^2}{me_0^2}, \quad (15)$$

and Z is the number of the electrons. The function $\varphi(x)$ is the solution of the TF differential equation

$$\frac{d^2\varphi}{dx^2} = \frac{\varphi^{3/2}(x)}{x^{1/2}} \quad (16)$$

satisfying the conditions

$$\varphi(0) = 1, \quad \varphi(x_0) = 0, \quad x_0\varphi'(x_0) = 0 \quad (17)$$

(x_0 denotes the limiting radius of the atom. For free neutral TF atoms $x_0 = \infty$).

Substituting these formulas in (8), (9), (11) and (12) we get the following general result for the TF atom. At the distance $r = \mu x$ the electron with the momentum components

$$p_\perp = \frac{4}{(6\pi)^{2/3}} \frac{\hbar}{a_0} Z^{2/3} \frac{a}{x}, \quad (18)$$

$$p_r = \frac{4}{(6\pi)^{2/3}} \frac{\hbar}{a_0} Z^{2/3} \left[\frac{\varphi(x)}{x} - \beta - \frac{a^2}{x^2} \right]^{1/2}. \quad (19)$$

is in the state characterized by the quantities

$$n_r^* = \left(\frac{3}{4\pi^2} \right)^{1/3} Z^{1/3} \Phi(a, \beta) \quad (20)$$

(radial quantum number) and

$$n^* = \left(\frac{3}{4\pi^2} \right)^{1/3} Z^{1/3} [\Phi(a, \beta) + \pi a] \quad (21)$$

(principal quantum number). The new symbols introduced here are

$$a = \frac{k^*}{\left(\frac{3\pi}{4} \right)^{1/3} Z^{1/3}}, \quad (22)$$

$$\beta = - \frac{(6\pi)^{2/3}}{8Z^{4/3}} \frac{a_0}{e_0^2} E, \quad (23)$$

$$\Phi(a, \beta) = \int_{x_1}^{x_2} [x\varphi(x) - \beta x^2 - a^2]^{1/2} \frac{dx}{x}, \quad (24)$$

where $x_1 = r_1/\mu$ and $x_2 = r_2/\mu$ are the roots of the equation

$$x\varphi(x) - \beta x^2 - a^2 = 0 \quad (25)$$

corresponding to the equ. (10). From these roots we get the data of the BOHR—SOMMERFELD orbit which may be considered to correspond to this state. The parameters a and β may vary in the intervals

$$0 \leq a \leq [x\varphi(x)]_{\max} = 0,6974$$

and

$$0 \leq \beta \leq \infty. \quad (26)$$

On this basis we can treat atoms with arbitrary atomic number Z if the function $\Phi(a, \beta)$ is known. The integral representing this function was computed numerically for several values of the parameters and is tabulated in Tables 1 and 2.

For the special case $\beta = 0$ the function $\Phi(a, \beta)$ is identical with the function $\Phi(a)$ introduced by FERMI [5]. In Table 2 the values denoted by + are those evaluated by FERMI.

Further in Table 3 we give some parameter values a_0 and β_0 for which $\Phi(a_0, \beta_0) = 0$.

For $\beta \ll 1$ and $a = 0$ the interval of integration in (24) is very small and lies very near to the nucleus. We can therefore replace $\varphi(x)$ by the series expansion [1]

$$\varphi(x) = 1 + \varphi'(0)x + \frac{4}{3}x^{3/2} + \dots \quad (27)$$

Table 1
Values of the function $\Phi(a, \beta)$

β	$a = 0$	$a = 0,075$	$a = 0,15$	$a = 0,30$	$a = 0,45$	$a = 0,575$
0	3,654	3,523	3,150	2,300	1,466	0,736
0,003288	3,014	2,772	2,497	1,855	1,223	0,605
0,005120	2,914	2,666	2,400	1,765	1,160	0,560
0,009904	2,758	2,492	2,247	1,631	1,045	0,475
0,01239	2,696	2,444	2,169	1,572	1,000	0,441
0,01576	2,630	2,377	2,124	1,519	0,951	0,399
0,02043	2,554	2,304	2,041	1,454	0,893	0,345
0,02710	2,474	2,223	1,971	1,376	0,825	0,289
0,03057	2,436	2,185	1,934	1,342	0,794	0,266
0,04526	2,309	2,054	1,800	1,226	0,691	0,181
0,07108	2,155	1,906	1,660	1,081	0,553	0,068
0,1215	1,961	1,712	1,468	0,895	0,395	
0,2378	1,704	1,457	1,217	0,668	0,169	
0,4240	1,484	1,252	0,999	0,449		
0,9353	1,179	0,926	0,686	0,131		
1,649	0,971	0,725	0,496	0,007		
3,965	0,694	0,435	0,202			
8,817	0,497	0,249	0,019			
18,70	0,351	0,103				
31,97	0,270	0,033				
50	0,219					
75	0,179					
100	0,156					
250	0,099					
500	0,070					
1000	0,050					
∞	0					

with

$$\varphi'(0) = -1,58807.$$

Retaining the first two terms only we get the asymptotic formula

$$\Phi(0, \beta) \simeq \frac{\pi}{2[\beta - \varphi'(0)]^{1/2}} \quad (28)$$

which may be used if $\beta \geq 40$.

Table 2
Values of the function $\Phi(a, \beta)$ for $a = 0$

a	$\Phi(a, 0)$	a	$\Phi(a, 0)$
0	3,654	0,4	1,739
0,025	3,635	0,425	1,612
0,05	3,584	0,4472	1,48 ⁺
0,075	3,523	0,45	1,466
0,1	3,415	0,475	1,324
0,125	3,292	0,5	1,187
0,15	3,170	0,525	1,040
0,175	3,017	0,5440	0,88 ⁺
0,2	2,897	0,55	0,885
0,225	2,748	0,575	0,736
0,25	2,606	0,6	0,587
0,275	2,456	0,625	0,430
0,3	2,310	0,6324	0,36 ⁺
0,3162	2,2 ⁺	0,65	0,282
0,325	2,186	0,675	0,132
0,35	2,017	0,6974	0
0,375	1,892		

4. The relation between the statistical quantities n_r^* , n^* and the wave-mechanical quantum numbers

Energy levels

As can be seen from (20) and (21) the quantities n_r^* and n^* belonging to the occupied states of the TF model have all possible values between zero and some maximum value depending on Z . The fact that these quantities are continuous variables is characteristic of the model just as is the continuity of the energy E and the angular momentum M .

When trying to correlate the TF model with the wave-mechanical atom the problem arises how to choose from this continuity the states which approximate those of the quantum-mechanical shell atom. Such a selection process must, of course, be based on some general principle which may be applied to all atoms and all types of states.

As was proved by FÉNYES [18] the TF model is an approximate solution of the wave-mechanical many-body problem, which may be obtained by the WKB method using first order approximation. On the other hand KRAMERS [12] and LANGER [13] were led to the conclusion that in the WKB

Table 3

Zeros of the function $\Phi(\alpha, \beta)$:
 $\Phi(\alpha_0, \beta_0) = 0$

α_0	β_0	α_0	β_0
0	∞	0,4291	0,5
0,075	42,35	0,4455	0,42401
0,0875	31,973	0,45	0,410
0,1111	18,704	0,4646	0,35
0,1145	17,5	0,5010	0,23779
0,1237	15,0	0,5405	0,15
0,1342	12,5	0,5570	0,12151
0,1485	10,0	0,575	0,095
0,15	9,80	0,5908	0,075
0,1572	8,8170	0,5941	0,07108
0,1688	7,5	0,6147	0,05
0,2002	5,0	0,6198	0,04526
0,2198	4,0	0,6380	0,03057
0,2203	3,9653	0,6426	0,02710
0,2435	3,0	0,6458	0,025
0,2805	2,0	0,6528	0,02043
0,30	1,73	0,6611	0,01576
0,3046	1,6489	0,6674	0,01239
0,3391	1,2	0,6724	0,00990
0,3555	1,0	0,6831	0,00512
0,3564	0,93527	0,6879	0,00329
0,3865	0,75	0,6974	0

method one should use the BOHR—SOMMERFELD quantum conditions with half-integer values of the quantum numbers in order to get an approximation of the wave-mechanical states.

From these statements one may conclude that an orbit in the TF model with

$$k^* = l + \frac{1}{2} \quad (l = 0, 1, 2, \dots) \quad (29)$$

corresponds to a quantum-mechanical state with the angular quantum number l . This correspondence was used by FERMI too [5]. In a similar manner an orbit in the model with

$$n_r^* = n_r + \frac{1}{2} \quad (n_r = 0, 1, 2, \dots) \quad (30)$$

corresponds to a quantum-mechanical state with the radial quantum number n_r . From (12) it follows that

$$n^* = n_r^* + k^* = n_r + l + 1 = n \quad (31)$$

and this means that wave-mechanical states with principal quantum number n are approximated by states with integer n^* -values ($n^* = n = 1, 2, 3, \dots$) in the TF model. Consequently, the orbits corresponding to the wave-mechanical states must satisfy the relation

$$\left(\frac{3}{4\pi^2} \right)^{1/3} Z^{1/3} [\Phi(a, \beta) + \pi a] = n. \quad (32)$$

Thus, in these cases the parameters a and β do not vary in the full intervals originally given by (26). From (31) we see that both k^* and n_r^* have minimum values 0 and maximum values n . This means that

$$0 \leq a \leq \frac{n}{\left(\frac{2\pi}{4} \right)^{1/3} Z^{1/3}} \quad (33)$$

and to a fixed a -value in (32) a unique β -value belongs which may be determined by numerical interpolation from Tables 1 and 3. Thus for given n and $k^* = 0$ ($n_r^* = n$) we obtain the parameter value $\beta_{n,0}$ and for $k^* = n$ ($n_r^* = 0$) the value $\beta_{n,n}$ both depending upon Z . As may be seen from the definition (24) of the function $\Phi(a, \beta)$, the relation $\beta_{n,0} > \beta_{n,n}$ is valid for any Z -value. Using the equ. (23) we get the minimum and maximum energies $E_{n,0}$ and $E_{n,n}$ of the electrons with the principal quantum number n in the TF model.

The energies $E_{n,0}$ and $E_{n,n}$ are shown in Fig. 2 as functions of Z for $n = 1, 2, 5/2, 3, 4$ and 5. For comparison the theoretical term values obtained by LATTER [19] when solving the one-electron SCHRÖDINGER equation with TF potential are also plotted for the cases $n = 2$ and $n = 3$. All LATTER's wave-mechanical term values belonging to a given n are lying between the two limiting curves $E_{n,0}$ and $E_{n,n}$ obtained here from the TF model. This justifies the selection rule (32) used for the determination of the states corresponding to the principal quantum number n .

It is also possible to determine the s -, p -, d - and f -states in a shell with given n . For this purpose for k^* the values (29a) have to be substituted in (22) and the $a_{l+\frac{1}{2}}$ — values so obtained in (32). This results in the relation

$$\left(\frac{3}{4\pi^2} \right)^{1/3} Z^{1/3} [\Phi(a_{l+\frac{1}{2}}, \beta_{n,l+\frac{1}{2}}) + \pi a_{l+\frac{1}{2}}] = n, \quad (34)$$

which is fulfilled only by certain values of $\beta_{n,l+\frac{1}{2}}$. For given n and l (i.e. for given $a_{l+\frac{1}{2}}$) (34) may be regarded as the secular equation for the determination

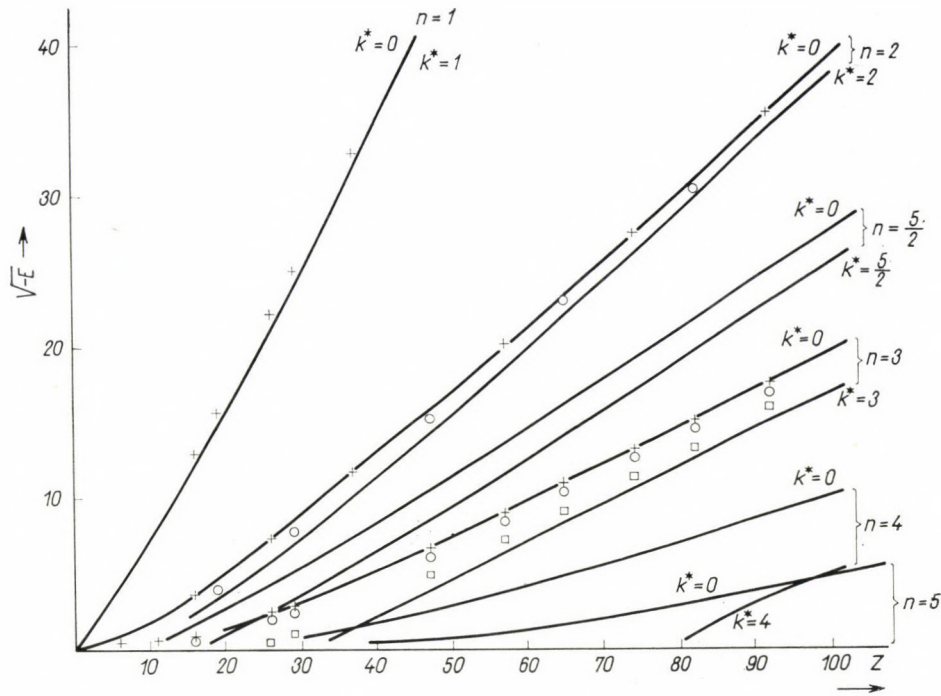


Fig. 2. The limiting energies $E_{n,0}$ and $E_{n,n}$ as functions of the atomic number.

Ordinate: $\sqrt{-E}$, E in Rydberg units.

$+$ term values for s -states
 \circ term values for p -states
 \square term values for d -states

calculated by LATTER [19]

of the parameter value $\beta_{l,n+\frac{1}{2}}$ and so for the approximation of the wave-mechanical energy eigenvalue $E_{n,l}$.

As an application of the method described we determine here the energy levels of the occupied states in the Ag atom.

The Ag atom with $Z = 47$ has the electron configuration

$$(1s)^2 (2s)^2 (2p)^6 (3s)^2 (3p)^6 (3d)^10 (4s)^2 (4p)^6 (4d)^10 (5s)^2.$$

According to (29) and (22) the parameter a has then the values $a_{l+\frac{1}{2}} = 0,1041$, $0,3123$ and $0,5205$, respectively, for the s -, p - and d -states. From Table 1 we first determine the values $\Phi(a_{l+\frac{1}{2}}, \beta)$ by interpolation and then with their help the $\beta_{n,l+\frac{1}{2}}$ values satisfying the condition (34) for $n = 1, 2, 3, 4$ and 5 .

The numerical results are summarized in Table 4. For comparison theoretical term values obtained by LATTER [19] and by GÁSPÁR [20] and further experimental energy values from LANDOLT-BÖRNSTEIN [21] are also given.

Table 4
Energy values of the occupied states in the Ag atom
(in Rydberg units)

	$\beta_{n,l+\frac{1}{2}}$	$-E_{n,l+\frac{1}{2}}$	%	$-E_{n,l}$		
				LATTER[19]	GÁSPÁR[20]	LANDOLT-BÖRNSTEIN[21]
1s	4,300	1648,0	1,6	1777,0	1831,9	1879,3
2s	0,625	239,5	4,8	251,7	261,6	280,4
3s	0,114	43,68	2,4	44,75	46,52	52,98
4s	0,015	5,747	3,1	5,934	6,44	7,14
5s	0,001	0,3832	4,7	0,4021	0,428	0,556
2p	0,550	210,7	9,6	232,2	245,30	253,3
3p	0,091	34,87	7,0	37,51	39,40	43,36
4p	0,009	3,448	8,5	3,768	4,24	4,28
3d	0,0617	23,64	1,6	24,04	25,30	27,34
4d	0,0012	0,4598	1,1	0,4652	0,75	0,390

Having obtained the values $a_{l+\frac{1}{2}}$ and $\beta_{n,l+\frac{1}{2}}$ we may determine now the BOHR-SOMMERFELD orbits corresponding to the occupied wave-mechanical states in the Ag atom. For this purpose we first solve equ. (25). The numerical results in units of a_0 are given in Table 5.

The radial charge densities of the electrons in the corresponding wave-mechanical states may be calculated from the eigenfunctions given by

Table 5
Data of the orbits corresponding to the occupied states in the Ag atom
(in units of a_0)

	r_1	r_2	r_{\max}
1s	0,002882	0,04121	0,02
2s	0,002748	0,1894	0,10
3s	0,002638	0,4445	0,38
4s	0,002453	1,3443	0,88
5s	0,002210	2,6592	2,50
2p	0,02895	0,1727	0,10
3p	0,02760	0,5076	0,33
4p	0,02735	1,3603	0,90
3d	0,1092	0,4563	0,30
4d	0,1023	1,6820	1,15

GÁSPÁR [20]. The maxima of these charge densities r_{\max} — given in Table 5 too — and the aphelion of the orbits lie nearly at the same distance from the nucleus.

5. Discussion

The method applied here to the treatment of the states existing in the TF model is closely related to some previous investigations that were carried out before the beginnings of quantum mechanics on the basis of the BOHR—SOMMERFELD theory. That theory gave orbits with definite energies and angular momenta for the electrons in a spherically symmetrical field. By using empirical term values it was possible to calculate effective electric fields $V(r)$ of the atoms with the help of formulas similar to (11). Publications of FUES [22], HARTREE [23] and JEFFREYS [24] are based on this idea. After the relation between the quantum numbers in the old and new quantum theory had been pointed out [12, 13] these investigations were repeated by SUGIURA and UREY [25, 26] with half-integral values of the quantum numbers. With the same method PROKOFJEV has calculated an effective potential field in analytic form for the sodium atom [27] which has often been used.

The way we have followed here is just the reverse. Starting from a given atomic potential field (the TF potential) we examined the states existing in this field of force and from the continuity of these states we selected those corresponding to the wave mechanical states.

The selection rule we obtained was as follows: In the states corresponding to the wave-mechanical ones the characteristic quantities n^* and k^* must have the values

$$n^* = n = 1, 2, 3, \dots,$$

$$k^* = l + \frac{1}{2} = \frac{1}{2}, \frac{3}{2}, \frac{5}{2}, \dots \quad (35)$$

As Fig. 2 shows the first condition defines energy intervals closely related to the wave-mechanical energy eigenvalues obtained from approximate calculations of the same order carried out by LATTER [19]. If we choose non-integer values for n^* (in Fig. 2 this is the case for $n^* = 5/2$) the obtained energy intervals do not agree with the quantum-mechanical term values.

The difference between the limiting energies $E_{n,0}$ and $E_{n,n}$ increases with increasing n^* . This property corresponds to the empirical observation, that the l -splitting of the term values grows as the principal quantum number n increases. The TF model also accounts for the fact, that for given n the energy values lie the lower the smaller the value of l .

In Fig. 2 one may observe an overlap of the neighbouring energy intervals. The limiting curves $E_{3,3}$ and $E_{4,0}$ further $E_{4,4}$ and $E_{5,0}$ intersect. This

behaviour corresponds to the fact known from the periodic system of the elements, that at several values of Z the sequence of the energy terms differs from that of the principal quantum numbers. It occurs e.g. that the $4s$ - or $5s$ -states precede the $3d$ - and $4f$ -states, respectively, etc.

A more detailed and quantitative investigation of this behaviour cannot be carried out by the examination of the limiting curves $E_{n,0}$ and $E_{n,n}$ only, one must also determine the s -, p ... states existing within every single energy interval.

This further selection can be made by applying the second condition (35).

By the simultaneous application of both the conditions (35) those states are selected which approximate the wave-mechanical ones as regards both the energy values and the spatial positions of the electrons in these states. This is shown by the Tables 4 and 5.

It is reasonable to compare the obtained energy values with those given by LATTER [19] because these are eigenvalues of one-electron SCHRÖDINGER equations with TF potential. The column in Table 4 marked % gives the difference in per cent between these two values. As may be seen the errors are of some per cent only, which may be regarded as satisfactory in view of the simplicity of the applied method. The errors are partly caused by inaccuracies in the values of the function $\Phi(a, \beta)$ and by the graphical interpolation.

Term values for several other atoms and further applications of the method developed here will be published in subsequent papers.

The author is greatly indebted to Prof. P. GOMBÁS for valuable discussions. His thanks are due to Mrs. J. HUSZÁR and Miss É. SZABÓ for carrying out the numerical calculations and for drawing the figures.

REFERENCES

1. P. GOMBÁS, Statistische Behandlung des Atoms, *Hb. d. Phys.* Vol. XXXVI, Springer, Berlin—Göttingen—Heidelberg, 1956.
2. L. H. THOMAS, *Rev. Mod. Phys.*, **35**, 508, 1963.
3. P. GOMBÁS, *Rev. Mod. Phys.*, **35**, 512, 1963.
4. L. C. R. ALFRED, *Phys. Rev.*, **125**, 214, 1962.
5. E. FERMI, *Zs. f. Phys.*, **48**, 73, 1928.
6. A. KÓNYA, *Acta Phys. Hung.*, **13**, 219, 1961.
7. P. GOMBÁS and K. LADÁNYI, *Acta Phys. Hung.* **5**, 313, 1955; **7**, 255, 1957; **7**, 263, 1957; **8**, 301, 1958.
8. P. GOMBÁS and K. LADÁNYI, *Zs. f. Phys.*, **158**, 261, 1960.
9. P. GOMBÁS and T. SZONDY, *Acta Phys. Hung.*, **14**, 335, 1962.
10. N. BOHR, *Phil. Mag.*, **26**, 1, 1913.
11. A. SOMMERFELD, *Ber. Akad. (München)*, 425, 1915.
12. H. A. KRAMERS, *Zs. f. Phys.*, **39**, 828, 1926.
13. R. E. LANGER, *Phys. Rev.*, **51**, 669, 1937.
14. G. WENTZEL, *Zs. f. Phys.*, **38**, 518, 1926.
15. L. BRILLOUIN, *Journal de Phys. et le Radium*, **7**, 353, 1926.
16. A short survey of the WKB method may be found in E. U. CONDON and G. H. SHORTLEY, *The Theory of the Atomic Spectra*, Cambridge University Press, 1952, pp. 339—344.
17. P. GOMBÁS, *Acta Phys. Hung.*, **12**, 329, 1960.
18. I. FÉNYES, *Zs. f. Phys.*, **125**, 336, 1948.

19. R. LATTER, Phys. Rev., **99**, 510, 1955.
20. R. GÁSPÁR, Acta Phys. Hung., **6**, 105, 1956.
21. LANDOLT-BÖRNSTEIN, Atom- und Molekularphysik, Bd. I., Springer, Berlin, 1950.
22. E. FUES, Zs. f. Phys., **11**, 369, 1922.
23. D. R. HARTREE, Proc. Cambridge Phil. Soc., **21**, 615, 1924.
24. H. JEFFREYS, Proc. London Math. Soc., **23**, 428, 1924.
25. Y. SUGIURA and H. C. UREY, Kgl. Danske Vid. Selskab. Math. fys., **7**, No. 13, 1926.
26. Y. SUGIURA, Phil. Mag., **4**, 495, 1927.
27. V. C. PROKOFJEV, Zs. f. Phys., **48**, 255, 1929.

КВАНТОВЫЕ ЧИСЛА И ЭНЕРГЕТИЧЕСКИЕ УРОВНИ
В АТОМЕ ТОМАСА—ФЕРМИ

А. КОНЬЯ

Р е з ю м е

Рассматриваются электроны в атоме Томаса—Ферми с одинаковыми энергией и моментом количества движения, находящиеся в том же квантовом состоянии. Исходя из квантового условия Бора—Зоммерфельда, эти состояния характеризуются непрерывно варьирующими величинами n_r^* и n^* , отвечающими радиальному и главному квантовым числам волновой механики. Состояния с целыми значениями n^* и полуцелыми n_r^* соответствуют одноэлектронным состояниям волновой механики.

В качестве применения развитого метода в работе определяется энергия и орбиты Бора—Зоммелфельда атома Ag, соответствующие занятым квантово-механическим состояниям. Результаты удовлетворительно согласуются с данными квантовой механики.

GRAPHICAL METHOD FOR THE CONSTRUCTION OF THE PATTERSON FUNCTION OF ONE-DIMENSIONAL STRUCTURE MODELS

By

MARIA FARKAS-JAHNKE

RESEARCH INSTITUTE FOR TECHNICAL PHYSICS OF THE HUNGARIAN ACADEMY OF SCIENCES,
BUDAPEST

(Presented by G. Szigeti. — Received 7. I. 1964)

A graphical method for the construction of Patterson functions of one-dimensional structure models is given. The method can be applied to the determination of the approximate electron density distribution along the large period of molecule chains too. Since in most cases the intensity of the first reflexions of X-ray diffraction patterns cannot be accurately measured, a correction for this case is also given.

In the case of three-dimensional crystal structure determinations by Fourier synthesis, the chemical composition of the matter, the number and atomic number of the atoms in the unit cell are usually known; the aim of the structure determination is the determination of the coordinates of the atoms[1]. One-dimensional structure determinations are generally undertaken to reveal the electron density distribution along relatively long periods in fibrous matter built up of molecule-chains. In this case we have fewer data, because the number, position and relative height of the maxima of the electron density distributions are unknown. For the approximate resolution of the phase problem in the Fourier synthesis [2] we have to construct an approximative model using also the informations derived from other investigations and changing the parameters of our model, to approximate the real distribution as well as possible, the Fourier synthesis is suitable only for the refinement of the structure determination. Changing the parameters successively, the correctness of the direction and the amount of alteration must be controlled in each case by a simple and rapid method. For this reason it is convenient to compare the Patterson function computed from the data of the X-ray diffraction pattern with the Patterson function belonging to each distribution. The following graphical method is well suitable for this purpose.

The definition of the Patterson function in one-dimensional case is the following, as it is well known:

$$P(x) = N \int_0^l \varrho(u) \cdot \varrho(x+u) du, \quad (1)$$

where $\varrho(u)$ means the electron density distribution along the u -axis, l the length and N the number of the periods in the sample, x the rate of transla-

tion of $\varrho(u)$ along the u -axis. It is clear, that after a translation in u the values of $P(x)$ will be different from zero only at such x ranges, where non-zero values of the original and translated electron density distribution functions overlap each other.

Let us decompose now the period to n intervals. In this way we put

$$\varrho(u) = \varrho_1(u) + \varrho_2(u) + \dots + \varrho_n(u), \quad (2)$$

where the functions $\varrho_i(u)$ differ from zero only in intervals not overlapping each other. We may now write $P(x)$ in the following form:

$$\begin{aligned} P(x) &= N \int_0^l [\varrho_1(u) + \varrho_2(u) + \dots + \varrho_n(u)] \cdot [\varrho_1(x+u) + \dots + \varrho_n(x+u)] du = \\ &= N \sum_{\substack{i,k=1 \\ i \neq k}}^n \left[\int_0^l \varrho_i(u) \cdot \varrho_i(x+u) du + \int_0^l \varrho_i(u) \cdot \varrho_k(u+x) du \right]. \end{aligned} \quad (3)$$

Integrals of the first type supply non-zero terms only in cases when x is smaller than the length of the greatest interval. Integrals of the second type will differ from zero when two different intervals overlap.

As $P(x)$ is the sum of these integrals, it can be determined, if we are able to evaluate both types of integrals.

The one-dimensional electron density distribution can be approximated by a gradual function consisting of steps of equal width. If for the limiting points of the intervals we choose the end points of the certain steps, all of the $\varrho_i(u)$ -s contain only one step, i.e. each $\varrho_i(u)$ will have a constant value inside the interval of the step and will be equal to zero outside it. In this case the integral of the product of $\varrho_i(u)$ and $\varrho_k(u+x)$ will be equal to the product of both heights of the steps multiplied by the length of the overlapping intervals. The resulting functions are represented therefore by triangles, with base equal to $2B$ and height equal to ABC (Fig. 1). Each $P_i(x)$ integral has its maximum value in the case, when x is equal to the distance between the middle points of the non-zero intervals of $\varrho_i(u)$ and $\varrho_k(u)$. It means that at x values, corresponding to the distances between the middle points of the steps we draw triangles with base of $2B$ and ABC of height, and after it we add the values of the functions at the suitable points, we obtain the Patterson function of the model.

The Patterson function constructed according to the method described contains all terms of the series:

$$P(x) = 1/l \sum_{h=0}^{\infty} |F_h|^2 \cos \frac{2\pi h}{l} x. \quad (4)$$

On the other hand, as the first reflexions do not appear on small-angle X-ray diffraction patterns, or cannot be measured accurately, the Patterson function computed from the data of the pattern does not contain the first terms of $P(x)$. The possible absence of terms belonging to higher h indices does not cause

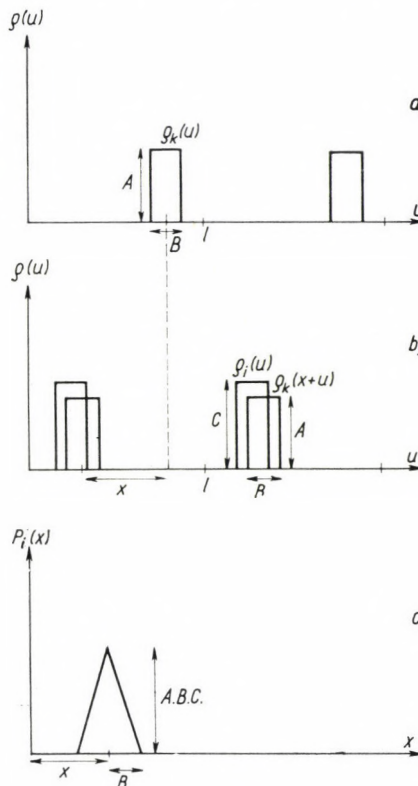


Fig. 1. The construction of the Patterson function for the case when two steps overlap

$$\text{a)} \quad \rho_k(u), \quad \text{b)} \quad \rho_i(u) \text{ and } \rho_k(x+u), \quad \text{c)} \quad P_i(x) = \int_0^l \rho_i(u) \cdot \rho_k(x+u) du$$

a great error because the values of $|F_h|^2$, i.e. the integral intensity of reflexions of higher order are small in these cases, but values of $|F_h|^2$ belonging to $h = 0, 1, 2$ may be considerable.

We therefore have to subtract also from the Patterson function constructed in the way described the terms belonging to the indices $h = 0, 1, 2$. The correction functions are being constructed as follows: each $|F_h|^2$ can be written in the form used in Fourier series:

$$|F_h|^2 = \int_0^l P(x) \cos 2\pi hu/l du. \quad (5)$$

Substituting $P(x)$ by its form decomposed to the sum of triangle functions, $P_i(x)$, this expression disintegrates into the sum of integrals containing now the $P_i(x)$ functions which can easily be given in analytical form. After the determination of these integrals the general form of $|F_h|^2$ will be:

$$|F_h|^2 = \sum_{i=1}^m AC - \frac{l^2}{(2\pi h)^2} \left[-\cos \frac{2\pi h}{l} (x_i + 2B) + 2 \cos \frac{2\pi h}{l} (x_i + B) - \right. \\ \left. - \cos \frac{2\pi h}{l} x_i \right], \quad (6)$$

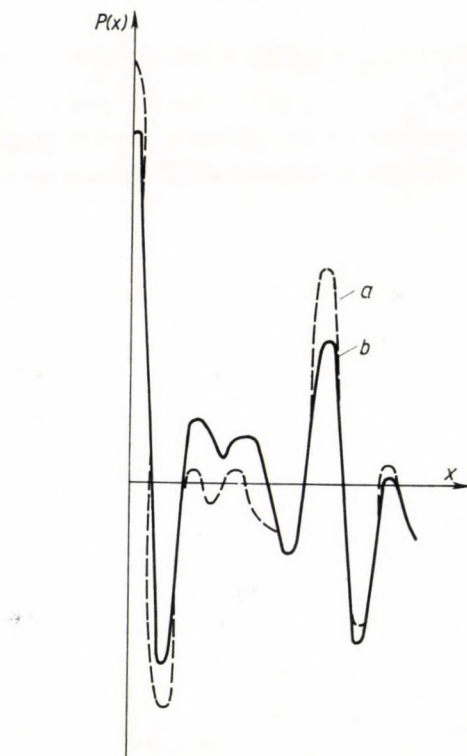


Fig. 2. a) Patterson function for native RTT (rat tail tendon) determined from the measured integral intensities on small angle X-ray patterns. b) Patterson function graphically constructed from the model of native RTT

where x_i means the value of x belonging to the maximum of $P_i(x)$, and m means the number of triangles.

Multiplying the values of $|F_h|^2$, corresponding to the reflexions which cannot be measured by $\cos 2\pi hu/l$, we obtain the terms which have to be subtracted as corrections from our graphically constructed Patterson function.

The data of the assumed model, i.e. the heights and coordinates of the steps have to be varied, until the graphically constructed Patterson function is similar to the Patterson function computed from the intensities measured on the X-ray diffraction pattern (Fig. 2). This model can then be treated as first approximation of the Fourier synthesis, and the determination of the structure can be then refined in the usual way.

REFERENCES

1. R. W. JAMES, *The Optical Principles of the Diffraction of X-rays*, G. Bell and Sons Ltd., London, 1958.
2. H. LIPSON and W. COCHRAN, *The Determination of Crystal Structures*, G. Bell and Sons Ltd., London, 1957.

ГРАФИЧЕСКИЙ МЕТОД ДЛЯ ОПРЕДЕЛЕНИЯ ФУНКЦИИ ПАТТЕРСОНА
ОДНОМЕРНОЙ СТРУКТУРНОЙ МОДЕЛИ

М. ФАРКАШ-ЯНКЕ

Р е з и м е

Даётся графический метод для составления функций Паттерсона одномерных постепенных структурных моделей. Метод может быть использован и при определении распределения электронной плотности вдоль большого периода молекулярных цепей. Так как интенсивность первичного отражения дифракционной картины рентгеновых лучей большей частью является не точно измеримой, даётся коррекция и для этого случая.

INELASTIC TWO-PRONG $\pi^- - p$ INTERACTIONS AT 17,2 GeV IN EMULSION

By

G. BOZÓKI, E. FENYVES, ÉVA GOMBOSI AND E. NAGY

CENTRAL RESEARCH INSTITUTE OF PHYSICS, BUDAPEST

(Presented by L. Jánossy. — Received 2. VII. 1964)

The angular and momentum distributions of pions and protons observed in two-prong $\pi^- - p$ interactions in emulsion are investigated. The results give further support to the assumption that in these events the incident pion undergoes a quasi-elastic scattering. The cross-section for this process is estimated to be $\sigma \approx 2$ mb.

1. Introduction

We have investigated the inelastic two-prong interactions at 17,2 GeV in emulsion. The aim of our work was to study the quasi-elastic diffraction character of inelastic processes at small multiplicities suggested originally by MORRISON [1, 2] and confirmed later by other authors [3—5], and extend our previous investigations carried out at 7 GeV [6] to higher energies.

2. Experimental

The measurements were made in Ilford G5 emulsion irradiated by a π^- -beam of $(17,2 \pm 0,2)$ GeV energy. The plates were $14,5 \text{ cm} \times 23,5 \text{ cm} \times 0,06 \text{ cm}$ in size.

Scanning the plates by following the tracks of primary pions and using appropriate selection criteria 100 two-prong inelastic $\pi^- - p$ interactions were found. In the analysis 40 more events of the same type, and having the same primary energy measured by the Alma-Ata groups are also included [7].

The mass and momentum of the particles were determined by a combination of blob-density and multiple scattering measurements on relativistic tracks having dip angle $\leq 5^\circ$. To the remaining relativistic particles geometrical correction was applied. For tracks, where $b/b_0 > 1,4$ irrespective of their dip angles two of the following three parameters were measured: blob density, multiple scattering and range.

For the scattering measurements a Koristka R4 microscope was used. The scattering of secondary particles was determined at cell lengths for which the ratio of the signal to noise was at least 2. The spurious scattering was determined by means of scattering measurements on primary tracks of well-known energies on a total length of about 15 m.

3. Results and discussion

In Figs. 1 and 2 we have plotted the momentum and transverse momentum distributions of secondary pions and protons originating in two-prong $\pi^- - p$ interactions in the center of mass system (CMS) of the colliding pion and nucleon.

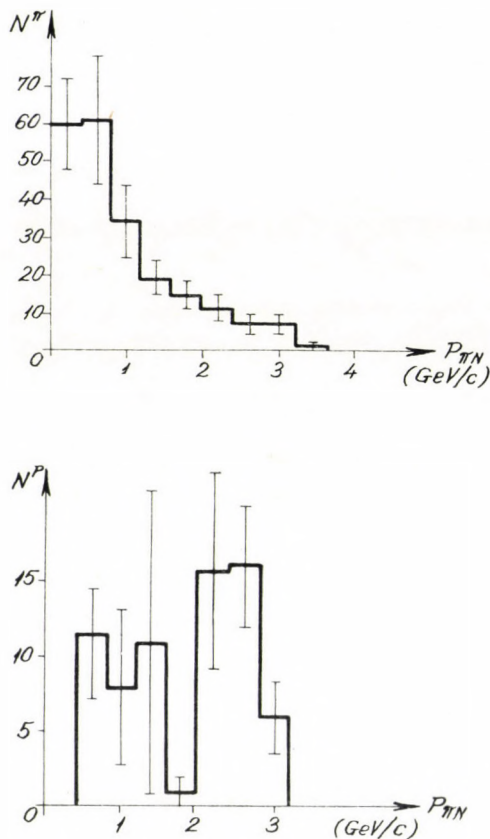


Fig. 1. The momentum distribution of secondary pions and protons in the CMS

The average momenta of pions and protons in the CMS are $\langle P_{\text{cms}}^\pi \rangle = (0.93 \pm 0.08) \text{ GeV}/c$ and $\langle P_{\text{cms}}^p \rangle = (1.8 \pm 0.3) \text{ GeV}/c$. The average transverse momenta of pions and protons are $\langle P_\perp^\pi \rangle = (0.29 \pm 0.02) \text{ GeV}/c$ and $\langle P_\perp^p \rangle = (0.34 \pm 0.05) \text{ GeV}/c$.

Fig. 3 shows the angular distribution of pions and protons in the CMS.

One can see clearly from Fig. 3 that all protons are emitted backward in the CMS. The distribution of pions is also very asymmetric, they are emitted, however, mostly in the forward direction.

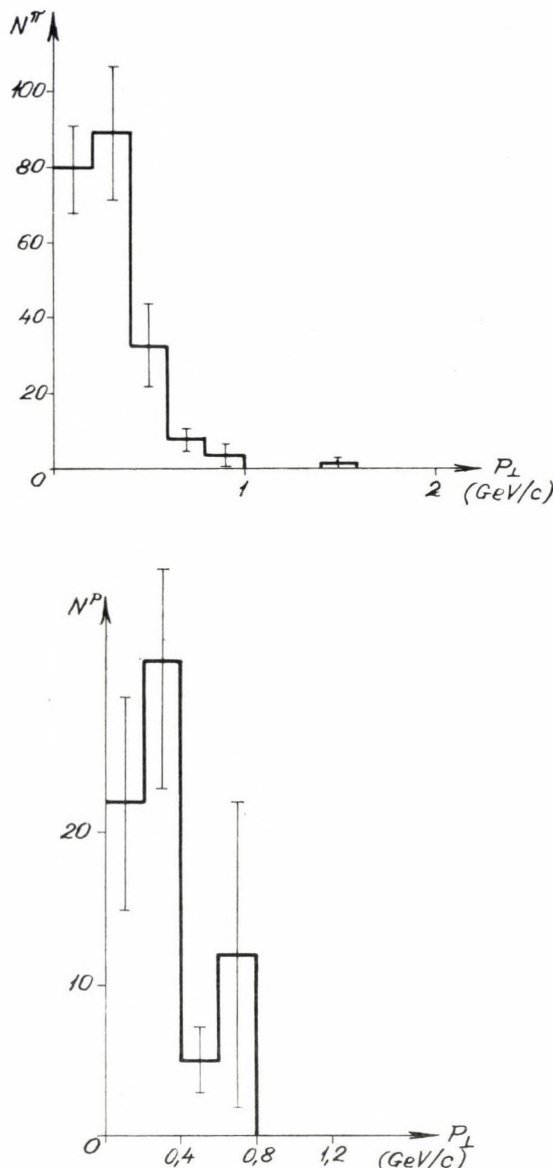


Fig. 2. The transverse momentum distribution of pions and protons in the CMS

The four-momentum transfer in the two-prong $\pi^- - p$ interactions was investigated in the way suggested by some of the authors in a previous paper [8]. We have calculated the four-momentum transfer squared, t , for π^- -mesons in the reaction:

$$\pi^- + p \rightarrow p + \pi^- + k \pi^\circ \quad (k = 1, 2, \dots), \quad (1)$$

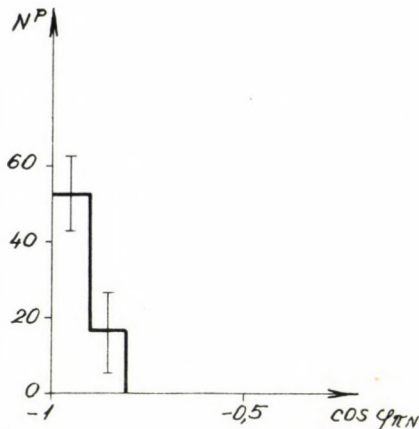
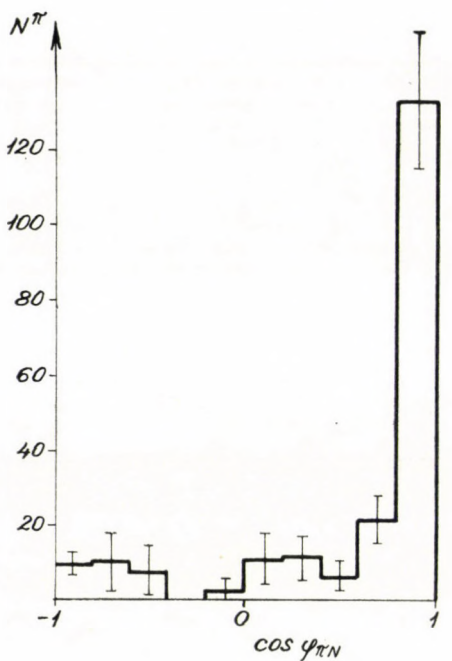
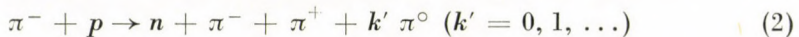


Fig. 3. The angular distribution of pions and protons in the CMS

and the four-momentum transfer squared for charged pions having the smaller four-momentum transfer (irrespective of their charge) in the reaction:



The distributions which were obtained applying appropriate geometrical correction [6] can be seen in Figs. 4a and 4b.

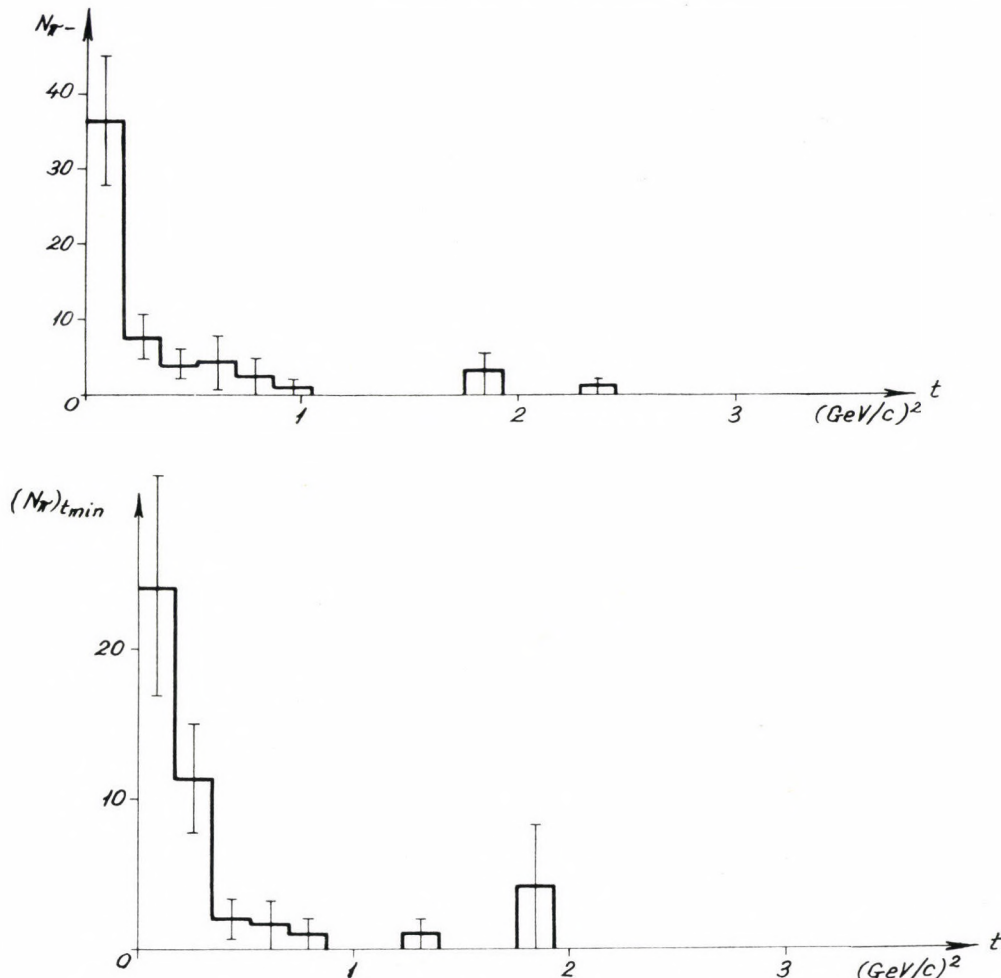


Fig. 4. The four-momentum transfer distribution: of π^- in reaction (1) and that of pions having the minimum four-momentum transfer in reaction (2) irrespective of their charge

The shape of these histograms is very similar to those obtained by some of the authors in the analysis of $\pi^- - p$ interactions in emulsions at 7 GeV and in bubble chambers at 7 and 16 GeV [8]. Both distributions are rapidly falling off with increasing $|t|$ quite similar to the characteristic four-momentum transfer distribution in high-energy elastic scattering. In [8] it was also shown from the bubble chamber data, that in reactions of the type (2) in the majority of cases the four-momentum transfer calculated for the π^- -meson is less than that obtained for the π^+ -meson. From these results the authors of [8] have concluded in accordance with MORRISON [1, 2] and other authors [3-5], that in the inelastic two-prong $\pi^- - p$ interactions the incident pion undergoes a quasi-elastic diffraction scattering and has a certain tendency to maintain

its charge. Our present experimental results give further support to this conclusion.

From the observed number of events having fast forward emitted pions the cross section of the quasi-elastic diffraction scattering can be roughly estimated. Taking into account the probability of collisions on free and quasi-free protons in emulsion, the cross section for the $\pi^- - p$ quasi-elastic diffraction scattering turns out to be $\sigma \approx 2$ mb at 17 GeV. This value is in good agreement with the results of MORRISON [1], who has found $\sigma = 2.25$ mb for the same type of events produced by 16 GeV π^- -mesons in a hydrogen bubble chamber.

Several attempts were made to explain these experimental results [9]. One interpretation was that the incident pion undergoes diffraction scattering on a virtual pion of the target nucleon. Another interpretation was given by the exchange of a Pomeranchukon between the incoming pion and the target proton or between the incoming pion and virtual target pion. All these models however, must be treated with great precaution. The only conclusion that cannot be disputed is that the *inelastic* interactions at small multiplicities have *quasi-elastic diffraction character*.

REFERENCES

1. D. R. O. MORRISON, Proc. Int. Conf. on Theor. Aspect of Very-High Energy Phenomena, CERN 61—62 (Geneva, 1961) p. 153; D. R. O. MORRISON, Proc. Int. Conf. on Elementary Particles, Aix-en-Provence, Vol. I (Saclay: C. E. N. 1961) p. 407.
2. D. R. O. MORRISON, 1962. Int. Conf. on High Energy Physics at CERN (Geneva, 1962), p. 606.
3. G. BELLINI, E. FIORINI, A. J. HERZ, P. NEGRI and S. RATTI, 1962. Int. Conf. on High Energy Physics at CERN (Geneva, 1962), p. 613; G. BELLINI, E. FIORINI, A. J. HERZ, P. NEGRI, S. RATTI, C. BAGLIN, H. BINGHAM, M. BLOCH, D. DRIJARD, A. LAGARRIGUE, P. MITTNER, A. ORKIN-LECOURTOIS, P. RANÇON, A. ROUSSET, B. DE RAAD, R. SALMERRON and R. VOSS, Nuovo Cim., **27**, 816, 1963.
4. D. K. KOPYLOVA, V. B. LJUBIMOV, M. N. PODGORECKIJ, X. RIZSEV, Z. TRKA, Z. E. T. F., **44**, 1481, 1963.
5. M. I. FERRERO, C. M. CARELLI, A. MARZARI CHIESA and M. VIGONE, Nuovo Cimento, **27**, 1066, 1963.
6. G. BOZÓKI, E. FENYVES, A. FRENKEL and E. GOMBOSI, Nuovo Cim., **27**, 668, 1963.
7. E. V. ANSON, A. H. VINICKY, A. A. LOKTIONOV, I. S. STRELCOV, D. S. TAKIBAEV, I. YA. CHASNIKOV and C. I. SHAHOVA, Communication at JINR Emulsion Experiments Committee held on 27—30 November, 1963.
8. G. BOZÓKI, E. FENYVES, A. FRENKEL and ÉVA GOMBOSI, Acta Phys. Hung., **16**, 335, 1964.
9. A summary of these papers is given by D. R. O. MORRISON, CERN report, 63—1, 1963,

ДВУХЛУЧЕВЫЕ НЕУПРУГИЕ ВЗАИМОДЕЙСТВИЯ В ЭМУЛЬСИИ ПРИ ЭНЕРГИИ 17,2 ГЕВ

Г. БОЗОКИ, Е. ФЕНЬВЕШ, Е. ГОМБОШИ и Е. НАДЬ

Р е з ю м е

Было исследовано угловое и импульсное распределение двухлучевых взаимодействий $\Pi^- + p$ в эмульсии. Полученные результаты подтверждают предположение, что при этих событиях пион рассеивается квазиупруго. Сечение этого процесса приблизительно равняется 2 мб.

COMMUNICATIONES BREVES

TRANSMISSION CURVE OF THE S³⁵ CONTINUOUS BETA-RADIATION IN AIR

By

T. VERTSE and D. BERÉNYI

INSTITUTE OF NUCLEAR RESEARCH OF THE HUNGARIAN ACADEMY OF SCIENCES (ATOMKI),
DEBRECEN

(Received 3. II. 1964)

It is not only in the fundamental research of nuclear physics but also in the applications in which radioactive nucleides are used and above all when standardizing pure beta-emitter sources that it becomes necessary to take the absorption in the air layer between the counter and the ion source into account.

However, some problems may arise in connection with carrying out such a correction. First of all, the absorption of the continuous β -radiation is supposed to be exponential, although deviations from this law were observed. On the other hand there are considerable differences in the literature between the values of μ/ρ determined on the basis of the exponential law. (The present state is summarized in [1].)

Further the measurements refer in most cases to Al and from these it is possible with the help of a correction formula only [2] to obtain the absorption coefficient for air. However, no transmission curve in air of any continuous β -radiation has been published in the literature. (There are some recent measurements in connection with the correction to the absorption in air [3].)

It was, therefore, found worthwhile to measure the transmission curve in air for the continuous β -radiation of S³⁵. This is one of the pure beta emitters with the lowest endpoint energy of the continuous beta-spectrum and therefore is very sensitive to the absorption in air.

The measurements were made with scintillation techniques, the detecting phosphor was a plastic scintillator (\varnothing 20 mm \times 3 mm in size) coupled to a RCA 6342/A multiplier. To the Al cylinder containing the multiplier a vacuum-chamber device was joined in such a way that allowed to produce a vacuum in the space between the source and the scintillator or to maintain there a certain pressure. The experimental arrangement can be seen in Fig. 1 where the respective dimensions are also indicated. The position of the source was changeable by placing appropriate insets into the vacuum chamber. Before the scintillator at a distance of about 10 mm was placed an Al diaphragm with an opening of \varnothing 16 mm and 2 mm thickness.

In the course of the measurements the pressure was changed in the vacuum chamber from one atmosphere to vacuum (10^{-2} Hgmm). In Fig. 2 the transmission curves taken at three different source-detector distances can be seen. The three curves satisfactorily coincide down to 75% transmission and even then only the curve corresponding to the largest source-detector

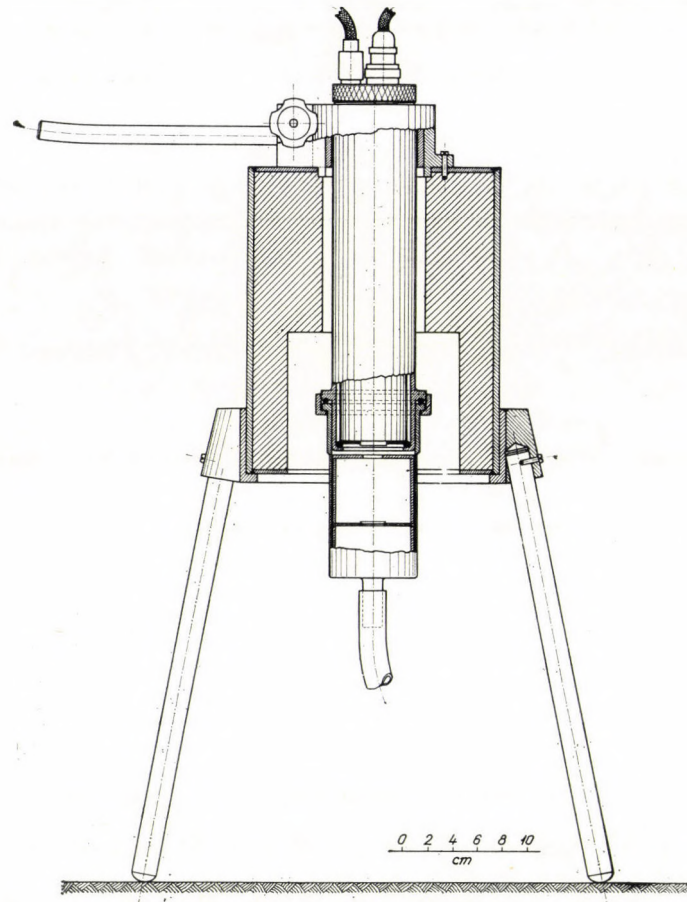


Fig. 1. Experimental arrangement for the investigation of the transmission of the S^{35} beta-rays in air of varying pressure

distance (84 mm) deviates from the two others. This can probably be explained by backscattering from the bottom of the vacuum chamber.

The coincidence of the transmission curves corresponding to the 27 and 42 mm source-detector distance (where backscattering from the bottom is negligible) shows that the measurement is practically not influenced by scattering from the side walls of the vacuum chamber. This means that if the trans-

mission is measured at a suitably fixed source-detector distance as function of the air pressure and the thickness of the air layer is expressed in mg/cm², the measured values immediately give the decrease of the intensity of the S³⁵ continuous beta-radiation, owing to the absorption of the air layer at different source-detector distances in atmospheric pressure. In Fig. 2 the transmission cur-

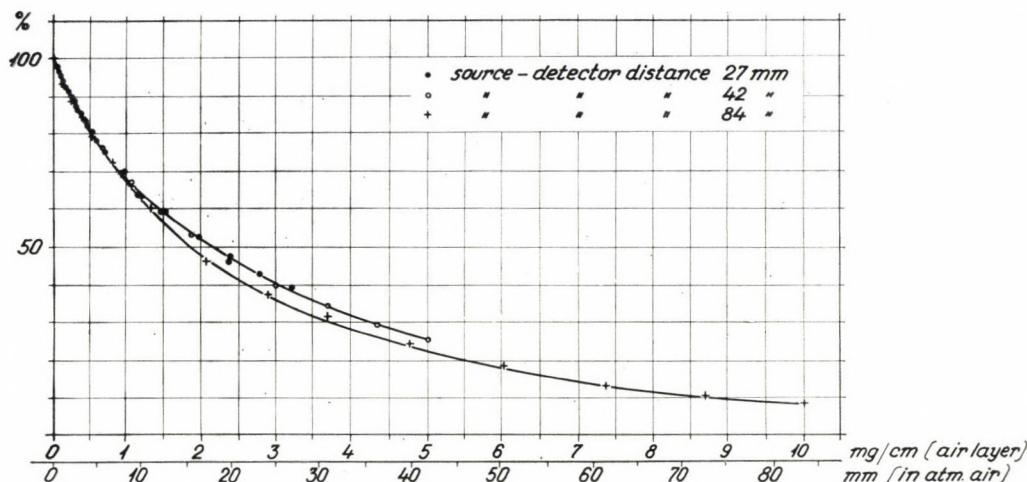


Fig. 2. Transmission curves of beta-rays with continuous spectral distribution of S³⁵ in air at different source-detector distances

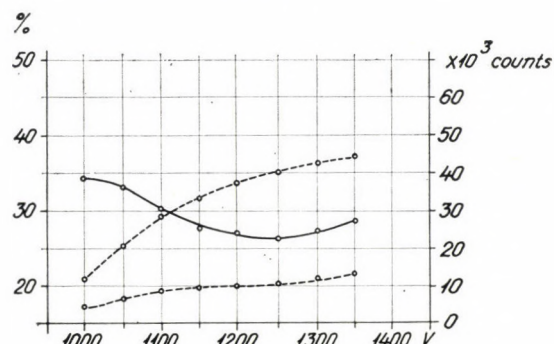


Fig. 3. The transmission as function of the high voltage applied to the multiplier at a given value of the absorber (solid curve). The upper dashed curve gives the counting rate without absorber, and the lower dashed curve that with the absorber

ves are reproduced which were obtained for various distances as function of the pressure. On the x-axis the values of the corresponding source-detector distance at atmospheric pressure in mm are also indicated. It can be seen that the intensity of the radiation investigated here decreased to about half its original value already after penetrating 15 mm of air at atmospheric pressure. We

should like to make the following remark on the role of the high voltage of the multiplier. If the transmission is measured as function of the high voltage at a given value of the absorber a change of the transmission will be observed (see the solid curve in Fig. 3). One can easily see that the minimum of the curve determines the real value of the transmission. As a matter of fact when using lower values of the high voltage that correspond to the minimum of the curve then the low-energy part of the spectrum will be cut off and at

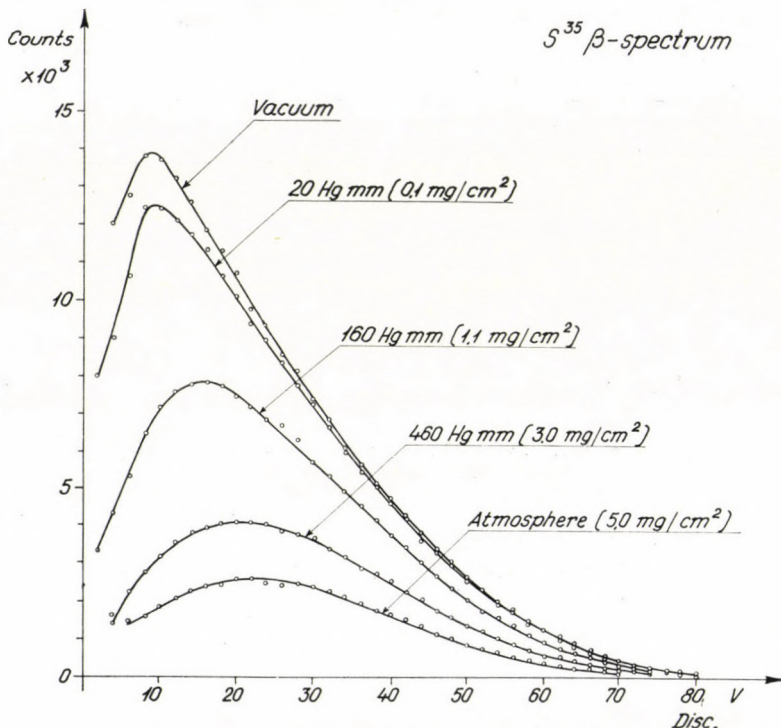


Fig. 4. The beta-spectrum of S^{35} at different air pressures between the source and the detector (the source-detector distance was 42 mm)

higher ones the dark current will make itself felt more and more. It may also be seen from Fig. 3 that at the value of the high voltage where the transmission has a minimum the counting rate attains its saturation value, it shows a plateau (cf. the dashed curves in Fig. 3). In our measurements the high voltage had a value of 1250 V.

In Fig. 4 the scintillation β -spectra of S^{35} are given at different values of the pressure between the source and the detector. In these measurements the source-detector distance was 42 mm (the data for the diaphragm were indicated earlier).

We also took the transmission curve for the β -rays of S³⁵ in aluminium absorbers. In these measurements the Al foils were placed on the top of the diaphragm (see Fig. 1). The value of the high voltage, as earlier, was 1250 V and the source-detector distance 42 mm. The form of the transmission curve obtained (Fig. 5) corresponds to the experimental [4, 5] and theoretical [6] curves recently published in the literature. It can be seen that the transmission curve taken for air has the same form when plotted in a half-logarithmic scale

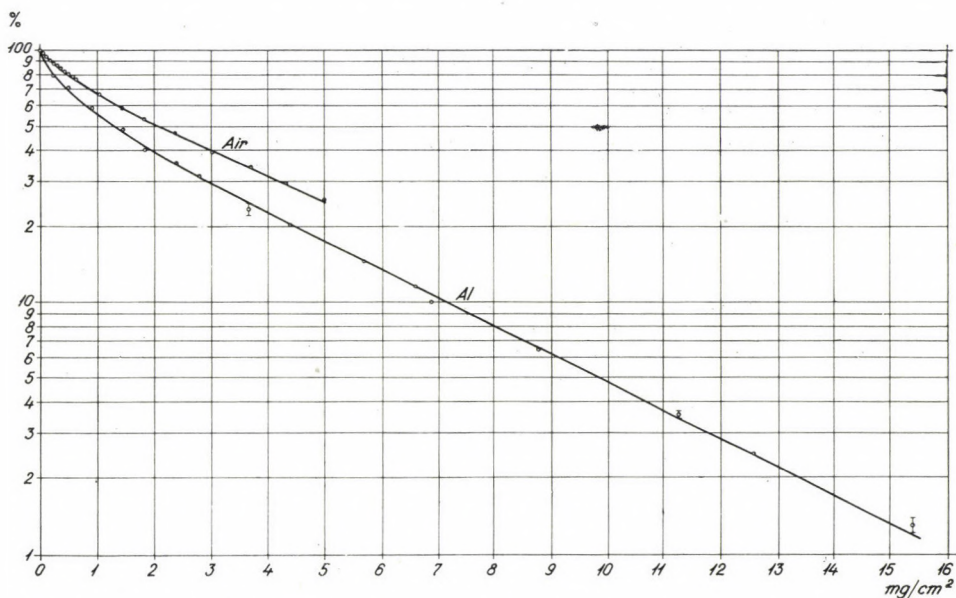


Fig. 5. The transmission of the S³⁵ beta-rays in air and in Al plotted in a half-logarithmic scale. The source-detector distance was 42 mm and the geometry was that of Fig. 1

(Fig. 5). A deviation from the straight line appears mainly at smaller values of the absorber. From the straight section of the curves (at larger thicknesses of the absorber: for air from about 1.5 mg/cm², i.e. at atmospheric pressure at 10–12 mm; for Al from at about 3 mg/cm²) the value of μ/ρ was determined as 246.7 for air. For Al it was found to be 256.7 cm²/g. From our experimental data for Al we calculated a value of 244.1 cm²/g for air on the basis of the Fournier formula [2]. This value agrees with our measured value very well. It is to be noted here that the mass absorption coefficients for Al to be found in the literature show considerable divergences: 290 cm²/g [7], 211 cm²/g [8], 277 cm²/g [1].

Finally, we note that in these measurements we disregarded the effect due to the backscattering from the surface of the scintillator. Owing to this effect we can define an effective window thickness the value of which is about 0.1 mg/cm² [9] according to an earlier measurement of ours.

The authors are indebted to Prof. A. SZALAY for the excellent working conditions at this Institute and to Dr. Cs. UJHELYI, radiochemist, for the careful preparation of the source.

REFERENCES

1. L. DADDI and V. D'ANGELO, Int. Journ. of App. Radiation and Isotopes, **14**, 97, 1963.
2. E. BLEULER and G. J. GOLDSMITH, Experimental Nucleonics, Rinehardt and Co. Inc., New York, 1952, p. 165.
3. H. E. Цветаева и М. Н. Брусенцова, Атомная Энергия, **4**, 583, 1958.
4. И. Б. Керим-Маркус и М. А. Львова, в сборнике статей «Исследования в области дозиметрии ионизирующих излучений». Изд. АН СССР, Москва, 1957. с. 3.
5. R. ENGELMANN, Nukleonik, **3**, 133, 1961.
6. H. E. Цветаева, Атомная Энергия, **9**, 507, 1960.
7. L. SEREN, H. N. FRIEDLANDER and S. H. TURKEL, Phys. Rev., **72**, 888, 1947. Quoted in Landolt-Börnstein, Bd. I. Teil 5, Springer Vlg., Berlin—Göttingen—Heidelberg 1952, p. 349.
8. G. I. GLEASON, I. D. TAYLOR and D. L. TABERN, Nucleonics, **8**, 12, 1951, No. 5. Quoted in Landolt-Börnstein, Bd. I. Teil. 5. Springer Vlg. Berlin—Göttingen—Heidelberg, 1952, p. 349.
9. D. BERÉNYI and Gy. MÁTHÉ, Nuclear Instruments, **13**, 161, 1961.

RESTRICTIONS ON THE VERTEX FUNCTIONS

By

G. PÓCSIK

INSTITUTE FOR THEORETICAL PHYSICS, ROLAND EÖTVÖS UNIVERSITY, BUDAPEST

(Received 19. III. 1964)

1. In the present note it is shown that in the theories possessing conserved currents the vertex functions are restricted by certain integral or differential relations. These restrictions are the necessary conditions for current conservation. Therefore, they are very useful 1. for the simplification of various calculations concerning the electromagnetic form factors and 2. to control the compatibility of the current conservation and the various approximate vertex functions.

2. The renormalized electron-photon vertex Γ_μ transforms as a four-vector under the Lorentz group, therefore, its most general form can be constructed from 12 invariants:

$$\begin{aligned} \Gamma_\mu(p, p') = & P_\mu F_1 + Q_\mu F_2 + \gamma_\mu F_3 + P_\mu(P\gamma F_4 + Q\gamma F_5) + \\ & + Q_\mu(P\gamma F_6 + Q\gamma F_7) + \sigma_{\mu\nu}(P^\nu F_8 + Q^\nu F_9) + \\ & + Q \cdot \sigma \cdot P(P_\mu F_{10} + Q_\mu F_{11}) + \varepsilon_{\mu\nu\rho\sigma} P^\nu Q^\rho \gamma^\sigma \gamma_5 F_{12}, \end{aligned} \quad (1)$$

where

$$P_\mu = p_\mu + p'_\mu, \quad Q_\mu = p_\mu - p'_\mu \quad \text{and} \quad F_j = F_j(p^2, p'^2, Q^2).$$

Let us assume that the physical vacuum is invariant under space inversion, charge conjugation and time inversion. It is easy to see that these lead in turn to the following restrictions:

$$1. \quad \pm \Gamma_\mu(p_1, p_2) = \gamma_0 \Gamma_\mu(-p_1, p_{10}, -p_2, p_{20}) \gamma_0. \quad (2)$$

The sign $+/-$ is valid for $\mu = 0/j$. (2) does not impose any restriction on (1).

$$2. \quad C \Gamma_\mu^\top(p_1, p_2) C^+ = - \Gamma_\mu(-p_2, -p_1). \quad (3)$$

This states that for $p \leftrightarrow p' F_{1, 3, 4, 7, 9, 10, 12}/F_{2, 5, 6, 8, 11}$ are even/odd functions.

$$3. \quad \Gamma_\mu^+(p_1, p_2) = \gamma_0 \Gamma_\mu(\sqrt{p_2}, p_1) \gamma_0. \quad (4)$$

Consequently, $F_1(p, p') = F_1^*(p', p)$ etc. From (3) and (4) we see that $F_1, \dots, F_7, F_{12}/F_8, \dots, F_{11}$ are real/imaginary.

Further restrictions are imposed by the asymptotics. Namely, for zero momentum transfer between free spinors for $p \rightarrow \infty$ the vertex function behaves as $\gamma_\mu/Z_1 \gamma_\mu$ and

$$2F_1(p, p) + 4mF_4(p, p) + \frac{1}{m}F_3(p, p) = \frac{1}{m}, \quad p^2 = m^2 \quad (5)$$

$$\lim_{p \rightarrow \infty} (2p_\mu F_1(p, p) + \gamma_\mu F_3(p, p) + 4p_\mu \gamma p F_4(p, p)) = Z_1 \gamma_\mu. \quad (6)$$

3. In the following we shall examine the conditions for gauge invariance.

From (1) and (3) it follows that only the invariants $F_{1, 3, 4, 9, 10, 12}$ can contribute to the electromagnetic form factors. Therefore, charge conjugation invariance of the vacuum state is a sufficient condition for "weak gauge invariance" [1]. In other words, charge conservation in one electron matrix element automatically holds:

$$Q_\mu \bar{u}(p) \Gamma^\mu(p, p') u(p') = 0. \quad (7)$$

As is well-known, a necessary condition for gauge invariance is just the WARD identity and the generalized WARD identity [2]. These can be combined into an equation which holds in each gauge

$$Q_\mu \int_0^1 dx \Gamma^\mu(p_x, p_x) = Q_\mu \Gamma^\mu(p, p'), \\ p_x = px + (1-x)p'. \quad (8)$$

For the invariants we obtain the restrictions

$$A(p, p') \equiv PQF_1(p, p') + Q^2 F_2(p, p') = \int_0^1 2Qp_x F_1(p_x, p_x) \\ B(p, p') \equiv F_3(p, p') + PQF_5(p, p') + Q^2 F_7(p, p') = \\ = \int_0^1 dx (F_3(p_x, p_x) + 2(2x-1)p_x QF_4(p_x, p_x)) \\ C(p, p') \equiv PQF_4(p, p') + Q^2 F_6(p, p') = 2 \int_0^1 dx p_x QF_4(p_x, p_x), \\ D(p, p') \equiv F_8(p, p') + PQF_{10}(p, p') + Q^2 F_{11}(p, p') = 0 \quad (9)$$

or in differential form

$$\frac{\partial A(p, p')}{\partial p_\lambda} = 2p^\lambda F_1(p, p), \quad B(p, p') + C(p, p') = F_3(p, p) \quad (10)$$

$$\frac{\partial B(p, p')}{\partial p_\lambda} = \frac{\partial}{\partial p_\lambda} C(p, p') = 2p^\lambda F_4(p, p), \quad D(p, p') = 0.$$

If a certain vertex does not satisfy the conditions (8)–(10), then it cannot be compatible with charge conservation. Furthermore, the invariants contributing to the electromagnetic form factors are not independent of the other invariants F_i . This immediately follows if we consider (10) on the mass shell. For instance, in case of small momentum transfer $(\partial F_1/\partial Q^2)Q^2 = 0 = -(\partial F_2/\partial p^2)Q^2 = 0$ etc.

4. As an example we shall examine whether or not EDWARDS' linear program [3] possesses the properties (8)–(10). First of all, it can be seen that the general equations are compatible with (8). However, the approximate vertex given by EDWARDS is

$$\Gamma_\mu(0, p) = \gamma_\mu \int_0^1 dx \frac{x^{-a/8\pi}}{1 - a/8\pi} \left(\frac{m^2(1-x)}{p^2 x + m^2} \right)^{1/8\pi} \quad (11)$$

and for large p

$$\Gamma_\mu(p, p) = \frac{\partial}{\partial p^\mu} \frac{(p^2)^{a/8\pi}}{\gamma p + m} \quad (12)$$

A simple calculation shows that for large p (11) and (12) contradict (10).

Similarly, it is true that in NAMBU's theory the approximate axial vector vertex part is not compatible with the conserved axial vector current [4].

REFERENCES

1. F. J. ERNST et al., Phys. Rev., **119**, 1105, 1960.
2. S. OKUBO, Nuovo Cim., **15**, 949, 1960.
3. S. F. EDWARDS, Phys. Rev., **90**, 284, 1953.
4. H. BANERJEE, Nuovo Cim., **23**, 587, 1962.

PRESSURE IN A RELATIVISTICALLY DEGENERATED FERMION GAS WITH SCALAR INTERACTION

By

G. MARX and J. NÉMETH

INSTITUTE FOR THEORETICAL PHYSICS, ROLAND EÖTVÖS UNIVERSITY, BUDAPEST

(Received 23. III. 1964)

For the analysis of the gravitational collapse in hyperstars it is necessary to know the pressure-density relation for the real baryon gas also in the extreme relativistic region [1]. The theory of nuclear matter enables us to compute the pressure-density relation in the state of nonrelativistic degeneracy. The case of relativistic degeneracy has been treated without any interaction [2] and when only the repulsive core was taken into account [3], as of course one has no detailed information about the baryon interactions at very short distances. An extrapolation of the pressure-density relation was tried under the assumption that the rest-mass density, given by the trace of the energy tensor, has to be positive. It possibly tends to zero if the density grows beyond all limits. This is equivalent to the conclusion

$$p \leq u \text{ and } \lim_{\eta \rightarrow \infty} \frac{p}{u} = \frac{1}{3}. \quad (1)$$

(Here p means the pressure, u the energy density and n the particle density.) (1) does not contain very much information about the behaviour of the functions $p(n)$, $u(n)$ at very high densities.

Here it is our aim to derive the pressure-density relation from a simple model interaction in the whole relativistic domain. We do not allow neglect of any relativistic effect, but we do make an over-simplification in respect of interactions. Because of this our results cannot be expected to be correct, they at most supply some information on the mathematical peculiarities of the pressure-density law in the extreme relativistic domain.

In our approximation a zero-range interaction will be used, the relativistic scalar version of the two-nucleon potential $V(r_{12}) = C \delta(r_{12})$ [4]. In a non-quantized scalar field the energy of a fermion gas with particle density n in the Thomas—Fermi approximation is known to be

$$E = \int \left[\eta(mc^2 + gf) \left\langle \frac{1}{\sqrt{1 - \beta^2}} \right\rangle + \frac{1}{8\pi} \left((\nabla f)^2 + \frac{1}{c^2} \dot{f}^2 + \mu^2 f^2 \right) \right] dV. \quad (2)$$

The field equation determining the scalar potential f is of the following form:

$$\nabla^2 f - \frac{1}{c^2} \ddot{f} - \gamma^2 f = 4\pi g n \langle \sqrt{1 - \beta^2} \rangle. \quad (3)$$

Here m is the bare mass constant of the fermions, g is the coupling constant and μ^{-1} is the range of the field. The kinetic energy of the particles is taken into account by calculating the mean values $\langle \rangle$ of the velocity (β)-dependent expression with the help of the Fermi distribution. Our aim is to evaluate the dependence of the pressure

$$p = - \frac{\partial E}{\partial V}$$

and of the energy density

$$u = \frac{E}{V}$$

on the particle density n at zero temperature. To make the evaluation of (1) possible, we go to the limit $\mu^{-1} = 0$ [4]. Let us introduce dimensionless quantities:

$$\varphi = - \frac{gf}{mc^2}, \quad v = \frac{n}{n_0}, \quad \pi = \frac{p}{p_0}, \quad \omega = \frac{u}{u_0}$$

with

$$n_0 = \frac{8\pi}{3} \left(\frac{h}{mc} \right)^{-3}, \quad u_0 = p_0 = mc^2 n_0, \quad \gamma = \frac{32\pi^2 g^2 m^2 c}{3\mu^2 h^3}.$$

Minimizing the energy E with respect to φ , we arrive at the relation (4)

$$\varphi = \frac{3}{2} \gamma (1 - \varphi)^3 \left[\frac{v^{1/3}}{1 - \varphi} \sqrt{1 + \frac{v^{2/3}}{(1 - \varphi)^2}} \right]$$

$$- \ln \left(\frac{v^{1/3}}{1 - \varphi} + \sqrt{1 + \frac{v^{2/3}}{(1 - \varphi)^2}} \right).$$

This is the explicit form of the field equation (3) in the limiting case $\mu^{-1} = 0$ and is equivalent to

$$\varphi = \gamma v \langle \sqrt{1 - \beta^2} \rangle. \quad (5)$$

(3) enables us to calculate φ for every density value ν . The pressure and the energy density turn out to be of the following form:

$$\begin{aligned}\pi &= \frac{1}{4} \nu \sqrt{\nu^{2/3} + (1 - \varphi)^2} - \gamma^{-1} \varphi(1 + \varphi), \\ \omega &= \frac{3}{4} \nu \sqrt{\nu^{2/3} + (1 - \varphi)^2} + \gamma^{-1} \varphi(1 + \varphi).\end{aligned}\quad (6)$$

When relation (4) is taken into account π and ω turn out to be functions of ν . These are shown in the Figure. Here we have chosen the parameter values $\gamma = 1,38$ and $m = 0,71 \cdot 10^{-24}$ g, because these reproduce the experimental density and energy of the nuclear matter at zero pressure. In this case

$$n_0 = 2,8 \cdot 10^{38} \text{ cm}^{-3}, \quad u_0 = 1,12 \cdot 10^{41} \text{ MeV cm}^{-3}, \quad p_0 = 1,79 \cdot 10^{29} \text{ atm.}$$

(This is not meant to be an explanation of the saturation in common nuclei, because, the equilibrium state $p = 0$ is — in the case of Wigner forces — in the relativistic domain [4] contradicted by the facts of nuclear physics.)

One sees that π at first has the nonrelativistic form $0,2\nu^{5/3}$, later it will be decreased by the attractive interaction, and for $\nu \rightarrow \infty$ it will increase as $0,25\nu^{4/3}$ like a neutrino gas without any interaction. The cause of this behaviour is clear: for $\nu \rightarrow \infty$ the potential $p \rightarrow 1$ and the physical rest mass

$$M = m + \frac{g\varphi}{c^2} = m(1 - \varphi),$$

occurring in the particle energy and momentum, disappear [4]. At the same time the maximum Fermi velocity approaches c since

$$\begin{aligned}\left\langle \frac{1}{\sqrt{1 - \beta^2}} \right\rangle &= \frac{3}{2} \frac{(1 - \varphi)^3}{\nu} \left[\frac{\nu^{1/3}}{1 - \varphi} \sqrt{1 + \frac{\nu^{2/3}}{(1 - \varphi)^2}} \right. \\ &\quad \left. - \ln \left(\frac{\nu^{1/3}}{1 - \varphi} + \sqrt{1 + \frac{\nu^{2/3}}{(1 - \varphi)^2}} \right) \right],\end{aligned}$$

tends to infinity for $\nu \rightarrow \infty$. According to the field equation (4) φ remains finite also for infinite densities, thus its influence loses in importance in the extreme relativistic region. The postulated relation (1) is verified for this type of interaction.

Above a critical density equation (3) can be satisfied not only by one, but by three different values of φ for a given density ν . (As a matter of fact,

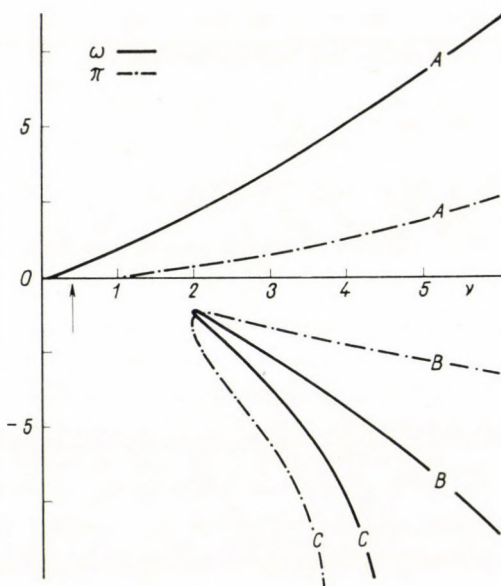


Fig. 1

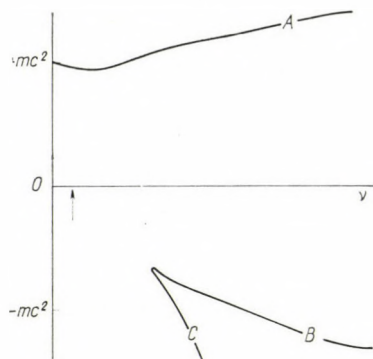


Fig. 2

not one, but three different values of potential and velocity can give the same Fermi momentum according to the relativistic formulas.) In the Figure along the branch B the potential decreases to 1 ($\varphi \rightarrow 1$) for $r \rightarrow \infty$, and the maximum Fermi velocity $\rightarrow c$. In this case (1) will be satisfied by negative values of p and u :

$$u \approx 3p \approx -\frac{3}{4} v^{4/3} \text{ for large } v,$$

In the branch C the interaction plays a decisive role in the relativistic region: For $v \rightarrow \infty$ the potential $\varphi \rightarrow \infty$, the maximum Fermi velocity $\rightarrow 0$, thus

$$p \approx u \approx -0,5 \gamma v^2.$$

(The inequality (1) has lost its validity, but $p/u \leq 1$ and so the sound velocity remains below the velocity of light also in this case.)

The negative energy states — in the sense of Dirac — are characterized by $<\sqrt{1-\beta^2}> < 0$, i.e. by $\varphi < 0$. We do not intend to investigate these solutions in the present paper.

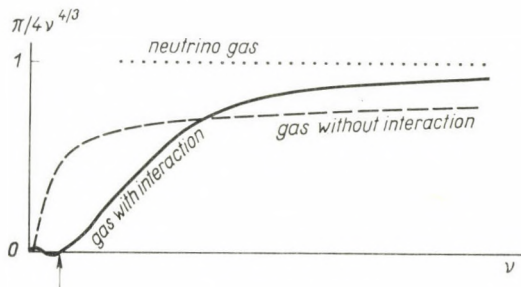


Fig. 3

The equilibrium state of the fermion gas is at $v = 0,42$, $p = 0$. If by compression the matter reaches higher and higher densities it moves along the branch A . It is problematic whether the strange branches B and C may have any physical meaning. If matter could jump from A to C the field would dominate and the gas would collapse. (This “scalar collapse” is somewhat similar to the gravitational collapse. It could be stopped only by a quantum fluctuational effect.) We note that the occurrence of states of negative pressure of the fermion gas at very high densities is not certain but only possible. This is, however, a very interesting possibility: Perhaps by compression the real many-neutron system may be brought to an extremely bound state, in which it has lost its positive mass but still has preserved its baryonic charge. (The transition of common terrestrial nuclei into this superbond state by tunnel effect is slowed down by the many degrees of freedom. As it is shown [5], for light nuclei — e.g. for deuteron — such a superbond state does not exist.) The formation of such supernuclei with negligible or negative rest mass may offer a possibility for the imploding hyperstar to decrease its gravitational mass below the Chandrasekhar limit. This may prevent the gravitational collapse inside the singularity. This mathematical possibility, suggested by our model, seems to deserve a more detailed (and more realistic) investigation.

The authors are indebted to Prof. P. GOMBÁS and to Dr. D. KISDI for valuable discussions on many-fermion systems. One of the authors (G. M.) is highly indebted to Prof. J. ROBINSON for the kind invitation to the Southwest Center for Advanced Studies in Dallas (Texas). The discussions on the problem of gravitational collapse have given the initiative for this work.

REFERENCES

1. E. E. SALPETER, Report on the John F. Kennedy Memorial Symposium on the Gravitational Collapse, Dallas, Texas, 16—19, Dec. 1963.
2. V. A. AMBARTSUMYAN and G. S. SAAKYAN, Astron. Thur. **37**, 193, 1960; ibid. **38**, 1016, 1961.
See also: Soviet Astron. A. M., **8**, 186, 1960; ibid **5**, 779, 1962.
3. L. GRATTON and G. SZAMOSI, Frascati preprint, 1963.
4. G. MARX, Nuclear Physics, **1**, 660, 1956.
5. G. MARX, Acta Phys. Hung., **6**, 48, 1955.

RECENSIONES

G. HERTZ

Lehrbuch der Kernphysik, Band III, Angewandte Kernphysik

B. G. Teubner Verlagsgesellschaft, Leipzig, 1962.

Im Band III des Lehrbuches der Kernphysik werden die wissenschaftlichen Grundlagen für die technische Anwendung kernphysikalischer Erscheinungen behandelt, ohne dass auf Einzelheiten der technischen Durchführung eingegangen würde. Dadurch ist das Buch einerseits gut übersichtlich, nicht allzu lang, andererseits jedoch genügend ausführlich um denjenigen, die kernphysikalische Methoden anzuwenden beabsichtigen, über die physikalischen beziehungsweise physiko-chemischen Grundlagen der einzelnen Anwendungsgebiete einen hinreichenden, wissenschaftlichen Überblick zu geben.

Das Buch hat einen Umfang von 320 Seiten und gliedert sich in 9 Kapitel. Die einzelnen Kapitel sind in mehrere, insgesamt 76 Paragraphen gegliedert. Das Buch ist klar und einfach geschrieben und für jeden mit entsprechender Vorbildung leicht verständlich. Der Wert des Buches wird durch die 79 schönen Abbildungen, 41 Tabellen und durch die zahlreichen Literaturangaben in grossem Masse erhöht.

Im folgenden geben wir einen kurzen Überblick über die im Buch behandelten Probleme.

Kapitel A gibt eine Einführung in die Theorie der Reaktoren. Es behandelt die im Reaktor ablaufenden Vorgänge, Fragen der Stabilität und der Ausnutzung des spaltbaren Materials, sowie die wichtigsten zur Ergänzung der theoretischen Berechnung benutzten experimentellen Methoden. Im Kapitel B werden die verschiedenen Methoden der Isotopen trennung besprochen. Es handelt sich hier um eine neuartige Darstellung dieses Gebietes, in der sämtliche, scheinbar sehr verschiedenen Verfahren unter einem einheitlichen Gesichtspunkt behandelt werden.

Das nächste Kapitel ist der Theorie der thermodynamischen Effekte der Isotopen gewidmet. Auf Grundlage der Methode der Zustandssummen werden die thermodynamischen Gleichgewichte in Isotopensystemen, vor allem die Berechnung des chemischen Isotopenaustausches behandelt, da diese für die technische Isotopen trennung von grosser Bedeutung ist.

Im Kapitel D wird eine kurze Übersicht über das Gebiet der Radiochemie gegeben. Wir finden hier die Behandlung der chemischen Eigenschaften der natürlichen radioaktiven Nukliden, der Transurane und der künstlich radioaktiven Isotope, sowie die Behandlung der speziellen Methoden, die für das Arbeiten mit den in extrem starker Verdünnung vorliegenden radioaktiven Elementen entwickelt worden sind.

Das nächste Kapitel behandelt die Anwendung der radioaktiven Nuklide in der Physik und Technik. Es wird neben zahlreichen Beispielen der Ausnutzung der ausgesandten hochenergetischen Strahlung und der Anwendung der Methode der Markierung auch kurz auf die Alterbestimmung mittels der Radioaktivität eingegangen.

Im Kapitel F werden die Verfahren zur Herstellung markierter Verbindungen, die Anwendung von radioaktiven Nukliden in der chemischen Analytik (Indikatoranalyse, Isotopenverdünnungs- und Aktivierungsanalyse) sowie in der chemischen Kinetik und der Strukturlehre erläutert.

Ein weiteres Kapitel behandelt die Verwendung der stabilen Isotope. Es werden ausführlich die Variationen in der natürlichen Isotopenzusammensetzung der Elemente und die neu entwickelten Verfahren zur Isotopenanalyse besprochen. Die Anwendung wird an einer Reihe von Beispielen beschrieben.

Über die umfangreiche Anwendung radioaktiver Nuklide in Medizin und Biologie wird im Kapitel H nur ein allgemeiner Überblick gegeben: an einer Reihe von typischen Beispielen werden die wichtigsten Arbeitsmethoden erläutert und ihre Fruchtbarkeit gezeigt.

Im letzten Kapitel schliesslich wird als Abschluss des Buches eine ausführliche Behandlung des Dosisbegriffes und der Dosismessung, sowie eine verhältnismässig eingehende Darstellung der möglichen Schädigungen, der zulässigen Belastungen und der notwendigen Strahlenschutzmassnahmen gegeben.

L. BOZÓKY

R. JANCEL—TH. KAHAN

Électrodynamique des plasmas

fondée sur la Mécanique statistique

Tome 1: Processes physiques et Méthodes mathématiques XX + 622 p. Dunod, Paris 1963.

Undoubtedly plasma physics is one of the most interesting topics of modern physics.

Specialists in quite a wide range of subjects from the theoretical astrophysicist to the electrical engineer, are engaged in research in this direction. The rapid development of this branch of physical science is influencing also the other branches and important results obtained in plasma physics will effect, directly or indirectly, the future life of mankind.

The ever-increasing speed of the rapid development of plasma physics has given rise to a didactic problem. It is perhaps true to say, that so far there has been no comprehensive textbook, that would be easier for the university student and at the same time for those starting to specialize in plasma physics, and that would deal systematically with the whole physical world of plasmas. To express our misgivings more clearly: the otherwise excellent, smaller or larger textbooks or monographies are either too short or too narrow in scope — i.e. too specialized — to be able to give an at once deep and many-sided survey in a self-contained form. But, in order to make teaching at the universities more effective in our opinion just this would be needed: to decrease the gap between the actual state of plasma physics research and the level of the text books.

The present volume, being the first part of a series, is a condensed version of the material of lectures delivered at the Sorbonne by the authors. They recognized that a comprehensive work of this kind is of interest to specialists of different branches, and they therefore give a self-contained review of the whole basic theory.

The present volume is divided into eight chapters.

In Chapter 1 the general properties and the fundamental processes going on among the constituents and the formation and decay of the plasmas are described.

Chapter 2 contains an excellent short summary of the basic principles of statistical mechanics together with a review also of some modern approaches relating to the evolution of nonequilibrium systems and their applications to the case of plasmas.

In Chapter 3 the dynamics of binary collisions is studied.

Chapter 4 is devoted to the detailed study of motion in different external electric and magnetic fields of given distributions and to the Brownian motion of charged particles.

Chapters 5 and 6 give a review of the theory of the Boltzmann equation, the transport equations, the macroscopic equations and the several-fluid-model of plasmas.

In Chapter 7 the mean free path theory of transport properties of equilibrium plasmas is expounded.

The last chapter is a comprehensive treatment of the general method for the approximate solutions of Boltzmann's integro-differential equation.

In the Appendix useful mathematical summaries are given.

The general impression of the present reviewer is that the authors have indeed reached their twofold aim: to provide up-to-date information and at the same time to remain on the solid ground of pedagogy, i.e. to give only "necessary elements" for the building of a very neat structure.

Excellent work has been done by the publishers as regards the careful printing and beautiful presentation of the volume.

We hope that this excellent book will soon be followed by the next volumes and that it will become an effective tool in the hands of the specialist as well as the scientist working in other branches of physics.

I. ABONYI

K. J. BINNS and P. J. LAWRENSON

Analysis and Computation of Electric and Magnetic Field Problems

Pergamon Press, Oxford—London—New York—Paris, 1963. 333 pages, 84 s net.

The book presents a very comprehensive treatment of the analytical and numerical methods for the solution of the two-dimensional stationary and quasi-stationary electric and magnetic field problems in not more than 333 pages.

The mathematical knowledge required of the reader is on the average engineer's level, assuming the normal calculus and some practice in the solution of ordinary differential equations, the use of simple Fourier series and of the elementary theory of functions of a complex variable. The more advanced mathematical methods used in the book are fully explained in the text such as the solution of partial differential equations, the use of double Fourier series and elliptic functions.

The book is divided into four parts. Part I gives a general introduction into the problem. It contains an introductory chapter pointing out the basic analogies in the methods of solution of several other important fields, such as the theory of heat conduction and the flow of fluids as well as static and quasistatic electric and magnetic problems. Chapter 2 is devoted to basic field theory giving in very concise form the theory of electric and magnetic fields and a clear explanation and definition of the physical quantities used in the later parts of the book. The basic physical requirements are collected in this part, in order that the other three parts of the book may be used independently of each other.

Part II entitled "Direct Methods" contains three chapters: Chapter 3 on the method of images, Chapter 4 on the direct method of the solution of Laplace's equation by separation of the variables and Chapter 5 on the solution of Poisson's equation for magnetic fields of distributed currents.

Part III, the longest of the four, is devoted to transformation methods. Its first chapter (Chapter 6) gives an introduction to conformal transformation. The next two chapters (Chapters 7 and 8) deal with curved and polygonal boundaries. Chapter 9 contains the necessary details of the elliptic integrals and functions, while Chapter 10 extends the transformation method to the general case.

Part IV on the numerical methods deals chiefly with the method of finite differences and with some possible uses of the Monte Carlo method.

At the end of each chapter a detailed list of references is given. At the end of the book four Appendices provide valuable tools for carrying out the necessary computations and an additional bibliography.

The book written in a very clear style contains many practical examples and figures referring to various field problems. It can be regarded as a valuable guide for engineers and physicists faced with two-dimensional static and quasistatic problems.

Published by Pergamon Press the book has the usual high standard of Pergamon publications.

J. ANTAL

Printed in Hungary

The *Acta Physica* publish papers on physics, in English, German, French and Russian. The *Acta Physica* appear in parts of varying size, making up volumes. Manuscripts should be addressed to:

Acta Physica, Budapest 502, Postafiók 24.

Correspondence with the editors and publishers should be sent to the same address.

The rate of subscription to the *Acta Physica* is 110 forints a volume. Orders may be placed with "Kultúra" Foreign Trade Company for Books and Newspapers (Budapest I., Fő u. 32. Account No. 43-790-057-181) or with representatives abroad.

Les *Acta Physica* paraissent en français, allemand, anglais et russe et publient des travaux du domaine de la physique.

Les *Acta Physica* sont publiés sous forme de fascicules qui seront réunis en volumes. On est prié d'envoyer les manuscrits destinés à la rédaction à l'adresse suivante:

Acta Physica, Budapest 502, Postafiók 24.

Toute correspondance doit être envoyée à cette même adresse.

Le prix de l'abonnement est de 110 forints par volume.

On peut s'abonner à l'Entreprise du Commerce Extérieur de Livres et Journaux «Kultúra» (Budapest I., Fő u. 32. — Compte-courant No. 43-790-057-181) ou à l'étranger chez tous les représentants ou dépositaires.

«*Acta Physica*» публикуют трактаты из области физических наук на русском, немецком, английском и французском языках.

«*Acta Physica*» выходят отдельными выпусками разного объема. Несколько выпусков составляют один том.

Предназначенные для публикации рукописи следует направлять по адресу:

Acta Physica, Budapest 502, Postafiók 24.

По этому же адресу направлять всякую корреспонденцию для редакции и администрации.

Подписная цена «*Acta Physica*» — 110 форинтов за том. Заказы принимает предприятие по внешней торговле книг и газет «Kultúra» (Budapest I., Fő u. 32. Текущий счет: № 43-790-057-181) или его заграничные представительства и уполномоченные.

INDEX

<i>J. Bitó: On the Anodic Side Oscillations of Low Pressure DC Gas Discharges.</i> — Й. Бито:	1
Об анодных колебаниях газовых разрядов постоянного тока низкого давления	
<i>Elisabeth Kovács-Csetényi: Electrical Resistivity Change in Cold-Worked Tungsten Wires During Recovery and Recrystallization.</i> — Е. Ковач-Четени:	11
Изменение сопротивления вольфрамовых проволок, разработанных в холодном состоянии, в сопропроцессах обновления и рекристаллизации.	
<i>S. Datta Majumdar: Wave Equations in Momentum Space.</i> — Ш. Датта Маюмдар:	19
Волновые уравнения в пространстве импульсов	
<i>G. Lakatos and J. Bitó: Some Parameters of the Moving Striations.</i> — Дь. Лакатош	27
и Й. Бито: О некоторых параметрах подвижного слоеобразования	
<i>A. Kónya: Quantum Numbers and Energy Levels in the Thomas-Fermi Atom.</i> —	39
А. Конья: Квантовые числа и энергетические уровни в атоме Томаса—Ферми	
<i>Maria Farkas-Jahnke: Graphical Method for the Construction of the Patterson Function of One-Dimensional Structure Models.</i> — М. Фаркаш-Янке:	55
Графический метод для определения функции Паттерсона одномерной структурой модели	
<i>G. Bozóki, E. Fenyves, Éva Gombosi and E. Nagy: Inelastic Two-Prong π^--p Interactions at 17,2 GeV in Emulsion.</i> — Г. Бозоки, Э. Феньвеш, Э. Гомбоши и Э. Надь:	61
Двухлучевые неупругие взаимодействия в эмульсии при энергии 17,2 Гев...	

COMMUNICACIONES BREVES

<i>T. Vertse and D. Berényi: Transmission Curve of the S³⁵ Continuous Beta-Radiation in Air</i>	67
<i>G. Pócsik: Restrictions on the Vertex Functions</i>	73
<i>G. Marx and J. Németh: Pressure in a Relativistically Degenerated Fermion Gas with Scalar Interaction</i>	77

RECENSIONES

<i>L. Bozóky: G. Hertz, Lehrbuch der Kernphysik, Band III.</i>	83
<i>I. Abonyi: R. Jancel—Th. Kahan, Électrodynamique des Plasmas</i>	84
<i>J. Antal: K. J. Binns and P. J. Lawrenson, Analysis and Computation of Electric and Magnetic Field Problems</i>	84

Acta Phys. Hung. Tom. XVIII. Fasc. 1. Budapest 30. XII. 1964

ACTA PHYSICA

ACADEMIAE SCIENTIARUM HUNGARICAE

ADIUVANTIBUS

Z. GYULAI, L. JÁNOSSY, I. KOVÁCS, K. NOVOBÁTZKY

REDIGIT

P. GOMBÁS

TOMUS XVIII

FASCICULUS 2



AKADÉMIAI KIADÓ, BUDAPEST

1965

ACTA PHYS. HUNG.

ACTA PHYSICA

A MAGYAR TUDOMÁNYOS AKADÉMIA FIZIKAI KÖZLEMÉNYEI

SZERKESZTŐSÉG ÉS KIADÓHIVATAL: BUDAPEST V., ALKOTMÁNY UTCA 21.

Az *Acta Physica* német, angol, francia és orosz nyelven közöl értekezéseket a fizika tárgyköréből.

Az *Acta Physica* változó terjedelmű füzetekben jelenik meg: több füzet alkot egy kötetet. A közlésre szánt kéziratok a következő címre küldendők:

Acta Physica, Budapest 502, Postafiók 24.

Ugyanerre a címre küldendő minden szerkesztőségi és kiadóhivatali levelezés.

Az *Acta Physica* előfizetési ára kötetenként belföldre 80 forint, külföldre 110 forint.

Megrendelhető a belföld számára az Akadémiai Kiadónál (Budapest V., Alkotmány utca 21. Bankszámla 05-915-111-46), a külföld számára pedig a „Kultúra” Könyv- és Hírlap Külkereskedelmi Vállalatnál (Budapest I., Fő u. 32. Bankszámla 43-790-057-181 sz.), vagy annak külföldi képviseleteinél és bizományosainál.

Die *Acta Physica* veröffentlichen Abhandlungen aus dem Bereich der Physik in deutscher, englischer, französischer und russischer Sprache.

Die *Acta Physica* erscheinen in Heften wechselnden Umfangs. Mehrere Hefte bilden einen Band.

Die zur Veröffentlichung bestimmten Manuskripte sind an folgende Adresse zu richten:

Acta Physica, Budapest 502, Postafiók 24.

An die gleiche Anschrift ist auch jede für die Redaktion und den Verlag bestimmte Korrespondenz zu senden.

Abonnementspreis pro Band: 110 Forint. Bestellbar bei dem Buch- und Zeitungs-Aussenhandels-Unternehmen »Kultúra« (Budapest I., Fő u. 32. Bankkonto Nr. 43-790-057-181) oder bei seinen Auslandsvertretungen und Kommissionären.

PERIODIC FOCUSING OF DENSE ELECTRON BEAMS WITH THIN LENSES

By

M. SZILÁGYI

RESEARCH INSTITUTE FOR TECHNICAL PHYSICS OF THE HUNGARIAN ACADEMY OF SCIENCES, BUDAPEST

(Presented by G. Szigeti. — Received 23. I. 1964)

In the first part of this paper the stability of an axially symmetric dense electron beam, focused by means of a periodic series of thin lenses is considered. The results here obtained are different from those given by J. R. PIERCE [1].

In the second part an investigation of the periodic focusing of a sheet electron beam by means of thin cylindrical lenses is given. The required value of the focal length of the lenses is determined. It is found that this kind of focusing is stable.

Introduction

Periodic focusing is a successful method for focusing dense electron beams. The main point of this method is the compensation of the space charge divergent effect of the beam by an alignment of identical lenses. The case when the focal length of the lenses (f) is far greater than the practically noticeable extension of their fields in the direction of the axis has been considered. Such lenses are called thin. Further we suppose that the space l between two neighbouring lenses is also far greater than the extension of the fields.

The first part of the paper is concerned with the stability of an axially symmetric dense electron beam, focused by means of a series of identical converging thin electron lenses i. e. with the change of the geometry of the beam when the initial conditions undergo small variations, taking into account the diverging effect of the space charge.

This problem was discussed primarily by J. R. PIERCE [1]. In the course of our investigation results quite different from those given by J. R. PIERCE have been obtained. We have drawn his attention to this discrepancy. On the initiation of PIERCE W. W. RIGROD repeated the calculation and obtained results agreeing with those given here [2].

In the second part the periodic focusing of sheet dense electron beams by means of a series of thin cylindrical lenses is dealt with. This problem is not treated in the literature. We give a simple expression for the required value of the focal length of the lenses. It is found that this kind of focusing of dense sheet beams is stable in all cases.

Both problems may be applied to electrostatic, magnetic and complementary thin lenses.

1. The stability of an axially symmetric electron beam focused by means of a series of thin lenses

Let us place a series of identical thin electron lenses, with a focal length f , periodically at an equal distance l from each other (Fig. 1). A laminar parallel electron beam arrives into the system, parallel to the z -axis. The beam radius is r_0 . The edge trajectory of the beam will be examined later. In the thin lens approximation it can be assumed that the beam motion in the section between any two lenses is determined only by space charge and the lenses change suddenly the slopes of the beam trajectories with respect to the z -axis. The slope $\frac{dr}{dz} = r'_0$ thus formed immediately after the lens, gives the value of the initial slope for the motion in the following section.

Parameters l and f characterizing the system may be chosen so that the configuration of the beam would be identical in all sections and symmetrical within the sections with respect to the centre of the section. These requirements are realized if the condition

$$\frac{r_0}{f} = -2r'_0 \quad (1)$$

is satisfied, where the value of r'_0 is determined by the length l , beam radius r_0 and beam perveance $P = \frac{I}{U_0^{3/2}}$, in the way given in [1], simultaneously satisfying the condition

$$l = 2z_{\min}.$$

(Here z_{\min} is the coordinate of the minimum beam cross-section, I the beam current in ampères and U_0 the accelerating potential in volts.) Evidently $r'_0 < 0$.

It should be mentioned that expression (1) is not concerned with the first lens placed in the plane $z = 0$. The convergence $\frac{1}{f_1}$ of this lens should be the half of the convergence $\frac{1}{f}$ of all the other lenses because this lens changes the slope of the edge path from zero to r'_0 .

Let us now pass to the question of *stability*. From a practical point of view this is a question of decisive importance because it is impossible to ensure a total identity and steadiness of the initial conditions. So unstable focusing is not practicable.

Suppose that in an arbitrary point z the deviations of the beam radius and slope from the ideal values r and r' given in Fig. 1 are δr and $\delta r'$ because

instead of r_0 and r'_0 the initial values are $r_0 + \delta r_0$ and $r'_0 + \delta r'_0$. (The primes represent derivation with respect to z). Then we can write

$$\delta r = \frac{\partial r}{\partial r_0} \delta r_0 + \frac{\partial r}{\partial r'_0} \delta r'_0 \quad (2)$$

and

$$\delta r' = \frac{\partial r'}{\partial r_0} \delta r_0 + \frac{\partial r'}{\partial r'_0} \delta r'_0. \quad (3)$$

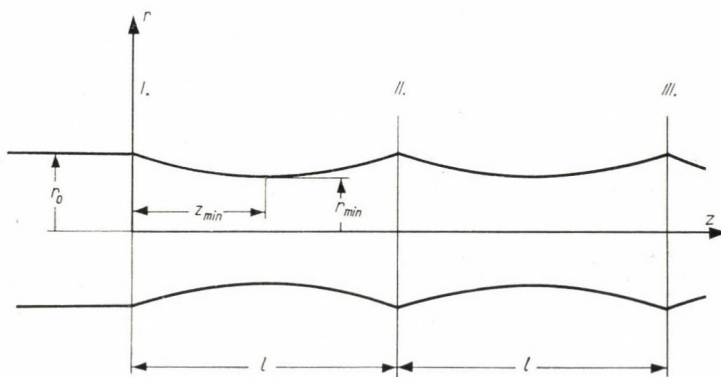


Fig. 1

The partial derivatives indicate the degree of deviation of the values r and r' , corresponding to an arbitrary point z , which originates in the variation of the initial values r_0 and r'_0 .

Let us consider the section between the n -th and $(n+1)$ -th lenses and rewrite expressions (2) and (3) for the point immediately after the $(n+1)$ -th lens. In this case the initial condition corresponds to the beginning of the section; thus $r_0 = r_n$ and $r'_0 = r'_n$. We obtain

$$\delta r_{n+1} = \left. \frac{\partial r}{\partial r_0} \right|_{n+1} \delta r_n + \left. \frac{\partial r}{\partial r'_0} \right|_{n+1} \delta r'_n \quad (4)$$

and

$$\delta r'_{n+1} = \left. \frac{\partial r'}{\partial r_0} \right|_{n+1} \delta r_n + \left. \frac{\partial r'}{\partial r'_0} \right|_{n+1} \delta r'_n - \frac{1}{f} \delta r_{n+1}. \quad (5)$$

Here the last term appears because the $(n+1)$ -th lens affects the deviation of the beam slope already at the point immediately after the lens.

Our task is now the determination of the partial derivatives. For this the expressions of the beam motion determined by space charge given in [1]

will be used. It is convenient to write these expressions in the following way:

$$\int_{\frac{r_0}{174\sqrt{P}}}^{\frac{r'}{174\sqrt{P}}} e^{u^2} du = \frac{174\sqrt{P}}{2r_0} z e^{\left(\frac{r'_0}{174\sqrt{P}}\right)^2} \quad (6)$$

and

$$\frac{r'}{174\sqrt{P}} = \pm \sqrt{\ln \frac{r}{r_0} + \left(\frac{r'_0}{174\sqrt{P}}\right)^2}. \quad (7)$$

If we consider the convergent part of the beam the negative sign should be chosen before the root, and the positive sign if the divergent part of the beam is considered.

Let us differentiate both sides of equation (6) with respect to r_0 and r'_0 . We have

$$\frac{\partial r'}{\partial r_0} \frac{1}{174\sqrt{P}} e^{\left(\frac{r'}{174\sqrt{P}}\right)^2} = -\frac{174\sqrt{P}z}{2r_0^2} e^{\left(\frac{r'_0}{174\sqrt{P}}\right)^2} \quad (8)$$

and

$$\frac{\partial r'}{\partial r'_0} \frac{1}{174\sqrt{P}} e^{\left(\frac{r'}{174\sqrt{P}}\right)^2} - \frac{1}{174\sqrt{P}} e^{\left(\frac{r'}{174\sqrt{P}}\right)^2} = \frac{174\sqrt{P}z}{2r_0} \cdot \frac{2r'_0}{(174\sqrt{P})^2} e^{\left(\frac{r'_0}{174\sqrt{P}}\right)^2}. \quad (9)$$

Let us now differentiate both sides of equation (7) with respect to the same parameters. We obtain:

$$\frac{\partial r'}{\partial r_0} \frac{1}{174\sqrt{P}} = \frac{\frac{1}{r} \frac{\partial r}{\partial r_0} - \frac{1}{r_0}}{\frac{2r'}{174\sqrt{P}}} \quad (10)$$

and

$$\frac{\partial r'}{\partial r'_0} \frac{1}{174\sqrt{P}} = \frac{\frac{1}{r} \frac{\partial r}{\partial r'_0} + \frac{2r'_0}{(174\sqrt{P})^2}}{\frac{2r'}{174\sqrt{P}}}. \quad (11)$$

The form of the expressions (8)–(11) does not depend on the fact whether the convergent or the divergent part of the beam is investigated.

In the case of the section considered we have $r_0 = r_n$ and $r'_0 = r'_n$. At the final point of the section $z = l$. In an ideal case we have: $r_n = r_{n+1}$ and $r'_n = r'_{n+1}$. So we have

$$r_0 = r_n = r_{n+1} \quad \text{and} \quad r'_0 = r'_n = r'_{n+1}. \quad (12)$$

Thus from expressions (8)–(11) the derivatives are

$$\left. \frac{\partial r}{\partial r_0} \right|_{n+1} = 1 - \frac{l r'_0}{r_0}, \quad (13)$$

$$\left. \frac{\partial r}{\partial r'_0} \right|_{n+1} = \frac{2 l r'^2_0}{(174 \sqrt{P})^2}, \quad (14)$$

$$\left. \frac{\partial r'}{\partial r_0} \right|_{n+1} = - \frac{(174 \sqrt{P})^2 l}{2 r_0^2}, \quad (15)$$

$$\left. \frac{\partial r'}{\partial r'_0} \right|_{n+1} = 1 + \frac{l r'_0}{r_0}. \quad (16)$$

From (4) we have

$$\delta r'_n = \frac{1}{\left. \frac{\partial r}{\partial r_0} \right|_{n+1}} \left[\delta r_{n+1} - \left. \frac{\partial r}{\partial r_0} \right|_{n+1} \delta r_n \right] \quad (17)$$

and

$$\delta r'_{n+1} = \frac{1}{\left. \frac{\partial r}{\partial r'_0} \right|_{n+2}} \left[\delta r_{n+2} - \left. \frac{\partial r}{\partial r_0} \right|_{n+2} \delta r_{n+1} \right]. \quad (18)$$

According to (13)–(16), the partial derivatives depend only on r_0 and r'_0 . Besides, for any values of k we have $r_0 = r_k$ and $r'_0 = r'_k$.

Therefore we may omit the indices. The fact should, however, be mentioned that these derivatives are concerned with the immediate beginning of the section. Substituting (17) and (18) into (5) we obtain

$$\begin{aligned} & \frac{1}{\left. \frac{\partial r}{\partial r_0} \right|} \left(\delta r_{n+2} - \left. \frac{\partial r}{\partial r_0} \right| \delta r_{n+1} \right) - \frac{\partial r'}{\partial r_0} \delta r_n - \\ & - \frac{\partial r'}{\left. \frac{\partial r}{\partial r'_0} \right|} \left(\delta r_{n+1} - \left. \frac{\partial r}{\partial r_0} \right| \delta r_n \right) + \frac{\delta r_{n+1}}{f} = 0. \end{aligned}$$

Reducing the equation we have

$$\begin{aligned} \delta r_{n+2} - & \left[\frac{\partial r}{\partial r_0} + \frac{\partial r'}{\partial r'_0} - \frac{1}{f} \frac{\partial r}{\partial r'_0} \right] \delta r_{n+1} + \\ & + \left[\frac{\partial r}{\partial r_0} \frac{\partial r'}{\partial r'_0} - \frac{\partial r'}{\partial r_0} \frac{\partial r}{\partial r'_0} \right] \delta r_n = 0 \end{aligned} \quad (19)$$

Let us now substitute the values of the derivatives from (13)–(16) and the value of $\frac{1}{f}$ from (1) into (19). The coefficient of δr_n is

$$\frac{\partial r}{\partial r_0} \frac{\partial r'}{\partial r'_0} - \frac{\partial r'}{\partial r_0} \frac{\partial r}{\partial r'_0} = \left(1 + \frac{lr'_0}{r_0}\right) \left(1 - \frac{lr'_0}{r_0}\right) + \frac{l^2 r'^2_0}{r_0^2} = 1.$$

The coefficient of δr_{n+1} is

$$\begin{aligned} \frac{\partial r}{\partial r_0} + \frac{\partial r'}{\partial r'_0} - \frac{1}{f} \frac{\partial r}{\partial r'_0} = & 1 - \frac{lr'_0}{r_0} + 1 + \frac{lr'_0}{r_0} + \\ & + \frac{2r'_0}{r_0} \cdot \frac{2lr'^2_0}{(174\sqrt{P})^2} = 2 \left[1 + \frac{2lr'^3_0}{(174\sqrt{P})^2 r_0}\right]. \end{aligned}$$

Therefore equation (19) may be written in the following way:

$$\delta r_{n+2} - 2M\delta r_{n+1} + \delta r_n = 0, \quad (20)$$

where

$$M = 1 + \frac{2lr'^3_0}{(174\sqrt{P})^2 r_0}. \quad (21)$$

The solution of equation (20) is [1]:

$$a) \quad \delta r_n = \text{const.} \cos [n \arccos M], \quad \text{if } |M| \leq 1, \quad (22)$$

$$b) \quad \delta r_n = \text{const.} \operatorname{ch} [n \operatorname{arc ch} |M|] \cos \gamma \pi n, \quad \text{if } |M| \geq 1, \quad (23)$$

where

$$\gamma = \begin{cases} 1, & \text{if } M \leq -1, \\ 0, & \text{if } M \geq 1. \end{cases}$$

The value of δr_n must not increase arbitrarily in the section between the n -th and $(n+1)$ -th lenses if the focusing is to be stable. Therefore expression (22) refers to the stable and expression (23) to the unstable focusing. Thus in the stable region of focusing the following condition must be satisfied:

$$|M| \leq 1. \quad (24)$$

Let us introduce the dimensionless variables

$$Z = 174 \sqrt{P} \frac{z}{r_0} \quad (25)$$

and

$$R = \frac{r}{r_0}. \quad (26)$$

Then

$$R'_0 = \frac{dR}{dZ} \Big|_{Z=0} = \frac{1}{174 \sqrt{P}} \frac{dr}{dz} \Big|_{z=0} = \frac{r'_0}{174 \sqrt{P}} \quad (27)$$

and

$$L = 174 \sqrt{P} \frac{l}{r_0}. \quad (28)$$

Expression (21) can be written in a dimensionless form by means of (27) and (28):

$$M = 1 + 2 R'_0 L. \quad (29)$$

If the value of L is given we know the value of R'_0 . To each value of L belong two values of R'_0 . These values may be read from Fig. 11.8 in [1], consequently to each value of L belong two values of M : the larger M belongs to the smaller $-R'_0$ and the smaller M belongs to the larger $-R'_0$.

The parameter M versus L is plotted in Fig. 2. We can see (the hatched section) that the stability condition (24) is satisfied for

$$0 \leq L \leq 2,116, \quad (30)$$

namely at the smaller values of $-R'_0$. Focusing is stable only for

$$0 \leq -R'_0 \leq 0,78. \quad (31)$$

Focusing is unstable along the whole lower portion of the curve. (This lower portion is given in the Figure only in part. If we increase the value of $-R'_0$ further, the value of M decreases rapidly and in the case $-R'_0 \rightarrow \infty$ we have $M \rightarrow -\infty$).

As already mentioned these results are quite different from those given in [1]. The form of the curve $M = M(L)$ differs very much from PIERCE's curve. He has found two stable sections: for the first section $0 < L < 2,04$, $0 < -R'_0 < 0,70$, and for the second $1,71 < L < 2,16$, $0,92 < -R'_0 < 1,51$.

According to our investigations the second section does not exist, and the first one proved to be a little wider. As $(-R'_0 L)_{\max} = 2,57$, with the aid of (1), (27) and (28) it can be seen easily that

$$\left(\frac{l}{f}\right)_{\max} = 5,14 . \quad (32)$$

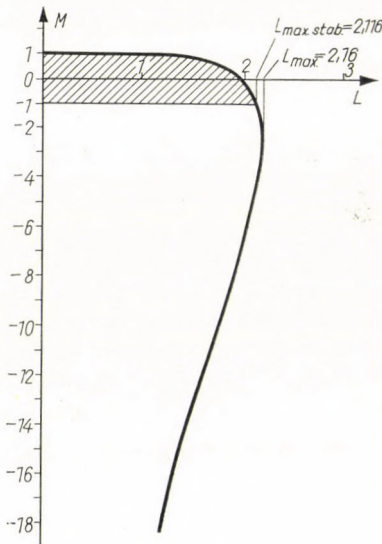


Fig. 2

According to Fig. 2 this value falls into the unstable region. In the stable region the maximum value of $(-R'_0 L)$ lies at the boundary of this region and its value is $(-R'_0 L)_{\max, \text{stab.}} = 1,65$.

Hence

$$\left(\frac{l}{f}\right)_{\max, \text{stab.}} = 3,30 . \quad (33)$$

Expression (33) determines the maximum applicable value of the lens convergence. That is a new result also, because in [1] the value $\left(\frac{l}{f}\right)_{\max} = 5,14$ fell into the boundary of the stable region. So we see that the value of $\left(\frac{l}{f}\right)_{\max, \text{stab.}}$ is smaller in the case when space charge is taken into account than in the absence of space charge when $\left(\frac{l}{f}\right)_{\max, \text{stab.}} = 4$ [1]. However, no special conclusion can be drawn from this fact, since in [1], in the absence of space charge, effects due to the deviation of the initial conditions were not studied.

2. Focusing of a sheet electron beam with a series of thin cylindrical lenses

Let us now consider the case of focusing a dense sheet beam. If the beam length is far greater than the other dimensions and the beam width W is far greater than the beam thickness $2y$, it may be assumed that space charge forces are acting only in the direction of the y coordinate. In this case we may apply the same approximation as in the case of an axially symmetrical beam. Evidently in this case thin cylindrical lenses must be put at a distance l from each other. The lenses may be electrostatic, magnetic or their combinations (but they all must have the same convergence $\frac{1}{f}$). If we replace l the coordinate r by y in Fig. 1 this Figure will be applicable for the case of sheet beams also because in the given approximation the beam width W in the direction of the x -coordinate (perpendicularly to the plane of the Figure) can be assumed to remain constant.

In order to keep the beam configuration identical in all sections and symmetrical within the sections with respect to the centre of the section the following condition must be satisfied:

$$\frac{y_0}{f} = -2y'_0, \quad (34)$$

where the value of y'_0 is determined by the requirement

$$l = 2z_m. \quad (35)$$

Here y_0 is the initial half-width of the beam, y'_0 the initial value of the slope of the edge path, f the focal length of the cylindrical lenses and z_m the coordinate of the minimum beam cross section.

Let us introduce the dimensionless new variables

$$Y = \frac{y}{y_0} \quad (36)$$

and

$$Z_s = 154 \sqrt{\frac{P}{W y_0}} z = \frac{z}{k y_0}. \quad (37)$$

Then the beam configuration determined only by space charge is given by the following equation [3]:

$$Y = Z_s^2 + Y'_0 Z_s + 1, \quad (38)$$

where

$$Y' = \frac{dY}{dZ_s} = \frac{1}{154} \sqrt{\frac{W}{Py_0}} \frac{dy}{dz} = ky'. \quad (39)$$

The value of the constant k , appearing in expressions (37) and (39), is

$$k = \frac{1}{154} \sqrt{\frac{W}{Py_0}}. \quad (40)$$

According to (38) the form of the beam boundary is parabolic. We know from the expression

$$Y' = 2Z_s + Y'_0 = 0 \quad (41)$$

that the apex of the parabola corresponds to the coordinate

$$Z_{sm} = -\frac{Y'_0}{2}. \quad (42)$$

This coordinate gives the location of the minimum beam cross-section. Thus we can rewrite (35) with the new variables in the form

$$L_s = 2Z_{sm} = -Y'_0, \quad (43)$$

where

$$L_s = Z_s(l) = \frac{l}{ky_0}. \quad (44)$$

From (39), (43) and (44) we have

$$\frac{l}{y_0} = -k^2 y'_0. \quad (45)$$

Now an exact expression can be obtained for the condition (34):

$$\frac{1}{f} = \frac{2l}{k^2 y_0^2} = \frac{2L_s}{ky_0} = \frac{2L_s^2}{l} = 4,74 \cdot 10^4 \frac{Pl}{Wy_0}. \quad (46)$$

Expression (46) gives the value of the focal length f of the applied thin cylindrical lenses required for the periodic focusing of a sheet beam with a perveance P , width W , initial thickness $2y_0$ and lens period l . If the beam enters into the system parallel to the z -axis the relation

$$\frac{1}{f_1} = \frac{1}{2} \cdot \frac{1}{f} \quad (47)$$

will be evidently valid in this case also, where f_1 is the focal length of the first lens.

If the variations of the beam boundary should not to be too large, evidently the value of l must be decreased, i.e. more lenses must be applied. It can be easily seen that in case $Z_{sm} \geq 1$ the beam boundary crosses the z -axis. As this is not desirable we can assume the value $L_{s\max} = 2$ as the limit, from the point of view of practical application. This — according to (46) — gives the condition

$$\left| \frac{l}{f} \right|_{\max} = 8, \quad (48)$$

which determines the practically applicable maximum values of the convergence and the lens space. Obviously, it must also be taken into account that both the focal length and the lens space must be considerably larger than the extension of the lens fields (thin lens approximation).

Let us now consider the problem of *stability*. For this the variation of the beam configuration under the influence of small variations of the initial values of beam thickness y_0 and beam boundary slope y'_0 must be considered.

Suppose that at an arbitrary point z the variations of the values y and y' are δy and $\delta y'$, respectively, as a consequence of the fact that the initial values are $y_0 + \delta y_0$ and $y'_0 + \delta y'_0$ instead of y_0 and y'_0 . Thus immediately after the $(n+1)$ -th lens we can write similarly to (4) and (5):

$$\delta y_{n+1} = \frac{\partial y}{\partial y_0} \Big|_{n+1} \delta y_n + \frac{\partial y}{\partial y'_0} \Big|_{n+1} \delta y'_n \quad (49)$$

and

$$\delta y'_{n+1} = \frac{\partial y'}{\partial y_0} \Big|_{n+1} \delta y_n + \frac{\partial y'}{\partial y'_0} \Big|_{n+1} \delta y'_n - \frac{\delta y_{n+1}}{f}. \quad (50)$$

Let us now determine the partial derivatives. Equation (38) can be rewritten in the form

$$Z_s^2 + Y'_0 Z_s + (1 - Y) = 0. \quad (51)$$

Hence

$$Z_s = \frac{1}{2} [-Y'_0 \pm \sqrt{Y'^2_0 - 4(1 - Y)}]. \quad (52)$$

Using (36), (37) and (39) equation (52) may be written as

$$\frac{z}{ky_0} = \frac{1}{2} \left[-ky'_0 \pm \sqrt{k^2 y'^2_0 - 4 \left(1 - \frac{y}{y_0} \right)} \right]. \quad (53)$$

From (41) and (52) follows

$$Y' = ky' = \pm \sqrt{Y_0'^2 - 4(1 - Y)} = \pm \sqrt{k^2 y_0'^2 - 4 \left(1 - \frac{y}{y_0}\right)}. \quad (54)$$

The sign before the root should be negative or positive depending on whether the convergent part or the divergent part, respectively, of the beam is considered.

By means of (54) expression (53) may be written thus:

$$\frac{z}{ky_0} = \frac{k}{2} (y' - y_0'). \quad (55)$$

Now let us rewrite expressions (53) and (55) by using (40). We obtain the following two formulae:

$$y' - y_0' = 4,74 \cdot 10^4 \frac{P}{W} z \quad (56)$$

and

$$\pm \sqrt{y_0'^2 + 9,48 \cdot 10^4 \frac{P}{W} (y - y_0)} - y_0' = 4,74 \cdot 10^4 \frac{P}{W} z. \quad (57)$$

Differentiating (56) and (57) with respect to y_0 we obtain

$$\frac{\partial y'}{\partial y_0} = 0 \quad (58)$$

and

$$\frac{9,48 \cdot 10^4 \frac{P}{W} \left(\frac{\partial y}{\partial y_0} - 1 \right)}{2 y'} = 0. \quad (59)$$

Let us now differentiate with respect to y_0' . The results are

$$\frac{\partial y'}{\partial y_0'} - 1 = 0 \quad (60)$$

and

$$\frac{2 y_0' + 9,48 \cdot 10^4 \frac{P}{W} \frac{\partial y}{\partial y_0'}}{2 y'} - 1 = 0. \quad (61)$$

In the case of the considered section between the n -th and $(n+1)$ -th lenses we have $y_0 = y_n$ and $y_0' = y_n'$. At the final point of the section $y = l$.

As $y'_n = y'_{n+1}$ and $y_n = y_{n+1}$ have been required we may write $y_0 = y_n = y_{n+1}$ and $y'_0 = y'_n = y'_{n+1}$. Thus the values of the partial derivatives are, from (58)–(61) (the indices may be omitted for the reason explained in the axially symmetrical case), given by

$$\frac{\partial y}{\partial y_0} = \frac{\partial y'}{\partial y'_0} = 1 \quad (62)$$

and

$$\frac{\partial y'}{\partial y_0} = \frac{\partial y}{\partial y'_0} = 0. \quad (63)$$

Substituting (62) and (63) into (49), we shall immediately see

$$\delta y_{n+1} = \delta y_n = \text{const. } (n) = \delta y_0. \quad (64)$$

Thus — independently of the value of f — the variation of the beam thickness remains constant during focusing, i.e. focusing is stable in all cases. We come to the same conclusion if the demonstration given in the axially symmetrical case is performed. Then we obtain

$$\delta y_{n+2} - 2\delta y_{n+1} + \delta y_n = 0, \quad (65)$$

which completely agrees with (20), if $M = 1$. In this case it follows from both (22) and (23) that $\delta y_n = \text{const.}$

Thus the sheet beam focusing with a series of thin cylindrical lenses is always stable. Practically, expression (48) determines the maximum value of $\frac{l}{f}$.

REFERENCES

1. J. R. PIERCE, Theory and Design of Electron Beams, Chapter XI. Van Nostrand, New York, 1954.
2. W. W. RIGROD, private communication.
3. J. R. PIERCE, op. cit. Chapter IX.

ПЕРИОДИЧЕСКАЯ ФОКУСИРОВКА ИНТЕНСИВНЫХ ЭЛЕКТРОННЫХ ПУЧКОВ ТОНКИМИ ЛИНЗАМИ

М. СИЛАДИ

Резюме

В первой части работы исследована стабильность интенсивного аксиально-симметричного электронного пучка, фокусируемого периодической системой тонких линз. Получены результаты, отличные от данных Дж. Пирса [1].

Во второй части рассматривается периодическая фокусировка ленточного пучка электронов системой, состоящей из тонких цилиндрических линз. Определена необходимая величина оптической силы линз. Установлено, что такая фокусировка является стабильной.

THE INTENSITY DISTRIBUTION OF THE TRIPLET BANDS OF THE CO MOLECULE

By

I. KOVÁCS and R. TŐRÖS

DEPARTMENT OF ATOMIC PHYSICS, POLYTECHNICAL UNIVERSITY, BUDAPEST

(Received 31. III. 1964)

The formulae for the intensity distribution of the $^3A - ^3\Pi$ transition are elaborated for the case when both terms taking part in the transition belong to HUND's intermediate case. The observed intensity values of the $d^3A - a^3\Pi$ transition of the CO molecule are compared with those calculated from the intensity formula derived. The good agreement confirms the assumption that the upper state of the mentioned transition is indeed a 3A state.

1. Introduction

The "triplet" bands of the CO molecule were first photographed under high resolution by GERŐ [1] who made a fine-structure analysis of several of the bands. According to GERŐ's findings the triplet bands arise from a $d^3\Pi - a^3\Pi$ transition, where both $^3\Pi$ terms belong to the intermediate case between HUND's cases *a*) and *b*). Recently, CARROLL [2] again photographed the 3—0 band under high resolution and carried out its rotational analysis. By means of a semi-quantitative method he also determined the intensity distribution within the band. Like MULLIKEN [3] CARROLL came to the conclusion that the upper state previously assumed to be $^3\Pi$ is, in all probability, an inverted 3A state, and it was in order to prove this that he measured the intensity distribution of the branches as well. The final decision as to the term state of the upper state can be reached — according to CARROLL — only by a comparison of the measured intensity distribution with that obtained by the theory.

The aim of the present paper is to derive such formulae for the intensity distribution of the $^3A - ^3\Pi$ transition when both states belong to HUND's intermediate case, and then to compare the theoretical results with CARROLL's measurements.

2. Intensity distribution

One of the reasons CARROLL gave for the upper state being 3A is that while for a $^3\Pi \rightarrow ^3\Pi$ transition the *Q* branch in the $^3\Pi_0 \rightarrow ^3\Pi_0$ component should be missing and in the $^3\Pi_1 \rightarrow ^3\Pi_1$ and $^3\Pi_2 \rightarrow ^3\Pi_2$ components it should

Table

Branches		<i>i</i> -factors
${}^3A - {}^3II$	${}^3II - {}^3A$	${}^3A_{\text{int}} - {}^3II_{\text{int}}$
$P_1(J)$	$R_1(J-1)$	$\frac{(J-2)(J-1)}{8JC'_1(J-1)C''_1(J)} \{(J-3)(J+2)u'_1 - (J-1)u''_1 - (J) + J(J+1)u'_1 + (J-1)u''_1 + (J) + 4(J-3)(J-1)(J+1)^2\}$
$Q_1(J)$	$Q_1(J)$	$\frac{(J-1)(J+2)(2J+1)}{8J(J+1)C'_1(J)C''_1(J)} \{(J-2)(J+3)u'_1 - (J)u''_1 - (J) + J(J+1)u'_1 + (J)u''_1 + (J) + 4(J-2)(J-1)(J+1)(J+2)\}$
$R_1(J)$	$P_1(J+1)$	$\frac{(J+2)(J+3)}{8(J+1)C'_1(J+1)C''_1(J)} \{(J-1)(J+4)u'_1 - (J+1)u''_1 - (J) + J(J+1)u'_1 + (J+1)u''_1 + (J) + 4(J-1)^2(J+1)(J+3)\}$
${}^Q P_{21}(J)$	${}^Q R_{12}(J-1)$	$\frac{(J-2)(J-1)}{8JC'_2(J-1)C''_1(J)} \{(J-3)(J+2)u''_1 - (J) - J(J+1)u''_1 + (J) + 4(J-1)(J+1)(Y'-2)\}$
${}^R Q_{21}(J)$	${}^P Q_{12}(J)$	$\frac{(J-1)(J+2)(2J+1)}{8J(J+1)C'_2(J)C''_1(J)} \{(J-2)(J+3)u''_1 - (J) - J(J+1)u''_1 + (J) + 4(J-1)(J+1)(Y'-2)\}$
${}^S R_{21}(J)$	${}^O P_{12}(J+1)$	$\frac{(J+2)(J+3)}{8(J+1)C'_2(J+1)C''_1(J)} \{(J-1)(J+4)u''_1 - (J) - J(J+1)u''_1 + (J) + 4(J-1)(J+1)(Y'-2)\}$
${}^R P_{31}(J)$	${}^P R_{13}(J-1)$	$\frac{(J-2)(J-1)}{8JC'_3(J-1)C''_1(J)} \{(J-3)(J+2)u'_3 + (J-1)u''_1 - (J) + J(J+1)u'_3 - (J-1)u''_1 + (J) - 4(J-2)(J-1)(J+1)(J+2)\}$
${}^S Q_{31}(J)$	${}^O Q_{13}(J)$	$\frac{(J-1)(J+2)(2J+1)}{8J(J+1)C'_3(J)C''_1(J)} \{(J-2)(J+3)u'_3 + (J)u''_1 - (J) + J(J+1)u'_3 - (J)u''_1 + (J) - 4(J-1)^2(J+1)(J+3)\}$
${}^T R_{31}(J)$	${}^N P_{13}(J+1)$	$\frac{(J+2)(J+3)}{8(J+1)C'_3(J+1)C''_1(J)} \{(J-1)(J+4)u'_3 + (J+1)u''_1 - (J) + J(J+1)u'_3 - (J+1)u''_1 + (J) - 4(J-1)J(J+1)(J+4)\}$
${}^O P_{12}(J)$	${}^S R_{21}(J-1)$	$\frac{(J-2)(J-1)}{JC'_1(J-1)C''_2(J)} \{(J-3)(J+2)u'_1 - (J-1) - J(J+1)u'_1 + (J-1) + (J-3)(J+1)(Y''-2)\}$
${}^P Q_{12}(J)$	${}^R Q_{21}(J)$	$\frac{(J-1)(J+2)(2J+1)}{J(J+1)C'_1(J)C''_2(J)} \{(J-2)(J+3)u'_1 - (J) - J(J+1)u'_1 + (J) + (J-2)(J+2)(Y''-2)\}$
${}^Q R_{12}(J)$	${}^Q P_{21}(J+1)$	$\frac{(J+2)(J+3)}{(J+1)C'_1(J+1)C''_2(J)} \{(J-1)(J+4)u'_1 - (J+1) - J(J+1)u'_1 + (J+1) + (J-1)(J+3)(Y''-2)\}$
$P_2(J)$	$R_2(J-1)$	$\frac{(J-2)(J-1)}{JC'_2(J-1)C''_2(J)} \{(J-3)(J+2) + J(J+1) + (Y'-2)(Y''-2)\}$

$Q_2(J)$	$Q_2(J)$	$\frac{(J-1)(J+2)(2J+1)}{J(J+1)C'_2(J)C''_2(J)}$ $\{(J-2)(J+3)+J(J+1)+(Y'-2)(Y''-2)\}^2$
$R_2(J)$	$P_2(J+1)$	$\frac{(J+2)(J+3)}{(J+1)C'_2(J+1)C''_2(J)}$ $\{(J-1)(J+4)+J(J+1)+(Y'-2)(Y''-2)\}^2$
${}^Q P_{32}(J)$	${}^Q R_{23}(J-1)$	$\frac{(J-2)(J-1)}{JC'_3(J-1)C''_2(J)}$ $\{(J-3)(J+2)u'_3+(J-1)-J(J+1)u'_3-(J-1)-(J-2)(J+2)(Y''-2)\}^2$
${}^R Q_{32}(J)$	${}^P Q_{23}(J)$	$\frac{(J-1)(J+2)(2J+1)}{J(J+1)C'_3(J)C''_2(J)}$ $\{(J-2)(J+3)u'_3+(J)-J(J+1)u'_3-(J)-(J-1)(J+3)(Y''-2)\}^2$
${}^S R_{32}(J)$	${}^O P_{23}(J+1)$	$\frac{(J+2)(J+3)}{(J+1)C'_3(J+1)C''_2(J)}$ $\{(J-1)(J+4)u'_3+(J+1)-J(J+1)u'_3-(J+1)-J(J+4)(Y''-2)\}^2$
${}^N P_{13}(J)$	${}^T R_{31}(J-1)$	$\frac{(J-2)(J-1)}{8JC'_1(J-1)C''_3(J)}$ $\{(J-3)(J+2)u'_1-(J-1)u''_3+(J)+J(J+1)u'_1+(J-1)u''_2-(J)-4(J-3)J(J+1)(J+2)\}^2$
${}^O Q_{13}(J)$	${}^S Q_{31}(J)$	$\frac{(J-1)(J+2)(2J+1)}{8J(J+1)C'_1(J)C''_3(J)}$ $\{(J-2)(J+3)u'_1-(J)u''_3+(J)+J(J+1)u'_1+(J)u''_3-(J)-4(J-2)J(J+2)^2\}^2$
${}^P R_{13}(J)$	${}^R P_{31}(J+1)$	$\frac{(J+2)(J+3)}{8(J+1)C'_1(J+1)C''_3(J)}$ $\{(J-1)(J+4)u'_1-(J+1)u''_3+(J)+J(J+1)u'_1+(J+1)u''_3-(J)-4(J-1)J(J+2)(J+3)\}^2$
${}^O P_{23}(J)$	${}^S R_{32}(J-1)$	$\frac{(J-2)(J-1)}{8JC'_2(J-1)C''_3(J)}$ $\{(J-3)(J+2)u''_3+(J)-J(J+1)u''_3-(J)-4J(J+2)(Y''-2)\}^2$
${}^P Q_{23}(J)$	${}^R Q_{32}(J)$	$\frac{(J-1)(J+2)(2J+1)}{8J(J+1)C'_2(J)C''_3(J)}$ $\{(J-2)(J+3)u''_3+(J)-J(J+1)u''_3-(J)-4J(J+2)(Y''-2)\}^2$
${}^Q R_{23}(J)$	${}^Q P_{32}(J+1)$	$\frac{(J+2)(J+3)}{8(J+1)C'_1(J+1)C''_3(J)}$ $\{(J-1)(J+4)u''_3+(J)-J(J+1)u''_3-(J)-4J(J+2)(Y''-2)\}^2$
$P_3(J)$	$R_3(J-1)$	$\frac{(J-2)(J-1)}{8JC'_3(J-1)C''_3(J)}$ $\{(J-3)(J+2)u'_3+(J-1)u''_3+(J)+J(J+1)u'_3-(J-1)u''_3-(J)+4(J-2)J(J+2)^2\}^2$
$Q_3(J)$	$Q_3(J)$	$\frac{(J-1)(J+2)(2J+1)}{8J(J+1)C'_3(J)C''_3(J)}$ $\{(J-2)(J+3)u'_3+(J)u''_3+(J)+J(J+1)u'_3-(J)u''_3-(J)+4(J-1)J(J+2)(J+3)\}^2$
$R_3(J)$	$P_3(J+1)$	$\frac{(J+2)(J+3)}{8(J+1)C'_3(J+1)C''_3(J)}$ $\{(J-1)(J+4)u'_3+(J+1)u''_3+(J)+J(J+1)u'_3-(J+1)u''_3-(J)+4J^2(J+2)(J+4)\}^2$

be very weak, in the present case, in general, it is just the Q branches that are the strongest among all the branches in all subbands. Recently one of the authors (I. K.) elaborated the formulae for the intensity distribution of the $^3A - ^3\Pi$ transition for all such cases where both states belong to HUND's case *a*) or *b*), as well as when one of them belongs to the intermediate case [4]. The case when both states belong simultaneously to the intermediate case was not dealt with. CARROLL's paper became accessible to the author only in the course of proofreading of [4]. It is, however, evident already from that paper that in the case of a $^3A - ^3\Pi$ transition the Q branches are actually much stronger than the corresponding P and R branches, in contrast to the $^3\Pi - ^3\Pi$ transition. This supports CARROLL's assumption. One might assume that further evidence may be provided by the comparison between the experimental and theoretical results already obtained. Since in the upper state $Y' = -12,92 \text{ cm}^{-1}$ and in the lower $Y'' = 24,7 \text{ cm}^{-1}$, it seems possible that among the elaborated cases the intensity formulae of the $^3A(\text{int}) \rightarrow ^3\Pi(a)$ transition (that is, where the 3A term belongs to HUND's intermediate case, and the $^3\Pi$ term to HUND's case *a*)) may be applied to the observed intensity values of the $d^3A_{\text{inv}} \rightarrow a^3\Pi_{\text{norm}}$ transition. Unfortunately the comparison shows that in the case of $J > 10$ HUND's case *a*) cannot be regarded as a good approximation even for the lower $a^3\Pi$ term, and further that for the quantitative comparison intensity distribution formulae are absolutely necessary where both 3A and $^3\Pi$ terms belong to HUND's intermediate case. These formulae, however, require complicated calculations for their application to all J which make the use of an electronic computer necessary. This was the reason why the author did not elaborate such formulae, since he assumed that the experimentally observed cases may be understood by means of some ordinary case already treated. Since, however, in the present case, this assumption was not justified, the intensity formulae, or to be more exact, the i -factors, corresponding to the $^3A(\text{int}) - ^3\Pi(\text{int})$ case, have been derived by means of the method described already in the paper mentioned [4]. The results are summarized in the Table. The denotations in the expressions given in the Table have the following meaning.

For a $^3A - ^3\Pi$ transition, if the 3A term is normal ($Y' = A_{3A}/B_{3A} > 0$)

$$\left. \begin{aligned} u_1'^{\pm}(J) &= [Y'(Y' - 4) + J^2]^{1/2} \pm (Y' - 2), \\ u_3'^{\pm}(J) &= [Y'(Y' - 4) + (J + 1)^2]^{1/2} \pm (Y' - 2), \\ C'_1(J) &= 2Y'(Y' - 4)(J - 1)(J + 2) + (2J - 1)(J - 1)J(J + 2), \\ C'_2(J) &= Y'(Y' - 4) + J(J + 1), \\ C'_3(J) &= 2Y'(Y' - 4)(J - 2)(J + 3) + (2J + 1)(J - 1)(J + 1)(J + 3), \end{aligned} \right\} \quad (1)$$

while for inverted 3A term ($Y' < 0$) the coefficient of $2Y'(Y' - 4)$ in $C'_1(J)$ is equal to $(J - 2)(J + 3)$ instead of $(J - 1)(J + 2)$; and in $C'_3(J)$ it is equal to $(J - 1)(J + 2)$ instead of $(J - 2)(J + 3)$.

For normal $^3\Pi$ state ($Y'' = A_{3\Pi}/B_{3\Pi} > 0$):

$$\left. \begin{aligned} u_3''^\pm(J) &= [Y''(Y'' - 4) + 4J^2]^{1/2} \pm (Y'' - 2), \\ u_3''^\pm(J) &= [Y''(Y'' - 4) + 4(J+1)^2]^{1/2} \pm (Y'' - 2), \\ C_1''(J) &= Y''(Y'' - 4)J(J+1) + 2(2J+1)(J-1)J(J+1), \\ C_2''(J) &= Y''(Y'' - 4) + 4J(J+1), \\ C_3''(J) &= Y''(Y'' - 4)(J-1)(J+2) + 2(2J+1)J(J+1)(J+2), \end{aligned} \right\} \quad (2)$$

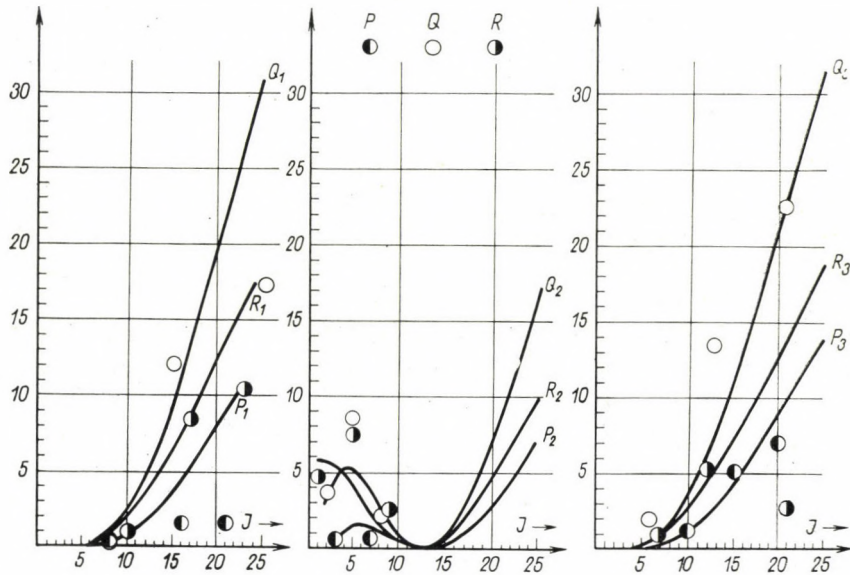


Fig. 1

while for inverted $^3\Pi$ term ($Y'' < 0$) the coefficient of $Y''(Y'' - 4)$ in $C_1''(J)$ is equal to $(J-1)(J+2)$ instead of $J(J+1)$ and in $C_3''(J)$ it is equal to $J(J+1)$ instead of $(J-1)(J+2)$. For a $^3\Pi - ^3\Delta$ transition the expressions with single prime will change to those with double prime and vice versa.

In the Figures the theoretical values of the i -factors as given in the Table and calculated with the values $Y' = -12,92 \text{ cm}^{-1}$ and $Y'' = 24,7 \text{ cm}^{-1}$ with the help of an electronic computer are shown by the curves, whereas the circles represent the experimental i -factors calculated by means of the observed data of the 3-0 band of the $d^3\Delta \rightarrow a^3\Pi$ transition of the CO molecule. For the calculation of the experimental i -factors according to the method published by NOLAN and JENKINS [5], we have first determined the emission temperature from the experimental data, and then, using this, the experimental data have been multiplied by the corresponding exponential factor. Finally, the proportionality factor has been evaluated with the least squares method. From the

Figures it can be seen that the agreement is good, especially, if it is considered that for the individual branches in general only three measured points were available which themselves resulted moreover from a semi-quantitative measurement, and that the i -factors were not directly observed data either, their values being influenced by the uncertainty of the determination of the temperature.

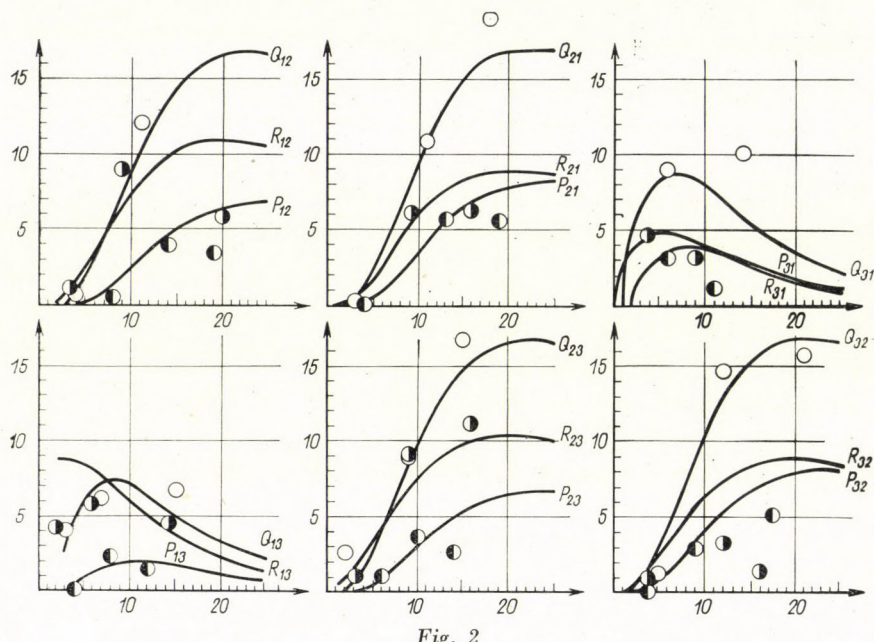


Fig. 2

The good agreement of the theoretical and experimental results shows without any doubt that the upper state of the "triplet" bands of the CO molecule is indeed a ${}^3\Delta_{\text{inv}}$ term.

REFERENCES

1. L. GERŐ, Ann. d. Phys., **35**, 597, 1939.
2. P. K. CARROLL, Journ. Chem. Phys., **36**, 2861, 1962.
3. R. S. MULLIKEN, Can. J. Chem., **36**, 10, 1958.
4. I. KOVÁCS, Nuovo Cim., **29**, 1089, 1963.
5. P. NOLAN and F. A. JENKINS, Phys. Rev., **50**, 943, 1936.

РАСПРЕДЕЛЕНИЕ ИНТЕНСИВНОСТИ В ТРИПЛЕТНОЙ СВЯЗИ МОЛЕКУЛЫ СО

И. КОВАЧ и Р. ТЭРЭШ

Резюме

Теоретическая формула распределения интенсивности в переходе ${}^3\Delta - {}^3\Pi$ была тщательно выведена для случая; когда оба терма, принимающие участие в переходе, отнесаются к среднему случаю Гунда. Формула интенсивности, выведенная теоретически, сравнивается с наблюдаемыми значениями интенсивности перехода $d^3\Delta - a^3\Pi$ в молекуле CO. Удовлетворительное совпадение упомянутых значений подтверждает предположение, согласно которому высшим состоянием данного перехода является именно состояние ${}^3\Delta$.

THE ROTATIONAL STRUCTURE OF THE d^3A STATE OF THE CO MOLECULE

By

I. KOVÁCS

DEPARTMENT OF ATOMIC PHYSICS, POLYTECHNICAL UNIVERSITY, BUDAPEST

(Received 31. III. 1964)

The multiplet splitting of the d^3A term of the CO molecule taken as a function of the rotational quantum number shows a deviation from the known triplet term formula. By taking into account the spin-spin interaction simultaneously with the perturbation of a 1A term arising from the spin-orbit interaction it was possible to give an interpretation for the deviation observed.

1. Introduction

CARROLL [1] investigated the rotational spin splitting of the $v' = 3$ level of the d^3A state of the CO molecule and found the experimental results to be in agreement only to a first approximation with the splitting calculated according to the known triplet formula established by BUDÓ [2]. Even after taking several corrections into account there still remains a systematic discrepancy of the order of about $1-2 \text{ cm}^{-1}$. These, essentially, consist in that mainly the middle component of the d^3A term, taken as a function of the rotational quantum number, runs differently from what is to be expected on the basis of the triplet formula. Deviations of a similar kind have already been observed in the case of Π terms, in particular, in the case of the $A^3\Pi$ state of the NH molecule [3], in that of the $^3\Pi$ states of the PH and PF molecules [4], [9] and the $^4\Pi$ state of the O_2^+ molecule [5]. These deviations could excellently be interpreted by simultaneously taking into account the spin-spin interaction neglected so far, and the perturbation of other Π terms of lower multiplicity due to the spin-orbit interaction [6], [7], [10]. With this method also the deviations observed by CARROLL may be interpreted, as we are showing below.

2. The interpretation of the anomalous spin splitting of the d^3A term

When the spin-spin interaction is taken into account simultaneously with the perturbation of a 1A term (completed by the interaction between rotation and spin), the method elaborated earlier and described in [6] and [7] gives the following results in the case of the 3A terms:

$$\begin{aligned} F'_1(J) &= F_1(J) - \frac{\beta}{3} + \beta S_{2,J-1}^2 + \gamma \left(J + \frac{1}{3} \right), \\ F'_2(J) &= F_2(J) - \frac{\beta}{3} + \beta S_{2,J}^2 + \frac{1}{3} \gamma, \\ F'_3(J) &= F_3(J) - \frac{\beta}{3} + \beta S_{2,J+1}^2 - \gamma \left(J + \frac{2}{3} \right), \end{aligned} \quad (1)$$

where $F'_1(J)$, $F'_2(J)$, $F'_3(J)$ represent the perturbed, i.e. actually observed terms, and $F_1(J)$, $F_2(J)$, $F_3(J)$ the term values calculated with the aid of the triplet formula established by BUDÓ. Further $\beta = a - 3\varepsilon$ with

$$a = \frac{|H(^3A_2, ^1A_2)|^2}{h\nu(^3A, ^1A)} \quad (2)$$

$H(^3A_2, ^1A_2)$ is the spin-orbit interaction matrix element of the perturbation between the 3A and 1A terms and $h\nu(^3A, ^1A)$ the distance of these two terms. ε is the constant of the spin-spin interaction, while γ is that of the interaction between rotation and spin. $S_{2,J-1}$, $S_{2,J}$, $S_{2,J+1}$ are the three elements of the transformation matrix in the intermediate case between HUND's cases a) and b) for the 3A term, the explicit expressions for which are the following [8]:

$$S_{2,J-1} = -\frac{(J-2)(J+3)}{\sqrt{C_1'(J)}}; S_{2,J} = \frac{Y' - 2}{\sqrt{C_2'(J)}}; S_{2,J+1} = \frac{(J-1)(J+3)}{\sqrt{C_3'(J)}}. \quad (3)$$

The value of these transformation matrix elements may be calculated numerically when Y' is known ($Y' = -12,92 \text{ cm}^{-1}$). For the values of $C_1'(J)$, $C_2'(J)$, $C_3'(J)$ see the preceding paper in this Journal.

For the differences between the multiplet splittings as observed and calculated by the aid of the triplet formula by means of (1) the following expressions are obtained:

$$\begin{aligned} (F_1 - F_2)_{\text{obs}} - (F_1 - F_2)_{\text{calc}} &= (F'_1 - F'_2) - (F_1 - F_2) = \beta(S_{2,J-1}^2 - S_{2,J}^2) + \gamma J, \\ (F_2 - F_3)_{\text{obs}} - (F_2 - F_3)_{\text{calc}} &= (F'_2 - F'_3) - (F_2 - F_3) = \beta(S_{2,J}^2 - S_{2,J+1}^2) + \gamma(J+1). \end{aligned} \quad (4)$$

In Fig. 1 the circles represent these differences (i.e. the left side of (4)), while the theoretical values (i.e. the right side of (4)) calculated with $\beta = -2,15 \text{ cm}^{-1}$ and $\gamma = -0,0178 \text{ cm}^{-1}$ lie on the full-drawn curves. The constants β and γ have been determined from the experimental data. As can be seen the agreement between theory and experiment is excellent.

CARROLL published also the individual observed and calculated values of the $F_2(J)$ term. Relation (1) gives the following expression for the deviations between these values:

$$F_2^{\text{obs}} - F_2^{\text{calc}} = F'_2 - F_2 = -\frac{\beta}{3} + \beta S_{2,J}^2 + \frac{1}{3} \gamma. \quad (5)$$

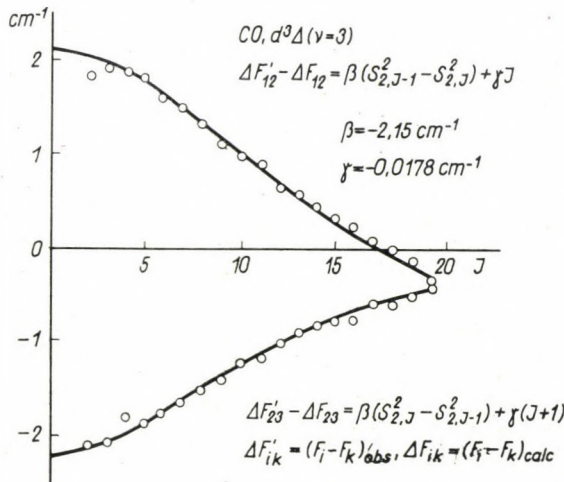


Fig. 1

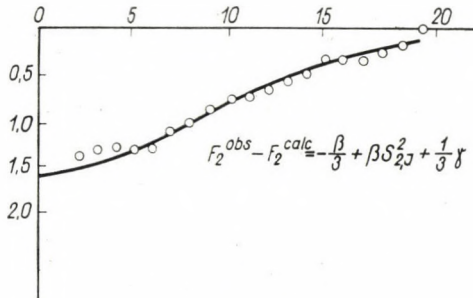


Fig. 2

In Fig. 2 the circles represent the observed values, i.e. the left side of (5), whereas the curve indicates the theoretical values calculated from the right side of (5). As can be seen the agreement between the experimental and theoretical results is excellent also here.

Summarizing, it may be stated that the deviation from the triplet formula may be satisfactorily interpreted by simultaneously taking into account the spin-spin and the spin-orbit interactions. For the multiplet splittings these two completely different mechanisms give formulas of the same structure.

REFERENCES

1. P. K. CARROLL, J. Chem. Phys., **36**, 2861, 1962.
2. A. BUDÓ, Z. Phys., **96**, 219, 1935.
3. R. N. DIXON, Can. J. Phys., **37**, 1171, 1959.
4. M. ISHAQUE and R. W. B. PEARSE, Proc. Roy. Soc., A **156**, 221, 1936; **173**, 265, 1939.
F. LEGAY, Can. J. Phys., **38**, 797, 1960.
5. T. E. NEVIN, Phil. Trans. Roy. Soc. (London), **237**, 471, 1938.
6. A. BUDÓ and I. KOVÁCS, Acta Phys. Hung., **4**, 273, 1954.
7. I. KOVÁCS, Acta Phys. Hung., **10**, 255, 1959; **12**, 67, 1960; **13**, 303, 1961; **17**, 67, 1964.
8. I. KOVÁCS, Can. J. Phys., **38**, 955, 1960.
9. A. E. DOUGLAS and M. FRACKOWIAK, Can. J. Phys., **40**, 832, 1962.
10. I. KOVÁCS, Can. J. Phys., **42**, 2180, 1964.

РОТАЦИОННАЯ СТРУКТУРА СОСТОЯНИЯ d^3A МОЛЕКУЛЫ СО

И. КОВАЧ

Р е з и о м е

Мультиплетное расщепление терма d^3A молекулы CO, взятое как функция от ротационного квантового числа, показывает некоторое отклонение от известной формулы триплетного терма. Принимая во внимание спин-спиновое взаимодействие одновременно с возмущением терма 1A ; обусловленным спин-орбитальным взаимодействием, стало возможным дать теоретическое объяснение упомянутого выше отклонения.

X-RAY POWDER DIFFRACTION STUDY OF THE $\text{WO}_3 \rightleftharpoons \text{W}_{20}\text{O}_{58}$ SHEAR TRANSFORMATION

By

P. GADÓ

INSTITUTE FOR TELECOMMUNICATION TECHNIQUE, DEPARTMENT FOR TESTING OF BASIC MATERIALS,
BUDAPEST

(Presented by T. Millner — Received 16. VII. 1964)

By means of continuous high-temperature diffractometry the shear model of the crystallographic transformation: $\text{WO}_3 \rightleftharpoons \text{W}_{20}\text{O}_{58}$ was experimentally studied. Solid state reaction in the range 500—600°C results in defective beta-tungsten-oxide structures, the shear between adjacent blocks being random instead of parallel-equidistant. A difference has been established between the mechanism of reduction and oxidation.

Introduction

In any attempt to throw light on the rearrangements and movements that take place on an atomic scale during the transformation of tungsten trioxide into beta-tungsten-oxide (described more precisely by the formula $\text{W}_{20}\text{O}_{58}$) and vice versa, it is first of all necessary to become familiar with these two structures.

Tungsten trioxide has a slightly distorted rhenium-trioxide type of lattice. For the study of the kinetics of the transformation it suffices to state that according to this structure each W ion is surrounded octahedrally by six O^{2-} ions, and each of these oxygens belongs to two adjacent octahedra, i.e. the co-ordination polyhedra are joined by sharing corners (Fig. 1a).

In beta-tungsten-oxide, on the other hand, the same mutual arrangement of W and O ions is restricted to the inside of particular blocks. These regions of ReO_3 -type structure form slabs which are large in two dimensions, but only seven octahedra wide in the third dimension. The neighbouring slabs join each other in boundary regions characterized by co-ordination octahedra sharing edges, instead of corners, as is normal in trioxide. — In a perfect $\text{W}_{20}\text{O}_{58}$ crystal these boundary regions form parallel equidistant running walls of “recurrent dislocations” as referred to by MAGNÉLI [1]. “Dislocation” as compared with the trioxide, because the three dimensional ReO_3 type network extending there throughout the entire crystallite is disturbed here periodically by the boundary regions between adjacent blocks (Fig. 1b).

This relation between the two structures is clear from MAGNÉLI’s description, and WADSLEY [2] mentions beta-tungsten-oxide as an outstanding example of “shear structures”. The reason for this is that if an extended

volume of tungsten-trioxide is taken, then oxygen ions are removed from certain appropriate positions (Fig. 2a), the remaining lattice can be sheared, and as a result beta-tungsten-oxide is formed — at least in a model or on a drawing (Fig. 2b).

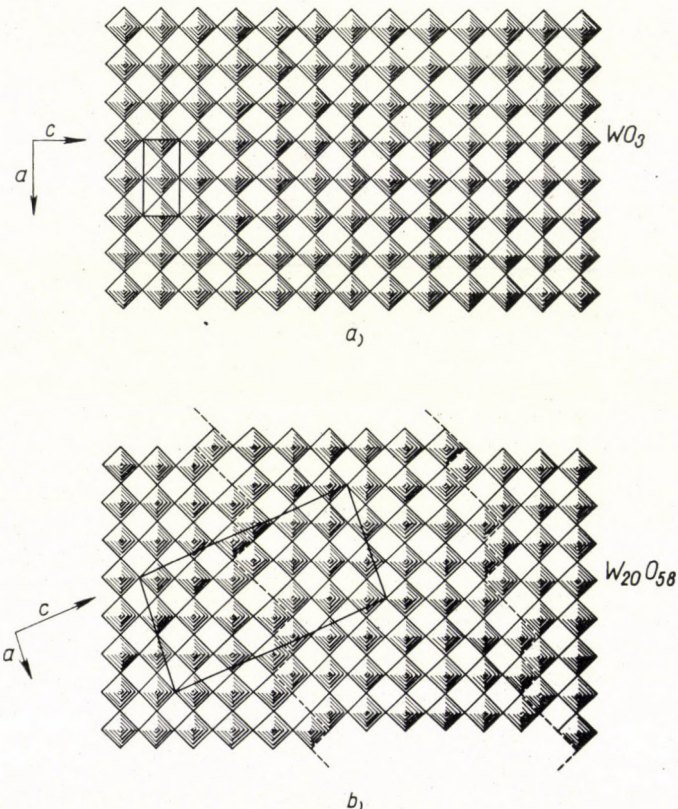


Fig. 1. Projection of the idealized WO_3 and $\text{W}_{20}\text{O}_{58}$ structures parallel to the [010] axis. Unit cells are outlined

- a) The ReO_3 -type structure of WO_3 , represented by one layer of co-ordination octahedra.
- b) Boundary regions between the ReO_3 -type slabs of $\text{W}_{20}\text{O}_{58}$. Along the dotted zig-zag lines octahedra share edges

The aim of our investigation was just to answer the question as to how far nature actually follows the proposed model of transition.

Results

Beta-tungsten-oxide was prepared in our Laboratory very many times in relatively different ways. The statistical interpretation of the powder photographs taken from these specimens revealed two facts:

1. The line breadth of the different hkl reflections varies just as in the case of a defect structure. The $010, 20\bar{8}, 403, 21\bar{8}, 413, 2,0,11, 60\bar{5}, 020$, etc. reflections are sharp, while those with indices $105, 30\bar{2}, 30\bar{3}, 106, 115, 31\bar{2}, 116$, etc. are often rather broadened. Thus the line breadth does not depend on the

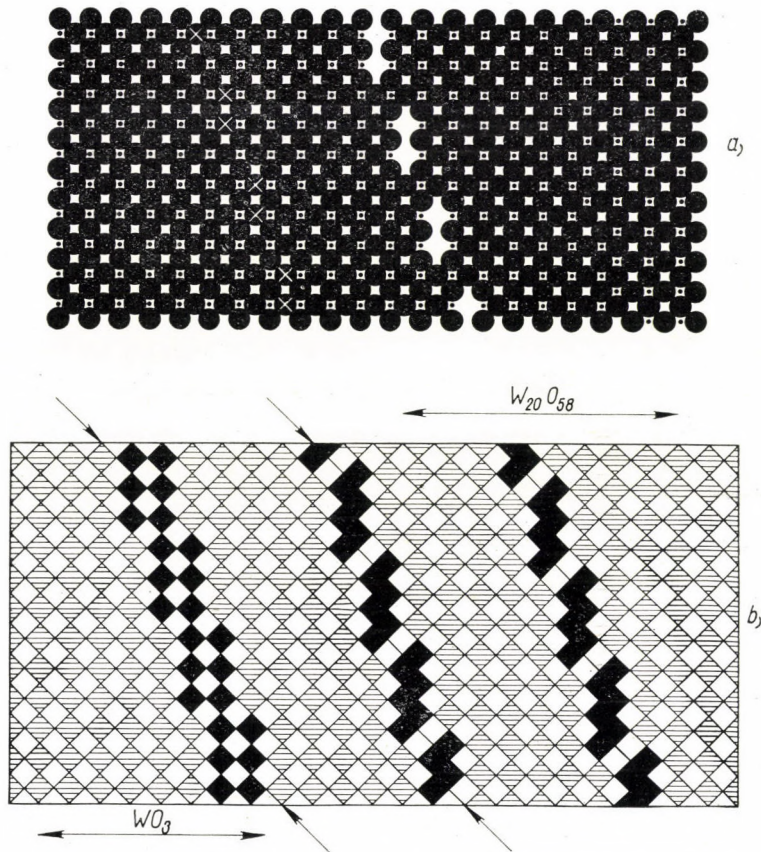


Fig. 2. Model of the shear mechanism of transformation

- a) Removing the O ions from appropriate sites.
- b) Shear of the adjacent blocks along the anion-vacancies

Bragg angle or any function of it, but lines belonging to a particular family are sharp and others broad.

2. Regarding powder specimens of different origins, it could be established that the scattering of d values belonging to the second group of lines mentioned above is much more important (1—3%) than that of the d values given by the first, sharper family of lines (0,2—0,3%).

In order to explain the different behaviour of the two groups of reflexions in respect of breadth and displacement of the lines, we accomplished a linear algebraic transformation between the (hkl) indices of trioxide and (HKL)

indices of beta-oxide, respectively. The results of this algebraic transformation are summarized in Fig. 3.

According to the algebraic behaviour taken up during linear transformation by the lines one can again distinguish definite groups of indices in both oxides.

In the first group we find on the beta-tungsten-oxide side indices 010, 208, 403, etc. which correspond to the sharp lines and transform into rational counterparts in the trioxide system (020, 201, 201, etc.) and vice versa.

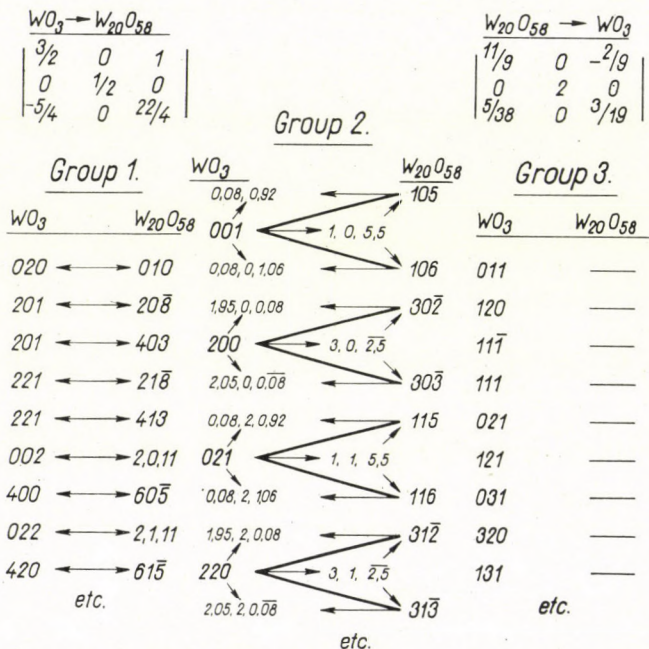


Fig. 3. The matrices of the linear algebraic transformation, and summary of its results (see text)

The second group of indices is identical with the previously mentioned family belonging to the usually broadened lines of the defect beta-oxide (105, 302, 303, etc.). The transformation selects from this group index-pairs which amalgamate into single indices in the trioxide system (105—106 → 001; 302—303 → 200; etc.). In the reverse direction of transformation a splitting of indices is observed, of course.

In the trioxide system there are still some other indices that have no counterparts in the $W_{20}O_{58}$ system. The absence of these reflexions in the latter case can be explained by space-group extinction.

Tracing the crystallographic planes of the beta-oxide structure, it can be stated that all the indices belonging to sharp reflexions describe planes which run continuously through the walls between neighbouring blocks, but those of

the second group belong to those planes which suffer serious distortion in the boundary region as a result of the shear which might create beta oxide out of trioxide.

To gain more information on the mechanism of transformation, we designed a glass-flow high temperature attachment to a Hilger recording diffractometer [3] and prepared continuous diffractograms during the reduction of tungsten trioxide in $N_2 + H_2$ gas mixture and during the oxidation of beta-tungsten-oxide in air. The reactions took place between 300 and 800°C.

$\beta(10^{-3})$		
$W_{20}O_{58}$	WO_3	$W_{20}O_{58}$
hkl	hkl	hkl
020	010	020
	238	337
403	201	403
	257	360
303	200	303
460	260	486

Fig. 4. Change in the breadth of the diffraction lines during transformation in both directions

Observing some selected diffraction lines with the aid of high temperature diffractometry, we found that the events in the direction of reduction differ from those in the direction of oxidation.

First of all, when reducing in a gas containing H_2 there is an intermediate phase between the two oxides, while oxidation seems to lead directly from beta-oxide to trioxide. This intermediate phase has not yet been determined in full detail, but it is very probably either a hydrogen-containing oxide (hydrogen-bronze) or an intermediate oxide, of the composition $WO_{2.96}$ [4]. In any case, it has been proved to have a ReO_3 -type lattice, thus its existence does not afford additional information regarding the geometric shear model of crystallographic transformation.

The diffraction observations reveal, however, some other interesting differences in the mechanism of transformations proceeding in opposite directions. Namely:

1. The overall line-breadth increases considerably in the direction of reduction, but shows no or negligible increase, or even a decrease in the direction of oxidation (Fig. 4).

2. Since beta-oxide powders consist of tiny needle-shaped crystals, flat powder specimens with strong preferred orientation can be prepared easily. This is generally regarded as undesirable in diffractometric practice. In our case, however, it led to additional information about the transformation,

because the anomalous intensity distribution of preferred orientation was retained during oxidation, but lost during reduction of the same specimen (Fig. 5).

With the aid of high temperature diffractometry it was also possible to observe that if the crystallite size of trioxide was extremely small (about 200—300 Å) then the reduced product did not show the characteristic pattern for $W_{20}O_{58}$, but only a strongly distorted WO_3 pattern. The transformation was in this case perfectly continuous.

$W_{20}O_{58} \rightarrow$	$WO_3 \rightarrow$	$W_{20}O_{58}$
hkl	hkl	
105_{20}		
	60	22
302_{55}	001_{100}	
	20	70 50
010_{100}	20	010_{95} 30 100
303_{55}	100	200_{100} 100 55
106_{60}	60	55

Fig. 5. Change in the intensity distribution given by specimens with preferred orientation, during reduction and oxidation, respectively

Discussion

On the basis of the described experimental findings the following model is suggested for the transformations:

During reduction of WO_3 , first an intermediate phase is formed, the oxygen atoms leave this at discrete positions, which form walls directly or by diffusion. In this way the crystal is broken up into blocks, the inside of which retain the co-ordination of the trioxide lattice. At the walls of vacant oxygens (in respect to WO_3) boundaries are formed by shear between adjacent blocks. The boundaries are not perfectly ordered and are distributed randomly at this stage. Thus the beta-tungsten-oxide prepared by solid state reaction (under the described conditions) has a defect structure compared with MAGNÉLI's ideal arrangement of parallel and equidistant walls of "recurrent dislocations". The perfection of the specimen can, of course, be increased by heat treatment: There is a continuous transition in the structure and degree of perfection from disordered trioxide — through disordered beta-oxide — to the perfect $W_{20}O_{58}$. This means, that the defect phase fills up the composition range between WO_3 and $WO_{2.90}$. The constancy of composition seems to be valid only for the perfect $W_{20}O_{58}$ crystals.

The mechanism of transformation is much more simple when starting with a beta-oxide specimen. Whether the crystals are defective or perfect, there are sites where oxygen ions are lacking compared with trioxide, and if the circumstances promote oxidation, the vacant places are filled by oxygens. The entering oxygens spring the boundary regions and shear takes place. The planes of shear are spaced uniformly or randomly according to the primary distribution of block-walls in the beta-tungsten-oxide.

A second part of this research is undertaken by using single-crystal methods.

Acknowledgements

Thanks are due to Drs. T. MILLNER, J. NEUGEBAUER and A. J. HEGEDÜS for their interest in this research, and to the Director of the Institute for Telecommunication Technique, Budapest for permitting the publication of this work.

REFERENCES

1. A. MAGNÉLI, Acta Cryst., **6**, 495, 1953.
2. A. D. WADSLY, Rev. Pure and Appl. Chem., **5**, 165, 1955.
3. P. GADÓ, Magyar Fizikai Folyóirat, **10**, 387, 1962.
4. R. J. ACKERMANN and E. G. RAUCH, J. Chem. Physics, **67**, 1146, 1963.

ИЗУЧЕНИЕ ПРЕОБРАЗОВАНИЯ СДВИГА $\text{WO}_3 \rightleftharpoons \text{W}_{20}\text{O}_{58}$ РЕНТГЕНОВЫМИ ЛУЧАМИ ПОРОШКО-ДИФФРАКЦИОННЫМ МЕТОДОМ

П. ГАДО

Р е з ю м е

Непрерывным высокотемпературным дифрактометром изучается экспериментально модель сдвига кристаллографического преобразования $\text{WO}_3 \rightleftharpoons \text{W}_{20}\text{O}_{58}$. Реакция твёрдого состояния в интервале температур 500—600° С результирует в дефекте структуры бетаокиси вольфрама, сдвиг между смежными блоками беспорядочен вместо параллельно-эквидистантного. Устанавливается различие между механизмами раскисления и окисления.

ON THE CONVERGENCE OF THE PERATIZATION METHOD

By

I. MONTVAY

INSTITUTE FOR THEORETICAL PHYSICS, ROLAND EÖTVÖS UNIVERSITY, BUDAPEST

(Presented by K. Novobátzky — Received 23. VI. 1964)

Recently G. FEINBERG and A. PAIS have found a method for the solution of the integral equation summing the ladder graphs in the theory of weak interactions. The present paper shows the convergence of their method in the case of zero incoming momenta and examines the connection between the regularized and unregularized equations. It is shown that it is possible to obtain the results of the regularization procedure directly from the original, unregularized equation.

1. Introduction

Since the field theory of weak interactions (the four-fermion interaction theory as well as the intermediate boson theory) is unrenormalizable, for a very long time it was not possible to calculate the probability of weak processes forbidden in the lowest order. The solution of this problem is of high importance in many respects. In their first paper G. FEINBERG and A. PAIS (FP) [1] have given a review of the unsolved questions which can be answered if the probability amplitudes can be calculated also in higher order. The procedure (peratization) proposed by them leads to finite corrections of the first order amplitude, due to the sum of higher order ladder graphs. This correction changes for example the coupling constant in the reaction $\nu_\mu e^- \rightarrow \mu^- \nu_e$ from g^2/m^2 to $3g^2/4m^2$. This can be seen from the zero momentum limit of the amplitude. The same result can be obtained also in a simpler way [2] if one deals directly with the case of zero incoming momenta. Denote the amplitudes of the processes $\nu_\mu e^- \rightarrow \mu^- \nu_e$ and $\nu_e e^- \rightarrow \nu_e e^-$ by M_{odd} and M_{even} , respectively, and introduce the amplitude

$$M^\pm = M_{\text{odd}} \pm M_{\text{even}} = M_{\mu\nu}^\pm \gamma_\mu^{(1)} (1 + \gamma_5^{(1)}) \gamma_\nu^{(1)} (1 + \gamma_5^{(2)}). \quad (1,1)$$

In the ladder approximation one gets for

$$T^\pm = \text{Trace } M_{\mu\nu}^\pm \quad (1,2)$$

the following Bethe—Salpeter equation:

$$T^\pm(p) = \frac{-ig^2(4 + m^{-2}p^2)}{p^2 + m^2} \pm \frac{4ig^2}{(2\pi)^4} \times \\ \times \int \frac{T^\pm(p') [4 + m^{-2}(p - p')^2]}{p'^2 [(p' - p)^2 + m^2]} d^4 p'. \quad (1,3)$$

Here the notations are the same as in the papers of FP ([1] and [2]). Regularizing the boson propagator in the kernel we are led to the equation

$$T^\pm(p, M) = \frac{-ig^2(4 + m^{-2}p^2)}{p^2 + m^2} \pm \frac{4ig^2 M^4}{(2\pi)^4} \times \\ \times \int \frac{T^\pm(p', M) [4 + m^{-2}(p - p')^2]}{p'^2 [(p' - p)^2 + m^2] (p'^2 + M^2)^2} \quad (1,4)$$

(see ref. [2], eq. (2,17)), where M is the regularization mass, thus we need the solution $\lim_{M \rightarrow \infty} T^\pm(p, M)$.

In the present paper we shall deal with the equations (1,3) and (1,4). In Section 2 we first reproduce the solution of (1,4) with the peratization method and show that the procedure converges if the coupling constant is small enough. We examine the connection between the solution and the unregularized equation (1,3) and prove a conjecture of FP. Equation (1,3) is investigated in Section 3. It is shown that the results of FP can be obtained directly from it, without the regularization. It is an interesting feature, however, that the unregularized equation splits into two coupled equations and it is not so easy to prove that these are not in contradiction with each other. We deal with this problem in the Appendix, where we prove under certain assumptions that the two equations do indeed not contradict each other.

2. The regularized equation for T^\pm

In the equation (1,4) the integration has to be extended over the whole p' space. For our purposes it will be more convenient to introduce new integration variables, since we want to prove the convergence of the Neumann series in terms of square integrability. First of all we perform the integration over the angular variables in the $p'_1 p'_2 p'_3$ space: these are ϑ' and φ' . The other two new variables are

$$R' = \sqrt{(p'^2_1 + p'^2_2 + p'^2_3)^2 + p'^4_0}, \\ \Phi' = \operatorname{arctg} \frac{p'^2_0}{p'^2_1 + p'^2_2 + p'^2_3}. \quad (2,1)$$

(These are polar coordinates in the $\varrho = p_1'^2 + p_2'^2 + p_3'^2; \pi = p_0'^2$ plane). Thus the connection between the old and new variables is the following

$$\begin{aligned} p'_0 &= \pm \sqrt{R' \sin \Phi'}, \\ p'_1 &= \sqrt{R' \cos \Phi'} \cdot \sin \vartheta' \cdot \sin \varphi', \\ p'_2 &= \sqrt{R' \cos \Phi'} \cdot \sin \vartheta' \cdot \cos \varphi', \\ p'_3 &= \sqrt{R' \cos \Phi'} \cdot \cos \vartheta'. \end{aligned} \quad (2,2)$$

Choosing $p_1 = p_2$ to be zero and $p_0 \geq 0$ one has

$$\begin{aligned} (p - p')^2 &= R(\cos \Phi - \sin \Phi) + R'(\cos \Phi' - \sin \Phi') - \\ &- 2 \cos \vartheta \sqrt{RR' \cos \Phi \cos \Phi'} \pm 2 \sqrt{RR' \sin \Phi \sin \Phi'}. \end{aligned}$$

The Jacobian can be obtained from (2,2)

$$\frac{\partial(p'_0 p'_1 p'_2 p'_3)}{\partial(R' \Phi' \vartheta' \varphi')} = \pm R' \frac{\sqrt{\operatorname{ctg} \Phi' \sin \vartheta'}}{4}.$$

It is now possible to write down the equation for $T^\pm(R\Phi, M)$. Introducing the new unknown function

$$T_S^\pm(R\Phi, M) = \frac{T^\pm(R\Phi, M) \operatorname{ctg}^{1/4} \Phi}{\sqrt{\cos \Phi - \sin \Phi}} \quad (2,3)$$

we obtain the following (more symmetrical) equation in the new variables

$$\begin{aligned} T_S^\pm(R\Phi, M) &= -ig^2 \frac{\operatorname{ctg}^{1/4} \Phi}{\sqrt{\cos \Phi - \sin \Phi}} \left(\frac{1}{m^2} + \frac{3}{R(\cos \Phi - \sin \Phi) + m^2} \right) \pm \\ &\pm \frac{4ig^2 \pi M^4}{(2\pi)^4} \int_0^{\infty} \int_0^{\pi/2} \frac{T_S^\pm(R' \Phi', M) \{ \operatorname{ctg} \Phi \cdot \operatorname{ctg} \Phi' \}^{1/4}}{\sqrt{(\cos \Phi - \sin \Phi)(\cos \Phi' - \sin \Phi')} [M^2 + R'(\cos \Phi' - \sin \Phi')]^2} \times \\ &\times \left\{ \frac{2}{m^2} - \frac{3 K_m^{(T)}(R\Phi R' \Phi')}{4 \sqrt{RR' \cos \Phi \cos \Phi'}} \right\} d\Phi' dR'. \end{aligned} \quad (2,4)$$

Here $K_m^{(T)}$ is an abbreviation standing for the expression

$$K_m^{(T)}(R\Phi R' \Phi') = \log \left| \frac{[R(\cos \Phi - \sin \Phi) + R'(\cos \Phi' - \sin \Phi') + m^2 - 2 \sqrt{RR' \cos \Phi \cos \Phi'}]^2 - 4RR' \sin \Phi \sin \Phi'}{[R(\cos \Phi - \sin \Phi) + R'(\cos \Phi' - \sin \Phi') + m^2 + 2 \sqrt{RR' \cos \Phi \cos \Phi'}]^2 - 4RR' \sin \Phi \sin \Phi'} \right|. \quad (2,5)$$

We must now find the solution of (2,4) in the limit $M \rightarrow \infty$. Following FP we suppose that

$$T_S^\pm(R\Phi, M) = T_{1S}^\pm(R\Phi, M) + T_{2S}^\pm(M) \frac{\operatorname{ctg}^{1/4} \Phi}{\sqrt{\cos \Phi - \sin \Phi}} . \quad (2,6)$$

Introducing the notations

$$K_m^{(S)}(R\Phi R'\Phi') = K_m^{(T)}(R\Phi R'\Phi') \frac{(\cos \Phi \sin \Phi \cos \Phi' \sin \Phi')^{-1/4}}{\sqrt{RR'(\cos \Phi - \sin \Phi)(\cos \Phi' - \sin \Phi')}} , \quad (2,7)$$

$$k_1 = -\frac{3ig^2}{16\pi^3}, \quad k_2 = \frac{ig^2}{2m^2 \pi^3} ,$$

and supposing

$$\begin{aligned} T_{1S}^\pm(R\Phi, M) &= \frac{-3ig^2}{R(\cos \Phi - \sin \Phi) + m^2} \cdot \frac{\operatorname{ctg}^{1/4} \Phi}{\sqrt{\cos \Phi - \sin \Phi}} \pm \\ &\pm k_1 M^4 \int_0^{\infty} \int_0^{\pi/2} \frac{T_{1S}^\pm(R'\Phi', M) + T_{2S}^\pm(M)}{[R'(\cos \Phi' - \sin \Phi') + M^2]^2} K_m^{(S)}(R\Phi R'\Phi') d\Phi' dR' , \end{aligned} \quad (2,8a)$$

$$T_{2S}^\pm(M) = \frac{-ig^2}{m^2} \pm k_2 M^4 \int_0^{\infty} \int_0^{\pi/2} \frac{[T_{1S}^\pm(R'\Phi', M) + T_{2S}^\pm(M)] \operatorname{ctg} \Phi' d\Phi' dR'}{[R'(\cos \Phi' - \sin \Phi') + M^2]^2 (\cos \Phi' - \sin \Phi')} \quad (2,8b)$$

one gets the solution of eq. (2,4). Eq. (2,8a) can be decomposed into the following two integral equations:

$$\begin{aligned} t_r^\pm(R\Phi, M) &= \frac{-3ig^2}{R(\cos \Phi - \sin \Phi) + m^2} \frac{\operatorname{ctg}^{1/4} \Phi}{\sqrt{\cos \Phi - \sin \Phi}} \pm \\ &\pm k_1 M^4 \int_0^{\infty} \int_0^{\pi/2} \frac{t_r^\pm(R'\Phi', M) K_m^{(S)}(R\Phi R'\Phi')}{[R'(\cos \Phi' - \sin \Phi') + M^2]^2} d\Phi' dR' , \end{aligned} \quad (2,9a)$$

$$\begin{aligned} t_s^\pm(R\Phi, M) &= \pm k_1 M^4 \int_0^{\infty} \int_0^{\pi/2} \frac{K_m^{(S)}(R\Phi R'\Phi') d\Phi' dR'}{[R'(\cos \Phi' - \sin \Phi') + M^2]^2} \pm \\ &\pm k_1 M^4 \int_0^{\infty} \int_0^{\pi/2} \frac{t_s^\pm(R'\Phi', M) K_m^{(S)}(R\Phi R'\Phi')}{[R'(\cos \Phi' - \sin \Phi') + M^2]^2} d\Phi' dR' . \end{aligned} \quad (2,9b)$$

In this way the solution $T_{1S}^\pm(R\Phi, M)$ is simply

$$T_{1S}^\pm(R\Phi, M) = t_r^\pm(R\Phi, M) + T_{2S}^\pm(M) t_s^\pm(R\Phi, M) . \quad (2,10)$$

The eq. (2,8b) for T_{2S}^{\pm} becomes now

$$\begin{aligned}
 T_{2S}^{\pm}(M) = & \left[\frac{-ig^2}{m^2} \pm k_2 M^4 \int_0^{\infty} \int_0^{\pi/2} \frac{t_r^{\pm}(R'\Phi', M) \sqrt{\operatorname{ctg} \Phi'} d\Phi' dR'}{[R'(\cos \Phi' - \sin \Phi') + M^2]^2 (\cos \Phi' - \sin \Phi')} \right] \times \\
 & \times \left\{ 1 \mp k_2 M^4 \int_0^{\infty} \int_0^{\pi/2} \frac{\sqrt{\operatorname{ctg} \Phi'} d\Phi' dR'}{[R'(\cos \Phi' - \sin \Phi') + M^2]^2 (\cos \Phi' - \sin \Phi')} \mp \right. \\
 & \left. \mp k_2 M^4 \int_0^{\infty} \int_0^{\pi/2} \frac{t_s^{\pm}(R'\Phi', M) \sqrt{\operatorname{ctg} \Phi'} d\Phi' dR'}{[R'(\cos \Phi' - \sin \Phi') + M^2]^2 (\cos \Phi' - \sin \Phi')} \right\}^{-1}. \quad (2,11)
 \end{aligned}$$

According to the meaning of regularization, in the solutions of the equations M must tend to infinity. (In our case only the quantity $\lim_{M \rightarrow \infty} T_S^{\pm}(0, \pi/4, M)$ has a physical meaning, since the point $p = 0, p^2 = 0$ corresponds to $R = 0, \Phi = \pi/4$.)

We solve (2,9a) and (2,9b) by iteration. If the iteration series converges, there is

$$\begin{aligned}
 \lim_{k \rightarrow \infty} t_r^{\pm(k)}(R\Phi, M) &= t_r^{\pm}(R\Phi, M), \\
 \lim_{k \rightarrow \infty} t_s^{\pm(k)}(R\Phi, M) &= t_s^{\pm}(R\Phi, M). \quad (2,12)
 \end{aligned}$$

In every iteration step we solve (2,11) exactly and so obtain $T_{2S}^{\pm(k)}(M)$. Thus in the k -th iteration step we obtain for $T_S^{\pm}(R\Phi, M)$ from (2,8) and (2,6)

$$T_S^{\pm(k)}(R\Phi, M) := t_r^{\pm(k)}(R\Phi, M) + T_{2S}^{\pm(k)}(M) \left[\frac{\operatorname{ctg}^{1/4} \Phi}{\sqrt{\cos \Phi - \sin \Phi}} + t_s(R\Phi, M) \right]. \quad (2,13)$$

Renouncing the summation of the Neumann series, we let M tend to infinity in every iteration step. The “solution” obtained in this way is

$$S_S^{\pm}(R\Phi) = \lim_{k \rightarrow \infty} \lim_{M \rightarrow \infty} T_S^{\pm(k)}(R\Phi, M). \quad (2,14)$$

The whole procedure converges if the Neumann series (2,12) converges. The functions

$$\begin{aligned}
 K_m^{(S)}(R\Phi R'\Phi') [R'(\cos \Phi' - \sin \Phi') + M^2 - i\varepsilon]^{-2}; \\
 - 3ig^2 \operatorname{ctg}^{1/4} \Phi \{ [R(\cos \Phi - \sin \Phi) + m^2 - i\varepsilon] (\sqrt{\cos \Phi - \sin \Phi} - i\varepsilon) \}^{-1};
 \end{aligned}$$

and

$$\int_0^\infty \int_0^{\pi/2} K_m^{(S)}(R\Phi R' \Phi') [R'(\cos \Phi' - \sin \Phi') + M^2 - i\varepsilon]^{-2}$$

that is the kernel and inhomogeneities in (2,9a) and (2,9b) are square integrable. Thus if $|k_1|$ (this means g^2) is small enough the convergence is assured. The remaining question is, whether the function (2,14) satisfies the original, unregularized equation, which can be obtained from (2,4) by omitting the factor $M^4 [R'(\cos \Phi' - \sin \Phi') + M^2]^{-2}$. Because of (2,11) it is obvious that

$$\lim_{M \rightarrow \infty} T_{2S}^{\pm(k)}(M) = 0. \quad (2,15)$$

Taking into account (2,13) one gets

$$\lim_{M \rightarrow \infty} T_S^{\pm(k)}(R\Phi, M) = \lim_{M \rightarrow \infty} t_r^{\pm(k)}(R\Phi, M). \quad (2,16)$$

Thus the solution obtained with the peratization method is $S_S^{\pm}(R\Phi) = \lim_{k \rightarrow \infty} t_r^{\pm(k)}(R\Phi, \infty)$ which satisfies the equation

$$S_S^{\pm}(R\Phi) = \frac{-3ig^2}{R(\cos \Phi - \sin \Phi) + m^2} \cdot \frac{\operatorname{ctg}^{1/4} \Phi}{\sqrt{\cos \Phi - \sin \Phi}} \pm \\ \pm k_1 \int_0^\infty \int_0^{\pi/2} K_m^{(S)}(R\Phi R' \Phi') S_S^{\pm}(R' \Phi') d\Phi' dR', \quad (2,17)$$

since S_S^{\pm} is the limit of the convergent Neumann series of this equation. By making use of (2,7) and (2,3) the corresponding integral equation in the four-momentum space is

$$S^{\pm}(p) = \frac{-3ig^2}{p^2 + m^2} \pm \frac{12ig^2}{(2\pi)^4} \int \frac{S^{\pm}(p') d^4 p'}{[(p - p')^2 + m^2] p'^2}, \quad (2,18)$$

where the relation between S^{\pm} and S_S^{\pm} is similar to that for T^{\pm} and T_S^{\pm} as given by (2,3):

$$S^{\pm}(R\Phi) = \frac{\sqrt{\cos \Phi - \sin \Phi}}{\operatorname{ctg}^{1/4} \Phi} S_S^{\pm}(R\Phi). \quad (2,19)$$

This result agrees exactly with the conjecture of FP in [2]. The solution of (2,18) and so the zero energy amplitude can be obtained with iteration.

3. The unregularized equation for T^{\pm}

Now we turn to the unregularized equation (1,3). Originally we wanted to solve this equation for $T^{\pm}(p)$. Since we have now found that $S^{\pm}(p)$, the solution obtained with the regularization procedure, satisfies (2,18) we investigate whether $S^{\pm} = T^{\pm}$. This can be true only if

$$0 = \frac{-ig^2}{m^2} \pm \frac{4ig^2}{m^2(2\pi)^4} \int \frac{S^\pm(p')}{p'^2} d^4 p',$$

this means if

$$\pm 4\pi^2 = \int \frac{S^\pm(p')}{p'^2} d^4 p' \quad (3,1)$$

is satisfied.

Before examining whether (3,1) is satisfied we show that (2,18) and (3,1) follow directly from the unregularized eq. (1,3). This means: 1. with the procedure discussed in Sec. 2 one gets the solution of the unregularized equation; 2. it is possible to get the same result without the regularization. Let us consider the integral equation:

$$\psi(x) = (\varphi(x) + \gamma)\chi(x) + \lambda \int_0^\infty [\Sigma(xx') + \chi(x)\sigma(x')] \psi(x') dx', \quad (3,2)$$

where φ and Σ are square integrable functions of their variables, $\chi(x)$ is bounded and $\int_0^\infty \chi(x')\sigma(x')dx'$ is divergent. (For the sake of simplicity let us suppose $\Sigma(xx') \rightarrow 0$ and $\chi(x')\sigma(x') \rightarrow \sigma_\infty \neq 0$ if $x' \rightarrow \infty$.) It is clear from (3,2) that the solution is of the form

$$\psi(x) = (\psi_1(x) + \psi_0)\chi(x), \quad (3,3)$$

where ψ_0 does not depend on x . Thus the integral on the right-hand side of (3,2) can exist only if $\psi_0 = 0$. (If the integral does not exist the equation has no meaning at all.) In this way (3,2) can be decomposed into two equations:

$$\begin{aligned} \psi(x) &= \varphi(x)\chi(x) + \lambda \int_0^\infty \Sigma(xx')\psi(x')dx', \\ 0 &= \gamma + \lambda \int_0^\infty \sigma(x')\psi(x')dx'. \end{aligned} \quad (3,4)$$

Let us apply now this decomposition to eq. (1,3). The two equations corresponding to (3,4) are (2,18) and (3,1). This is easily seen when writing the equations in the new variables introduced in (2,2). One gets the unregularized equation by omitting the factor $M^4 [R'(\cos \Phi' - \sin \Phi') + M^2]^{-2}$ from (2,4). Thus the correspondence between the functions in (3,2) and the functions in the unregularized equation is the following:

$$\begin{aligned} \varphi &\rightarrow \frac{-3ig^2}{R(\cos \Phi - \sin \Phi) + m^2 - i\varepsilon}; & \gamma &\rightarrow \frac{-ig^2}{m^2}; \\ \chi &\rightarrow \frac{\operatorname{ctg}^{1/4} \Phi}{\sqrt{\cos \Phi - \sin \Phi - i\varepsilon}}; & \Sigma &\rightarrow K_m^{(S)}(R\Phi R'\Phi'); \\ \sigma &\rightarrow -\frac{8}{3m^2} \frac{\operatorname{ctg}^{1/4} \Phi}{\sqrt{\cos \Phi' - \sin \Phi' - i\varepsilon}}; & \lambda &\rightarrow \pm k_1. \end{aligned}$$

Writing the equations in the old variables one gets (2,18) and (3,1).

The remaining problem is the proof of (3,1). The direct proof seems to be rather difficult. Writing the equation in the new variables one obtains a complicated equation:

$$\pm 2\pi^3 = \int_0^\infty \int_0^{\pi/2} \frac{T^\pm(R'\Phi') d\Phi' dR'}{(\cos\Phi' - \sin\Phi') \sqrt{\operatorname{tg}\Phi'}} . \quad (3,5)$$

The problem becomes simpler when one supposes that the path of integration in the complex p'_0 plane may be rotated so as to coincide with the imaginary axis. The proof of (3,1) on this assumption is outlined in the Appendix.

4. Conclusion

In the case of zero incoming momenta it is possible to sum up the higher order ladder graphs with the aid of the Bethe—Salpeter equation. Solving this equation one does not need to regularize or make a cut off, since the eq. (1,3) reduces to (2,18) which has an iterative solution if g^2 is small enough. The iteration becomes possible because only a part of the boson propagator appears in (2,18). One may say, that in this case the “divergent” part of the propagator does not give any interaction in the ladder approximation.

It would be very interesting to investigate the case of non-vanishing incoming momenta. In this case the problem is much more complicated, however, the summation of the most divergent parts of the graphs leads to an equation similar to (1,1) [1].

Concerning the peratization method we have found the following results.
 1. The method leads to the correct result in the case of the equation for $T^\pm(p)$.
 2. This equation can be solved also without this method. It is another question, whether generally peratization gives the correct answer. The method (as a mathematical one) seems to be general enough. PAIS et al. [3—4] have utilized it for instance in the scattering theory of singular potentials. There also the correct solutions are obtained which seems to show that the method is mathematically exact.

The author would like to thank Prof. K. NAGY and Dr. G. PÓCSIK for stimulating discussions.

Appendix

The integration path in (1,3) can be rotated in the complex p'_0 plane so as to fall on the imaginary axis if the functions $T^\pm(p')$ have suitable analytical properties. In this case one can perform the integration over the angular variables in an Euclidian $p'_1 p'_2 p'_3 p'_4$ space. This reduces the mathematical difficulties. For example also the proof of the convergence becomes simpler.

Now we prove (3,1) assuming these analytical properties of T^\pm . The unregularized integral equation becomes after the angular integration

$$T^\pm(s) = \frac{-ig^2}{m^2} - \frac{3ig^2}{s+m^2} \pm \frac{g^2}{4m^2\pi^2} \int_0^\infty T^\pm(s') \{1+3m^2 K_m(ss')\} ds'. \quad (\text{A},1)$$

Here the following notations were introduced:

$$s = p^2 \quad ; \quad s' = p'^2; \\ K_m(ss') = \frac{s+s'+m^2}{2ss'} \left\{ 1 - \sqrt{1 - \frac{4ss'}{(s+s'+m^2)^2}} \right\}. \quad (\text{A},2)$$

First of all one notes the asymptotic form of the kernel:

$$K_m(ss') \simeq \begin{cases} \frac{1}{s} & \text{if } s > s' \\ & \text{and } s \text{ or } s' \gg m^2. \\ \frac{1}{s'} & \text{if } s' > s \end{cases} \quad (\text{A},3)$$

The functions $-3ig^2(s+m^2)^{-1}$ and $K_m(ss')$ are square integrable, so eq. (A,1) is of the type (3,2). Here the corresponding functions are

$$\varphi \rightarrow \frac{-3ig^2}{s+m^2}; \quad \gamma \rightarrow \frac{-ig^2}{m^2}; \quad \chi \rightarrow 1; \\ \Sigma \rightarrow K_m(ss'); \quad \sigma \rightarrow \frac{1}{3m^2}; \quad \lambda \rightarrow \pm \frac{3g^2}{4\pi^2}. \quad (\text{A},4)$$

Thus eq. (A,1) can be split (like (3,2) into (3,4)) into the equations:

$$T^\pm(s) = \frac{-3ig^2}{s+m^2} \pm \frac{3g^2}{4\pi^2} \int_0^\infty K_m(ss') T^\pm(s') ds' \quad (\text{A},5a)$$

and

$$\int_0^\infty T^\pm(s') ds' = \pm 4\pi^2 i. \quad (\text{A},5b)$$

For the proof of (A,5b) it is useful to examine first the asymptotic behaviour of $T^\pm(s)$. If $s \gg m^2$ we have from (A,3)

$$T^\pm(s) \simeq \frac{-3ig^2}{s+m^2} \pm \frac{3g^2}{4\pi^2} \left[\frac{1}{s} \int_0^s T^\pm(s') ds' + \int_s^\infty \frac{T^\pm(s')}{s'} ds' \right]. \quad (\text{A},6)$$

Supposing now $\int_0^\infty T^\pm(s')ds' < \infty$ it is possible to prove (A,5b). Because of (A,6) we can write

$$T^\pm(s) \simeq \frac{1}{s} \left\{ -3ig^2 \pm \frac{3g^2}{4\pi^2} \int_0^\infty T^\pm(s')ds' \right\} + o\left(\frac{1}{s^2}\right). \quad (\text{A},7)$$

Here the coefficient of the s^{-1} term vanishes if $\int_0^\infty T^\pm(s')ds'$ exists. This means that (A,5b) holds. The existence of $\int_0^\infty T^\pm(s')ds'$ follows from the asymptotic differential equation

$$T''^\pm(s) + \frac{2}{s} T'^\pm(s) \pm \frac{3g^2}{4\pi^2 s^2} T^\pm(s) \simeq \frac{6ig^2 m^2}{s^4} \quad (\text{A},8)$$

obtained from (A,6). The solution of this equation is of the form

$$T^\pm(s) \simeq a_1^\pm s^{k_1^\pm} + a_2^\pm s^{k_2^\pm} + \frac{6g^2 im^2}{s^2 \left(2 \pm \frac{3g^2}{4\pi^2}\right)}, \quad (\text{A},9)$$

where

$$k_1^\pm = \frac{1}{2} \left(-1 + \sqrt{1 \mp \frac{3g^2}{4\pi^2}} \right)$$

and

$$k_2^\pm = \frac{1}{2} \left(-1 - \sqrt{1 \mp \frac{3g^2}{4\pi^2}} \right).$$

If the constants a_1^\pm, a_2^\pm are chosen in (A,9) in a way which guarantees that also (A,6) is satisfied, the existence of $\int_0^\infty T^\pm(s')ds'$ can be easily shown. This completes the proof of (A,5b).

REFERENCES

1. G. FEINBERG and A. PAIS (referred to in the present paper as FP), Phys. Rev., **131**, 2724, 1963.
2. G. FEINBERG and A. PAIS, Phys., Rev., **133B**, 477, 1964.
3. N. N. KHURI and A. PAIS, Rev. Mod. Phys., **36**, 590, 1964.
4. T. T. WU and A. PAIS, J. Math. Phys., **5**, 799, 1964.

О СХОДИМОСТИ ПЕРАТИЗАЦИОННОГО МЕТОДА

И. МОНТВАЙ

Р е з и о м е

В последнее время Г. Фейнбергом и А. Пайсом был найден метод для решения интегрального уравнения, суммирующего лестничную диаграмму в теории слабого взаимодействия. В данной работе показывается сходимость упомянутого метода в случае нулевого входного момента и исследуется связь между регулированным и нерегулированным уравнениями. Оказывается возможным получить результаты регулированного процесса непосредственно из оригинального, нерегулированного уравнения.

THEORETICAL INTERPRETATION OF SOME PROPERTIES OF THE PERIODIC SYSTEM BY THE THOMAS—FERMI MODEL

By

A. KÓNYA

RESEARCH GROUP FOR THEORETICAL PHYSICS, HUNGARIAN ACADEMY OF SCIENCES, BUDAPEST

(Received 1. VIII. 1964)

By means of quantities defined in the statistical theory of atoms as analogous quantities to the quantum numbers of wave mechanics [7] several problems of the atomic shell structure are dealt with: the maximal principal quantum number and the first appearance of the principal quantum numbers in the periodic system of the elements, the completion of the electron shells and the anomalous sequence of the electronic states with higher angular quantum numbers. The THOMAS—FERMI model gives a theoretical description for all these characteristic properties of the atomic structure, averaging the discontinuous changes in the periodic system of the elements.

I. Introduction

FERMI was the first to apply the THOMAS—FERMI (TF) atom to the theoretical interpretation of the anomalous filling of the one-electron quantum levels in the periodic system of the elements [1]. Since that time his method has been investigated by several authors [2—6]. The main problem discussed here is in what order the “quantum states” defined in this model are occupied by the electrons.

In [1] the following interpretation of the angular quantum number was given by FERMI for the TF atom. If we treat the electrons in each volume element dv of the atom as totally free, then these electrons are fully characterized by their momentum vector \bar{p} having absolute values from zero to

$$P(r) = (3\pi^2)^{1/3} \hbar \varrho^{1/3}(r), \quad (1)$$

the radius of the Fermi sphere ($\varrho(r)$ denotes the electronic charge density). The angular momentum of an electron with the momentum \bar{p} has the absolute value

$$M = rp_{\perp}, \quad (2)$$

where p_{\perp} is the azimuthal component of \bar{p} . The maximal angular momentum occurring in dv is then

$$M_{\max} = rP(r). \quad (3)$$

The definition given by FERMI for the quantity k^* corresponding to the azimuthal quantum number k of quantum mechanics is now

$$k^* = \frac{1}{\hbar} M. \quad (4)$$

He considered the electrons with

$$l \leq k^* \leq l + 1 \quad (5)$$

as the electrons with the angular quantum number l , commonly characterized by the quantity

$$k^* = l + \frac{1}{2}. \quad (6)$$

As was shown by A. KÓNYA in an earlier publication [7] the quantity

$$n_r^* = \frac{1}{\pi \hbar} \int_{r_1}^{r_2} \left[2 m e_0 V(r) + 2 m E - \frac{M^2}{r^2} \right]^{1/2} dr \quad (7)$$

and

$$n^* = n_r^* + k^* \quad (8)$$

can also be defined using the BOHR—SOMMERFELD quantization conditions.

In (7) E denotes the energy of the electron

$$E = \frac{p^2}{2m} - e_0 V(r), \quad (9)$$

e_0 is the elementary charge and $V(r)$ is the electrostatic potential due to the nucleus and to the electronic charge around the nucleus. The integral must be extended to the interval where the integrand is positive.

The quantity n_r^* corresponds to the radial quantum number if we introduce half integer quantum numbers

$$n_r^* = n_r + \frac{1}{2}. \quad (10)$$

From (8), (6) and (10) it follows that

$$n^* = n_r + l + 1, \quad (11)$$

which means that the quantity n^* corresponds to the principal quantum number and that the integer values of n^* correspond to the discrete values of the principal quantum number.

The TF model is chosen here as the basic model. In this case one can use the variables introduced by FERMI

$$x = \frac{r}{\mu}, \quad \mu = \frac{1}{4} \left(\frac{9\pi^2}{2Z} \right)^{1/3} a_0, \quad a_0 = \frac{\hbar^2}{me_0^2}, \quad (12)$$

$$\varphi(x) = \frac{\mu x}{Ze_0} \cdot V(x). \quad (13)$$

Substituting these variables into (7) and using the relations (8) and (4) we obtain the following expression for the quantity n^* :

$$n^* = \left(\frac{3}{4\pi^2} \right)^{1/3} Z^{1/3} [\Phi(a, \beta) + \pi a], \quad (14)$$

where

$$a = \frac{k^*}{\left(\frac{3\pi}{4} \right)^{1/3} Z^{1/3}}, \quad (15)$$

$$\beta = -\frac{(6\pi)^{2/3}}{8Z^{4/3}} \frac{a_0}{e_0^2} E \quad (16)$$

and

$$\Phi(a, \beta) = \int_{x_1}^{x_2} [x\varphi(x) - \beta x^2 - a^2]^{1/2} \frac{dx}{x}. \quad (17)$$

The interval of integration in (17) is limited by the zeros x_1 and x_2 of the function under the square root. The numerical values of the function $\Phi(a, \beta)$ are given in [7] in Tables 1 and 2.

The results briefly summarized here enable a more detailed investigation of the properties of the periodic system to be made than that of FERMI using the angular quantum number only. In the following we determine the maximal principal quantum number of the atoms in their ground states (Section 2), the first appearance of the principal quantum numbers (Section 3), the completion of the electron shells (Section 4) and the appearance of the states with different angular and principal quantum numbers (Section 5).

The most striking phenomenon in the periodic system is that the states with higher angular quantum numbers are occupied later as may be supposed on the basis of the energy sequence of the hydrogenic terms. It will be shown that this anomaly may be described by the ratio of the maximal angular quantum number to the maximal principal quantum number and that the value of this ratio for the TF model lies very near to that for the wave mechanical shell model (Section 6).

2. The maximal principal quantum number of the atoms

From (14) we obtain directly the maximal value of the quantity n^* for the TF atom with the atomic number Z

$$n_{\max}^* = \left(\frac{3}{4\pi^2} \right)^{1/3} Z^{1/3} [\Phi(a, \beta) + \pi a]_{\max}. \quad (18)$$

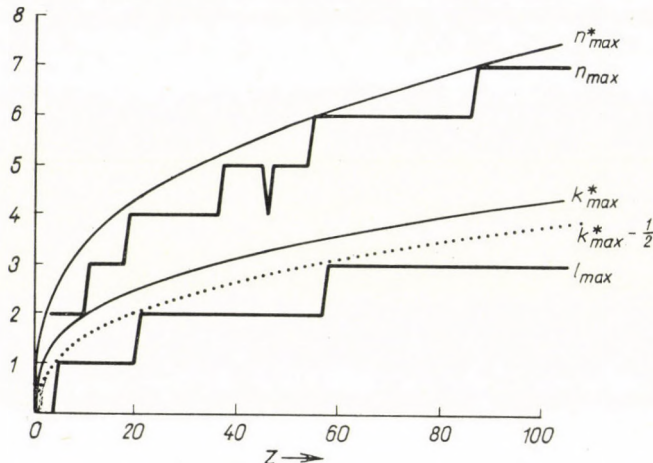


Fig. 1. The maximal principal quantum number n_{\max} and the maximal angular quantum number l_{\max} of the atoms in the ground state as functions of the atomic number Z

By numerical interpolation from Tables 1 and 2 given in [7] we obtain

$$[\Phi(a, \beta) + \pi a]_{\max} = 3.76 \quad (19)$$

and this maximum belongs to the parametric values

$$a = 0.067 \quad \text{and} \quad \beta = 0. \quad (20)$$

From (18) then follows

$$n_{\max}^* = 1.59 Z^{1/3}. \quad (21)$$

This relation is graphically shown by the upper smooth curve in Fig. 1 together with the values of n_{\max} taken from the BOHR-STONER table of electron configurations. The result may be considered as a good approximation. It is characteristic that the TF atom has, in general, somewhat greater n_{\max}^* values than the wave mechanical shell atom, but the difference decreases with increasing atomic number.

From the value of the parameter α under (20) we reach the following interesting conclusion. According to (15) and (4) the state specified by n_{\max}^* has the angular momentum $M < \hbar$ if $Z < 1000$. On the basis of (5) this means that the electrons begin to occupy first the s -states of a new shell — in full agreement with the BOHR—STONER table.

The result (21) for the principal quantum number may be compared with that for the angular quantum number. As SOMMERFELD [8] and IVANENKO and LARIN [4] have shown, the maximal value of the angular momentum in an atom, as can be seen from (3), is

$$M_{\max}^{(Z)} = [rP(r)]_{\max} = \left(\frac{3\pi}{4}\right)^{1/3} Z^{1/3} [x\varphi(x)]_{\max}. \quad (22)$$

From numerical tables for the function $\varphi(x)$ it follows [9] that

$$[x\varphi(x)]_{\max} = 0,70. \quad (23)$$

So, from (4), we obtain

$$k_{\max}^* = 0,93Z^{1/3}. \quad (24)$$

This relation is graphically shown by the lower smooth curve in Fig. 1 together with the values of l_{\max} taken from the BOHR—STONER table.

A correspondence between the quantities k_{\max}^* and l_{\max} may be obtained, as follows from (6), by reducing the values of k_{\max}^* by the constant $1/2$. These reduced values are graphically shown by the curve with dotted line in Fig. 1. So one has an approximation of the same character as obtained above for the principal quantum number.

3. First appearance of the principal quantum numbers

FERMI has given a theoretical calculation of the atomic numbers Z_l at which a state with an angular quantum number l first appears [1]. SOMMERFELD [8] gave the relation

$$Z_l = 1,25 \left(l + \frac{1}{2}\right)^3, \quad l = 0, 1, 2, 3 \quad (25)$$

easily obtainable from (24) and (6).

Having the expression (21) for the maximal principal quantum number we can calculate similarly the atomic numbers Z_n at which a state with the principal quantum number n first appears. From relations (21) and (11) we get

$$Z_n = 0,25 n^3. \quad (26)$$

(As follows from the continuous change of n^* in the statistical theory of atoms, the results obtained for Z_n must be treated as lower limits of the empirical data).

In Table 1 the results rounded up to the next integer numbers are compared with the Z_n values taken from the BOHR-STONER table.

If the states were occupied by the electrons all over the periodic system of the elements without any anomaly, that is in the sequence of the hydrogenic terms, the values of Z_n should be 1, 3, 11, 29, 61, 111, 183 and 281 for the values of n given in Table 1. As we can see, the Z_n values obtained from (26) approximate the values taken from the BOHR-STONER table and not those of the shell model without anomaly.

We get more detailed information if we compare the values of Z_n and Z_l also given in Table 1.

A d -state (the $3d$ -state) appears in the TF model first if $Z_l = 20$. At this atomic number the electrons have already begun to occupy the shell with the principal quantum number $n = 4$, too, since the value Z_n for $n = 4$ is 16. Similarly we found that at the first appearance of the state $4f(l = 3)$ at $Z_3 = 54$ there are electrons already in states with $n = 5$ and $n = 6$, that is in the O- and P-shells too. Further the electrons in the TF model begin to occupy the shells with $n = 6$ and $n = 7$ before the first appearance of a $5g$ -state.

All these statements are in accordance with the table of electron configurations.

4. Completed shells

The completion of a shell in the statistical theory of atoms may be described as follows.

For a given value of the quantity n^* the other quantum variable k^* may have the values

Table 1

First appearance of the principal and angular quantum numbers

Shell	n	Z_n		Sub-shell	l	Z_l	
		(26)	BOHR-STONER table			(25)	BOHR-STONER table
<i>K</i>	1	1	1	<i>s</i>	0	1	1
<i>L</i>	2	2	3	<i>p</i>	1	5	5
<i>M</i>	3	7	11	<i>d</i>	2	20	21
<i>N</i>	4	16	19	<i>f</i>	3	54	58
<i>O</i>	5	32	37	<i>g</i>	4	114	—
<i>P</i>	6	54	55				
<i>Q</i>	7	86	87				
<i>R</i>	8	128	—				

$$0 \leq k^* \leq n^* \quad (27)$$

as is shown by (8). At the first appearance of the quantum number n^* the value of k^* is given by (20) and (15):

$$k^* = 0,067 \left(\frac{3\pi}{4} \right)^{1/3} Z^{1/3}. \quad (28)$$

With increasing Z the quantity k^* increases from this value to its maximal value $l^* = n^*$. The states characterized by n^* may be treated as com-

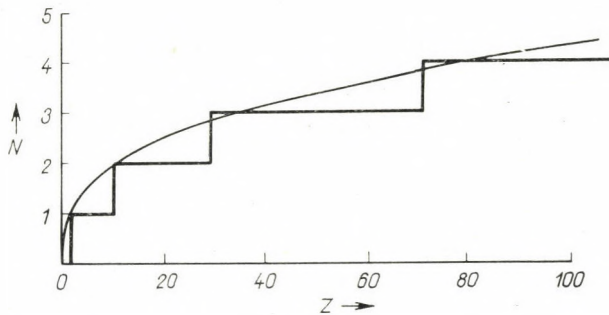


Fig. 2. The principal quantum number N of the outer completed shell of the atoms as a function of the atomic number Z

pletely filled by electrons at the atomic number Z at which k^* attains its maximal value $k^* = n^*$.

If in the TF atom with the atomic number Z the outer completed shell has the principal quantum number N , then the state with the maximal k^* value in this shell is the maximal k^* value in the whole atom. This means that the shell characterized by N is completely filled by electrons, if $N = k_{\max}^*$, where k_{\max}^* is given by (24):

$$N = 0,93Z^{1/3}. \quad (29)$$

So the expression (24) without the reduction by $1/2$ has the following direct physical meaning: it gives the principal quantum number of the outer completed shell in the TF atom as a function of the atomic number.

The result (29) is shown graphically in Fig. 2 compared with the empirical data taken from the BOHR-STONER table. Here, too, we have an approximation characteristic of the TF theory. The theoretical curve averages the discontinuous changes in the periodic system of the elements.

5. The filling of the states in the shells

In the definition of n^* in (8) the parameter a contains the quantity k^* as can be seen from (14) and (15). So formula (14) distinguishes among electrons with the same angular quantum number according to their energy value E .

The commonly occurring two quantities n^* and k^* in (14) make it possible to investigate more detailed properties in the periodic system, determined by the simultaneous occurrence of the two quantum numbers n and l .

Here we wish to discuss the problem of what are the maximal principal quantum numbers N_l of the shells having occupied s -, p -, d -, and f -states.

The discontinuous curves in Fig. 3a und 3b show graphically the empirical data N_l taken from the table of electron configurations for the cases $l = 0, 1, 2$ and 3 .

The quantities N_l^* corresponding to the quantum numbers N_l as functions of the atomic number Z may be calculated in the TF model as follows:

Corresponding to (15) and (6) the value of the parameter a must be chosen as

$$a_{l+\frac{1}{2}} = \frac{l + \frac{1}{2}}{\left(\frac{3\pi}{4}\right)^{1/3} Z^{1/3}}, \quad l = 0, 1, 2, 3. \quad (30)$$

For given values of l the maximum of the quantity n^* is, according to (14),

$$N_l^* = \left(\frac{3}{4\pi^2}\right)^{1/3} Z^{1/3} [\Phi(a_{l+\frac{1}{2}}, \beta) + \pi a_{l+\frac{1}{2}}]_{\max}. \quad (31)$$

The integral $\Phi(a, \beta)$ as shown by Table 1 in [7], is a monotonically decreasing function of the parameter β for $a = \text{const}$, form which we obtain

$$N_l^* = \left(\frac{3}{4\pi^2}\right)^{1/3} Z^{1/3} [\Phi(a_{l+\frac{1}{2}}, 0) + \pi a_{l+\frac{1}{2}}]. \quad (32)$$

This relation may be evaluated easily for any Z and l values with the aid of the Table 2 in [7].

The results are shown by the continuous curves in Fig. 3a and 3b. The approximation here is also of the type usual in the TF theory. The theoretical curves describe the general behaviour of the empirical curves, but they do not account for the abrupt changes.

6. The anomaly in the periodic system of the elements

The theoretical discussions given above allow us to conclude, in accordance with the earlier results of FERMI [1], that the TF model is able to describe

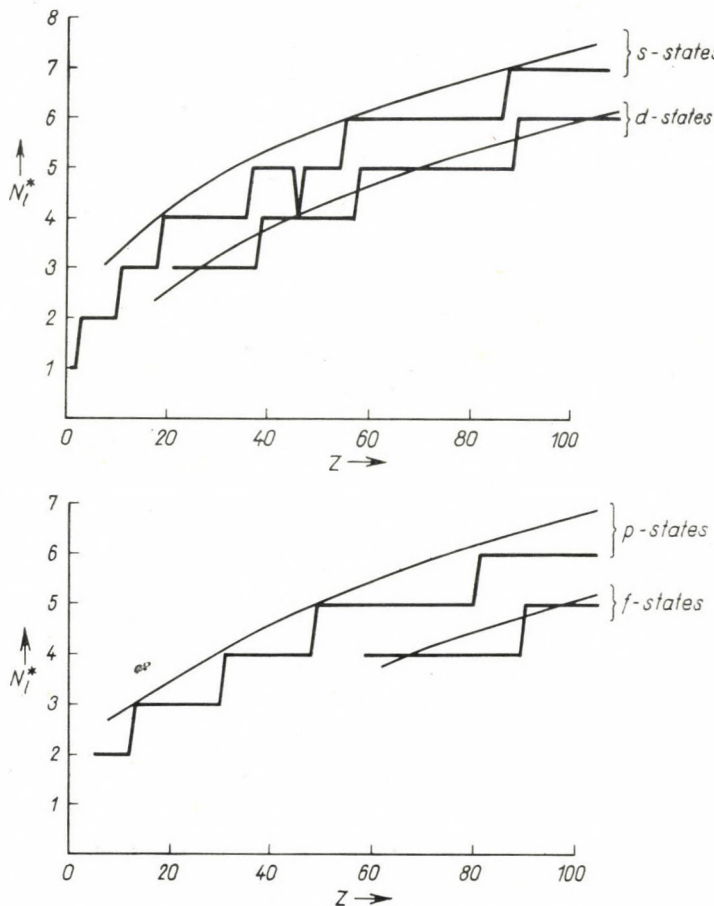


Fig. 3a and 3b. The maximal principal quantum numbers N_l having occupied l -states as functions of the atomic number Z

approximately the anomalous sequence in the filling of the electronic states with higher angular quantum numbers.

Here we want to prove this characteristic behaviour of the TF atom in a direct and very simple manner.

Let us investigate the ratio of the maximal angular and principal quantum numbers of the atoms. The values of this quotient, determined from the BOHR-STONER table, are shown in Fig. 4 as a function of the atomic number Z . This function has values between 0 and $1/2$ and for large Z it approaches

the limit 1/2. This specific property is caused by the anomalous order of filling the electronic levels.

In an atomic shell model with regular filling (i.e. occurring in the sequence of the hydrogenic terms) the maximal angular quantum number l_{\max} would be equal to $n_{\max} - 1$ for the atoms with completed shells. Consequently in this case the ratio l_{\max}/n_{\max} tends to unity as the atomic number Z increases.

In the case of the anomalous filling of the quantum states, as was shown in [6], only the value $l_{\max} = [n_{\max}/2]$ belongs to n_{\max} , $[n_{\max}/2]$ denoting the integer part of the fraction. Thus in the wave mechanical shell atom with

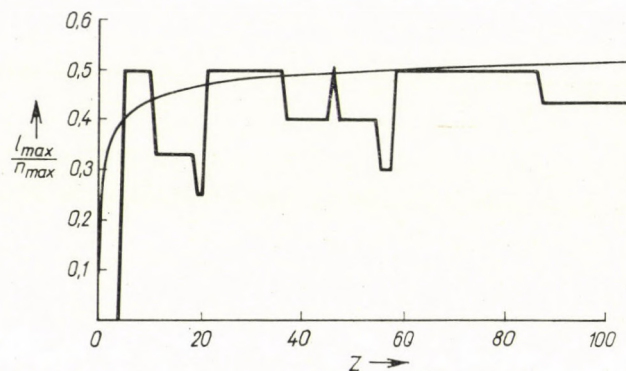


Fig. 4. The ratio of the maximal angular quantum number to the maximal principal quantum number in the atoms as a function of the atomic number Z

anomaly l_{\max}/n_{\max} tends to 1/2, in accordance with the periodic system of the elements.

For the TF atom with Z electrons the ratio of the two maximal quantum numbers is, according to (24), (6) and (21),

$$l_{\max}/n_{\max} = 0.58 - 0.31Z^{-1/3} \quad (33)$$

with the limiting value 0.58 for $Z \rightarrow \infty$.

This ratio lies very near to that of the shell model with anomaly, indicating the tendency of the electrons in the TF atom to favour the states with lower angular momentum. Fig. 4 shows that in some intervals of Z the approximation given by the TF atom is even better as in the limit for large Z . This is why the TF atom is able to represent the characteristic anomaly in the periodic system of the elements with a good approximation.

REFERENCES

1. E. FERMI, Z. Physik, **48**, 73, 1928; Nature, **121**, 502, 1928.
2. J. H. D. JENSEN and J. M. LUTTINGER, Phys. Rev., **86**, 907, 1952.
3. W. R. THEIS, Z. Physik, **140**, 1, 1955.

4. D. D. IVANENKO and S. I. LARIN, D. A. A. N., **88**, 45, 1953;
S. I. LARIN, J. E. T. F., **28**, 498, 1955.
5. T. A. OLIPHANT, jr., Phys. Rev., **104**, 954, 1956.
6. A. KÓNYA, Acta Phys. Hung., **13**, 219, 1961.
7. A. KÓNYA, Acta Phys. Hung., **18**, 39, 1964.
8. A. SOMMERFELD, Atombau und Spektrallinien, 2. Auflage, Bd. II. S. 690—703. F. Vieweg u. Sohn, Braunschweig, 1951.
9. P. GOMBÁS, Statistische Behandlung des Atoms, Hb. d. Phys. Bd. XXXVI, Springer, Berlin—Göttingen—Heidelberg, SS. 124 u. 127.

ТЕОРЕТИЧЕСКАЯ ИНТЕРПРЕТАЦИЯ НЕКОТОРЫХ СВОЙСТВ ПЕРИОДИЧЕСКОЙ СИСТЕМЫ ЭЛЕМЕНТОВ МОДЕЛЬЮ ТОМАСА—ФЕРМИ

А. КОНЬЯ

Р е з ю м е

С помощью некоторых величин, определённых в статистической теории атома как аналоги квантовым числам волновой механики [7], рассматриваются некоторые проблемы оболочечной структуры атома: максимальное главное квантовое число в периодической системе элементов, комплекtnость электронных оболочек и аномальный порядок заполнения электронных состояний с большим значением побочного квантового числа. Модель Томаса—Ферми даёт теоретическое описание всех этих характерных свойств атомной структуры, усредняя прерывисто меняющиеся свойства в периодической системе элементов.

COMMUNICATIONES BREVES

ELECTRON SCATTERING BY ATOMS
AND THE EXISTENCE OF NEGATIVE IONS

By

T. TIETZ

DEPARTMENT OF THEORETICAL PHYSICS, UNIVERSITY OF ŁÓDŹ ŁÓDŹ, POLAND

(Received 12. III. 1964)

It is well known that the study of the scattering of electrons by neutral atoms near zero energy is of great interest in connection with the physics of the upper atmosphere as well as in astrophysics. Since the energy of the scattered electrons is of the order of zero to 50 eV the Born approximation loses its validity. A convenient method for the calculation of the phase shifts is, in this case, the variational method. In order to find a suitable solution of the Schrödinger equation

$$\left[\frac{d^2}{dr^2} + k^2 - \frac{l(l+1)}{r^2} - 2V(r) \right] R_l(r) = 0 \quad (1)$$

we shall here apply the variational methods of HULTHÉN [1], KOHN [2] and MALIK [3]. In eq. (1) $k = 2E$, where E is the energy of the scattered electron. For in eq. (1) one may use the charge density as given by the HARTREE or HARTREE—FOCK wave functions for the bound electrons. This can be very well approximated by series of exponential functions as was done by HOLTS-MARK [4], RUARK [5] and BYATT [6] in the following way:

$$V(r) = -\frac{Z}{r} \sum_n A_n \exp(-\gamma_n r), \quad (2)$$

where A_n and γ_n are constants depending on the atomic number Z . Their numerical values can be found in the paper of BYATT [7]. Let L_l be equal to

$$L_l \equiv \int_0^\infty R_l(r) \left[\frac{d^2}{dr^2} - \frac{l(l+1)}{r^2} - 2V(r) + k^2 \right] R_l(r) dr \quad (3)$$

and let $R_l(r)$ have the following asymptotic forms:

$$\lim_{r \rightarrow \infty} R_l(r) \rightarrow \sin kr + (-1)^l a \cos kr, \quad (4)$$

$$\lim_{r \rightarrow 0} R_l(r) = 0.$$

In this case the variation of eq. (3) with respect to $R_l(r)$ gives

$$\delta L_l = -k\delta a \quad \text{or} \quad \delta(L_l + ka) = 0 . \quad (5)$$

In eqs. (4) and (5) $a = \tan \lambda_l$, where λ_l denotes the phase shift. For the study of the scattering of electrons by neutral atoms near zero energy it is enough to calculate the phase shift for $l = 0$. Hence we omit the index l from L , R and λ . According to HULTHÉN's method the phase shift λ can be calculated from the following relations:

$$L = 0 , \quad \partial L / \partial c_i = 0 , \quad i = 1, \dots, n \quad \text{and} \quad \lambda = \arctan a . \quad (6)$$

The KOHN method is given by

$$\left(\frac{\partial L}{\partial a} \right)_{a=a_K} = -k , \quad \partial L / \partial c_i = 0 \quad \text{and} \quad \lambda_K = \arctan (L_K/k + a_K) . \quad (7)$$

The subscript K refers to KOHN's method. In eqs. (6) and (7) c_1, \dots, c_n denote independent parameters in the trial function $R(r)$.

MALIK's method is given by

$$\int_0^\infty R^2 V(r) j_0(kr) dr = -ak , \quad \partial L / \partial c_i = 0 \quad \text{and} \quad \lambda_M = \arctan (a_M + L_M/k) , \quad (8)$$

where the subscript M refers to the MALIK method and $j_0(kr)$ denotes the spherical Bessel function which is regular at the origin. Denoting the Bessel functions by $j_\nu = (\pi kr/2)^{1/2} J_{\nu+\frac{1}{2}}(kr)$, where $\nu = 0, 1, 2, 3, 4, \dots$, we can fit $R(r)$ by

$$\begin{aligned} {}_1R_0(r) &= c_0(j_0 + j_2) + c_1(j_1 + j_3) + j_4 - aj_5 , \\ {}_2R_0(r) &= c_0(j_0 + j_2) + c_1(j_1 + j_3) + c_2(j_4 + j_6) + c_3(j_5 + j_7) + j_8 - aj_9 , \\ {}_3R_0(r) &= c_0(j_0 + j_2) + c_1(j_1 + j_3) + c_2(j_4 + j_6) + c_3(j_5 + j_7) + c_4(j_8 + j_{10}) + \\ &\quad + c_5(j_9 + j_{11}) + j_{12} - aj_{13} , \end{aligned} \quad (9)$$

where c_0, c_1, c_2, c_3, c_4 and c_5 are constants. The last equation shows that ${}_1R_0(r)$, ${}_2R_0(r)$ and ${}_3R_0(r)$ satisfy the same boundary conditions as $R(r)$ of eq. (4). The trial wave function ${}_1R_0(r)$ depends only on the two constants c_0 and c_1 and the trial wave function ${}_3R_0(r)$ depends on six constants c_i . Eq. (9) shows that it is possible to write the trial wave function in terms of the Bessel function j_ν , ν depending on the number of constants c_i . To obtain an expression for the phase shifts λ we substitute ${}_1R_0(r)$ into eq. (3), in this special case we have

$$L = c_0^2 A + c_1^2 B + a^2 C + c_0 c_1 D + c_0 a E + c_1 a F + c_0 G + c_1 H + a I + J, \quad (10)$$

where the constants A, B, C, \dots, J are given by

$$\begin{aligned} A &= -\frac{3\pi k}{5} - 2 \int_0^\infty V(r) [j_0(r) + j_2(r)]^2 dr, \\ B &= \frac{25\pi k}{21} - 2 \int_0^\infty V(r) [j_1(r) + j_3(r)]^2 dr, \\ C &= \frac{15\pi k}{11} - 2 \int_0^\infty V(r) j_5^2(r) dr, \\ D &= 5k - 4 \int_0^\infty V(r) [j_1(r) + j_3(r)] [j_0(r) + j_2(r)] dr, \\ E &= \frac{k}{2} + 4 \int_0^\infty V(r) [j_0(r) + j_2(r)] j_5(r) dr, \\ F &= 4 \int_0^\infty V(r) [j_1(r) + j_3(r)] j_5(r) dr, \\ G &= -4 \int_0^\infty V(r) [j_0(r) + j_2(r)] j_4(r) dr, \\ H &= \frac{25k}{9} - 4 \int_0^\infty V(r) [j_1(r) + j_3(r)] j_4(r) dr, \\ I &= -5k + 4 \int_0^\infty V(r) j_5(r) j_4(r) dr. \\ J &= \frac{10\pi k}{9} - 2 \int_0^\infty V(r) j_4^2(r) dr. \end{aligned} \quad (11)$$

The last formula for A, B, \dots, J has been calculated by the aid of the integrals

$$\int_0^\infty J_p(ax) J_q(ax) \frac{dx}{x} = \frac{2}{\pi} \frac{\left[\frac{p-q}{2} \pi \right]}{p^2 - q^2}, \quad \operatorname{Re}(p+q) > 0, \quad a > 0 \quad (12)$$

$$\int_0^\infty J_p(ax) J_p(ax) \frac{dx}{x} = \frac{1}{2p},$$

as also by the help of the differential equation for the $j_\nu(r)$. Since the scattering potential $V(r)$ is a continuous function of r and

$$\int_0^1 r |V(r)| dr + \int_1^\infty r^2 |V(r)| dr < \infty, \quad (13)$$

the phase shift λ ($k = 0$) of zero energy scattering is related to the number of eigenvalues m as follows [8]: $\lambda(k = 0) = m\pi$. From the study of the behaviour of the phase shift λ near zero energy one can get information on the number of bound states m and say whether the existence [9] of negative ions is possible or not. In the Table we have listed some numerical results for λ_H and λ_K for a neutral carbon atom.

Table

The phase shift of low energy electrons scattered by neutral carbon

k^2	λ_H	λ_K
0,005	2,82	2,82
0,01	2,69	2,69
0,1	1,96	1,96
1,0	0,91	0,91

From the Table we see that the zero-energy phase shift confirms the existence of the already established C⁻-ion. If we put $R(r) = {}_2R_0(r)$ or $R(r) = {}_3R_0$ in the expression for L (eq. (3)) and $l = 0$ we obtain more accurate results. Our trial wave functions given by eq. (9) have the following convenient property for practical calculations. The constants A, B, C, \dots are independent of the variational parameters c_i and a and further they can be obtained analytically by simple integrations of the potential given by eq. (2).

REFERENCES

1. L. HULTHÉN, K. Fys. Sällsk. Lund Förk, 14, Nr. 21, 1944.
2. W. KOHN, Phys. Rev., **74**, 1763, 1948.
3. F. B. MALIK, Zs. Naturforschg., **14a**, 172, 1959.
4. J. HOLTSMARK, Zs. Phys., **66**, 49, 1930.
5. A. E. RUARK, Phys. Rev., **57**, 62, 1940.
6. W. O. BYATT, Phys. Rev., **104**, 1298, 1956.
7. see ref. [6].
8. N. LEVINSON, Kgl. Danske Videnskab. Selskab. Mat. Fys. Medd. **25**, No. 1949.
9. T. TIETZ, J. Chem. Phys., **38**, 102, 1963;
F. B. MALIK and A. TREFFTZ, Zs. Naturforschg., **16**, 492, 1961.

CONTRIBUTION TO THE PROBLEM OF THE ENTROPY INCREASE OF QUANTUM MECHANICAL MANY-BODY SYSTEMS

By

J. I. HORVÁTH

INSTITUTE OF THEORETICAL PHYSICS, JÓZSEF ATTILA UNIVERSITY, SZEGED

(Received 20. IV. 1964)

One of the fundamental problems in the statistical mechanics of irreversible processes is to understand why and in what way many-particle systems approach equilibrium. As is well known, the main point of this problem becomes clear, when we try to reconcile the irreversible behaviour of macroscopic systems with the reversibility of the underlying microscopic equations of motion. In the last few years several authors [1—4] have dealt with this problem and reasonable progress has been made.

The usual approach to these problems is based on GIBBS' idea of the fine-grained and coarse-grained statistical ensembles which can be translated into the language of quantum statistical mechanics in terms of the fine-grained and coarse-grained density operators corresponding to von NEUMANN's micro- and macro-observables. We should like to emphasize that the concept of the micro- and macro-observables — at least as this was used especially by N. G. VAN KAMPEN [5] — can be based on the objective properties of the measuring apparatus. In fact, this means that the distinction between these two kinds of operators — or rather between the two kinds of complete sets of commutable physical quantities characterizing the system under consideration — leads to an adequate description of reality.

The time evolution of the fine-grained statistical ensemble is described by von NEUMANN's equation of motion of the fine-grained density operator

$$i\hbar \dot{\varrho} = [\mathbf{H}, \varrho], \quad (1)$$

(where \mathbf{H} means the Hamiltonian of the system) which can be derived from the reversible SCHRÖDINGER equation. The solution of eq. (1) is obtained in the form

$$\varrho(t) = \mathbf{U}(-t) \varrho(0) \mathbf{U}(t), \quad (2)$$

where the unitary operator

$$\mathbf{U}(t) = \exp \left\{ \frac{i}{\hbar} \mathbf{H} t \right\} \quad (3)$$

determines a reversible time evolution. This means that the statistical average value of an arbitrary operator \mathbf{A} representing a physical quantity

$$\langle \mathbf{A} \rangle = \text{Tr} \{ \mathbf{A} \varrho \} \quad (4)$$

is independent of time; *i.e.* the fine-grained ensemble describes an equilibrium system, and the entropy of the ensemble

$$S(t) = -k \text{Tr} \{ \varrho(t) \log \varrho(t) \} \quad (5)$$

does not increase (k is the Boltzmann constant).

On the other hand, the coarse-grained density operator characterizing the coarse-grained ensemble — according to its usual definition — has a different evolution law which can be determined, *e.g.* by PAULI's master equation [6], or the generalized master equation of L. VAN HOVE [7] and that of I. PRIGOGINE and P. RÉSIBOIS [8], respectively. From this new evolution law of the ensemble the increase of the entropy of the coarse-grained ensemble can be obtained.

Recently, V. M. FAĬN, in his otherwise very interesting review article [9], pointed out that the increase of entropy has nothing to do with the coarsening of the ensembles and the entropy of the fine-grained ensemble increases, too. We can, however, not agree with FAĬN's objections, since he has not taken into account the different evolution laws of the fine-grained and coarse-grained density operators.

To prove that the increase of the entropy is indeed independent of the coarsening method but depends on the evolution law of the system, we will suggest a reasonable coarsening without changing the evolution operator $\mathbf{U}(t)$ and show that in this case no increase of the entropy is obtained.

Let us introduce as a coarse-grained density operator the time average of the fine-grained density operator:

$$\mathbf{P}(t) = \frac{1}{t} \int_0^t \varrho(\tau) d\tau, \quad (6)$$

which in the energy representation has the matrix elements

$$\langle n | \mathbf{P}(t) | m \rangle = \langle n | \varrho(0) | m \rangle \frac{1 - e^{-i\omega_{nm} t}}{i\omega_{nm} t} \quad \left(\omega_{nm} \equiv \frac{E_n - E_m}{\hbar} \right). \quad (7)$$

One immediately obtains the following properties of $\mathbf{P}(t)$:

$$\mathbf{P}(o) = \varrho(o), \quad \langle n | \mathbf{P}(o) | m \rangle = \langle n | \varrho(o) | m \rangle, \quad (8)$$

as well as

$$\langle n | \mathbf{P}(\infty) | m \rangle = \begin{cases} \langle n | \varrho(0) | m \rangle, & \text{if } n = m \\ 0, & \text{if } n \neq m \end{cases} \quad (9)$$

and

$$\langle n | \mathbf{P}(t) | m \rangle = 0 \quad \text{for } t = 2l\hbar/|E_n - E_m| \quad \text{and } n \neq m \quad (l = 1, 2, \dots), \quad (10)$$

i.e., the matrix elements of $\mathbf{P}(t)$ oscillate around zero with frequencies depending on the energy differences. Furthermore

$$T_r \{ \mathbf{P}(t) \} = 1, \quad (11)$$

$$T_r \{ \mathbf{P}^2(t) \} = \begin{cases} < Tr \{ \varrho^2(0) \}, & \text{if } t < \infty, \\ \rightarrow Tr \{ \varrho^2(0) \}, & \text{if } t \rightarrow \infty. \end{cases} \quad (12)$$

The latter statements are very important and not at all trivial. They can be proved as follows:

$$\begin{aligned} Tr \{ \mathbf{P}^2(t) \} &= \sum_n \sum_m \langle n | \mathbf{P}(t) | m \rangle \langle m | \mathbf{P}(t) | n \rangle = \\ &= \sum_n \sum_m |\langle n | \varrho(0) | m \rangle|^2 2 \frac{1 - \cos \omega_{nm} t}{\omega_{nm}^2 t^2} < \\ &< \sum_n \sum_m |\langle 0 | \varrho(0) | m \rangle|^2 = Tr \{ \varrho^2(0) \}, \end{aligned}$$

because

$$\frac{1 - \cos x}{x^2} < \frac{1}{2} (x \neq 0).$$

Indeed, the function given by the equation

$$y(x) = 1 - \frac{1}{2} x^2 - \cos x$$

is negative for $x \neq 0$ and zero for $x = 0$. (This property of $y(x)$ follows most easily from the fact that $y(0)=0$ and $y' = -x + \sin x$ has the opposite sign to that of x). The second statement follows from eq. (9).

It is well known that a pure state of the statistical ensemble is characterized by $Tr \{ \varrho^2(t) \} = 1$ and $Tr \{ \varrho^2(t) \} < 1$ corresponds to a mixture. Owing to this, eq. (12) means that even if for $t = 0$ the fine-grained ensemble is in a pure state, the coarse-grained ensemble represents a mixture for $t < \infty$, but for $t \rightarrow \infty$ the state of the system tends again to a pure state.

Due to the facts that

$$\mathbf{P}(t + \Delta t) - \mathbf{P}(t) = \frac{1}{t(t + \Delta t)} \left\{ t \int_0^t \varrho(\tau) d\tau + t \int_t^{t + \Delta t} \varrho(\tau) d\tau - (t + \Delta t) \int_0^t \varrho(\tau) d\tau \right\}$$

and

$$\lim_{\Delta t \rightarrow 0} \frac{1}{\Delta t} \int_t^{t + \Delta t} \varrho(\tau) d\tau = \varrho(t)$$

for the time derivative of $\mathbf{P}(t)$ the equation

$$\dot{\mathbf{P}}(t) = \lim_{\Delta t \rightarrow 0} \frac{\mathbf{P}(t + \Delta t) - \mathbf{P}(t)}{\Delta t} = \frac{\varrho(t) - \mathbf{P}(t)}{t} \quad (13)$$

can be obtained. This equation of motion for $\mathbf{P}(t)$ has been derived by von NEUMANN's equation of motion for $\varrho(t)$, i.e. by eq. (1), and

$$\dot{\mathbf{P}}(0) = 0, \quad \dot{\mathbf{P}}(\infty) = 0. \quad (14)$$

The entropy of the coarse-grained ensemble is defined as

$$\mathcal{S}(t) = -k \text{Tr} \{ \mathbf{P}(t) \log \mathbf{P}(t) \} \quad (15)$$

and it can easily be shown that its time derivative is given by

$$\begin{aligned} \dot{\mathcal{S}} &= -k \text{Tr} \{ \dot{\mathbf{P}}(t) \log \mathbf{P}(t) \} = 0 \quad \text{for } t = 0, \\ t &= 2l\hbar/|E_n - E_m|, \quad t = \infty \quad (l = 1, 2, \dots). \end{aligned} \quad (16)$$

This means, however, that $\mathcal{S}(t)$ oscillates around zero (with decreasing amplitude) and, the equation of motion indeed does not result in an entropy increase of the coarse-grained statistical ensemble.

REFERENCES

1. D. TER HAAR, Rev. Mod. Phys., **27**, 289, 1955.
2. P. CALDIROLA, Ergodic Theories, Acad. Press, New York, 1961.
3. E. G. D. COHEN, Fundamental Problems in Statistical Mechanics, North-Holland, Amsterdam, 1962.
4. K. W. FORD, Brandeis Univ. Summer Institute, Vol. 3, Statistical Physics, Benjamin, New York, 1963.
5. N. G. VAN KAMPEN, Physica, **20**, 603, 1954.
6. W. PAULI, Über das H-Theorem vom Anwachsen der Entropie vom Standpunkt der neuen Quantenmechanik from P. DEBYE, Probleme der modernen Physik, Hirzel, Leipzig, 1928.
7. L. VAN HOVE, Physica **23**, 441, 1957; **25**, 268, 1958.
8. I. PRIGOCINE and P. RÉSIBOIS, Physica **27**, 418, 1961.
9. V. M. FAĬN, UPN, SSSR, **79**, 641, 1963; Fortschr. Phys., **11**, 525, 1963.

Theoretical Interpretation of Upper Atmosphere Emissions

Edited by D. R. BATES, Pergamon Press, New York, Oxford, London, Paris, 1963, 264 pages

The origin of upper atmosphere emission has been the subject of research for a long time. In the early 20th century the idea still prevailed that the glow of the night sky was entirely due to telescopic stars. This assumption was rejected when the stars were assigned orders of magnitude and it was found that they gave about 1/5th part of the glow of the night sky. In view of the fact that the brightness increases from the zenith to the horizon it was assumed that the rest was due to upper atmospheric emission. It is known that in the aurorae the energy required for the emission of the bands N_2 , N_2^+ and O_2 is supplied by drifting particles originating in the Sun. The spectrum of the glow of the night sky is, however, characterized by the fact that it can be attributed to weaker excitation, and can be explained without recourse to an external supply of energy. Earlier investigations also lead to infer that upper atmosphere emission is due to the release of energy accumulated during the day.

The first international conference on upper atmosphere emission was held in 1947, where it was stated that information on this process was quite insufficient.

At the Symposium arranged in 1955 many more results were reported, which was due to the fact that by the application of mains spectrographs, more sensitive emulsions and electron multipliers introduced after the first conference, such data became available that made possible a more thorough investigation of the problems connected with sky glow and aurorae. Important results were obtained from the photoelectric measurements introduced early in the International Geophysical Year in 1955, providing a further basis for studies on the intensity variation and geographical distributions of various radiations.

In recent years, following the evaluation of more precise observations and measurements, the situation still improved and it became possible to refine theoretical hypo-

theses. The papers collected in the work reviewed here summarize the results of recent investigations discussed at the Symposium held in 1962.

P. A. FORSYTH presented a method to determine the degree of ionization in the auroral atmosphere by radar measurements. G. S. IVANOV-KHOLODNY dealt with the source and acceleration of electrons that penetrate deep into the atmosphere and the connections which these electrons have with aurorae. Investigating the interactions of solar plasma with the geomagnetic field J. W. DUNGEY interpreted theoretically the auroral zones. P. J. KELLOGG discussed the properties of energetic particles incident on the top of the atmosphere. Y. I. GALPERIN described the characteristics of proton aurorae, showing that — under quiet magnetic conditions — they appear usually in the auroral zone, and — while moving towards the equator — cause increasing magnetic disturbance.

A thorough investigation of upper atmosphere emission was facilitated by the observations on sodium and lithium clouds emitted by rockets. Thus e.g. according to the investigations of A. DALGARNO, the sodium vapour released above 190 kms contributes a great deal to the transfer of vibrational energy. Based on lithium cloud measurements J. E. BLAMONT proved his theoretical consideration regarding the turbulence conditions prevailing in the layer between 90 to 130 kms of the atmosphere and found that above 100 kms the equations of molecular diffusion and below that level those of turbulent diffusion were valid. G. F. J. MACDONALD's results are also worth mentioning: his investigations show that at heights between 40—80 kms the prevailing wind is zonal, blowing from east to west in summer and from west to east in winter.

From experience gained in nuclear explosion tests carried out at altitudes ranging from 400 to 500 kms some conclusions may also be drawn as regards upper atmospheric

emission processes. T. OBAYASHI described light phenomena of the upper atmosphere due to the high-energy nuclear explosions which took place in the period 1958 to 1961. As is known such explosions produce a large amount of radioactive material and emit various radiations exciting and ionizing the air in the high atmosphere; they also cause magnetic and ionospheric storms, aurorae and night glow of the sky. In the lower ionosphere increased ionization causes a severe attenuation of radio waves passing through it and an artificial radiation belt is formed

from the charged particles injected above the ionosphere and trapped by the geomagnetic field.

In the opinion of the authors of the present volume the Symposium was a good example for the fruitful cooperation of UAI and UIGG, in striving to clear the common problems of astronomy and geophysics. The future is also promising: steadily improving methods of observation and measurement will make possible the expansion of theoretical research.

F. DÉSI

Absorption Spectra in the Ultraviolet and Visible Region

Volumes III and IV, Publishing House of the Hungarian Academy of Sciences, Budapest 1962 and 1963 (424 and 414 pp., resp.)

Edited by L. LÁNG

The introductory and first volumes of the compilation of spectra, issued at the initiative of L. LÁNG, was first reviewed in the Hungarian Journal of Physics (*Magyar Fizikai Folyóirat*, in 1959 (7, 400, 1959). In 1962 the publication of volume II and the second edition of the previous volumes prompted a more extensive account of these publications in the *Acta Phys. Hung.*, (15, 86, 1962), as well as in the Hungarian Journal of Physics (10, 249, 1962). As volumes III and IV of this series and the third edition of the introductory volume have also been published since, it seems well worth to recall some of the data of the preceding volumes when discussing the more recent issues. The four volumes of the compilation published so far, contain the spectra of 706 substances, on 1660 pages. A very useful table of contents has also been annexed as a separate supplement to each of the volumes, in which the names of the substances are given (both according to the official and the practical nomenclature), together with their formulae arranged in accordance with the system of Chemical Abstracts and indicating the corresponding numbers of figures and pages as well as the names and respective places of work of the co-authors and summarizing the bibliographic data of articles published on the relevant subject, arranged in alphabetical order according to authors. In the cases of most of the substances the authors have used more than one solvent for the investigation of spectra, which is most advantageous and useful from just the point of view of this compilation. Quite naturally all absorption spectra throughout the series are given on uniform scales — a

point facilitating the comparability of the spectra and thus affording a synoptical presentation of the compiled material. On the verso of each of the figures the data necessary for a quantitative analysis can be found in the original registrations of the measurements, with the help of which the user of the volumes may be able to draw the spectra for himself on the desired scale. In order to obtain a uniform level in a work where spectra taken with different apparatuses are to be published side by side, various difficulties have to be overcome by both the editor and his collaborators. In the latest volume (and it is hoped also in the forthcoming ones) an increasing number of such spectra were published for which the necessary measuring data were obtained by means of registering apparatuses. The editors had also considered publishing the original data. Fortunately, however, the idea has been abandoned, for one of the most outstanding merits of this series lies in the fact that the spectra can be found on identical scales and that the tables are arranged uniformly, which could not have been the case with the original data. Had the original data been given in the compilation, the user of the series would have had to convert these for himself, making it much more difficult for him to use the data required, not to mention the fact that the original registrations could be fitted into the volume obviously only on a reduced scale, thus making a precise reading of them impossible. The firm stand of the editorial committee ensuring the uniformity of the volumes is, in my view, greatly to be appreciated.

To come back to volumes III and IV, it can be said that contributions from some new

co-authors have lent new colour to the compilation. From among the authors of volume III we wish to mention the publications of A. R. KATRITZKY and R. A. JONES, as well as those of J. MOSTEW and his collaborators; from among the contributors to volume IV the publications submitted by L. LÁNG, K. LEMPERT and G. DOLESCHALL, as well as C. PÁRKÁNYI and R. ZAHRADNIK ought to be mentioned, for — in comparison to the previous edition — they give information on new fields of research. It should be stressed that from the very outset this compilation of spectra has not aimed at completeness, its main purpose being to supplement other similar compilations by publishing the most recent results of its contributors. Thus no system has been followed when compiling the material, the only aim being publications of — as far as possible — the latest data available in spectroscopic research. The above principle is exemplified fully by the material of volume IV.

A selection from nine of the lectures of the 7th European Congress on Molecular Spectroscopy, held in Budapest in July 1963, was published in volume IV of this series, the volume appearing just in time for the opening of the Congress. It should be mentioned that the staffs both of the Publishing House and the Printers of the Hungarian Academy of Sciences, together with the editorial committee and their collaborators did their utmost to bring about this happy co-incidence of events.

In the single volumes more and more coauthors from abroad have submitted their latest scientific results for publication. Thus, the original aim of the publication, its international character, may well be considered to have been realized. It is hoped that in the forthcoming volumes we shall be able to witness a further development of this most fruitful international cooperation.

I. KOVÁCS*

Zur Physik und Chemie der Kristallphosphore

II.

Herausgegeben von Dr. Ing. HENRY ORTMANN
(Akademie-Verlag, Berlin, 1962. 236 Seiten DM 55)

Die Unterkommission Leuchstoffe der Sektion für Physik der Deutschen Akademie der Wissenschaften zu Berlin veranstaltete vom 27.—29. November, 1961 eine internationale Tagung über die Physik und Chemie der Kristallphosphore.

Der vorliegende Band ist eine Sammlung der im Rahmen des Kolloquiums vorgetragenen 37 Arbeiten, in denen über Forschungen aus den folgenden Gebieten der Physik und Chemie der Kristallphosphore berichtet wurde:

- a/ theoretische Probleme des Lumineszenzmechanismus;
- b/ Lumineszenz der Alkali-Halogenide;
- c/ Lumineszenz der II—IV-Verbindungen;
- d/ Silberhalogenide;
- e/ organische Phosphoren,
- f/ technische Anwendungen.

Ein verhältnismässig grosser Teil der Referate beschäftigte sich mit den Untersuchungen an Zink- und Calciumsulfid und den dabei gewonnenen Resultaten. Verfahren der Einkristallzüchtung von Phosphoren und Luminophoren und deren Nachbehandlung, sowie optische und elektrische Messmethoden bei der Untersuchung dieser Stoffe wurden behandelt. Die Anzahl der Mitteilungen bezüglich der III—VI Verbindungen — 16 Vorträge — zeigt, dass dieses Thema in der Festkörperphysik im Mittelpunkt des

Interesses steht und von vielen Forschern bearbeitet wird.

Im Rahmen der theoretisch-physikalischen Untersuchungen wurde die Frage der Ladungsträger und deren Diffusion, ferner der Mechanismus des Lumineszenzentrums behandelt.

Weiterhin wurden über die traditionellen Alkali- und Silberhalogenide, organische Phosphore und schliesslich Ergebnisse auf dem Gebiet der praktischen Anwendungen für die Dosimetrie und die Lumineszenzbildschirme berichtet.

Das Organisationskomitee hatte es sich zum Ziel gesetzt, Forscher von den verschiedenen Weisheitsplätzen einzuladen, um auf A den stene in den Vorträgen und nachfolgenden Diskussionen einen möglichst breiten Überblick über den Stand dieses interessanten Gebietes der Festkörperphysik zu erhalten, und die Perspektiven der weiteren Forschung zur Diskussion zu stellen.

Die Zahl der Teilnehmer war aus verschiedenen Gründen bedauerlicherweise geringer als vorausgesehen. Der Sammelband enthält deswegen nicht Beiträge aus allen Spezialgebieten, die einzelnen Beiträge zeugen jedoch von sorgfältiger Forschungsarbeit.

Die Redaktion des schön ausgestatteten Bandes wurde von Dr. Ortmann gewissenhaft besorgt, man vermisst jedoch die Dis-

* Department of Atomic Physics, Polytechnical University, Budapest

kussionen, die das rege Interesse der Teilnehmer an der Tagung widerspiegeln würden. Auch die Auswertung der Konferenz wäre dem Leser erleichtert, wenn die Eröffnungsansprachen von Prof. R. Rompe und Dr.

H. Ortmann wiedergegeben worden wären, sowie auch die Schlussworte des letzteren, in denen festgestellt wurde, dass das Ziel der Konferenz erreicht wurde.

Pál Kovács

F. SAUTER : Festkörperprobleme I

(Halbleiterprobleme VII), Friedr. Vieweg & Sohn, Braunschweig 1962. Preis DM 58.

Festkörperprobleme I or, to quote it under its oldstyle title, *Halbleiterprobleme VII* deals mainly with the general lectures of the 1961 Bad Pyrmont conference. This widening of the scope is reflected and explained in the foreword by Prof. SAUTER, where the indivisibility of solid state physics is clearly emphasized. The reviewer completely agrees with this view, allowing for a separate semiconductor literature for technical applications only, where rough and sometimes even macroscopic concepts are sufficient. I feel that it is imperative to forge further links with theoretical physics, particularly with field theory and quantum statistics, which seem to inject new blood and add further impetus to the rapidly developing science of solid state physics.

The first paper, written by VINK, deals with interactions among defects in semiconductors. The treatment is along the familiar lines of the mass action law. The paper by GREMMELMAIER gives a lucid description of the tunnel diode, while that of BÖER deals with the field and current inhomogeneities observed in CdS in high fields. The paper by CARDONA gives a very good account of the FARADAY rotation in semiconductors, one of the few effects, which although not the easiest to measure accurately, are nevertheless capable of furnishing an unambiguous value of the carrier effective mass.

The next two papers are complementary to each other, that of REIK dealing with the theoretical, that of SCHMIDT-TIEDEMANN with the experimental aspects of hot electrons in semiconductors. The subject is in the stage of rapid development, contributing to the clarification of quite a few theoretical concepts, and simultaneously to the possible construction of some new semiconductor devices. Next comes HUND's paper on the electronic energy bands and properties of metals. It describes in very simple terms the new theoretical ideas and some experimental methods used in recent years for Fermi-

surface determination. This task, which was regarded as almost hopeless for two decades is now in the forefront of research activity in the most advanced laboratories, and offers real hope for a quantitative determination of the properties of solids in the foreseeable future.

Now follows the paper of SCHWAB on the catalytic effect of semiconductors. A close relationship is established between the number of free electron places in a Brillouin zone and the activation energy for catalysis. The next two papers deal with the problem of noise, that of BITTEL summarizing the more elementary theoretical aspects, while that of KLEINKNECHT and SEILER the special cases encountered in semiconductors, mainly in germanium.

The paper of NEUERT contains some technical data on the decay of a few inorganic scintillators, as a result of nuclear irradiation. SEVERIN's paper introduces the reader to a new, fascinating subject: the magnetic properties of ferromagnetic oxides, with special emphasis on the recently much investigated yttrium-iron garnets. In these materials various spin wave and magnetostatic resonances can be established, which make the determination of the internal field possible.

The last two papers deal with transport theory. Both are detailed, the former, that of EGGERT giving a comprehensive, easily readable account on the mobility of semiconductors, while the second, by SCHOTTKY, tackles the problem of the solution of the Boltzmann-equation for semiconductors. It amounts to an iterative solution of the transport equation, with the introduction of higher order relaxation times.

It is usual for the reviewer to complete his review by referring to printing standards, errors, etc. This is not a difficult task at all. This book from F. Vieweg and Sohn is, in all such respects, as excellent as usual.

E. NAGY

М. А. Сапожков

Защита трактов радио и проводной телефонной связи от помех и шумов

Государственное издательство литературы по вопросам связи и радио, Москва, 1963

Телефонная связь получила широкое распространение в конце XIX века. На первом этапе развития — до появления электронных ламп — внимание научной мысли было сосредоточено на повышении эффективности электроакустических преобразователей и уменьшении потерь в соединительных линиях. Изобретение усилителей с электронными лампами значительно увеличило дальность проводной телефонной связи и способствовало быстрому развитию радиотелефонной связи, а затем и многоканальной проводной связи.

Расширение области применения телефонной связи потребовало решить задачу по повышению ее качества. Известно, что качество передачи речи с достаточной полнотой определяется величиной разборчивости речи, обеспечиваемой телефонным трактом. Поэтому было обращено особое внимание на разработку теории разборчивости речи, включая создание методов расчета и измерения. Материалы, связанные с разработкой этих вопросов, рассредоточены по различным изданиям.

Книга М. А. Сапожкова представляет собой попытку обобщить эти материалы и, пополнив их данными из малоизвестных источников, ведомственных изданий и работ автора, создать пособие по вопросам защиты трактов связи от помех и шумов. Ценной является книга и потому, что, несмотря на то, что вопросам помехозащиты трактов связи посвящено сравнительно много работ, все же целый ряд вопросов до сих пор не нашел требуемого освещения. Кроме того, материалы по помехозащите трактов не обобщены.

Поэтому в настоящей книге сделаны попытки разрабатывать методы повышения разборчивости речи; уделять особое внимание дополнению теории шумов в части амплитудных распределений и учета маскирующего действия сложных помех; изложить сущность методики измерений помехозащищенности трактов и их элементов; дать анализ различных способов снижения уровня помех, попадающих в тракты телефонной связи; рассмотреть методы достижения возможно большей разборчивости речи, передаваемой по трактам связи, путем осуществления соответствующих частотных и амплитудных характеристик, исследовать влияние искажений, вносимых трактом связи, на разборчивость речи и определить условия, при которых искажения не оказывают существенного влия-

ния на помехозащиту тракта; определить эффективность различных способов помехозащиты применительно к конкретным типам трактов.

Для легкого чтения и полного понимания книги автором предполагается прочное знание таких разделов математики, как алгебра, дифференциальное и интегральное исчисления, теория комплексных чисел и т. д., далее основы анализа Фурье, специальные функции, например, функции Бесселя, Гамма-функция. В отношении подготовленности читателя в области физики, здесь в первую очередь необходимо твердое значение разделов акустики (акустические величины и их измерение).

Монография М. А. Сапожкова состоит из следующих глав:

- I. Помехи и их маскирующие действия.
- I. Методы оценки и измерения помехозащищенности трактов.
- III. Анализ методов прямой помехозащиты трактов.
- IV. Методы косвенной помехозащиты трактов.
- V. Влияние искажений в трактах телефонной связи на их помехозащищенность.
- VI. Защита трактов телефонной связи от помех и шумов.

Глава I. В ней рассматривается общая теория помех, в первую очередь исследуются вопросы, не достаточно освещенные в литературе. Даётся перечень различных видов помех, исследуется маскирующее действие помех, затрудняющее восприятие речи. Для определения влияния помех на разборчивость речи истолкуются как их частотная, так и амплитудная структуры. В главе можно найти далее методы измерения и оценки спектра помех, причем при рассмотрении данного вопроса наряду со схемами экспериментальных установок читатель может уяснить себе физические основы измерений, дискутируемые автором в закрытом математическом виде.

Глава содержит 20 рисунков, 2 таблицы и 57 соотношений.

Глава II. После определения необходимых при оценке помехозащищенности трактов понятий автор переходит к определению количественных соотношений между этими величинами. С измерением помехозащищенности трактов в действительности занимается 2-й § главы, в котором одновременно с уяснением теоретических основ дается блок-схема устройства для измере-

ния разборчивости речи тональным методом.

Глава содержит 11 рисунков, 2 таблицы и 45 соотношений.

Глава III. При анализе методов прямой помехозащищенности трактов автор не останавливается на электрической защите, теория и практика которой подробно разработана. Рассматриваются методы акустической защиты. В главе получили место такие измерительные приемы, как метод пространственной дискриминации, широко использованной в телефонной связи метод компенсации и другие важные методы измерения.

Глава содержит 22 рисунка и 111 соотношений.

Глава IV. В главе рассматриваются вопросы оптимальной чувствительности, рациональной чувствительности тракта, вариации чувствительности и мощности, компрессии динамического диапазона речи.

Глава содержит 11 рисунков и 95 соотношений.

Глава V. Среди всех глав наряду с 3-й главой обладает высокой математической потребностью. Коротко упомянуты линей-

ные искажения. Краткость трактовки обусловливается тем, что влияние этого вида искажений на разборчивость речи достаточно изучено. Необходимой обоснованностью дискутируются нелинейные искажения в последующих пяти параграфах.

В главе содержатся 6 рисунков и 40 соотношений.

Глава VI. В первой части рассматриваются характеристики и шумозащита электроакустической аппаратуры, затем следуют тракты телефонной проводной связи и радиотелефонные тракты связи. В данной главе читатель находит и схемы различных аппаратов техники связи.

В главе содержатся 48 рисунков, 1 таблица и 35 соотношений.

В заключение следует упомянуть о современности книги М. А. Сапожкова «Задачи трактов радио и проводной телефонной связи от помех и шумов», она будет полезной для студентов вузов связи, инженеров, аспирантов и научных сотрудников, специализирующихся в области радио и проводной телефонной связи.

3. Фюзэши

М. А. Сапожков

Речевой сигнал в кибернетике и связи

Государственное издательство литературы по вопросам связи и радио, Москва, 1963

Вопросами, поставленными в книге М. А. Сапожкова «Речевой сигнал в кибернетике и связи», занимались во многих литературных изданиях середины XX столетия. Главным образом эти работы посвящены вопросам сжатия и расширения объема сигналов речи, автоматического распознавания звуков речи и их синтеза. Если рассматривать упомянутые работы более конкретно, то в ранних изданиях ставили вопрос о преобразовании динамического диапазона речи, позже появились работы по вопросам частотной и временной компрессии сигналов речи, далее по фонемному кодированию, автоматическому распознаванию и синтезу речи и их приложениям в кибернетике и технике связи. Общее число подобных и тесно связанных с ними работ доходит до тысячи.

Автор книги ставит своей целью объединить материалы по этой проблеме, дать их критическое обобщение. В монографии М. А. Сапожкова рассматриваются наиболее важные для настоящего периода развития кибернетики и связи вопросы. Ценным для читателя является обширный

список литературы, включающий в себе 715 изданий и состоящий главным образом из иностранных источников.

Книга разделена на две части. В первой части рассматриваются общие вопросы теории информации, речеобразования, принципов преобразования и восприятия речи, т. е. тот фундамент, на котором построена теория сжатия и расширения объема речевого сигнала, автоматического распознавания и синтеза речи. Во второй части рассматриваются методы непосредственного компандирования и ограничения, лингвистического и параметрического компандирования, а также методы автоматического распознавания и синтеза речи. Из параметрических методов рассмотрены полосные, гармонические и формантные методы. Особое внимание уделено проблеме основного тона. Кроме этого рассмотрены практические применения этих методов как для связи, так и для целей автоматики и кибернетики, в частности для речевого управления и для читающих и говорящих машин. В приложении рассмотрены методы анализа речевых сигналов, аппаратура и методы

оценки качества преобразованной речи, принятая терминология.

Для беглого чтения и полного понимания книги автор предполагает знание таких разделов математики, как алгебра, дифференциальное и интегральное исчисления, теория комплексных чисел, преобразования Фурье, Лапласа и другие, связанные с перечисленными разделами области математики. В области физики читатель должен быть знаком с общей физикой, особенно желательно твёрдое знание основ акустики (акустические величины и их изменение).

Книга М. А. Сапожкова состоит из следующих глав:

- I. Теория информации в применении к речевому сигналу.
- II. Теория речеобразования.
- III. Характеристики русской речи.
- IV. Преобразование речи. Влияние помех.
- V. Восприятие речи.
- VI. Методы непосредственной компрессии, экспандирования ограничения.

- VII. Параметрические методы компандирования речи и генерирование (воспроизведение) речевых колебаний.
- VIII. Спектрально полосные методы.
- IX. Гармонические и корреляционные методы.
- X. Формантные методы.
- XI. Фонемные и другие лингвистические методы.
- XII. Практические применения методов компандирования, автоматического распознавания и синтеза речи.

В книге нумеруются 450 страниц. Она содержит 203 рисунка, 221 соотношение и 39 таблиц.

В заключение следует ещё раз упомянуть о важности книги М. А. Сапожкова, она будет являться, по нашему мнению, настольной книгой специалистов, работающих в области техники связи, автоматики, кибернетики, в смежных с ними областях и, в первую очередь, для инженеров, аспирантов и научных сотрудников, изучающих вопросы преобразования речи.

3. Фюзети

Printed in Hungary

A kiadásért felel az Akadémiai Kiadó igazgatója

A kézirat nyomdába érkezett: 1964. XI. 30. — Terjedelem: 6,25 (A/5) iv, 16 ábra

Műszaki szerkesztő: Farkas Sándor

64.59942 Akadémiai Nyomda, Budapest — Felelős vezető: Bernát György

The *Acta Physica* publish papers on physics, in English, German, French and Russian.
The *Acta Physica* appear in parts of varying size, making up volumes.
Manuscripts should be addressed to :

Acta Physica, Budapest 502, Postafiók 24.

Correspondence with the editors and publishers should be sent to the same address.
The rate of subscription to the *Acta Physica* is 110 forints a volume. Orders may be placed with "Kultúra" Foreign Trade Company for Books and Newspapers (Budapest I., Fő u. 32. Account No. 43-790-057-181) or with representatives abroad.

Les *Acta Physica* paraissent en français, allemand, anglais et russe et publient des travaux du domaine de la physique.

Les *Acta Physica* sont publiés sous forme de fascicules qui seront réunis en volumes.
On est prié d'envoyer les manuscrits destinés à la rédaction à l'adresse suivante:

Acta Physica, Budapest 502, Postafiók 24.

Toute correspondance doit être envoyée à cette même adresse.

Le prix de l'abonnement est de 110 forints par volume.

On peut s'abonner à l'Entreprise du Commerce Extérieur de Livres et Journaux «Kultúra» (Budapest I., Fő u. 32. — Compte-courant No. 43-790-057-181) ou à l'étranger chez tous les représentants ou dépositaires.

«*Acta Physica*» публикуют трактаты из области физических наук на русском, немецком, английском и французском языках.

«*Acta Physica*» выходят отдельными выпусками разного объема. Несколько выпусков составляют один том.

Предназначенные для публикации рукописи следует направлять по адресу:

Acta Physica, Budapest 502, Postafiók 24.

По этому же адресу направлять всякую корреспонденцию для редакции и администрации.

Подписная цена «*Acta Physica*» — 110 форинтов за том. Заказы принимает предприятие по внешней торговле книг и газет «Kultúra» (Budapest I., Fő u. 32. Текущий счет: № 43-790-057-181) или его заграничные представительства и уполномоченные.

INDEX

<i>M. Szilágyi: Periodic Focusing of Dense Electron Beams with Thin Lenses.</i> — <i>М. Силади: Периодическая фокусировка интенсивных электронных пучков</i> тонкими линзами	87
<i>I. Kovács and R. Törös: The Intensity Distribution of the Triplet Bands of the CO Molecule.</i> — <i>И. Ковач и Р. Тэреш: Распределение интенсивности в триплетной связи</i> молекулы CO	101
<i>I. Kovács: The Rotational Structure of the $d^3\Delta$ State of the CO Molecule.</i> — <i>И. Ковач:</i> Ротационная структура состояния $d^3\Delta$ молекулы CO	107
<i>P. Gadó: X-Ray Powder Diffraction Study of the $\text{WO}_3 \rightleftharpoons \text{W}_{20}\text{O}_{58}$ Shear Transformation.</i> — — <i>П. Гадо: Изучение преобразования сдвига $\text{WO}_3 \rightleftharpoons \text{W}_{20}\text{O}_{58}$ рентгеновыми</i> лучами порошко-дифракционным методом	111
<i>I. Montvay: On the Convergence of the Peratization Method.</i> — <i>И. Монтвай:</i> О сходимости ператизационного метода	119
<i>A. Kónya: Theoretical Interpretation of Some Properties of the Periodic System by the Thomas—Fermi Model.</i> — <i>А. Конья:</i> Теоретическая интерпретация некоторых свойств периодической системы элементов моделью Томаса—Ферми	129

COMMUNICACIONES BREVES

<i>T. Tietz: Electron Scattering by Atoms and the Existence of Negative Ions</i>	141
<i>J. I. Horváth: Contribution to the Problem of the Entropy Increase of Quantum Mechanical Many-Body Systems</i>	145

RECENSIONES

<i>F. Dési: D. R. Bates, Theoretical Interpretation of Upper Atmosphere Emissions</i>	149
<i>I. Kovács; L. Láng, Absorption Spectra in the Ultraviolet and Visible Region</i>	150
<i>P. Kovács: H. Ortmann, Zur Physik und Chemie der Kristallphosphore</i>	151
<i>E. Nagy: F. Sauter, Festkörperprobleme I</i>	152
<i>З. Фюзэши: М. А. Сапожков, Защита трактов радио и проводной телефонной связи</i> от помех и шумов	153
<i>З. Фюзэши: М. А. Сапожков, Речевой сигнал в кибернетике и связи</i>	154

Acta Phys. Hung. Tom. XVIII. Fasc. 2. Budapest, 10. III. 1965

ACTA PHYSICA

ACADEMIAE SCIENTIARUM HUNGARICAE

ADIUVANTIBUS

Z. GYULAI, L. JÁNOSSY, I. KOVÁCS, K. NOVOBÁTZKY

REDIGIT
P. GOMBÁS

TOMUS XVIII

FASCICULUS 3



AKADÉMIAI KIADÓ, BUDAPEST
1965

ACTA PHYS. HUNG.

ACTA PHYSICA

A MAGYAR TUDOMÁNYOS AKADÉMIA FIZIKAI KÖZLEMÉNYEI

SZERKESZTŐSÉG ÉS KIADÓHIVATAL: BUDAPEST V., ALKOTMÁNY UTCA 21.

Az *Acta Physica* német, angol, francia és orosz nyelven közöl értekezéseket a fizika tárgyköréből.

Az *Acta Physica* változó terjedelmű füzetekben jelenik meg: több füzet alkot egy kötetet. A közlésre szánt kéziratok a következő címre küldendők:

Acta Physica, Budapest 502, Postafiók 24.

Ugyanerre a címre küldendő minden szerkesztőségi és kiadóhivatali levelezés.

Az *Acta Physica* előfizetési ára kötetenként belföldre 80 forint, külföldre 110 forint. Megrendelhető a belföld számára az Akadémiai Kiadónál (Budapest V., Alkotmány utca 21. Bankszámla 05-915-111-46), a külföld számára pedig a „Kultúra” Könyv- és Hírlap Külkereskedelmi Vállalatnál (Budapest I., Fő u. 32. Bankszámla 43-790-057-181 sz.), vagy annak külföldi képviseleteinél és bizományosainál.

Die *Acta Physica* veröffentlichen Abhandlungen aus dem Bereiche der Physik in deutscher, englischer, französischer und russischer Sprache.

Die *Acta Physica* erscheinen in Heften wechselnden Umfangs. Mehrere Hefte bilden einen Band.

Die zur Veröffentlichung bestimmten Manuskripte sind an folgende Adresse zu richten:

Acta Physica, Budapest 502, Postafiók 24.

An die gleiche Anschrift ist auch jede für die Redaktion und den Verlag bestimmte Korrespondenz zu senden.

Abonnementspreis pro Band: 110 Forint. Bestellbar bei dem Buch- und Zeitungs-Aussenhandels-Unternehmen »Kultúra« (Budapest I., Fő u. 32. Bankkonto Nr. 43-790-057-181) oder bei seinen Auslandsvertretungen und Kommissionären.

ELEMENTARY CALCULATIONS OF THE MADELUNG CONSTANTS OF SOME CUBIC LATTICES

By

F. BUKOVSZKY*

INSTITUTE OF EXPERIMENTAL PHYSICS, TECHNICAL UNIVERSITY, BUDAPEST

(Presented by Z. Gyulai — Received in revised form 10. I. 1964)

An elementary method (the so-called “chain method”) [1] is applied to the evaluation of the Madelung constant of crystal lattices both of the NaCl and the CsCl-type. The binding energies are summed up over suitably chosen cylinder shells resulting in very good approximate values for the Madelung constant. The Madelung constants both of CaF₂ and ZnS-type lattices are determined from linear relations given by BENSON and VAN ZEGGEREN [2].

I. Introduction

The first calculations concerning crystal structure energies were published by E. MADELUNG [3] about forty years ago, and a simple and clear theory for the mechanism of crystal growth was given by KOSSEL and STRANSKI in 1927 [4]. The methods applied in the calculations were mostly rather complicated and therefore physicists, chemists and mineralogists have for long been trying to develop simpler and more accurate methods. We mention the method by FRANK [5] and that worked out by FÁTHY and the author [1]. The main features of the latter method may briefly be outlined in the following.

The chains or half-chains consisting of equidistant ions of alternating sign are considered as the basic elements of a crystal body. The binding energies are first summed up along such chains or half-chains; this method may therefore be called “*chain method*”. By the aid of certain lemmata the difficulties arising in such summations can be overcome.

The ions with positive and negative charges, playing symmetrical roles, will be simply called “red” and “black” ions and in the figures will be marked by empty (○) or filled (●) circles, respectively.

Let the charge of the ions forming the chain be $\pm e$, e being the charge of an electron, and let d be the distance of two neighbours in the chain. The binding energy of a pair of ions is then

$$u = \frac{e^2}{d}$$

* Present address: The Federal Advanced Teachers' College, Lagos, Nigeria

and the energy required to bind the next ion to the lattice is some multiple this expression, e.g.

$$U_1 = \varphi \cdot \frac{e^2}{d} \quad \text{or} \quad U_2 = \chi \frac{e^2}{d}.$$

In the following we shall use d as the unit of length and e^2/d as the unit of energy. Their values are collected in Table I.

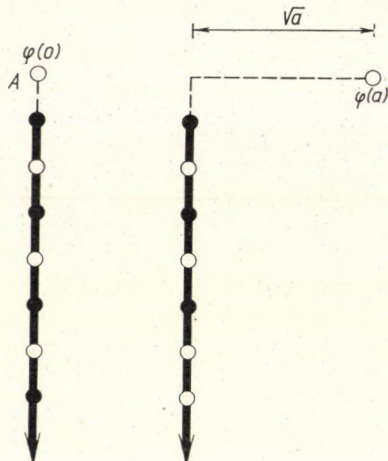


Fig. 1. The ion joins the half-chain with the binding energy $\varphi(0)$ or $\varphi(a)$, respectively

The binding energy of an ion joining a half-chain and continuing it is (Fig. 1)

$$\varphi(0) = \sum_{n=1}^{\infty} (-1)^{n-1} \cdot \frac{1}{n} = \ln 2$$

and for an ion being at the distance \sqrt{a} , the binding energy has the value

$$\varphi(a) = \sum_{n=1}^{\infty} (-1)^{n+a-1} \frac{1}{\sqrt{n^2 + a}}. \quad (1)$$

Table I

Length and energy units used in the present calculations

	d angström	e^2/d electronvolt
NaCl	2,81	5,13
CsCl	3,56	4,05

For greater distances ($a \geq 40$) the simple asymptotic formula

$$\varphi(a) \sim (-1)^a \cdot \frac{1}{2\sqrt{a}}$$

holds to an accuracy sufficient for most practical purposes. Finally, the binding energy of a complete chain at the distance \sqrt{a} is (Fig. 2)

$$\chi(a) = \sum_{n=-\infty}^{+\infty} (-1)^{n+a-1} \frac{1}{\sqrt{n^2 + a}} \quad (2)$$

as can be proved in a simple way.

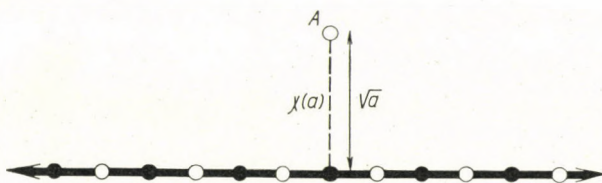


Fig. 2. The contribution of a complete chain, infinite in both directions, to the binding energy of the ion A is $\chi(a)$

In the following the place of the joining ion, or of the ion for which the binding energy is to be calculated, usually denoted by A , will be called the point of reference. The ion of a chain or half-chain nearest to the point of reference will be called the *initial link* of the chain or half-chain. The chain or half-chain will be called a red (black) chain or half-chain if its initial link is a red (black) ion. In the sodium-chloride lattice these chains run parallel to the edge, in the lithium-chloride lattice parallel to the diagonal of the elementary cell.

II. The Madelung constant of NaCl

Let a red ion in the interior of the crystal body be the point of reference. We shall call the plane containing the point of reference and being perpendicular to the direction of the chain the "basic plane". In the NaCl crystal this basic plane is a lattice plane which contains the initial links of the parallel chains (Fig. 3). The lattice points are to be found along concentric circles around the point of reference and the chains represented by these lattice points (initial links) form co-axial cylindric shells. These shells contain either red chains or black chains and may be called red shells or black shells, respectively.

The radii of these successive shells can be given by the simple formula

$$\varrho_k = \varrho_1 \sqrt{x_k} \quad (3)$$

with $\varrho_1 = 1$ and

$$\begin{array}{c|c|c|c|c|c|c|c|c|c|c|c|c|c|c|c|c} k = & 1 & 2 & 3 & 4 & 5 & 6 & 7 & 8 & 9 & 10 & 11 & 12 & 13 & 14 \\ x_k = & 1 & 2 & 4 & 5 & 8 & 9 & 10 & 13 & 16 & 17 & 18 & 20 & 25 & 26 \end{array}$$

(See Fig. 3).

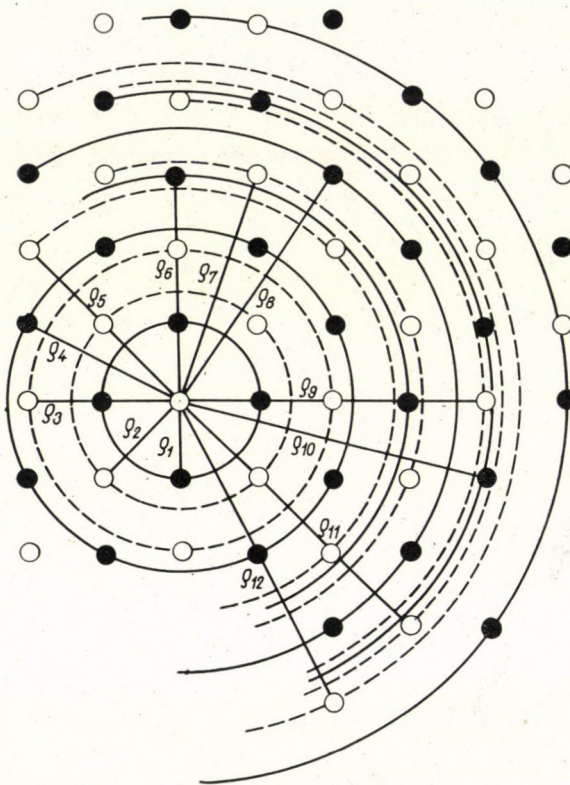


Fig. 3. The basic plane of a NaCl crystal with the radii of a few concentric circles. The initial links of the chains form a geometric quadratic lattice

The numerical values of the functions φ and χ which were already given in [1] have been newly computed to an eight-digit accuracy (see Table II).

These values make possible to calculate the energies of the cylindrical shells as well as their sums. These are given in Table II.

The first column of the Table shows the serial numbers of the shells, the second the quantity

$$a = \varrho_k^2 \triangleq x_k$$

Table II
Binding energy in the NaCl lattice

<i>k</i>	<i>a</i>	Chain energy		Energy of a shell	Total energy
0	0	1,38629436	1	1,38629436	1,38629436
1	1	,11816506	4	,47266024	1,85895462
2	2	—,02727194	4	—,10908776	1,74986686
3	4	—,00366634	4	—,01466536	1,73552015
4	5	,00165470	8	,01323760	1,74843910
5	8	—,00022957	4	—,00091828	1,74752082
6	9	,00013013	4	,00052052	1,74804134
7	10	—,00007617	8	—,00060936	1,74743198
8	13	,00001774	8	,00014192	1,74757390
9	16	—,00000488	4	—,00001952	1,7475438
10	17	,00000327	8	,00002616	1,74758054
11	18	—,00000222	4	—,00000888	1,74757166
12	20	—,00000104	8	—,00000832	1,74756334
13	25	,00000018	12	,00000216	1,74756550
14	26	—,00000014	8	—,00000112	1,74756438
15	29	,00000006	8	,00000048	1,74756486
16	32	—,00000002	4	—,00000008	1,74756478
17	34	—,00000001	8	—,00000008	1,74756470
18	36	—,00000001	4	—,00000004	1,74756466
19	37	,00000001	8	,00000008	1,74756474
20	40	—,00000000	8	—,00000000	1,74756474

and the third column the binding energies of the chains. This column contains the values

$$\chi(a) = \sum_{n=-\infty}^{+\infty} (-1)^{n+a-1} \frac{1}{\sqrt{n^2 + a}} = (-1)^{a-1} \frac{1}{\sqrt{a}} + 2 \cdot \varphi(a)$$

except for the first row, since $\chi(a)$ is not defined for $a = 0$. Here, instead,

$$2\varphi(0)$$

is to be found. The fourth column shows the number of chains in each shell, and the fifth the corresponding binding energy. The last column contains the sum of the energies of the preceding shells, that is the energy of the cylinder of radius ϱ_k . These latter energy values are approximate values of the Madelung constant of NaCl. Their accuracy may be judged from the Table below:

$k =$	1	3	5	8	9	13	15
number of exact digits	1	2	3	4	5	6	7

They can be easily checked by comparison with the values given by O. EMERSLEBEN and Y. SAKAMOTO [6].

III. Application of the chain method to the CsCl lattice

The lattice of CsCl is quite different from the lattice of NaCl though the chemical behaviour of the two substances is very similar. Each ion of NaCl is

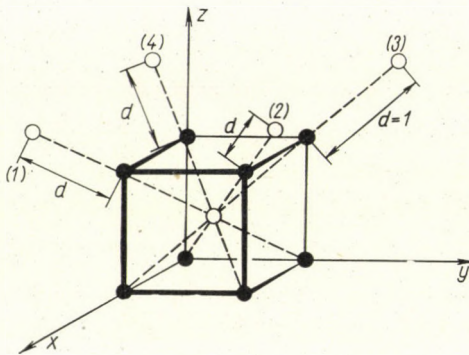


Fig. 4. Elementary cell of the CsCl lattice. The smallest ion-ion distance is d

surrounded by six neighbours of opposite charge, while in the case of CsCl a (say) red ion has eight black neighbouring ions situated at the corners of a cube in the centre of which the red ion sits (Fig. 4). The role of red and black ions may be interchanged. The length of the diagonal, according to our choice of unit of length, is 2. The elementary cell lies at the origo of the system of reference as shown in Fig. 4. As the basic plane is orthogonal to the direction of the chain, e.g., the direction (2) shows the (1,1,1)-plane to be a basic plane.

We project the initial links of the black chains also on this basic plane. In the Figure these points are marked by crossed circles. As can be seen we have for the longest side of the triangle (Fig. 5)

$$\sqrt{u^2 + v^2 + u v}$$

and with this we obtain for the radii of the cylindric shells

$$\varrho_k = \varrho_1 \sqrt{x_k} . \quad (4)$$

This formula is similar to that obtained for NaCl. Here the x_k have the following values:

$k = 1$	2	3	4	5	6	7	8	9	10	11	12	13	14	15
$x_k = 1$	3	4	7	9	12	13	16	19	21	25	27	28	31	36

and

$$\varrho_1(\text{CsCl}) \neq \varrho_1(\text{NaCl}).$$

The numerical calculation of the chain energies is in principle the same as for NaCl [1]. A red chain consists of two symmetrical black half-chains and

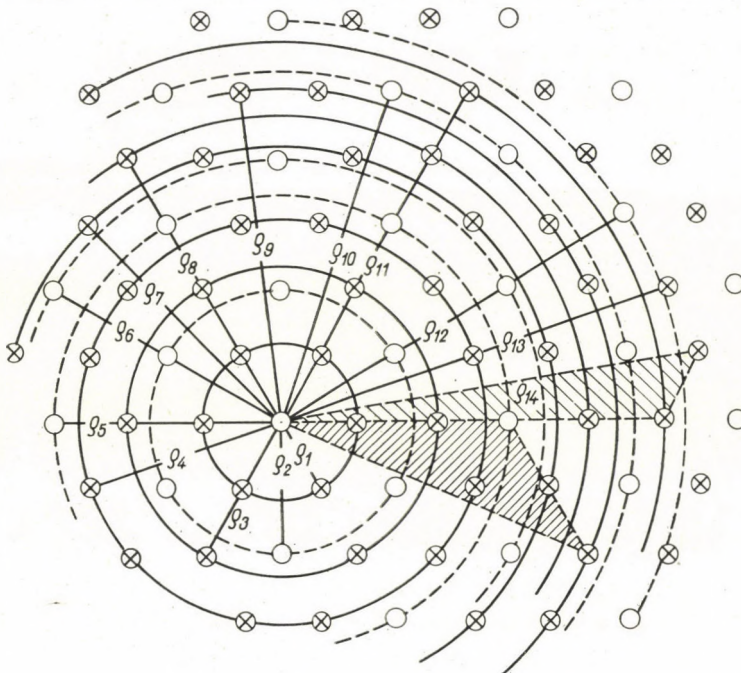


Fig. 5. The basic plane of the CsCl crystal with the radii of the first 15 concentric circles. The intersections of the chains form a geometric lattice of regular triangles

one red ion which is the initial link at the distance \sqrt{a} (see Fig. 2). The binding energy for each half chain is

$$\varphi_k = 3 \sum_{n=1}^{\infty} (-1)^{n-1} \frac{1}{\sqrt{(3n)^2 + 8x_k}},$$

from which we obtain for the chain-energy

$$\begin{aligned} \chi_k = -\frac{1}{\varrho_k} + 2\varphi_k &= -\frac{3}{\sqrt{8x_k}} + 6 \sum_{n=1}^{\infty} (-1)^{n-1} \frac{1}{\sqrt{(3n)^2 + 8x_k}} = \\ &= -\frac{3}{\sqrt{8x_k}} + 6 \Sigma_{k,0}, \end{aligned} \quad (5)$$

with

$$\frac{k}{x_k} = \frac{2, 5, 6, 10, 12, 15}{3, 9, 12, 21, 27, 36}.$$

The calculation is somewhat different in the case of black chains. In the lattice type considered a black chain consists of an "upper" (black) and a "lower" (red) half-chain (Fig. 6). The symmetry is lost, and both half-chains have to be treated separately. The words "upper" and "lower" refer to Fig. 6. The initial link of the upper half-chain is at the distance $1/3$ and that of the lower half-chain at the distance $2/3$ from the basic plane.

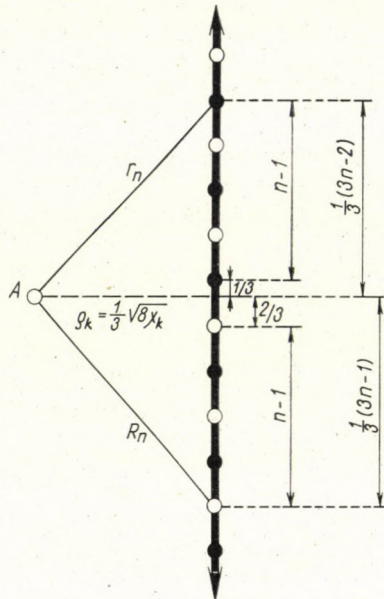


Fig. 6. A black chain consists of an "upper" (black) and a "lower" (red) half-chain. The chain is in the k^{th} cylindric shell. $k = 1, 3, 4, 7, 8, 9, 11, 13, 14$

The distance of the n^{th} link of the k^{th} lower half-chain from A is

$$R_{k,n} = \frac{1}{3} \sqrt{(3n-1)^2 + 8x_k}$$

and the binding energy of this lower half-chain in respect of the point A is

$$\varphi_{k,1} = 3 \sum_{n=1}^{\infty} (-1)^n \frac{1}{\sqrt{(3n-1)^2 + 8x_k}} = -3 \Sigma_{k,1}. \quad (6)$$

Similar formulas can be obtained for the upper half-chain also:

$$\begin{aligned} r_{k,n} &= \frac{1}{3} \sqrt{(3n-2)^2 + 8x_k}, \\ \varphi_{k,2} &= 3 \sum_{n=1}^{\infty} (-1)^{n-1} \frac{1}{\sqrt{(3n-2)^2 + 8x_k}} = +3 \cdot \Sigma_{k,2} \end{aligned} \quad (7)$$

with

$k = 1$	3	4	7	8	9	11	13	14
$x_k = 1$	4	7	13	16	19	25	28	31

Table III
Energy values for red chains

x_k	$\frac{3}{\sqrt{8X_k}}$	$\Sigma_{k,0}$	Chain energy
3	0,61237243	0,09992815	-0,01280353
9	,35355339	,05888730	-,00022959
12	,30618621	,5102202	-,00005409
21	,23145502	,03857555	-,00000172
27	,20412414	,03402065	-,00000024
36	,17677670	,02946277	-,00000008

The energy of the chain from (6) and (7) is therefore

$$\varphi_{k,1} + \varphi_{k,2} = 3 [\Sigma_{k,2} - \Sigma_{k,1}]. \quad (8)$$

The computation of the sums $\Sigma_{k,0}$, $\Sigma_{k,1}$ and $\Sigma_{k,2}$ in the formulas (5), (6) and (7) can be significantly simplified by the use of the method of the successive arithmetical means discussed briefly in the Appendix.

IV. The Madelung constant of CsCl

We give the results of our calculations in a few tables. Tables III and IV contain energy values for red and black chains calculated according to the formulas (5) and (6), respectively.

Table IV
Energy values for black chains

x_k	$\Sigma_{k,2}$	$\Sigma_{k,1}$	$3 [\Sigma_{k,2} - \Sigma_{k,1}]$
1	0,20707332	0,18294707	0,07237875
4	,09245585	,09155538	,00270141
7	,06832757	,06821142	,00034845
13	,04955419	,04954837	,00001746
16	,04456887	,04456715	,00000516
19	,04084023	,04083966	,00000171
25	,03554059	,03554051	,00000024
28	,03356305	,03356301	,00000012
31	,03188282	,03188281	,00000003

Table V
Binding energy in the CsCl lattice

<i>k</i>	<i>x_k</i>	<i>a</i>	Energy of a chain		Energy of a shell	Total energy
0	—	0	1,38629436	1	1,38629436	1,38629436
1	1	8/9	,07237875	6	,43427250	1,82056686
2	3	24/9	—,01280353	6	—,07682118	1,74374568
3	4	32/9	,00270141	6	,01620846	1,75995414
4	7	56/9	,00034845	12	,00418140	1,76413554
5	9	72/9	—,00022959	6	—,00137754	1,76275800
6	12	96/9	—,00005409	6	—,00032454	1,76224346
7	13	104/9	,00001746	12	,00020952	1,76264298
8	16	128/9	,00000516	6	,00003096	1,76267394
9	19	152/9	,00000171	12	,00002052	1,76269446
10	21	168/9	—,00000172	12	—,00002064	1,76267382
11	25	200/9	,00000024	6	,00000144	1,76267526
12	27	216/9	—,00000024	6	—,00000144	1,76267382
13	28	224/9	,00000012	12	,00000144	1,76267526
14	31	248/9	,00000003	12	,00000036	1,76267562
15	36	288/9	—,00000008	6	—,00000048	1,76267514

The negative energy values mean that the red ion which is situated in the point of reference is repulsed by the red chains which have initial links of the same charge. The energies of the black chains are for the same reason positive.

With the energy values in Tables III and IV we can evaluate the Madelung constant of CsCl. The results are given in Table V in an arrangement similar to that of Table II.

Here, too we obtain in the last column the approximate values of the Madelung constant. Their accuracy is shown below:

$$k = \frac{1}{\text{number of exact digits} = 1} \left| \begin{array}{c} 3 \\ 2 \end{array} \right| \left| \begin{array}{c} 5 \\ 3 \end{array} \right| \left| \begin{array}{c} 7 \\ 4 \end{array} \right| \left| \begin{array}{c} 9 \\ 5 \end{array} \right| \left| \begin{array}{c} 11 \\ 6 \end{array} \right| \left| \begin{array}{c} 14 \\ 7 \end{array} \right| .$$

Our result agrees with that obtained by other authors.

V. The Madelung constant of ZsS and CaF₂ lattices

There exist certain simple relations between some of the constants for cubic-type crystals. These relations, suspected by WHEELER and determined by HOPPE [7] and BENSON and VAN ZEGGEREN [2], may be written as

$$M(\text{Ca F}_2) = \frac{\sqrt{3}}{2} M(\text{Na Cl}) + 2 \cdot M(\text{CsCl}),$$

$$M(\text{Zn S}) = \frac{\sqrt{3}}{4} M(\text{Na Cl}) + \frac{1}{2} M(\text{CsCl}).$$

With the help of our results (Tables II and V)

$$M(\text{NaCl}) = 1,747565,$$

$$M(\text{CsCl}) = 1,762675$$

and we have for calcium fluorite

$$M(\text{CaF}_2) = 5,038785$$

and for zinc blende

$$M(\text{ZnS}) = 1,638055.$$

These results agree with those known from the literature.

VI. Summary

The results of the present paper may be briefly summarized as follows.

a) The chain method developed originally for lattices of the NaCl-type can be applied to the lattice of CsCl also.

b) Parallel chains are considered along co-axial cylindric shells, the radii of which are given by the formula

$$\varrho_h = \varrho_1 \sqrt{x_k}.$$

The quantities ϱ_1 and x_k have different values for the lattice of NaCl and for that of CsCl-type, they can easily be determined.

c) The numerical calculations may be carried out using only elementary mathematical operations. The results which are given in a few Tables, are correct to six decimal digits.

d) The Madelung constant of CaF₂-type and ZnS-type lattices are computed from linear relations between their Madelung constants and those of NaCl- and CsCl-type crystals.

e) The values of the Madelung constant of NaCl, CsCl, CaF₂ and ZnS are shown in column 1. of Table VI which, for comparison, includes in column 2. the values published by BENSON and VAN ZEGGEREN [2].

Table VI

	1.	2.
NaCl	1,747565	
CsCl	1,762675	1,7626747730
CaF ₂	5,038785	5,0387848798
ZnS	1,638055	1,6380550533

Acknowledgements

The author wishes to express his thanks to Prof. Z. GYULAI for constant interest in this work; to the Mathematical Research Institute of the Hungarian Academy of Sciences, Department for Differential Equations, and especially to DR. G. FREUD, for the proof given in the Appendix; to the Hungarian Central Statistical Office, Department of Electronic Computers, and especially to Mrs. F. JÁNCSSÓ for help in numerical calculations; and to his colleagues at the Institute, where this work was carried out, for detailed and helpful discussions.

Appendix*Method of the successive arithmetical means***I**

We consider the following infinite sum

$$\varphi(a) = (-1)^a \sum_{n=1}^{\infty} (-1)^{n-1} \frac{1}{\sqrt{n^2 + a}}$$

and denote the series of its partial sums by

$$a_1, a_2, \dots, a_n, \dots,$$

the successive arithmetical means of which are

$$\beta_n = \frac{a_n + a_{n+1}}{2}, \quad n = 1, 2, 3, \dots$$

The common limes both of a_n and β_n be a . We shall prove that

$$|a_n - a| = \frac{1}{2n} + O\left(\frac{1}{n^2}\right)$$

and

$$|\beta_n - a| = \frac{1}{(2n)^2} + O\left(\frac{1}{n^3}\right),$$

which means that the series of the successive arithmetical means converges better than the original series.

We shall first prove that

$$|a_n - a| \leq \frac{1}{2n} + O\left(\frac{1}{n^2}\right). \quad (1)$$

For this purpose we write

$$\begin{aligned} (-1)^a \varphi(a) &= \sum_{n=1}^{\infty} (-1)^{n-1} \frac{1}{\sqrt{n^2 + a}} = \\ &= \sum_{k=0}^{\infty} \frac{1}{\sqrt{(2k+1)^2 + a}} - \sum_{k=1}^{\infty} \frac{1}{\sqrt{(2k)^2 + a}}. \end{aligned}$$

The n -th partial sum of this, for $n = 2l$, is

$$\begin{aligned} a_n &= \sum_{x=0}^{l-1} \frac{1}{\sqrt{(2x+1)^2 + a}} - \sum_{x=1}^l \frac{1}{\sqrt{(2x)^2 + a}} = \\ &= \sum_{x=0}^{l-1} f_1(x) - \sum_{x=1}^l f_2(x) = a_n^{(1)} - a_n^{(2)}. \end{aligned}$$

$a_n^{(1)}$ and $a_n^{(2)}$ can be expressed by the so-called *Eulersche Summenformel* (the sum formula of EULER) in the following way:

$$a_n^{(1)} = \int_0^{l-1} f_1(x) dx + \frac{1}{2} [f_1(l-1) + f_1(0)] + \int_0^{l-1} \bar{B}_1(x) f'_1(x) dx,$$

where $\bar{B}_1(x)$ is the polynom of BERNOULLI of index 1. So we obtain

$$\begin{aligned} a_n &= \left\{ \int_0^{l-1} f_1(x) dx - \int_1^l f_2(x) dx \right\} + \frac{1}{2} \left(\frac{1}{\sqrt{(n-1)^2 + a}} - \frac{1}{\sqrt{n^2 + a}} \right) + \\ &\quad + \left[\int_0^{l-1} \bar{B}_1(x) f'_1(x) dx - \int_1^l \bar{B}_1(x) f'_2(x) dx \right] + \text{const}, \end{aligned}$$

where

$$\int_0^{l-1} f_1(x) dx - \int_1^l f_2(x) dx = \frac{1}{2} \int_n^{n-1} \frac{du}{\sqrt{u^2 + a}} + \text{const.}$$

The limit a can be expressed also with the help of the *Eulerschen Summenformeln*:

$$a = \left\{ \int_0^\infty [f_1(x) - f_2(x)] dx \right\} + \int_0^\infty \bar{B}_1(x) f'_1(x) dx - \int_1^\infty \bar{B}_1(x) f'_2(x) dx.$$

Hence, because of

$$|\bar{B}_1(x)| \leq \frac{2}{\pi}$$

after some changes we obtain

$$\begin{aligned} |a_n - a| &\leq \frac{1}{2} \left| \int_{n-1}^n \frac{du}{\sqrt{u^2 + a}} \right| + \frac{1}{2} \left(\frac{1}{\sqrt{(n-1)^2 + a}} - \frac{1}{\sqrt{n^2 + a}} \right) + \\ &+ \left(\frac{1}{\sqrt{(n-1)^2 + a}} - \frac{1}{\sqrt{(n+2)^2 + a}} \right) + \frac{2}{\pi} \left(\frac{1}{\sqrt{n^2 + a}} - \frac{1}{\sqrt{(n+2)^2 + a}} \right). \end{aligned}$$

The three last terms are of the order $O\left(\frac{1}{n^2}\right)$. The first term can be checked against the first mean-value theorem of the integral calculus:

$$\int_{n-1}^n \frac{du}{\sqrt{u^2 + a}} = \frac{1}{\sqrt{(n-\vartheta)^2 + a}}, \quad 0 \leq \vartheta \leq 1.$$

Hence

$$|a_n - a| \leq \frac{1}{2} \frac{1}{\sqrt{(n-\vartheta)^2 + a}} + O\left(\frac{1}{n^2}\right) = \frac{1}{2n} + O\left(\frac{1}{n^2}\right).$$

On the other hand it can be similarly shown that

$$|a_n - a| \geq \frac{1}{2n} + O\left(\frac{1}{n^2}\right).$$

From the two last expressions it follows that

$$|a_n - a| = \frac{1}{2n} + O\left(\frac{1}{n^2}\right).$$

qu.e.d

II

We discuss now the β_n -series.

$$\begin{aligned}\beta_n &= \frac{\alpha_n + \alpha_{n+1}}{2} = \\ &= \frac{1}{2} \left(\sum_{x=0}^{k-1} \frac{1}{\sqrt{(2x+1)^2 + a}} + \sum_{x=0}^l \frac{1}{\sqrt{(2x+3)^2 + a}} - \sum_{x=1}^l \frac{1}{\sqrt{(2x)^2 + a}} \right) = \\ &= \sum_{x=0}^{l-1} f_3(x) - \sum_{x=1}^l \frac{1}{\sqrt{(2x)^2 + a}} = \beta_n^{(1)} - \beta_n^{(2)}.\end{aligned}$$

Using again the *Eulersche Summenformel* we obtain

$$\begin{aligned}|\beta_n - a| &= \frac{1}{2^2} \left| \int_n^{n+1} \frac{du}{\sqrt{u^2 + a}} - \int_{n-1}^n \frac{du}{\sqrt{u^2 + a}} \right| + O\left(\frac{1}{n^3}\right) \\ \int_n^{n+1} \frac{du}{\sqrt{u^2 + a}} - \int_{n-1}^n \frac{du}{\sqrt{u^2 + a}} &= \frac{1}{\sqrt{(n-\vartheta_1)^2 + a}} - \frac{1}{\sqrt{(n-\vartheta_2)^2 + a}} = \\ &= \frac{1}{n^2} + O\left(\frac{1}{n^3}\right),\end{aligned}$$

where

$$0 \leq \left\{ \begin{array}{l} \vartheta_1 \\ \vartheta_2 \end{array} \right\} \leq 1.$$

Hence

$$|\beta_n - a| \leq \frac{1}{(2n)^2} + O\left(\frac{1}{n^3}\right).$$

As, on the other hand, it can be shown that

$$|\beta_n - a| \geq \frac{1}{(2n)^2} + O\left(\frac{1}{n^3}\right),$$

it follows that

$$|\beta_n - a| = \frac{1}{(2n)^2} + O\left(\frac{1}{n^3}\right).$$

The proof continues in a similar way also for the case $n = 2l + 1$ and gives the same result as above. Our statement is thus fully proved.

REFERENCES

1. F. FÁTHY and F. BUKOVSKY, *Acta Phys. Hung.*, **8**, 89, 1957; **9**, 275, 1959.
2. G. C. BENSON and F. VAN ZEGGEREN, *J. Chem. Phys.*, **26**, 1083, 1957.
3. E. MADELUNG, *Phys. Zs.*, **19**, 524, 1918.
4. W. KOSSEL, *Die molekularen Vorgänge beim Kristallwachstum*, Leipziger Vorträge, Hirzel, Leipzig, 1928.
H. E. BUCKLEY, *Crystal Growth*, John Wiley and Sons, New York, 1951.
5. F. C. FRANK, *Phil. Mag.*, **41**, 1287, 1950.
6. O. EMERSLEBEN, *Der Wert der Madelungkonstanten des Steinsalzgitters. Kritische Zusammenfassung*. *Wiss. Zs. d. Univ. Greifswald*, III, 607, 1953/54;
Y. SAKAMOTO, *J. Sci. Hiroshima Univ. Ser. A.*, **16**, 569, 1953.
7. R. HOPPE, *Z. Anorg. Allgem. Chem.*, **283**, 196, 1956.

ВЫЧИСЛЕНИЕ ПОСТОЯННОЙ МАДЕЛУНГА ЭЛЕМЕНТАРНЫМ ПУТЕМ
ДЛЯ НЕСКОЛЬКИХ КУБИЧЕСКИХ РЕШЕТОК

Ф. БУКОВСКИ

Р е з и о м е

Соответствующим применением цепного метода автором вычисляется постоянная Маделунга для решёток NaCl и CsCl . На основе этих результатов, используя линейные зависимости Бензона и Цеггера, определяется значение постоянной Маделунга для решёток CaF_2 и ZnS .

SOME DEVELOPMENTS IN THE SEMIEMPIRICAL THEORIES OF MOLECULAR CRYSTALS. I. THE HÜCKEL APPROXIMATION

By

J. LADIK

CENTRAL RESEARCH INSTITUTE FOR CHEMISTRY OF THE HUNGARIAN ACADEMY OF SCIENCES, BUDAPEST

(Presented by G. Schay. — Received 11. VI. 1964)

The paper reviews the calculation of energy bands in the HÜCKEL approximation of one-dimensional periodic and nearly periodic polymers, which have an arbitrary number of atoms in the elementary cell. In the derivation the BORN—KÁRMÁN periodic boundary condition has been used and only nearest neighbour interactions have been taken into account. The matrix formulation of the problem is extended also to three-dimensional molecular crystals by taking into account only interactions between first, second and third neighbours with arbitrary symmetry and with an arbitrary number of atoms in the elementary cell. Finally, appropriate expressions are given also for the case when we have slightly different types of units in the three-dimensional polymers.

Introduction

For the investigation of the physical properties of different organic synthetic- and biopolymers the semiempirical theories of molecular crystals have an increasing importance. We shall discuss here only those semiempirical theories, which refer to polymers in which 1) there is a small, but non-negligible overlap-type interaction between atoms belonging to different molecules as compared to the interactions within the molecules and 2) it is possible to define an elementary cell (periodic polymers) or an approximate elementary cell (pseudoperiodic polymers). Further 3) the van der Waals type interactions between the different molecules of the molecular crystal are not included in these theories.

Using the simple LCAO MO method in its semiempirical form and neglecting the overlap integrals (HÜCKEL approximation), we can derive comparatively simple expressions for the calculation of the energy band structure of a molecular crystal, if we introduce the BORN—KÁRMÁN periodic boundary condition and we take into account only interactions between nearest neighbours in the one-dimensional case and between the first, second and third neighbours* in the three-dimensional case. In this paper we review the

* We shall call first neighbours of a given elementary cell characterized by the lattice vector $R_j = j_1 a_1 + j_2 a_2 + j_3 a_3$ (a_1 , a_2 and a_3 are the primitive translation vectors) in a three-dimensional solid those cells which have such $R_h = h_1 a_1 + h_2 a_2 + h_3 a_3$ lattice vectors, that $h_1 = j_1 \pm 1$ and $h_2 = j_2$, $h_3 = j_3$, or $h_2 = j_2 \pm 1$ and $h_1 = j_1$, $h_3 = j_3$ holds, or finally (footnote continued on page 174)

resulting expressions for one- and three-dimensional periodic and pseudo-periodic molecular crystals. In a subsequent paper we give the appropriate expressions for the semiempirical SCF LCAO MO and CI methods (PARISER—PARR—POPLE approximation [1, 2]).

One-dimensional case

If we have in a linear chain N elementary cells and n atoms within the elementary cell, which contribute electrons to the delocalized electron system, we may write for the crystal orbitals in the tight binding (LCAO) approximation (see for instance [3])

$$\Psi_{p,t}(\underline{r}) = \sum_{j=1}^N \sum_{l=1}^n c_{p,t;j,l} \Phi_l(\underline{r}_l - j\underline{a}), \quad p = 1, 2, \dots, N, \quad t = 1, 2, \dots, n. \quad (1)$$

Here $c_{p,t;j,l}$ is the coefficient of the l -th atom in the j -th elementary cell in the crystal orbital characterized by the two quantum numbers p and t , $\Phi_l(\underline{r}_l - j\underline{a})$ is the atomic orbital belonging to the l -th atom of the j -th elementary cell and \underline{a} is the primitive translation vector. Introducing the BORN—KÁRMÁN periodic boundary condition

$$\Psi_{p,t}(\underline{r} + N\underline{a}) = \Psi_{p,t}(\underline{r}), \quad (2)$$

for the coefficients the BLOCH condition [3]

$$c_{p,t;j,l} = \exp\left(\frac{i 2 \pi p}{N} j\right) c_{p,t;l} \quad (3)$$

follows. If N is a large number we may substitute the integer $p(p = 1, 2, \dots, N)$ by the continuous variable

$$k = \frac{2 \pi p}{N}, \quad 0 \leq k \leq 2 \pi \quad (4)$$

and may rewrite (3) in the form

$$c_{k,t;j,l} = e^{ikj} c_{k,t;l}. \quad (5)$$

(continued)

$h_3 = j_3 \pm 1$ and $h_1 = j_1$, $h_2 = j_2$. We define as second neighbours those cells for which two components of the lattice vector are simultaneously different, e.g. $h_1 = j_1 \pm 1$, $h_2 = j_2 \pm 1$ and $h_3 = j_3$. Finally, we shall call third neighbours those cells for which all three components are different $h_1 = j_1 \pm 1$, $h_2 = j_2 \pm 1$ and $h_3 = j_3 \pm 1$. It should be mentioned that the second and third neighbours defined in this way are in most cases (but not always) the second and third nearest neighbours in a geometrical sense. The number of the first neighbours of an elementary cell is 6 and the number of the second and third neighbours (as defined above) is 12 and 8, respectively.

Substituting the wave function (1) with condition (5) into the expression of the expectation value of the effective one-electron Hamiltonian of the system and applying the variation principle, it is possible to arrive at an eigenvalue problem of a Hermitian complex matrix. Although this has already been demonstrated for the one-dimensional case [3], it will be repeated here in detail, because on its basis it will be easy to generalize the resulting expressions for the three-dimensional case.

For the expectation value of the effective one-electron Hamiltonian we may write

$$\begin{aligned} \langle H \rangle &= \frac{\int \Psi_k^* H \Psi_k dV}{\int \Psi_k^* \Psi_k dV} = \\ &= \frac{\int \left[\sum_{j=1}^N \sum_{l=1}^n e^{-ikj} c_{k;l}^* \Phi_l^*(\underline{r}_l - j\underline{a}) \right] H \left[\sum_{h=1}^N \sum_{s=1}^n e^{ikh} c_{k;s} \Phi_s(\underline{r}_s - h\underline{a}) \right] dV}{\int \left[\sum_{j=1}^N \sum_{l=1}^n e^{-ikj} c_{k;l}^* \Phi_l^*(\underline{r}_l - j\underline{a}) \right] \left[\sum_{h=1}^N \sum_{s=1}^n e^{ikh} c_{k;s} \Phi_h(\underline{r}_s - h\underline{a}) \right] dV}, \\ &\quad 0 \leq k \leq 2\pi \end{aligned} \quad (6)$$

where for the sake of simplicity we have dropped the index t .

Introducing further the simplifying condition that we take into account only interactions between nearest neighbours, we find that from the summation according to h we have to keep only the terms

$$h = j \quad \text{or} \quad j \pm 1. \quad (7)$$

In this way we obtain the expression

$$\langle H \rangle = \frac{N \sum_{l=1}^n \sum_{s=1}^n c_{k;l}^* c_{k;s} [\beta_{l,s} + \beta_{l,s}^+ e^{ik} + \beta_{l,s}^- e^{-ik}]}{N \sum_{l=1}^n \sum_{s=1}^n c_{k;l}^* c_{k;s} [S_{l,s} + S_{l,s}^+ e^{ik} + S_{l,s}^- e^{-ik}]}, \quad (8)$$

where

$$\begin{aligned} \beta_{l,s} &= \langle \Phi_l(\underline{r}_l - j\underline{a}) | H | \Phi_s(\underline{r}_s - j\underline{a}) \rangle, \quad \beta_{l,s}^\pm = \\ &= \langle \Phi_l(\underline{r}_l - j\underline{a}) | H | \Phi_s(\underline{r}_s - (j \pm 1)\underline{a}) \rangle \end{aligned}$$

and

$$\begin{aligned} S_{l,s} &= \langle \Phi_l(\underline{r}_l - j\underline{a}) | \Phi_s(\underline{r}_s - j\underline{a}) \rangle, \quad S_{l,s}^\pm = \\ &= \langle \Phi_l(\underline{r}_l - j\underline{a}) | \Phi_s(\underline{r}_s - (j \pm 1)\underline{a}) \rangle. \end{aligned}$$

In equ. (8) the first term in the brackets of the nominator and the denominator refers to the case $h = j$, while the second and the third to the cases

$h = j + 1$ and $h = j - 1$. Since the terms of the double sums in equ. (8) do not depend on j , the summation according to j gives merely a factor N in the nominator and the denominator.

Applying the variation principle we obtain in the usual way with the aid of the minimum conditions

$$\frac{\partial \langle H \rangle}{\partial c_{k;l}^*} = \frac{\partial \langle H \rangle}{\partial c_{k;s}} = 0, \quad l = 1, 2, \dots, n, \quad 0 \leq k \leq 2\pi \quad (9)$$

the secular equation

$$\frac{\partial \langle H \rangle}{\partial c_{k;l}^*} = \sum_{s=1}^n [\beta_{l,s} - S_{l,s} \varepsilon(k) + e^{ik} (\beta_{l,s}^+ - S_{l,s}^+ \varepsilon(k)) + e^{-ik} (\beta_{l,s}^- - S_{l,s}^- \varepsilon(k))] c_{k;s} = 0. \quad (10)$$

Here we have denoted by $\varepsilon(k)$ the minimum values of $\langle H \rangle$ as a function of the coefficients $c_{k;l}^*$ and $c_{k;s}$.

If we neglect the overlap integrals, as is usual in the simple HÜCKEL approximation,

$$S_{l,s} = \delta_{l,s}, \quad S_{l,s}^\pm = 0, \quad (11)$$

we obtain the matrix eigenvalue problem

$$\gamma c_{k;l} = \varepsilon(k)_t c_{k;l}. \quad (12)$$

Here the elements of the matrix γ are

$$\gamma_{l,s} = \beta_{l,s} + \beta_{l,s}^+ e^{ik} + \beta_{l,s}^- e^{-ik}. \quad (13)$$

Since even in the most general case, when we have not only a translation of the elementary cells but also a screw, the relation

$$\beta_{l,s}^+ = \beta_{s,l}^- \quad (14)$$

holds, we have always $\gamma_{l,s} = \gamma_{s,l}$. Therefore γ is a Hermitian complex matrix with real $\varepsilon(k)_t$ eigenvalues but complex eigenvectors. The eigenvalues $t = 1, 2, \dots, n$ of γ for a given k value belong to the n different energy bands, and the $\varepsilon(k)_t$ values for given t but k varying from 0 to 2π form the t -th energy band.

For the solution of the complex matrix eigenvalue problem (12) standard mathematical methods are known. The most simple one is to rewrite the

eigenvalue problem of a complex matrix of order n as the eigenvalue problem of a real matrix of order $2n$ (for the details and for the determinations of the limits of the energy bands see [4]).

For actual numerical computations we have to substitute the values of the $\beta_{l,s}$ and $\beta_{s,l}^\pm$ integrals into equations (13) and (14). In the simple HÜCKEL approximation the $\beta_{l,s}$ integrals are taken as empirical parameters. The $\beta_{l,s}^\pm$ integrals can be calculated with the aid of the relation

$$\frac{\beta_{l,s}(R_1)}{\beta_{l,s}^\pm(R_2)} = \frac{S_{l,s}(R_1)}{S_{l,s}^\pm(R_2)}, \quad (15)$$

if we know the values of the parameters $\beta_{l,s}(R_1)$. (Here R_1 and R_2 denote two different distances between the centres l and s).

In the case when we have N units in the linear chain, which are not all identical, but differ only slightly, it is yet possible to determine the energy bands approximately. If the BORN-KÁRMÁN periodic boundary condition is valid for the chain and we take into account only nearest neighbour interactions, we can write down for the chain in the HÜCKEL LCAO MO approximation the equation

$$D = \begin{vmatrix} \mathbf{A}_1 & \mathbf{B}_{1,2} & 0 & \dots & 0 & \mathbf{B}_{1,N} \\ \mathbf{B}_{1,2}^t & \mathbf{A}_2 & \mathbf{B}_{2,3} & \dots & 0 & 0 \\ 0 & \mathbf{B}_{2,3}^t & \mathbf{A}_3 & \dots & 0 & 0 \\ \vdots & \vdots & \vdots & \ddots & \vdots & \vdots \\ \vdots & \vdots & \vdots & \ddots & \vdots & \vdots \\ 0 & 0 & 0 & \dots & \mathbf{A}_{N-1} & \mathbf{B}_{N-1,N} \\ \mathbf{B}_{1,N}^t & 0 & 0 & \dots & \mathbf{B}_{N-1,N}^t & \mathbf{A}_N \end{vmatrix} = 0. \quad (16)$$

Here in the diagonal the matrices \mathbf{A}_i refer to the different units including in their diagonal elements the $-\lambda$ terms (where λ is the root of the determinantal equation (16)) and the matrices $\mathbf{B}_{i,i+1}$ and their transposed $\mathbf{B}_{i,i+1}^t$ refer to the interaction between the neighbouring units. If we have m different kinds

of units, the order of determinant D will be $r = \sum_{i=1}^m q_i n_i$, where n_i is the order

of the i -th type matrix and q_i its frequency in the chain $\left(\sum_{i=1}^m q_i = N \right)$. The exact solution of that matrix eigenvalue problem of order r which is equivalent to the determinantal equation (16), is practically impossible because of the extremely high order involved.

By a generalization of a method due to ORLOV and MEN [5] BELEZNAY and BICZÓ [6] were able to show that by neglecting only second and higher order terms, equation (16) may be substituted by the equation

$$\bar{D} = \begin{vmatrix} \bar{\mathbf{A}} & \bar{\mathbf{B}} & 0 & \dots & 0 & \bar{\mathbf{B}} \\ \bar{\mathbf{B}}^t & \bar{\mathbf{A}} & \bar{\mathbf{B}} & \dots & 0 & 0 \\ 0 & \bar{\mathbf{B}}^t & \bar{\mathbf{A}} & \dots & 0 & 0 \\ \vdots & \vdots & \vdots & \ddots & \vdots & \vdots \\ \vdots & \vdots & \vdots & & \vdots & \vdots \\ \bar{\mathbf{B}}^t & 0 & 0 & \dots & \bar{\mathbf{B}}^t & \bar{\mathbf{A}} \end{vmatrix} = 0. \quad (17)$$

Here the average matrices $\bar{\mathbf{A}}$ and $\bar{\mathbf{B}}$ are defined by

$$\bar{\mathbf{A}} = \sum_{i=1}^m p_i \mathbf{A}_i \quad ; \quad \bar{\mathbf{B}} = \sum_{j=1}^m p_{j,k} \mathbf{B}_{j,k}, \quad (18)$$

where p_i is the probability of the occurrence of the i -th type of unit and $p_{j,k}$ is the probability to have the unit k after j in the chain (nearest neighbour frequency).

The neglected terms, as is possible to show [6], are $O(\alpha_i^2, \beta_{i,i+1}^2)$, where the deviation matrices α_i $\beta_{i,i+1}$ are defined by

$$\alpha_i = \mathbf{A}_i - \bar{\mathbf{A}}, \quad \beta_{i,i+1} = \mathbf{B}_{i,i+1} - \bar{\mathbf{B}}. \quad (18a)$$

It should be mentioned that in order to keep small the errors due to the neglection of the second and higher order terms, as BELEZNAY and BICZÓ [6] have pointed out, it is advantageous to use the diagonalized forms of the matrices \mathbf{A}_i instead of the original ones. By doing this we have of course to perform an appropriate transformation also on the matrices $\mathbf{B}_{j,k}$ in (18) [6], which have, in general, in the case of molecular crystals, elements smaller by an order of magnitude than the elements of the \mathbf{A}_i matrices. It should be emphasized further that the performance of the average matrices according to equations (18) and the substitutions of equation (16) by (17) will lead to small errors only in that case if the units of the chain differ only slightly (pseudoperiodic polymers).

Equation (17) refers to a periodic structure for which we can write, in analogy with equation (12) and (13), the complex Hermitian matrix eigenvalue problem

$$\bar{\gamma} \underline{c}_{k;t} = (\bar{\mathbf{A}} + \bar{\mathbf{B}} e^{ik} + \bar{\mathbf{B}}^t e^{-ik}) \underline{c}_{k;t} = \varepsilon(k)_t \underline{c}_{k;t}, \quad (19)$$

which can be solved in the above mentioned way.

Three-dimensional case

In the case of a three-dimensional molecular crystal, if the BORN-KÁRMÁN boundary condition is valid, we may write

$$\psi_{k,t}(\underline{r} + \underline{R}_N) = \psi_{k,t}(\underline{r}), \quad (20)$$

where

$$\underline{R}_N = N_1 \underline{a}_1 + N_2 \underline{a}_2 + N_3 \underline{a}_3. \quad (21)$$

N_1, N_2, N_3 are large integers ($N_1 N_2 N_3$ is the number of elementary cells in the crystal) and $\underline{a}_1, \underline{a}_2$ and \underline{a}_3 are the primitive translation vectors. In contradiction to the one-dimensional case k is now also a vector. If we introduce for $\psi_{k,t}(\underline{r})$ again LCAO crystal orbitals, we can write

$$\Psi_{k,t}(\underline{r}) = \sum_{j_1, j_2, j_3=1}^{N_1 N_2 N_3} \sum_{l=1}^n c_{k,t;j_l,l} \Phi_l(\underline{r}_l - \underline{R}_{j_l}), \quad (22)$$

where the symbol j stands as an abbreviation of j_1, j_2 and j_3 and the summation index l runs from 1 to n , the number of atoms within the elementary cell, which contribute electrons to the delocalized electron system. \underline{R}_j in the argument of $\Phi_l(\underline{r}_l - \underline{R}_j)$, the atomic orbital of the l -th atom in the elementary cell characterized by j , is the lattice vector

$$\underline{R}_j = j_1 \underline{a}_1 + j_2 \underline{a}_2 + j_3 \underline{a}_3. \quad (23)$$

If we put equation (22) into equation (20) we obtain for the coefficients $c_{k,t;j_l,l}$ the Bloch condition

$$c_{k,t;j_l,l} = c_{k,t;l} e^{ik \cdot \underline{R}_j}. \quad (24)$$

Since the possible vectors \underline{k} of a Brillouin zone are usually given by the possible values of their rectangular components, it is advantageous to express also the primitive translation vectors $\underline{a}_1, \underline{a}_2, \underline{a}_3$, which are not always rectangular, and thus also the vectors \underline{R}_j in their rectangular components. In this way we obtain

$$k \underline{R}_j = k_x j_x + k_y j_y + k_z j_z, \quad (25)$$

where

$$j_r = j_1 a_{1r} + j_2 a_{2r} + j_3 a_{3r}. \quad (r = x, y, z) \quad (26)$$

Substituting equations (26), (25) and (24) into the expression (22) of the crystal orbitals, we form with the aid of the latter the expectation value of the Hamiltonian

$$\begin{aligned}
 \langle H \rangle &= \frac{\int \Psi_{k,t}^* H \Psi_{k,t} dV}{\int \Psi_{k,t}^* \Psi_{k,t} dV} = \\
 &= \frac{\int \left[\sum_{j_1, j_2, j_3}^{N_1 N_2 N_3} \sum_{l=1}^n \exp \left(\sum_{r=x,y,z} -ik_r [j_1 a_{1r} + j_2 a_{2r} + a_{3r}] \right) \right]}{\int \left[\sum_{h_1 h_2 h_3}^{N_1 N_2 N_3} \sum_{f=1}^n \exp \left(+ \right. \right.} \\
 &\quad \cdot [c_{k,t;l}^* \Phi_l^*(r_l - R_j)] H \left. \sum_{h_1 h_2 h_3}^{N_1 N_2 N_3} \sum_{f=1}^n \exp \left(+ \right. \right. \\
 &\quad \left. \left. + \sum_{r=x,y,z} ik_r [h_1 a_{1r} + h_2 a_{2r} + h_3 a_{3r}] \right) \cdot c_{k,t;f} \Phi_f(r_f - k_h) \right] dV,
 \end{aligned} \tag{27}$$

where in the brackets in the denominator we have the same expressions as in the nominator. Taking into account only first, second and third neighbour interactions (for their definition see the Introduction) we have the conditions

$$\begin{aligned}
 h_1 &= j_1 \quad \text{or} \quad j_1 \pm 1, \\
 h_2 &= j_2 \quad \text{or} \quad j_2 \pm 1, \\
 h_3 &= j_3 \quad \text{or} \quad j_3 \pm 1.
 \end{aligned} \tag{28}$$

With the aid of these conditions and by introducing the neglections customary in the HÜCKEL approximation, after a somewhat lengthy but simple calculation quite similar to the procedure described in detail in the one-dimensional case (equs. (8)—(14)), we arrive again at the eigenvalue problem of a complex matrix:

$$\gamma c_{k,t} = \varepsilon(k)_t c_{k,t}. \tag{29}$$

The elements of γ are defined by

$$\begin{aligned}
 \gamma_{i,j} &= \beta_{i,j} + \sum_{s=1}^3 [(\beta_{i,j}^+)_s e^{ins} + (\beta_{i,j}^-)_s e^{-ins}] + \sum_{s>t}^3 [(\beta_{i,j}^{++})_{s,t} e^{i(n_s+n_t)} + \\
 &\quad + (\beta_{i,j}^{+-})_{s,t} e^{i(n_s-n_t)} + (\beta_{i,j}^{-+})_{s,t} e^{-i(n_s-n_t)} + (\beta_{i,j}^{--})_{s,t} e^{-i(n_s+n_t)}] + \\
 &\quad + (\beta_{i,j}^{+++})_{1,2,3} e^{i(n_1+n_2+n_3)} + (\beta_{i,j}^{++-})_{1,2,2} e^{i(-n_1+n_2+n_3)} + \\
 &\quad + (\beta_{i,j}^{+-+})_{1,2,3} e^{i(n_1-n_2+n_3)} + (\beta_{i,j}^{+-})_{1,2,2} e^{i(n_1+n_2-n_3)} + \\
 &\quad + (\beta_{i,j}^{--+})_{1,2,3} e^{-i(-n_1+n_2+n_3)} + (\beta_{i,j}^{-+-})_{1,2,3} e^{-i(n_1-n_2+n_3)} + \\
 &\quad + (\beta_{i,j}^{--+})_{1,2,3} e^{-i(n_1+n_2-n_3)} + (\beta_{i,j}^{--})_{1,2,3} e^{-i(n_1+n_2+n_3)},
 \end{aligned} \tag{30}$$

where

$$n_s = \sum_{r=x,y,z} k_r a_{sr} \quad (s = 1, 2, 3). \tag{31}$$

The rather complicated expression (30) refers to the general case, in actual cases it is simplified considerably by the symmetry of the crystal. The first term of equation (30) refers to the case $h_1 = j_1$, $h_2 = j_2$, $h_3 = j_3$, the 6 terms of the first sum arise from the cases $h_1 = j_1 \pm 1$, $h_2 = j_2$, $h_3 = j_3$ or $h_1 = j_1$, $h_2 = j_2 \pm 1$, $h_3 = j_3$ or $h_1 = j_1$, $h_2 = j_2$, $h_3 = j_3 \pm 1$. The 12 terms of the second sum originate from the cases, when two of the three h_s ($s = 1, 2, 3$) differ simultaneously from the appropriate j_s -s by ± 1 . Finally, the last 8 terms refer to the cases when all three h_s -s differ from the appropriate j_s -s by ± 1 .

It should be pointed out that in general for a given i and j pair of atoms in all above-mentioned cases the integrals $\beta_{i,j}$ may have different values. This is indicated by the subscripts, where the lower indices of the $\beta_{i,j}$ -s refer to the components of h which differ from those of j by $|1|$ and the + or - signs indicate whether the components of h differ from those of j by +1 or -1. Thus we have for instance for $(\beta_{i,j}^{-+})_{1,2,3}$

$$(\beta_{i,j}^{-+})_{1,2,3} = \langle \Phi_i(r_i - j_1 \underline{a}_1 - j_2 \underline{a}_2 - j_3 \underline{a}_3 | H | \Phi_j(r_j - (j_1 - 1) \underline{a}_1 - (j_2 - 1) \underline{a}_2 - (j_3 + 1) \underline{a}_3) \rangle.$$

It can easily be shown that $\gamma_{i,j} = \gamma_{j,i}^*$, i.e. γ is a Hermitian complex matrix with real eigenvalues. The appropriate integrals $\beta_{i,j}$ can be determined again on the basis of the overlap integrals with the aid of equ. (15). We can then write down for an actual case the elements of the γ matrix numerically and can determine the eigenvalues $\varepsilon(\underline{k})_t$ of γ , which are functions of \underline{k} . Substituting different components of the vectors \underline{k} into the γ matrix, for which the vectors \underline{k} lie within the first Brillouin zone, we can determine the minima and maxima of the energy surfaces in the \underline{k} space. In this way the energy band structure of an arbitrary molecular crystal can be obtained in the HÜCKEL approximation.

It is possible to generalize our results (29)—(30) also to the case of three-dimensional pseudoperiodic polymers. We have to substitute in this case the appropriate elements of the average matrices $\bar{\mathbf{A}}$ and $\bar{\mathbf{B}}$ into equation (30). We can then formulate our results on the basis of equations (20) and (30) in the form

$$\begin{aligned} \bar{\gamma} \underline{c}_{\underline{k},t} = & \left[\bar{\mathbf{A}} + \sum_{s=1}^3 (\bar{\mathbf{B}}_s^+ e^{ins} + (\bar{\mathbf{B}}_s^+)^t e^{-ins}) + \right. \\ & + \sum_{\substack{s>v \\ v=1,2}} (\bar{\mathbf{B}}_{s,v}^{++} e^{im_{s,v}} + (\bar{\mathbf{B}}_{s,v}^{++})^t e^{-im_{s,v}} + \bar{\mathbf{B}}_{s,v}^{+-} e^{ip_{s,v}} + (\bar{\mathbf{B}}_{s,v}^{+-})^t e^{-ip_{s,v}}) + \quad (32) \\ & \left. + 8 \text{ terms} \right] \underline{c}_{\underline{k},t} = \varepsilon(\underline{k})_t \underline{c}_{\underline{k},t}, \end{aligned}$$

where we have used the abbreviations

$$\begin{aligned} n_s &= \sum_{r=x,y,z} k_r a_{sr} & (s = 1, 2, 3), \\ m_{s,v} &= \sum_{r=x,y,z} k_r (a_{sr} + a_{vr}) & \left. \begin{array}{l} v = 1, 2 \\ s > v \end{array} \right\}, \\ p_{s,v} &= \sum_{r=x,y,z} k_r (a_{sr} - a_{vr}) & \left. \begin{array}{l} v = 1, 2 \\ s > v \end{array} \right\}. \end{aligned} \quad (33)$$

The last 8 terms of the $\bar{\gamma}$ matrix, which are not shown here for brevity, correspond to the last 8 terms of equation (30) in which all three components h_1 , h_2 and h_3 differ from j_1 , j_2 and j_3 by ± 1 .

If we have m slightly different kinds of units in our molecular crystal with the probabilities $p^{(i)}$, $\bar{\mathbf{A}}$ is defined again, as in the one-dimensional case by

$$\bar{\mathbf{A}} = \sum_{i=1}^m p^{(i)} \mathbf{A}^{(i)}. \quad (34)$$

The elements of the matrices $\mathbf{A}^{(i)}$ consist of only the integrals $\beta_{i,j}^{(i)}$, which correspond to interactions within the i -th kind of unit.

The average matrices $\bar{\mathbf{B}}$ are defined by the equations

$$\begin{aligned} \bar{\mathbf{B}}_s^+ &= \sum_{j,k=1}^m p^{+(j,k)} \mathbf{B}_s^{+(j,k)} & (s = 1, 2, 3), \\ \bar{\mathbf{B}}_{s,v}^{++} &= \sum_{j,k=1}^m p_{s,v}^{++(j,k)} \mathbf{B}_{s,v}^{++(j,k)} & \left. \begin{array}{l} v = 1, 2 \\ s > v \end{array} \right\}, \\ \bar{\mathbf{B}}_{s,v}^{+-} &= \sum_{j,k=1}^m p_{s,v}^{-(j,k)} \mathbf{B}_{s,v}^{-(j,k)} & \left. \begin{array}{l} v = 1, 2 \\ s > v \end{array} \right\} \end{aligned} \quad (35)$$

and similar expressions for the average matrices $\bar{\mathbf{B}}$ occurring in the 8 further terms in equation (32). We have among them for instance the matrix

$$\bar{\mathbf{B}}_{1,2,3}^{-++} = \sum_{j,k=1}^m p_{1,2,3}^{-++(j,k)} \mathbf{B}_{1,2,3}^{-++(j,k)}. \quad (36)$$

The nearest neighbour frequencies $p^{(j,k)}$ (the probabilities to have the unit k after j) may generally depend on the direction in the pseudoperiodic crystal. This is indicated by the further lower and upper indices of the $p^{(j,k)}$ -s. The elements of matrices $\mathbf{B}^{(j,k)}$ are the interaction integrals between the atoms of the neighbouring j and k type of units. We can write for instance for the u, z element of the matrix $\mathbf{B}_{1,2,3}^{-++(j,k)}$

$$(\mathbf{B}_{1,2,3}^{-+,+(j,k)})_{u,z} = (\beta_{u,z}^{-+,+(j,k)})_{1,2,3} = \langle \Phi_u^{(j)}(r_u - j_1 \underline{a}_1 - j_2 \underline{a}_2 - j_3 \underline{a}_3) | H | \cdot \Phi_z^{(k)}(r_z - (j_1 - 1) \underline{a}_1 - (j_2 + 1) \underline{a}_2 - (j_3 + 1) \underline{a}_3) \rangle, \quad (37)$$

where $\Phi_u^{(j)}$ denotes the u -th atomic orbital of the j -th type of unit and $\Phi_z^{(k)}$ the z -th one of the k -th type of unit.

Just as for the periodic case it is also true for the average matrices that the interchange of their + and — indices is equivalent to the transposition of their elements:

$$\begin{aligned} \bar{\mathbf{B}}_s^- &= (\bar{\mathbf{B}}_s^+)^t & (s = 1, 2, 3), \\ \bar{\mathbf{B}}_{s,v}^- &= (\bar{\mathbf{B}}_{s,v}^{++})^t & \left| \begin{array}{l} v = 1, 2 \\ s > v \end{array} \right., \\ \bar{\mathbf{B}}_{s,v}^{-+} &= (\bar{\mathbf{B}}_{s,v}^{+-})^t & \left| \begin{array}{l} v = 1, 2 \\ s > v \end{array} \right., \\ \bar{\mathbf{B}}_{1,2,3}^{+--} &= (\bar{\mathbf{B}}_{1,2,3}^{-++})^t \end{aligned} \quad (38)$$

and so on. We have used these relations when we have written down the eigenvalue problem of the $\bar{\gamma}$ matrix. From relations (38) we have the result that the $\bar{\gamma}$ matrix is always Hermitian and has therefore real eigenvalues, which can be determined.

It should be emphasized again that we can use equation (32) only if the different units of a molecular crystal differ from each other only very little. Otherwise the neglection of the second and higher order correction terms (see equations (18a)) will cause serious errors in our results.

In an actual case the unpleasant looking expression (32) is simplified greatly because of the symmetry of the crystal. By determining all necessary integrals $\beta_{u,z}$ on the basis of the appropriate overlap integrals and knowing the composition and the nearest neighbour frequencies of the pseudo-periodic molecular crystal, it is possible to determine the eigenvalues $\varepsilon(k)_t$ of the $\bar{\gamma}$ matrix. Calculating the minima and maxima in the k space of the different energy surfaces obtained we can also determine the band structure of a pseudoperiodic polymer.

Acknowledgment

The author would like to express his gratitude to Professor P.-O. Löwdin for his critical remarks and for making possible the carrying out of part of this work during the author's stay at the Uppsala Quantum Chemistry Group. The author is very grateful to Professor G. DEL RE for having called his attention to the problem of arbitrary three-dimensional molecular crystals and to Mr. G. BICZÓ and Mr. F. BELEZNAY for making their results available before publication.

REFERENCES

1. R. PARISER and R. G. PARR, J. Chem. Phys., **21**, 466, 1953; **21**, 767, 1953.
2. J. A. POPLE, Trans-Far. Soc., **49**, 1357, 1953.
3. J. KOUTECKÝ and R. ZAHRADNÍK, Coll. Czech. Chem. Comm., **15**, 811, 1960.
4. J. LADÍK and K. APPEL, J. Chem. Phys., **40**, 2470, 1964.
5. A. N. ORLOV and A. N. MEN, Fiz. Metallov i Metallovedenie USSR, **7**, 335, 1959.
6. F. BELEZNAY and G. BICZÓ, J. Chem. Phys., **41**, 2351, 1964.

О ПОЛУЭМПИРИЧЕСКИХ ТЕОРИЯХ МОЛЕКУЛЯРНЫХ КРИСТАЛЛОВ

I. ПРИБЛИЖЕНИЕ ГЮККЕЛЯ

Я. ЛАДИК

Резюме

Работа ознакомляет читателя с определением энергии связи в приближении Гюккеля одноразмерных периодических и близко периодических полимеров, имеющих в элементарном ячейке произвольное число атомов. При выводе формулы используются периодические граничные условия Борна—Кармана и принимаются во внимание взаимодействия лишь самых ближайших соседей. Полученный матричный формализм обобщается и для трёхмерных молекулярных кристаллов с произвольной симметрией и с произвольным числом атомов в элементарной ячейке. Данный формализм обобщается, наконец, для случая, когда в трёхмерных полимерах встречаются элементы немного различного типа.

SOME DEVELOPMENTS IN THE SEMIEMPIRICAL THEORIES OF MOLECULAR CRYSTALS. II. THE PARISER-PARR-POPLE APPROXIMATION

By

J. LADIK

CENTRAL RESEARCH INSTITUTE FOR CHEMISTRY OF THE HUNGARIAN ACADEMY OF SCIENCES, BUDAPEST

(Presented by G. Schay. — Received 11. VI. 1964)

Using the BORN-KÁRMÁN periodic boundary condition and taking into account only nearest neighbour interactions in the one-dimensional case and interactions between the first, second and third neighbours in the three-dimensional case, general matrix formulation is given for the calculation of energy bands of one- and three-dimensional arbitrary molecular crystals in the PARISER-PARR-POPLE approximation. The expressions are generalized to the case, when we have in the one- or three-dimensional molecular crystals slightly different types of units.

Introduction

The semiempirical SCF LCAO MO and semiempirical CI methods (PARISER-PARR-POPLE approximation) are important tools for the better understanding of the electronic structure of molecules with delocalized π -electron systems. Therefore it seems useful to extend these methods also to the calculation of the energy band structure of one- and three-dimensional periodic or pseudoperiodic molecular crystals (see the preceding paper [1]). Using the BORN-KÁRMÁN periodic boundary condition and taking into account only interactions between nearest neighbours in the one-dimensional case and between first, second and third neighbours (see the Introduction of [1]) in the three-dimensional case, it is possible to calculate the energy levels and wave functions of a molecular crystal in a comparatively simple way as the eigenvalues and eigenvectors of a complex Hermitian matrix (as in the HÜCKEL case, see [1]). It should be mentioned that in the application of the CI method to crystals the difficulty arises that in principle we have to take into account an infinite number of configurations. In the case of a molecular crystal, however, the interaction between molecules in different elementary cells is comparatively small and thus it is probable that if we take into account in the semiempirical CI method only a limited number of selected configurations, this will not cause very serious errors. For the definite solution of the problem it is necessary of course to perform detailed numerical calculations on molecular crystals with the semiempirical CI method.

One-dimensional case

In the case of a linear chain with N -elementary cells and with n atoms within in each elementary cell we can write down an LCAO crystal orbital in the form of equ. (1) of [1]. Introducing the BORN—KÁRMÁN boundary condition we obtain for the coefficients the BLOCH condition (equ. (5) of [1]).

On the other hand for a molecule of m atoms we can obtain the coefficients of the SCF MO-s in the PARISER—PARR—POPLE approximation [2, 3] as the eigenvectors of the matrix \mathbf{F} , which has the elements

$$F_{l,l} = -I_l + \frac{1}{2} p_{l,l} (I_l - E_l) + \sum_{s \neq l}^m p_{s,s} - z_s \gamma_{l,s} \equiv \tilde{a}_l, \quad (1)$$

$$F_{l,s} = \beta_{l,s} - \frac{1}{2} p_{l,s} \gamma_{l,s} \equiv \tilde{\beta}_{l,s} (l \neq s), \quad (2)$$

Here I_l and E_l are the ionization potential and electron affinity on the l th atom in the molecule, z_s is the effective nuclear charge of the s th atom, the charge density, $p_{s,s}$ is defined by

$$p_{s,s} = 2 \sum_{r=1}^{n_f} c_{r,s}^* c_{r,s} \quad (3)$$

and the $p_{l,s}$ bond order by

$$p_{l,s} = 2 \sum_{r=1}^{n_f} c_{r,l}^* c_{r,s}, \quad (4)$$

where n_f is the number of the filled orbitals. The two-centre integrals $\beta_{l,j}$ and $\gamma_{l,j}$ are defined by the expressions

$$\beta_{l,s} = \int \varphi_l^*(\underline{r}_l) H_c \varphi_s(\underline{r}_s) dV_1, \quad (5)$$

$$\gamma_{l,s} = \int \varphi_l^*(\underline{r}_l) \varphi_l(\underline{r}_l) \frac{1}{r_{12}} \varphi_s^*(\underline{r}_s) \varphi_s(\underline{r}_s) dV_1 dV_2, \quad (6)$$

where in the one-electron integral $\beta_{l,j} H_c = -\frac{1}{2} A + V_c$ (V_c is the core potential) [2, 3]. In actual calculations the integrals $\beta_{l,s}$ are treated as adjustable parameters and are taken to be different from zero only between neighbouring atoms, while the integrals $\gamma_{l,s}$ are approximated in a systematic way [2, 3, 4]. For starting we can use the values $p_{s,s}^{(0)}$ and $p_{l,s}^{(0)}$ resulting from a HÜCKEL calculation, which are substituted into equations (1) and (2). Then the eigenvalue problem of the matrix is solved and from the resulting eigenvectors, with the aid of equations (3) and (4), a new set of $p_{s,s}^{(1)}$ and $p_{l,s}^{(1)}$ is obtained. The procedure is repeated until self-consistency is reached.

We may imagine our linear chain as one molecule of $m = n$, N atoms and the equations (1) and (2) hold of course also for the whole linear chain. It is, however, impossible to solve the eigenvalue problem of the resulting matrix \mathbf{F} because of the very large order of nN . If we introduce, however, the BLOCH condition for the LCAO coefficients in the expression of δE (the variation of the total energy of the many electron system) in ROOTHAAN's first paper [6], we take into account only nearest neighbour interactions and introduce the neglections used by POPLE [3] in the molecular case, after a somewhat lengthy but simple calculation it is possible to show that the matrix \mathbf{F} will have only the order n and its elements can be written in the form

$$F_{l,l} = -I_l + \frac{1}{2} p_{l,l}(I_l - E_l) + \sum_{s \neq l}^n (p_{s,s} - z_s) \gamma_{l,s} + \sum_{s=1}^n (p_{s,s} - z_s) (\gamma_{l,s}^+ +$$

$$+ \gamma_{l,s}^-) + \beta_{l,l}^+ e^{ik} + \beta_{l,l}^- e^{-ik} - \frac{1}{2} (p_{l,l}^+ \gamma_{l,l}^+ + p_{l,l}^- \gamma_{l,l}^-) = \tilde{a}_l + \tilde{a}_l^+ + \tilde{a}_l^- \quad (7)$$

$$\left[\tilde{a}_l^\pm = \sum_{s=1}^n - (p_{s,s} - z_s) \gamma_{l,s}^\pm - \frac{1}{2} p_{l,l}^\pm \gamma_{l,l}^\pm + \beta_{l,l}^\pm e^{\pm ik} \right],$$

$$F_{l,s} = \beta_{l,s} - \frac{1}{2} p_{l,s} \gamma_{l,s} - \frac{1}{2} (p_{l,s}^+ \gamma_{l,s}^+ + p_{l,s}^- \gamma_{l,s}^-) + \beta_{l,s}^+ e^{ik} + \beta_{l,s}^- e^{-ik} = \\ = \tilde{\beta}_{l,s} + \tilde{\beta}_{l,s}^+ + \tilde{\beta}_{l,s}^- \quad (l \neq s) \quad (8)$$

$$\left[\tilde{\beta}_{l,s}^\pm = - \frac{1}{2} p_{l,s}^\pm \gamma_{l,s}^\pm + \beta_{l,s}^\pm e^{\pm ik} \right].$$

In these equations

$$\beta_{l,s}^\pm = \int \varphi_l^*(\underline{r}_{l_1} - j\underline{a}) H_C \varphi_s(\underline{r}_{s_1} - (j \pm 1)\underline{a}) dV_l, \quad (9)$$

$$\gamma_{l,s}^\pm = \int \varphi_l^*(\underline{r}_{l_1} - j\underline{a}) \varphi_l(\underline{r}_{l_1} - j\underline{a}) \frac{1}{r_{l_2}} \varphi_s^*(\underline{r}_{s_2} - (j \pm 1)\underline{a}) \cdot \varphi_s(\underline{r}_{s_2} + (j \pm 1)\underline{a}) dV_1 dV_2, \quad (10)$$

where $\Phi_l(\underline{r}_l - ja)$ is the atomic orbital centred on the l -th atom of the j -th elementary cell. $p_{l,l}^\pm$, $p_{l,s}^\pm$ are the bond orders between the l -th atom of an elementary cell and the l -th, s -th atom, respectively, in the right (+ sign) or left (- sign) neighbouring cell. Their starting values can be determined from a HÜCKEL calculation of a molecule consisting of two interacting elementary cells of the chain.

Having formed the elements of the matrix \mathbf{F} its eigenvalue problem

$$\mathbf{F}(k) \underline{c}(k)_t = \varepsilon(k)_t \underline{c}(k)_t \quad (11a)$$

can be solved in the usual way by separating its real and imaginary part [6]:

$$\begin{pmatrix} \mathbf{F}_{(k)}^{(\text{Re})} & -\mathbf{F}_{(k)}^{(\text{Im})} \\ \mathbf{F}_{(k)}^{(\text{Im})} & \mathbf{F}_{(k)}^{(\text{Re})} \end{pmatrix} \begin{pmatrix} \underline{u}(k) \\ \underline{v}(k) \end{pmatrix}_t = \varepsilon(k)_t \begin{pmatrix} \underline{u}(k) \\ \underline{v}(k) \end{pmatrix}_t. \quad (11b)$$

Here $\mathbf{F}_{(k)}^{(\text{Re})}$ is the real and $\mathbf{F}_{(k)}^{(\text{Im})}$ the imaginary part of the matrix \mathbf{F} and $\underline{u}(k)_t$ is the real and $\underline{v}(k)_t$ the imaginary part of the complex eigenvector $\underline{c}(k)_t$. It should be mentioned that the eigenvalue problem (11b) is twofold degenerate. The eigenvectors belonging to a given eigenvalue $\varepsilon(k)_t$ are, as is easy to show, $\underline{u}_t + i\underline{v}_t$ and $+i(\underline{u}_t + i\underline{v}_t)$ or $-i(\underline{u}_t + i\underline{v}_t)$.

After solving the eigenvalue problem (11) it is possible to form the new, always real charge densities $p_{l,l}$ and complex bond orders $p_{l,s}$, $p_{l,l}^{\pm}$, $p_{l,s}^{\pm}$

$$p_{l,s} = 2 \sum_{r=1}^{n_f} c_{r,l}^* c_{r,s} = p_{l,s}^{(\text{Re})} + i p_{l,s}^{(\text{Im})}, \quad (12a)$$

$$p_{l,s}^{\pm} = 2 \sum_{r=1}^{n_f} c_{r,l}^* e^{-ikj} c_{r,s} e^{ik(j\pm 1)} = 2 \sum_{r=1}^{n_f} c_{r,l}^* c_{r,s} e^{\pm ik} = p_{l,s}^{(\text{Re})\pm}(k) + \\ + i p_{l,s}^{(\text{Im})\pm}(k) = p_{l,s} \cos k \pm i p_{l,s} \sin k, \quad (12b)$$

where $p_{l,s}^{(\text{Re})}$ is the real and $p_{l,s}^{(\text{Im})}$ the imaginary part of $p_{l,s}$. Substituting equations (12) into equations (8) we obtain for the elements of the real and imaginary part of the matrix \mathbf{F} the following results

$$\mathbf{F}_{l,l}^{(\text{Re})}(k) = \tilde{a}_l + \sum_{s=1}^n (p_{s,s} - z_s) (\gamma_{l,s}^+ + \gamma_{l,s}^-) + (\beta_{l,l}^+ + \beta_{l,l}^-) \cos k - \\ - \frac{1}{2} (p_{l,l}^{(\text{Re})+} \gamma_{l,l}^+ + p_{l,l}^{(\text{Re})-} \gamma_{l,l}^-), \quad (13a)$$

$$\mathbf{F}_{l,s}^{(\text{Re})}(k) = \beta_{l,s} - \frac{1}{2} p_{l,s}^{(\text{Re})} \gamma_{l,s} + (\beta_{l,s}^+ + \beta_{l,s}^-) \cos k - \frac{1}{2} (p_{l,s}^{(\text{Re})+} \gamma_{l,s}^+ + p_{l,s}^{(\text{Re})-} \gamma_{l,s}^-) \quad (13b)$$

$$\mathbf{F}_{l,l}^{(\text{Im})}(k) = (\beta_{l,l}^+ - \beta_{l,l}^-) \sin k - \frac{1}{2} (p_{l,l}^{(\text{Im})+} \gamma_{l,l}^+ + p_{l,l}^{(\text{Im})-} \gamma_{l,l}^-), \quad (13c)$$

$$\mathbf{F}_{l,s}^{(\text{Im})}(k) = -\frac{1}{2} p_{l,s}^{(\text{Im})} \gamma_{l,s} + (\beta_{l,s}^+ - \beta_{l,s}^-) \sin k - \frac{1}{2} (p_{l,s}^{(\text{Im})+} \gamma_{l,s}^+ + p_{l,s}^{(\text{Im})-} \gamma_{l,s}^-). \quad (13d)$$

We have the relations for the integrals β and γ

$$\beta_{l,s} = \beta_{s,l}, \beta_{l,s}^+ = \beta_{s,-l}, \gamma_{l,s} = \gamma_{s,l}, \gamma_{l,s}^+ = \gamma_{s,-l}^- \quad (14)$$

and by the definition of the complex bond orders

$$p_{l,s} = p_{s,l}^* \text{ és } p_{l,s}^+ = p_{s,-l}^- \quad (15)$$

or

$$\begin{aligned} p_{l,s}^{(Re)} &= p_{s,l}^{(Re)} & p_{l,s}^{(Re)+} &= p_{s,l}^{(Re)-} \\ p_{l,s}^{(Im)} &= -p_{s,l}^{(Im)} & p_{l,s}^{(Im)+} &= -p_{s,l}^{(Im)-} \end{aligned} \quad (16)$$

hold. Therefore, as we can see from inspection of their elements, the submatrix $F^{(Re)}$ is a symmetrical matrix and $F^{(Im)}$ an antisymmetrical one. So the whole matrix of order $2n$ occurring in equation (11) is a symmetrical matrix and has therefore always real eigenvalues.

Continuing the procedure described here in an interative way to self-consistency we can obtain the SCF eigenvalues and eigenvectors as a function of k . Determining the limits of each band (the maxima and minima of the functions $\varepsilon(k)_l$) we can obtain the energy band structure of the linear chain in the PARISER—PARR—POPLE approximation.

After having performed this calculation we can introduce also a limited CI for the excited states. As first step we can take into account CI only between singlet excited configurations. We can write the interconfigurational matrix elements for a molecule in this case in the PARISER—PARR approximation [2] in the form [4]

$$\begin{aligned} {}^1G_{i \rightarrow m}^{h \rightarrow l} &\equiv ({}^1\Phi_{i \rightarrow m} | H | {}^1\Phi_{h \rightarrow l}) = \sum_{p=1}^n \sum_{r=1}^n (2 c_{i,p}^* c_{h,p}^* c_{m,r} c_{i,r} - c_{i,p} c_{h,p}^* c_{m,r} c_{i,r}^*) \gamma_{p,r} + \\ &+ (\varepsilon_m - \varepsilon_i) \delta_{i,h} \delta_{m,l} \end{aligned} \quad (17)$$

where ${}^1\Phi_{i \rightarrow m}$ is the singlet excited many electron wave function for the state in which one electron is promoted from the i th MO to the m th one and $\delta_{i,h}$ is a Kronecker delta. In the double sum the first terms are the exchange terms and the second ones the Coulomb terms.

Forming these matrix elements between all the considered configurations we obtain the interconfigurational matrix (G). Solving the eigenvalue problem

$$\mathbf{G} \underline{b}_v = E_v \underline{b}_v \quad (18)$$

of this matrix, we obtain the different excitation energies E_v of the many-electron system.

If we introduce for the coefficients the BLOCH condition (see equ. (5) of [1]) and take into account only nearest neighbour interactions, after a simple calculation we obtain, in the case of a linear chain, for the interconfigurational matrix elements between singlet excited states in the PARISER—PARR approximation for a given value k the expression

$$\begin{aligned} {}^1G_{i \rightarrow m}^{h \rightarrow l}(k) = & \sum_{p=1}^n \sum_{r=1}^n [2 c_{l,p}^*(k) c_{h,p}^*(k) c_{m,r}(k) c_{i,r}(k) \cdot (\gamma_{p,r} + \gamma_{p,r}^+ e^{2ik} + \gamma_{p,r}^- e^{-2ik}) - \\ & - c_{i,p}(k) c_{h,p}^*(k) c_{m,r}(k) c_{i,r}^*(k) (\gamma_{p,r} + \gamma_{p,r}^+ + \gamma_{p,r}^-)] + [\varepsilon(k)_m - \varepsilon(k)_i] \delta_{i,b} \delta_{m,l}. \quad (19) \end{aligned}$$

In this expression we obtain in the exchange terms the factors $e^{\pm 2ik}$ because we have such a combination of the coefficients that for both coefficients belonging to the p -th atom of the j -th elementary cell we have to take their complex conjugate and for both coefficients of the r -th atom of the $(j \pm 1)$ -th cell we need not do so. Thus we have for the exponential factors the expression $e^{-2ijk} \cdot e^{2i(j \pm 1)k} = e^{\pm 2ik}$. At the same time in the Coulomb terms we always have for a given centre the complex conjugate of a coefficient only once (e.g. $c_{m,r}(k) \cdot c_{i,r}^*(k)$). Therefore the exponential factors cancel.

Expression (19) shows that

$${}^1G_{i \rightarrow m}^{h \rightarrow l} = ({}^1G_{h \rightarrow l}^{i \rightarrow m})^* \quad (20)$$

holds and thus the matrix $\mathbf{G}(k)$ is Hermitian with real eigenvalues. These can be determined for a given k value in the usual way.

It should be mentioned that transitions between levels belonging to different k values are spectroscopically forbidden. Therefore in a CI calculation such excitations should not be taken into account. Further it is possible to show that singly excited configurations belonging to different k values do not interact. Therefore the remaining interconfigurational matrix elements are those given by equ. (19).

As we have already mentioned in the introduction, in the application of the CI method the difficulty arises that, in principle, we have to take into account an infinite number of configurations for crystals. In the case of molecular crystals with weakly interacting units we can, however, hope that if we include in our interconfigurational matrix elements only nearest neighbour interactions, this will not cause very serious errors. The justification of this assumption will be possible only on the basis of actual numerical calculations. To be able to do this we have derived the formula (19) for the interconfigurational matrix elements for a given k value.

In the case of nearly periodic (pseudoperiodic) linear chains with j kinds of units, which are only slightly different, we can calculate the energy band structure in the PARISER—PARR—POPLE approximation, as in the HÜCKEL case, again with the aid of an average matrix (see [1]),

$$\bar{\mathbf{F}}(k) \underline{c}_{k,t} = \varepsilon(k)_t \underline{c}_{k,t} \quad (21)$$

Here

$$\bar{\mathbf{F}} = \bar{\mathbf{F}}_A + \bar{\mathbf{F}}_B^+ + \bar{\mathbf{F}}_B^-, \quad (22)$$

where

$$\bar{\mathbf{F}}_A = \sum_{d=1}^s P_d \mathbf{F}_d \quad (23)$$

is the average matrix of the units and

$$\bar{\mathbf{F}}_B^\pm = \sum_{d,f=1}^s P_{d,f}^\pm \mathbf{F}_{d,f}^\pm \quad (24)$$

is the average interaction matrix between the units. In equ. (23) P_d is the frequency of the d th type of unit and the matrix \mathbf{F}_d is defined by

$$(\mathbf{F}_d)_{i,i} = (\tilde{a}_i)_d = \left[-I_i + \frac{1}{2} p_{i,i} (I_i - E_i) + \sum_{j \neq i}^n (p_{j,j} - z_j) \gamma_{i,j} \right]_d \quad (25)$$

and

$$(\mathbf{F}_d)_{i,j} = (\tilde{\beta}_{i,j})_d = (\beta_{i,j} - \frac{1}{2} p_{i,j} \gamma_{i,j})_d. \quad (26)$$

In equ. (24) $P_{d,f}$ is the probability to have the unit f after the unit d , going from left to right (+) or in the opposite (-) direction and the matrices $\mathbf{F}_{d,f}^\pm$ are defined by

$$(\mathbf{F}_{d,f}^\pm)_{i,i} = (\tilde{a}_i^\pm)_{d,f} = \left(\sum_{j=1}^n (p_{j,j} - z_j) \gamma_{i,j}^\pm - \frac{1}{2} p_{i,i}^\pm \gamma_{i,i}^\pm + \beta_{i,i}^\pm e^{\pm ik} \right)_{d,f} \quad (27)$$

and

$$(\mathbf{F}_{d,f}^\pm)_{i,j} = (\tilde{\beta}_{i,j}^\pm)_{d,f} = \left(\frac{1}{2} p_{i,j}^\pm \gamma_{i,j}^\pm + \beta_{i,j}^\pm e^{\pm ik} \right)_{d,f}. \quad (28)$$

To perform an actual calculation we have to begin with some starting charge densities $(p_{i,i})_d$ and bond orders $(p_{i,i}^\pm)_{d,f}$, $(p_{i,j})_{d,f}$, $(p_{i,j}^\pm)_{d,f}$ taken from a HÜCKEL calculation. With their aid we can form the different matrices \mathbf{F}_d and $\mathbf{F}_{d,f}$ and from the latter the average matrices $\bar{\mathbf{F}}_A$ and $\bar{\mathbf{F}}_B^\pm$. Solving the eigenvalue problem (21) of the Hermitian complex matrix $\bar{\mathbf{F}}$ we obtain the eigenvalues $\varepsilon(k)_t$ and eigenvectors $\underline{c}(k)_t$. From the latter we can obtain the new average charge densities $p_{i,i}$ and the average complex bond orders $p_{i,j}$, $p_{i,i}^\pm$, $p_{i,j}^\pm$. After that we can use equations (13a)—(13d) for the further calculation substituting in these the average charge densities and bond orders

and using everywhere the average values of the different quantities occurring here:

$$\bar{I}_i = \sum_{d=1}^s P_d (I_i)_d, \quad \bar{E}_i = \sum_d P_d (E_i)_d, \quad \bar{Z}_i = \sum_d P_d (z_i)_d, \quad (29)$$

$$\bar{\gamma}_{i,j} = \sum_d P_d (\gamma_{i,j})_d, \quad \bar{\gamma}_{i,j}^{\pm} = \sum_{d,f=1}^s P_{d,f} (\gamma_{i,j}^{\pm})_{d,f}, \quad (30)$$

$$\bar{\beta}_{i,j} = \sum_d P_d (\beta_{i,j})_d, \quad \bar{\beta}_{i,j}^{\pm} = \sum_{d,f} P_{d,f} (\beta_{i,j}^{\pm})_{d,f}. \quad (31)$$

Continuing this iterative procedure until self-consistency is reached we can obtain the self-consistent eigenvalues and eigenvectors $\varepsilon(k)_t^{SCF}$, $c(k)_t^{SCF}$ of the average matrix \bar{F} . Determining the minima and maxima of the different functions $\varepsilon(k)_t^{SCF}$ we can obtain the energy band structure of a pseudo-periodic linear chain in the semiempirical SCF LCAO approximation.

It should be mentioned, however, that since the individual values $(I_i)_d$ and $(E_i)_d$ may differ considerably, the applicability of the method is still more restricted to units which differ only slightly than it is in the HÜCKEL approximation. To keep the errors due to the neglections of the average matrix method [7] as small as possible, it is again advantageous to start with the diagonalized forms of the different matrices F_d (together with the appropriate transformations on the matrices $F_{d,f}$).

Having the SCF eigenvalues of the average matrices $\bar{F}(k)$ we can perform again a limited CI calculation for the excited states. For this purpose we can use again the expression (19), but with the average integrals (30) $\bar{\gamma}_{i,j}$ and $\bar{\gamma}_{i,j}^{\pm}$.

Three-dimensional case

By using the crystal orbitals for a three-dimensional lattice given by equ. (22) of [1] we obtain an expression for the elements of the matrix F similar to that in the HÜCKEL case (see equ. (30) of [1]), we have only to replace the $\beta_{i,j}$ -s occurring there by the quantities $\tilde{\beta}_{i,j}$ defined by equations (1), (2), (7) and (8). Thus we can formulate the problem of the calculation of the energy bands of a three-dimensional molecular crystal as the eigenvalue problem defined by

$$F c_{k,t} = \varepsilon(k)_t c_{k,t}, \quad (32)$$

where the elements of the matrix F are defined now by

$$\begin{aligned}
F_{i,j} = & \tilde{\beta}_{i,j} + \sum_{s=1}^3 [(\tilde{\beta}_{i,j}^+)_s + (\tilde{\beta}_{i,j}^-)_s] + \sum_{\substack{s>t \\ t=1,2}}^3 [(\tilde{\beta}_{i,j}^{++})_{s,t} + (\tilde{\beta}_{i,j}^{+-})_{s,t} + (\tilde{\beta}_{i,j}^{-+})_{s,t} + (\tilde{\beta}_{i,j}^{--})_{s,t}] + \\
& + (\tilde{\beta}_{i,j}^{+++})_{1,2,3} + (\tilde{\beta}_{i,j}^{-++})_{1,2,3} + (\tilde{\beta}_{i,j}^{+-+})_{1,2,3} + (\tilde{\beta}_{i,j}^{++-})_{1,2,3} + (\tilde{\beta}_{i,j}^{--+})_{1,2,3} + (\tilde{\beta}_{i,j}^{-+-})_{1,2,3} + \\
& + (\tilde{\beta}_{i,j}^{--+})_{1,2,3} + (\tilde{\beta}_{i,j}^{---})_{1,2,3}. \tag{33}
\end{aligned}$$

In equation (33) we have, if $i = j$

$$\tilde{\beta}_{i,i} = \tilde{a}_i = -I_i + \frac{1}{2} p_{i,i} (I_i - E_i) + \sum_{j \neq i}^n (p_{j,j} - z_j) \gamma_{i,j}, \tag{34}$$

$$\begin{aligned}
(\tilde{\beta}_{i,i}^\pm)_s = (\tilde{a}_i^\pm)_s = & \sum_{j=1}^n (p_{j,j} - z_j) (\gamma_{i,j}^\pm)_s - \frac{1}{2} (p_{i,i}^\pm)_s (\gamma_{i,i}^\pm)_s + (\beta_{i,i}^\pm)_s e^{\pm i n_s} \\
\left(n_s = \sum_{r=x,y,z} k_r a_{s_r}, s = 1, 2, 3 \right), \tag{35}
\end{aligned}$$

$$\begin{aligned}
(\tilde{\beta}_{i,i}^{\pm\pm})_{s,t} = (\tilde{a}_i^{\pm\pm})_{s,t} = & \sum_{j=1}^n (p_{j,j} - z_j) (\gamma_{i,j}^{\pm\pm})_{s,t} - \frac{1}{2} (p_{i,i}^{\pm\pm})_{s,t} (\gamma_{i,i}^{\pm\pm})_{s,t} + (\beta_{i,i}^{\pm\pm})_{s,t} e^{\pm i(n_s + n_t)} \\
(s < t \quad t = 1, 2), \tag{36}
\end{aligned}$$

$$\begin{aligned}
(\tilde{\beta}_{i,i}^{\mp\mp})_{s,t} = (\tilde{a}_i^{\mp\mp})_{s,t} = & \sum_{j=i}^n (p_{j,j} - z_j) (\gamma_{i,j}^{\mp\mp})_{s,t} - \frac{1}{2} (p_{i,i}^{\mp\mp})_{s,t} (\gamma_{i,i}^{\mp\mp})_{s,t} + (\beta_{i,i}^{\mp\mp})_{s,t} e^{\pm i(n_s - n_t)} \\
(s > t \quad t = 1, 2) \tag{37}
\end{aligned}$$

and e.g.

$$\begin{aligned}
(\tilde{\beta}_{i,i}^{-+-})_{1,2,3} = (\tilde{a}_i^{-+-})_{1,2,3} = & \sum_{j=1}^n (p_{j,j} - z_j) (\gamma_{i,j}^{-+-})_{1,2,3} - \frac{1}{2} (p_{i,i}^{-+-})_{1,2,3} (\gamma_{i,i}^{-+-})_{1,2,3} + \\
& + (\beta_{i,i}^{-+-})_{1,2,3} e^{-i(n_1 - n_2 + n_3)} \tag{38}
\end{aligned}$$

with similar definitions for the other integrals $(\tilde{\beta}_{i,i})_{1,2,3}$. If $i \neq j$, the terms in $F_{i,j}$ are defined by

$$\tilde{\beta}_{i,j} = \beta_{i,j} - \frac{1}{2} P_{i,j} \gamma_{i,j}, \tag{39}$$

$$(\tilde{\beta}_{i,j}^\pm)_s = -\frac{1}{2} (p_{i,j}^\pm)_s (\gamma_{i,j}^\pm)_s + (\beta_{i,j}^\pm)_s e^{\pm i n_s} (s = 1, 2, 3), \tag{40}$$

$$(\tilde{\beta}_{i,j}^{\pm\pm})_{s,t} = -\frac{1}{2} (p_{i,j}^{\pm\pm})_{s,t} (\gamma_{i,j}^{\pm\pm})_{s,t} + (\beta_{i,j}^{\pm\pm})_{s,t} e^{\pm i(n_s + n_t)} \quad (s > t \quad t = 1, 2), \tag{41}$$

$$(\tilde{\beta}_{i,j}^{\pm\mp})_{s,t} = -\frac{1}{2}(p_{i,j}^{\pm\mp})_{s,t}(\gamma_{i,j}^{\pm\mp})_{s,t} + (\beta_{i,j}^{\pm\mp})_{s,t} e^{\pm i(n_s - n_t)} \quad (s > t \quad t = 1, 2) \quad (42)$$

and e.g.

$$(\tilde{\beta}_{i,j}^{+-+})_{1,2,3} = -\frac{1}{2}(p_{i,j}^{+-+})_{1,2,3}(\gamma_{i,j}^{+-+})_{1,2,3} + (\beta_{i,j}^{+-+})_{1,2,3} e^{i(n_1 - n_2 + n_3)} \quad (43)$$

with similar definitions for the other integrals $(\tilde{\beta}_{i,j})_{1,2,3}$. For the definitions on the various integrals $\beta_{i,j}$ we refer to the example given by equation (32) of [1]. There the meaning of the different indices is also explained. The integrals $\gamma_{i,j}$ are defined in a similar manner as the integrals $\beta_{i,j}$. E.g.

$$(\gamma_{i,j}^{+-})_{2,3} = \int \left| \varphi_i(r_{i_1} - j_1 \underline{a}_1 - j_2 \underline{a}_2 - j_3 \underline{a}_3) \right|^2 \frac{1}{r_{12}} \left| \varphi_j(r_{j_2} - j_1 \underline{a}_1 - (j_2 + 1) \underline{a}_2 - (j_3 - 1) \underline{a}_3) \right|^2 dV_1 dV_2, \quad (44)$$

$$(\gamma_{i,j}^{-+-})_{1,2,3} = \int \left| \varphi_i(r_{i_1} - j_1 \underline{a}_1 - j_2 \underline{a}_2 - j_3 \underline{a}_3) \right|^2 \frac{1}{r_{12}} \left| \varphi_j(r_{j_2} - (j_1 - 1) \underline{a}_1 - (j_2 + 1) \underline{a}_2 - (j_3 - 1) \underline{a}_3) \right|^2 dV_1 dV_2. \quad (45)$$

In the course of an actual calculation we can start with the HÜCKEL values $p_{i,i}$, $p_{i,i}^{\pm}$ etc. and $p_{i,j}$, $p_{i,j}^{\pm}$ etc. After solving the eigenvalue problem of the complex Hermitian matrix (32) for a given vector \underline{k} , which has an end point within the first Brillouin zone of the crystal, we have to form the new charge densities and bond orders from the eigenvectors so obtained. We have to take care, however, in the calculation of their definitions:

$$p_{i,j} = 2 \sum_{l=1}^{n_f} c_{l,i}^* c_{l,j} \quad (i = j \text{ or } i \neq j), \quad (46a)$$

$$(p_{i,j}^{\pm})_s = 2 \sum_{l=1}^{n_f} c_{l,i}^* c_{l,j} e^{\pm i n_s} = p_{i,j} e^{\pm i n_s}$$

$$\left(n_s = \sum_{r=x,y,z} k_r a_{s_r} \quad s = 1, 2, 3 \right) \quad (46b)$$

and e.g.

$$(p_{i,j}^{+-})_{2,3} = p_{i,j} e^{i(n_2 - n_3)} \quad (47a)$$

$$(p_{i,j}^{-+-})_{1,2,3} = p_{i,j} e^{-i(n_1 - n_2 + n_3)} \quad (47b)$$

with similar definitions for the other complex bond orders.

Continuing the iterations until self-consistency is reached the SCF eigenvectors and eigenvalues of \mathbf{F} can be determined for a given vector \underline{k} . Repeating this procedure for other vectors \underline{k} within the first Brillouin zone the maxima and minima of the eigenvalues as functions of \underline{k} or in other words the energy band structure of the three-dimensional molecular crystal in the semiempirical SCF LCAO approximation can be determined.

It should be pointed out that for a real crystal the rather complicated expression (34) is much simplified by the symmetry of the crystal. Therefore it seems to be possible to carry out such calculations in the near future.

Having performed a semiempirical SCF LCAO calculation for a three-dimensional molecular crystal, we can write down again with the aid of the resulting eigenvectors the interconfigurational matrix elements between singlet excited states for a given vector \underline{k} by generalizing the one-dimensional expression (19)

$$\begin{aligned} {}^1G_{i \rightarrow m}^{h \rightarrow l}(\underline{k}) = & \sum_{p=1}^n \sum_{r=1}^n [2 c_{l,p}^*(\underline{k}) c_{h,p}^*(\underline{k}) c_{m,r}(\underline{k}) c_{i,r}(\underline{k}) \cdot \left(\gamma_{p,r} + \right. \\ & + \sum_{s=1}^3 \{(\gamma_{p,r}^+)_s e^{2in_s} + (\gamma_{p,r}^-)_s e^{-2in_s}\} + \sum_{\substack{s>t \\ t=1,2}} \{(\gamma_{p,r}^{++})_{s,t} e^{2i(n_s+n_t)} + (\gamma_{p,r}^{--})_{s,t} e^{-2i(n_s+n_t)} + \right. \\ & + (\gamma_{p,r}^{+-})_{s,t} e^{2i(n_s-n_t)} + (\gamma_{p,r}^{-+})_{s,t} e^{-2i(n_s-n_t)}\} + (\gamma_{p,r}^{++})_{1,2,3} e^{2i(n_1+n_2+n_3)} + \\ & + (\gamma_{p,r}^{++})_{1,2,3} e^{2i(-n_1+n_2+n_3)} + (\gamma_{p,r}^{++})_{1,2,3} e^{2i(n_1-n_2+n_3)} + (\gamma_{p,r}^{+-})_{1,2,3} e^{2i(n_1+n_2-n_3)} + \\ & + (\gamma_{p,r}^{+-})_{1,2,3} e^{-2i(-n_1+n_2+n_3)} + (\gamma_{p,r}^{+-})_{1,2,3} e^{-2i(n_1-n_2+n_3)} + (\gamma_{p,r}^{--})_{1,2,3} e^{-2i(n_1+n_2-n_3)} + \\ & \left. \left. + (\gamma_{p,r}^{--})_{1,2,3} e^{-2i(n_1+n_2+n_3)} \right) - c_{i,p}(\underline{k}) c_{h,p}^*(\underline{k}) c_{m,r}(\underline{k}) c_{i,r}^*(\underline{k}) \right)'] + (\varepsilon(\underline{k}))_m - \\ & - \varepsilon(\underline{k})_i \delta_{i,h} \delta_{m,l}. \end{aligned} \quad (48)$$

Here the symbol $(\)'$ means an expression in the integrals similar to that we have in the first part of ${}^1G_{i \rightarrow m}^{h \rightarrow l}$ but without the exponential factors. It can be shown that

$${}^1G_{i \rightarrow m}^{h \rightarrow l}(\underline{k}) = ({}^1G_{h \rightarrow l}^{i \rightarrow m}(\underline{k}))^* \quad (49)$$

holds again and therefore \mathbf{G} is Hermitian with real eigenvalues.

It should be mentioned, as it was pointed out already in the one-dimensional case, that CI calculations should be applied to molecular crystals only with great caution. It will be possible to decide only after performing actual calculations, which excited configurations are important and should therefore be included in the CI calculations.

In case we have v kinds of units only slightly different in the three-dimensional molecular crystal, we can calculate the energy bands from the equation

$$\bar{\mathbf{F}} \underline{c}_{k,t} = \varepsilon(\underline{k})_t \underline{c}_{k,t}. \quad (50)$$

Here the average matrix $\bar{\mathbf{F}}$ is defined by

$$\begin{aligned} \bar{\mathbf{F}} = \bar{\mathbf{F}}_A + \sum_{s=1}^3 (\bar{\mathbf{F}}_s^+ + \bar{\mathbf{F}}_s^-) + \sum_{\substack{s>t \\ t=1,2}}^3 (\bar{\mathbf{F}}_{s,t}^{++} + \bar{\mathbf{F}}_{s,t}^{+-} + \bar{\mathbf{F}}_{s,t}^{-+} + \bar{\mathbf{F}}_{s,t}^{--}) + \bar{\mathbf{F}}_{1,2,3}^{++} + \bar{\mathbf{F}}_{1,2,3}^{-+} + \\ + \bar{\mathbf{F}}_{1,2,3}^{+-} + \bar{\mathbf{F}}_{1,2,3}^{++} + \bar{\mathbf{F}}_{1,2,3}^{+-} + \bar{\mathbf{F}}_{1,2,3}^{-+} + \bar{\mathbf{F}}_{1,2,3}^{--}. \end{aligned} \quad (51)$$

The component average matrices of $\bar{\mathbf{F}}$ have as elements the averages of the matrix elements (34)—(43). Thus we have e.g.

$$(\bar{\mathbf{F}}_A)_{i,i} = \sum_{d=1}^v P_d (\tilde{\alpha}_i)_d, \quad (\bar{\mathbf{F}}_A)_{i,j} = \sum_{d=1}^v P_d (\tilde{\beta}_{i,j})_d, \quad (52)$$

$$(\bar{\mathbf{F}}_{s,t}^{+-})_{i,i} = \sum_{d,f=1}^v P_{s,t}^{+(d,f)} (\tilde{\alpha}_i^{+(d,f)})_{s,t}, \quad (53)$$

$$(\bar{\mathbf{F}}_{s,t}^{+-})_{i,j} = \sum_{d,f=1}^v P_{s,t}^{+(d,f)} (\tilde{\beta}_{i,j}^{+(d,f)})_{s,t}$$

and

$$(\bar{\mathbf{F}}_{1,2,3}^{+-})_{i,i} = \sum_{d,f=1}^v P_{1,2,3}^{+(d,f)} (\tilde{\alpha}_i^{+(d,f)})_{1,2,3}, \quad (54)$$

$$(\bar{\mathbf{F}}_{1,2,3}^{+-})_{i,j} = \sum_{d,f=1}^v P_{1,2,3}^{+(d,f)} (\tilde{\beta}_{i,j}^{+(d,f)})_{1,2,3}.$$

Here e.g. $(\tilde{\beta}_{i,j}^{+(d,f)})_{1,2,3}$ is defined by equ. (43), if index i refers to the i -th atom of the d -th type of unit and index j to the j -th atom of the f -th type of unit and $P_{1,2,3}^{+(d,f)}$ is the frequency to have a d -th type of unit at the elementary cell characterized by the lattice vector $\underline{R}_j = j_1 \underline{a}_1 + j_2 \underline{a}_2 + j_3 \underline{a}_3$ and an f -th type of unit at the lattice point $\underline{R}_{i,j} = (j_1 + 1) \underline{a}_1 + (j_2 - 1) \underline{a}_2 + (j_3 + 1) \underline{a}_3$.

Starting with the appropriate charge densities and bond orders known from a previous HÜCKEL calculation we can form, with the aid of equations (34)—(43), all quantities $\tilde{\alpha}_i$ and $\tilde{\beta}_{i,j}$ for the different units and different interactions. Substituting these into the appropriate equations ((52)—(54) type) we can construct the terms of the average matrix $\bar{\mathbf{F}}$. Solving the eigenvalue problem of the latter for a given \underline{k} vector, with the aid of the resulting eigen-

vectors we can form the charge densities and bond orders belonging to the average system. After obtaining these we can continue our calculation by solving the eigenvalue problem of the matrix $\bar{\mathbf{F}}$ defined by equations (33)–(43), but using for I_i , E_i , z_i , $\beta_{i,j}$, $\gamma_{i,j}$ their average values over all units (see equations (29)–(31)) and for $(\beta_{i,j}^{\pm})_s$, $(\gamma_{i,j}^{\pm})_s$, $(\beta_{i,j}^{++})_{s,t}$, $(\gamma_{i,j}^{++})_{s,t}$ etc. their average values for all types of interactions (e.g.) $(\bar{\gamma}_{i,j}^{++})_{s,t} = \sum_{d,f=1}^v P_{s,t}^{++(d,f)} (\gamma_{i,j}^{++(d,f)})_{s,t}$.

Continuing this iterative procedure we can determine the SCF eigenvectors and eigenvalues of $\bar{\mathbf{F}}$ for a given vector k . Repeating this procedure for different vectors k lying within the first Brillouin zone of the average lattice, we can determine the limits of the different energy bands.

Having obtained the SCF eigenvectors we can determine the inter-configurational matrix elements between singlet excited states for a given vector k also for nearly periodic three-dimensional molecular crystals, if we use equation (48) with the average integrals $\bar{\gamma}_{p,r}$.

Acknowledgment

The author would like to express his gratitude to Professor P.-O. Löwdin for his critical remarks and for making possible to perform part of this work during the author's stay at the Uppsala Quantum Chemistry Group. He is also indebted to Mr. F. BELEZNAY and Mr. G. BICZÓ for some useful remarks.

REFERENCES

1. J. LADÍK, Acta Phys. Hung., **18**, 23, 1965.
2. R. PARISER, and R. G. PARR, J. Chem. Phys., **21**, 466, 1953; **21**, 767, 1953.
3. J. A. POPPLE, Trans. Far. Soc., **49**, 1375, 1953.
4. N. MATAGA and K. NISHIMOTO, Z. Physik. Chemie, **13**, 140, 1957.
5. J. LADÍK and K. APPEL, J. Chem. Phys., **40**, 2470, 1964.
6. C. C. J. ROOTHAAN, Rev. Mod. Phys., **21**, 61, 1951.
7. F. BELEZNAY and G. BICZÓ, J. Chem. Phys., **43**, 2351, 1964.

О ПОЛУЭМПИРИЧЕСКИХ ТЕОРИЯХ МОЛЕКУЛЯРНЫХ КРИСТАЛЛОВ II. ПРИБЛИЖЕНИЕ ПАРИЗЕРА—ПАРРА—ПОПЛА

Я. ЛАДИК

Р е з и о м е

Даётся общий матричный формализм для определения энергетических полос одно- и трёхмерных произвольных молекулярных кристаллов в приближении Паризера—Парра—Попла при периодических граничных условиях Борна—Кармана, в котором принимаются во внимание только взаимодействия самых близких соседей. Выражения обобщаются и для случая, когда в одно- или трёхмерных кристаллах встречаются немного различные подэлементы.

INTENSITY CORRELATION OF COHERENT LIGHT BEAMS

By

GY. FARKAS, L. JÁNOSSY, Zs. NÁRAY and P. VARGA

CENTRAL RESEARCH INSTITUTE OF PHYSICS, BUDAPEST

(Received 12. VI. 1964.)

By making use of the coincidence technique, the intensity correlation between two coherent light beams produced by splitting a light beam by means of a semitransparent mirror could be verified. The data obtained in this way are in good agreement with the result predicted by a semi-classical theory.

Introduction

§ 1. More than ten years ago we started a series of measurements in this Laboratory which aimed at the investigation of the dual nature of light. In our first experiment [1] we split a weak beam of light into two components and showed, that the pulses registered by two photomultipliers placed in the paths of the beams were distributed at random. The rate of coincidences between the signals registered by the multipliers did not exceed the rate of random coincidences which are obtained if the multipliers are exposed to independent beams of light.

When considering the beam of light as consisting of single photons the above result could be interpreted by saying that "photons falling on the semitransparent mirror are not split — but at random pass on in the one or the other of the components of the beam". From the evaluation of the experimental results it was concluded that if there were photons in the beam which were split after all, their relative rate could not have exceeded $\varepsilon = (-0,29 \pm 0,30)\%$ of the total intensity. The value of the standard error $\delta\varepsilon = \pm 0,30\%$ of ε was obtained from the expression

$$\delta\varepsilon = \frac{2}{p} \sqrt{\frac{\tau}{T}}, \quad (1)$$

where $\tau = 2 \mu\text{sec}$ was the resolving time of the measuring arrangement [1], $T = 10$ hours the total time of measurement and p the efficiency of the multipliers in respect of the recording of a single photon. By the comparison of the energy carried in the beam as measured by a thermoelement with the rate of pulses recorded, it was found that $p \sim 1/300$.

Similar results were obtained later by BRANNEN and FERGUSON [2], their analysis was also based on similar arguments.

I. Theory of the experiment

§ 2. The above analysis of the coincidence experiments has, however, a weakness. If we were to assume that photons are split in two by the semi-transparent mirror, then we may argue that because of previous splitting processes the photons which are contained in the primary beam are already small fractions of an original photon. Indeed, suppose, e. g. that an excited atom emits one photon in one emission process. The radiation emitted by the atom spreads like a dipole wave into all directions and only a very small part of this wave is fed into the arrangement. Therefore, if photons can be split at all this means that only small fractions of photons will enter the arrangement, to begin with. The probability of response of the photocathode to one such fraction is very much smaller than the value p obtained for the efficiency of the cathode.

In order to express the above argument in more usual terms we state that the wave function representing the beam entering the arrangement is the superposition of very many photon states, each having a very small amplitude only. Thus, even a very weak beam contains many overlapping photon states, each with a rather small probability. When the beam falls on the dividing mirror, each of the components of the wave function is separated into two components. The correct value of p , which must be used in (1), is therefore $p = P_{\text{eff}} P$, where P_{eff} is the effective efficiency of the cathode and P the average square of the probability amplitude of the photon states in the beam. Since $P \ll 1$, the correct estimation of the value of $\delta\varepsilon$ gives a much larger value than that obtained by using p in (1) and given in our first publication [1]. Thus the fact that no systematic coincidences were then observed does not contradict the assumption, that the individual photon states are divided by the mirror.

§ 3. The nature of a beam of light emitted by a macroscopic source has recently been investigated from the theoretical and experimental points of view by several authors [3], [4], [5]. Some of the investigations were carried out in a semi-classical manner, i. e. it was assumed that the atoms of the source emit dipole radiation in accordance with the concepts of classical electrodynamics and further that the propagation of the waves also takes place according to classical theory. It was, however, assumed [3], [4] that such a beam when falling on a photocathode produces photo electrons such that the probability density of the emission of an electron is proportional to the energy absorbed by the cathode. More precisely, the probability of the emission

of a photo electron during a time dt from a surface element dS of the cathode is given by

$$dP = \alpha E^2 dS dt, \quad (2)$$

where α is a constant of proportionality and E the instantaneous electric field strength of the beam.

§ 4. Consider a beam of light of constant intensity that falls on a cathode. The probabilities of the emission of photo electrons in various intervals of time are according to (2) independent of each other and we expect emissions at random times. If the beam is split into two components in such a way that these are both of constant intensity and fall on two separate cathodes, then the emission of photo electrons from the cathodes takes place at random and therefore no correlation between the times of emission from the two cathodes is to be expected. Thus, recording the coincidences between the signals obtained from the cathodes, we expect only random coincidences, as it was indeed found in the early experiments.

A real beam of light shows fluctuations of intensity as was shown by several authors (e. g. [3], [4]). The fluctuations are mainly caused by the interference of the wave bands which are emitted by the individual atoms of the source. The relative fluctuations are independent of intensity and are of the order of 100 %.

When such a fluctuating beam of light is split into two components it must be assumed that the components show identical fluctuations. Owing to the fluctuations the probability densities for emission of electrons by the cathodes also vary in time. Denoting by $P_1(t, Q_1)$, $P_2(t, Q_2)$ the probability densities for emissions from the surface elements dS_1 , dS_2 , respectively, around the points Q_1 and Q_2 of the two cathodes 1 and 2, we expect for the rate of coincidences registered by a coincidence arrangement

$$C_s = \int \langle P_1(t, Q_1) P_2(t', Q_2) \rangle dt dt' dS_1 dS_2. \quad (3)$$

The rate of the accidental coincidences which are to be expected if there were no correlation between the intensities of the beams falling on the two cathodes is given by the following expression:

$$C_0 = \int \langle P_1(t, Q_1) \rangle \langle P_2(t', Q_2) \rangle dt dt' dS_1 dS_2. \quad (4)$$

The integration must be extended over $|t - t'| < \tau$ and over the cathode surfaces S_1 , S_2 . We find

$$C_s > C_0.$$

The excess of the observed coincidences C_s over the random rate C_0 which is caused by the correlation of the fluctuations may be written

$$\alpha = \frac{C_s - C_0}{C_0} = \frac{1}{C_0} \int \langle \delta P_1(t, Q_1) \delta P_2(t', Q_2) \rangle dt dt' dS_1 dS_2. \quad (5)$$

The effect is largest, i. e. α has its maximum if the resolving time τ of the apparatus is of the same order of magnitude as the period of the fluctuations of the beam. The theory shows that the period of the fluctuations of the beam is of the same order of magnitude as the time the beam takes to traverse its effective coherence length.

The detailed calculations show similarly, that the fluctuations are in phase in respect of surfaces on which the illumination is coherent. In the experiment it is therefore necessary to ensure that the illumination of the whole cathode is coherent.

Summarizing the theoretical considerations one expects a close connection between the coherence length A of the beam as observed directly by a Michelson type of interferometer and the quantity α .

One finds

$$\alpha = \frac{C_s - C_0}{C_0} = g^2 \frac{A}{c\tau}, \quad (6)$$

where g^2 is a factor describing the degree of coherence of the illumination of the cathodes and c is the velocity of light.

In the following it will be shown that the quantities A and g^2 can be expressed by the visibility of an interference pattern when this is produced by the same light beam as that used for the investigation of the correlation of the fluctuations.

From the theory [4] we obtain the expression

$$A = \int_0^{c\tau} V^2(x) dx, \quad (7)$$

where

$$V(x) = \frac{I_{\max} - I_{\min}}{I_{\max} + I_{\min}} \quad (8)$$

is the visibility of the interference pattern (produced e. g. in a Michelson interferometer) and x is the path difference between the interfering beams. In eq. (8) I_{\max} stands for the maximum of the intensity and I_{\min} for the minimum of the intensity of the interference pattern. Further, on the basis of the theory g^2 is given by the following expression:

$$g^2 = \frac{1}{S_1 S_2} \iint V^2(Q_1, Q_2) dS_1 dS_2, \quad (9)$$

where

$$V(Q_1, Q_2)$$

stands for the visibility of the interference pattern when beams going through points Q_1 and Q_2 of the cathodes 1 and 2, respectively are brought to interference by a suitable arrangement, and it is certain that the path difference between the interfering beams is considerably smaller than Λ .

It should be noted that eqs. (7) and (9) are valid only for the case when the intensities of the interfering beams are equal. If this condition is not satisfied, instead of eq. (7) one has to put

$$\Lambda = \int_0^{c\tau} |\gamma_{12}(x)|^2 dx, \quad (7a)$$

where $\gamma_{12}(x)$ is the complex degree of the longitudinal coherence defined by ZERNIKE [6]. In an analogous manner one obtains then

$$g^2 = \frac{1}{S_1 S_2} \iint |\gamma_{12}(Q_1, Q_2)|^2 dS_1 dS_2, \quad (9a)$$

where $\gamma_{12}(Q_1, Q_2)$ denotes the complex degree of the transversal coherence.

II. The experiment

§ 5. The experimental task was thus the following. A monochromatic beam of light was to be divided by a suitable optical device into two coherent components. The components were to be registered by photomultipliers by pulse technique. The excess of the rate of coincidences obtained from the coherent beams over the rate of coincidences obtained from independent beams was to be measured and compared with the coherence properties of the beam used in the experiment using eq. (6). As the rate of coincidences must be supposed to be affected not only by the micro-fluctuations as described in §§ 1—4 but also by macroscopic fluctuations of the intensity of the light source, special precautions were to be taken to exclude the possible effects of such macroscopic fluctuations.

The method

§ 6. The block diagram of the experimental setup is shown in Fig. 1. The beam \mathcal{B}_0 emitted by the light source \mathcal{F} of finite size is split into two coherent components \mathcal{B}_1 and \mathcal{B}_2 by the semi-transparent mirror \mathcal{M}_0 . The coherent beams thus obtained are passed to multipliers PM_1 and PM_2 , respectively. By means of a coincidence circuit of resolution time τ the number C_s of coincidences in unit time between the output pulses of the multipliers can be counted. Exposing the same two multipliers to two incoherent beams

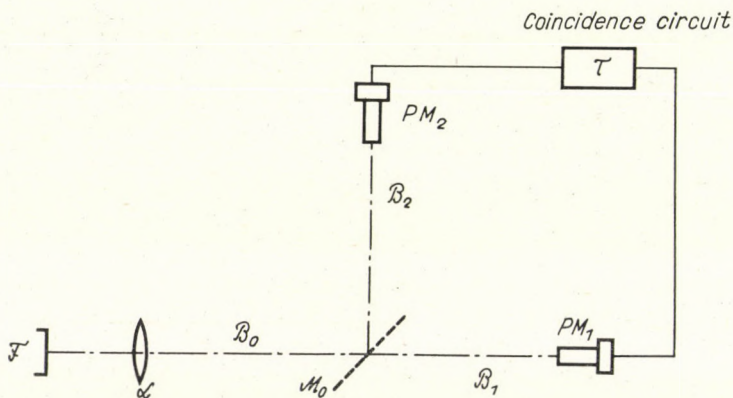


Fig. 1. The block diagram of the experimental arrangement

(which are of the same intensity, wave length, etc. as the two coherent beams \mathcal{B}_1 and \mathcal{B}_2) the accidental coincidences C_0 per unit time can be counted at the output of the coincidence circuit.

Light source

§ 7. Before describing in detail our experiment let us consider some aspects of previous measurements [5] referred to in § 3.

The light source used in all these experiments was a gaseous discharge tube excited by microwaves. The possibility cannot be excluded altogether that such an excitation might give rise to intensity modulation in the beams \mathcal{B}_0 , \mathcal{B}_1 and \mathcal{B}_2 , in addition to the natural fluctuations which are to be investigated. At excitation frequencies of 1000—2500 Mc/s needed for the light sources used in these experiments the period of the macroscopic intensity fluctuations of the beam \mathcal{B}_0 may range from 0,2 to 0,5 μ sec. Now, in the papers quoted above the coherence length of the light source used was given as $A = 30$ cm. With this value one obtains for the average duration of emission $T = A/c \sim 10^{-9}$ sec, i. e. the period of the possible intensity modulation due to the excitation is found to be of the same order of magnitude as that of the natural intensity fluctuations. Consequently, the results of the measurements of the intensity fluctuations of coherent light beams carried out with sources of this kind are unsuitable as a precise check on the theory. We have therefore used a gaseous discharge lamp supplied by d. c. as light source \mathcal{F} , to avoid the additional modulation caused by the high-frequency excitation.

It must be noted, however, that d. c. excitation by itself does not necessarily guarantee the absence of macroscopic fluctuations of intensity of the source. One might suppose, e. g. that in the avalanches developing in the gas discharge several atoms may simultaneously emit wave trains which are

not independent of each other. Checking, however, the light source applied in our experiment we found that the intensity fluctuations due to avalanche processes did not affect the results of the measurement (see § 14).

Optical arrangement

§ 8. In order to eliminate possible instabilities in the electronic and optical part of the measuring apparatus which may cause slow variations, the multipliers registering the coincidences were illuminated alternately by coherent and incoherent light beams in an arrangement shown in Fig. 2.

Let us consider first the measurement of systematic coincidences between two coherent light beams. The light beam emitted by the source \mathcal{T} (a krypton discharge lamp supplied by d. c.) passes through the glass plate \mathcal{Q} to the input of the monochromator which selects the wave length $\lambda = 5570 \text{ \AA}$ from the beam. The output slit \mathcal{S} (width 80μ , height 80μ) of the monochromator acts as a secondary source. The beam formed by the collimator lens \mathcal{L} (with a focal length of 30 cm) passes through the polarizer \mathcal{P} to the mirror \mathcal{M}_0 , where it is split into two coherent beams \mathcal{B}_1 and \mathcal{B}_2 . The intensity correlation of these two beams was investigated by registering the coincidences between the output pulses of the multipliers PM_1 and PM_2 , placed in the way of the beams. To provide well-defined apertures for the beams incident on the multipliers, the mirrors \mathcal{M}_1 and \mathcal{M}_2 were provided at their centres with holes of 3 mm in diameter.

For the recording of random coincidences multipliers PM_1 and PM_2 had to be illuminated by incoherent light beams. For this purpose the mirror \mathcal{M}_3 was moved into the position \mathcal{M}'_3 blocking the way of beam \mathcal{B}_2 , while the beam \mathcal{B}_1 was directed as beforehand towards multiplier PM_1 . Multiplier PM_2 was illuminated by a beam \mathcal{B}_3 obtained from that part of the original light beam which is reflected on the glass plate \mathcal{Q} . This beam avoiding the monochromator is reflected on the mirrors \mathcal{M}_4 and \mathcal{M}_5 and reaches multiplier PM_2 after having covered a path which is by 6 meters longer than the path of beam \mathcal{B}_1 . In order to obtain, in the case of incoherent illumination, a pulse rate approximately equal to that obtained when illuminating multiplier PM_2 by the beam coherent to beam \mathcal{B}_1 , i. e. in order to adjust the intensity of the incoherent beam to a value approximately equal to the intensity of the coherent one, a grey wedge \mathcal{W} was put in the way of the beam.

Arrangement for the determination of $V(x)$

§ 9. The optical system of the measuring arrangement can be checked by the telescope \mathcal{T} . The mirrors \mathcal{M}_1 and \mathcal{M}_2 and the semi-transparent mirror \mathcal{M}_0 constitute a Michelson interferometer, the interference pattern of which can be observed in the telescope \mathcal{T} . Replacing the mirrors \mathcal{M}_1 and \mathcal{M}_2 by mirrors without holes and placing the multiplier PM_3 in the way of the beam \mathcal{B}_4 ,

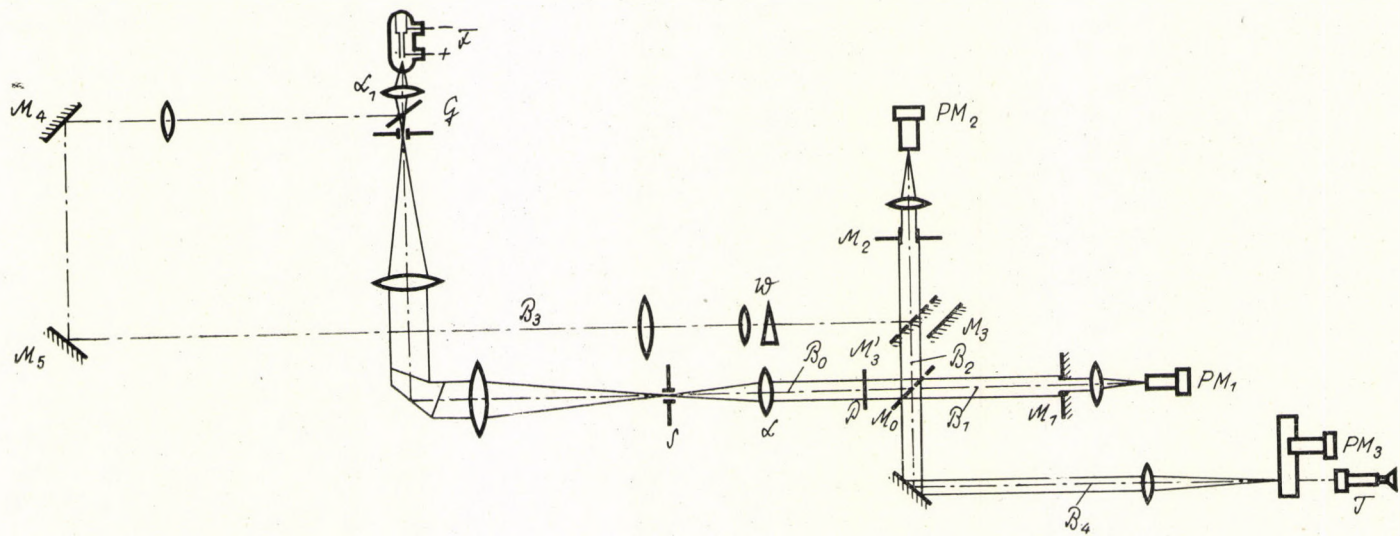


Fig. 2. The optical arrangement

the visibility $V(x)$ of the interference pattern can be determined for a given difference x between the armlengths under the same experimental conditions as those obtained in the coincidence experiment. Repeating the measurement of visibility for different values of x the function $V(x)$ can be established.

Electronics

§ 10. For counting systematic and random coincidences the outputs of the multipliers PM_1 and PM_2 are connected to a slow-fast coincidence circuit. In addition to the systematic and random coincidences, the numbers of pulses appearing during the measuring time on the output of multipliers PM_1 and PM_2 (denoted by N_1 and N_2 , respectively) are also counted. As mentioned above measurements with either coherent or incoherent illumination followed each other alternately. The duration of each run was 200 sec. A programmed automatic remote control was used to adjust the optical arrangement for the two kinds of illumination. Control measurements (e. g. measurement of the dark current pulse rate of the multipliers) were also provided for by this automatic control.

Method of evaluation

§ 11. As we have seen above, in order to compare the experimental and theoretical results relating to the intensity correlation of coherent light beams the systematic coincidences of two coherent light beams as well as the random coincidences had to be measured in the same arrangement. However, the comparison of these two kinds of coincidences cannot be carried out directly as the numbers of pulses counted by multipliers PM_1 and PM_2 cannot be made exactly identical for coherent and incoherent illuminations. To overcome this difficulty a method already described in connection with a previous experiment [1] was used.

Expressing the so-called effective resolution time Θ by the number C_s of the systematic coincidences and the numbers N_1 and N_2 of pulses registered by the multipliers, we have in case of coherent light beams

$$\Theta = \frac{C_s}{2 N_1 N_2} . \quad (10)$$

Correspondingly, the resolution time τ of the coincidence circuit in case of incoherent illumination — denoting the random coincidences by C'_0 and the numbers of pulses registered by N'_1 and N'_2 — can be expressed as

$$\tau = \frac{C'_0}{2 N'_1 N'_2} \quad (11)$$

or expressing τ by the numbers of pulses measured during the coherent illumination

$$\tau = \frac{C_0}{2 N_1 N_2} . \quad (12)$$

From eqs. (10) and (12) together with eq. (6) one obtains the relation

$$\alpha\tau = \theta - \tau = g^2 \frac{A}{c} . \quad (13)$$

For the evaluation of our results also the dark current pulses of the multipliers used in the measurement have to be taken into account. Denoting the dark current pulses of multipliers PM_1 and PM_2 by v_1 and v_2 , respectively, we obtain instead of (13)

$$\alpha' = \frac{\theta - \tau}{\left(1 - \frac{v_1}{N_{t_1}}\right)\left(1 - \frac{v_2}{N_{t_2}}\right)} , \quad (14)$$

where

$$N_{t_1} = N_1 + v_1 , \quad N_{t_2} = N_2 + v_2 .$$

Evaluating the quantities defined by (10) and (11) separately for each consecutive pair of readings taken with coherent and incoherent illumination, respectively (measuring run), we may compute the mean value of their difference, i. e. $\overline{\theta - \tau}$ and the error $\Delta(\overline{\theta - \tau})$.

As the secular change in both the number of counts N_{t_1} and N_{t_2} and in the dark current pulses v_1 and v_2 was negligibly small during the few hundred measuring runs it was not necessary to use eq. (14), i. e. the corrected form of (13) for each individual run, but it was sufficient to take the correction into account in the mean value only, i. e. finally the quantity

$$\bar{\alpha}' = \frac{(\overline{\theta - \tau}) \pm \Delta(\overline{\theta - \tau})}{\left(1 - \frac{v_1}{N_{t_1}}\right)\left(1 - \frac{v_2}{N_{t_2}}\right)} \quad (15)$$

had to be determined. It should be noted that the dark current correction amounted to about 10%.

§ 12. The visibility $V(x)$ was determined at different values of x from the intensity distribution of the respective interference pattern using on average 8—10 fringes for every value of x . The effective coherence length A was then computed according to eq. (7). The visibility as a function of the path difference is shown in Fig. 3.

As the direct measurement of $V(Q_1, Q_2)$ is very difficult from the technical point of view, the function $V(Q_1, Q_2)$ which is needed for the determination of g^2 (see eq. (9)) was determined from the expression

$$V(Q_1, Q_2) = \frac{\sin \pi \frac{Y(y_1 - y_2)}{\lambda f}}{\pi \frac{Y(y_1 - y_2)}{\lambda f}} \frac{\sin \pi \frac{Z(z_1 - z_2)}{\lambda f}}{\pi \frac{Z(z_1 - z_2)}{\lambda f}}, \quad (16)$$

where y_1, z_1 and y_2, z_2 are the coordinates of Q_1 and Q_2 , respectively, Y and Z are the sizes of the exit slit \mathcal{S} of the monochromator, and f is the focal length of the second collimating lens \mathcal{L} . The validity of eq. (16) was proved by experiments [7]. The results derived in this way for A and g^2 are listed in Table 1.

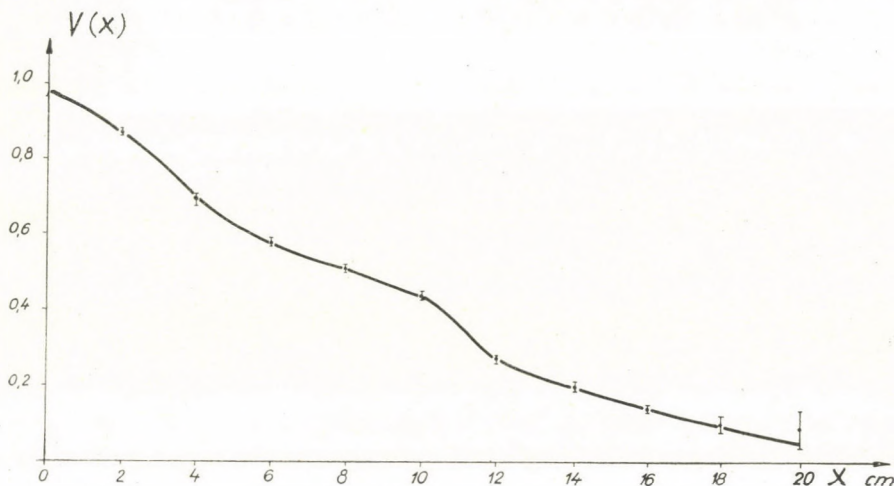


Fig. 3. The measured visibility curve

III. Results and conclusions

§ 13. Two series of measurements were performed: the first consisted of 440, the second of 634 runs. The main parameters of the measurements and the results are listed in Table 1.

For the sake of illustration a sample of the results of one measuring series is reproduced in Table 2. It should be mentioned that although the intensity of the light beams \mathcal{B}_1 and \mathcal{B}_2 were equal, the difference in the sensitivities and dark currents of the multipliers PM_1 and PM_2 resulted in a fairly large difference of N_{t_1} and N_{t_2} .

From the set of values obtained for the individual runs (see the histogram of Fig. 4) it could be established that the distribution of $\Theta - \tau$ is Gaussian. A χ^2 -test was carried out to prove that no systematic variation affected the value of $\Theta - \tau$.

§ 14. Finally, measurements were carried out to determine whether the individual emissions of the light source used in our experiment were really

Table I

Number of measuring runs	τ 10^{-12} sec	\bar{N}_{t_1} 10^3 sec $^{-1}$	\bar{N}_{t_2} 10^3 sec $^{-1}$	$\bar{\nu}_1$ 10^3 sec $^{-1}$	$\bar{\nu}_2$ 10^3 sec $^{-1}$	$\overline{\Theta - \tau}$ 10^{-12} sec	$\bar{\chi}'$ 10^{-12} sec	A cm	g^2	$\frac{g^2 A}{c}$ 10^{-12} sec
440	1,2	34	54	2,6	0,6	$49,3 \pm 2,8$	54 ± 3	$5,3 \pm 0,2$	0,314	55 ± 2
634	1,2	24	35	2,4	0,5	$47,3 \pm 3,4$	53 ± 4	$4,6 \pm 0,2$	0,314	48 ± 2
361	1,2	44	50	2,3	0,6	$-0,37 \pm 2,7$	$0,4 \pm 3$	~ 0	0,03	~ 0

Table II

Sample of a measuring series containing 10 measuring runs.
The number of pulses refers to a measuring time of 200 sec each.

$N_{t_1} \times 10^{-6}$	$N_{t_2} \times 10^{-6}$	C_s	Θ_i $(10^{-12}$ sec)	$N'_{t_1} \times 10^{-6}$	$N'_{t_2} \times 10^{-6}$	C'_0	τ_i $(10^{-12}$ sec)	$\Theta_i - \tau_i$ $(10^{-12}$ sec)	$(\Theta_i - \tau_i)^2$ $(10^{-24}$ sec)
6,6211	10,7056	837	1 181	6,5831	10,7128	856	1 214	- 33	1 089
6,6568	10,7518	874	1 221	6,6149	10,7889	841	1 178	+ 43	1 849
6,6683	10,7744	858	1 194	6,6250	10,7846	821	1 149	+ 45	2 025
6,6640	10,8062	912	1 266	6,5883	10,7662	821	1 157	+ 109	11 881
6,6201	10,7610	851	1 194	6,5431	10,7735	777	1 102	+ 92	8 464
6,6168	10,7407	841	1 183	6,5647	10,7210	749	1 064	+ 119	14 400
6,5883	10,7118	866	1 227	6,5113	10,7099	806	1 156	+ 71	5 041
6,5575	10,7046	819	1 167	6,5238	10,7138	806	1 153	+ 14	196
6,6014	10,7581	796	1 121	6,5739	10,7653	837	1 183	- 62	3 844
6,6693	10,7816	896	1 246	6,6149	10,7928	846	1 185	+ 61	3 721
66,2636	107,4958	8550	12 000	65,7430	107,5288	8160	11 541	459	52 510

$$\bar{\tau} = 1154 \times 10^{-12} \text{ sec.}$$

$$\overline{\Theta - \tau} = 46 \times 10^{-12} \text{ sec.}$$

$$\Delta(\bar{\tau} - \overline{\Theta}) = 19 \times 10^{-12} \text{ sec.}$$

independent of one another (see § 5 and 7). In these checking measurements the conditions were so chosen as to allow registration of only such systematic coincidences that resulted from simultaneous emission processes in the avalanches of the kind mentioned in § 7. These incidental emission processes affect the intensity of the whole spectrum emitted by the source and therefore their effect can be measured even if the beam \mathcal{B}_0 is obtained by using the entire spectrum of the source \mathcal{F} . In this case $A \sim 0$ and according to (6)

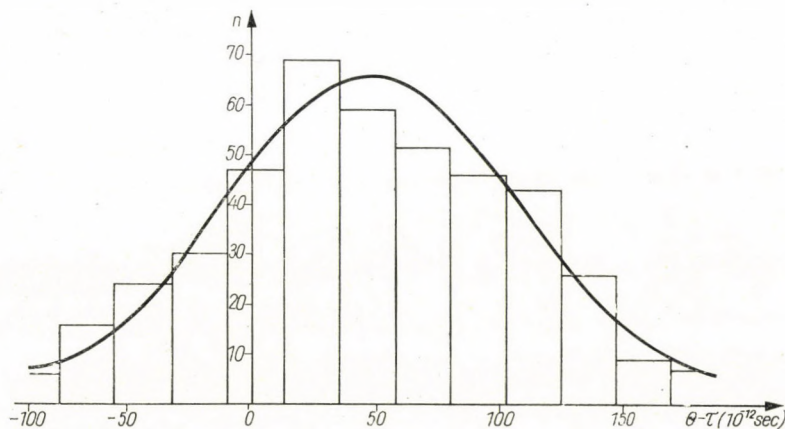


Fig. 4. The histogram representing the measured frequency $\Theta - \tau$ and the theoretical curve

the correlation effect disappears. By analysing in the same way, as was described above, the results obtained when the light beam \mathcal{B}_0 contains the entire spectrum of the source, the contribution of the avalanche effect to the intensity fluctuation can be evaluated.

361 runs of measurement were carried out to determine the avalanche fluctuations. As a result we obtained

$$\bar{\tau}' = (-0.4 \pm 3) \cdot 10^{-12} \text{ sec.}$$

The respective quantities are listed in the last row of Table 1. The fact that the error is of the same order as in the two measurements described in § 13 shows that within the experimental accuracy the light source did not influence the experimental results.

It can be seen from Table 1 that there is a very good agreement between the measured and the theoretically predicted values. This quantitative agreement supports the semi-classical theory of light which we made use of when interpreting the phenomenon.

Thanks are due to our collaborators Mr. K. TITSCHKA, Mr. I. CZIGÁNY and Mr. L. IMRE for their valuable assistance in the experiments.

REFERENCES

1. A. ÁDÁM, L. JÁNOSSY and P. VARGA, *Acta Phys. Hung.*, **4**, 4, 1955; *Ann. Phys.* **16**, 409, 1955
2. E. BRANNEN and H. I. S. FERGUSON, *Nature* **177**, 481, 1956.
3. R. HANBURY-BROWN and A. G. LITTLE, *Phil. Mag.*, **45**, 663, 1954.
R. HANBURY-BROWN and R. Q. TWISS, *Proc. Roy. Soc., A* **242**, 300, 1957.
E. WOLF, *Phil. Mag.*, **2**, 351, 1957.
4. E. M. PURCELL, *Nature*, **178**, 1149, 1956.
L. MANDEL, *Proc. Phys. Soc.*, **72**, 1037, 1958.
5. L. JÁNOSSY, *Nuovo Cim.*, **6**, 111, 1957.
L. JÁNOSSY, *Nuovo Cim.*, **12**, 369, 1959.
6. R. Q. TWISS and R. HANBURY-BROWN, *Nature*, **117**, 27, 1957.
G. A. REBKA and R. V. POUND, *Nature*, **180**, 1035, 1957.
E. BRANNEN, H. I. S. FERGUSON and W. WEHLAU, *Can. J. Phys.*, **36**, 371, 1958.
R. Q. TWISS and A. G. LITTLE, *Aust. J. Phys.*, **12**, 77, 1959.
7. F. ZERNIKE, *Physica*, **5**, 875, 1938.
M. BORN and E. WOLF, *Principles of Optics*, Pergamon Press, London, 1959.
8. J. BAKOS, K. KÁNTOR and P. VARGA, *Reports of the Central Research Inst. of Phys.*, **9**, 207, 1961.
J. BAKOS and K. KÁNTOR, *Optik*, **18**, 554, 1961.
Z. ERDŐKÜRTI and K. KÁNTOR, *Optik*, **20**, 304, 1963.

КОРРЕЛЯЦИЯ ИНТЕНСИВНОСТИ КОГЕРЕНТНЫХ ПУЧКОВ СВЕТА

ДЬ. ФАРКАШ, Л. ЯНОШИ, Ж. НАРАИ и П. ВАРГА

Р е з ю м е

Использование техники совпадений позволило проверить корреляцию интенсивности между двумя когерентными пучками света, полученными разделением пучка при помощи полупрозрачного зеркала. Результаты измерения хорошо согласуются с предсказаниями выработанной нами квазиклассической теории.

THEORETICAL ESTIMATION OF THE CONDUCTIVITY OF DNA

By

F. BELEZNAY

RESEARCH INSTITUTE FOR TECHNICAL PHYSICS OF THE HUNGARIAN ACADEMY OF SCIENCES, BUDAPEST

G. BICZÓ and J. LADIK

CENTRAL RESEARCH INSTITUTE FOR CHEMISTRY OF THE HUNGARIAN ACADEMY OF SCIENCES,
BUDAPEST

(Presented by G. Schay. — Received 30. VI. 1964)

We have calculated the specific conductivity (σ_0) values of adenylic acid assuming for it a stereo-structure of a chain in the WATSON-CRICK model of DNA. The deformation potential approximation has been used for the calculation of the interaction of the charge carriers with the phonons correspondig 1. to vibrations perpendicular to the planes of the bases; 2. to the C-N bond stretching vibration of the carbon atom and the N atom of the NH₂-group of adenine. We have found in the first case $\sigma_0 = 3,58 \cdot 10^4 \Omega^{-1} \text{ cm}^{-1}$ and in the second $\sigma_0 = 8,81 \cdot 10^4 \Omega^{-1} \text{ cm}^{-1}$.

Introduction

Conductivity measurements of DNA have been reported several times in the literature. DUCHESNE et al. [1] give 0,80 eV, ELEY and SPIVEY [2] 1,21 eV, while O'KONSKI and SHIRAI [3] give 1,15—1,20 eV for the activation energy of d. c. conduction. If the mechanism of conduction were electronic and DNA were an intrinsic semiconductor, these results would give for the forbidden band width 1,60 eV, 2,42 eV, 2,30—2,40 eV, respectively. ELEY and SPIVEY have found σ_0 in

$$\sigma = \sigma_0 e^{-\frac{W_{\text{act}}}{kT}} \quad (1)$$

to have the order of magnitude $10^3 \Omega^{-1} \text{ cm}^{-1}$, while from O'KONSKI's and SHIRAI's data [3] $\sigma_0 = 10^7 \Omega^{-1} \text{ cm}^{-1}$ is obtained. The origin of this discrepancy is not clear.

On the other hand O'KONSKI and SHIRAI [3, 4] give about 0,12 eV for the activation energy and $10^{-3} \Omega^{-1} \text{ cm}^{-1}$ for σ_0 (4) of the high frequency (10^9 c. p. s.) a. c. conductivity of desiccated DNA.

ELEY and SPIVEY interpret their results on the basis of intrinsic electronic conductivity due to the overlap of the electrons of the superimposed base pairs in DNA [5]. O'KONSKI and SHIRAI take this possibility also as probable. To be able to compare the experimental results with the theoretical ones it seemed interesting to estimate also theoretically the value of σ_0 assuming an intrinsic electronic conductivity in DNA.

Method

To estimate the specific conductivity of the intrinsic conduction of DNA we have to calculate the mobility of the electrons and holes. The latter depends on the band structure of DNA and on the scattering of these particles on those lattice vibrations *inside* the macromolecule which correspond to the acoustic phonons. We can write for the mobility of the electrons and holes in the deformation potential approximation [6] for the three-dimensional case

$$\mu_e = \frac{2^{3/2} \pi^{1/2}}{3} \frac{c_{l,l} \hbar^4 e}{\varepsilon_{1e}^2 m_e^{*5/2} (kT)^{3/2}}, \quad (2)$$

and

$$\mu_h = \frac{2^{3/2} \pi^{1/2}}{3} \frac{c_{l,l} \hbar^4 e}{\varepsilon_{1h}^2 m_h^{*5/2} (kT)^{3/2}}, \quad (3)$$

respectively. Here $c_{l,l}$ is the elastic constant for longitudinal acoustic waves, T is the absolute temperature, ε_{1e} and ε_{1h} are the deformation potentials of the electron, and hole, respectively:

$$\varepsilon_{1e} = \frac{\delta W c_l}{\Delta}, \quad (4)$$

$$\varepsilon_{1h} = \frac{\delta W v_u}{\Delta}, \quad (5)$$

where $\delta W c_l$ denotes the change of the lower limit of the lowest unfilled energy band with the dilatation Δ of the lattice and $\delta W v_u$ has a similar meaning for the upper limit of the highest filled band. Further m_e^* and m_h^* are the effective masses of the electron and hole, resp. which, assuming a parabolic energy wave number connection, can be written in the form

$$m_e^* = \frac{\hbar^2 \pi^2}{2 a^2 \Delta W_c}; \quad m_h^* = \frac{\hbar^2 \pi^2}{2 a^2 \Delta W_v}, \quad (6)$$

where a is the lattice constant and ΔW_c , ΔW_v are the widths of the conductivity and valence band, respectively.

For the specific conductivity we can write

$$\sigma = e (n \mu_e + p \mu_h), \quad (7)$$

where n is the density of mobile electrons and p the density of holes, which are given by

$$n = e^{-(W_{cl} - W_F)/kT} \cdot 2 (2\pi m_e^* kT/\hbar^2)^{3/2} \quad (8)$$

and

$$p = e^{-(W_F - W_{cv})/kT} \cdot 2 (2\pi m_h^* kT/\hbar^2)^{3/2}, \quad (9)$$

where $W_F = \frac{W_{cl} + W_{cv}}{2}$ in a good approximation. Substituting equations (2), (3) and (8), (9) into (7) we obtain

$$\sigma = \frac{2}{3\pi} e^2 \hbar c_{l,l} \left[\frac{1}{m_e^* \varepsilon_{1e}^2} + \frac{1}{m_\mu^* \varepsilon_{1h}^2} \right] e^{-\frac{\Delta W}{2kT}} = \sigma_0 e^{-\frac{\Delta W}{2kT}}, \quad (10)$$

where ΔW is the forbidden band width between the conduction and valence bands.

In the one-dimensional case¹ it is possible to show that

$$\mu_e = 4 \sqrt{\frac{2}{\pi}} \frac{c_\perp \hbar^2 e}{m_e^{*3/2} (kT)^{1/2}} \quad (11)$$

and a similar expression holds for μ_h . Here c_\perp is the elastic constant parallel with the directions of the linear chains. In the one-dimensional case we have for the dilatation $\Delta = \frac{\delta a}{a}$ and this should be substituted into equations (4) and (5). In this case the acoustic vibrations correspond to such vibrations in which the distance between the planes of the base pairs changes.

For the number of mobile electrons in the one-dimensional case one obtains

$$n = \frac{1}{2\sqrt{2\pi}} \frac{m_e^{*1/2}}{\hbar} (kT)^{1/2} e^{-(W_{cl} - W_F)/kT} \quad (12)$$

and a similar expression for the number of holes. Substituting (11) and (12) into (7) we obtain

$$\sigma = \frac{2}{\pi} c_\perp \hbar e^2 \left[\frac{1}{m_e^* \varepsilon_{1e}^2} + \frac{1}{m_h^* \varepsilon_{1h}^2} \right] e^{-\frac{\Delta W}{2kT}} = \sigma_0 e^{-\frac{\Delta W}{2kT}}. \quad (13)$$

In the calculation we have taken for c_\perp the appropriate value found for graphite [7],² $c_\perp = 3,60 \cdot 10^{11}$ din/cm². In the determination of the effective masses and deformation potentials as first approximation we used the energy band data calculated for polyadenylic acid in the tight binding approximation [8].³ For the calculation of the effective masses (equ. 6) we have taken $a = 3,36 \text{ \AA}$ and $\Delta W_c = 0,246 \text{ eV}$, $\Delta W_v = 0,320 \text{ eV}$ [8].

¹. We call that case one dimensional, when we have linear chains parallel to each other.

To determine ε_{1e} and ε_{1h} we have calculated δW_{C_l} and δW_{V_u} for $\delta a = 0,05a = 0,05 \cdot 3,36 = 0,17 \text{ \AA}$. Assuming that the $\beta'_{i,j}$ resonance integrals between atom i belonging to one base and atom j belonging to its superimposed neighbour are proportional to the appropriate overlap integrals $S'_{i,j}$, as a first step we have determined all these integral values between two superimposed adenine molecules for a distance of $3,36 + 0,17 = 3,53 \text{ \AA}$. (The $S'_{i,j}$ and $\beta'_{i,j}$ integral values for $3,36 \text{ \AA}$ between two adenine molecules have been determined previously [5, 9]). On the basis of these values we have calculated the new $\beta'_{i,j}$ integral values for $3,53 \text{ \AA}$. Substituting these in the eigenvalue problem of the complex Hermitian matrix $\mathbf{C} = \mathbf{A} + \mathbf{B}^{ik} + \mathbf{B}^{tr-ik}$ which gives the energy bands of polyadenylic acid [8], one could obtain directly the energy bands at the changed adenine-adenine distance (in matrix \mathbf{C} matrix \mathbf{A} contains the integrals $a_i = (\psi_i, H\psi_i)$ and $\beta_{i,j} = (\psi_i, H\psi_j)$ which contribute to the matrix elements of the one-electron effective Hamiltonian with atomic wave function belonging to the same molecule, while \mathbf{B} contains the interaction parameters $\beta'_{i,j}$ between atoms belonging to different neighbouring adenine molecules. For further details see [8]).

Since we are interested only in the change of the lower limit of the lowest unfilled and of the upper limit of the highest filled band, we have not solved again the matrix eigenvalue problem, but we have performed a perturbation treatment. We may rewrite

$$\mathbf{C}(1,05a) = \mathbf{A} + (\mathbf{B}(a) + \Delta\mathbf{B}) e^{ik} + (\mathbf{B}^{tr}(a) + \Delta\mathbf{B}^{tr}) e^{-ik}, \quad (14)$$

where the matrix $\Delta\mathbf{B}$ contains the change of the integrals $\beta'_{i,j}$ e. g. we have

$$(\Delta\mathbf{B})_{i,j} = \beta'_{i,j}(1,05a) - \beta'_{i,j}(a). \quad (15)$$

From the numerical results we could see that all the elements of the $\Delta\mathbf{B}$ matrix are small. Therefore it was enough to perform only a first order perturbation calculation. By taking the eigenvectors \underline{u} belonging to the limits of the bands under consideration and by taking into account that these limits have occurred at $k = 0, \pi$, we can write [8]

$$\delta W_{C_l} = - \underline{u}_{c,\pi}^{tr} (\Delta\mathbf{B} + \Delta\mathbf{B}^{tr}) \underline{u}_{c,\pi}, \quad (k = \pi), \quad (16a)$$

$$\delta W_{V_u} = \underline{u}_{v,0}^{tr} (\Delta\mathbf{B} + \Delta\mathbf{B}^{tr}) \underline{u}_{v,\pi}, \quad (k = 0), \quad (16b)$$

² In graphite the distance between the different layers ($3,36 \text{ \AA}$) is the same as the distance between nucleotide base pairs in DNA and we can assume that their density is not very different.

³ In the energy band calculation for polyadenylic acid it was assumed that the adenine molecules have the same position relative to each other as the one within one chain of DNA, i. e. they are parallel to each other. The distance between them is $3,36 \text{ \AA}$ and they are distorted relative to each other by an angle of 36° .

where $\underline{u}_{c,\pi}$ is the eigenvector belonging to the lower limit of the conduction band and $\underline{u}_{v,0}$ belonging to the upper level of the valence band. With the aid of these expressions we could determine ε_{1e} and ε_{1h} .

To obtain some information about the effect of scattering of the electrons and holes on vibrations in the plane of the adenine molecules (optical phonons) we have calculated the specific conductivity belonging to the vibration of the C—N bond between a ring carbon atom and the NH₂-group of adenine. As a first approximation we have used the elastic constant $c_{||} = 8,53 \cdot 10^{12}$ din/cm² [7] of graphite in the plane of the layers. The effective masses will be the same as in the previous case. The deformation potentials have now been calculated with the aid of the expressions

$$\delta W_{c_l} = -\underline{u}_{c,\pi}^{tr} \Delta \mathbf{A} \underline{u}_{c,\pi}, \quad (17)$$

$$\delta W_{v_v} = \underline{u}_{v,0}^{tr} \Delta \mathbf{A} \underline{u}_{v,0}. \quad (18)$$

This calculation became very simple because the matrix $\Delta \mathbf{A}$ consisted of only two elements $\Delta \beta_{C,N(H_2)} = \Delta \beta_{N(H_2),C} = \beta_{C,N(H_2)}(1,05a_{C,N}) - \beta_{C,N(H_2)}(a_{C,N})$ ($a_{C,N} = 1,34 \text{ \AA}$). For $\beta_{C,N(H_2)}$ (a) we have taken 3,33 eV [9] and we have calculated $\beta_{C,N(C_2)}$ ($1,05a$) again on the basis of the appropriate overlap integrals.

Results

We have obtained in the case of the vibrations perpendicular to the planes of the bases $\varepsilon_{1e} = 0,448$ eV and $\varepsilon_{1h} = 0,352$ eV. For the C—N vibration between the NH₂-group and the adjacent carbon atom the results are $\varepsilon_{1e} = 0,999$ eV, $\varepsilon_{1h} = 1,465$ eV, resp.

With the aid of these we have obtained in the first case

$$\sigma_0 = \sigma_{0e} + \sigma_{0h} = (1,15 \cdot 10^4 + 2,43 \cdot 10^4) \Omega^{-1} \text{ cm}^{-1} = 3,58 \cdot 10^4 \Omega^{-1} \text{ cm}^{-1} \quad (19)$$

and in the second case

$$\sigma_0 = \sigma_{0e} + \sigma_{0h} = (5,47 \cdot 10^4 + 3,34 \cdot 10^4) \Omega^{-1} \text{ cm}^{-1} = 8,81 \cdot 10^4 \Omega^{-1} \text{ cm}^{-1}. \quad (20)$$

Discussion

We can see from the above results that the theoretically computed σ_0 values fall between the experimental values for d.c. conductivity given by ELEY and SPIVEY [2] ($10^3 \Omega^{-1} \text{ cm}^{-1}$) and by O'KONSKI and SHIRAI [3] ($10^7 \Omega^{-1} \text{ cm}^{-1}$). Since our calculation was only an approximate one, in which

we have used the energy band structure of polyadenylic acid instead of the band structure of real DNA we can assume that the theoretically found σ_0 values, calculated for interactions with different types of phonons do not differ very strongly from the d. c. conductivity of DNA.

Assuming an intrinsic electronic mechanism for conduction in DNA we have for the width of the forbidden band between the highest filled and lowest unfilled energy band of DNA from the d. c. conductivity measurements the value $\Delta W = 2,40$ eV [2, 3]. The theoretical value from band structure calculations for the forbidden band width between the highest filled and lowest unfilled singlet band is 3,50 eV [10]. For the width between the highest filled and lowest unfilled triplet band we find about 2,00 eV [11]. Since the experimentally found lowest triplet excited state has 2,55 eV energy [12] it is probable that the forbidden band width determined by d. c. conduction measurements refers to the first unfilled triplet band.

Our theoretical σ_0 values do not agree, however, with the experimental ones found by high frequency a. c. conductivity measurements ($10^{-3} \Omega^{-1} \text{cm}^{-1}$) [3]. The band gap (0,24 eV) determined by high frequency a. c. conductivity measurements [3] does not agree with the appropriate theoretical value ($\sim 2,00$ eV) either.

A priori, one would expect that data determined by high frequency a. c. conductivity measurements should agree with the computed ones. Namely in d. c. measurements we have an electric current not only along the macromolecule, but the current flows also through the junctions between different macromolecules. Therefore the measured values refer rather to these junctions than to the inside of the macromolecules. On the other hand in high frequency a. c. measurements the current alternates practically only along single macromolecules and therefore the measured values are more characteristic of the intrinsic conductivity of the macromolecule. The fact that the experimental and theoretical σ_0 and ΔW values agree for d. c. measurements, but not for a. c. measurements indicates that the conduction mechanism of DNA is more complicated than it has been supposed and further experimental and theoretical work is required to clear up the situation.

Acknowledgment

We should like to express our gratitude to Professor M. KOTANI for stimulating discussions and to Professor C. T. O'KONSKI for valuable remarks. We are indebted to Miss A. JESZENÁK for performing the numerical calculations.

REFERENCES

1. J. DUCHESNE, J. DEPIREUX, A. BERTINCHAMPS, N. CORNET and VAN DER J. M. KAA, Nature, **188**, 405, 1960.
2. D. D. ELEY and D. I. SPIVEY, Trans. Far. Soc., **58**, 411, 1962.
3. C. T. O'KONSKI and M. SHIRAI, Biopolymers, **1**, 557, 1963.
4. C. T. O'KONSKI, Rev. Mod. Phys., **35**, 722, 1963.
5. J. LADIK, Acta Phys. Hung., **11**, 239, 1960.
6. W. SHOCKLEY, Electrons and Holes in Semiconductors, 278, D. Van Nostrand Company, Inc. New York, 1950.
7. K. KOMATSU and T. NAGAMYA, J. Phys. Soc. Japan, **6**, 438, 1951.
8. J. LADIK and K. APPEL, J. Chem. Phys., **40**, 2470, 1964.
9. T. A. HOFFMANN and J. LADIK, Adv. Chem. Phys., **7**, 83, 1964.
10. J. LADIK and G. BICZÓ, J. Chem. Phys., **42**, 817, 1965.
11. J. LADIK and K. APPEL, Preprint QB 20, Quantum Chemistry Group, Uppsala University, 1965.
12. P. DOUZOU, J. C. FRANCQ, M. HAUSS and M. PTAK, J. Chem. Phys., **58**, 926, 1961.

ТЕОРЕТИЧЕСКОЕ ОПРЕДЕЛЕНИЕ ЭЛЕКТРИЧЕСКОЙ ПРОВОДИМОСТИ DNS

Ф. БЕЛЕЗНАИ, Г. БИЦО и Я. ЛАДИК

Резюме

Вычисляются значения удельной электропроводимости полиадениловой кислоты (σ_0), предполагая, что пространственная структура полиадениловой кислоты и единичной цепи DNS в модели Ватсона—Крика одинакова. Для описания взаимодействия между электронами и фононами применено приближение деформационного потенциала. Фононы, принятые во внимание при вычислениях I. соответствуют колебаниям, перпендикулярным к плоскости базисов и 2, соответствуют валентным колебаниям С—N связи между атомом углерода и атомом азота в NH₂ группе адениловой кислоты. В первом случае для электропроводности получено значение $\sigma_0 = 3,58 \cdot 10^4 \Omega^{-1} \text{ см}^{-1}$, а во втором — $\sigma_0 = 8,81 \cdot 10^4 \Omega^{-1} \text{ см}^{-1}$.

A SUPERCONDUCTIVE MODEL WITH TWO KINETIC ENERGIES

By

J. NÉMETH

INSTITUTE OF THEORETICAL PHYSICS, ROLAND EÖTVÖS UNIVERSITY, BUDAPEST
and
NUCLEAR RESEARCH INSTITUTE, DEBRECEN

(Presented by K. Novobátzky — Received 24. VIII. 1964)

A superconductive model is examined with two kinetic energies. The energy values are determined in second order approximation with an exact wave function and with the BCS wave function. The correction of the BCS method is examined in this special case.

1. Introduction

Recently BARDEEN, COOPER and SCHRIEFFER have had great success in explaining the superconductivity with their approximation method [1]. Their results gave the initiative to BOHR, MOTTELSON and PINES [2] to raise the possibility of applying the BCS method to atomic nuclei. Although the superfluid nuclear model proved to be very successful for the explanation of certain nuclear properties [3] it raised some problems connected with the application of the BCS method to nuclei. The BCS model wavefunction is not an exact particle number eigenfunction, and in the case of systems with low particle numbers this fact may cause significant errors. To estimate these errors it becomes important to consider in more detail the so-called degenerate model [4]. In this case the kinetic energy of different states is supposed to be a constant, and it is possible to diagonalise the Hamilton operator exactly. In the degenerate model the error of the BCS approximation turned out to be [5]

$$\Delta E = E_{\text{exact}} - E_{\text{BCS}} = -\frac{1}{2} \frac{d^2 E_{\text{exact}}}{dN^2} (\delta N)^2, \quad (1)$$

where $(\delta N)^2 = \langle N^2 \rangle - \langle N \rangle^2$ is the mean square deviation of the particle number operator. If we add this energy correction to the energy obtained by the BCS method for the case of the degenerate model we get back the exact energy. The question arises, however, to what extent this correction method is applicable if we have no constant kinetic energy. To decide this problem it seems to be useful to examine the simplest model with no constant kinetic energy in a more detailed manner, namely a model where the kinetic energy has two possible values.

2. The exact treatment of a model with two kinetic energies

Let the number of the possible states be Ω . In $\Omega/2$ state the kinetic energy is ε_1 , in $\Omega/2$ it is ε_2 . The model Hamilton operator of the system is the following

$$H = \sum_{k=1}^{\Omega/2} \varepsilon_1 (a_{k+}^+ a_{k+}^- + a_{k-}^+ a_{k-}^-) + \sum_{l=\Omega/2+1}^{\Omega} \varepsilon_2 (a_{l+}^+ a_{l+}^- + a_{l-}^+ a_{l-}^-) - V \sum_i \sum_j a_{i+}^+ a_{i-}^+ a_{j-}^- a_{j+}^- . \quad (2)$$

From (2) it can be seen that the first $\Omega/2$ states and the second $\Omega/2$ states are completely equivalent. The most general exact wavefunction of this system is the superposition of terms of the type

$$b_{n_i} [a_{k_i+}^+ a_{k_i-}^- \dots a_{k_{n_i}+}^+ a_{k_{n_i}-}^-] [a_{e_i+}^+ a_{e_i-}^- \dots a_{l_{N/2-n_i}+}^+ a_{l_{N/2-n_i}-}^-],$$

where the b_{n_i} -s should be determined by minimizing the ground state energy. Here n_i means the number of particle pairs which have kinetic energy ε_1 , and $N/2 - n_i$ that of kinetic energy ε_2 . There are $\binom{\Omega/2}{n_i} \binom{\Omega/2}{N/2 - n_i}$ different states with the same b_{n_i} factor and the summation over n_i runs from 0 to $N/2$. The normalization condition for b_{n_i} is

$$\sum_{n_i=0}^{N/2} b_{n_i}^2 \binom{\Omega/2}{n_i} \binom{\Omega/2}{N/2 - n_i} = 1 . \quad (3)$$

The energy of the system turns out to be

$$E = 2 \sum b_{n_i}^2 \binom{\Omega/2}{n_i} \binom{\Omega/2}{N/2 - n_i} \left[\frac{N}{2} \varepsilon_2 - n_i (\varepsilon_2 - \varepsilon_1) \right] - \frac{VN}{2} - V \sum b_{n_i}^2 \binom{\Omega/2}{n_i} \binom{\Omega/2}{N/2 - n_i} n_i \left(\frac{\Omega}{2} - n_i \right) - V \sum b_{n_i}^2 \binom{\Omega/2}{n_i} \binom{\Omega/2}{N/2 - n_i} \left(\frac{N}{2} - n_i \right) \left(\frac{\Omega}{2} - \frac{N}{2} - n_i \right) - V \sum b_{n_i} b_{n_{i+1}} \binom{\Omega/2}{n_i} \binom{\Omega/2}{N/2 - n_i} \left(\frac{\Omega}{2} - n_i \right) \left(\frac{N}{2} - n_i \right) - V \sum b_{n_i} b_{n_{i-1}} \binom{\Omega/2}{n_i} \binom{\Omega/2}{N/2 - n_i} n_i \left(\frac{\Omega}{2} - \frac{N}{2} + n_i \right) . \quad (4)$$

To obtain the b_{n_i} factors let us minimize the energy by taking into account the normalization condition

$$\frac{\partial \left(E - \lambda \sum b_{n_i}^2 \binom{\Omega/2}{n_i} \binom{\Omega/2}{N/2 - n_i} \right)}{\partial b_{n_i}} = 0.$$

From this we get

$$\begin{aligned} b_{n_i} & \left[N\varepsilon_2 - 2n_i(\varepsilon_2 - \varepsilon_1) - \lambda - Vn_i \left(\frac{\Omega}{2} - n_i \right) - \right. \\ & \quad \left. - V \left(\frac{N}{2} - n_i \right) \left(\frac{\Omega}{2} - \frac{N}{2} + n_i \right) \right] = \\ & = b_{n_i+1} V \left(\frac{\Omega}{2} - n_i \right) \left(\frac{N}{2} - n_i \right) + b_{n_i-1} Vn_i \left(\frac{\Omega}{2} - \frac{N}{2} + n_i \right). \end{aligned} \quad (5)$$

If we express b_{n_i+1} from (5) and put it back into (4), we get for the energy

$$E = \lambda - \frac{VN}{2}. \quad (6)$$

We may determine the value of λ with the help of (3) and (5). The solution of (5) is possible only approximately. In the following we shall deal with two different approximations, i.e. with the case a), when $A = (\varepsilon - \varepsilon_1)/V\Omega \ll 1$ and with the case b), when $B = \frac{V\Omega}{(\varepsilon_2 - \varepsilon_1)} \ll 1$.

Let us consider approximation a) first. The solution of (5) in this case, if we take only second order terms in A into account, turns out to be

$$\begin{aligned} b_{n_i} &= \frac{1}{\sqrt{\left(\frac{\Omega}{N/2} \right)}} \left[1 + A \left(n_i - \frac{N}{4} \right) + 2A^2 \frac{\Omega}{\Omega - 1} (n_i - N/4)^2 - \right. \\ & \quad \left. - A^2 \frac{N\Omega(2\Omega - 1)}{4(\Omega - 1)^2} \left(1 - \frac{N}{2\Omega} \right) \right], \end{aligned} \quad (7)$$

$$\lambda = N\bar{\varepsilon} - \frac{V}{2} N(\Omega - N/2) - \frac{NA^2\Omega^2V}{2(\Omega - 1)} (1 - N/2\Omega),$$

where

$$\bar{\varepsilon} = \frac{\varepsilon_1 + \varepsilon_2}{2}.$$

Substituting (7) back into (6), we get

$$E = N\bar{\varepsilon} - \frac{V}{2} N(\Omega - N/2 + 1) - \frac{N(\varepsilon_2 - \varepsilon_1)^2}{2V(\Omega - 1)} \left(1 - \frac{N}{2\Omega} \right). \quad (8)$$

In the case of approximation b), taking only second order terms in B into account, we get as a solution of (5) and (3)

$$\begin{aligned} b_{N/2} &= \frac{1}{\sqrt{\frac{\Omega/2}{N/2}}} [1 + OB^2], \\ b_{\frac{N}{2}-1} &= \frac{1}{\sqrt{\frac{\Omega/2}{N/2}}} \left[\frac{N}{4} B + OB^2 \right], \\ b_{\frac{N}{2}-2} &= \frac{1}{\sqrt{\frac{\Omega/2}{N/2}}} OB^2, \\ \lambda &= \varepsilon_1 N - V \frac{N}{2} \left(\frac{\Omega}{2} - \frac{N}{2} \right) - \frac{V^2}{\varepsilon_2 - \varepsilon_1} \frac{\Omega N}{8} \left(\frac{\Omega}{2} - \frac{N}{2} + 1 \right), \end{aligned} \quad (9)$$

and the energy is

$$E = \varepsilon_1 N - \frac{VN}{2} \left(\frac{\Omega}{2} - \frac{N}{2} + 1 \right) - \frac{V^2}{\varepsilon_2 - \varepsilon_1} \frac{\Omega N}{8} \left(\frac{\Omega}{2} - \frac{N}{2} + 1 \right). \quad (10)$$

In the following the energy of the system in the BCS approximation will be evaluated and the results will be compared with (8) and (10), respectively. In this way it is possible to get information about the error of the BCS method for this model.

3. The determination of the energy with the BCS method

The energy computed with the BCS method, turns out to be

$$E = \sum 2\varepsilon_k v_k^2 - V \sum \sum u_k v_k u_{k'} v_{k'} - V \sum v_k^4,$$

or in the case of our simple model

$$E = \Omega(\varepsilon_1 v_1^2 + \varepsilon_2 v_2^2) - \frac{V\Omega^2}{4} (u_1 v_1 + u_2 v_2)^2 - \frac{V\Omega}{2} (v_1^4 + v_2^4), \quad (11)$$

$$N = \Omega(v_1^2 + v_2^2), \quad (12)$$

Let us minimize the energy, taking into account the given particle number

$$\frac{\partial(E - \lambda N)}{\partial v_i} = 0.$$

We get for v_i after eliminating λ

$$2(\varepsilon_2 - \varepsilon_1) - \frac{V\Omega}{2}(u_1 v_1 + u_2 v_2) \left[\frac{1 - 2v_1^2}{u_1 v_1} - \frac{1 - 2v_2^2}{u_2 v_2} \right] - 2V(v_2^2 - v_1^2) = 0. \quad (13)$$

In approximation a) the following expression is obtained for v_1^2 and v_2^2 with the help of (12) and (13)

$$v_1^2 = \frac{N}{2\Omega} + \frac{N \left(1 - \frac{N}{2\Omega}\right) \frac{\varepsilon_2 - \varepsilon_1}{V\Omega}}{\Omega - 2 \frac{N}{\Omega} (1 - N/2\Omega)}, \quad (14)$$

$$v_2^2 = \frac{N}{2\Omega} - \frac{N \left(1 - \frac{N}{2\Omega}\right) \frac{\varepsilon_2 - \varepsilon_1}{V\Omega}}{\Omega - 2 \frac{N}{\Omega} (1 - N/2\Omega)}.$$

Substituting this into (11), the energy becomes

$$E = \bar{\varepsilon}N - \frac{VN}{2}\Omega - \frac{N}{2} + \frac{N}{2\Omega} - \frac{(\varepsilon_2 - \varepsilon_1)^2}{V\Omega} N \frac{1 - N/2\Omega}{\Omega - 2 \frac{N}{\Omega} \left(1 - \frac{N}{2\Omega}\right)}. \quad (15)$$

Let us evaluate now the mean square deviation of the particle number

$$(\delta N)^2 = \langle N^2 \rangle - \langle N \rangle^2 = 2N - 4 \sum v^4 = 2N \left(1 - \frac{N}{2\Omega}\right) - \frac{\frac{4N^2}{\Omega} \left(1 - \frac{N}{2\Omega}\right)^2 \frac{(\varepsilon_2 - \varepsilon_1)^2}{V^2}}{[\Omega - 2N/\Omega(1 - N/2\Omega)]}. \quad (16)$$

and from (8) the second derivative of the energy turns out to be

$$\frac{d^2 E}{dN^2} = \frac{V}{2} + \frac{1}{2V\Omega} \frac{(\varepsilon_2 - \varepsilon_1)^2}{\Omega - 1}. \quad (17)$$

Now from (1), (16) and (17) we obtain for the energy

$$\begin{aligned} E = & -\frac{V}{4} \left(1 + \frac{(\varepsilon_2 - \varepsilon_1)^2}{V^2 \Omega (\Omega - 1)} \right) (\delta N)^2 = N \bar{\varepsilon} - \frac{VN}{2} \left(\Omega - \frac{N}{2} + 1 \right) - \\ & - \frac{N(\varepsilon_2 - \varepsilon_1)^2}{2V\Omega} \left(1 - \frac{N}{2\Omega} \right) + O \frac{(\varepsilon_2 - \varepsilon_1)^2}{V} \frac{N}{\Omega}. \end{aligned} \quad (18)$$

Comparing (8) and (18) we see that the deviation between them is only of the order N/Ω^2 . A better result is obtained if one starts from the following consideration. The energy

$$E(N) = \left\langle H(N) - \frac{1}{2} \frac{d^2 E(N)}{dN^2} (\delta N)^2 \right\rangle$$

and the wave function are chosen in such a way that not $\langle H(N) \rangle$, but $E(N)$ should be minimalized. The result is

$$\begin{aligned} v_1^2 &= \frac{N}{2\Omega} + \frac{(\varepsilon_2 - \varepsilon_1)N}{V\Omega^2} \left(1 - \frac{N}{2\Omega} \right), \\ v_2^2 &= \frac{N}{2\Omega} - \frac{(\varepsilon_2 - \varepsilon_1)N}{V\Omega^2} \left(1 - \frac{N}{2\Omega} \right), \end{aligned}$$

and the energy is

$$E = N \bar{\varepsilon} - \frac{V}{2} N \left(\Omega - \frac{N}{2} + 1 \right) - \frac{N(\varepsilon_2 - \varepsilon_1)^2}{2V(\Omega - 1)} (1 - N/2\Omega). \quad (19)$$

Comparing (19) with (8) we see that they are just equal.

In the b) approximation the results are (up to orders of B^2)

$$\begin{aligned} v_1^2 &= \frac{N}{2\Omega} - \frac{V^2 N \Omega}{(\varepsilon_2 - \varepsilon_1)^2} \frac{1}{16} \left(1 - \frac{N}{\Omega} \right), \\ v_2^2 &= \frac{V^2 N \Omega}{16(\varepsilon_2 - \varepsilon_1)^2} \left(1 - \frac{N}{\Omega} \right). \end{aligned} \quad (20)$$

The energy is

$$E = \varepsilon_1 N - \frac{VN}{2} \left(\frac{\Omega}{2} - \frac{N}{2} + \frac{N}{\Omega} \right) - \frac{V^2 \Omega}{8(\varepsilon_2 - \varepsilon_1)} N \left(\frac{\Omega}{2} - \frac{N}{2} \right), \quad (21)$$

and the mean square deviation is given by

$$(\delta N)^2 = 2N \left(1 - \frac{N}{\Omega} \right). \quad (22)$$

The second derivative of the energy is

$$\frac{d^2 E}{dN^2} = \frac{V}{2} + \frac{V^2 \Omega}{8(\varepsilon_2 - \varepsilon_1)}. \quad (23)$$

With the help of (1), (21) (22) and (23) the energy turns out to be

$$\begin{aligned} E' = E - \frac{1}{2} \frac{d^2 E}{dN^2} (\delta N)^2 &= \varepsilon_1 N - \frac{VN}{2} \left(\frac{\Omega}{2} - \frac{N}{2} + 1 \right) - \\ &- \frac{V^2}{\varepsilon_2 - \varepsilon_1} \frac{\Omega N}{8} \left(\frac{\Omega}{2} - \frac{N}{2} + 1 - \frac{N}{\Omega} \right). \end{aligned} \quad (24)$$

Comparing (24) with (10), the deviation is again of the order of $1/\Omega$, but now it is not possible to get better results even by minimizing E' . The reason for this may be that the energy operator does not depend only on N , but on other operators too.

The results obtained by the model with two kinetic energies shows that we arrive at better results by adding the correction term $\frac{1}{2} \frac{d^2 E}{dN^2} (\delta N)^2$ to the BCS energy expression. If we do not know the form of $E(N)$ to determine the energy correction, we may get better and better results by successive approximation.

4. The determination of the energy with the quasi-spin formalism

In the following we want to get the approximate energy for the cases discussed above with the help of the quasi-spin formalism [5]. The basis of this method, as is known, is the following.

Let us introduce the pair creation and absorption operators

$$\begin{aligned} \beta_i &= a_{i-} a_{i+}, \\ \beta_i^+ &= a_{i+}^+ a_{i-}^+ \end{aligned}$$

and define the following quantities:

$$S_{xi} = \frac{\beta_i + \beta_i^+}{2}, \quad S_{yi} = \frac{\beta_i - \beta_i^+}{2}, \quad S_{zi} = \frac{1 - n_i}{2},$$

where

$$n_i = 2 \beta_i^+ \beta_i.$$

With the help of these definitions it is easy to show that the $S_x = \Sigma S_{x_i}$, $S_y = \Sigma S_{y_i}$, $S_z = \Sigma S_{z_i}$ operators obey just the usual spin commutator rules. The energy operator in the degenerate model will be the following

$$H = \varepsilon(\Omega - 2S_z) - V[\bar{S}^2 - S_z(S_z + 1)], \quad (25)$$

where

$$\bar{S}^2 = S_x^2 + S_y^2 + S_z^2.$$

Using this formalism for our model, let us denote by \bar{S}_1 the spin of the first $\Omega/2$ state and with \bar{S}_2 the second $\Omega/2$ state.

The energy operator will be the following

$$H = \varepsilon_1(\Omega/2 - 2(\bar{S}_1)_z) + \varepsilon_2(\Omega/2 - 2(\bar{S}_2)_z) - V[\bar{S}^2 - S_2(S_2 + 1)]. \quad (26)$$

The energy in the a) and b) approximations can be determined by second order perturbation calculation. In case a) the unperturbed ground state wave function is the following

$$(\psi_{s,m})^0 = \sum (S_1 m_1 S_2 m_2 | Sm) \psi_{s_1 m_1} \psi_{s_2 m_2}, \quad (27)$$

where m_1 , m_2 , m are the eigenvalues of $(\bar{S}_1)_z$, $(\bar{S}_2)_z$ and $(\bar{S})_z$ and S_1 , S_2 , S^0 are the eigenvalues of \bar{S}_1^2 , \bar{S}_2^2 and \bar{S}^2 , respectively.

The Hamilton operator is

$$H_0 = \bar{\varepsilon}(\Omega - 2S_z) - V[\bar{S}^2 - S_2(S_2 + 1)], \quad (28)$$

$$H_1 = -(\varepsilon_2 - \varepsilon_1)[(\bar{S}_2)_z - (\bar{S}_1)_z]. \quad (29)$$

The energy turns out to be

$$E = E_0 + E_1 + E_2, \quad (30)$$

where

$$\begin{aligned} E_0 &= \bar{\varepsilon}(\Omega - 2m) - V[S^0(S^0 + 1) - m(m + 1)] = \\ &= \bar{\varepsilon}N - \frac{VN}{2}\left(\Omega - \frac{N}{2} + 1\right), \end{aligned} \quad (31)$$

where we took into account that

$$m = \frac{\Omega}{2} - \frac{N}{2} \quad \text{and} \quad S^0 = \Omega/2, \quad S_1 = S_2 = \Omega/4.$$

$$E_1 = (\psi_0 H_1 \psi_0) = -(\varepsilon_2 - \varepsilon_1) \sum_{m_1, m_2} (S_1 m_1 S_2 m_2 | S^0 m)^2 (m_2 - m_1) = 0 \quad (32)$$

$$E_2 = \sum_r (\psi_0 H_1 \psi_r)^2 \frac{1}{E_r - E_0} = -(\varepsilon_2 - \varepsilon)^2 \sum_r \frac{1}{E_r - E_0} \times \\ \times \left[\sum_{m_1, m_2} (S_1 m_1 S_2 m_2 | S^0 m) \times (S_1 m_1 S_2 m_2 | S^r m) \cdot (m_2 - m_1) \right]^2, \quad (33)$$

where $E_r - E_0$ is the excitation energy

$$E_r - E_0 = Vr(\Omega - r + 1), \quad (34)$$

and S is the quasi-spin of the excited state

$$S^r = \frac{\Omega}{2} - r.$$

E_2 can be evaluated with the help of the calculation rules of the Clebsch—Gordan coefficients

$$\sum_{m_1 m_2} S_1 m_1 S_1 m_2 | S^0 m) (S_1 m_1 S_1 m_2 | S^r m) (m_1 - m_2) = \\ = (1 - (-1)^{S^r - S^0}) [(2 S_1 + 1) (2 S^r + 1) S]^{1/2} \times \\ \times (1 O S^r m | S^0 m) \cdot W(1 S_1 S^0 S_1; S_1 S^r). \quad (35)$$

Here the only term differing from zero will be that for which $S^0 = S^r + 1$ and in this case the value of (35) will be

$$\sqrt{\frac{S^{02} - m^2}{2 S^0 - 1}}. \quad (36)$$

Substituting (36) into (33) and taking into account (34), E_2 is the following

$$E_2 = -\frac{(\varepsilon_2 - \varepsilon_1)^2}{V(\Omega - 1)} \frac{N}{2} \left(1 - \frac{N}{2\Omega} \right). \quad (37)$$

With the help of (31), (32) and (37) the energy turns out to be

$$E = \bar{\varepsilon} N - \frac{V}{2} N \left(\frac{\Omega}{2} - \frac{N}{2} + 1 \right) - \frac{(\varepsilon_2 - \varepsilon_1)^2}{V(\Omega - 1)} \frac{N}{2} \left(1 - \frac{N}{2\Omega} \right). \quad (38)$$

(38) is just equivalent to (8).

In the b) approximation the unperturbed wave function is

$$\psi = \psi_{S_1 m_1} \psi_{S_2 m_2}, \quad (39)$$

and the energy operator is

$$H_0 = \varepsilon_1 \left(\frac{\Omega}{2} - 2(\bar{S}_1)_2 \right) + \varepsilon_2 \left(\frac{\Omega}{2} - 2(\bar{S}_2)_2 \right), \quad (40)$$

$$\begin{aligned} H_1 = & -V [\bar{S}_1^2 + S_2^2 - (S_1)_2 \{ (\bar{S}_1)_2 + 1 \} - (\bar{S}_2)_2 \{ (\bar{S}_2)_2 + 1 \} + \\ & + 2 \{ (\bar{S}_1)_+ (\bar{S}_2)_- + (\bar{S}_1)_- (\bar{S}_2)_+ \}]. \end{aligned} \quad (41)$$

The energy terms will be the following

$$E_0 = \varepsilon_1 N, \quad (42)$$

$$\begin{aligned} E_1 = & -V [S_1(S_1 + 1) + S_2(S_2 + 1) - m_1^0(m_2^0 + 1) - \\ & - m_2^0(m_2^0 + 1)] = -\frac{VN}{2} \left(\frac{\Omega}{2} - \frac{N}{2} + 1 \right), \end{aligned} \quad (43)$$

where we took into account that

$$m_1^0 = \frac{\Omega}{4} - \frac{N}{2}, \quad m_2^0 = \frac{\Omega}{4},$$

and

$$\begin{aligned} E_2 = & -\sum_r \frac{V^2}{2(\varepsilon_2 - \varepsilon_1)} [(S_1(S_1 + 1) - m_1^r(m_1^r - 1))^{1/2} \times \\ & \times (S_2(S_2 + 1) - m_2^r(m_2^r + 1))^{1/2} \cdot \delta m_1^r - 1, m_1^0 \delta m_2^r + 1, m_2^0 + \\ & + (S_1(S_1 + 1) - m_1^r(m_1^r + 1))^{1/2} \cdot (S_2(S_2 + 1) - m_2^r(m_2^r - 1))^{1/2} \times \\ & \times \delta m_1^r + 1, m_1^0 \delta m_2^r - 1, m_2^0]^2 = -\frac{V^2}{2(\varepsilon_2 - \varepsilon_1)} \frac{\Omega}{2} \left[\frac{\Omega}{4} \left(\frac{\Omega}{4} + 1 \right) - \right. \\ & \left. - \left(\frac{\Omega}{4} - \frac{N}{2} + 1 \right) \left(\frac{\Omega}{4} - \frac{N}{2} \right) \right]^2 = -\frac{V^2}{\varepsilon_2 - \varepsilon_1} \frac{\Omega N}{8} \left(\frac{\Omega}{2} - \frac{N}{2} + 1 \right). \end{aligned} \quad (44)$$

Here the excitation energy is

$$E_r = E_0 + 2r(\varepsilon_2 - \varepsilon_1)$$

and the quasi-spin values in the excited states are

$$m_1^r = \frac{\Omega}{4} - \frac{N}{2} + r,$$

$$m_2^r = \frac{\Omega}{4} - r.$$

Substituting (42), (43) and (44) into (30) we get for the energy the following expression

$$E = \varepsilon_1 N - \frac{VN}{2} \left(\frac{\Omega}{2} - \frac{N}{2} + 1 \right) - \frac{V^2}{\varepsilon_2 - \varepsilon_1} \frac{\Omega N}{8} \left(\frac{\Omega}{2} - \frac{N}{2} + 1 \right), \quad (45)$$

which is equivalent to (10). The advantage of the quasi-spin formalism is that we may use it even in those more complex cases where the exact calculation is not possible, and we may get the excitation energy in a certain approximation exactly.

It is a pleasure for the author to express her thanks to Prof. G. MARX for his valuable advices and to Dr. J. ZIMÁNYI for a useful discussion.

REFERENCES

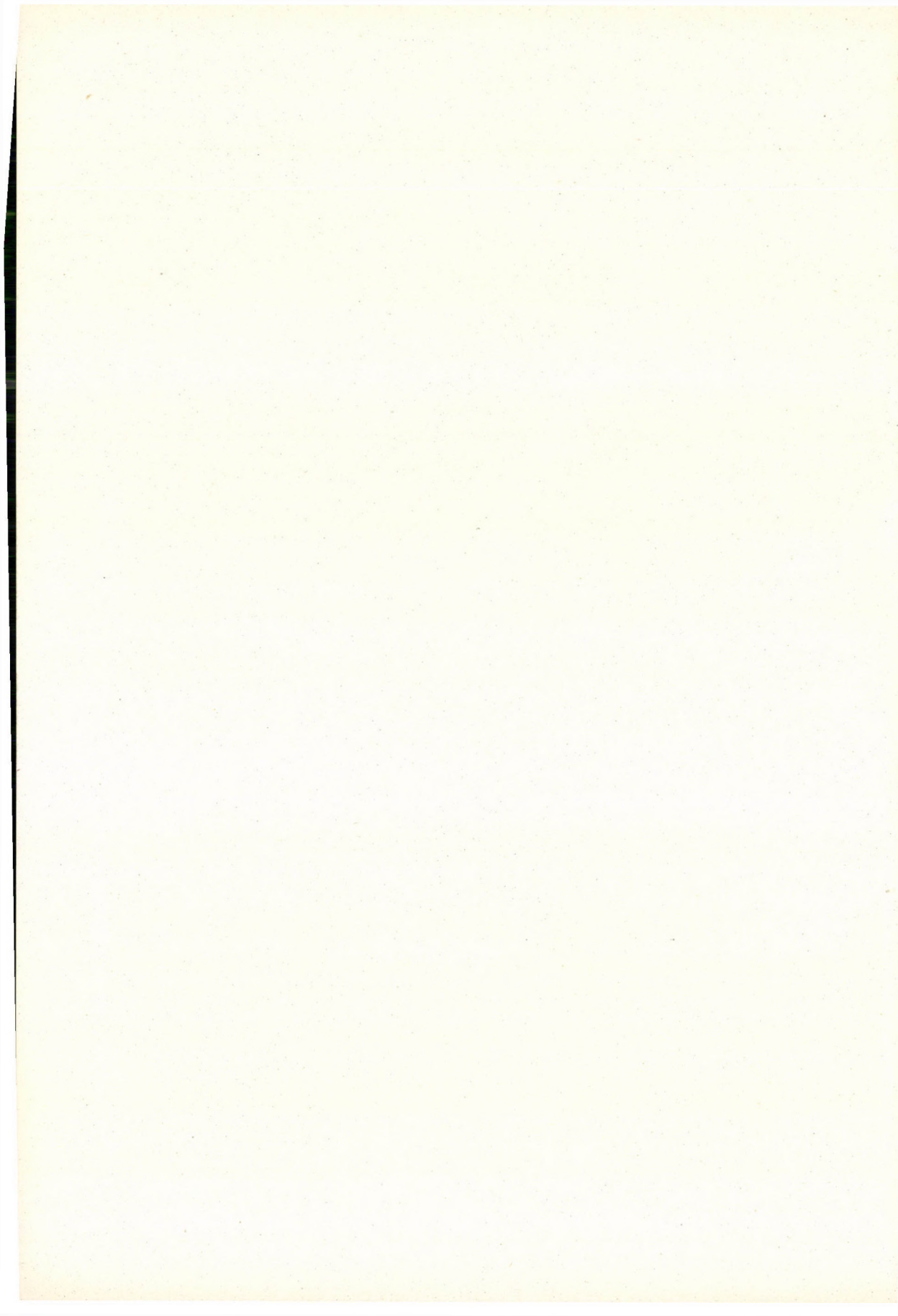
1. J. BARDEEN, L. N. COOPER and J. R. SCHRIEFFER, Phys. Rev., **108**, 1175, 1957.
2. A. BOHR, B. R. MOTTELSON and D. PINES, Phys. Rev., **110**, 936, 1958.
3. S. T. BELYAEV, Mat. Fys. Medd. Dan. Vid. Selsk., **31**, no 11, 1959.
4. K. BAUMANN, G. EDER, R. SELL, W. THIRRING, Ann. of Phys., **16**, 14, 1961.
5. S. G. NILSSON (to be published).

МОДЕЛЬ СВЕРХПРОВОДИМОСТИ С ДВУМЯ ЗНАЧЕНИЯМИ КИНЕТИЧЕСКОЙ ЭНЕРГИИ

Й. НЭМЕТ

Р е з и о м е

Исследуется модель сверхпроводимости с двумя значениями кинетической энергии. Значения энергии определяются во втором приближении применением точной волновой функции и применением BCS волновой функции. Коррекция метода BCS исследуется в данном специальном случае.



ZUR THEORIE UND PRAXIS DER BERECHNUNG DER ÜBERTRAGUNGSFUNKTION OPTISCHER SYSTEME*

Von

WERNER REICHEL

VEB CARL ZEISS JENA, JENA, DDR

(Vorgelegt von N. Bárány. — Eingegangen 25. VIII. 1964)

Die optische Übertragungstheorie wird kurz erläutert und eine Methode zur Berechnung der Frequenzübertragungsfunktion (FÜF) für ein in der geometrisch-optischen Korrektion vorgegebenes System entwickelt. Die Bedeutung der FÜF als Gütemass für die optische Abbildung und zur Korrektion optischer Systeme wird diskutiert.

Die geometrisch-optischen Aberrationen werden auf die Öffnung normiert und in die Wellenaberrationsbeträge durch graphische Integration überführt.

Einige charakteristische Zusammenhänge der verschiedenen Bildfehler mit der FÜF werden an optischen Systemen aus der Praxis aufgezeigt. Besonderer Wert wurde dabei auf das ausseraxiale Gebiet gelegt.

1. Einleitung

Die Anwendung der Übertragungstheorie aus der Nachrichtentechnik auf die Optik hat für ausgedehnte Objektstrukturen ein objektives Mass für die Abbildungsgüte optischer Systeme bei inkohärenter Beleuchtung ergeben, welches sich relativ einfach berechnen und messen lässt. Ein optisches System wird natürlich nicht durch *eine* Übertragungsfunktion, sondern durch eine Schar solcher Funktionen charakterisiert, deren Anzahl jeweils durch die Objektivparameter wie Blende (Öffnung), Fokussierung, Bildformat und Lichtart bestimmt wird. Es bedeutet jedoch gegenüber der bisherigen Testung einen Fortschritt, denn für die Bildgüte eines optischen Systems wurde hauptsächlich das Auflösungsvermögen herangezogen, die Fähigkeit zwei benachbarte Objektelemente (Punkt oder Linien) getrennt wiederzugeben. Eine solche subjektive Beobachtung läuft aber auf eine Schwellenmessung hinaus und ist daher starken Schwankungen unterworfen. Außerdem genügt es für die Abbildungsqualität eines Objektives durch ein optisches System im allgemeinen nicht, getrennte Objektelemente wieder als getrennte Bildelemente abzubilden (aufzulösen), sondern es ist notwendig dieselben mehr oder weniger nach Phase und Amplitude der Originalfunktion getreu als Bildfunktion wiederzugeben. Die Qualität eines optischen Bildes wird also so definiert dass das Objekt dem Bild möglichst ähnlich wird.

Um solche allgemeinen Zusammenhänge zu klären, ist die optische Übertragungstheorie entwickelt worden. Sie unterscheidet sich von der elektro-

* Vorgetragen auf der II. Optischen Konferenz in Budapest, 1963.

trischen Übertragung allein dadurch, dass die dort zeitlich nacheinander zu übertragenden Signale in der Optik durch räumliche (ein- oder zweidimensional) nebeneinander ersetzt werden. Es liegt dann nahe, das optische System als Übertragungsglied (Filter) von Objekt zum Bild oder umgekehrt aufzufassen. Charakteristische Übertragungseigenschaften des Systems werden durch die sogenannte Übertragungsfunktion (response) beschrieben. Sie wird im wesentlichen durch Restfehler und Beugung vom Objektiv bestimmt, wenn man von Streulicht, Transparenz u. a. absieht. Sind diesem elementaren Prozess noch weitere Abbildungsschritte wie photographische Emulsionen, Zwischenabbildungen, Projektion usw. angeschlossen, dann kann man aus diesen Funktionen der Einzelglieder, sofern es sich um lineare Prozesse handelt, durch Produktbildung die Gesamtübertragungsfunktion berechnen. Das schwächste Glied bestimmt in dieser Kette natürlich die resultierende Qualität, doch soll hier nur der elementare Prozess der eindimensionalen Abbildung vom Objekt zum Bild verfolgt werden.

Grundsätzlich kann man jede als Objekt vorhandene Lichtverteilung als zweidimensionales Fourierintegral oder als Fouriersumme darstellen. Mit anderen Worten kann durch Superposition von sinusförmigen Helligkeitsverteilungen jede im Objekt vorhandene Helligkeitsverteilung erreicht werden. Oder umgekehrt lässt sich jeder beliebigen Objektsintensitätsverteilung ein Frequenzspektrum zuordnen.

Bei der Verschiedenartigkeit optischer Bilder, deren Intensitätsverteilungen in grossen Grenzen variieren, ist es jedoch nicht möglich, eine universelle Verteilung bzw. Spektrum anzugeben. Man geht deshalb von ein- oder zweidimensionalen elementaren periodischen Strukturen mit konstanter Intensitätsverteilung aus, die man in der Frequenz (Gitterkonstante) variiert und ermittelt nacheinander rechnerisch oder experimentell die Übertragungseigenschaften. Diese Gitter stellen dann durch Variation in ihren Abmessungen annähernd natürlich ausgedehnte Objekte dar. Die Frequenzübertragungsfunktion gibt dann an, wie das gesamte Frequenzspektrum, welches durch das Auflösungsvermögen begrenzt wird, in seinen Frequenzen nach Amplitude und Phase gegenüber dem Objektgitter mit konstanter Amplitude und Phase durch das optische System übertragen wird. Dabei ist allerdings Voraussetzung, dass die Grundform des Elementargitters objektseitig im Bild erhalten bleibt. Wegen dieser Voraussetzung hat sich ein Strichgitter mit cosinusförmiger Lichtverteilung, auch kurz oft Sinusgitter genannt, bewährt. Kompliziertere Strukturen wie z. B. ein Rechteckgitter, welches wegen seiner leichteren Herstellung zum Messen der Übertragungseigenschaften oft benutzt wird, lässt sich ja bekanntlich auf Sinusgitter zurückführen. Welchen charakteristischen Verlauf solche Übertragungskurven für ein optisches System jeweils besitzen, soll dann später am Beispiel erörtert werden. Der Frequenzbereich oder die Bandbreite und die Kontrast- bzw. Modulationstiefe werden

durch relative Öffnung und Restfehler bestimmt. Auf Grund von Bildanalysen weiss man bereits, welche Frequenzen für die jeweiligen Verwendungszwecke durch Steuerung der Aberrationen anzustreben sind. Hierin liegt die praktische Bedeutung der Übertragungstheorie für den Objektivkonstrukteur. Der Begriff *Frequenz* wird hier nicht als zeitabhängige Grösse, sondern als reziproke Länge in Form der Linienfrequenz gebraucht.

Obwohl die mathematischen Grundlagen der Übertragungstheorie für optische Systeme heute allgemein bekannt sind, sollen kurz die Zusammenhänge aufgezeigt werden. Die wesentlichen Gedankengänge sind von DUFFIEUX 1946 und später von MARÉCHAL und H. H. HOPKINS 1951 aufgegriffen und weiter entwickelt worden. Der optische Abbildungsprozess kann für inkohärente Beleuchtung in Form des Faltungsintegrals beschrieben werden. Allerdings ist hierfür eine wesentliche Voraussetzung, dass die Abbildung isoplanatisch ist, die Abbildung also ein linearer Vorgang ist. Der Ausdruck linear besagt, dass zwischen Objekt und Bild lineare mathematische Beziehungen bestehen, die sich durch das Faltungsintegral beschreiben lassen. Nun ist die Abbildung bei korrigierten Systemen selten über die ganze Öffnung isoplanatisch, sondern nur für einen kleinen Bereich. Das bedingt allerdings, dass die Objekte so klein sind, dass sie in einen solchen Bereich hineinfallen.

Andererseits ändern sich die Aberrationen eines korrigierten Systems — nur solche sind Gegenstand der folgenden Betrachtungen — und damit auch die Punktbildintensität relativ langsam, so dass man, um eine Änderung derselben innerhalb eines Feldes beobachten zu können, sich um wesentliche Beträge bewegen muss, die gemessen in den Dimensionen des Beugungsbildes beträchtlich sind. Demzufolge kann man die Abbildung kleiner Details in einem solchen isoplanatischen Gebiet untersuchen. Die Punktbildintensität ist demzufolge vom Ort in diesem Bereich unabhängig. Die Ausdehnung des Punktbildes wird aber für ein korrigiertes System praktisch in keinem Falle grösser als ca. 1 mm im Durchmesser sein. Ausserhalb kann der Intensitätsbeitrag, wie zahlreiche Punktbildintensitätsberechnungen für verschiedene Aberrationstypen zeigten [1], vernachlässigt werden. Streng mathematisch ist natürlich das Lichtgebirge unendlich ausgedehnt.

2. Theoretische Grundlagen der optischen Übertragungstheorie

In Bild 1 ist der Abbildungsvorgang schematisch mit den jeweiligen Koordinatensystemen skizziert. Für die Objekt- und Bildebene sowie Ein-(EP) und Austrittspupille (AP) werden normierte Koordinaten verwendet. Es lässt sich dann die Bildintensitätsverteilung B' als Faltungsintegral aus Objektintensität B und Punktbildintensität (Lichtgebirge) G schreiben

$$B'(u', v') = \iint B(u, v) G(u' - u, v' - v) du dv. \quad (2.1)$$

Die Punktbildintensität wird durch Restaberrationen bestimmt und ist andererseits proportional dem Amplitudenquadrat

$$G(u', v') \sim |F(u', v')|^2. \quad (2.2)$$

Unter gewissen Voraussetzungen kann die Amplitude als zweidimensionales Fourierintegral auf Grund der Kirchhoffschen Beugungstheorie geschrieben werden.

$$F(u', v') = \text{const} \iint f(\bar{x}', \bar{y}') \exp \{2\pi i(u' \bar{x}' + v' \bar{y}')\} d\bar{x}' d\bar{y}'. \quad (2.3)$$

Die Funktion $f(\bar{x}', \bar{y}')$ wird Wellen- oder Pupillenfunktion genannt und ist die inverse Fouriertransformierte der Amplitude $F(u', v')$. Für die Größen

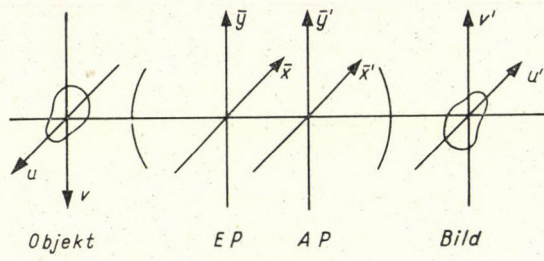


Bild 1

B' , B und G gelten die gleichen mathematischen Beziehungen, die entsprechenden kleinen Buchstaben sind jeweils die inversen Fouriertransformierten. Es gilt dann

$$G(u', v') = \iint g(s', t') \exp \{2\pi i(s' u' + t' v')\} ds' dt', \quad (2.4)$$

$$g(s', t') = \iint G(u', v') \exp \{-2\pi i(s' u' + t' v')\} du' dv'. \quad (2.5)$$

Setzt man diese Transformationsformeln in Gl. (2.1) ein, dann erhält man

$$B'(u', v') = \iint g(s', t') b(s', t') \exp \{2\pi i(s' u' + t' v')\} ds' dt' \quad (2.6)$$

oder

$$b'(s', t') = g(s', t') \cdot b(s', t'). \quad (2.7)$$

Da Intensitäten immer reell sind, muss für die inversen Fouriertransformationen in Gl. (2.7) gelten

$$b(-s', -t') = b^*(s', t')^1 \quad (2.8)$$

¹ konjugiert komplex

und entsprechend für

$$g(-s', -t') \quad \text{und} \quad b'(-s', -t'). \quad (2.9)$$

Als Übertragungsmass definiert man nun nicht das Lichtgebirge G selbst, sondern seine inverse Fouriertransformierte

$$g(s', t') = \frac{b'(s', t')}{b(s', t')}, \quad (2.10)$$

das Frequenzspektrum der Intensitäten von G . Man ordnet also ganz analog wie in der elektrischen Nachrichtenübertragung den Orts- oder Originalfunktionen B , B' und G eine gleichwertige Darstellung auf den Frequenzkoordinaten s' , t' mit Hilfe der Fouriertransformation — in der elektrischen Nachrichtenübertragung ist es die speziellere Laplace-Transformation — in Form der Frequenz (Spektral)- oder Bildfunktion b , b' und g zu. Es ist das Verdienst von H. H. HOPKINS [2], diese Grösse, die sogenannte Frequenzübertragungsfunktion (frequency response function) $g(s', t')$, auch kurz FÜF genannt, als Mass für die Bildgüte ausgedehnter einfacher Objekte erkannt zu haben, denn dieselbe lässt sich für inkohärente Beleuchtung als Autokorrelation der Pupillenfunktion ausdrücken.

Nach DUFFIEUX [3] ergibt sich dann

$$g(s', t') = \iint f(\bar{x}', \bar{y}') f^*(\bar{x}' - s', \bar{y}' - t') d\bar{x}' d\bar{y}'. \quad (2.11)$$

Zur Berechnung dieses Ausdrückes ist also nur die aus den Konstruktionsdaten des optischen Systems berechenbare Wellenfunktion $f(\bar{x}', \bar{y}')$ notwendig, während man ohne Anwendung der Fouriertransformation aus der Wellenaberration $W(\bar{x}', \bar{y}')$ das Lichtgebirge G berechnen muss und durch Faltung die Bildintensität meistens graphisch gewinnt und erst dann für die entsprechenden Frequenzen das Übertragungsmass nach Amplitude und Phase bestimmen kann [1].

Es ist nun vorteilhaft, nicht die Grösse $g(s', t')$, sondern eine relative Frequenzübertragungsfunktion D auf die Frequenz Null bezogen, einzuführen:

$$D(s', t') = \frac{g(s', t')}{g(0,0)} = r(s', t') + i \Re(s', t') = T(s', t') \cdot \exp \{i \Theta(s', t')\}. \quad (2.12)$$

Die Funktion $D(s', t')$ tritt im allgemeinen komplex auf und kann deshalb nach Real- und Imaginärteil oder Betrag (Amplitude) und Phase getrennt werden.

Nach einem Vorschlag von H. H. HOPKINS kann man noch aus Symmetriegründen eine Verschiebung um die Strecke $\bar{x}' + s'/2$ und $\bar{y}' + t'/2$ vornehmen, so dass sich die normierte Frequenzübertragungsfunktion wie folgt ergibt

$$D(s', t') = \frac{\iint f(\bar{x}' + s'/2, \bar{y}' + t'/2) f^*(\bar{x}' - s'/2, \bar{y}' - t'/2) d\bar{x}' d\bar{y}'}{\iint |f(\bar{x}', \bar{y}')|^2 d\bar{x}' d\bar{y}'} = \frac{S}{G}. \quad (2.13)$$

Dieser Ausdruck bedeutet anschaulich nichts anderes als den gemeinsamen Flächeninhalt der um s', t' bezüglich ihres Koordinatenursprunges versetzten Pupillenfunktion bezogen auf die Pupillenfläche S . Nur im überdeckten Gebiet C (auch Durchschnitt genannt) in Bild 2 ist das Integral von Null

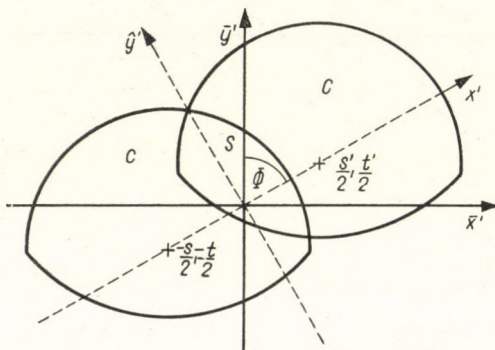


Bild 2

verschieden. Für den Spezialfall kreisförmiger Pupillenflächen errechnet sich für ein aberrationsfreies Objektiv

$$D(s') = \pi [2 \arccos(s'/2) - \sin[2 \arccos(s'/2)]]. \quad (2.14)$$

Führt man noch ein um den Winkel Φ gedrehtes Koordinatensystem \hat{x}', \hat{y}' ein und verwendet ein eindimensionales Strichgitter parallel zur \hat{y}' -Achse ausgerichtet, dann lässt sich eine Frequenz \hat{s}' längs der \hat{x}' -Achse definieren und die Übertragungsfunktion in Abhängigkeit von Azimut und Frequenz \hat{s}' darstellen

$$D(\hat{s}', \Phi) = \frac{1}{C} \iint f(\hat{x}' + \hat{s}'/2, \hat{y}') f^*(\hat{x}' - \hat{s}'/2, \hat{y}') d\hat{x}' d\hat{y}'. \quad (2.15)$$

Der Übergang zur eindimensionalen Darstellung und Einbeziehung des Azimutes vereinfacht sowohl den experimentellen Aufwand zur Ermittlung der Übertragungsfunktion als auch die Rechnung. Außerdem lassen sich ja die Aberrationen nach Azimuten und Einfallshöhen klassifizieren.

3. Verfahren und Möglichkeiten zur Ermittlung der Übertragungsfunktionen optischer Systeme

In den letzten Jahren sind verschiedene Verfahren zur Berechnung der Übertragungsfunktion optischer Systeme nach der im Abschnitt 2 geschilderten Theorie entwickelt worden. Bild 3 gibt als Schema die einzelnen Schritte und die bestehenden Zusammenhänge wieder.

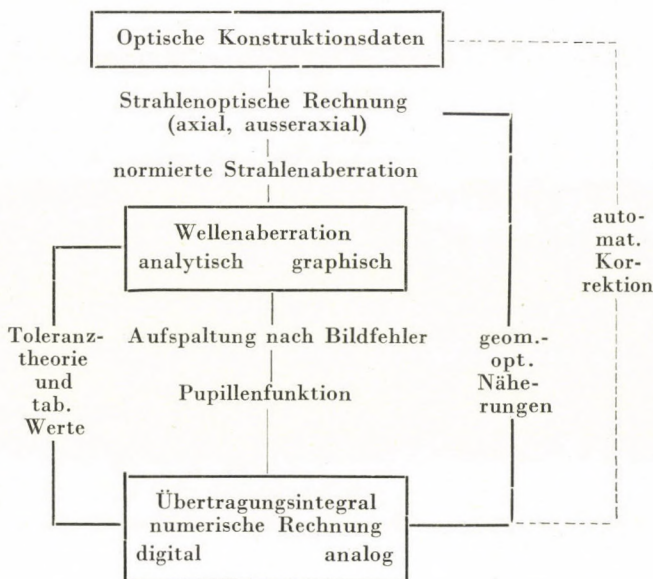


Bild 3

Ausgangspunkt ist im allgemeinen das optische System, dessen Konstruktionsdaten bekannt sind. Das Objektiv sei nach den bekannten geometrisch-optischen Strahldurchrechnungsformeln axial und ausseraxial etwa mit einem Rechenautomaten durchgerechnet und die geometrisch-optischen Aberrationen liegen demzufolge in der üblichen Darstellung vor. Es soll nun entschieden werden, welche Abbildungseigenschaften vom System in Form der Übertragungsfunktionen zu erwarten sind. Diese Aufgabenstellung ist am gebräuchlichsten, da man in der Praxis stets von einem System ausgeht, welches für den jeweiligen Zweck weiter- oder umkorrigiert wird. Die Übertragungsfunktion soll also neben einer Masszahl bzw. Gütekriterium hauptsächlich dazu verwendet werden, bestimmte Abbildungseigenschaften durch Variation der Restfehler in einem Objektiv rechnerisch zu ermitteln bzw. einen exakten Zusammenhang zwischen Restfehler und Bildgüte zu liefern, der dem Optikkonstrukteur bisher fehlte. Der Optikrechner war bis jetzt nur auf Erfahrungswerte und gewisse Faustformeln angewiesen, die er sich auf

Grund der Restfehler und Bildleistung am sehr sorgfältig ausgeführten Muster sammeln konnte.

Es wäre natürlich auch denkbar, dass man sich die Abbildungseigenschaften vorgibt und ein System zu berechnen versucht. Solche allgemeinen Ansätze erfordern grossen Rechenaufwand bis man auf die bekannten Objektivtypen kommt und werden deshalb in der Praxis kaum angewendet; es sei denn, es werden systematische Untersuchungen für einen speziellen Zweck gefordert.

Um jedoch die Übertragungsfunktion aus den Konstruktionsdaten berechnen zu können, müssen die Restfehler in normierter Form als Wellenaberration vorliegen; diese für praktisch ausgeführte Systeme zu ermitteln, sind verschiedene Wege beschritten worden.

Einmal ist es möglich, am Muster die Wellenaberration interferometrisch mit dem TWYMAN—GREEN-Interferometer bzw. KRUG—LAU-Interferometer zu ermitteln, zum anderen rechnerisch durch einen Integrationsprozess aus den geometrisch-optischen Restfehlern. Für die rechnerische Gewinnung der Wellenaberration, die hier allein betrachtet werden soll, sind analytische Methoden speziell für Rechenautomaten entwickelt worden, die gleichzeitig eine Potenzreihendarstellung nach Bildfehlern liefern [4], [5], [6], doch sind diese Methoden für mehrlinsige Systeme recht aufwendig und nur mit grossen programmgesteuerten Rechenautomaten möglich. Es soll deshalb im folgenden Abschnitt eine graphische Methode ausführlich behandelt werden, die bei relativ wenig Rechenaufwand exakt die Wellenaberration aus den geometrisch-optischen Restfehlern zu ermitteln gestattet. Diese so gewonnene Wellenaberration wird dann anschliessend nach Bildfehlerkoeffizienten mittels der Methode der kleinsten Quadrate aufgespalten [7].

Eine Möglichkeit, die Berechnung der Wellenaberration zu umgehen und direkt aus den Restaberrationen in Näherung die Übertragungswerte zu berechnen, wird im 5. Abschnitt erwähnt. Aus Bild 3 ist weiterhin durch die Toleranztheorie von MARÉCHAL und HOPKINS bzw. durch den allgemeinen Zusammenhang zwischen Wellenaberration und Übertragungsfunktion ein exakter Weg aufgezeigt, schon gewisse Übertragungseigenschaften aus dem normierten Wellenaberrationskoeffizienten zu erkennen, zumal für einige Koeffizientenkombinationen aus der Schule von H. H. HOPKINS tabellierte Werte vorliegen. Es wird so möglich, in vielen Fällen einige Besonderheiten an optischen Systemen bereits an den normierten Wellenaberrationskoeffizienten zu erkennen, ohne die Übertragungsfunktion im einzelnen mit relativ grossem Rechenaufwand berechnen zu müssen. Ein Schritt weiter wäre nun, die Restfehler so zu verändern, dass die gesuchten Übertragungswerte realisiert werden. Hierzu müsste man durch systematische Variationen automatisch die Restfehler in diese Schranken einengen. Als Bewertungsfunktion wird hierfür die FÜF als sogenannte Merit-Funktion für die entsprechenden

Linienfrequenzen gewählt. Es ist üblich, die verschiedenen Aberrationsanteile noch mit entsprechenden Gewichten zu versehen, da die FÜF ein integrales Gütekriterium des optischen Systems darstellt und die Beträge der Restfehleranteile unterschiedlich eingehen. In einem weiteren Schritt könnte durch Variation versucht werden, die Konstruktionsparameter des Systems so zu verändern, dass die Restaberrationen in diesen vorgegebenen Schranken etwa nach der Methode von GIRARD—WYNNE [8] oder nach FIALOVSKY [9] eingeengt werden. Doch sind für solche Rechenverfahren zunächst systematische Untersuchungen über die Zusammenhänge von Aberrationen und Bild-eigenschaften Voraussetzung. Erste Erfahrungen mit grösseren Rechenautomaten haben an Systemen gezeigt, dass eine sinnvolle automatische Korrektion nur durch das grundlegende Verständnis der Bildfehlertheorie und die Voraussetzung des Erfahrungsschatzes des Optikkonstrukteurs erreicht werden kann.

Zur numerischen Berechnung der Frequenzübertragungsfunktion für die einzelnen Linienfrequenzen sind verschiedene Verfahren speziell für Rechenautomaten entwickelt worden. Eine recht genaue Methode von HOPKINS und GOODBODY [10] soll noch detailliert im Abschnitt 5 dieser Arbeit für die Berechnung einiger Beispiele benutzt werden. Neben den bekannten numerischen Näherungsverfahren (SIMPSON, STIRLING), das Integral zu lösen, hat BARAKAT [5] jetzt mit Hilfe der Gaußschen Quadraturtheorie für höhere Ordnungen in Verbindung mit Legendreschen Polynomen eine Methode vorgeschlagen, die geeignet ist, auch nicht äquidistante Integrationselemente zu verwenden. Da die bisher geschilderten Verfahren grössere Rechenautomaten erfordern, sei noch erwähnt, dass mit geringerem Zeitaufwand unter Verwendung der exakten mathematischen Beziehungen ohne Vernachlässigung die Berechnung auch auf Analogrechenmaschinen durchgeführt wurde. Man hat hier den Vorteil, systematisch durch Eingeben der Aberrationskoeffizienten in die Potentiometer relativ schnell ein System zu optimieren; natürlich hattet diesem Verfahren naturgemäß eine beschränkte Genauigkeit an. Welche Verfahren sich jemals für die gesamte praktische Objektivberechnung durchsetzen werden oder ob alle diese Überlegungen nur gelegentlich für Spezialzwecke angewendet werden — wo ihre Brauchbarkeit schon erwiesen ist — kann wohl heute noch nicht entschieden werden, da noch nicht genügend Erfahrungen vorliegen.

4. Ermittlung der Wellenaberration in normierter Darstellung aus den geometrisch-optischen Restfehlern durch graphische Integration

Jede Objektivberechnung wird zunächst von der geometrischen Optik ausgehen und erst, wenn die Aberrationen klein sind, einer wellenoptischen Feinkorrektion bedürfen, denn eine wellenoptische Betrachtung ist unum-

gänglich, wenn die durch Aberrationen verursachten Abweichungen der Wellenfläche gegenüber der Referenzfläche klein sind. Daher erscheint es wichtig, aus der geometrischen Strahldurchrechnung gewonnene Aberrationen in die Wellenaberration umzurechnen. Dies ist nicht schwierig, da die Strahlen auch nach beliebig vielen Brechungen und Spiegelungen (Satz von MALUS) stets senkrecht auf den Wellenflächen stehen und man deshalb dem Strahlensbündel geometrisch eine Wellenflächenschar zuordnen kann. Eine Wellenfläche (Isoikonalfäche) nennt man innerhalb einer Welle jede Fläche, deren sämtliche Punkte im betrachteten Zeitpunkt sich in gleicher Phase befinden. Unter der Wellenaberration versteht man nun die Abweichung der durch Aberrationen deformierten Wellenfläche längs eines Strahles von einer geeigneten Bezugs- oder Referenzfläche (z. B. Kugel), die als optische Wegdifferenz gemessen wird. Die so definierte Wellenaberration wird positiv gezählt, wenn die deformierte Welle innerhalb der Referenzkugel liegt. Legt man das Zentrum der Referenzkugel in die ideale Bildende und die Referenzkugel in die Austrittspupille des aus sphärischen Flächen aufgebauten zentrierten Systems, dann besteht zwischen den optischen Wegdifferenzen und der Abweichung des Strahles (Aberration) vom Zentrum der Referenzkugel nach einigen Umformungen und Integration der bekannte Zusammenhang [12]

$$W_1(a') = \int_0^{a'} (\xi'_1 \sin \Phi + \eta'_1 \cos \Phi) \cos a' da', \quad (4.1)$$

wobei allerdings rechtwinkelige Koordinaten (ξ'_1, η'_1) senkrecht zum Bezugs- oder Referenzstrahl mit der Bildebene in der ξ'_1, η'_1 -Ebene benutzt sind, a' der Winkel zwischen Strahl- und Bezugs(Referenz)strahl und Φ der Azimutwinkel in der Bildebene bedeuten. Man erhält so die Wellenaberration in der üblichen Schreibweise eines unbestimmten Integrals, die wegen ihrer Wellenlängenabhängigkeit in Einheiten von λ ermittelt wird. Dabei ist die Änderung des Zentrums der Referenzkugel um den Betrag ΔR vom Radius der Referenzkugel R infolge des mit Aberration behafteten Strahles unberücksichtigt geblieben. Da es sich jedoch aber nach Voraussetzung um korrigierte Systeme mit kleinen Aberrationen handelt und die Grösse ΔR für die verschiedenen Strahlen gegenüber R klein bleibt, ist dieser Ansatz erlaubt.

Nach Gl. (4.1) lässt sich nunmehr die Wellenaberration aus der Strahlaberration berechnen, wenn letztere aus der geometrisch-optischen Durchrechnung bekannt ist. Dies soll in Anlehnung an die geometrische Optik für das axiale und ausseraxiale Gebiet getrennt erfolgen. In einem zentrierten System tritt im axialen Gebiet wegen der Rotationssymmetrie nur der Abbildungsfehler der sphärischen Aberration auf, der vom Azimut Φ unabhängig ist. Die Bezugsachse ist mit der optischen Achse identisch. Gl. (4.1) spezialisiert sich zu

$$W(a') = \int_0^{a'} \eta' \cos a' da', \quad (4.2)$$

da $\Phi = 0$ und $\partial W / \partial \Phi = 0$. Die Größe η' ist aber als sphärische Queraberration bekannt und ergibt sich sofort aus der bei der Strahldurchrechnung ermittelten sphärischen Längsaberration ($\Delta s' = \tilde{s}' - s'$)*

$$\eta' = -\Delta s' \tan \tilde{\sigma}' . \quad (4.3)$$

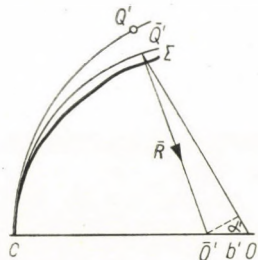


Bild 4

Dem bisherigen Winkel α' entspricht jetzt der Winkel σ' in der technischen Strahlenoptik (Bild 4), der für kleine Aberrationen $\Delta s'$ — die Winkelaberration $\Delta \sigma'$ ist gegen $\tilde{\sigma}'$ zu vernachlässigen — gleich $\tilde{\sigma}'$ für die Integration angenommen werden kann und es ergibt sich

$$W(\tilde{\sigma}') = \int_0^{\tilde{\sigma}'} -\Delta s' \sin \tilde{\sigma}' d\tilde{\sigma}' . \quad (4.4)$$

Eine negative Schnittweitenaberration $\Delta s'$ wird also eine positive Wellenaberration ergeben. Die Schnittweitenaberrationen sind für die einzelnen Strahlen aus der Strahldurchrechnung in Millimeter oder kleineren Längeneinheiten für die entsprechende Lichtwellenlänge bekannt, so dass die Wellenaberration W in die zugehörigen Lichtwellenlängeneinheiten leicht umzurechnen ist.

Für das ausseraxiale Gebiet fällt nun die Rotationssymmetrie weg, die Wellenaberration wird vom Azimut Φ abhängig. Es soll deshalb die Ermittlung der Wellenaberration für $\Phi = 0$ und π (Meridionalschnitt) und $\Phi = \pi/2$ und $3\pi/2$ (Sagittalschnitt) im einzelnen aufgezeigt werden. Dies bedeutet keine grundsätzliche Beschränkung nach Gl. (4.1), vielmehr bieten sich diese Ebenen auf Grund der üblichen geometrischen Durchrechnung eines Systems zwangsläufig an.

* s. hierzu TIEDEKEN, Lehrbuch f. Optikkonstrukteur Bdn. 1. S. 42 (Berlin 1963)

Für den Meridionalschnitt dient als Referenzstrahl der Bezugs (Haupt)- oder besser Schwerstrahl mit dem Neigungswinkel σ'_B gegen die optische Achse und als Zentrum der Referenzebene der Schnittpunkt O' vom Bezugsstrahl mit der Gaußschen Bildebene ($0'_o$, $0'$) nach Bild 5. Im übrigen gelten die entsprechenden Formeln und Vereinbarungen aus Gl. 4.4 auch für die Queraberration η'

$$W_m(\tilde{\sigma}'_m) = \int_0^{\tilde{\sigma}'_m} -\eta' \cos \sigma'_m d\tilde{\sigma}'_m. \quad (4.5)$$

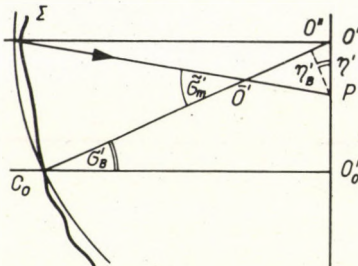


Bild 5

Da der Wert der Längsaberration $\Delta s'_m$ in der Regel bei der Strahldurchrechnung nicht anfällt, lässt sich nach dem Sinussatz diese Grösse nach η' wie in Bild 5 angedeutet, umrechnen. Für den Meridionalschnitt sei darauf hingewiesen, dass die Wellenfläche in beiden Azimuten $\Phi = 0$ und π d. h. für positive und negative Werte von $\tilde{\sigma}'_m$ selbstverständlich gesondert berechnet werden muss und die Begrenzung des oberen und unteren Randstrahles durch Vignettierung bestimmt wird.

Für den Sagittalschnitt ($\Phi = \pi/2$ und $3\pi/2$) reicht aber wegen der Symmetrie zum Meridionalschnitt die Hälfte der Apertur aus. Nach. Gl. 4.1 ergibt sich dann die Wellenaberration W'_s , wenn ξ' aus der geometrischen Strahldurchrechnung* bekannt ist, zu

$$W_s(\tilde{\sigma}'_s) = \int_0^{\tilde{\xi}'} -\xi' \cos \tilde{\sigma}'_s d\tilde{\sigma}'_s. \quad (4.6)$$

Somit hat man die Wellenaberration auch für den Sagittalschnitt gewonnen. Es erscheint angebracht, um die Aberrationen für die verschiedenen Aperaturen miteinander vergleichen zu können, auf die Randaperturen $\tilde{\sigma}'_{\max}$ zu normieren. Es hat sich die folgende Substitution nach Richter für die verschiedenen Winkel $\tilde{\sigma}'$ zur erleichterten Integration als vorteilhaft erwiesen:

$$q' = \frac{p'}{P'_{\max}} = \frac{1 - \cos \tilde{\sigma}'}{1 - \cos \tilde{\sigma}'_{\max}} \approx \frac{\sin^2 \tilde{\sigma}'}{\sin^2 \tilde{\sigma}'_{\max}} \quad 0 \leq q' \leq 1 \quad (4.7)$$

Die Variable p in Gl. 4.7 ist der Pfeilhöhe des Meridianbogens der Wellen-

fläche proportional und die Entwicklung der Aberrationen nach p ist bis zu beliebig grossen Öffnungen der Wellenfläche brauchbar. Aus diesem Grunde wird auch die jeweilige maximale Apertur mit p_{\max} normiert.

Die neue Variable q' , die vom Verfasser [7] schon in einer früheren Arbeit benutzt wurde, kennzeichnet nicht den Raumwinkel, sondern die Apertur und es ergibt sich in guter Näherung

$$q' \sim \bar{r}'^2. \quad (4.8)$$

Für eine kreisförmige Pupille gilt dann $\bar{r}'^2 = \bar{x}'^2 + \bar{y}'^2$. Die Wellenaberration wird so eine Funktion der normierten Polarkoordinaten \bar{r}' bzw. q' und Φ für den jeweiligen Bildwinkel σ'_B .

Führt man in Gl. 4.4, 4.5, 4.6 die neue normierte Öffnungskoordinate q' ein, dann erhält man die Wellenaberration für das axiale Gebiet

$$W(q') = \int_0^{q'} -\Delta s' p_{\max} dq' = \int_0^{q'} -\bar{\Delta}s' dq' \quad (4.9)$$

für den Meridionalschnitt

$$W_m(q'_m) = \int_0^{q'_m} -\eta \frac{\cos \sigma'_m}{\sin \sigma'_m} p'_{\max} dq'_m = \int_0^{q'_m} -\bar{\eta}' dq'_m \quad (4.10)$$

und für den Sagittalschnitt

$$W_s(q'_s) = \int_0^{q'_s} -\xi \operatorname{ctg} \tilde{\sigma}'_s p'_{\max} dq'_s = \int_0^{q'_s} -\bar{\xi}' dq'_s. \quad (4.11)$$

Die Integration wird wie erwähnt, graphisch numerisch in Stufen von $\Delta q' = 0,1$ durchgeführt. An Beispielen in Bild 6 soll die Methode erläutert werden.

Im oberen Teil des Bildes ist für ein Objektiv auf Grund der Strahl-durchrechnung die normierte sphärische Aberration $\bar{\Delta}s'$ gegen die Öffnungs-koordinate q' aufgetragen. Es wurden jeweils 5 Strahlen durch das Objektiv nach den üblichen trigonometrischen Formeln gerechnet, so dass die Kurve eindeutig zu zeichnen möglich war. Bei entsprechendem Zeichnungsmassstab lassen sich durch graphische Integration dann in äquidistanten Schritten zehn Werte der Wellenaberration gewinnen, wie sie in Wellenlängeneinheiten in Bild 6 links oben aufgetragen sind. Die Integrationsschritte werden dadurch von den Höhenabstufungen der Strahlen unabhängig, während die äquidistante Stufung bei der nachfolgenden Potenzreihenentwicklung sich dagegen sehr günstig und vereinfachend auswirkt. Eine analytische Darstellung der Aberrationskurve (etwa in Form einer Potenzreihe für die Einfalls Höhen) würde eine weit grössere Anzahl von Strahldurchrechnungen erfordern.

Grundsätzlich wäre damit die Wellenaberration für die verschiedenen Azimute gewonnen und die Berechnung des Frequenzübertragungsintegrals

* hierzu TIEDEKEN, Lehrbuch f. Optikkonstrukteur Bdn. 1. S. 63 (Berlin 1963)

möglich. Jedoch hat es sich als nützlich erwiesen, um allgemeinere Zusammenhänge zu erfassen, dieselbe nach den verschiedenen Bildfehlern aufzuspalten. Dadurch ist man in der Lage, den Einfluss der auftretenden Bildfehler quantitativ einzeln oder kombiniert in ihren Auswirkungen auf das Integral der FÜF zu studieren und Dank der Normierung die verschiedenen

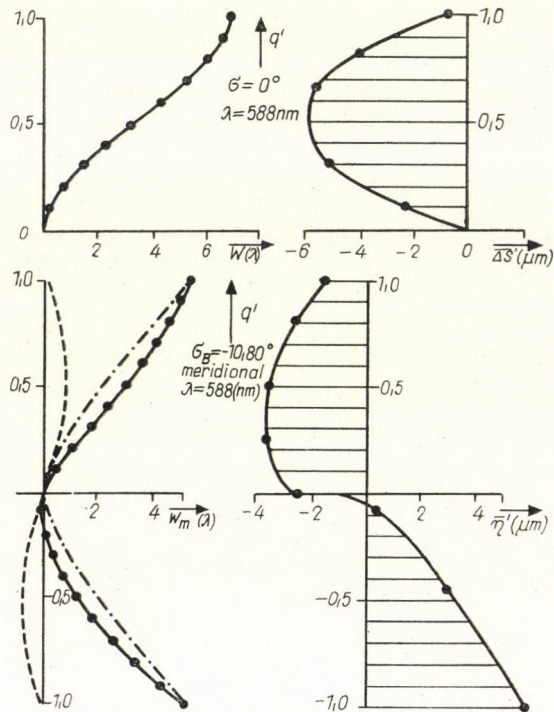


Bild 6

Objektive untereinander zu vergleichen. Ausserdem lassen sich die Werte der FÜF für die einzelnen Bildfehler besser tabellieren und zusätzlich gewisse Toleranzen in Verbindung mit dem Rayleigh-Kriterium festlegen, wie bei H. H. HOPKINS [13] und MARÉCHAL [14] näher ausgeführt.

In Anlehnung an NIJBOER lässt sich die Wellenaberration in normierten Polarkoordinaten (\tilde{r}' , Φ) für eine kreisförmige Pupille schreiben

$$\begin{aligned}
 W(\tilde{r}', \Phi) = & \boxed{W_{20} \tilde{r}'^2 + W_{40} \tilde{r}'^4 + W_{60} \tilde{r}'^6 \\
 & + (W_{11} \tilde{r}' + W_{31} \tilde{r}'^3 + W_{51} \tilde{r}'^5 \\
 & + (W_{22} \tilde{r}'^2 + W_{42} \tilde{r}'^4 \\
 & + (W_{33} \tilde{r}'^3 \\
 & + (W_{80} \tilde{r}'^8 \\
 & + W_{71} \tilde{r}'^7) \cos \Phi \\
 & + W_{62} \tilde{r}'^6) \cos 2\Phi \\
 & + W_{53} \tilde{r}'^5) \cos 3\Phi \\
 & + W_{44} \tilde{r}'^4) \cos 4\Phi
 }
 \end{aligned}$$

Die einzelnen Koeffizienten charakterisieren die folgenden Bildfehler

W_{20}	Defokussierung
W_{40}, W_{60}, W_{80}	Sphärischer Öffnungsfehler
W_{11}	Verzeichnung
W_{31}, W_{51}, W_{71}	Koma
W_{22}	Zweischalenfehler (Astigmatismus)
W_{42}, W_{62}	Astigmatischer Öffnungsfehler
W_{33}, W_{53}	Dreiblattfehler (treffil)
W_{44}	Vierblattfehler (tetrafil)

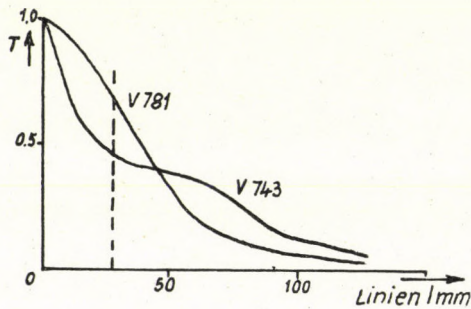
Die hier gegebene Darstellung berücksichtigt alle Fehler bis zur 7. Ordnung, doch reicht erfahrungsgemäss für normale Aufnahme- und Wiedergabekomplexe die Darstellung bis zur 5. Ordnung (in Gl. 4.12 eingerahmt) aus. Spezialkomplexe und Mikrokomplexe verlangen gelegentlich auch Entwicklungen bis zur 7. Ordnung, doch ist damit ein erhöhter Rechenaufwand und Genauigkeit der Ermittlung der Wellenaberration verbunden.

Zu bemerken ist noch, dass in der hier gewählten Darstellung für jeden Bildwinkel σ'_B ein neues Koordinatensystem verwendet wurde, so dass der Bildwinkel in die Aberrationsfunktion wie ursprünglich bei NIJBOER nicht eingeht und die Berechnung der einzelnen Koeffizienten für jeden Bildwinkel einschliesslich Vignettierung erfolgen kann. Ferner wird für das ausseraxiale Gebiet der Referenzpunkt in den realen Bildpunkt gelegt, so dass die Verzeichnung nicht in die Aberrationsfunktion eingeht. Die Verzeichnung ist ja auch kein Abbildungsfehler, der auf Unvollkommenheiten der Strahlenvereinigung zurückzuführen ist, sondern nur die geometrische Ähnlichkeit der Bildfigur verfälscht und ist deshalb einfach zu bewerten. Es gibt allerdings auch Bestrebungen, den Verzeichnungsterm mit in die Phase der komplexen Frequenzübertragungsfunktion einzubeziehen, hier soll aber aus praktischen Gründen davon Abstand genommen werden.

Und nun zur Berechnung der Aberrationskoeffizienten selbst. Durch graphische Integration wurde die Wellenaberration in äquidistanten Schritten von q' bzw. \bar{r}' gemessen und es kann nun für den entsprechenden Azimutwinkel Φ der Polynomausdruck aus Gl. 4.12 zugeordnet werden. Die Bestimmung der Koeffizienten wurde nach der Methode der kleinsten Quadrate vorgenommen und es bleiben durch die bereits erfolgte Aufspaltung der Wellenaberration höchstens drei Koeffizienten zu bestimmen übrig. Die Aberrationskoeffizienten werden so bestimmt, dass die Summe der Fehlerquadrate ein Minimum wird. Das wird durch Nullsetzen der partiellen Differentialquotienten erreicht. Man erhält dann die sogenannten Normalgleichungen, aus denen sich die Koeffizienten bestimmen lassen. Da die Wellenaberration aber stets in 10

Tabelle 1

$V \ 1.6/77.5 \ V \ 743$			$V \ 1.6/77 \ V \ 781$		
MERIDIONALSCHNITT ($\Phi = 0, \pi$)					
$\sigma_B =$	-9,50	-7,75°	-3,20°	-9,60°	-7,90°
$+w_2 =$	2,42	1,02	,70	1,60	-,21
$+w_4 =$	5,02	7,61	5,41	2,95	6,50
$w_{60} =$	-2,08	-4,08	-5,00	-1,19	-3,27
$+w_3 =$	4,68	1,67	4,10	6,27	3,54
$w_{51} =$	-4,50	-3,25	-2,25	-2,85	-2,05
$+ w_2 = w_{20} + w_{22} \quad w_4 = w_{40} + w_{42} \quad w_3 = w_{31} + w_{33}$					

Bild 7. Sagittalschnitt $\sigma = -7,8^\circ$, $\lambda = 588 \text{ nm}$

äquidistanten Schritten von q' ermittelt wird, bedeutet es eine wesentliche Rechenerleichterung, wenn man nur einmal die verschiedenen Summen von q' zu berechnen hat. Bei Benutzung einer vollautomatischen Rechenmaschine lassen sich dann die Koeffizienten in wenigen Minuten bestimmen. Tab. 1 zeigt für zwei Versuchsrechnungen den Korrektionszustand in Form normierter Wellenaberrationskoeffizienten für das axiale Gebiet und den Meridionalschnitt in drei Bildfeldwinkeln. Wie man sofort erkennt, enthält der Meridionalschnitt alle Koeffizienten doch lassen sich bestimmte Kombinationen nur durch Hinzunahme weiterer Azimute (z. B. Sagittalschnitt) aufspalten. Es ist aus Gl. 4.12 abzulesen, dass um alle Koeffizienten 5. Ordnung einzeln zu erfassen, eine Stufung der Wellenfläche mit $\Phi = 60^\circ$ erforderlich ist. In der praktischen Objektivberechnung begnügt man sich aber meistens mit der Stufung $\Phi = 90^\circ$ (Meridional- und Sagittalschnitt). Es wird später ins-

besondere an Bild 7 noch erläutert werden, dass die Koeffizientendarstellung für den Meridionalschnitt bereits wichtige Schlussfolgerungen auf die Übertragungseigenschaften zulässt.

Die Fehler durch die Potenzreihenentwicklung blieben bei zahlreichen Beispielen unter 0,1 Wellenlängen. Diese Genauigkeiten sind für die Praxis ausreichend, wenn man bedenkt, dass diese Methode mit relativ wenig Aufwand für erste systematische Untersuchungen an praktisch ausgeführten Systemen angewendet worden ist.

Kürzlich hat BARAKAT [5] eine analytische Methode zur Berechnung der Wellenaberration direkt aus der Strahldurchrechnung veröffentlicht und die Aberrationskoeffizienten mit Hilfe Tschebyscheffscher Polynome mit grosser Genauigkeit berechnet. Der Rechenaufwand ist dabei erheblich und nur mit grossen Rechenmaschinen zunächst für Spezialfälle zu bewältigen. Es können jedoch solche Verfahren in Zukunft bei entsprechender Rechenkapazität für die sogenannte automatische Korrektion optischer Systeme übernommen werden, wobei die Frequenzübertragungsfunktion als Meritfunktion, wie im vorigen Abschnitt angedeutet, benutzt werden kann. Erste Ansätze sind bereits vorhanden [15], es lässt sich aber noch kein abschliessendes Urteil darüber für die praktische Optikkonstruktion abgeben.

5. Berechnung der Frequenzübertragungsfunktion aus der Wellenaberration und einige bemerkenswerte Zusammenhänge

Die numerische Berechnung der komplexen Frequenzübertragungsfunktion soll, wie bereits angedeutet, nach einem Verfahren von HOPKINS und GOODBODY [10], [16] vorgenommen werden. Es wurde speziell für Rechenautomaten entwickelt und gewinnt nunmehr an praktischer Bedeutung, da es gelingt, die Restfehler eines aus der Praxis vorliegenden Systems in Form normierter Wellenaberrationskoeffizienten nach NIJBOER darzustellen, die Ausgangspunkt für die Berechnung sind.

Die Wellenaberration wird zunächst in die Pupillenfunktion umgerechnet, die innerhalb der Pupille wie folgt verknüpft sind

$$f(\bar{x}', \bar{y}') = \tau(\bar{x}', \bar{y}') \exp\{ikW(\bar{x}', \bar{y}')\}. \quad (5.1)$$

Die Amplitudendurchlässigkeit τ wird bis auf einen unwesentlichen Faktor gleich der tatsächlichen Amplitude der Welle gesetzt, da die ideale Amplitude über der gesamten Referenzfläche als konstant angenommen und auf Eins normiert werden kann. Es wird hierbei vorausgesetzt, dass die Welle weder durch Absorption noch durch Reflexion oder Streuung geschwächt ist, mit anderen Worten sei die gesamte Pupille als gleichmässig durchlässig ange-

nommen. Mit dieser in der Praxis meist erfüllten Bedingung lässt sich dann Gl. 2.15 mit Gl. 5.1 kombiniert schreiben

$$D(\hat{s}', \Phi) = \frac{1}{C} \iint \exp \{ik [W(\hat{x}' + \hat{s}'/2, \hat{y}') - W(\hat{x}' - \hat{s}'/2, \hat{y}')] \} d\hat{x}' d\hat{y}' \quad (5.2)$$

oder unter Einführung einer zweckmässigen Abkürzung,

$$V = \frac{1}{\hat{s}'} [W(\hat{x}' + \hat{s}'/2, \hat{y}) - W(\hat{x}' - \hat{s}'/2, \hat{y})], \quad (5.3)$$

ergibt sich dann

$$D(\hat{s}', \Phi) = \frac{1}{C'} \iint \exp \{ik \hat{s}' V(\hat{x}', \hat{y}', \hat{s}') \} d\hat{x}' d\hat{y}'. \quad (5.4)$$

Für die numerische Integration teilt man zweckmässig die $\hat{x}' - \hat{y}'$ -Ebene in rechteckförmige Elemente mit den Längen $2\Delta\hat{x}'$ und $2\Delta\hat{y}'$ und den Zeigern n, m auf. Die Funktion V wird durch eine Taylorentwicklung

$$\begin{aligned} V(\hat{x}', \hat{y}'; \hat{s}) &= W'_{\hat{x}'}(\hat{x}', \hat{y}') + \frac{1}{3!} (\hat{s}'/2)^2 W'''_{\hat{x}'}(\hat{x}', \hat{y}') + \\ &\quad + \frac{1}{5!} (\hat{s}'/2)^4 W^v_{\hat{x}'}(\hat{x}', \hat{y}') + \dots \end{aligned} \quad (5.5)$$

im Punkt (\hat{x}'_n, \hat{y}'_m) mit den Mittelpunktskoordinaten $\hat{x}'_n = (2n - 1)\Delta\hat{x}'$ und $\hat{y}'_m = (2m - 1)\Delta\hat{y}'$ eines solchen Elementes ersetzt, so dass die Gl. 5.4 für das Flächenelement lautet

$$D_{n,m}(\hat{s}', \Phi) = \frac{1}{4\Delta\hat{x}'\Delta\hat{y}'} \int_{\hat{x}'_n-\Delta\hat{x}'}^{\hat{x}'_n+\Delta\hat{x}'} \int_{\hat{y}'_m-\Delta\hat{y}'}^{\hat{y}'_m+\Delta\hat{y}'} \exp \{ik \hat{s}' V(\hat{x}', \hat{y}'; \hat{s}')\} d\hat{x}' d\hat{y}'. \quad (5.6)$$

Die Beiträge der einzelnen Flächenelemente, deren Zentren innerhalb des Integrationsgebietes S liegen, werden summiert, so dass man das Integral, abgesehen von einem Restglied wie bei GOODBODY [16] näher ausgeführt, als Doppelsumme schreiben kann.

$$D(\hat{s}', \Phi) = \frac{1}{N_C} \sum_n \sum_m \exp \{i \mathfrak{B}_{n,m}\} \frac{\sin \mathfrak{X}_{n,m} \sin \mathfrak{Y}_{n,m}}{\mathfrak{X}_{n,m} \cdot \mathfrak{Y}_{n,m}}, \quad (5.7)$$

$$\mathfrak{R}(\hat{s}', \Phi) = \frac{1}{N_C} \sum_n \sum_m \cos \mathfrak{B}_{n,m} \cdot \operatorname{sinc} \mathfrak{X}_{n,m} \cdot \operatorname{sinc} \mathfrak{Y}_{n,m}, \quad (5.8)$$

* Die Ausdrücke in Gl. 5.5 wie $W'_{\hat{x}'}$, $W'''_{\hat{x}'}$ und $W^v_{\hat{x}'}$ sind Differentialquotienten.

$$\mathfrak{J}(\hat{s}', \Phi) = \frac{1}{N_C} \sum_n \sum_m \sin \mathfrak{B}_{n,m} \cdot \text{sinc } \mathfrak{X}_{n,m} \cdot \text{sinc } \mathfrak{Y}_{n,m}, \quad (5.9)$$

mit

$$\mathfrak{B}_{n,m} = k \cdot \hat{s}' \cdot V, \quad (5.10)$$

$$\mathfrak{Y}_{n,m} = k \cdot \hat{s}' \cdot \Delta \hat{y}' \frac{\partial}{\partial \hat{y}'} V, \quad (5.11)$$

$$\mathfrak{X}_{n,m} = k \cdot \hat{s}' \cdot \Delta \hat{x}' \frac{\partial}{\partial \hat{x}'} V. \quad (5.12)$$

N_C sei die Anzahl der Flächenelemente der aufgeteilten Pupillenfläche C . Diese Aufteilung des Integrationsgebietes in elementare Gebiete ist sehr vorteilhaft, da man beliebig gestaltete Integrationsflächen damit erfassen kann. Für die nachfolgenden Beispiele wurden die Pupillenelemente $2\Delta \hat{x}' = 2\Delta \hat{y}' = 0,1$ gewählt, so dass für einen Quadranten einer kreisförmigen Pupillenfläche (C) 79 Pupillenelemente zu bestimmen waren. Auf die Einzelheiten der Berechnung und Programmierung sei in dieser Darstellung verzichtet. Die aus der Praxis ausgewählten Beispiele konnten leider nicht auf die tabellierten Werte der FÜF von HOPKINS zurückgeführt werden, so dass die Berechnung auf der Rechenmaschine „Oprema“ des VEB Carl Zeiss Jena vorgenommen wurde. Es seien hier einige Bemerkungen über die geometrisch-optischen Näherungsmethoden eingeschoben. Nach einem Vorschlag von HOPKINS [17] kann die Grösse V in geometrischer Näherung wie folgt in das Übertragungsintegral eingehen

$$V = W'_{\hat{x}'}(\hat{x}', \hat{y}') = \text{const} \cdot L' \cdot \xi'. \quad (5.13)$$

Die Grösse L' ist als Linienfrequenz in Linien/mm des verwendeten Sinusgitters mit der normierten Frequenzvariablen \hat{s}' durch die folgende Beziehung verknüpft

$$L' = \frac{\hat{s}'}{2\lambda\Omega}, \quad (5.14)$$

wobei λ die Lichtwellenlänge und Ω die wirksame Blendenzahl bedeuten. Die Grösse der normierten Queraberration setzt sich aus den verschiedenen Anteilen der normierten Strahlaberration wie folgt zusammen

$$\xi' = \bar{\xi}' \cos \Phi + \bar{\eta}' \sin \Phi. \quad (5.15)$$

Diese Näherung d. h. Vernachlässigung der höheren Ableitungen aus Gl. 5.5 ist nur für bestimmte Beträge der einzelnen Aberrationskoeffizienten, die sehr unterschiedlich ist und nur für kleine Linienfrequenzen \hat{s}' zulässig. Mehrere Autoren haben diese Näherungen untersucht und man findet bei

MIYAMOTO [19] eine zusammenfassende Darstellung. Diese Verfahren sind z. B. von LUKOSZ [18], ZÖLLNER, STUTTER und HÄUSER [20] weiter ausgebaut worden. Der Vorteil solcher Näherungsmethoden besteht darin, dass man nicht erst die Wellenaberration durch Integration aus der Strahlaberration gewinnen muss, da letztere (Strahlaberrationsbetrag ξ') direkt in das Übertragungsintegral eingeht und zusätzlich das Integrationsglied unabhängig von der Frequenz wird. Natürlich bedingt das für die Mittelpunktskoordinaten \hat{x}_n', \hat{x}_m' , jedes Pupillenelementes eine geometrische Strahldurchrechnung zur Ermittlung der Queraberration, dass für komplizierte optische Systeme mit 5—10 Linsen auch mit Rechenautomaten einen nicht geringen Rechenaufwand bedeutet. Die in dieser Arbeit benutzte graphische Methode kommt dagegen mit einer sehr viel geringeren Anzahl von Strahldurchrechnungen aus und lässt durch die normierte Aberrationskoeffizientendarstellung bereits eine Bewertung der Bildgüte und Tabellierung der FÜF zu. Will man dann noch die Pupillenelemente für die Integration als Rechnerleiterung äquidistant wählen, dann wird man die Strahlen in der entsprechend aufgeteilten Eintrittspupille auswählen und dieselbe anstatt der Austrittspupille auch als Integrationsgebiet verwenden, denn eine gleich abständige Aufteilung der Austrittspupille ist schwierig. Die Voraussetzung, die Eintrittspupille bei der Integration gleich der Austrittspupille setzen zu dürfen, gilt aber nur, wenn die Puppen aberrationsfrei ineinander abgebildet werden und ist für die meisten Objektive auch nur in Näherung erfüllt. Allerdings eignet sich die graphische Methode zur Ermittlung der Wellenaberration für Rechenautomaten wenig, hat aber, wie aufgezeigt, einige andere Vorteile und war auch ursprünglich nicht dafür bestimmt. Abschliessend sei festgestellt, dass bei Anwendung der geometrischen Näherungsverfahren jeweils zu überprüfen ist, ob diese vereinfachten Annahmen gerechtfertigt sind. Ausserdem ist der rechnerische Aufwand nicht so viel geringer wie gelegentlich behauptet wird. Das schliesst natürlich nicht aus, dass charakteristische Merkmale der Wellenaberration im Zusammenhang mit der Übertragungsfunktion auf die Strahlaberration übertragen werden können unter den obigen Voraussetzungen. Doch ist es besser, prinzipielle Überlegungen zunächst mit der Wellenaberration korrekt zu klären, wie es in den folgenden Beispielen durchgeführt werden soll.

Bild 8 zeigt im unteren Teil den Korrektionszustand und im oberen die Übertragungswerte für die günstigste Einstellebene. Es handelt sich hier um eine Versuchsrechnung eines Spezialobjektives, welches für Fernsehzwecke verwendet werden sollte. Die eingezeichnete Frequenzgrenze lässt sehr schön erkennen, dass für das Fernsehen nur ein relativ kleiner Frequenzteil benötigt wird [21], dieser jedoch optimal auskorrigiert sein muss. Die strichpunktiierte Kurve stellt zum Vergleich ein aberrationsfreies Objektiv der gleichen Öffnung dar. Im Bild 9 ist dagegen selbst für die günstigste Einstellebene diese Fernsehforderung nur schlecht erfüllt. Der Optikkonstrukteur

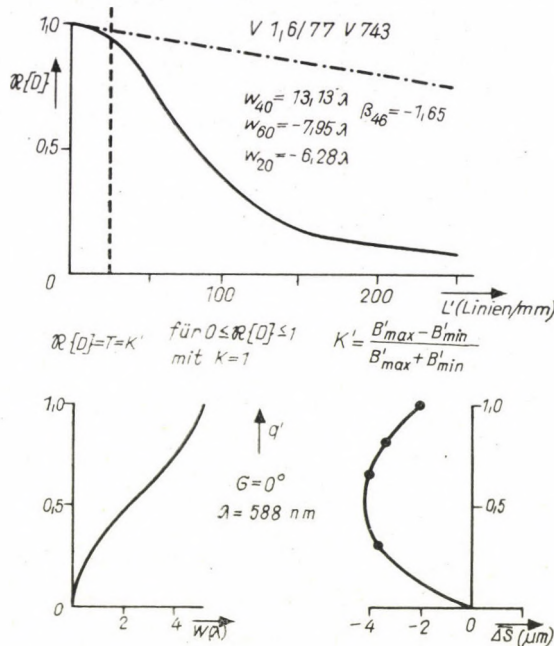


Bild 8

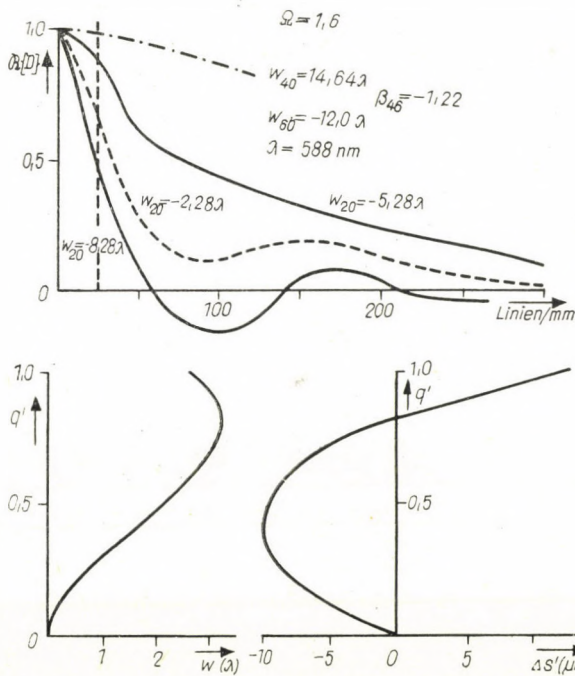


Bild 9

weiss bereits aus der Erfahrung, dass überkorrigierte Objektive kontrastarm sind. Hier lässt sich aber ein quantitativer Vergleich anstellen. Man erkennt diese Zusammenhänge auch am Verhältnis der Aberrationskoeffizienten β_{46} ($\beta_{46} = W_{40}/W_{60}$) in Verbindung mit der Toleranztheorie [13]. Ein weiteres Beispiel zeigt Bild 10 ebenfalls für das axiale Gebiet. Es handelt sich um ein Spezialobjektiv mit geringer Öffnung und sehr kleinen Restfehlern. Hier macht sich schon die Beugung sehr stark bemerkbar und geometrisch-optische Näherungsrechnungen würden in diesem Fall schon zu beträchtlichen Fehlern führen. Durch eine entsprechende Dehnung der Abszisse für die Linienführungen.

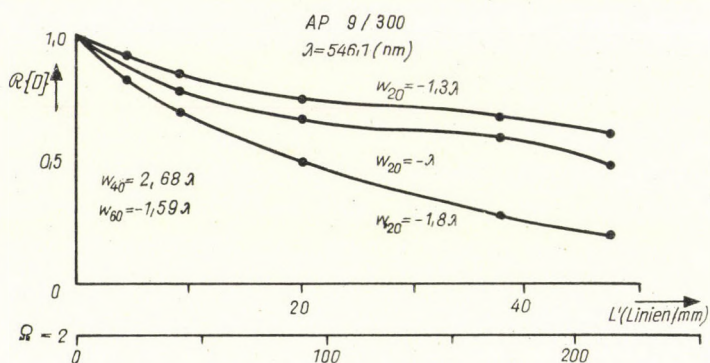


Bild 10

frequenz kann man sofort auf Systeme mit grösserer Öffnung (z. B. $\Omega = 2$) bei gleicher Korrektion übergehen.

Auch das ausseraxiale Gebiet wurde an praktischen Beispielen untersucht und in Bild 11 ist für ein Projektionssystem die FÜF in komplexer Darstellung aufgetragen. In diesem Zusammenhang sei nochmals kurz auf Bild 7 eingegangen. Die Versuchsrechnung V 743 sollte auf Grund ihrer günstigen axialen Kontrastverhältnisse (vgl. Bild 8) für Fernsehzwecke Verwendung finden, jedoch genügten für den Rand des Bildformats die Kontrastverhältnisse nicht. Der tiefere Grund lag hierfür in der negativen Komasumme für den Bildwinkel $\sigma'_B = 7,75^\circ$. Durch Änderung der Konstruktionsparameter ist es gelungen, die Komasumme ($W_3 + W_{51}$) auch für den Rand des Fernsehformats positiv zu bekommen. Allerdings wurde wie aus der Tabelle zu entnehmen ist, die axiale Bildqualität wenig verschlechtert, doch ist der Gewinn im Kontrast für die Randzone für den ohnedies etwas schlechteren Sagittalschnitt gegenüber dem Meridionalschnitt erheblich (Bild 7).

An einigen Beispielen konnte auch experimentell, nachdem die Wellenaberration mit einem Interferometer nach KRUG—LAU ermittelt wurde und mit der Rechnung übereinstimmte, die Kontrastübertragungsfunktion [7] gemessen werden (Bild 12).

Den Optikkonstrukteur interessieren aber in erster Linie die Berechnung und Zusammenhänge, wie man zu einer guten Bildqualität kommt und erst in zweiter Linie die Bestätigung durch praktische Messung am ausgeführten Typ, deshalb wurde auch in dieser Arbeit ausschliesslich die Berechnung der

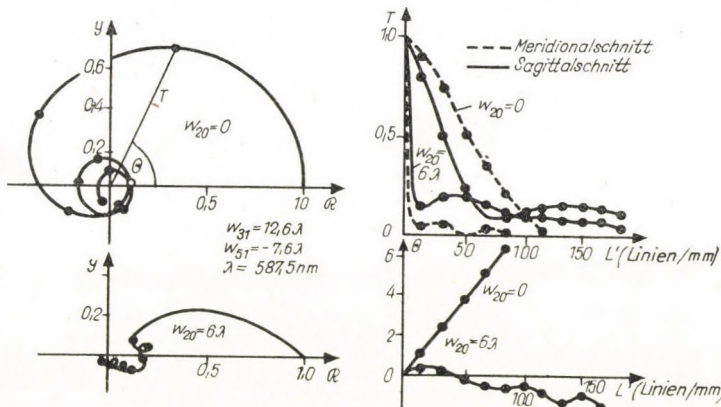


Bild 11

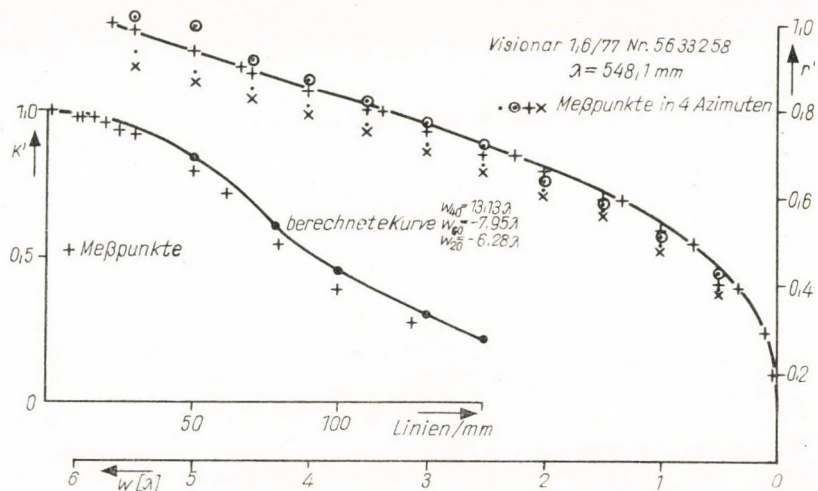


Bild 12

FÜF behandelt und das Experiment nur zur Bestätigung der Theorie herangezogen.

Diese Beispiele mögen genügen, um zu zeigen, dass mit Hilfe der FÜF speziell in der optischen Rechenpraxis mit dieser entwickelten Methode [22] bereits einige quantitative Schlüsse über die Bildleistung von optischen Systemen möglich sind.

LITERATUR

1. G. SCHMIDT und W. REICHEL, Untersuchungen über die Intensitätsverteilung im Bild von Objektpunkten mit Gittern verschiedener Gitterkonstanten, Berichtsheft »Optik aller Wellenlängen« 1958, Akademieverlag, Berlin, 1959.
2. H. H. HOPKINS, Proc. Roy. Soc., A **217**, 408, 1953.
3. P. M. DUFFIEUX, L'integrale de Fourier et ses applications à l'optique, Besançon, 1946.
4. P. W. FORD, Aberration Coefficients and Optical Design, Proceedings of the Conference on Optical Instruments, Chapman and Hall, London, 1962, pp. 121—132.
5. R. BARAKAT, Journ. Opt. Amer., **52**, 985, 1962.
6. H. A. BUCHDAL, Optical Aberration Coefficients, Oxford, 1954.
7. W. REICHEL, Jenaer Jahrbuch 1961/I, 23—34.
8. G. WYNNE und M. NUNN, Proc. Phys. Soc., **74**, 316, 1959.
C. G. WYNNE, The Relevance of Aberration Theory to Computing Machine Methods, Proc. Conf. Optical Instr., London, 1961, Chapman and Hall Ltd., 1962.
9. L. FIALOVSKY, Anwendung einer Differentialmethode und der Ausgleichsrechnung zur Feinkorrektion optischer Systeme, Compte rendu du premier symposium international sur les calculs géodésiques, Krakau 1959, 1961; s. Opt. Act., **10**, 341, 1963.
10. H. H. HOPKINS, Proc. Phys. Soc., B **70**, 1002, 1957.
11. K. ROSENHAUER, K. J. ROSENBRUCH und H. SIEMS, Ztschr. f. Instrumentenk., **71**, 14, 1963.
12. A. NIJBOER, The Diffraction Theory of Aberrations, Diss. Groningen, 1942.
13. H. H. HOPKINS, Proc. Phys. Soc., B **70**, 449, 1957.
14. A. MARÉCHAL, Rev. Opt., **26**, 257, 1947.
15. K. SAYANAGI, The Role of Optical Transfer Function in Optical Design Techniques, Proc. Confer. Optical Instr., London 1961, Chapman and Hall, London 1962, pp. 95—106.
K. SAYANAGI, Journ. Opt. Soc. Amer., **53**, 494, 1963.
16. A. M. GOODBODY, Proc. Phys. Soc., **72**, 411, 1958.
17. H. H. HOPKINS, Proc. Phys. Soc., B **70**, 1162, 1957.
18. W. LUKOSZ, Opt. Acta, 5, Sdhft. 299, 1958; s. auch Diss. Braunschweig, 1958.
19. K. MIYAMOTO, Wave Optics and Geometrical Optics in Optical Design aus Progress in Optics I, v. E. WOLF, Amsterdam, 1961.
20. W. HÄUSER, J. SCHILLING und H. ZÖLLNER, Die Kontrastübertragungsfunktion in geometrisch-optischer Näherung als Korrektionskriterium, Berichtsheft »Optik und Spektroskopie aller Wellenlängen« 1960, Akademieverlag 1962, 249.
21. W. REICHEL, Jenaer Rundschau, 7, 64, 1962; s. auch Bild und Ton, **16**, 146, 1963.
22. W. REICHEL, Zur Theorie und Praxis der Berechnung der Frequenzübertragungsfunktion optischer Systeme für die inkohärente Abbildung, Diss. Jena, 1962. Veröffentlichung im Jenaer Jahrbuch in Vorbereitung.

О ТЕОРИИ И ПРАКТИКЕ ОПРЕДЕЛЕНИЯ ПЕРЕДАТОЧНОЙ ФУНКЦИИ
ОПТИЧЕСКИХ СИСТЕМ

В. РЕЙХЕЛ

Резюме

Коротко рассматриваются вопросы оптической передаточной теории и разрабатывается метод для определения передаточной функции частоты системы, заданной в коррекции геометрической оптики. Истолкуется значение передаточной функции частоты как подходящей для оптического отображения и к коррекции оптической системы.

Аберрации геометрической оптики урегулированы на восходное отверстие и сумма волновых aberrаций определена через графическое интегрирование. Передаточной функцией частоты показывается несколько характеристических зависимостей различных ошибок изображения оптических систем, взятых из практики. При этом отдельное значение будет лежать вне аксиальной области.

MONOCRYSTALS OF Mn-PHTHALATE

By

EDMOND LENDVAY

RESEARCH INSTITUTE FOR TECHNICAL PHYSICS OF THE HUNGARIAN ACADEMY OF SCIENCES, BUDAPEST

(Presented by G. Szigeti — Received 29. IX. 1964)

Investigation of luminescent Mn-phthalate monocrystals, prepared by diffusion growing method, was carried out. It was observed that the crystals have different morphology and the crystals so grown are needles, platelets and twins.

1. Introduction

In the course of investigating the luminescent properties of Mn-salts it is essential to take into consideration the physical and luminescent characteristics of the Mn-phthalate. This compound shows a very intensive red luminescence probably due to the excess of Mn-ions in the lattice. It is characteristic for this emission that the temperature and the exciting wavelength strongly influence the intensity and the shape of the spectrum [1]. Generally at room temperature the intensity of the luminescence is much higher than of other pure Mn-salts. The compound is of special interest, because the anion in the lattice is organic and the interaction between the lattice and the activator seems to be simpler than in the case of crystal phosphors.

The samples earlier investigated were microcrystalline powders. The X-ray patterns show a definite crystal structure. A detailed study of them made possible to determine the data of the unit cell. According to these investigations the unit cell is monoclinic. The cell data are: $a = 4,436 \pm 0,010 \text{ \AA}$; $b = 13,690 \pm 0,020 \text{ \AA}$; $c = 5,720 \pm 0,002 \text{ \AA}$; $\beta = 108^\circ 27' \pm 10'$ [2].

As the investigation of microcrystalline materials is not sufficient in many respects, we prepared single crystals for the further experiments. The present paper deals with the problem of the preparation of Mn-phthalate crystals and their properties.

2. Growth method

The problem of the preparation of Mn-phthalate is complicated by the fact that the compound is practically insoluble in solvents, and decomposes without melt. Its vapor pressure before its decomposition is practically negligible, and the resistivity against acidic and basical reagents is low. All

these mean that the usual crystal growth methods are unsuccessful for the preparation of the single crystals of Mn-phthalate. The only method for producing single crystals is the diffusion growth method, which was applied first by JOHNSTON and FRENELIUS for the preparation of sparingly soluble crystals [3, 4].

In our experiments this method of crystal growth was used. The ground materials were K-phthalate and different Mn-salts (e.g. $MnCl_2$, Mn-acetate, etc.). The saturated solutions of the mentioned compounds were put separately into cylindrical vessels of 7,0 cm in length. First both "ion source" vessels were immersed into a bath of distilled water, and then the disposing of the

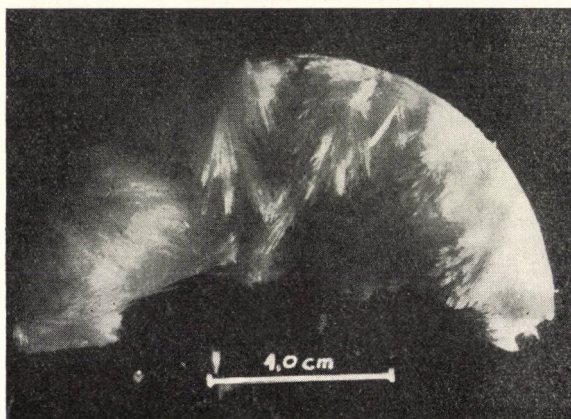


Fig. 1. Mn-phthalate crystals developed by the diffusion crystal growth method

saturated solutions into the cylindrical vessels was carefully done. The distance between the two vessels was 0,5 cm. As the formation of Mn-phthalate takes place only above $70^\circ C$, during the diffusion growth process the whole crystallisator was in a Höpler ultrathermostat at $80^\circ C$. For the prevention of the strong vaporisation of solvent, the water surface in the crystallisator was covered by paraffin oil. At the mentioned temperature the diffusion rate of reactants was sufficient, and after 3 days pink Mn-phthalate crystals with different sizes developed between the vessels and on the top of the cylinder containing the K-phthalate. In Fig 1 such a characteristic Mn-phthalate crystal group is shown. This group was formed after 4 days. The length of certain needles in the group reaches 4,0—6,0 mm with thickness of $\sim 0,1$ mm. Among the crystals one can find not only needles, but other types of crystals, too.

3. Different types of crystals

During the diffusion process and reaction at 80°C in water different types of crystals develop. Generally these crystals are needles or platelets. The needles usually appear in branches as it is well observable in Fig. 1. The microphotograph of such a branch is shown in Fig. 2. Sometimes interesting platelike crystals appear together with a needle-branch. These crystals develop at the end point of the needle-branch where the growth of the needles began. In some cases the symmetrical distribution of these platelets can be observed in a definite plane on both sides of the branch. This situation is shown in Fig. 3/a. In a very usual case the platelike crystals develop only on one side of the

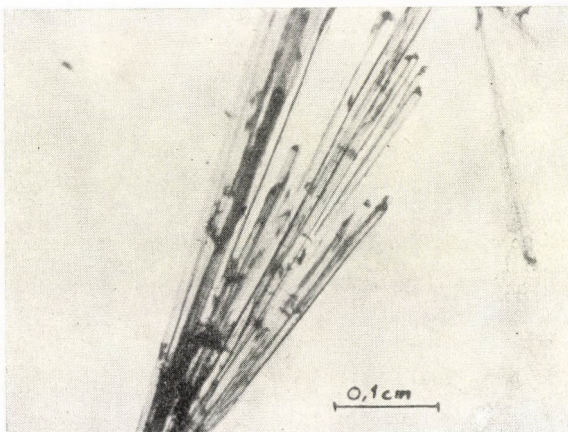


Fig. 2. Mn-phthalate needles. The length of certain crystals reaches 4–6 mm with a thickness of 0,1 mm

branch. All of these crystals lie in the same plane without any twist around the branch axes, similarly to the type of distribution mentioned before. A very interesting growth feature consists of needles and platelets of the mentioned type. In this latter case the crystal group contains only a few short needles but the mentioned thin platelike crystals appear in a great number. In the group the arrangement of platelets is very similar to that of Fig. 3/a, but certain platelike crystals partly overlap on both sides of the branch. (See Fig. 3/b.) It seems possible that in the latter case there is a connection between the high density of platelike crystals and the moderate development of needles but the verification of this requires a further detailed study of the growth process.

Corresponding to the monoclinic structure all types of Mn-phthalate crystals show a very strong birefringence in polarized light. Between crossed nicols at a suitable orientation of crystals the needles are homogeneously

extinguished or illuminated. The platelike crystals behave similarly, but the phenomenon is not homogeneous. In Fig. 4 a big, but thin platelet is shown in polarized light. From Fig. 4 and from Fig. 3 (both of which were photographed in polarized light) it can be determined that these crystals are twins. These twins show the abnormal interference colours characteristic of a mono-



Fig. 3.a — Mn-phthalate needle-branch with shield-shaped thin twin crystals in symmetrical distribution on both sides of the branch; *b* — Characteristic thin twinplatelets and repeated twins overlapping each other

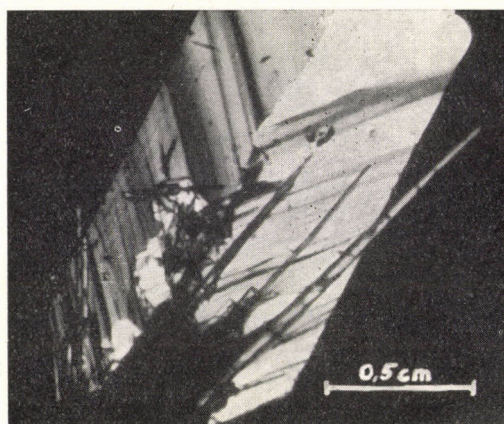


Fig. 4. Big, thin twin in polarized light. The plane of the plate corresponds to the $\langle 010 \rangle$ plane. The twin plane is the $\langle 100 \rangle$ plane

clinic system in polarized light when the crystal is lying on its $\langle 010 \rangle$ face. In this case the b-axis is normal to the face, and certain parts of the crystal are reddish for one setting of the polarizers and bluish when the polarizers are turned [5]. This is not possible for monoclinic crystals lying on any face parallel to the b-axis.

The mentioned facts mean that the c-axis of the crystal lies in the plane of the platelets and parallel to its long edges. Furthermore, the twin-plane corresponds to the $\langle 100 \rangle$ plane, and all the optical and other properties are related to each other by this plane of symmetry. In the Figures it is easily

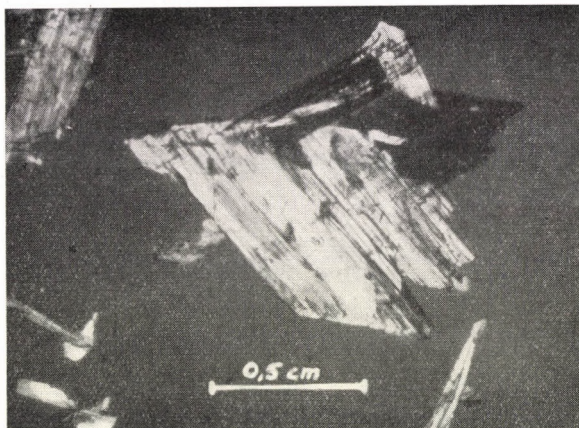


Fig. 5. Thick, twinned Mn-phthalate crystal in polarized light. One wing is completely extinguished, the other is illuminated

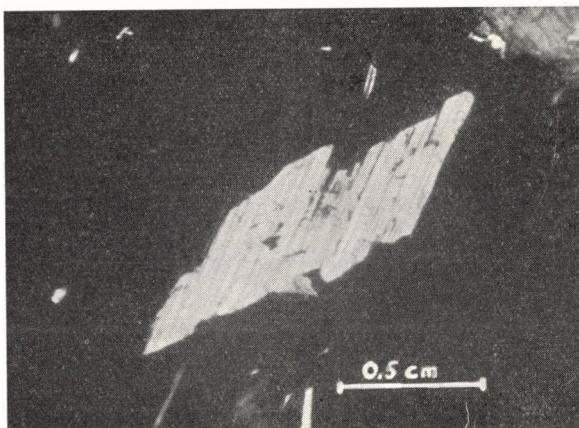


Fig. 6. Characteristic Mn-phthalate platelike crystal in polarized light

visible that the two wings incline to the c-axis with an angle of approximately 41° . These observations are also valid for another type of twinned crystals of Mn-phthalate. These crystals have not so perfect a morphology as the mentioned, but they are larger and thicker than that of the previous twins. In Fig. 5 such a characteristic, thick twinned crystal is shown in polarized light. In the left lower corner of the picture some small twins of the previous type are also

visible, therefore the comparison is very easy. In the Figure one wing of the twin is completely extinguished, but on the other wing the strong striations on the surface are observable. During a complete revolution the middle part of the crystal may not extinguish at any position of the polarizers. It means that the differently oriented wings overlap and this leads to confusing effects. In the left upper corner of the Figure a normal, untwinned plate can be seen. This type of crystal is also common. In Fig. 6 a characteristic, untwinned platelike crystal is shown. The morphology of it is almost entirely similar to the twinned crystal in Fig. 5.

All these crystals are large enough for physical investigations. They exhibit a brilliant red luminescence, if we excite them with a HP mercury lamp, but on irradiation with 265 or 254 nm mercury line the crystals do not show luminescence. The intensity of lighting is higher than that of powders.

REFERENCES

1. E. LENDVAY and J. SCHANDA, *Acta Phys. Hung.*, **13**, 469, 1961.
2. E. ZSOLDOS, *Magy. Kém. Folyóirat*, **69**, 463, 1963.
3. J. JOHNSTON, *J. Am. Chem. Soc.*, **36**, 16, 1964.
4. W. C. FRENELIUS and K. D. DETTING, *J. Chem. Educ.*, **11**, 176, 1954.
5. C. W. BUNN, *Chemical Crystallography*, The Clarendon Press, Oxford, 1961.

МОНОКРИСТАЛЛЫ ФТАЛАТА Mn

Э. ЛЕНДВАИ

Резюме

Проводились исследования люминесценции монокристаллов фталата Mn, полученных диффузионным методом выращивания. В ходе исследования выявлялось, что кристаллы имеют различную морфологию. Полученные данным методом кристаллы являются игольчатыми, пластинчатыми и двойными.

COMMUNICATIONES BREVES

HILBERT TRANSFORM AND THE DIFFERENTIAL EQUATIONS OF HAMILTON'S CANONICAL FORM

By

PARESH KUMAR BISWAS

DEPARTMENT OF THEORETICAL PHYSICS, INDIAN ASSOCIATION FOR THE CULTIVATION OF SCIENCE,
JADAVPUR, CALCUTTA-32, INDIA

(Received 3. VIII. 1964)

Let $u(t)$ and $v(t)$ be Hilbert transforms of each other so that we have the relations

$$u(t) = \frac{1}{\pi} P \int_{-\infty}^{\infty} \frac{v(\xi) d\xi}{\xi - t}, \quad v(t) = \frac{1}{\pi} P \int_{-\infty}^{\infty} \frac{u(\xi) d\xi}{\xi - t}. \quad (1)$$

Further, let q and p be defined by

$$u(t) = \frac{dq}{dt}, \quad v(t) = \frac{dp}{dt}. \quad (2)$$

We shall show that (1) implies certain relations between q and p , which are similar to the partial differential equations of Hamilton's canonical form of the equations of motion

$$\frac{dq}{dt} = \frac{\partial H}{\partial p}, \quad \frac{dp}{dt} = -\frac{\partial H}{\partial q}, \quad (3)$$

where H is a suitable function of q and p .

Clearly, $q = \Phi(t)$, $p = \psi(t)$, so that q and p are certain functions of t . Inversely, there exist functions χ and Λ such that

$$t = \chi(q) \quad (4a)$$

$$t = \Lambda(p). \quad (4b)$$

If the inverse relations are not single valued, we can still obtain an H . Of course it will not be unique as can be realised from (9).

Let us put

$$q_{\pm} = \Phi(\pm a), \quad p_{\pm} = \psi(\pm a). \quad (5)$$

The first relation of (1) gives us after substitution of the values of $u(t)$ and $v(t)$ as given in (2)

$$\begin{aligned} \frac{dq}{dt} &= \frac{1}{\pi} P \int_{-\infty}^{\infty} \frac{dp/dx dx}{x-t} = \frac{1}{\pi} P \int_{p_-}^{p_+} \frac{dp}{A(p)-t} = \frac{1}{\pi} M(t) = \\ &= \frac{1}{\pi} M\{A(p)\} = \frac{d}{dp} \left[\int_{p_-}^p \frac{1}{\pi} M\{A(p')\} dp' \right]; \end{aligned} \quad (6)$$

here use has been made of the relation (4b) twice and $M(t)$ has been written for $P \int_{p_-}^{p_+} \frac{dp}{A(p)-t}$ in the above deduction.

Similarly, we shall use (4a) and substitute $N(t)$ for $P \int_{q_-}^{q_+} \frac{dq}{\chi(q)-t}$ to

show that the second relation of (1) gives

$$\begin{aligned} \frac{dp}{dt} &= -\frac{1}{\pi} P \int_{-\infty}^{\infty} \frac{dq/dx dx}{x-t} = -\frac{1}{\pi} P \int_{q_-}^{q_+} \frac{dq}{\chi(q)-t} = \\ &= -\frac{1}{\pi} N(t) = -\frac{1}{\pi} N\{\chi(q)\} = -\frac{d}{dq} \left[\int_{q_-}^q \frac{1}{\pi} \cdot N\{\chi(q')\} dq' \right]. \end{aligned} \quad (7)$$

Let

$$H = \int_{p_-}^{p_+} \frac{1}{\pi} M\{A(p')\} dp' + \int_{q_-}^q \frac{1}{\pi} N\{\chi(q')\} dq'; \quad (8)$$

with H thus chosen (6) and (7) can be written in the form (3) as required.

Recalling that $M(t) = P \int_{p_-}^{p_+} \frac{dp}{A(p)-t}$ and $N(t) = P \int_{q_-}^{q_+} \frac{dq}{\chi(q)-t}$ we have from (8)

$$H = \int_{p_-}^q \frac{1}{\pi} \cdot dp' \int_{p_-}^{p_+} \frac{dp''}{A(p'')-A(p')} + \int_{q_-}^q \frac{1}{\pi} \cdot dq' \int_{q_-}^{q_+} \frac{dq''}{\chi(q'')-\chi(q')}; \quad (9)$$

(9) then shows the existence of an H .

Thanks are due to Professor D. BASU, Ph. D., (Dublin) for valuable comments and encouragement.

MAGNETIC CHARACTERISTIC CURVE FOR A SPECIAL PERMANENT-MAGNET BETA-RAY SPECTROGRAPH SET OF TWO UNITS

By

F. ILLÉS and D. BERÉNYI

INSTITUTE OF NUCLEAR RESEARCH (ATOMKI) OF THE HUNGARIAN ACADEMY OF SCIENCES, DEBRECEN

(Received 22. IX. 1964)

Based mainly on the work of ELLIS [1] and SLÄTIS [2] the permanent-magnet beta-ray spectrograph has become one of the fundamental instruments of nuclear spectroscopy. As is well known, these spectrographs operate on the classical principle of semicircular focusing in a homogeneous magnetostatic field. Recently, this type of instrument developed especially in two directions: in order to obtain high resolving power, large beta-ray spectrographs (ϱ_{\max} : 40—50 cms) were introduced [3], whereas SLÄTIS [4] built a set of spectrographs, which was soon followed by others.*

At this Institute a large special permanent-magnet beta-ray spectrograph, the so-called *Band Spectrograph* [5] was constructed, the maximum curvature radius of which is 75 cms. The spectrograph is half-ring shaped. The width of the operating band is 15 cms. This makes measurements in the range from $\varrho_{\min.} = 60$ to $\varrho_{\max.} = 75$ cms possible. The length of the air gap is 4 cms. The adjustment of the Band Spectrograph is now in progress.

In the course of the construction of the Band Spectrograph it became also necessary to build a small conventional permanent-magnet beta-ray spectrograph. This instrument, the so-called *Spectrograph Baby* [6] plays an important role not only in connection with some construction problems, but also as an essential supplement to the Band Spectrograph in research work. As a matter of fact, the two spectrographs together form one operative unit. The maximum ϱ of the Spectrograph Baby is 7,5 cms. The area of the pole-pieces is $13 \times 18 \text{ cm}^2$ and the air gap is 2,5 cms long. The yoke is U-shaped.

In both spectrographs the pole-pieces serve as the upper and lower walls of the vacuum chambers of the horizontal state. (Here the source- and film-holders, in which the entrance slit and the film are in the same plane, are mounted.) The magnetic fields of the instruments are excited by small permanent-magnet prisms, which are mounted directly on the upper pole-piece and surrounded by a common magnetizing coil. The opposite ends of the prisms fit into the upper part of the yoke. The material of the pole-pieces

* E. g. at the Centre of Nuclear Spectroscopy, Orsay (France) and at California University, Berkeley (USA)

is soft iron "Fermax" (made by the Hungarian firm "Csepel Vas- és Fémművek" in Budapest) and the yokes are made of ordinary soft iron. The permanent-magnet pieces are made of "Alnico-5"** steel (of a size of $13 \times 33 \times 37$ mm³ in the Band Spectrograph and $13 \times 33 \times 37,5$ mm³ in the Spectrograph Baby). At present, 50 of these pieces are being built into the larger spectrograph and 10 into the smaller one.

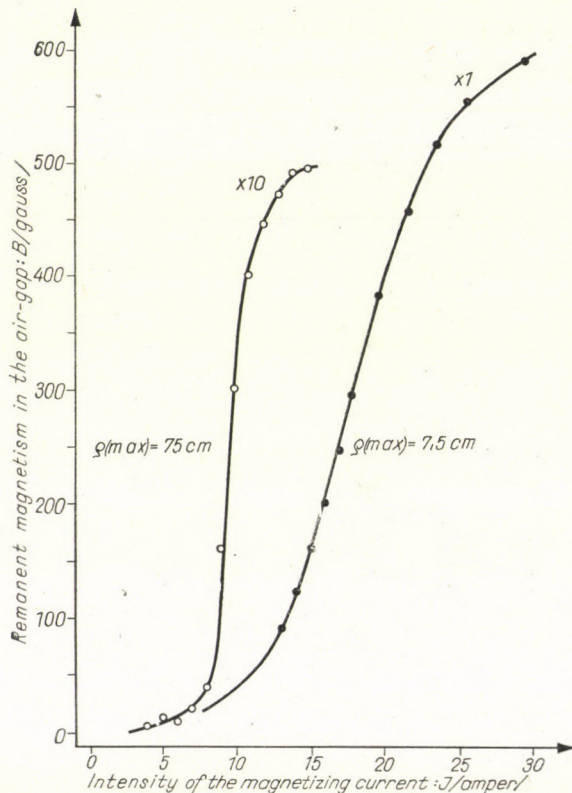


Fig. 1. Magnetic characteristic curves of the Band-Spectrograph (○) and the Spectrograph Baby (●). The points indicated are the averages of several independent measurements

In permanent-magnet beta-ray spectrographs it is also necessary to change the intensity of the magnetic field. By SLÄTIS' magnetization procedure [4] one can produce magnetic fields constant in time both in spectrograph sets and in single spectrographs. The quick setting of different values of the constant magnetic field is especially important in our case, where the operating band of the spectrograph includes different energy ranges depending on the intensity of the magnetic field in the air gap. The changing of the magnetization state of the permanent magnets, and thus the setting of the whole magnetic

** Made by the Hungarian firm "Kőbányai Vas- és Acélöntőde" (Budapest).

circuit of the spectrograph takes place by the coil surrounding the permanent magnet prisms. To solve the whole problem *quantitatively* it is necessary to know a unique relation between the remanent magnetic field intensity in the air gap after magnetization with a certain current in the coil, and the intensity of the magnetizing current. This relation is called the *magnetic characteristic curve* of beta-ray spectrographs of permanent-magnet type [1].

The theoretical deduction of the characteristic curve is too difficult a task. Thus, we determined it *experimentally* by measuring the remanent magnetism in the air-gap as a function of the magnetizing current (after switching off the current). The uniqueness and applicability of the function are assured by degaussing after every measurement of the remanence. It is to be noted here that the characteristic curve concerned is evidently *not* identical with the magnetization curve of the spectrograph [1].

In Fig. 1. the characteristic curves of the Band Spectrograph and the Spectrograph Baby can be seen. The intensity of the magnetic field in the air-gap was measured by a test coil connected to a fluxmeter. The coil was calibrated in the Spectrograph Baby by means of the well-known conversion lines of the Th ($B + C + C'$). The degaussing was carried out in the case of the Band Spectrograph by direct current and in the case of the Spectrograph Baby by alternating current.

In practice, of course, the inverse of the magnetic characteristic curve is to be used and even the energy characteristic curve [6] can be obtained from the magnetic one in a simple way.

REFERENCES

1. J. D. COCKROFT, C. D. ELLIS and H. KERSHAW, Proc. Roy. Soc. A, **135**, 628, 1932.
2. H. SLÄTIS, Ark. Fys., **6**, 415, 1953.
3. M. MLADJENOVIC', Bull. "B. Kidrich" Inst. **6**, 53, 1956.
H. NIEWODNICZAŃSKI, Beta-ray spectrometers of Cracow Institute of Nuclear Physics;
Lecture on the Balatonöszöd Colloquium for Low Energy Nuclear Physics, 1960 (unpublished).
4. H. SLÄTIS, Nucl. Instr., **2**, 332, 1958.
5. D. BERÉNYI and F. ILLÉS, ATOMKI Közl., **3**, 83, 1961.
F. ILLÉS and D. BERÉNYI, ATOMKI Közl., **3**, 91, 1961.
J. SCHADEK, D. BERÉNYI and F. ILLÉS, ATOMKI Közl., **3**, 105, 1961.
6. F. ILLÉS and D. BERÉNYI, ATOMKI Közl., **6**, 157, 1964.

RECENSIONES

MILTON KERKER

Electromagnetic Scattering

International Series of Monographs on Electromagnetic Waves Vol. 5, Pergamon Press,
Oxford—London—New York—Paris, 1963, 592 pages, £ 7 net

The volume gives a collection of papers presented at the Interdisciplinary Conference on Electromagnetic Scattering (ICES) held at Clarkson College of Technology, Potsdam N. Y. August 1962. As MILTON KERKER, the Editor of these proceedings, points out in the Preface the six sections of the book correspond to the six scientific sessions of the conference: (the chairmen are shown in parentheses)

1. Particle Scattering (H. C. VAN DE HULST).
2. Light Scattering in the Atmosphere and Space (P. SWINGS),
3. Microwave and Radiowave Scattering in the Atmosphere (J. STEWART MARSHALL),
4. Light Scattering in Solution (PETER DEBYE),
5. Interaction in Solids and Liquids (VICTOR K. LA MER),
6. Multiple Scattering (VICTOR TWERSKY).

The Preface is followed by a short Introduction by Professor VAN DE HULST, outlining the purpose and the spirit of this meeting "The problem of 'keeping in touch' with developments in related fields becomes really bewildering" — he says. "In this situation great benefit can be derived from a meeting of experts in widely varying fields on what seems to be common ground, an interdisciplinary conference." "The Interdisciplinary Conference on Electromagnetic Scattering set a fine example of such mutual inspiration across widely different fields of specialisation".

As for the subjects treated in the conference and this volume: about one-third of the program was devoted to the scattering properties of single particles while the other end of the scale of problems was formed by multiple scattering. Between these limits are treated the problems in which the distinction of individual scattering particles in the medium is itself not an easy question.

Part 1 contains papers on "Particle Scattering". J. B. KELLER and B. R. LEVY report on "Scattering of Short Waves", P. J. WYATT on "Light Scattering from Objects with Spherical Symmetry" and S. LEVINE and M. KERKER on "Scattering of Electromagnetic Waves from Two Concentric

Spheres, when Outer Shell has a Variable Refractive Index". Y. IKEDA gives an "Extension of the Rayleigh-Gans Theory", W. A. FARONE, M. KERKER and E. MATIJEVIĆ discuss "Scattering by Infinite Cylinders at Perpendicular Incidence". R. PENNDORF deals with "Scattering Diagrams in the Mie Region", J. R. HODKINSON with "Light Scattering and Extinction by Irregular Particles larger than the Wavelength" and W. HELLER with "Theoretical and Experimental Investigation of the Light Scattering of Colloidal Spheres".

Part 2 entitled "Light Scattering in the Atmosphere and Space" contains J. M. GREENBERG, A. C. LIND, R. T. WANG and L. F. LIBELO's paper on "The Polarisation of Starlight by Oriented Nonspherical Particles", M. F. INGHAM's paper on "Scattering by Interplanetary and Cislunar Dust Particles". Further B. DONN and R. S. POWELL deal with "Angular Scattering from Irregularly shaped Particles with Application to Astronomy", P. SWINGS with "Scattering by Cometary Particles". "Scattering and Polarisation Properties of Polydispersed Suspensions with Partial Absorption" is treated by D. DEIRMENDJIAN, "Mie Scattering of an Atmospheric Air Volume" by K. BULLRICH and "Rayleigh Scattering and Polarization in the Atmosphere" by T. GEHRELS.

Part 3 on "Microwave and Radiowave Scattering in the Atmosphere" contains the following papers: "Back-Scatter by Dielectric Spheres with and without Metal Caps" by D. ATLAS and M. GLOVER, "Surface Waves Associated with the Back-Scattering of Microwave Radiation by Large Ice Spheres" by J. R. PROBERT-JONES, "Calculations of the Total Attenuation and Angular Scatter of Ice Spheres" by B. M. HERMAN and L. J. BATTAN, "The Role of Radio Wave Scattering in the Study of Atmospheric Microstructure" by R. BOLCIANO Jr. and "Atmospheric Scatter Reflection Phenomena in Radio Wave Propagation" by A. SPIZZICHINO and J. VOGUE.

"Light Scattering in Solution" is treated in Part 4 in various conditions: by dilute solution of high polymers, by nonideal solutions, by electrolyte solutions containing charged colloidal particles, by non-Gaussian macromolecular coils and by soap films in the respective papers of H. BENOIT, D. STIGTER, J. TH. G. OVERBEEK, A. VRIJ, H. F. HUISMAN, A. PETERLIN and A. VRIJ. The rest of this Part is concerned with "The Application of Light Scattering and Small-Angle X-Ray Scattering to Interacting Biological Systems" (S. N. TIMASHEFF) and "Light Scattering Studies on Monodisperse Silver Bromide Sols" (D. H. NAPPER and R. H. OTTEWILL).

Part 5 is entitled "Interaction in Solids and Liquids", where P. DEBYE's article on "Light Scattering and Molecular Forces" is followed by "Scattering of Electromagnetic Radiation as a Tool for Investigating Critical Phenomena (The Low-Angle X-Ray Scattering of the Nitrobenzene-n-Heptane System in the Critical Region)" by H. BRUMBERGER and W. C. FARRAR, "Optical Extinction by Metal Precipitates in Semiconductors and Insulators" by B. R. GOSICK, "The Scattering of Light by Heterogeneities in Crystalline Polymeric Solids" by R. S. STEIN, "Absolute Intensity of Small Angle X-Ray Scattering in Solid High Polymer Research" by O. KRATKY and finally "Light Scattering from Elastic Strains" by M. GOLDSTEIN.

The last part of the book, Part 6, is devoted to Multiple Scattering. C. C. GROSJEAN reports on "Recent Progress in the Development of a New Approximate General Theory of Multiple Scattering". A paper by C. M.

CHU, S. W. CHURCHILL and S. C. PANG considers "A Variable-Order Diffusion-Type Approximation for Multiple Scattering". "Multiple Scattering of Waves" is treated in "Dense Distributions of Large Tenuous Scatterers" by V. TWERSKY and in "Media with Anisotropic Scattering" by Z. SEKERA. T. W. MULLIKIN deals with "Uniqueness Problems in the Mathematics of Multiple Scattering", C. M. CHU, J. A. LEACOCK, J. C. CHEN and S. W. CHURCHILL with "Numerical Solutions for Multiple, Anisotropic Scattering." The book concludes with H. C. VAN DE HULST's "Remarks on Multiple Scattering".

The above list of papers may show quite clearly that the volume gives valuable information in a very wide field of science. Its interdisciplinary character makes it in some respects more inspirative than the usual proceedings of other, much more conventional symposia. The book is not a Treatise on Electromagnetic Scattering, its aim being to give a collection of interesting and inspirative individual contributions in this field, where the common denominator is the electromagnetic scattering. It can be used to advantage primarily by research workers, but it may also be of value for the beginners and students who may even obtain some general perspectives of the entire field.

Credit is due to MILTON KERKER for careful editing. The book was published as Volume 5 of the International Series of Monographs on Electromagnetic Waves by Pergamon Press at the usual high standard of this Publisher.

J. ANTAL

J. THEWLIS (HARWELL)

Encyclopaedic Dictionary of Physics

Vol. 6, Pergamon Press, Oxford, London, New York, Paris, 1962

The volume contains 883 pages in large octavo form. The preparatory committee of the complete work included more than 150 famous personalities. The number of contributors to this volume was approximately 400. The title words of volume 6 begin with "Radiation, continuous" and end with the expression "Stellar luminosity".

As regards its dimensions this book is almost equivalent to large handbooks, yet its vocabulary character makes everything in it easily accessible. Young researchers may even use it as a textbook, if one has patience to look up for the title words following each

other. Thus e. g. the words of radioactivity occupy approximately 140 pages. The text of each title word is immediately followed by the literature of the subject.

Title words are given as commonly used in the English speaking countries. Thus it may occur that e. g. instead of the expression "screw dislocations" one finds "screw displacements". The reader has to try to find a corresponding synonym, if any word seems to be missing.

References are ample and well selected, yet e. g. under the title word "Schlieren" reference is missing to SCHARDIN's detailed

article in the *Ergebnisse der exakten Naturwissenschaften*, **20**, 303—439, 1942, where all aspects of the phenomenon are treated.

Naturally, it is impossible to avoid some printer's errors. Thus e. g. on page 198 under the title word Rate Process H_{act} = activation energy should probably be replaced by ΔH_{act} = activation energy and accordingly S_{act} = should read ΔS_{act} = activation entropy.

Similarly, it should be mentioned that on page 223 the title word Recombination should include, in addition to the positive ion as electron capturing place, the positive hole, also as electron capturing place.

On page 537 under the title word Solenoid it would be desirable to give the formula of the magnetic field intensity appearing inside the coil.

On page 637 the title word Specific Resistance is said to increase in general with temperature. It could perhaps be mentioned that this assertion is in general valid for metals, but the case is just the opposite for semiconductors.

Such small deficiencies, which may cause

difficulties for the young physicists, ought to be corrected.

The book gives a precise historic background of concepts of major importance, which is useful in many cases. References to related fields are carefully selected, thus particularly to biology and biophysics, an important advantage regarding the rapid development of physics in our days. As a whole the book is equally useful for the researcher and the applied physicist.

The layout, printing, figures and tables are all exemplary.

This book can be used by all who have already acquainted themselves with the fundamentals of experimental and theoretical physics. However, certain self-discipline is required of the reader to look up for the precise definition of any concept with which he may not be familiar. Doing so for years one may obtain precise information on many subjects at the expense of a comparatively small amount of work. It is, however, necessary that the reader has access to all volumes of the Dictionary.

Z. GYULAI

R. K. WANGNESS

Introduction to Theoretical Physics (Classical Mechanics and Electrodynamics)

John Wiley and Sons Inc., New York and London 1963. Pp X + 413

This textbook will be found useful by anybody who wants to learn theoretical physics, and in particular by those who want to work in the field of quantum mechanics. The book requires only the knowledge of the very elements of experimental physics and of differential and integral calculus, and although its style always remains easy-to-read and clear, it gradually digs deeper not only into physics but also into mathematics, providing thereby an excellent starting point for further studies. Care has been taken

throughout the book to teach not only the subject-matter itself, but also the physical way of thinking.

The book consists of three main parts: Mechanics, Electrodynamics and Interactions of Electromagnetic Fields and Matter. These parts deal not only with the basic laws, but discuss also many applications in detail, in particular those which may be important for the study of quantum mechanics.

T. SZONDY

Printed in Hungary

A kiadásért felel az Akadémiai Kiadó igazgatója

A kézirat nyomdába érkezett: 1965. I. 18. — Terjedelem: 10 (A/5) ív, 30 ábra

Műszaki szerkesztő: Farkas Sándor

65. 60144 Akadémiai Nyomda, Budapest — Felelős vezető: Bernát György

The *Acta Physica* publish papers on physics, in English, German, French and Russian. The *Acta Physica* appear in parts of varying size, making up volumes.

Manuscripts should be addressed to:

Acta Physica, Budapest 502, Postafiók 24.

Correspondence with the editors and publishers should be sent to the same address.

The rate of subscription to the *Acta Physica* is 110 forints a volume. Orders may be placed with "Kultúra" Foreign Trade Company for Books and Newspapers (Budapest I., Fő u. 32. Account No. 43-790-057-181) or with representatives abroad.

Les *Acta Physica* paraissent en français, allemand, anglais et russe et publient des travaux du domaine de la physique.

Les *Acta Physica* sont publiés sous forme de fascicules qui seront réunis en volumes.

On est prié d'envoyer les manuscrits destinés à la rédaction à l'adresse suivante:

Acta Physica, Budapest 502, Postafiók 24.

Toute correspondance doit être envoyée à cette même adresse.

Le prix de l'abonnement est de 110 forints par volume.

On peut s'abonner à l'Entreprise du Commerce Extérieur de Livres et Journaux «Kultúra» (Budapest I., Fő u. 32. — Compte-courant No. 43-790-057-181) ou à l'étranger chez tous les représentants ou dépositaires.

«*Acta Physica*» публикуют трактаты из области физических наук на русском, немецком, английском и французском языках.

«*Acta Physica*» выходят отдельными выпусками разного объема. Несколько выпусков составляют один том.

Предназначенные для публикации рукописи следует направлять по адресу:

Acta Physica, Budapest 502, Postafiók 24.

По этому же адресу направлять всякую корреспонденцию для редакции и администрации.

Подписная цена «*Acta Physica*» — 110 форинтов за том. Заказы принимает предприятие по внешней торговле книг и газет «Kultúra» (Budapest I., Fő u. 32. Текущий счет: № 43-790-057-181) или его заграничные представительства и уполномоченные.

INDEX

F. Bukovszky: Elementary Calculations of the Madelung Constants of Some Cubic Lattices	157
J. Ladik: Some Developments in the Semiempirical Theories of Molecular Crystals. I. The Hückel Approximation. — Я. Ладик: О полуэмпирических теориях молекулярных кристаллов I. Пирближение Гюкеля	173
J. Ladik: Some Developments in the Semiempirical Theories of Molecular Crystals. II. The Pariser-Parr-Pople Approximation. — Я. Ладик: О полуэмпирических теориях молекулярных кристаллов II. Приближение Паризера—Парра—Попла	185
Gy. Farkas, L. Jánossy, Zs. Náray and P. Varga: Intensity Correlation of Coherent Light Beams. — Дь. Фаркаш, Л. Яноши, Ж. Нараи и П. Варга: Корреляция интенсивности когерентных световых лучей	199
F. Beleznay, G. Biczó and J. Ladik: Theoretical Estimation of the Conductivity of DNA. — Ф. Белезнаи, Г. Бицо и Я. Ладик: Теоретическое определение электрической проводимости DNS	213
J. Németh: A Superconductive Model with Two Kinetic Energies. — Й. Немет: Модель сверхпроводимости с двумя значениями кинетической энергии	221
W. Reichel: Zur Theorie und Praxis der Berechnung der Übertragungsfunktion optischer Systeme. — В. Рейхел: О теории и практике определения передаточной функции оптических систем	233
E. Lendvay: Monocrystals of Mn-Phthalate. — Э. Лендвай: Монокристаллы фталата-Mn	257

COMMUNICATIONES BREVES

P. K. Biswas: Hilbert Transform and the Differential Equations of Hamilton's Canonical Form	263
F. Illés and D. Berényi: Magnetic Characteristic Curve for a Special Permanent-Magnet Beta-Ray Spectrograph Set of Two Units	265

RECENSIONES

J. Antal: Milton Kerker, Electromagnetic Scattering	269
Z. Gyulai: J. Thewlis, Encyclopaedic Dictionary of Physics Vol. 6.	270
T. Szondy: R. K. Wangsness, Introduction to Theoretical Physics	271

Acta Phys. Hung., Tom. XVIII. Fasc. 3. Budapest, 15. IV. 1965.

ACTA PHYSICA

ACADEMIAE SCIENTIARUM HUNGARICAE

ADIUVANTIBUS

Z. GYULAI, L. JÁNOSSY, I. KOVÁCS, K. NOVOBÁTZKY

REDIGIT

P. GOMBÁS

TOMUS XVIII

FASCICULUS 4



AKADÉMIAI KIADÓ, BUDAPEST

1965

ACTA PHYS. HUNG.

ACTA PHYSICA

A MAGYAR TUDOMÁNYOS AKADÉMIA FIZIKAI KÖZLEMÉNYEI

SZERKESZTŐSÉG ÉS KIADÓHIVATAL: BUDAPEST V., ALKOTMÁNY UTCA 21.

Az *Acta Physica* német, angol, francia és orosz nyelven közöl értekezéseket a fizika tárgyköréből.

Az *Acta Physica* változó terjedelmű füzetekben jelenik meg: több füzet alkot egy kötetet.
A közlésre szánt kéziratok a következő címre küldendők:

Acta Physica, Budapest 502, Postafiók 24.

Ugyanerre a címre küldendő minden szerkesztőségi és kiadóhivatali levelezés.

Az *Acta Physica* előfizetési ára kötetenként belföldre 80 forint, különöldre 110 forint. Megrendelhető a belföld számára az Akadémiai Kiadónál (Budapest V., Alkotmány utca 21. Bankszámla 05-915-111-46), a különöld számára pedig a „Kultúra” Könyv- és Hírlap Külkereskedelmi Vállalatnál (Budapest I., Fő u. 32. Bankszámla 43-790-057-181 sz.), vagy annak különöldi képviseleteinél és bizományosainál.

Die *Acta Physica* veröffentlichen Abhandlungen aus dem Bereich der Physik in deutscher, englischer, französischer und russischer Sprache.

Die *Acta Physica* erscheinen in Heften wechselnden Umfangs. Mehrere Hefte bilden einen Band.

Die zur Veröffentlichung bestimmten Manuskripte sind an folgende Adresse zu richten:

Acta Physica, Budapest 502, Postafiók 24.

An die gleiche Anschrift ist auch jede für die Redaktion und den Verlag bestimmte Korrespondenz zu senden.

Abonnementspreis pro Band: 110 Forint. Bestellbar bei dem Buch- und Zeitungs-Aussenhandels-Unternehmen »Kultúra« (Budapest I., Fő u. 32. Bankkonto Nr. 43-790-057-181 oder bei seinen Auslandsvertretungen und Kommissionären.

NOTES ON THE QUANTUM-MECHANICAL DISCUSSION OF THE GIBBS PARADOX

By

GY. FÁY

DEPARTMENT OF ATOMIC PHYSICS, POLYTECHNICAL UNIVERSITY, BUDAPEST*

(Presented by I. Kovács. — Received 3. III. 1964)

Starting from the deductive development of quantum theory as worked out by NEUMANN and making use of the quantum-theoretical propositional calculus it will be shown that the quantum theoretical entropy of any physical property increases if the property is replaced by a logically weaker one.

Introduction

It has been the recognition that the entropy is an information-theoretical concept, i. e. that its value depends on the conditions under which the given thermodynamical system is investigated, that led to the resolution of the thermodynamical GIBBS paradox¹ [1]. More strictly speaking: one can assign to a thermodynamical system such properties, which, although unimportant concerning its macroscopical behaviour, may affect the value of its entropy. L. SZILÁRD [2] made the first quantitative investigations concerning the change of the entropy of a system due to some external action originating in the knowledge of certain microscopical properties of it.

Before exposing the aims of the paper let us formulate the GIBBS paradox in general.

Let us consider two samples of gases isolated by a wall. Let the state of the gases be determined by their pressures (P_1, P_2), their volumes ($V_1 = V_2 = V$) and the numbers of their molecules (N_1, N_2). If the system $1 + 2$ is thermally homogeneous it has entropy the value of which is

$$S = S_1 + S_2.$$

Let us remove now the wall and let us consider the thermodynamical system obtained in this way. Let the entropy of the new system be S_{12} . Then it follows from thermodynamics that

* Present address: Department of Physics, Technical University for Heavy Industry, Miskolc, Hungary.

¹ In the paper [1] FÉNYES has completely resolved the GIBBS paradox. The present paper actually does not deal with the thermodynamical GIBBS paradox, but it gives a more general discussion of a property of the entropy recognized in the course of investigating the GIBBS paradox.

$$\Delta S = S_{12} - (S_1 + S_2) > 0.$$

This change ΔS of the entropy does not vanish even if the systems 1 and 2 are "completely equivalent" meaning by this, that they are thermodynamically equivalent, i.e. the observables (P, V, N) describing their state and their equations of state are identical. This latter means in the case of ideal gases that their molecular weights are the same. As we could have devided the system $1 + 2$ by the wall purely *mentally*, it appears paradoxical that this purely mental action can change the entropy.²

This purely mental dividing means, however, that while we assigned to every molecule of the system $1 + 2$ (without wall) the property that it can move in the volume $2V$, the volume available for any molecule of the system $1 + 2$ (with wall) is only V .³ This can also be formulated so that the mental removing of the wall is equivalent to replacing a certain property of the molecules (subsystems)⁴ comprising the gas (the thermodynamical system) by a consequence of it.

Naturally *phenomenological* thermodynamics cannot make statements concerning such " V " and " $2V$ " type properties of molecules (more generally: subsystems) making up a thermodynamical system, since of the "properties" of the molecules (meant in a general sense) only their number N enters explicitly.⁵

Consequently, this problem must be investigated in the framework of a theory which explicitly investigates the properties of the subsystems of a physical system. Our aim is evidently to show: *Whenever a property of a system is replaced by a (weaker) consequence of it, the entropy of the system increases*. The theory which makes possible such investigations is the *quantum theory*.⁶

2. The macroentropy of quantum-mechanical ensembles

Let us consider a quantum-mechanical ensemble with the statistical operator U , and let us investigate how a macroscopical observer can characterize it. His procedure is always the following: he considers some property ε_1 and measures the probability with which ε_1 occurs in the ensemble. Besides,

² Naturally only if we assume that the state of the system is uniquely determined by its pressure P , and its volume $2V$. In this case the system is not changed by mentally deviding it by a wall, as we do not take notice of the fact that the gas is made up of molecules. The paradox lies in the fact that if we take into account also the mixing of the gas caused by the removing of the wall, that is, if we take into account that the original system $(P, V) + (P, V)$ has been converted into the system $(P, 2V) + (P, 2V)$, the entropy of the latter system will differ from the entropy of the former one.

³ Thus here we already abandoned the phenomenological attitude.

⁴ These are already not thermodynamical systems.

⁵ Or not even this, in more restricted considerations (cf.²).

⁶ Detailed quantitative investigations concerning properties of physical systems have been carried out by NEUMANN ([3], Chapter III. p. 5., and Chapter IV. p. 3.).

however, he inevitably measures also the complementary property $\bar{\varepsilon}_1$. Namely, by stating that the property ε_1 is not present in some system picked out at random, he shows at the same time that the property $\bar{\varepsilon}_1$ ("not ε_1 ") is present. Denoting $\bar{\varepsilon}_1$ by ε_2 , the method of measuring of the macroscopical observer interested only in one property can be characterized by the operators E_1 and E_2 which belong to the properties ε_1 and ε_2 and which satisfy the relations

$$E_1 + E_2 = 1,$$

$$E_1 \cdot E_2 = 0.$$

Let us assume now that the observer wants to obtain information about the properties $\varepsilon_1, \varepsilon_2, \varepsilon_3, \dots, \varepsilon_N$. Similarly as previously it follows also in this case, that

$$\sum_{i=1}^N E_i = 1. \quad (1)$$

We shall show, however, that also the "orthogonality relations"

$$E_i \cdot E_k = 0 \quad (i \neq k) \quad (2)$$

can always be fulfilled in the sense that if the set $E_1, E_2, E_3, \dots, E_N \equiv \{E_i\}$ is not orthogonal but is "complete", i.e. it satisfies (1), one can always assign in a unique way to the set $\{E_{i_N}\}$ ($i = 1, 2, 3, \dots, N$) a set $\{F_n\}$ ($n = 1, 2, 3, \dots, M = 2$) for which the orthogonality relations

$$F_i \cdot F_k = 0 \quad (i \neq k) \quad (2')$$

hold.

This set $\{F_n\}$ can be constructed in the following way. Let us recast the operator E_i by making use of the fact, that for every k ($k = 1, 2, 3, \dots, N$)

$$1 = E_k + (1 - E_k).$$

Thus

$$\begin{aligned} E_i &= 1 \cdot 1 \cdot 1 \dots 1 \cdot E_i \cdot 1 \dots 1 = [E_1 + (1 - E_1)] \cdot [E_2 + (1 - E_2)] \cdot \\ &\dots [E_{i-1} + (1 - E_{i-1})] \cdot E_i \dots [E_N + (1 - E_N)]. \end{aligned} \quad (3)$$

In order to simplify the expression let us introduce the notation⁷

$$E_k = E_k^+, \quad 1 - E_k = E_k^- \quad (k = 1, 2, 3, \dots, N).$$

⁷ These symbols have been used by NEUMANN [3], pp. 217–8.

Let us denote the symbols $+$, $-$ collectively by $s_k \cdot s_k = +$ or $s_k = -$, and these symbols can occur in the k 'th factor of the following expression obtained from (3) in a straightforward manner

$$E_i = \sum_{\varepsilon_k = \pm} \prod_{j=1}^N E_j^{s_j} \quad (s_i = +). \quad (4)$$

The summation must be extended to every possible combination of the symbols $+$ and $-$, keeping thereby $s_i = +$. Let us denote the n 'th term on the right hand side of (4) by F_n . The number of the F_n 's is evidently equal to 2^N , the number of ways in which the symbols $+$ and $-$ can be distributed over N factors. Evidently also zeros can occur among the F_n 's. Now it is easily verified that the F_n 's satisfy the orthogonality relations (2'). Namely, if $i \neq k$, the only difference between F_i and F_k can be that there exists a subscript m with the property that while in the m 'th factor of F_i E_m or E_m^- stands, in the m 'th factor of F_k E_m^- or E_m stands, respectively. However, as

$$E_m \cdot E_m^- \equiv E_m^- \cdot E_m \equiv 0, \quad (5)$$

(2') can be satisfied by means of (3). Here we made use of the fact that the E_i 's commute, which means that the macroscopical properties ε_i can be measured simultaneously. This is just a consequence of the *macroscopical* character of these properties. Naturally by (1)

$$\sum_{n=1}^{2N} F_n = \sum_{i=1}^N E_i = 1.$$

Consequently, we can say that the method of measuring of the macroscopical observer can be characterized by the set $\{E_i\}$ of operators satisfying the conditions (1) and (2). Such sets will be called in the following *normalized*. Consequently, the normalized set $\{E_i\}$ determines completely the probability distribution e_i of the mixture having the statistical operator U

$$e_i = \text{Trace } UE_i, \quad (6)$$

and by (1) for such e_i 's

$$\sum_{i=1}^N e_i = 1. \quad (7)$$

Thus it is essentially this discrete probability distribution that characterizes the view-points of the macroscopical observer. As to the gauge of the uncertainty in the value of the probability variable e_i — which is characteristic of the methods of the observer — it is suitable to choose the mathematical entropy of the distribution e_i

$$\text{Entr } (S) = - K \sum_{i=1}^N e_i \log e_i, \quad (8)$$

$(K > 0, \text{constant}).$

There remains the question, how the entropy (8) belonging to the set $\{E_i\}$ can be compared with the entropy of the set $\{E_i\}'$ obtained from the set $\{E_i\}$ by replacing the j 'th property by a consequence of it belonging to the projection operator E'_j ; that is, replacing E_j by such an E'_j for which

$$E_j \cdot E'_j = E_j. \quad (9)$$

This problem will be investigated in the next section.

3. The replacement of the macroscopical property

Let us now consider the case when the macroscopical observer wants to obtain information about the ensemble with the statistical operator U^8 in such a way that instead of investigating the j 'th property ε_j he investigates the weaker property ε'_j . This method of observation can be represented instead of the set $\{\varepsilon_i\}$ by a set $\{\varepsilon_i\}'$, the difference between $\{\varepsilon_i\}$ and $\{\varepsilon_i\}'$ being that the j 'th property e_i in $\{\varepsilon_j\}$ is replaced by a consequence e'_i of it. Evidently the set $\{E_i\}'$ of projection operators belonging to $\{\varepsilon_j\}'$ will no longer have the properties (2.1) and (2.2), i.e. it will not be normalized. Thus although we can formally define the entropy of the corresponding set of probabilities $\{e_i\}'$, $\{e_i\}'$ is no longer a probability distribution and consequently the expression

$$-K \sum_{i=1}^N e_i \log e_i = K (e_1 \log e_1 + e_2 \log e_2 + \dots + e'_j \log e'_j + \dots + e_N \log e_N)$$

$$e'_j = \text{Trace } UE'_j$$

cannot be regarded as entropy and there is no reason for comparing it with the original expression

$$-K \sum_{i=1}^N e_i \log e_i.$$

Consequently, the set $\{E_i\}'$ must be orthogonalized and must be completed, i.e. by a procedure similar to that carried out in Section 2 a set $\{F_n\}$ must be assigned to it in a unique way for which

⁸ This is naturally possible, as U does not depend on the E_i 's.

$$\sum_{n=1}^M F_n = 1 \quad (M = 2^N)^9 \quad (1)$$

$$F_i \cdot F_k = 0 \quad (i \neq k). \quad (2)$$

The entropy can be constructed only for this normalized set $\{F_n\}$ by the definition

$$\text{Entr}'(S) = -K \sum_{n=1}^M f_n \log f_n,$$

where

$$f_n = \text{Trace } UF_n.$$

This will essentially be the entropy to be compared with $\text{Entr}(S)$ and for which we shall show¹⁰ that

$$\text{Entr}'(S) > \text{Entr}(S).$$

In order to do this, let us normalize the set $\{E_i\}$. Let us begin with the orthogonalization. Be

$$E_i = \sum_{s_1 \dots s_{i-1}, s_{i+1} \dots s_N = \pm} E_1^{s_1} \cdot E_2^{s_2} \cdot E_3^{s_3} \dots E_i \dots E_N^{s_N} \quad (i \neq j), \quad (3)$$

while for the case $i = j$

$$E'_j = \sum_{s_1 \dots s_{j-1}, s_{j+1} \dots s_N = \pm} E_1^{s_1} \cdot E_2^{s_2} \dots E'_j \dots E_N^{s_N}.$$

Denoting the expression to be summed by F_n ($n = 1, 2, 3, \dots, M = 2^N$) we have obtained the set $\{F_n\}$ which is the orthogonalization of the set $\{E_i\}'$. This set $\{F_n\}$ can, however, be simplified by taking into account that the set $\{E_i\}$ is normalized. Let us therefore introduce the notation

$$\begin{aligned} F(s_h, s_j) &= E_1^- E_2^- \dots E_{h-1}^- E_h^{s_h} E_{h+1}^- \dots E_{j-1}^- E_j^{s_j} E_{j+1}^- \dots E_{N-1}^- E_N^- \\ F(s_h, s_j, s_i) &= E_1^- E_2^- \dots E_{i-1}^- E_i^{s_i} E_{i+1}^- \dots E_{h-1}^- E_h^{s_h} E_{h+1}^- \dots E_{j-1}^- E_j^{s_j} E_{j+1}^- \dots \\ &\quad \dots E_{N-1}^- E_N^- \\ &\quad (i \neq j, h \neq j). \end{aligned} \quad (4)$$

⁹ We should essentially write $M = 2^N + 1$, where $F_M = 1 - \sum_{n=1}^{2^N} F_n$, but we shall see that this makes no essential difference.

¹⁰ With the difference that the summation should be extended from 1 to $2^N + 1$, where $f_{2^N+1} = 1 - \sum f_n$, but the statement for this case is a consequence of the statement (3).

It can be verified that the F_n 's of all the other types are zero, as if — apart from the j 'th factor — at least two + signs occur, the operator product is zero because of the orthogonality of the set $\{E_i\}$.¹¹ Thus if $s_h = +$, $s_i = -$, $i \neq j$, $h \neq j$,

$$F(+, s_j, +) = 0. \quad (5)$$

This simplification of the set $\{F_n\}$ can be expressed also in the form

$$E_i = \sum_{\substack{h \neq i \\ h \neq j}} F(-, +, +) + F(-, -, +) \quad (i \neq j). \quad (6)$$

We shall also need the relation

$$E_j = F(-, +) \quad (7)$$

corresponding to the case $i = j$.¹²⁻¹³ This may be proved as follows.

According to the definition

$$F(-, +) = F_1^- \dots E'_j \dots E_N^- = E'_j \prod_{i \neq j} E_i^- = E'_j \prod_{i \neq j} (1 - E_i),$$

where use has been made of the fact that E'_j commutes with the E_i 's.¹⁴ Thus it is sufficient to show that

$$\prod_{i \neq j} (1 - E_i) = E_j, \quad (7')$$

as in this case by $E'_j \cdot E_j = E_j \cdot E'_j = E_j$ the relation (7) follows immediately.

(7') expresses, however, a self-evident fact if we formulate it in terms of the decisions $\{\varepsilon_i\}$ belonging to the normalized set $\{E_i\}$. The corresponding statement for the ε_i 's is

$$\varepsilon_j = \bar{\varepsilon}_1 \& \bar{\varepsilon}_2 \& \dots \& \bar{\varepsilon}_{j-1} \& \bar{\varepsilon}_{j+1} \& \dots \& \bar{\varepsilon}_N. \quad (7'')$$

This is, however, certainly true, as any of the properties ε_i e.g. ε_j means that neither ε_1 nor ε_2 nor any of the ε_i 's different from ε_j is present. One of the ε_i 's must namely be present inevitably.

¹¹ Making use of the fact that the E_i 's commute among themselves and they also commute with E_j . Namely if E_i commutes with E_j and E_j commutes with E'_j , because of the transitivity of the commutabilities (cf. [3], p. 92.) also the E_i 's commute with E'_j : The commutability of E_j and E_j follows from the fact that $E'_j \cdot E_j$ is a hermitian operator (cf. [3], p. 51.).

¹² This is, naturally, independent of h , as in $F(-, +)$ apart from the j 'th term the symbol — stands in every term.

¹³ I express my thanks to my colleague R. TÖRÖS for the simplification of this proof.

¹⁴ Cf. footnote 11.

Finally, we shall need also the following relation: when $x_i > 0$, ($i = 1, 2, \dots, n$) and $\sum_{i=1}^n x_i < 1$,

$$\sum x_i \log \sum x_i > \sum x_i \log x_i. \quad (8)$$

Before proving the increase of the entropy we have to investigate the completeness of the set $\{F_n\}$. It can be seen, that the F_n 's obtained from (3.3) form already an orthogonal set, i.e. (3.2) is fulfilled,

$$F_i \cdot F_k = 0 \quad (i \neq k; \quad i, k = 1, 2, \dots, 2^N). \quad (9)$$

The set $\{F_n\}$ is, however, not complete, as

$$\begin{aligned} \sum_{n=1}^{2N} F_n &= E_1 + \dots + E'_j + \dots + E_N = \sum_{i=1}^N E_i - E_j + E'_j = \\ &= 1 - (E_j - E'_j) \neq 1, \end{aligned} \quad (10)$$

unless E'_j is not a trivial consequence of E_j , that is if $E'_j \neq E_j$. It has been shown in Section 2 that a set of projection operators representing the measurement of a macroscopical observer must be complete. Therefore the set $\{F_n\}$ must be completed by adding to it the term $F_{2N+1} = 1 - \sum_{n=1}^{2N} F_n$, for which (as can easily be shown)

$$F_n \cdot F_{2N+1} = F_{2N+1} \cdot F_n = 0 \quad (n = 1, 2, \dots, 2^N).$$

It is now this modified set for which the expression¹⁵

$$\begin{aligned} &- K \sum_{n=1}^{2N+1} f_n \log f_n, \\ &f_n = \text{Trace } UF_n \end{aligned}$$

must be regarded as entropy in the sense of Section 2, and this expression must be compared with the original expression

$$- K \sum_{i=1}^N e_i \log e_i.$$

This will be done in the following Section.

¹⁵ Cf. footnote 11.

4. The increase of the entropy

Making use of the relations (3.6) (3.7) and (3.8) it can easily be shown that

$$-K \sum_{n=1}^{2^N+1} f_n \log f_n > -K \sum_{i=1}^N e_i \log e_i. \quad (1)$$

As $-K < 0$, it is sufficient to show that

$$\sum_{n=1}^{2^N+1} f_n \log f_n < \sum_{i=1}^N e_i \log e_i$$

or what is the same, introducing the notation $f_{2^N+1} = 1 - \sum_{i=1}^{2^N} f_n = 1 - f$, it is sufficient to show that

$$\sum_{i=1}^{2^N} f_n \log f_n + (1-f) \log (1-f) < \sum_{i=1}^N e_i \log e_i.$$

Instead of this, however, we shall prove the stronger statement

$$\sum_{i=1}^{2^N} f_n \log f_n < \sum_{i=1}^N e_i \log e_i \quad (2)$$

which implies, because of $(1-f) \log (1-f) < 0$, the relation (1).

In order to prove (2) let us express the e_i 's in terms of the f_n 's, making use of (3.6).

$$e_i = \sum_{h \neq i} f_{hi},$$

$$(f_{hi} = \text{Trace } UF_{hi}, \quad F_{hi} = F \begin{pmatrix} -, & +, & + \\ (h) & (j) & (i) \end{pmatrix} + F \begin{pmatrix} -, & -, & + \\ (h) & (j) & (i) \end{pmatrix}).$$

Substituting this into (2) we obtain

$$\sum_{n=1}^{2^N} f_n \log f_n < \sum_{i=1}^N \left(\sum_{h \neq i} f_{hi} \right) \log \left(\sum_{h \neq i} f_{hi} \right), \quad (3)$$

$$(\sum f_{hj} = f_j = f(-, +) = \text{Trace } UF(-, +)).$$

Let us take now into account that of the f_n 's only the $f_{hi}(+)$'s and the $f_{hi}(-)$'s differ from zero: $f_{hi}(+) = \text{Trace } UF_{hi}(-, +, +)$, $f_{hi}(-) = \text{Trace } UF_{hi}(-, -, +)$

$$\sum_{h \neq j} f_{hj}(+) \log f_{hj}(+) = f_{hj}(+) \log f_{hj}(+),$$

$$\sum_{h \neq j} f_{hj}(-) \log f_{hj}(-) = 0.$$

Thus the left hand side of (3) can be decomposed into two parts

$$\sum_{n=1}^{2^N} f_n \log f_n = \sum_{i=1}^N \left[\sum_{h \neq i} f_{hi}(+) \log f_{hi}(+) + \sum_{h \neq i} f_{hi}(-) \log f_{hi}(-) \right].$$

Making use of this result it is sufficient to prove that

$$\begin{aligned} & \sum_{i=1}^N \left\{ \left[\sum_{h \neq i} f_{hi}(+) \log f_{hi}(+) + \sum_{h \neq i} f_{hi}(-) \log f_{hi}(-) \right] - \right. \\ & \left. - \left[\sum_{h \neq i} (f_{hi}(+) + f_{hi}(-)) \log \sum_{h \neq i} (f_{hi}(+) + f_{hi}(-)) \right] \right\} < 0 \end{aligned}$$

or what is the same

$$\begin{aligned} & \sum_{i=1}^N \left\{ \left[\sum_{h \neq i} (f_{hi}(+) \log f_{hi}(+) - \left(\sum_{h \neq i} f_{hi}(+) \right) \log \left(\sum_{h \neq i} f_{hi}(+) \right)) \right] + \right. \\ & \left. + \left[\sum_{h \neq i} f_{hi}(-) \log f_{hi}(-) - \left(\sum_{h \neq i} f_{hi}(-) \right) \log \left(\sum_{h \neq i} f_{hi}(-) \right) \right] \right\} < 0. \end{aligned}$$

This is, however, trivial because of (3.8).¹⁶

We have thus completed our task.

It should be noted that the probabilities $f_{1j}(+), f_{2j}(+), \dots$, and $f_{1j}(-), f_{2j}(-), \dots$ express the correlation of the set $\{E_i\}'$ in the sense that they measure the probability of the simultaneous occurrence of the properties ε'_j and $\bar{\varepsilon}'_j$, respectively, with one of the ε_i 's.

Acknowledgement

I express my thanks to Prof. I. FÉNYES for conversations during which the problems presented have been clarified.

¹⁶ Apart from the j 'th term all terms give a negative contribution to the sums $\sum_{h \neq i}$. In the case of the j 'th term we have (cf. footnote 5.):

$$\begin{aligned} \sum_{h \neq j} f_{hj}(\pm) \log \sum_{h \neq j} f_{hj}(\pm) &= \sum_{h \neq j} f_{hj}(\pm) \log f_{hj}(\pm) = \\ &= f_{hj}(\pm) \log f_{hj}(\pm) - f_{hj}(\pm) \log f_{hj}(\pm) = 0. \end{aligned}$$

Naturally in the sums $\sum_{h \neq j}$ the value $h \neq j$ does not occur.

REFERENCES

1. I. FÉNYES, M. T.A. Mat. Kut. Int. Közl., to be published.
2. L. SZILÁRD, Z. Phys., **53**, 840, 1929.
3. J. NEUMANN, Mathematische Grundlagen der Quantenmechanik, Springer, Berlin, 1932.
4. R. CARNAP, Physikalische Begriffsbildung, Karlsruhe, 1926.
5. D. HILBERT and P. BERNAYS, Grundlagen der Mathematik. I. pp. 53—60, Springer, Berlin, 1934.
6. J. BALATONI and A. RÉNYI, M. T. A. Mat. Kut. Int. Közl., **1**, 9, 1956.
7. L. BRILLOUIN, Science and Information Theory. pp. 115, 122, 152, 153, 170. (Academic Press, New York, 1956).
8. N. I. ACHIESER and I. M. GLASSMANN, Theorie der linearen Operatoren im Hilbert-Raum. Akademie Vlg., Berlin, 1954.

ЗАМЕЧАНИЯ К КВАНТОВОМЕХАНИЧЕСКОМУ РАССМОТРЕНИЮ
ПАРАДОКСА ГИББСА

Д. ФАИ

Р е з ю м е

На основе дедуктивного построения квантовой теории, разработанного Найманном, и также с помощью оценивающего вычисления квантовой теории доказывается, что квантовомеханическая энтропия любого физического свойства возрастает при замещении данного свойства более слабым в логическом смысле.

NEW ALPHA-DECAY BARRIER PENETRABILITIES WITH ICO POTENTIAL: EVEN- AND ODD-MASS NUCLEI

By

L. KOHLMANN and T. VÖRÖS

CENTRAL RESEARCH INSTITUTE FOR PHYSICS, BUDAPEST

(Presented by L. Jánossy. — Received 8. VI. 1964)

The Igo potential is used for the calculation of barrier penetrabilities for ground and excited state transitions of even mass nuclei and for transitions of odd-mass nuclei, measured after 1959. The barrier penetration factors were calculated by numerical integration in the WKB approximation, taking into account centrifugal barrier effects for even-even nuclei, but ignoring noncentral interactions. Using the calculated penetration factors and the experimental alpha half-lives, the reduced level widths were calculated in each case. Hindrance factors for odd-mass alpha-particle emitters are also given.

Introduction

In 1959 RASMUSSEN [1], [2] discussed in detail the calculation of alpha-decay barrier penetration factors using Igo potential and gave numerical results for all known ground and excited-state transitions of even-even nuclei and for alpha decay groups of odd-mass nuclei. Since then a lot of experimental data have been collected which require the calculation of penetration factors and reduced widths.

Like in RASMUSSEN's paper, the nuclear potential used here is the real part of the potential derived by Igo [3] from data on elastic scattering of alpha particles of 10 MeV, and valid in the surface region. The potential is of the form

$$V(r) = -1100 \exp \left\{ - \left[\frac{r - 1,17 A^{1/3}}{0,574} \right] \right\} \text{MeV},$$

where r is the distance in fermis and A is the mass number of the daughter nucleus.

Method of calculation

As is well known [4], the natural logarithm of the penetration factor P equals the WKB integral

$$-I = -\frac{(8M)^{1/2}}{\hbar} \int_{R_i}^{R_o} \left[V(r) + \frac{2Ze^2}{r} + \frac{\hbar l(l+1)}{2Mr^2} - E \right]^{1/2} dr$$

Table I

Variation in the values of
 I and P with the number of intervals

Calculated results		
Number of intervals n	I	Barrier penetration factors ^a P
112	72,7284	2,60 (-32)
224	72,7246	2,61 (-32)
336	72,7237	2,61 (-32)
448	72,7233	2,61 (-32)

^a The number in parentheses is the power of ten by which the preceding number is to be multiplied.

evaluated between the inner and outer classical turning points, where the integrand vanishes. Here $M = \frac{M_a M_r}{M_a + M_r}$ is the reduced mass of the system, Z_e is the charge of the daughter nucleus, l is the orbital angular momentum of the alpha particle emitted and E is the total decay energy, i.e., alpha-particle energy, plus electron-screening correction given by $E_{sc} = 65,3(Z+2)^{7/5} - 80(Z+2)^{2/5}$ eV, plus recoil energy $E_{rc} = \frac{E_a M_a}{M_r}$. The exact value for M_a , 4,00278 a. m. u. is from AJZENBERG and LAURITSEN's [5] measurement on the mass of the He atom, for M_r JELEPOV and PEKER's data [6] are used. The numerical constants were taken from the paper by COHEN—DU MOND—LAYTON—ROLLETT [7].

Numerically the integrations were carried out on an Ural I type electronic computer. The outer and the inner turning points were found by Newton iteration. The barrier integral was evaluated by a Gauss quadrature with the barrier region divided into 336 intervals.

Table II
Calculated results for an error of 10 keV

Experimental data			Calculated results				
α -particle energy with screening + recoil corrections (MeV)	Partial half-life for α decay	α -group intensity %	R_i (fermis)	R_o (fermis)	I	Barrier penetration factor P	Reduced width δ^2 (MeV)
5,165	1,482 (13)	100	9,525	52,409	75,467	1,68 (-33)	0,115
5,175			9,525	52,308	75,315	1,95 (-33)	0,0989
5,185			9,525	52,207	75,163	2,27 (-33)	0,0850

Table III
Ground-state transitions of even-even nuclei

Experimental data					Calculated results		
Atomic No. <i>Z</i>	Mass No. <i>A</i>	α -particle energy with screening + recoil corrections (MeV)	Partial half-life for α -decay (sec)	α -group intensity %	R_t (fermis)	Barrier penetration factor <i>P</i>	Reduced width δ^a (MeV)
86	216	8,194	1,67 (-3)	100	9,35	2,65 (-16)	0,00649
88	220	7,602	0,03	100	9,35	7,98 (-19)	0,120
94	234	6,335	3,24 (4)	100	9,42	3,36 (-26)	0,263
94	244	4,663	2,396 (15)	100	9,48	5,41 (-36)	0,221
96	238	6,649	9,00 (3)	100	9,46	1,28 (-25)	2,49
96	240	6,392	2,316 (6)	70	9,47	9,09 (-27)	0,0874
96	246	5,500	1,261 (11)	100	9,51	2,01 (-31)	0,113
96	248	5,185	1,482 (13)	100	9,53	2,27 (-33)	0,0850
98	244	7,330	1,50 (3)	100	9,52	1,50 (-23)	0,128
98	246	6,905	1,285 (5)	78	9,53	2,92 (-25)	0,0595
98	248	6,372	2,938 (7)	82	9,54	1,14 (-27)	0,0700
100	250	7,592	1,800 (3)	100	9,58	2,78 (-23)	0,0573
100	252	7,205	1,08 (5)	100	9,59	8,94 (-25)	0,0297

In the case of $^{94}\text{Pu}^{240}$ (α -particle energy with screening correction $E_a + E_{sc} = 5,202$ MeV) the variation of *I* and *P* with the interval number *n* was investigated. In Table I some typical data are given for *n* = 112, 224, 336, 448. With the barrier region divided into 336 intervals, it may be seen that the values of *I* are in agreement to three figures.

The dependence of the penetration factor on the experimental error of alpha particle energy was investigated. Assuming after HANNA [8] an experimental error of 10 kev for an alpha particle of an energy of 5 MeV the case of $^{96}\text{Cm}^{248}$ (with $E_a + E_{sc} + E_{rc}$) was studied. The results are shown

Table IV
Excited state transitions

Atomic No. <i>Z</i>	Mass No. <i>A</i>	Experimental data				Calculated results	
		α -particle energy with screening + recoil corrections (MeV)	Partial half-life for α -decay (sec)	α -group intensity (%)	Spin and parity	Barrier penetration factor <i>P</i>	Reduced width δ^a (MeV)
94	240	5,044	2,075 (11)	3,1 (-3)	6+	6,24 (-35)	0,00686
98	246	6,862	1,285 (5)	22	2+	1,16 (-25)	0,0423

in Table II. The fact is that a change of 10 kev in the value of E causes change in the first figure in I . So the required accuracy of two figures in the integration is greater than that required by the experimental accuracy of E .

Let us now do the calculation of the reduced alpha emission width δ^2 using the experimental decay rate data from the following expression

$$\lambda = \frac{P\delta^2}{h},$$

where λ is the decay constant and h is Planck's constant.

Results

Table III lists the data used for even-even nuclei taken from [9], and the calculated results. The results were calculated with total decay energy ($E_a + E_{sc} + E_{rc}$). The Tables are of the same form as that of RASMUSSEN. The calculated quantities are R_i , P and δ^2 .

The calculated results are consistent with those of RASMUSSEN's and complete RASMUSSEN's Tables.

Table IV presents the results of the calculations on excited-state transitions of even-even nuclei. Only two data are given here, taken from [9].

Table V lists for odd-odd nuclei the results of the calculations on excited and ground state transitions. The experimental data were taken from [9—10]. Here the penetration factors were calculated with $l = 0$.

Table VI shows the result of the calculations for transitions of odd-mass nuclei. The experimental data used are taken from [9, 11—14]. The penetration factors of odd-mass nuclei are calculated with $l = 0$, as by RASMUSSEN. The reason for this is that one usually expects a mixture of two or more l values in the alpha groups of odd nuclei that are generally not known from experiments.

Table VI also lists the hindrance factor F , expressed by

$$F = \frac{\delta_1^2 + \delta_2^2}{2\delta_{odd}^2},$$

where δ_1^2 and δ_2^2 are the reduced widths for ground-state transitions of the nearest-neighbour even-even nuclei. In cases where the data for one or both of the nearest even-even neighbours are unknown, the next available data have been taken to calculate F .

Table V
Alpha groups of odd-odd nuclei

Atomic No. <i>Z</i>	Mass No. <i>A</i>	Neutron No. <i>N</i>	α -particle energy with screening + recoil correction (MeV)	Partial half-life for α -decay (sec)	α -group intensity (%)	Barrier penetration factor <i>P</i>	Reduced width δ^2 (MeV)
						Calculated results	
	Experimental data						
85	214	129	8,979	3,33 (-2)	100	6,35 (-14)	0,135 (-5)
	216	131	7,969	5,00 (-3)	100	1,44 (-15)	0,00397
	218	133	6,786	1,5	100	1,83 (-20)	0,105
87	218	131	8,030	8,33 (-2)	100	3,97 (-17)	0,000866
	220	133	6,847	27,5	100	4,46 (-21)	0,0234
89	222	133	7,123	5,5	100	7,14 (-21)	0,0730
	224	135	6,317	1,044 (4)	100	4,19 (-24)	0,0655
91	226	135	6,969	108	100	2,97 (-22)	0,0892
	228	137	6,284	7,920 (4)	2,5	4,00 (-25)	0,00226
			6,259		10,5	3,07 (-25)	0,0124
			6,246		12,0	2,67 (-25)	0,0163
			6,232		2,3	2,30 (-25)	0,00363
			6,218		20,7	1,97 (-25)	0,0379
			6,206		1,0	1,73 (-25)	0,00209
			6,181		2,3	1,32 (-25)	0,00630
			6,168		9,0	1,15 (-25)	0,0284
			6,150		0,8	9,42 (-26)	0,00307
			6,137		0,3	8,17 (-26)	0,00307
			6,128		1,1	7,40 (-26)	0,00538
			6,121		2,8	6,85 (-26)	0,0148
			6,114		2,7	6,34 (-26)	0,0154
			6,085		0,6	4,59 (-26)	0,00473
			6,179		0,5	4,29 (-26)	0,00422
			6,060		0,8	3,47 (-26)	0,00835
			6,044		1,1	2,90 (-26)	0,0137
			6,011		1,4	1,99 (-26)	0,0254
			5,995		0,3	1,66 (-26)	0,00653
			5,979		0,4	1,38 (-26)	0,0105
			5,941		7,3	8,93 (-27)	0,296
			5,935		11,3	8,33 (-27)	0,491
			5,914		1,4	6,52 (-27)	0,0777
			5,900		2,0	5,54 (-27)	0,131
			5,895		1,4	5,22 (-27)	0,0970
			5,891		2,5	4,98 (-27)	0,182
			5,845		1,0	2,89 (-27)	0,125
97	240	147	6,820	1,584 (4)	100	3,26 (-25)	0,556
99	246	147	7,512	4,2 (2)	100	3,08 (-23)	0,221
	248	149	7,023	1,5 (3)	100	3,63 (-25)	5,27
	252	153	6,787	1,210 (7)	100	4,02 (-26)	0,00590

Table VI
Alpha groups of odd-odd nuclei

Experimental data					Calculated results			
Atomic No. <i>Z</i>	Mass No. <i>A</i>	Neutron No. <i>N</i>	α -particle energy (MeV) $E_\alpha + E_{\text{sc}} + E_{\text{rec}}$	Partial half-life for α decay (sec)	α -group intensity %	Barrier penetration factor <i>P</i>	Reduced width δ^2 (MeV)	Hindrance factor <i>F</i>
85	213	128	9,408	2	100	6,00 (-13)	0,239 (-8)	0,382 (-8)
86	215	129	8,796	1,67 (-2)	100	1,03 (-14)	0,166 (-4)	0,353 (4)
87	217	130	8,489	2	100	7,63 (-16)	0,188 (-5)	0,375 (6)
	221	134	6,482	2,88 (2)	84	1,62 (-22)	0,517 (-1)	3,11
			6,262		16	1,84 (-23)	0,867 (-1)	1,86
88	213	125	7,066	1,62 (2)	100	8,09 (-21)	0,219 (-2)	0,281 (2)
	219	131	8,183	1,67 (-2)	100	4,80 (-17)	0,359 (-2)	0,616 (2)
	223	135	6,008	1,011 (6)	1	4,55 (-25)	0,624 (-4)	0,228 (4)
			5,994		0,3	3,90 (-25)	0,210 (-4)	0,0674 (5)
			5,971		0,5	3,02 (-25)	0,468 (-5)	0,303 (5)
			5,881		10,5	1,10 (-25)	0,270 (-2)	0,526 (2)
			5,850		50	7,74 (-26)	0,183 (-1)	0,0775 (2)
			5,738		24	2,11 (-26)	0,323 (-1)	0,420 (1)
			5,669		10,3	9,27 (-27)	0,315 (-1)	0,507 (1)
			5,631		0,9	5,86 (-27)	0,436 (-2)	0,326 (2)
			5,562		2,4	2,51 (-27)	0,271 (-1)	0,524 (1)
			5,492		0,2	1,05 (-27)	0,542 (-2)	0,262 (2)
			5,465		0,07	7,43 (-28)	0,267 (-2)	0,532 (2)
89	223	134	6,814	1,32 (2)	40	4,92 (-22)	0,177 (-1)	0,0803 (2)
			6,800		46	4,33 (-22)	0,231 (-1)	0,0617 (2)
			6,716		14	1,99 (-22)	0,153 (-1)	0,0932 (2)
	225	136	5,958	8,64 (5)	54	9,22 (-26)	0,194 (-1)	0,744 (1)
			5,922		30,7	6,13 (-26)	0,166 (-1)	0,871 (1)
			5,860		8,1	3,01 (-26)	0,891 (-2)	0,162 (2)
			5,851		2,1	2,72 (-26)	0,256 (-2)	0,564 (2)
			5,810		0,95	1,69 (-26)	0,187 (-2)	0,773 (2)
			5,764		2,9	9,80 (-27)	0,982 (-2)	0,147 (2)
			5,735		0,5	6,94 (-27)	0,239 (-2)	0,605 (2)
			5,706		0,6	4,90 (-27)	0,406 (-2)	0,356 (2)
			5,678		0,08	3,49 (-27)	0,760 (-3)	0,191 (3)
227	138	5,073	6,938 (8)	48,7	1,26 (-30)	0,160 (1)	0,863 (-1)	
		5,060		36,1	1,04 (-30)	0,143 (1)	0,0962	
		4,988		6,9	3,62 (-31)	0,788	0,178	
		4,971		5,5	2,81 (-31)	0,809	0,171	

Table VI (continued)

Atomic No. Z	Mass No. A	Neutron No. N	Experimental data		Calculated results			
			α -particle energy (MeV) $E_{\alpha} + E_{se} +$ $+ E_{rec}$	Partial half-life for α decay (sec)	α -group intensity %	Barrier penetration factor P	Reduced width δ^2 (MeV)	Hindrance factor F
90	223	133	4,907		1,0	1,07 (-31)	0,386	0,358
			4,879		1,8	6,98 (-32)	0,107 (1)	0,129
			4,848		0,1	4,32 (-32)	0,956 (1)	0,145 (1)
			4,823		0,4	2,93 (-32)	0,564	0,245
			4,633		0,2	1,36 (-33)	0,605 (1)	0,228 (-1)
			7,723	0,1	100	3,48 (-19)	0,823 (-9)	0,173 (9)
			6,679	2,298 (3)	2,3	2,08 (-23)	0,138 (-2)	0,0871 (3)
			6,668		0,3	1,87 (-23)	0,200 (-3)	0,600 (3)
			6,612		49,5	1,08 (-22)	0,569 (-1)	0,211 (1)
			6,569		11,5	7,11 (-24)	0,202 (-1)	0,594 (1)
91	227	136	6,561		14,8	6,56 (-24)	0,281 (-1)	0,427 (1)
			6,547		9,3	5,71 (-24)	0,203 (-1)	0,591 (1)
			6,521		2,6	4,41 (-24)	0,736 (-2)	0,163 (2)
			6,501		7,8	3,61 (-24)	0,270 (-1)	0,445 (1)
			6,481		0,7	2,95 (-24)	0,296 (-2)	0,405 (2)
			6,470		0,4	2,64 (-24)	0,189 (-2)	0,635 (2)
			6,443		0,8	2,00 (-24)	0,498 (-2)	0,241 (2)
			5,802	1,296 (5)	19,1	1,81 (-27)	0,234 (1)	0,528 (-1)
			5,761		9,8	1,10 (-27)	0,197 (1)	0,627 (-1)
			5,746		13,4	9,17 (-28)	0,323 (1)	0,382 (-1)
229	138	138	5,721		4,7	6,75 (-28)	0,154 (1)	0,802 (-1)
			5,710		36,8	5,90 (-28)	0,138 (2)	0,0891 (-1)
			5,695		39	4,90 (-28)	0,176 (1)	0,0701 (-1)
			5,665		8,9	3,37 (-28)	0,583 (1)	0,211 (-1)
			5,646		0,6	2,66 (-28)	0,499	0,248
			5,630		0,74	2,18 (-28)	0,752	0,164
			5,607		1,77	1,63 (-28)	0,241 (1)	0,514 (-1)
			5,549		0,07	7,75 (-29)	0,200	0,618
			5,542		0,15	6,90 (-29)	0,481	0,257
			5,446		0,05	2,02 (-29)	0,549	0,225
231	140	140	5,170	1,082 (12)	11,0	4,85 (-31)	0,601 (-3)	0,198 (3)
			5,142		2,5	3,23 (-31)	0,205 (-3)	0,584 (3)
			5,140		20	3,14 (-31)	0,169 (-2)	0,708 (2)
			5,123		25,4	2,45 (-31)	0,274 (-2)	0,436 (2)
			5,096		1,4	1,65 (-31)	0,225 (-3)	0,531 (3)
			5,084		0,4	1,38 (-31)	0,766 (-4)	0,156 (4)

Table VI (continued)

Experimental data					Calculated results			
Atomic No.	Mass No. <i>A</i>	Neutron No. <i>N</i>	α -particle energy (MeV) $E_\alpha + E_{se} + E_{rec}$	Patrial half-life for α decay (sec)	α -group intensity %	Barrier penetration factor <i>P</i>	Reduced width δ^2 (MeV)	Hindrance factor <i>F</i>
93	237	144	5,061		22,8	9,84 (-32)	0,614 (-2)	0,195 (2)
			5,043		3,0	7,53 (-32)	0,106 (-2)	0,113 (3)
			5,009		2 (-3)	4,52 (-32)	0,117 (-5)	0,102 (6)
			4,960		1,4	2,14 (-32)	0,173 (-2)	0,690 (2)
			4,901		4 (-2)	8,59 (-33)	0,123 (-3)	0,0970 (4)
			4,943		8,4	3,44 (-33)	0,647 (-1)	0,184 (1)
			4,818		1	2,31 (-33)	0,115 (-1)	0,104 (2)
			4,785		1,5	1,36 (-33)	0,293 (-1)	0,408 (1)
			4,748		1 (-1)	7,41 (-34)	0,357 (-2)	0,334 (2)
			4,735		1 (-1)	5,99 (-34)	0,443 (-2)	0,270 (2)
			4,703		1,5 (-2)	3,52 (-34)	0,113 (-2)	0,106 (3)
			4,669		8,0 (-3)	1,99 (-33)	0,106 (-2)	0,113 (3)
			4,609		3 (-3)	7,18 (-34)	0,111 (-2)	0,108 (3)
			4,993	7,096 (13)	0,441	3,47 (-33)	0,513 (-4)	0,177 (4)
			4,991		0,925	3,37 (-33)	0,111 (-3)	0,0819 (4)
			4,982		0,242	2,93 (-33)	0,334 (-4)	0,272 (4)
			4,936		1,487	1,42 (-33)	0,423 (-3)	0,215 (3)
			4,921		1,565	1,12 (-33)	0,564 (-3)	0,161 (3)
			4,906		51,42	8,82 (-34)	0,236 (-1)	0,385 (1)
			4,889		19,38	6,72 (-34)	0,118 (-1)	0,0777 (2)
			4,883		16,82	6,10 (-34)	0,111 (-1)	0,0819 (2)
			4,858		0,119	4,07 (-34)	0,188 (-4)	0,482 (4)
			4,829		0,126	2,54 (-34)	0,200 (-3)	0,453 (3)
			4,825		0,293	2,38 (-34)	0,497 (-3)	0,182 (3)
			4,816		0,067	2,05 (-34)	0,132 (-3)	0,0688 (4)
94	239	145	4,811		0,178	1,89 (-34)	0,380 (-3)	0,170 (3)
			4,780		1,605	1,13 (-34)	0,573 (-2)	0,159 (2)
			4,775		0,573	1,04 (-34)	0,222 (-2)	0,409 (2)
			4,775		4,617	7,46 (-35)	0,250 (-1)	0,363 (1)
			4,713		0,063	3,67 (-35)	0,693 (-3)	0,131 (3)
			4,710		0,085	3,49 (-35)	0,984 (-3)	0,0922 (3)
			4,696		0,024	2,75 (-35)	0,353 (-3)	0,257 (3)
			4,688		0,054	2,40 (-35)	0,910 (-3)	0,0997 (3)
			4,628		0,01	8,49 (-36)	0,476 (-3)	0,191 (3)
			4,497		0,02	8,18 (-37)	0,988 (-2)	0,0922 (2)
94	239	145	5,282	7,569 (11)	73,3	8,03 (-32)	0,346 (-1)	0,268 (1)

Table VI (continued)

Experimental data				Calculated results				
Atomic No. <i>Z</i>	Mass No. <i>A</i>	Neutron No. <i>N</i>	α -particle energy (MeV) $E_\alpha + E_{\text{ge}} + E_{\text{rec}}$	Partial half-life for α decay (sec)	α -group intensity %	Barrier penetration factor <i>P</i>	Reduced width δ^2 (MeV)	Hindrance factor <i>F</i>
95	241	146	5,270		1,5	6,75 (-32)	0,847 (-2)	0,110 (2)
			5,231		11,5	3,83 (-32)	0,114 (-1)	0,816 (1)
			5,201		3,2 (-2)	2,47 (-32)	0,492 (-4)	0,189 (4)
			5,189		9 (-4)	2,06 (-32)	0,165 (-5)	0,562 (5)
			5,179		2,1 (-2)	1,78 (-32)	0,447 (-4)	0,208 (4)
			5,154		5 (-3)	1,23 (-32)	0,154 (-4)	0,601 (4)
			5,132		8 (-3)	8,81 (-33)	0,344 (-4)	0,270 (4)
			5,123		6 (-4)	7,69 (-33)	0,295 (-5)	0,314 (5)
			5,110		5 (-3)	6,32 (-33)	0,300 (-4)	0,309 (4)
			5,084		3 (-3)	4,25 (-33)	0,267 (-5)	0,347 (4)
			5,078		5 (-4)	3,88 (-33)	0,488 (-5)	0,190 (5)
			5,058		3 (-3)	2,85 (-33)	0,398 (-4)	0,233 (4)
			5,035		8 (-4)	2,00 (-33)	0,151 (-4)	0,613 (4)
			4,993		7 (-4)	1,04 (-33)	0,255 (-4)	0,363 (4)
			4,988		7 (-4)	9,59 (-34)	0,276 (-4)	0,336 (4)
			4,949		1,5 (-3)	5,17 (-34)	0,110 (-3)	0,846 (3)
			4,920		6 (-4)	3,25 (-34)	0,699 (-4)	0,133 (4)
			4,861		2,6 (-3)	1,25 (-34)	0,789 (-3)	0,118 (3)
			4,857		2,6 (-3)	1,17 (-34)	0,842 (-3)	0,110 (3)
			4,812		4 (-4)	5,56 (-35)	0,273 (-3)	0,340 (3)
			4,752		2 (-4)	2,03 (-35)	0,373 (-3)	0,248 (3)
			5,675	1,454 (10)	0,25	5,66 (-30)	0,872 (-4)	0,101 (4)
			5,641		0,12	3,62 (-30)	0,653 (-4)	0,135 (4)
			5,716		86	9,62 (-30)	0,176 (-1)	0,501 (1)
			5,598		0,04	2,05 (-30)	0,385 (-4)	0,230 (4)
			5,572		12,7	1,45 (-30)	0,173 (-1)	0,512 (1)
			5,545		1 (-2)	1,01 (-30)	0,196 (-4)	0,451 (4)
			5,516		1,33	6,80 (-31)	0,386 (-2)	0,229 (2)
			5,448		1,5 (-2)	2,67 (-31)	0,111 (-3)	0,797 (3)
			5,418		1 (-4)	1,76 (-31)	0,124 (-5)	0,715 (5)
			5,404		5 (-4)	1,44 (-31)	0,683 (-5)	0,129 (5)
			5,399		3 (-4)	1,34 (-31)	0,440 (-5)	0,200 (5)
			5,368		2,4 (-3)	8,67 (-32)	0,546 (-4)	0,162 (4)
			5,348		1,3 (-3)	6,52 (-32)	0,393 (-4)	0,224 (4)
			5,318		6 (-4)	4,24 (-32)	0,279 (-4)	0,316 (4)
			5,305		9 (-4)	3,51 (-32)	0,505 (-4)	0,175 (4)
			5,301		3 (-4)	3,32 (-32)	0,178 (-4)	0,495 (4)
			5,280		7 (-4)	2,44 (-32)	0,565 (-4)	0,157 (4)
			5,262		3 (-4)	1,88 (-32)	0,315 (-4)	0,280 (4)
			5,237		4 (-4)	1,30 (-32)	0,606 (-4)	0,146 (4)
			5,223		7 (-4)	1,06 (-32)	0,131 (-3)	0,677 (3)
			5,217		3 (-4)	9,67 (-33)	0,612 (-4)	0,144 (4)
			5,210		3 (-4)	8,72 (-33)	0,679 (-4)	0,130 (4)
99	247	148	7,511	4,380 (2)	100	3,19 (-23)	0,205	0,250

Conclusion

The present investigation gives a great number of new data on barrier penetrability collected since the excellent papers of RASMUSSEN were published. They complete RASMUSSEN's Tables for the ground and excited state transitions of even- and odd-mass nuclei and offer a possibility for new investigations of odd-odd nuclei, which have not been dealt with by RASMUSSEN.

Acknowledgements

The authors are indebted to Dr. T. SIKLÓS and Dr. I. TÓTH for their helpful discussions, further to Mr. G. KRAMMER for furnishing the Gauss-subroutine.

LITERATURE

1. J. O. RASMUSSEN, Phys. Rev., **113**, 1593, 1959.
2. J. O. RASMUSSEN, Phys. Rev., **115**, 1675, 1959.
3. G. IGO, Phys. Rev. Letters, **1**, 72, 1958.
4. I. PERLMAN and J. O. RASMUSSEN, in Handbuch der Physik (Springer Verlag, Berlin, 1957). Vol. 42.
5. F. AJZENBERG and T. LAURITSEN, Rev. Mod. Phys., **24**, 321, 1952.
6. B. S. JELEPOV and L. K. PEKER: Decay schemes of radioactive nuclei. Izd. A. N. Soviet Union, Moscow—Leningrad, 1958.
7. E. R. COHEN, J. W. M. DUMOND, T. W. LAYTON and J. S. ROLLETT, Rev. Mod. Phys., **27**, 363, 1955.
8. G. C. HANNA, Alpha-Radioactivity Experimental Nuclear Physics Vol. III. New York, 1959.
9. LANDOLT—BÖRNSTEIN New Series: Energy Levels of Nuclei A = 5 to A = 257, Springer-Verlag, Berlin—Göttingen—Heidelberg, 1961.
10. B. S. JELEPOV, R. B. IVANOV and L. N. MOSKVEN, JETP, **43**, 2077, 1962.
11. S. A. BARANOV, V. M. KULAKOV, A. G. ZELENKOV and V. M. SASINSKI, JETP, **43**, 1135, 1962.
12. S. A. BARANOV, V. M. KULAKOV and S. N. BELENKI, JETP, **43**, 1135, 1962.
13. S. A. BARANOV, V. M. KULAKOV, P. S. SAMOILOV, A. G. ZELENKOV, U. F. RADIONOV and S. V. PERESKOV, JETP, **41**, 1475, 1961.
14. S. A. BARANOV, V. M. KULAKOV, P. S. SAMOILOV, A. G. ZELENKOV and U. F. RADIONOV, JETP, **41**, 1733, 1961.

НОВАЯ ПРОХОДИМОСТЬ ЧЕРЕЗ ПОТЕНЦИАЛЬНЫЙ БАРЬЕР
С ПОТЕНЦИАЛОМ ИГО ПРИ α -РАСПАДЕ: ЧЁТНЫЕ И НЕЧЁТНЫЕ ЯДРА

Л. КОЛЬМАНН и Т. ВЕРЕШ

Р е з ю м е

Потенциал Иго используется при определении проходимости через потенциальный барьер для переходов чётных и нечётных ядер в основное и возбуждённые состояния, измеренных после 1959 г. Фактор проходимости через потенциальный барьер определялся численным интегрированием в приближении ВКБ, принимающем во внимание центробежный барьерный эффект чётно-чётных ядер, пренебрегая нецентральным взаимодействием. Используя полученный фактор проходимости и экспериментальное значение периода полураспада α -частиц, в каждом случае определяется уменьшенная ширина уровней. Приводятся также и барьерные факторы для излучателей α -частиц с нечётной массой.

INVESTIGATION OF Mo⁹²(n, 2n)Mo^{91,91m} REACTION

By
J. BACSÓ, J. CSIKAI

INSTITUTE OF NUCLEAR RESEARCH OF THE HUNGARIAN ACADEMY OF SCIENCES, DEBRECEN
and

A. PÁZSIT

INSTITUTE FOR EXPERIMENTAL PHYSICS, KOSSUTH UNIVERSITY, DEBRECEN

(Presented by A. Szalay. — Received 24. IX. 1964)

The occurrence of Mo⁹²(n, 2n)Mo^{91m} reaction has been demonstrated at 14,8 MeV neutron energy and the isomeric cross-section ratio $\frac{\sigma_g}{\sigma_m} = 10,6$ has been determined. For the reactions Mo⁹²(n, 2n)Mo^{91g,91m} the cross-section values $\sigma_g = 159$ mb, $\sigma_m = 15$ mb were found.

Introduction

Previous investigations of (γ , n) and (n, 2n) reactions in Mo⁹² nuclei [1, 2, 3, 4, 5] have shown that no short-life (nearly 1 minute) isomeric state of Mo⁹¹ will be produced by an (n, 2n) reaction [3], whereas in (γ , n) reaction at energy $E_\gamma = 14,5$ MeV the cross-section ratio of isomeric and ground states has been found to be 0,2 [4].

For the (n, 2n) reaction, the activity of the short half-life isomeric state was found only in traces at a bombarding neutron energy of even 18 MeV [4]. The threshold energy of the process (13,2 MeV) [6] permits to produce a level of 658 keV above the ground state at a bombarding neutron energy of 14,8 MeV. The purpose of our investigations has been to demonstrate the existence of the above mentioned isomeric state under the conditions of (n, 2n) reaction at an energy of 14,8 MeV, and to determine the isomer cross-section ratio (σ_g/σ_m).

Measurement and evaluation

Natural Mo metal was irradiated for 3 minutes by neutrons produced in D + T reaction at a bombarding energy of $E_d = 250$ keV. The beta activity of the foil was measured by an end-window GM counter. The decay curve obtained is shown in Fig. 1. By analysing the complex decay curve, components with the following half lives were obtained: 60,5 hours, 74 minutes, 15,7 minutes, 60,4 seconds.

In addition to the 15,7 minute half life (pertaining to the ground state of Mo⁹¹), there appeared two components with half lives of 60,4 second and 74 minutes, respectively. The latter may be assigned to an Nb⁹⁷ isotope coming from the Mo⁹⁷(n, p) reaction also having a gamma-decay isomeric

state with a half life of 1 minute and an energy of 750 keV, which may as well be responsible for the production of a component with a half life of 1 minute. The end-window GM counter employed has a sensitivity of 0,5 per cent for gamma particles of 750 keV. To determine unambiguously the production

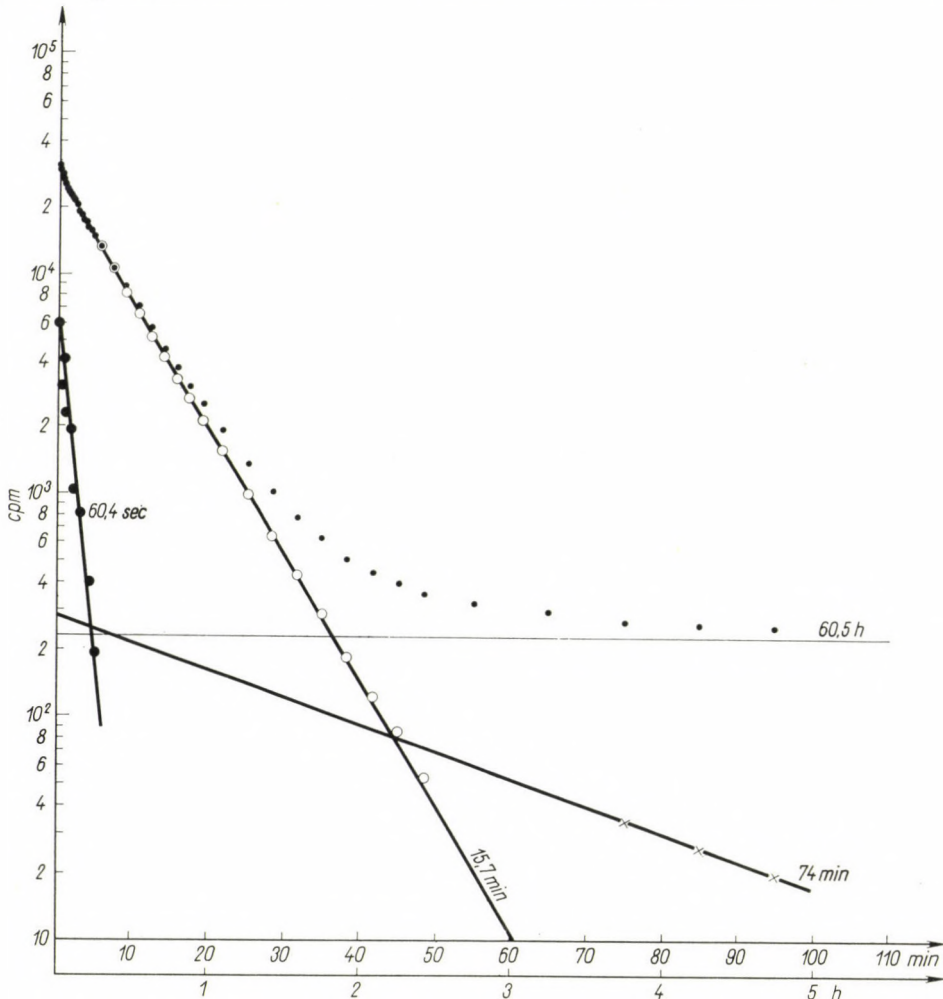


Fig. 1. The analysed complex decay curve

of Mo^{91m} , the decay curve was measured by means of a gamma spectrometer in such a way that only particles over 850 keV were detected. Under such circumstances, the activity with a half life of 1 minute was also obtained, which could only be produced by the positron decay of Mo^{91m} (Fig. 2) [7]. In order to determine the Mo^{91} isomer cross-section ratio, we had to study a possible contribution of the Nb^{97m} activity to the 1-minute half-life component measured by GM counter.

The least unfavourable condition was assumed, i.e. that Nb⁹⁷ nuclei in the ground state can only be produced through the decay of the isomeric state. By measuring the activity of the 74-minute half life, we determined the number and activity of the Nb^{97m} nuclei. The activity value so obtained is the greatest possible contribution of Nb^{97m} to the measured 1-minute activity. The above assumption does not appreciably affect the value obtained for the

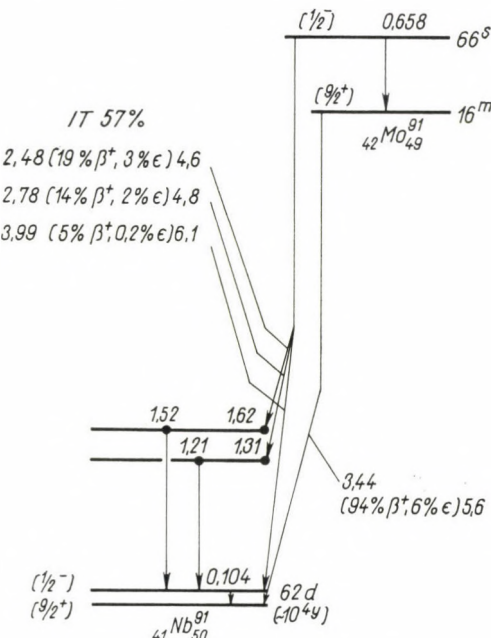


Fig. 2. The decay scheme

isomeric cross-section ratio since the Nb^{97m} could contribute to the measured activity of the 1-minute half life by not more than 5 per cent. For the decay scheme in Fig. 2 the relationship between cross-sections and activities will be

$$\frac{\sigma_g}{\sigma_m} = \frac{A_g^0}{A_m^0} \frac{(1 - e^{-\lambda_m t})(\lambda_g - 0.43 \lambda_m)}{(1 - e^{-\lambda g t})(\lambda_g - \lambda_m)} + \frac{0.57 \lambda_m}{\lambda_g - \lambda_m} .$$

Taking the above relationship into account, for the isomeric cross-section ratio the value $\sigma_g/\sigma_m = 10.6 \pm 0.3$ was obtained in the Mo⁹² (*n*, 2*n*) Mo^{91g,91m} reaction at a bombarding energy of 14.8 MeV.

In addition to the isomeric cross-section ratio at 14.8 MeV bombarding energy the absolute cross-section of the reaction Mo⁹² (*n*, 2*n*) Mo^{91g} was also determined. Accepting the result $\sigma_g = 159$ mb obtained by us, the isomeric cross-section value $\sigma_m = 15$ mb is obtained by means of the measured ratio.

REFERENCES

1. F. B. SMITH, Jr. N. B. GOVE, R. W. HENRY and R. A. BECKER, Phys. Rev., **104**, 706, 1956.
2. R. B. DUFFIELD and J. D. KNIGHT, Phys. Rev., **76**, 573, 1949.
3. J. E. BROLLEY, Jr., J. L. FOWLER and L. K. SCHLACKS, Phys. Rev., **88**, 618, 1952.
4. J. E. BROLLEY, Jr., Phys. Rev., **89**, 877, 1953.
5. P. AXEL, J. D. FOX and R. H. PARKER, Phys. Rev., **97**, 975, 1955.
6. UCRL-5419 (1959).
7. K. H. HELLWEGE: Landolt-Börnstein, I/I Springer-Verlag, Berlin, Göttingen, Heidelberg, 1961.

ИССЛЕДОВАНИЕ РЕАКЦИИ $\text{Mo}^{92}(n, 2n)\text{Mo}^{91g, 91m}$

Й. БАЧО, Й. ЧИКАИ и А. ПАЖИТ

Р е з ю м е

Реакция $\text{Mo}^{92}(n, 2n)\text{Mo}^{91m}$ наблюдается при энергии нейтронов 14,8 MeV; определяется отношение изомерного поперечного сечения $\frac{\sigma_g}{\sigma_m} = 10,6$. При реакциях $\text{Mo}^{92}(n, 2n)$ $\text{Mo}^{91g, 91m}$ для поперечного сечения найдены значения $\sigma_g = 159$ mb; $\sigma_m = 15$ mb.

ИССЛЕДОВАНИЕ ДИФФУЗИОННОГО ПРОЦЕССА В ГЕРМАНИИ

Д. Нергеш, М. Ш. Силади и Б. Визкеleti

НАУЧНО-ИССЛЕДОВАТЕЛЬСКИЙ ИНСТИТУТ, ПРОМЫШЛЕННОСТИ ТЕХНИКИ СВЯЗИ,
БУДАПЕШТ

(Представлено Г. Сигети. — Поступило 23. X. 1964)

Авторы исследовали диффузию сурьмы в германии с помощью четырехзондового измерения и послойного травления. По нашему опыту n^-n слои измеряются легче, чем диффузионные $p-n$ переходы. Измерения проводили на экзо- и эндодиффузионных слоях.

1. Введение

В технологии производства высокочастотных полупроводниковых приборов для формирования дырочного, или электронного слоя наиболее часто применяется метод диффузии. Несколько сообщений посвящены оценке слоев, в которых концентрация примесей переменная, и которые созданы путем диффузии. Простейшим из известных методов является послойное измерение поверхностного сопротивления, применимый Фуллером и Диценбергером [1]. Применяемый ими метод для измерения толщины удаленного слоя не пригоден при небольшой глубине проникновения диффузии. Айлес и Лайбенгаут [2] применяли метод измерения веса удаленного слоя для определения его толщины, пригоден для весьма неглубокой диффузии ($\sim 1 \text{ мк}$).

Предполагая, что форма распределения диффузии и концентрация примесей в исходном материале известны, измеряя поверхностную проводимость и толщину диффузионного слоя можно просто определить концентрацию на поверхности с помощью диаграммы, имеющейся в статье Катриса [3], и, зная это, можно определить концентрацию примеси для любого лежащего под поверхностью слоя. Но это не применимо в общем случае. Так, например, по опыту нескольких авторов [2, 4, 5] распределение концентрации примесей, диффундируемых в кремний, не соответствует функции erfc , а концентрация у поверхности уменьшается только медленно, но в области перехода изменяется очень резко. В случае такого распределения примеси, которое нельзя описать простой аналитической функцией, метод Катриса неприменим. Кроме того, этот метод предполагает, что в образце параллельно его поверхности имеется электронно-дырочный переход, т. е., например, в пластинку из полупроводника p -типа диффундирует примесь, создающая на поверхности слой электронной проводимости.

2. Метод измерения

Применяемый нами метод для определения распределения диффундируемой примеси во многом аналогичен методу, применяемому Айлесом и Лайбенгаутом [2]. Метод состоит в последовательном травлении слоев, и в определении их толщины путем взвешивания, на травленных поверхностях измеряли четырехзондовую поверхностную проводимость.

Основой вычисления служил следующий расчет: поверхностная проводимость, определенная непосредственно четырехзондовом методом на расстоянии x от поверхности, выражается следующей зависимостью:

$$S(x) = \int_x^l \sigma(t) dt. \quad (1)$$

Здесь $\sigma(x)$ — удельная проводимость в точке x , t — переменная интегрирования и l — глубина проникновения диффузии. Определение $S(x)$ с помощью четырехзондового метода возможно из следующего выражения [6]:

$$S(x) = \frac{1}{4,53} \frac{I}{U}, \quad (2)$$

где I — ток, протекающий через два крайних контакта, а U — измеряемая разность потенциалов на внутренних контактах. Дифференцируя выражение (1) получим

$$\sigma(x) = - \frac{dS(x)}{dx} \quad (3)$$

и концентрацию примесей $-N$ можно определить, зная $N = N(\sigma)$.

Измерения проводились на соответственно подготовленных германиевых пластинках толщиной в 200—300 мк. На их поверхности сформировался слой с неоднородной концентрацией примесей, с глубиной проникновения 5—13 мк, в результате диффузии из паровой фазы. (В случае $p - n^+$ перехода глубиной проникновения, как правило, называется расстояние от поверхности до электронно-дырочного перехода, а в случае $n^+ - n$ перехода глубиной проникновения называется расстояние от поверхности образца до такой поверхности внутри образца, где концентрация примесей в два раза больше, чем исходная концентрация в образце). С обратной стороны пластиинки легированный слой удалялся шлифовкой.

Пригодный состав травителя для удаления слоев: 1 вес. ч. HF (38%), 1 вес. ч. H_2O_2 (30%) и 4 вес. ч. дистиллированной воды. Применяя данный травитель для травления слоя с упомянутой глубиной проникновения достаточно время в 20—30 сек. при 0° С. Толщину удаленного слоя

определяли взвешиванием на микроаналитических весах, и она была около 0,4 мк. Наши эксперименты показали, что тефлон и пицеин подготовленные в царской водке и в применяемом травителе свой вес не меняли в ходе травления. Поэтому германиевые образцы наклеивали на подкладку из тефлона и все измерения проводились без снятия образца с подкладки. Таким образом обратная сторона пластинки защищалась от травителя, и травление происходило достаточно быстро, так как покрытие перед травлением и растворение перед взвешиванием стали ненужными. Применение тефлона и пицеина не влияет заметно на точность измерения.

Измерение поверхностной проводимости проводилось обычным четырехзондовым прибором. Расстояние между контактами — 1 мм. Все данные поверхностной проводимости вычислялись как среднее 10-и измерений, сделанных в различных местах поверхности. Место измерений на поверхности кристалла после каждого травления были одни и те же с точностью в $\pm 0,1$ мм. Поверхностную проводимость, определенную как среднее измерений по выражению (2), изобразили как функцию расстояния от поверхности, и после этого кривую проходящую через измеренные точки графически дифференцировали по каждый 0,5 мк. Так по выражению (3) определяли функцию $\sigma = \sigma(x)$. Для того, чтобы определить концентрацию примеси $N(x)$ применяли кривую, изготовленную по приближенной формуле, в первой таблице статьи Катриса. Соответствующие формулы для кремния имеются в статье Ирвина [7].

3. Результаты

a. Измерение диффузии $n^+ - n$.

Выше описанным методом исследовали распределение примеси полученного диффузией сурьмы в образце германия n — типа. В случае упомянутых размеров толщина образца меньше, чем половина расстояния между контактами четырехзондового аппарата [6], итак перпендикулярным к поверхности кристалла компонентом напряжения можно пренебречь по сравнению с параллельным компонентом, т. е. можно определить поверхностную проводимость по выражению (2).

На рис. 1 изображена концентрация примеси в зависимости от расстояния измеренной поверхности от первоначальной поверхности в диффундированном образце.

Как видно на рисунке, распределение примеси хорошо согласуется с теоретической зависимостью $erfc$ и коэффициент диффузии приблизительно совпадает с рассчитанной величиной [8] ($D = 1 \cdot 2 \cdot 10^{-11}$ см²/сек при температуре 770° С).

Относительные отклонения десяти измерений, как функция расстояния показаны на рис. 2. Видно, что отклонение измерений при последова-

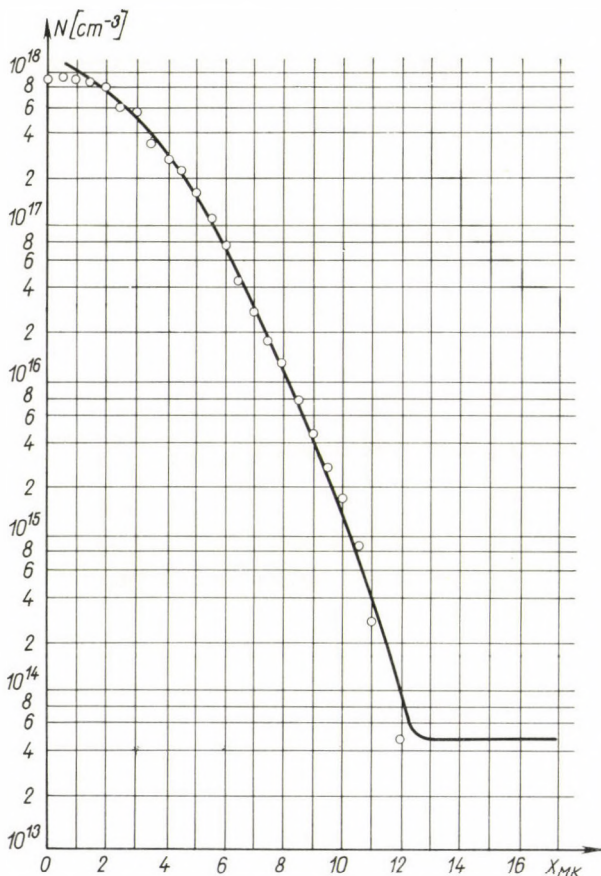


Рис. 1. Диффузионный профиль слоя

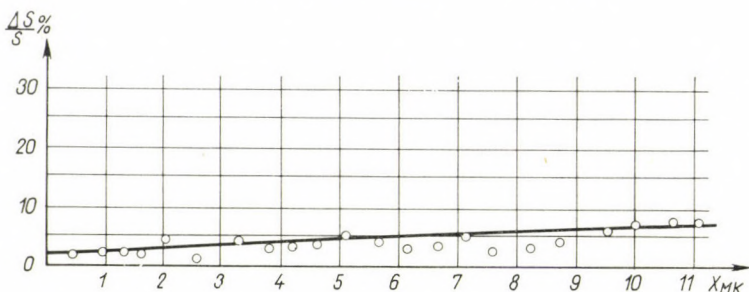


Рис. 2. Средние отклонения измерения слоя

тельном травлении ничтожно возрастает. В однородной части материала вышеописанным методом нельзя было определить концентрацию примеси, т. к. изменения вследствии травления были одного порядка с разбросами. Кроме этого в данной области инжекция токовых контактов также мешала

измерению, но это можно было устранить уменьшением тока. Поэтому концентрацию примесей в однородной части материала определили непосредственно из проводимости, измеренной обычно четырехзондовым методом.

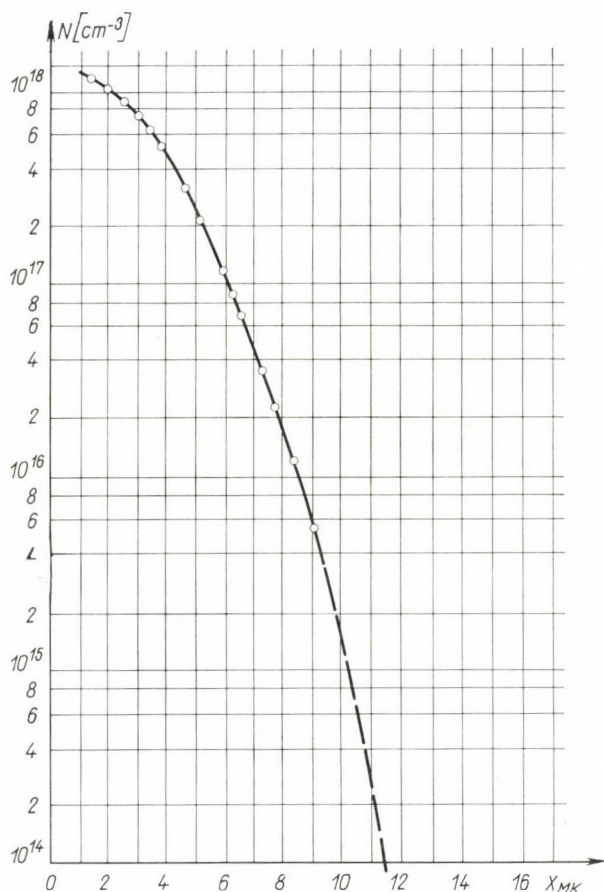


Рис. 3. Диффузионный профиль слоя

б. Измерение диффузии $n-p$.

Распределение примеси в образце p — типа, который подвергли операции диффузии одновременно с предыдущим образцом n — типа, показано на рис. 3. Измерение считали приемлемым только до тех пор, пока относительное отклонение значений поверхностной проводимости, измеренных в десяти местах, не превышает 10%. Это отклонение изображено на рис. 4, как функция расстояния измеренной поверхности от первоначальной поверхности образца, отсюда видно, что концентрацию примеси уверенно определить удается только на первых 8,5 мк. Начиная от расстояния в 9 мк от

первоначальной поверхности образца, измеренные значения поверхностной проводимости с большими отклонениями от среднего постепенно увеличивались. Это явление нельзя объяснить тем, что стравили уже весь диффузионный слой, и достигли основной материал *p*-типа. Дело в том, что при достижении материала *p*-типа поверхностная проводимость должна была быть резко увеличиваться, так как большое сопротивление *p* — *n* перехода уже не препятствует проникновению тока в область *p*-типа. В последствии поверхностная проводимость очень медленно и постепенно уменьшается также, как толщина образца *p*-типа из-за последовательных травлений несколько уменьшается. В нашем случае положение было иным, на наличие поверх-

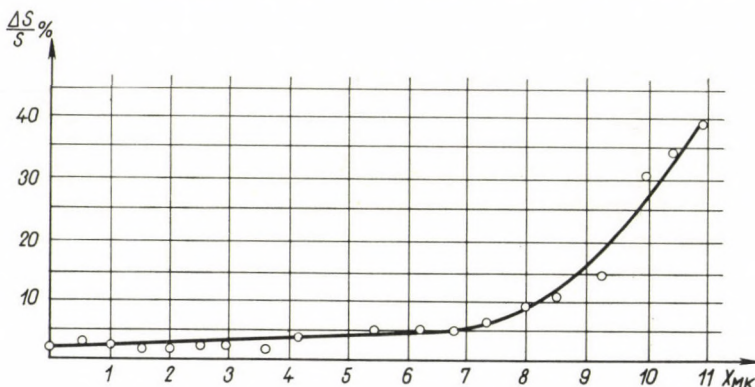


Рис. 4. Средние отклонения измерения слоя

ности *n*-слоя указали также измерения методом термозонда. По нашему мнению объяснение данного явления следующее: приближаясь к *p* — *n* переходу падение напряжения между токовыми контактами достигает очень большой величины, под влиянием которой может произойти пробой смешенного в обратном направлении *p* — *n* перехода, так его сопротивление уменьшается, часть тока проходит через вглуб лежащие слои, и поэтому падение напряжения, измеренное между внутренними контактами, уменьшается.

6. Измерение экзодиффузии

В качестве примера более сложного случая, определяли распределение примеси в образце, подвергающемуся предварительно сначала процессу диффузии из паровой фазы, а после диффузии еще определенное время выдерживался при температуре диффузии в вакууме.

Используя выведенное Номура [9] выражение для двойной диффузии получим, что

$$C_1(x, t) = C_0 \operatorname{erfc} \left[\frac{x}{2(Dt_0 + Dt)^{1/2}} \right] - (C_0 - C_2) \operatorname{erfc} \frac{x}{2(Dt)^{1/2}}, \quad (4)$$

где $C_1(x, t)$ концентрация, полученная после экзодиффузии, протекающей время t , C_2 — поверхностная концентрация в конце процесса диффузии, D — коэффициент диффузии, который из-за постоянства температуры во время диффузии не менялся, и t_0 — время эндодиффузии. Значение C_0 и D определили из данных диффузии, проведенной в таких же условиях с про-

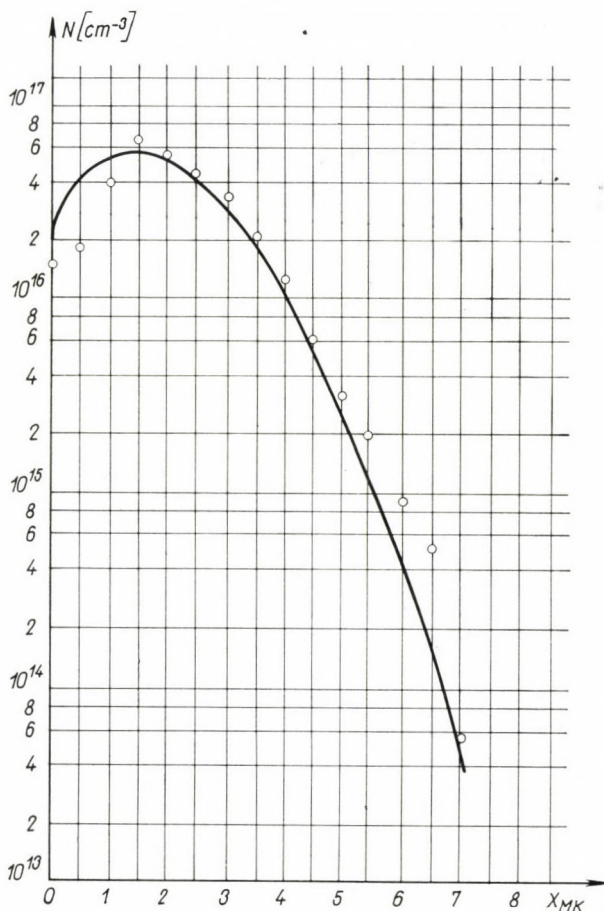


Рис. 5. Профиль экзодиффузии слоя

должительностью $t_0 + t$. C_2 принимали равной среднему значению поверхностной концентрации, полученной при проведении в идентичных условиях нескольких диффузий.

На рис. 5. видно распределение концентрации в таком случае и определенная по (4) кривая. Результаты эксперимента сравнимы с кривой, полученной из (4).

4. Выводы

По нашим измерениям в образцах, имеющих $p-n$ переход, созданный диффузией, в определении концентрации вблизи глубины проникновения появляются трудности из-за больших отклонений и постепенного роста значений поверхностной проводимости. Распределение примеси хорошо можно определить в таких тонких образцах, в которых нет изменения типа проводимости. В случае проведения после энодиффузии и экзодиффузии распределение примеси в пределах ошибки соответствует теоретическому.

5. Благодарность

Приносим глубокую благодарность доктору И. Сеп, Э. Рожа и П. Себени, за внимание и ценные советы, и далее М. Немет, которая передала нам свой опыт по вопросам травления.

ЛИТЕРАТУРА

1. C. S. FULLER, J. A. DIETZENBERGER, Journal of Applied Physics **27**, 544, 1956.
2. P. A. ILES, B. LEIBENHAUT, Solid-State Electronics, **5**, 331, 1962.
3. D. B. CUTTRISS, Bell System Technical Journal, **40**, 509, 1961.
4. Субашиев, Ландсман, Кухарский, Физика Твердого Тела 2 II. 2703. 1960.
5. G. KSOLL, Phys. Status Sol., **1**, 181, 1961.
6. A. UHLIR, Bell System Technical Journal, **34**, 105, 1955.
7. J. C. IRVIN, Bell System Technical Journal, **41**, 387, 1962.
8. F. M. SMITS, Proc. IRE, **46**, 1049, 1958.
9. K. C. NOMURA, Journal of Applied Physics, **32**, 1167, 1961.

INVESTIGATION OF THE DIFFUSION PROCESS IN GERMANIUM

By

G. NYERGES, M. S. SZILÁGYI and B. VIZKELETY

A b s t r a c t

The authors investigated diffusion of antimony in germanium by the four-point probe and gradual etching. In the experiments the n^+-n layer could be more easily measured than the $p-n$ junction made by diffusion. The measurements were carried out on in-diffused and out-diffused layers.

DIE BERECHNUNGEN DER $1sns^1S$ -ZUSTÄNDE DES WASSERSTOFFMOLEKÜLS AUF GRUND DER METHODE DER MOLEKÜLBAHNEN II.

Von

F. BERENCZ

INSTITUT FÜR THEORETISCHE PHYSIK, JÓZSEF ATTILA UNIVERSITÄT, SZEGED

(Vorgelegt von A. Kónya. — Eingegangen: 16. XI. 1964)

Es wurde die Elektronenergie des $1s3s^1S$ -Zustandes des Wasserstoffmoleküls auf Grund der Methode der Molekülbahnen berechnet. Es wurde weiterhin festgestellt, dass die auf Grund der Methode der Molekülbahnen berechneten Energien der $1sns^1S$ -Zustände ($n = 1, 2, 3$) des Wasserstoffmoleküls von dem empirischen Wert eine Differenz von 4,5%-en zeigen. Die Methode der Molekülbahnen ist also für eine theoretische Behandlung sowohl des Grundzustandes als der angeregten Zustände geeignet.

Einleitung

Es ist wohlbekannt, dass die Lösung der Schrödingergleichung schon im Falle von Atomen auf unüberwindliche mathematische Schwierigkeiten stößt, die bei Molekülproblemen noch gesteigert werden. Deshalb ist man bei Lösung von Molekülproblemen auf Näherungsmethoden angewiesen. Die eine sehr oft erfolgreich gebrauchte Näherungsmethode ist die sogenannte MO (Molecular Orbital)-Methode, zu deren Ausarbeitung HUND [1], MULLIKEN [2], HÜCKEL [3] und LENNARD-JONES [4] beigetragen haben. Bei der MO-Methode wird angenommen, dass die Elektronen im Molekül nicht den einzelnen Atomen, sondern dem Molekül als ganzes angehören, d. h. dass sich die Eigenfunktion eines Elektrons auf das ganze Molekül erstrecke. Dementsprechend werden die Molekülbahnen der einzelnen Elektronen mehrzentrig im Gegensatze zu den einzentrischen Atombahnen. Die mehrzentrischen Molekülbahnen der einzelnen Elektronen lassen sich aber auf Grund der LCAO (Linear Combination of Atomic Orbitals)-Methode als Linearkombination der einzelnen einzentrischen Atombahnen angeben. Die Eigenfunktion des Moleküls, d. h. die MO des Moleküls wird als Produkt der Molekülbahnen der einzelnen Elektronen angegeben. Es muss aber bemerkt werden, dass zwischen zwei Atombahnen nur dann eine effektive Linearkombination sich verwirklichen kann, wenn die Grösse der Energien berechnet mit den einzelnen Atombahnen vergleichbare Grösse haben, ihre Ladungswolken sich maximal bedecken und betrefflich der Molekülachse dieselbe Symmetrie besitzen. WEINBAUM [5] führte zuerst bezüglich des Grundzustandes des Wasserstoffmoleküls quantenmechanische Berechnungen auf Grund der sogenannten LCAO—MO-Methode mit verhältnismässig guten Resultaten durch. In einer früheren Arbeit [6]

berechneten wir den angeregten $1s2s^1S$ -Zustand des Wasserstoffmoleküls auf Grund der Methode der Molekülbahnen, in dieser Arbeit werden die vorigen Berechnungen auf den angeregten $1s3s^1S$ -Zustand ausgebretet. Schiesslich werden die WEINBAUMSchen und unsere Resultate mit den empirischen Werten verglichen.

Die Rechenmethode

Die Wasserstoffeigenfunktionen der ns -Zustände werden durch den folgenden Zusammenhang geliefert:

$$ns(r) = \frac{1}{n^{3/2} \sqrt{\pi}} \exp\left(-\frac{r}{n}\right) R_n(r), \quad (1)$$

wo

$$R_n(r) = 1 - \frac{n-1}{1! 2!} \left(\frac{2r}{n}\right) + \frac{(n-1)(n-2)}{2! 3!} \left(\frac{2r}{n}\right)^2 - \dots \quad (2)$$

ist. Die Molekülbahn des $1s3s^1S$ -Zustandes des Wasserstoffmoleküls wird als Produkt der Molekülbahnen der einzelnen Elektronen angegeben, bei welchen sich das erste Elektron im Grundzustand und das zweite Elektron im angeregten Zustand befindet. Die Molekülbahnen der einzelnen Elektronen haben nach (1) und (2) die folgende Gestalt:

$$1s(r_{a1}) + 1s(r_{b1}) = \frac{1}{\sqrt{\pi}} [\exp(-r_{a1}) + \exp(-r_{b1})], \quad (3)$$

$$\begin{aligned} 3s(r_{a2}) + 3s(r_{b2}) &= \frac{1}{3\sqrt{3}\pi} \left\{ \left[\exp\left(-\frac{r_{a2}}{3}\right) \right] \left(1 - \frac{2}{3} r_{a2} + \frac{2}{27} r_{a2}^2 \right) + \right. \\ &\quad \left. + \left[\exp\left(-\frac{r_{b2}}{3}\right) \right] \left(1 - \frac{2}{3} r_{b2} + \frac{2}{27} r_{b2}^2 \right) \right\}. \end{aligned} \quad (4)$$

Unter Berücksichtigung von (3) und (4) kann die Molekülbahn des $1s3s^1S$ -Zustandes des Wasserstoffmoleküls in der folgenden Form angegeben werden:

$$\begin{aligned} \psi_3 &= \frac{1}{3\sqrt{3}\pi} [\exp(-r_{a1}) + \exp(-r_{b1})] \times \\ &\quad \times \left\{ \left[\exp\left(-\frac{r_{a2}}{3}\right) \right] \left(1 - \frac{2}{3} r_{a2} + \frac{2}{27} r_{a2}^2 \right) + \right. \\ &\quad \left. + \left[\exp\left(-\frac{r_{b2}}{3}\right) \right] \left(1 - \frac{2}{3} r_{b2} + \frac{2}{27} r_{b2}^2 \right) \right\}. \end{aligned} \quad (5)$$

Die Elektronenergie wird dann auf Grund des folgenden Zusammenhanges berechnet:

$$E_3 = \frac{\int \psi_3 H \psi_3 d\tau}{\int \psi_3^2 d\sigma}, \quad (6)$$

wo

$$H = H_a + H_b - \frac{1}{r_{b1}} - \frac{1}{r_{a2}} + \frac{1}{r_{12}} + \frac{1}{R} \quad (7)$$

und

$$H_a = -\frac{1}{2} A_1 - \frac{1}{r_{a1}} \quad (8)$$

$$H_b = -\frac{1}{2} A_2 - \frac{1}{r_{b2}}. \quad (9)$$

ist.

Die Resultate der Berechnungen

WEINBAUM [5] führte bezüglich des Grundzustandes des Wasserstoffmoleküls quantenmechanische Berechnungen auf Grund der sogenannten LCAO—MO-Methode durch und gelangte mit der Molekülbahn von der Gestalt:

$$\psi_1 = [1s(r_{a1}) + 1s(r_{b1})] [1s(r_{a2}) + 1s(r_{b2})] \quad (10)$$

zu einer Elektronenergie von 1,12755 a. u. Verfasser berechnete in einer früheren Arbeit [6] den $1s2s^1S$ -Zustand des Wasserstoffmoleküls auf Grund der Molekülbahn von der Gestalt

$$\psi_2 = [1s(r_{a1}) + 1s(r_{b1})] [2s(r_{a2}) + 2s(r_{b2})] \quad (11)$$

und erhielt eine Elektronenergie von 0,68086 a. u. In dieser Arbeit wurde der $1s3s^1S$ -Zustand des Wasserstoffmoleküls auf Grund der Molekülbahn von der Gestalt

$$\psi_3 = [1s(r_{a1}) + 1s(r_{b1})] [3s(r_{a2}) + 3s(r_{b2})] \quad (12)$$

berechnet mit einem Resultat von 0,63400 a. u. für die Elektronenergie.

Vergleichen wir die oben angeführten Resultate mit den empirischen Werten, die der Reihe nach die folgenden sind:

$(1s)^2 1S$	1,17442 a. u.
$1s2s^1S$	0,71188 a. u.
$1s3s^1S$	0,65975 a. u. [7].

Die Differenzen zwischen den berechneten und empirischen Werten in den einzelnen Zuständen sind wie folgen:

$(1s)^2 \ ^1S$	0,04687 a. u. (4,00%),
$1s2s^1S$	0,03102 a. u. (4,36%),
$1s3s^1S$	0,02575 a. u. (3,90%).

Die Differenzen zwischen den auf Grund der LCAO—MO-Methode erhaltenen Resultaten und den empirischen Werten bleiben unter einer minimalen Fehler-Grenze von 4,5%-en in allen drei Fällen. Aus dieser Tatsache kann man die Schlussfolgerung ziehen, dass die in der Einleitung beschriebene Form der MO-Methode zu einer theoretischen Behandlung sowohl des Grundzustandes als der angeregten Zustände mit einem verhältnismässig guten Resultat geeignet ist.

Ich danke auch an dieser Stelle Fräulein A. BOLDIZSÁR für die Hilfe bei den numerischen Rechnungen.

Anhang

Bei der Berechnung der Elektronenergie mussten mehrere Integrale bestimmt werden, welche bisher in der Literatur nicht vorgekommen sind. Diese seien folgendermassen bezeichnet:

$$\begin{aligned} I(a, \beta, \gamma, \delta s t u v) &= \\ &= \frac{1}{\pi^2} \int \int \exp(-\alpha r_{a1} - \beta r_{b1}) \exp(-\gamma r_{a2} - \delta r_{b2}) \times \\ &\quad \times r_{a1}^s r_{b1}^t r_{a2}^u r_{b2}^v \cdot \frac{1}{r_{12}} d\tau_1 d\sigma_2. \end{aligned}$$

Bei der Berechnung der Integrale wird die Methode von KOTANI und seinen Mitarbeitern benutzt. Der Integrand wird in elliptischen Koordinaten dargestellt und die gegenseitige Entfernung der beiden Elektronen wird durch die NEUMANNSCHE Reihenentwicklung berücksichtigt. Unsere Integrale wurden mit Hilfe der von KOTANI, AMEMIYA und SIMOSE [8], gleichwie von MILLER, GERHAUSER und MATSEN [9] tabellierten folgenden Hilfsintegralen ausgedrückt:

$$A_n(a) = \int_1^\infty e^{-a\mu} \mu^n d\mu,$$

$$B_n(\beta) = \int_{-1}^{+1} e^{-\beta v} v^n dv,$$

$$G_{\tau}^v(l, \beta) = \int_{-1}^{+1} P_{\tau}^v(\nu_i) e^{-\beta \nu_i} \nu_i^l (1 - \nu_i^2)^{v/2} d\nu_i,$$

$$H_{\tau}^v(i, a; k, \beta) = \int_1^{\infty} \int_1^{\infty} e^{-(\alpha \mu_1 + \beta \mu_2)} \mu_1^i \mu_2^k Q_{\tau}^v(\mu_+) P_{\tau}^v(\mu_-) \times \\ \times (\mu_1^2 - 1)^{v/2} (\mu_2^2 - 1)^{v/2} d\mu_1 d\mu_2.$$

Die neuen Integrale ergaben sich wie folgt.

$$I\left(2, 0, \frac{2}{3}, 0, 0, 0, 0, 0, 0\right) = \frac{R^5}{8} \left[H_0^0\left(2, R; 2, \frac{1}{3}R\right) G_0^0(0, R) G_0^0\left(0, \frac{1}{3}R\right) + C_1 - \right. \\ - H_0^0\left(2, R; 0, \frac{1}{3}R\right) G_0^0(0, R) G_0^0\left(2, \frac{1}{3}R\right) - C_2 - \\ - H_0^0\left(0, R; 2, \frac{1}{3}R\right) G_0^0(2, R) G_0^0\left(0, \frac{1}{3}R\right) - C_3 + \\ \left. + H_0^0\left(0, R; 0, \frac{1}{3}R\right) G_0^0(2, R) G_0^0\left(2, \frac{1}{3}R\right) + C_4 \right].$$

$$I\left(2, 0, \frac{2}{3}, 0, 0, 0, 1, 0\right) = \frac{R^6}{16} \left[H_0^0\left(2, R; 3, \frac{1}{3}R\right) G_0^0(0, R) G_0^0\left(0, \frac{1}{3}R\right) + C_5 + \right. \\ + H_0^0\left(2, R; 2, \frac{1}{3}R\right) G_0^0(0, R) G_0^0\left(1, \frac{1}{3}R\right) + C_6 - \\ - H_0^0\left(2, R; 1, \frac{1}{3}R\right) G_0^0(0, R) G_0^0\left(2, \frac{1}{3}R\right) - C_7 - \\ - H_0^0\left(2, R; 0, \frac{1}{3}R\right) G_0^0(0, R) G_0^0\left(3, \frac{1}{3}R\right) - C_8 - \\ - H_0^0\left(0, R; 3, \frac{1}{3}R\right) G_0^0(2, R) G_0^0\left(0, \frac{1}{3}R\right) - C_9 - \\ - H_0^0\left(0, R; 2, \frac{1}{3}R\right) G_0^0(2, R) G_0^0\left(1, \frac{1}{3}R\right) - C_{10} + \\ + H_0^0\left(0, R; 1, \frac{1}{3}R\right) G_0^0(2, R) G_0^0\left(2, \frac{1}{3}R\right) + C_{11} + \\ \left. + H_0^0\left(0, R; 0, \frac{1}{3}R\right) G_0^0(2, R) G_0^0\left(3, \frac{1}{3}R\right) + C_{12} \right].$$

$$I\left(2, 0, \frac{2}{3}, 0, 0, 0, 2, 0\right) = \frac{R^7}{32} \left[H_0^0\left(2, R; 4, \frac{1}{3}R\right) G_0^0(0, R) G_0^0\left(0, \frac{1}{3}R\right) + C_{13} + \right. \\ + 2H_0^0\left(2, R; 3, \frac{1}{3}R\right) G_0^0(0, R) G_0^0\left(1, \frac{1}{3}R\right) + 2C_{14} - \\ - 2H_0^0\left(2, R; 1, \frac{1}{3}R\right) G_0^0(0, R) G_0^0\left(3, \frac{1}{3}R\right) - 2C_{15} - \\ - H_0^0\left(2, R; 0, \frac{1}{3}R\right) G_0^0(0, R) G_0^0\left(4, \frac{1}{3}R\right) - C_{16} - \\ \left. + H_0^0\left(2, R; 0, \frac{1}{3}R\right) G_0^0(0, R) G_0^0\left(5, \frac{1}{3}R\right) + C_{17} \right].$$

$$\begin{aligned}
& - H_0^0 \left(0, R; 4, \frac{1}{3} R \right) G_0^0 (2, R) G_0^0 \left(0, \frac{1}{3} R \right) - C_{17} - \\
& - 2H_0^0 \left(0, R; 3, \frac{1}{3} R \right) G_0^0 (2, R) G_0^0 \left(1, \frac{1}{3} R \right) - 2C_{18} + \\
& + 2H_0^0 \left(0, R; 1, \frac{1}{3} R \right) G_0^0 (2, R) G_0^0 \left(3, \frac{1}{3} R \right) + 2C_{19} + \\
& + H_0^0 \left(0, R; 0, \frac{1}{3} R \right) G_0^0 (2, R) G_0^0 \left(4, \frac{1}{3} R \right) + C_{20} \Big].
\end{aligned}$$

$$\begin{aligned}
I \left(2, 0, \frac{2}{3} 0, 0, 0, 3, 0 \right) = & \frac{R^8}{64} \left[H_0^0 \left(2, R; 5, \frac{1}{3} R \right) G_0^0 (0, R) G_0^0 \left(0, \frac{1}{3} R \right) + C_{21} + \right. \\
& + 3H_0^0 \left(2, R; 4, \frac{1}{3} R \right) G_0^0 (0, R) G_0^0 \left(1, \frac{1}{3} R \right) + 3C_{22} + \\
& + 2H_0^0 \left(2, R; 3, \frac{1}{3} R \right) G_0^0 (0, R) G_0^0 \left(2, \frac{1}{3} R \right) + 2C_{23} - \\
& - 2H_0^0 \left(2, R; 2, \frac{1}{3} R \right) G_0^0 (0, R) G_0^0 \left(3, \frac{1}{3} R \right) - 2C_{24} - \\
& - 3H_0^0 \left(2, R; 1, \frac{1}{3} R \right) G_0^0 (0, R) G_0^0 \left(4, \frac{1}{3} R \right) - 3C_{25} - \\
& - H_0^0 \left(2, R; 0, \frac{1}{3} R \right) G_0^0 (0, R) G_0^0 \left(5, \frac{1}{3} R \right) - C_{26} - \\
& - H_0^0 \left(0, R; 5, \frac{1}{3} R \right) G_0^0 (2, R) G_0^0 \left(0, \frac{1}{3} R \right) - C_{27} - \\
& - 3H_0^0 \left(0, R; 4, \frac{1}{3} R \right) G_0^0 (2, R) G_0^0 \left(1, \frac{1}{3} R \right) - C_{28} - \\
& - 2H_0^0 \left(0, R; 3, \frac{1}{3} R \right) G_0^0 (2, R) G_0^0 \left(2, \frac{1}{3} R \right) - C_{29} + \\
& + 2H_0^0 \left(0, R; 2, \frac{1}{3} R \right) G_0^0 (2, R) G_0^0 \left(3, \frac{1}{3} R \right) + C_{30} + \\
& + 3H_0^0 \left(0, R; 1, \frac{1}{3} R \right) G_0^0 (2, R) G_0^0 \left(4, \frac{1}{3} R \right) + C_{31} + \\
& \left. + H_0^0 \left(0, R; 0, \frac{1}{3} R \right) G_0^0 (2, R) G_0^0 \left(5, \frac{1}{3} R \right) + C_{32} \right].
\end{aligned}$$

$$\begin{aligned}
I \left(2, 0, \frac{2}{3} 0, 0, 0, 4, 0 \right) = & \frac{R^9}{128} \left[H_0^0 \left(2, R; 6, \frac{1}{3} R \right) G_0^0 (0, R) G_0^0 \left(0, \frac{1}{3} R \right) + C_{33} + \right. \\
& + 4H_0^0 \left(2, R; 5, \frac{1}{3} R \right) G_0^0 (0, R) G_0^0 \left(1, \frac{1}{3} R \right) + C_{34} + \\
& + 5H_0^0 \left(2, R; 4, \frac{1}{3} R \right) G_0^0 (0, R) G_0^0 \left(2, \frac{1}{3} R \right) + 5C_{35} - \\
& - 5H_0^0 \left(2, R; 2, \frac{1}{3} R \right) G_0^0 (0, R) G_0^0 \left(4, \frac{1}{3} R \right) - 5C_{36} - \\
& - 4H_0^0 \left(2, R; 1, \frac{1}{3} R \right) G_0^0 (0, R) G_0^0 \left(5, \frac{1}{3} R \right) - 4C_{37} -
\end{aligned}$$

$$\begin{aligned}
& - H_0^0 \left(2, R; 0, \frac{1}{3} R \right) G_0^0 (0, R) G_0^0 \left(6, \frac{1}{3} R \right) - C_{38} - \\
& - H_0^0 \left(0, R; 6, \frac{1}{3} R \right) G_0^0 (2, R) G_0^0 \left(0, \frac{1}{3} R \right) - C_{39} - \\
& - 4H_0^0 \left(0, R; 5, \frac{1}{3} R \right) G_0^0 (2, R) G_0^0 \left(1, \frac{1}{3} R \right) - C_{40} - \\
& - 5H_0^0 \left(0, R; 4, \frac{1}{3} R \right) G_0^0 (2, R) G_0^0 \left(2, \frac{1}{3} R \right) - C_{41} + \\
& + 5H_0^0 \left(0, R; 2, \frac{1}{3} R \right) G_0^0 (2, R) G_0^0 \left(4, \frac{1}{3} R \right) + C_{42} + \\
& + 4H_0^0 \left(0, R; 1, \frac{1}{3} R \right) G_0^0 (2, R) G_0^0 \left(5, \frac{1}{3} R \right) + C_{43} + \\
& + H_0^0 \left(0, R; 0, \frac{1}{3} R \right) G_0^0 (2, R) G_0^0 \left(6, \frac{1}{3} R \right) + C_{44} \Big].
\end{aligned}$$

$$\begin{aligned}
I \left(1, 1, \frac{2}{3}, 0, 0, 0, 0, 0, 0 \right) = & \frac{R^5}{12} \left\{ \left[3H_0^0 \left(2, R; 2, \frac{1}{3} R \right) - H_0^0 \left(0, R; 2, \frac{1}{3} R \right) \right] G_0^0 \left(0, \frac{1}{3} R \right) - \right. \\
& - \left[3H_0^0 \left(2, R; 0, \frac{1}{3} R \right) - H_0^0 \left(0, R; 0, \frac{1}{3} R \right) \right] G_0^0 \left(2, \frac{1}{3} R \right) - \\
& \left. - 2H_2^0 \left(0, R; 2, \frac{1}{3} R \right) G_2^0 \left(0, \frac{1}{3} R \right) 2H_2^0 \left(0, R; 0, \frac{1}{3} R \right) G_2^0 \left(2, \frac{1}{3} R \right) \right\}.
\end{aligned}$$

$$\begin{aligned}
I \left(1, 1, \frac{2}{3}, 0, 0, 0, 1, 0 \right) = & \frac{R^6}{24} \left\{ \left[3H_0^0 \left(2, R; 3, \frac{1}{3} R \right) - H_0^0 \left(0, R; 3, \frac{1}{3} R \right) \right] G_0^0 \left(0, \frac{1}{3} R \right) + \right. \\
& + \left[3H_0^0 \left(2, R; 2, \frac{1}{3} R \right) - H_0^0 \left(0, R; 2, \frac{1}{3} R \right) \right] G_0^0 \left(1, \frac{1}{3} R \right) - \\
& - \left[3H_0^0 \left(2, R; 1, \frac{1}{3} R \right) - H_0^0 \left(0, R; 1, \frac{1}{3} R \right) \right] G_0^0 \left(2, \frac{1}{3} R \right) - \\
& - \left[3H_0^0 \left(2, R; 0, \frac{1}{3} R \right) - H_0^0 \left(0, R; 0, \frac{1}{3} R \right) \right] G_0^0 \left(3, \frac{1}{3} R \right) - \\
& - 2H_2^0 \left(0, R; 3, \frac{1}{3} R \right) G_2^0 \left(0, \frac{1}{3} R \right) - 2H_2^0 \left(0, R; 2, \frac{1}{3} R \right) G_2^0 \left(1, \frac{1}{3} R \right) + \\
& \left. + 2H_2^0 \left(0, R; 1, \frac{1}{3} R \right) G_2^0 \left(2, \frac{1}{3} R \right) + 2H_2^0 \left(0, R; 0, \frac{1}{3} R \right) G_2^0 \left(3, \frac{1}{3} R \right) \right\}.
\end{aligned}$$

$$\begin{aligned}
I \left(1, 1, \frac{2}{3}, 0, 0, 0, 2, 0 \right) = & \frac{R^7}{48} \left\{ \left[3H_0^0 \left(2, R; 4, \frac{1}{3} R \right) - H_0^0 \left(0, R; 4, \frac{1}{3} R \right) \right] G_0^0 \left(0, \frac{1}{3} R \right) + \right. \\
& + 2 \left[3H_0^0 \left(2, R; 3, \frac{1}{3} R \right) - H_0^0 \left(0, R; 3, \frac{1}{3} R \right) \right] G_0^0 \left(1, \frac{1}{3} R \right) - \\
& - 2 \left[3H_0^0 \left(2, R; 1, \frac{1}{3} R \right) - H_0^0 \left(0, R; 1, \frac{1}{3} R \right) \right] G_0^0 \left(3, \frac{1}{3} R \right) - \\
& - \left[3H_2^0 \left(2, R; 0, \frac{1}{3} R \right) - H_2^0 \left(0, R; 0, \frac{1}{3} R \right) \right] G_0^0 \left(4, \frac{1}{3} R \right) -
\end{aligned}$$

$$\begin{aligned}
& - 2H_0^2 \left(0, R; 4, \frac{1}{3}R \right) G_2^0 \left(0, \frac{1}{3}R \right) - 4H_2^0 \left(0, R; 3, \frac{1}{3}R \right) G_2^0 \left(1, \frac{1}{3}R \right) + \\
& + 4H_0^0 \left(0, R; 1, \frac{1}{3}R \right) G_2^0 \left(3, \frac{1}{3}R \right) + 2H_2^0 \left(0, R; 0, \frac{1}{3}R \right) G_2^0 \left(4, \frac{1}{3}R \right) \}.
\end{aligned}$$

$$\begin{aligned}
I \left(1, 1, \frac{2}{3}, 0, 0, 0, 3, 0 \right) = & \frac{R^8}{96} \left\{ \left[3H_0^0 \left(2, R; 5, \frac{1}{3}R \right) - H_0^0 \left(0, R; 5, \frac{1}{3}R \right) \right] G_0^0 \left(0, \frac{1}{3}R \right) + \right. \\
& + 3 \left[3H_0^0 \left(2, R; 4, \frac{1}{3}R \right) - H_0^0 \left(0, R; 4, \frac{1}{3}R \right) \right] G_0^0 \left(1, \frac{1}{3}R \right) + \\
& + 2 \left[3H_0^0 \left(2, R; 3, \frac{1}{3}R \right) - H_0^0 \left(0, R; 3, \frac{1}{3}R \right) \right] G_0^0 \left(2, \frac{1}{3}R \right) - \\
& - 2 \left[3H_0^0 \left(2, R; 2, \frac{1}{3}R \right) - H_0^0 \left(0, R; 2, \frac{1}{3}R \right) \right] G_0^0 \left(3, \frac{1}{3}R \right) - \\
& - 3 \left[3H_0^0 \left(2, R; 1, \frac{1}{3}R \right) - H_0^0 \left(0, R; 1, \frac{1}{3}R \right) \right] G_0^0 \left(4, \frac{1}{3}R \right) - \\
& - \left[3H_0^0 \left(2, R; 0, \frac{1}{3}R \right) - H_0^0 \left(0, R; 0, \frac{1}{3}R \right) \right] G_0^0 \left(5, \frac{1}{4}R \right) - \\
& - 2H_0^0 \left(0, R; 5, \frac{1}{3}R \right) G_2^0 \left(0, \frac{1}{3}R \right) - 6H_2^0 \left(0, R; 4, \frac{1}{3}R \right) G_0^0 \left(1, \frac{1}{3}R \right) - \\
& - 4H_2^0 \left(0, R; 3, \frac{1}{3}R \right) G_2^0 \left(2, \frac{1}{3}R \right) + 4H_2^0 \left(0, R; 2, \frac{1}{3}R \right) G_2^0 \left(3, \frac{1}{3}R \right) + \\
& \left. + 6H_2^0 \left(0, R; 1, \frac{1}{3}R \right) G_2^0 \left(4, \frac{1}{3}R \right) + 2H_2^0 \left(0, R; 0, \frac{1}{3}R \right) G_2^0 \left(5, \frac{2}{3}R \right) \right\}.
\end{aligned}$$

$$\begin{aligned}
I \left(1, 1, \frac{2}{3}, 0, 0, 0, 4, 0 \right) = & \frac{R^9}{192} \left\{ \left[3H_0^0 \left(2, R; 6, \frac{1}{3}R \right) - H_0^0 \left(0, R; 6, \frac{1}{3}R \right) \right] G_0^0 \left(0, \frac{1}{3}R \right) + \right. \\
& + 4 \left[3H_0^0 \left(2, R; 5, \frac{1}{3}R \right) - H_0^0 \left(0, R; 5, \frac{1}{3}R \right) \right] G_0^0 \left(1, \frac{1}{3}R \right) + \\
& + 5 \left[3H_0^0 \left(2, R; 4, \frac{1}{3}R \right) - H_0^0 \left(0, R; 4, \frac{1}{3}R \right) \right] G_0^0 \left(2, \frac{1}{3}R \right) - \\
& - 5 \left[3H_0^0 \left(2, R; 2, \frac{1}{3}R \right) - H_0^0 \left(0, R; 2, \frac{1}{3}R \right) \right] G_0^0 \left(4, \frac{1}{3}R \right) - \\
& - 4 \left[3H_0^0 \left(2, R; 1, \frac{1}{3}R \right) - H_0^0 \left(0, R; 1, \frac{1}{3}R \right) \right] G_0^0 \left(5, \frac{1}{3}R \right) - \\
& - \left[3H_0^0 \left(2, R; 0, \frac{1}{3}R \right) - H_0^0 \left(0, R; 0, \frac{1}{3}R \right) \right] G_0^0 \left(6, \frac{1}{3}R \right) - \\
& - 2H_2^0 \left(0, R; 6, \frac{1}{3}R \right) G_2^0 \left(0, \frac{1}{3}R \right) - 8H_2^0 \left(0, R; 5, \frac{1}{3}R \right) G_2^0 \left(1, \frac{1}{3}R \right) - \\
& - 10H_2^0 \left(0, R; 4, \frac{1}{3}R \right) G_2^0 \left(2, \frac{1}{3}R \right) + 10H_2^0 \left(0, R; 2, \frac{1}{3}R \right) G_2^0 \left(4, \frac{1}{3}R \right) + \\
& \left. + 8H_2^0 \left(0, R; 1, \frac{1}{3}R \right) G_2^0 \left(5, \frac{1}{3}R \right) + 2H_2^0 \left(0, R; 0, \frac{1}{3}R \right) G_2^0 \left(6, \frac{1}{3}R \right) \right\}.
\end{aligned}$$

$$I \left(2, 0, \frac{1}{3}, \frac{1}{3}, 0, 0, 0, 0 \right) = \frac{R^5}{12} \left\{ \left[3H_0^0 \left(2, R; 2, \frac{1}{3} R \right) - H_0^0 \left(2, R; 0, \frac{1}{3} R \right) \right] G_0^0(0, R) - \right.$$

$$- \left[3H_0^0 \left(0, R; 2, \frac{1}{3} R \right) - H_0^0 \left(0, R; 0, \frac{1}{3} R \right) \right] G_0^0(2, R) -$$

$$\left. - 2H_2^0 \left(2, R; 0, \frac{1}{3} R \right) G_0^0(0, R) + 2H_2^0 \left(0, R; 0, \frac{1}{3} R \right) G_2^0(2, R) \right\}.$$

$$I \left(2, 0, \frac{1}{3}, \frac{1}{3}, 0, 0, 1, 0 \right) = \frac{R^6}{120} \left\{ 5 \left[3H_0^0 \left(2, R; 3, \frac{1}{3} R \right) - H_0^0 \left(2, R; 1, \frac{1}{3} R \right) \right] G_0^0(0, R) - \right.$$

$$- 5 \left[3H_0^0 \left(0, R; 3, \frac{1}{3} R \right) - H_0^0 \left(0, R; 1, \frac{1}{3} R \right) \right] G_0^0(2, R) +$$

$$+ 3 \left[5H_1^0 \left(2, R; 2, \frac{1}{3} R \right) - 3H_1^0 \left(2, R; 0, \frac{1}{3} R \right) \right] G_1^0(0, R) -$$

$$- 3 \left[5H_1^0 \left(0, R; 2, \frac{1}{3} R \right) - 3H_1^0 \left(0, R; 0, \frac{1}{3} R \right) \right] G_1^0(2, R) -$$

$$- 10H_2^0 \left(2, R; 1, \frac{1}{3} R \right) G_2^0(0, R) + 10H_2^0 \left(0, R; 1, \frac{1}{3} R \right) G_2^0(2, R) -$$

$$\left. - 6H_3^0 \left(2, R; 0, \frac{1}{3} R \right) G_3^0(0, R) + 6H_3^0 \left(0, R; 0, \frac{1}{3} R \right) G_3^0(2, R) \right\}.$$

$$I \left(2, 0, \frac{1}{3}, \frac{1}{3}, 0, 1, 0, 0 \right) = \frac{R^6}{120} \left\{ 5 \left[3H_0^0 \left(2, R; 3, \frac{1}{3} R \right) - H_0^0 \left(2, R; 1, \frac{1}{3} R \right) \right] G_0^0(0, R) - \right.$$

$$- 5 \left[3H_0^0 \left(0, R; 3, \frac{1}{3} R \right) - H_0^0 \left(0, R; 1, \frac{1}{3} R \right) \right] G_0^0(2, R) +$$

$$- 3 \left[5H_1^0 \left(2, R; 2, \frac{1}{3} R \right) - 3H_1^0 \left(2, R; 0, \frac{1}{3} R \right) \right] G_1^0(0, R) +$$

$$+ 3 \left[5H_1^0 \left(0, R; 2, \frac{1}{3} R \right) - 3H_1^0 \left(0, R; 0, \frac{1}{3} R \right) \right] G_1^0(2, R) -$$

$$- 10H_2^0 \left(2, R; 1, \frac{1}{3} R \right) G_2^0(0, R) + 10H_2^0 \left(0, R; 1, \frac{1}{3} R \right) G_2^0(2, R) +$$

$$\left. + 6H_3^0 \left(2, R; 0, \frac{1}{3} R \right) G_3^0(0, R) - 6H_3^0 \left(0, R; 0, \frac{1}{3} R \right) G_3^0(2, R) \right\}.$$

$$I \left(2, 0, \frac{1}{3}, \frac{1}{3}, 0, 0, 1, 1 \right) = \frac{R^7}{1680} \left\{ \left[105H_0^0 \left(2, R; 4, \frac{1}{3} R \right) - 70H_0^0 \left(2, R; 2, \frac{1}{3} R \right) + \right. \right.$$

$$+ 21H_0^0 \left(2, R; 0, \frac{1}{3} R \right) \left. \right] G_0^0(0, R) -$$

$$- \left[105H_0^0 \left(0, R; 4, \frac{1}{3} R \right) - 70H_0^0 \left(0, R; 2, \frac{1}{3} R \right) + \right.$$

$$+ 21H_0^0 \left(0, R; 0, \frac{1}{3} R \right) \left. \right] G_0^0(2, R) -$$

$$\left. - \left[140H_2^0 \left(2, R; 2, \frac{1}{3} R \right) - 60H_2^0 \left(2, R; 0, \frac{1}{3} R \right) \right] G_2^0(0, R) + \right.$$

$$\begin{aligned}
& + \left[140 H_2^0 \left(0, R; 2, \frac{1}{3} R \right) - 60 H_2^0 \left(0, R; 0, \frac{1}{3} R \right) \right] G_2^0 (2, R) + \\
& + 24 H_4^0 \left(2, R; 0, \frac{1}{3} R \right) G_4^0 (0, R) - 24 H_4^0 \left(0, R; 0, \frac{1}{3} R \right) G_4^0 (2, R) \Big\}.
\end{aligned}$$

$$\begin{aligned}
I \left(2, 0, \frac{1}{3}, \frac{1}{3}, 0, 0, 2, 0 \right) = & \frac{R^8}{1120} \left\{ 7 \left[5 H_0^0 \left(2, R; 4, \frac{1}{3} R \right) - H_0^0 \left(2, R; 0, \frac{1}{3} R \right) \right] G_0^0 (0, R) - \right. \\
& - 7 \left[5 H_0^0 \left(0, R; 4, \frac{1}{3} R \right) - H_0^0 \left(0, R; 0, \frac{1}{3} R \right) \right] G_0^0 (2, R) + \\
& + 14 \left[5 H_1^0 \left(2, R; 3, \frac{1}{3} R \right) - 3 H_1^0 \left(2, R; 1, \frac{1}{3} R \right) \right] G_1^0 (0, R) - \\
& - 14 \left[5 H_1^0 \left(0, R; 3, \frac{1}{3} R \right) - 3 H_1^0 \left(0, R; 1, \frac{1}{3} R \right) \right] G_1^0 (2, R) - \\
& - 20 H_2^0 \left(2, R; 0, \frac{1}{3} R \right) G_2^0 (0, R) + 20 H_2^0 \left(0, R; 0, \frac{1}{3} R \right) G_2^0 (2, R) - \\
& - 28 H_3^0 \left(2, R; 1, \frac{1}{3} R \right) G_3^0 (0, R) + 28 H_3^0 \left(0, R; 1, \frac{1}{3} R \right) G_3^0 (2, R) - \\
& \left. - 8 H_4^0 \left(2, R; 0, \frac{1}{3} R \right) G_4^0 (0, R) + 8 H_4^0 \left(0, R; 0, \frac{1}{3} R \right) G_4^0 (2, R) \right\}.
\end{aligned}$$

$$\begin{aligned}
I \left(2, 0, \frac{1}{3}, \frac{1}{3}, 0, 0, 0, 2 \right) = & \frac{R^8}{1120} \left\{ 7 \left[5 H_0^0 \left(2, R; 4, \frac{1}{3} R \right) - H_0^0 \left(2, R; 0, \frac{1}{3} R \right) \right] G_0^0 (0, R) - \right. \\
& - 7 \left[5 H_0^0 \left(0, R; 4, \frac{1}{3} R \right) - H_0^0 \left(0, R; 0, \frac{1}{3} R \right) \right] G_0^0 (2, R) - \\
& - 14 \left[5 H_1^0 \left(2, R; 3, \frac{1}{3} R \right) - 3 H_1^0 \left(2, R; 1, \frac{1}{3} R \right) \right] G_1^0 (0, R) + \\
& + 14 \left[5 H_1^0 \left(0, R; 3, \frac{1}{3} R \right) - 3 H_1^0 \left(0, R; 1, \frac{1}{3} R \right) \right] G_1^0 (2, R) - \\
& - 02 H_2^0 \left(2, R; 0, \frac{1}{3} R \right) G_2^0 (0, R) + 20 H_2^0 \left(0, R; 0, \frac{1}{3} R \right) G_2^0 (2, R) + \\
& + 28 H_3^0 \left(2, R; 1, \frac{1}{3} R \right) G_3^0 (0, R) + 28 H_3^0 \left(0, R; 1, \frac{1}{3} R \right) G_3^0 (2, R) - \\
& \left. - 8 H_4^0 \left(2, R; 0, \frac{1}{3} R \right) G_4^0 (0, R) + 8 H_4^0 \left(0, R; 0, \frac{1}{3} R \right) G_4^0 (2, R) \right\}.
\end{aligned}$$

$$\begin{aligned}
I \left(2, 0, \frac{1}{3}, \frac{1}{3}, 0, 0, 2, 1 \right) = & \frac{R^9}{20 \cdot 160} \left\{ 21 \left[15 H_0^0 \left(2, R; 5, \frac{1}{3} R \right) - 10 H_0^0 \left(2, R; 3, \frac{1}{3} R \right) \right] + \right. \\
& + 3 H_0^0 \left(2, R; 1, \frac{1}{3} R \right) \Big] G_0^0 (0, R) - \\
& - 21 \left[15 H_0^0 \left(0, R; 5, \frac{1}{3} R \right) - 10 H_0^0 \left(0, R; 3, \frac{1}{3} R \right) \right] + \\
& \left. + 3 H_0^0 \left(0, R; 1, \frac{1}{3} R \right) \right] G_0^0 (2, R) +
\end{aligned}$$

$$\begin{aligned}
& + 9 \left[35H_1^0 \left(2, R; 4, \frac{1}{3} R \right) - 42H_1^0 \left(2, R; 2, \frac{1}{3} R \right) + \right. \\
& + 15H_1^0 \left(2, R; 0, \frac{1}{3} R \right) \Big] G_0^0 (0, R) - \\
& - 9 \left[35H_1^0 \left(0, R; 4, \frac{1}{3} R \right) - 42H_1^0 \left(0, R; 2, \frac{1}{3} R \right) + \right. \\
& + 15H_1^0 \left(0, R; 0, \frac{1}{3} R \right) \Big] G_1^0 (2, R) - \\
& - 60 \left[7H_2^0 \left(2, R; 3, \frac{1}{3} R \right) - 3H_2^0 \left(2, R; 1, \frac{1}{3} R \right) \right] G_2^0 (0, R) + \\
& + 60 \left[7H_2^0 \left(0, R; 3, \frac{1}{3} R \right) - 3H_2^0 \left(0, R; 1, \frac{1}{3} R \right) \right] G_2^0 (2, R) - \\
& - 20 \left[9H_3^0 \left(2, R; 2, \frac{1}{3} R \right) - 7H_3^0 \left(2, R; 0, \frac{1}{3} R \right) \right] G_3^0 (0, R) + \\
& + 20 \left[9H_3^0 \left(0, R; 2, \frac{1}{3} R \right) - 7H_3^0 \left(0, R; 0, \frac{1}{3} R \right) \right] G_3^0 (2, R) + \\
& \left. + 72H_4^0 \left(2, R; 1, \frac{1}{3} R \right) G_4^0 (0, R) - 72H_4^0 \left(0, R; 1, \frac{1}{3} R \right) G_4^0 (2, R) \right].
\end{aligned}$$

$$\begin{aligned}
I \left(2, 0, \frac{1}{3}, \frac{1}{3}, 0, 0, 1, 2 \right) = & \frac{R^9}{20 \cdot 160} \left\{ 21 \left[15H_0^0 \left(2, R; 5, \frac{1}{3} R \right) - 10H_0^0 \left(2, R; 3, \frac{1}{3} R \right) + \right. \right. \\
& + 3H_0^0 \left(2, R; 1, \frac{1}{3} R \right) \Big] G_0^0 (0, R) - \\
& - 21 \left[15H_0^0 \left(0, R; 5, \frac{1}{3} R \right) - 10H_0^0 \left(0, R; 3, \frac{1}{3} R \right) + \right. \\
& + 3H_0^0 \left(0, R; 1, \frac{1}{3} R \right) \Big] G_0^0 (2, R) - \\
& - 9 \left[35H_1^0 \left(2, R; 4, \frac{1}{3} R \right) - 42H_1^0 \left(2, R; 2, \frac{1}{3} R \right) + \right. \\
& + 15H_1^0 \left(2, R; 0, \frac{1}{3} R \right) \Big] G_1^0 (0, R) + \\
& + 9 \left[35H_1^0 \left(0, R; 4, \frac{1}{3} R \right) - 42H_1^0 \left(0, R; 2, \frac{1}{3} R \right) + \right. \\
& + 15H_1^0 \left(0, R; 0, \frac{1}{3} R \right) \Big] G_1^0 (2, R) - \\
& - 60 \left[7H_2^0 \left(2, R; 3, \frac{1}{3} R \right) - 3H_2^0 \left(2, R; 1, \frac{1}{3} R \right) \right] G_2^0 (0, R) + \\
& + 60 \left[7H_2^0 \left(0, R; 3, \frac{1}{3} R \right) - 3H_2^0 \left(0, R; 1, \frac{1}{3} R \right) \right] G_2^0 (2, R) + \\
& + 20 \left[9H_3^0 \left(2, R; 2, \frac{1}{3} R \right) - 7H_3^0 \left(2, R; 0, \frac{1}{3} R \right) \right] G_3^0 (0, R) - \\
& - 20 \left[9H_3^0 \left(0, R; 2, \frac{1}{3} R \right) - 7H_3^0 \left(0, R; 0, \frac{1}{3} R \right) \right] G_3^0 (2, R) + \\
& \left. + 72H_4^0 \left(2, R; 1, \frac{1}{3} R \right) G_4^0 (0, R) - 72H_4^0 \left(0, R; 1, \frac{1}{3} R \right) G_4^0 (2, R) \right\}.
\end{aligned}$$

$$\begin{aligned}
I\left(2, 0, \frac{1}{3}, \frac{1}{3}, 0, 0, 2, 2\right) = & \frac{R^{10}}{1034880} \left\{ 231 \left[35H_0^0\left(2, R; 6, \frac{1}{3}R\right) - 35H_0^0\left(2, R; 4, \frac{1}{3}R\right) + \right. \right. \\
& + 21H_0^0\left(2, R; 2, \frac{1}{3}R\right) - 5H_0^0\left(2, R; 0, \frac{1}{3}R\right) \Big] G_0^0(0, R) - \\
& - 231 \left[35H_0^0\left(0, R; 6, \frac{1}{3}R\right) - 35H_0^0\left(0, R; 4, \frac{1}{3}R\right) + \right. \\
& + 21H_0^0\left(0, R; 2, \frac{1}{3}R\right) - 5H_0^0\left(0, R; 0, \frac{1}{3}R\right) \Big] G_0^0(2, R) - \\
& - 770 \left[21H_2^0\left(2, R; 4, \frac{1}{3}R\right) - 18H_2^0\left(2, R; 2, \frac{1}{3}R\right) + \right. \\
& + 5H_2^0\left(2, R; 0, \frac{1}{3}R\right) \Big] G_2^0(0, R) + \\
& + 770 \left[21H_2^0\left(0, R; 4, \frac{1}{3}R\right) - 18H_2^0\left(0, R; 2, \frac{1}{3}R\right) + \right. \\
& + 5H_2^0\left(0, R; 0, \frac{1}{3}R\right) \Big] G_2^0(2, R) + \\
& + 72 \left[77H_4^0\left(2, R; 2, \frac{1}{3}R\right) - 35H_4^0\left(2, R; 0, \frac{1}{3}R\right) \right] G_4^0(0, R) - \\
& - 72 \left[77H_4^0\left(0, R; 2, \frac{1}{3}R\right) - 35H_4^0\left(0, R; 0, \frac{1}{3}R\right) \right] G_4^0(2, R) \}.
\end{aligned}$$

$$\begin{aligned}
I\left(1, 1, \frac{1}{3}, \frac{1}{3}, 0, 0, 0, 0\right) = & \\
= & \frac{R^5}{90} \left[45H_0^0\left(2, R; 2, \frac{1}{3}R\right) - 15H_0^0\left(2, R; 0, \frac{1}{3}R\right) - 15H_0^0\left(0, R; 2, \frac{1}{3}R\right) + \right. \\
& \left. + 5H_0^0\left(0, R; 0, \frac{1}{3}R\right) + 4H_2^0\left(0, R; 0, \frac{1}{3}R\right) \right].
\end{aligned}$$

$$\begin{aligned}
I\left(1, 1, \frac{1}{3}, \frac{1}{3}, 0, 0, 1, 0\right) = & \\
= & \frac{R^6}{18} \left[45H_0^0\left(2, R; 3, \frac{1}{3}R\right) - 15H_0^0\left(2, R; 1, \frac{1}{3}R\right) - 15H_0^0\left(0, R; 3, \frac{1}{3}R\right) + \right. \\
& \left. + 5H_0^0\left(0, R; 1, \frac{1}{3}R\right) + 4H_2^0\left(0, R; 1, \frac{1}{3}R\right) \right].
\end{aligned}$$

$$\begin{aligned}
I\left(1, 1, \frac{1}{3}, \frac{1}{3}, 0, 0, 1, 1\right) = & \\
= & \frac{R^7}{2520} \left[315H_0^0\left(2, R; 4, \frac{1}{3}R\right) - 210H_0^0\left(2, R; 2, \frac{1}{3}R\right) + \right. \\
& + 63H_0^0\left(2, R; 0, \frac{1}{3}R\right) - 105H_0^0\left(0, R; 4, \frac{1}{3}R\right) + \\
& + 70H_0^0\left(0, R; 2, \frac{1}{3}R\right) - 21H_0^0\left(0, R; 0, \frac{1}{3}R\right) + \\
& \left. + 56H_2^0\left(0, R; 2, \frac{1}{3}R\right) - 24H_2^0\left(0, R; 0, \frac{1}{3}R\right) \right].
\end{aligned}$$

$$\begin{aligned} I\left(1, 1, \frac{1}{3}, \frac{1}{3}, 0, 0, 2, 0\right) = \\ = \frac{R^7}{840} \left[105 H_0^0 \left(2, R; 4, \frac{1}{3} R\right) - 21 H_0^0 \left(2, R; 0, \frac{1}{3} R\right) - 35 H_0^0 \left(0, R; 4, \frac{1}{3} R\right) + \right. \\ \left. + 7 H_0^0 \left(0, R; 0, \frac{1}{3} R\right) + 8 H_2^0 \left(0, R; 0, \frac{1}{3} R\right) \right]. \end{aligned}$$

$$\begin{aligned} I\left(1, 1, \frac{1}{3}, \frac{1}{3}, 0, 0, 2, 1\right) = \frac{R^8}{5040} \left[315 H_0^0 \left(2, R; 5, \frac{1}{3} R\right) - 210 H_0^0 \left(2, R; 3, \frac{1}{3} R\right) + \right. \\ + 63 H_0^0 \left(2, R; 1, \frac{1}{3} R\right) - 105 H_0^0 \left(0, R; 5, \frac{1}{3} R\right) + \\ + 70 H_2^0 \left(0, R; 3, \frac{1}{3} R\right) - 21 H_0^0 \left(0, R; 1, \frac{1}{3} R\right) + \\ \left. + 56 H_2^0 \left(0, R; 3, \frac{1}{3} R\right) - 24 H_2^0 \left(0, R; 1, \frac{1}{3} R\right) \right]. \end{aligned}$$

$$\begin{aligned} I\left(1, 1, \frac{1}{3}, \frac{1}{3}, 0, 0, 2, 2\right) = \frac{10080}{R^9} \left[315 H_0^0 \left(2, R; 6, \frac{1}{3} R\right) - 315 H_0^0 \left(2, R; 4, \frac{1}{3} R\right) + \right. \\ + 189 H_0^0 \left(2, R; 2, \frac{1}{3} R\right) - 45 H_0^0 \left(2, R; 0, \frac{1}{3} R\right) - \\ - 105 H_0^0 \left(0, R; 6, \frac{1}{3} R\right) + 105 H_0^0 \left(0, R; 4, \frac{1}{3} R\right) - \\ - 63 H_0^0 \left(0, R; 2, \frac{1}{3} R\right) + 15 H_0^0 \left(0, R; 0, \frac{1}{3} R\right) + 108 H_2^0 \left(0, R; 4, \frac{1}{3} R\right) - \\ \left. - 72 H_2^0 \left(0, R; 2, \frac{1}{3} R\right) + 20 H_2^0 \left(0, R; 0, \frac{1}{3} R\right) \right]. \end{aligned}$$

$C_i = 3H_1^0 G_1^0 G_1^0 + 5H_2^0 G_2^0 G_2^0 + 7H_3^0 G_3^0 G_3^0 + 9H_4^0 G_4^0 G_4^0$ mit den Argumenten in den betreffenden Reihen.

LITERATUR

1. F. HUND, Z. Phys., **73**, 1, 1931.
2. R. S. MULLIKEN, J. Chem. Phys., **1**, 492, 1933; **3**, 375, 1935; Chem. Rev., **9**, 347, 1931.
3. E. HÜCKEL, Z. Phys., **60**, 423, 1930; **72**, 310, 1931.
4. T. LENNARD-JONES, Trans. Faraday Soc., **25**, 668, 1929.
5. L. PAULING und E. B. WILSON: Introduction to Quantum Mechanics, Mc Graw-Hill Book Comp. Inc., New York and London, 1935. S. 347.
6. F. BERENCI, Acta Phys. Hung., **16**, 49, 1963.
7. H. SPONER, Molekülspektren, Springer, Berlin, 1935.
8. M. KOTANI, A. AMEMIYA und T. SIMOSE, Proc. Phys. Math. Soc. Japan, **20**, extra No 1, 1938; **22**, extra No 2, 1940.
9. J. MILLER, I. M. GERHAUSER und F. A. MATSEN, Quantum Chemistry Integrals and Tables, University of Texas Press, 1959.

ОПРЕДЕЛЕНИЕ СОСТОЯНИЯ $1sns^1S$ МОЛЕКУЛЫ ВОДОРОДА МЕТОДОМ
МОЛЕКУЛЯРНЫХ ОРБИТ II

Ф. БЕРЕНЦ

Р е з ю м е

В работе определяется энергия электрона в состоянии $1s3s^1S$ молекулы водорода на основе метода молекулярных орбит. Далее определяется, что энергия, найденная методом молекулярных орбит для состояния $1sns^1S$ ($n = 1, 2, 3$) молекулы водорода, отличается от эмпирического значения на 4,5%. Метод молекулярных орбит годен для теоретического рассмотрения как основного, так и возбуждённых состояний.

CALCULATION OF NUCLEAR QUADRUPOLE MOMENTS

By

M. TISZA

PHYSICAL INSTITUTE, UNIVERSITY FOR TECHNICAL SCIENCES,, BUDAPEST

(Presented by A. Kónya. — Received 24. XI. 1964)

The aim of this paper is to determine the quadrupole moments of some nuclei, starting from SKYRME's semiempirical energy formula for a nucleon gas, and minimizing the energy by means of a three-parameter variational expression for the nucleon density.

The quadrupole moments are calculated from the obtained densities and the results are compared with the empirical data.

1. The calculation of the energy and quadrupole moment of nuclei

For the calculation of the energy of the nucleus, we made use of the expression derived by SKYRME [1] for the sum of the Fermi kinetic and the interaction energy resulting from the nuclear forces. SKYRME's expression is given by

$$E_v = \int W_v(\varrho) dv, \quad (1)$$

where

$$W_v(\varrho) = \varepsilon_0 \varrho_0 \left[\left(\frac{\varrho}{\varrho_0} \right)^3 - 2 \left(\frac{\varrho}{\varrho_0} \right)^2 \right], \quad (2)$$

ϱ is the total density of the nucleon gas, while ε_0 and ϱ_0 are constants given by

$$\varepsilon_0 = 15 \text{ MeV}, \quad \varrho_0 = 1,4 \cdot 10^{38} \text{ cm}^{-3}. \quad (3)$$

Following SKYRME we use the expression

$$E_i = \frac{1}{2} B \int (\text{grad } \varrho)^2 dv \quad (4)$$

for the energy resulting from the inhomogeneity of the nucleon gas, where

$$B = 1,2 \cdot 10^{-63} \text{ MeV} \cdot \text{cm}^5. \quad (5)$$

In addition to the SKYRME terms we take into account also the energy resulting from the Coulomb repulsion of the protons

$$E_c = \frac{1}{2} e^2 \iint \frac{\varrho_P(\mathbf{r}) \varrho_P(\mathbf{r}')}{|\mathbf{r} - \mathbf{r}'|} dv dv', \quad (6)$$

where $\varrho_p(\mathbf{r})$ denotes the proton density. Thus the binding energy of the nucleus consists of the following terms

$$E = E_v + E_i + E_c. \quad (7)$$

Our approximate normalized density of the nucleon gas is the following variational expression

$$\varrho(r, \vartheta) = \frac{A}{\pi^{3/2} (\lambda_1^{-3} + \varkappa \lambda_2^{-5})} \{ e^{-\lambda_1^2 r^2} + 2\varkappa r^2 e^{-\lambda_1^2 r^2} \cos^2 \vartheta \}, \quad (8)$$

where A is the mass number and \varkappa , λ_1 and λ_2 are variational parameters. This expression makes it possible to investigate the deviations from spherical symmetry of the nucleus. The spherically symmetric case belongs to $\varkappa = 0$. The deviation from spherical symmetry is generally characterized by the quadrupole moment of the nucleus. The quadrupole moment

$$q = \frac{z}{A} \int \varrho(r; \vartheta) [3 \cos^2 \vartheta - 1] r^2 dv \quad (9)$$

can be calculated by means of (8) and we obtain

$$q = \frac{2z \mu x^3}{\lambda^2 (1 + \mu x^2)}, \quad (10)$$

where

$$\mu = \frac{\varkappa}{\lambda_2^2} \quad \lambda = \lambda_1 \quad x = \frac{\lambda_1}{\lambda_2}. \quad (11)$$

Using (8) we obtain for the energy terms

$$E_c = \frac{z^2 e^2 \lambda}{\sqrt{2\pi} (1 + \mu x^3)^2} \left\{ 1 + \frac{49}{60} \mu^2 x^5 + \mu \left(\frac{2x^2}{x^2 + 1} \right)^{3/2} \left(1 + \frac{2}{3} x^2 \right) \right\}, \quad (12)$$

$$\begin{aligned} E_v = \varepsilon_0 & \left\{ \frac{A^3 \lambda^6}{(\sqrt{3}\pi)^3 \varrho_0^2 (1 + \mu x^3)^3} \left[1 + \mu x^3 \left(\frac{3}{2x^2 + 1} \right)^{5/2} + \right. \right. \\ & \left. \left. + \mu^2 x^2 \left(\frac{3}{x^2 + 2} \right)^{7/2} + \frac{5}{9} \mu^3 x^3 \right] - \right. \end{aligned} \quad (13)$$

$$\left. - \frac{A^2 \lambda^3}{\sqrt{2} \pi^{3/2} \varrho_0 (1 + \mu x^3)^2} \left[1 + \mu x^3 \left(\frac{2}{x^2 + 1} \right)^{5/2} + \frac{3}{4} \mu^2 x^3 \right] \right\},$$

$$E_i = \frac{3A^2 B\lambda^5}{2(2\pi)^{3/2} (1 + \mu x^2)^2} \left\{ 1 + \mu x^3 \left(1 - \frac{2}{3} x^2 \right) \left(\frac{2}{x^2 + 1} \right)^{7/2} + \right. \\ \left. + \mu^2 x \left[\frac{37}{12} - 2 \left(\frac{2}{x^2 + 1} \right)^{7/2} \right] \right\}. \quad (14)$$

In the following we consider only the simpler case when $x = 1$, i.e. $\lambda_1 = \lambda_2$ and $\varrho(r; \vartheta)$ has the following form

$$\varrho(r; \vartheta) = N (1 + 2\mu\lambda^2 r^2 \cos^2 \vartheta) e^{-\lambda r^2}, \quad (15)$$

where

$$N = \frac{A\lambda^3}{\pi^{3/2} (1 + \mu)}. \quad (16)$$

The energy terms reduce then to the form

$$E_v = \varepsilon_0 \left\{ \frac{A^3 \lambda^6}{(\sqrt{3}\pi)^3 \varrho_0^2 (1 + \mu)^3} \left[1 + \mu + \mu^2 + \frac{5}{9} \mu^3 \right] - \right. \\ \left. - \frac{A^2 \lambda^3}{\sqrt{2}\pi^{3/2} \varrho_0 (1 + \mu)^2} \left[1 + \mu + \frac{3}{4} \mu^2 \right] \right\}, \quad (17)$$

$$E_i = \frac{3BA^2 \lambda^5}{2(2\pi)^{3/2} (1 + \mu)^3} \left[1 + \frac{1}{3} \mu + \frac{13}{12} \mu^2 \right], \quad (18)$$

$$E_c = \frac{Z^2 e^2 \lambda}{\sqrt{2\pi} (1 + \mu)^2} \left[1 + \frac{5}{3} \mu + \frac{49}{60} \mu^2 \right]. \quad (19)$$

In this simpler case we have calculated the energy of the nucleus Ta_{73}^{181} . We have minimum energy when $\lambda = 0,2199 \cdot 10^{13} \text{ cm}^{-1}$, $\mu = 0,992$ and the value of the energy per nucleon number is $E/A = -6,32019 \text{ MeV}$. Having obtained the values of the parameters λ and μ we can compute the quadrupole moment by using (10) and the result is $q = 15 \cdot 10^{-24} \text{ cm}^2$. Our results must be compared with the measured quantities $E/A = -8,03089 \text{ MeV}$ and $q = 6,6 \cdot 10^{-24} \text{ cm}^2$.

2. Discussion

In the following the cause of the discrepancy between the calculated and the experimental results obtained for the energy as well as for the quadrupole moment will be discussed.

Let us begin with the energy. SKYRME determined the constants in the energy by disregarding the Coulomb term. Consequently, the discrepancy in the energy values is probably due to the fact that we took into account also the Coulomb term without changing the parameters [3].

Additional problems arise in the case of the quadrupole moment. First of all we notice that this quantity is not a smoothly varying function of the mass number A , and therefore we can only estimate the order of magnitude of the quadrupole moment on the basis of our model. There may be cases, where the agreement between the computed and measured moments is worse than in our example, while in other cases the agreement may be better.

It is well known that in unfortunate cases the error in the densities obtained by the method of energy variation may be significant even if the energy value is fairly accurate. (This can be readily seen e.g. in an example given by PREUSS [2]. He showed that we can construct a wave function for the hydrogen atom satisfying all the conditions required of a variational wave function and approximating the energy up to any required accuracy, nevertheless leading to wrong values for the diamagnetic susceptibility, the error of which indefinitely increases.)

It seems, however, more probable in our case that the error is not primarily due to an unfortunate choice of the variational function, but the semiempirical energy expression of SKYRME gives erroneous results if deviations from spherical symmetry are allowed for the nucleon density.

In connection with this we refer to a paper by GOMBÁS and KISDI [3], where a nuclear molecule consisting of two C^{12} nuclei is investigated. This investigation is also based on the semiempirical energy expression of SKYRME, and the authors obtain the result that the energy of the system consisting of two C^{12} nuclei shows a minimum at a distance of $R = 3,6 \cdot 10^{-13}$ cm between the centres of the nuclei. This minimum actually corresponds to a stable state of a strongly deformed Mg^{24} nucleus. This fact also indicates that a variational calculation based on the energy expression of SKYRME leads to a nucleon density which deviates much more from spherical symmetry than the experimental density does.

3. Acknowledgement

Thanks are due to Professor Dr. P. GOMBÁS and Dr. D. KISDI for many helpful discussions and advices.

REFERENCES

1. T. H. R. SKYRME, Phil. Mag., **1**, 1043, 1956.
2. H. PREUSS, Z. Naturforschg., **16a**, 598, 1961.
3. P. GOMBÁS and D. KISDI, Z. Phys. **167**, 250, 1962.

ВЫЧИСЛЕНИЕ ЯДЕРНОГО КВАДРУПОЛЬНОГО МОМЕНТА

М. ТИСА

Р е з и о м е

Целью данной работы является определение квадрупольного момента некоторых ядер, исходя из полуэмпирической формулы энергии для нуклонного газа Скарма и минимизируя энергию с помощью вариационного выражения для плотности нуклонов, содержащего три параметра. Квадрупольный момент вычисляется на основе полученной плотности и сравнивается с опытными данными.

РАСЧЕТ ТРАЕКТОРИИ ЭЛЕКТРОНА, ДВИЖУЩЕГОСЯ МЕЖДУ КОАКСИАЛЬНЫМИ ТРУБАМИ, В ПРИСУТСТВИИ ПОЛОГО ЭЛЕКТРОННОГО ПУЧКА

М. Силади

ИНСТИТУТ ТЕХНИЧЕСКОЙ ФИЗИКИ ВЕНГЕРСКОЙ АН, БУДАПЕШТ

(Представлено Г. Сигети. — Поступило 24. XI. 1964)

В работе определена траектория электрона, исходящего с внутренней границы аксиально-симметричного трубчатого интенсивного электронного пучка, движущегося между двумя коаксиальными длинными проводящими цилиндрами. Исследовано влияние различных параметров системы на движение электрона. Даются формулы для определения максимального первеанса пучка и максимальной длины системы.

В различных электронных приборах часто применяются полые интенсивные электронные пучки. Как известно, в таких пучках действуют силы электростатического отталкивания между электронами, которые приводят к изменению формы пучка. Точное исследование расширения пучка является чрезвычайно сложной задачей, так как необходимо совместно решать уравнение Пуассона и уравнения движения. В настоящей статье проблема аппроксимируется решением следующей задачи.

Рассмотрим идеально фокусированный полый электронный пучок с постоянным поперечным сечением, ограниченный цилиндрическими поверхностями. С границы пучка начинают свое движение электроны, внесенные в систему извне. В дальнейшем исследуется движение такого — не относящегося к пучку — электрона в электростатическом поле, созданном пространственным зарядом пучка с конечной и постоянной толщиной. Траектория электрона, исходящего с внешней границы пучка, рассмотрена в статье [1]. Частному случаю бесконечно тонкого пучка посвящена работа [2]. В настоящей работе определяется траектория электрона, начавшего свое движение на внутренней границе пучка. Применяется нерелятивистское приближение.

Пусть длинный аксиально-симметричный интенсивный полый электронный пучок движется между двумя длинными коаксиальными проводящими цилиндрами по направлению, перпендикулярному плоскости чертежа (рис. 1.). Примем общую ось системы за ось z цилиндрической системы координат r, a, z . Оба цилиндра находятся на одинаковом потенциале U_0 . Радиус внутреннего цилиндра обозначим через R_1 , радиус внешнего цилиндра — через R_2 . Пучок ограничен цилиндрическими поверхностями с радиусом a с внутренней стороны и с радиусом b с внешней стороны. Поперечное сечение всей системы показано на рис. 1. Сечение пучка заштриховано.

В такой системе на электроны действуют только силы пространственного заряда. Вследствие большой длины пучка, а также вращательной симметрии, эти силы действуют лишь в радиальном направлении. Как известно, распределение потенциала по сечению полого пучка имеет вид, показанный на рис. 2. Имеется некоторый радиус r_e , при котором потенциал достигает минимального значения. На электроны, которые движутся при этом равновесном радиусе, силы не действуют. Электроны, находящиеся во внешней части пучка ($r > r_e$), отклоняются от оси. В случае $r < r_e$ силы пространственного заряда действуют в обратном направлении.

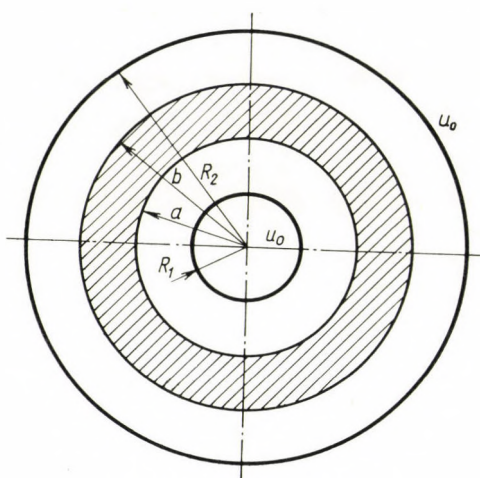


Рис. 1

Прежде чем приступить к исследованию внутренней границы пучка, примем следующие *допущения*:

1. Распределение потенциала будем учитывать только при вычислении силы, действующей на электрон. Скорости всех электронов приближенно определяются потенциалом U_0 .

2. Считаем, что плотность тока равномерно распределяется по поперечному сечению пучка.

Оба допущения верны при обычных интенсивностях и не очень больших величинах отношения $\frac{R_2}{R_1}$.

Будем применять практическую систему единиц МКСА.

Теперь рассмотрим движение электрона, исходящего с внутренней границы пучка. Для этого электрона

$$R_1 \leq r \leq a.$$

Если имеет место второе допущение, то в этой области распределение потенциала определяется следующим выражением [3]:

$$U(r) = U_0 - \frac{I}{2\pi\epsilon_0 \sqrt{2\eta} \sqrt{U_0}} \frac{r_e^2 - a^2}{b^2 - a^2} \ln \frac{r}{R_1}, \quad (1)$$

где

$$r_e^2 = \frac{1}{\ln \frac{R_2}{R_1}} \left[b^2 \ln \frac{R_2}{b} + a^2 \ln \frac{a}{R_1} + \frac{1}{2} (b^2 - a^2) \right]. \quad (2)$$

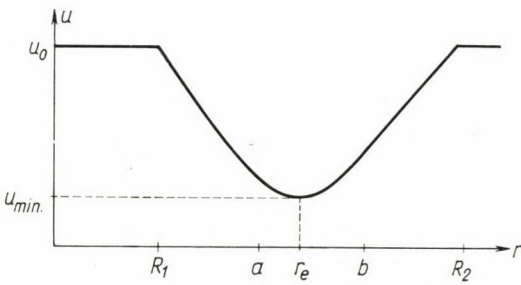


Рис. 2

Здесь I — полная сила тока пучка, ϵ_0 — величина диэлектрической проницаемости вакуума, а $\eta = \frac{e}{m}$ — абсолютная величина отношения заряда электрона к его массе.

Уравнение движения электрона имеет вид:

$$\frac{d^2 r}{dt^2} = \eta \frac{dU}{dr}. \quad (3)$$

Приближенно можно считать, что

$$\frac{dz}{dt} \approx \sqrt{2\eta U_0}, \quad (4)$$

так как поперечная составляющая скорости электрона в рассматриваемом приближении мала по сравнению с продольной составляющей. Учитывая соотношение (4), из (1) и (3) получим уравнение траектории:

$$\frac{d^2 r}{dz^2} = - \frac{I}{4\pi\epsilon_0 \sqrt{2\eta} U_0^{3/2}} \frac{r_e^2 - a^2}{b^2 - a^2} \frac{1}{r}. \quad (5)$$

Начальные условия имеют следующий вид:

$$\left. \begin{array}{l} r(0) = a \\ \frac{dr}{dz} \Big|_{z=0} = 0 \end{array} \right\} \quad (6)$$

Интегрируем уравнение (5) один раз с учетом (6). Получается:

$$\left(\frac{dr}{dz} \right)^2 = - \frac{I}{2\pi\varepsilon_0 \sqrt{2\eta} U_0^{3/2}} \frac{r_e^2 - a^2}{b^2 - a^2} \ln \frac{r}{a}, \quad (7)$$

откуда

$$dz = \frac{dr}{-\sqrt{-\frac{I}{2\pi\varepsilon_0 \sqrt{2\eta} U_0^{3/2}} \frac{r_e^2 - a^2}{b^2 - a^2} \ln \frac{r}{a}}} . \quad (8)$$

Перед корнем выбрали отрицательный знак, так как при положительном приращении координаты z величина координаты r должна уменьшаться. Интегрируя уравнение (8), получим:

$$\frac{z}{a} = \sqrt{\frac{2\pi\varepsilon_0 \sqrt{2\eta} U_0^{3/2}}{I}} \frac{b^2 - a^2}{r_e^2 - a^2} \int_1^{r/a} \frac{dw}{-\sqrt{-\ln w}}, \quad (9)$$

где w переменная интегрирования, которую заменим новой переменной u по формуле

$$u = \sqrt{-\ln w}, \quad (10)$$

откуда

$$dw = -2ue^{-u^2} du. \quad (11)$$

С помощью (10) и (11) можно написать:

$$\int_1^{r/a} \frac{dw}{-\sqrt{-\ln w}} = 2 \int_0^{\sqrt{-\ln \frac{r}{a}}} e^{-u^2} du = \sqrt{\pi} \operatorname{erf} \left(\sqrt{-\ln \frac{r}{a}} \right), \quad (12)$$

где

$$\operatorname{erf} x = \frac{2}{\sqrt{\pi}} \int_0^x e^{-u^2} du \quad (13)$$

(интеграл вероятности). Из (9) и (12) получим выражение для траектории электрона:

$$\frac{z}{a} = \sqrt{\frac{2\pi^2 \varepsilon_0 \sqrt{2\eta} U_0^{3/2}}{I}} \cdot \frac{b^2 - a^2}{r_e^2 - a^2} \operatorname{erf}\left(\sqrt{-\ln \frac{r}{a}}\right). \quad (14)$$

Выражение (14) с учетом (2) после простых преобразований приводится к следующему виду:

$$\frac{z}{a} = \frac{\operatorname{erf}\left(\sqrt{\ln \frac{a}{r}}\right)}{\sqrt{\frac{P}{2\pi^2 \varepsilon_0 \sqrt{2\eta}}} \cdot F\left(\frac{R_2}{R_1}, \frac{b}{a}, \frac{R_2}{b}\right)}, \quad (15)$$

где

$$F\left(\frac{R_2}{R_1}, \frac{b}{a}, \frac{R_2}{b}\right) = \sqrt{\frac{\frac{1}{2} + \ln \frac{R_2}{b} - \frac{\ln \frac{b}{a}}{\left(\frac{b}{a}\right)^2 - 1}}{\ln \frac{R_2}{R_1}}}, \quad (16)$$

а

$$P = \frac{I}{U_0^{3/2}}, \quad \frac{a}{b^{3/2}} \quad (17)$$

— первеанс пучка. Отклонение электрона тем сильнее, чем меньше величина $\frac{z}{a}$ при данном $\frac{r}{a}$, т. е. чем больше величины первеанса P и параметра F . Из формулы (16) сразу видно, что с ростом отношения $\frac{R_2}{b}$ величина F растет, а с ростом $\frac{R_2}{R_1}$ она убывает. Анализ формулы показывает, что величина F монотонно растет с ростом величины $\frac{b}{a}$.

Представляет также интерес поведение функции F при фиксированных значениях $\frac{b}{a}$ и $\frac{b}{R_1}$. Обозначим

$$\gamma = \frac{R_1}{b}, \quad (18)$$

где $\frac{1}{R_2} < \gamma < 1$. Учитывая, что $\frac{R_2}{b} = \gamma \cdot \frac{R_2}{R_1}$, перепишем формулу (16).

Получится следующее соотношение:

$$F\left(\frac{R_2}{R_1}, \frac{b}{a}, \gamma\right) = \sqrt{1 + \frac{A}{\ln \frac{R_2}{R_1}}}, \quad (19)$$

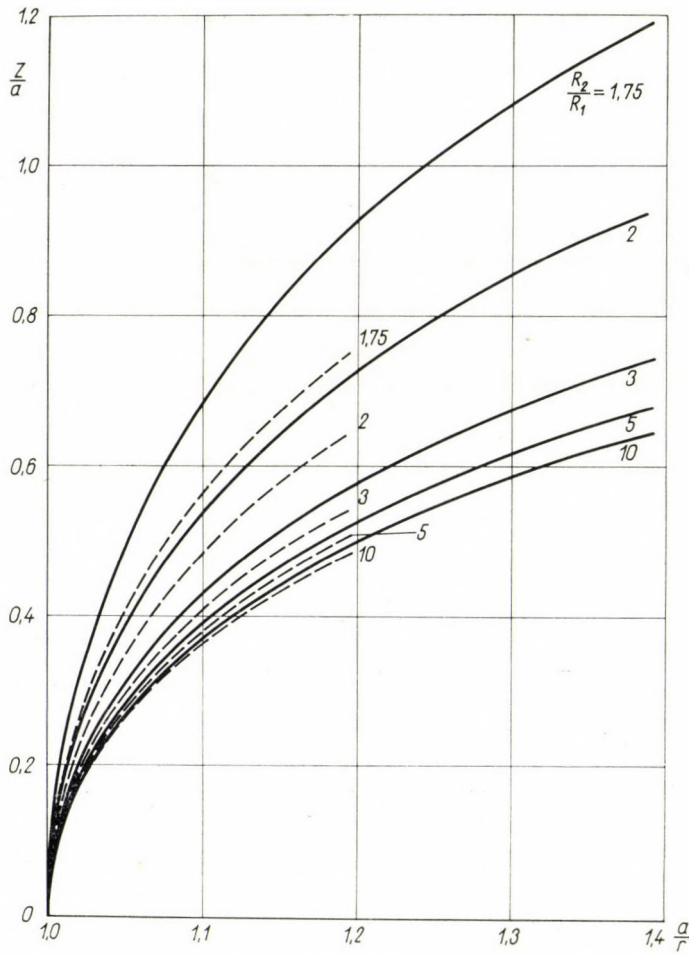


Рис. 3

Где

$$A = \frac{1}{2} + \ln \gamma - \frac{\ln \frac{b}{a}}{\left(\frac{b}{a}\right)^2 - 1} = \text{const.} \quad (20)$$

Анализ показывает, что при всех возможных значениях параметров γ и $\frac{b}{a}$

имеет место $A < 0$. (При этом необходимо помнить, что $R_1 < a < b < R_2$ по определению). Из формулы (19) видно, что в этом случае $0 < F < 1$ и величина F растет с ростом $\frac{R_2}{R_1}$, а также с ростом A .

В качестве примера на рис. 3. покажем графики зависимости безразмерной величины

$$\frac{Z}{a} = \sqrt{\frac{P}{2\pi^2 \varepsilon_0 \sqrt{2\eta}}} \frac{z}{a} \quad (21)$$

от $\frac{a}{r}$, построенные на основании соотношений (15) и (19) при $\gamma = 0,6$. Сплошные кривые относятся к случаю $\frac{b}{a} = 1, 2$, а штриховые — к случаю $\frac{b}{a} = 1,4$.

Величины отношения $\frac{R_2}{R_1}$ указаны на кривых.

Из соотношения (15) легко можно определить максимальную величину первеанса пучка, который может быть пропущен через рассматриваемую систему с длиной l . Очевидно, что условием максимального первеанса будет равенство расстояния от оси рассмотренного электрона радиусу внутреннего цилиндра, т. е.

$$\frac{a}{r} = \frac{a}{R_1} \quad \text{при} \quad \frac{z}{a} = \frac{l}{a}. \quad (22)$$

Подставляя эти равенства, а также значения универсальных постоянных в (15), получим следующее выражение:

$$P_{\max} = 1,04 \cdot 10^{-4} \left(\frac{a}{l} \right)^2 \left[\frac{\operatorname{erf} \left(\sqrt{\ln \frac{a}{R_1}} \right)}{F \left(\frac{R_2}{R_1}, \frac{b}{a}, \frac{R_2}{b} \right)} \right]^2 \frac{a}{\theta^{3/2}}. \quad (23)$$

Вследствие принятых допущений, а также потому, что длина l по определению должна быть намного больше всех поперечных размеров системы, величина P_{\max} не может быть очень большой. Величина $\frac{a}{R_1}$ связана с остальными параметрами следующим простым соотношением:

$$\frac{a}{R_1} = \frac{\frac{R_2}{R_1}}{\frac{b}{a} \cdot \frac{R_2}{b}}.$$

При данной величине первенца длина системы также ограничена условиями (22). Отсюда следует, что

$$\left(\frac{l}{a}\right)_{\max} = \frac{1 \cdot 02 \cdot 10^{-2}}{\sqrt{P}} \cdot \frac{\operatorname{erf}\left(\sqrt{\ln \frac{a}{R_1}}\right)}{F\left(\frac{R_2}{R_1}, \frac{b}{a}, \frac{R_2}{b}\right)}, \quad (24)$$

В заключение для полноты рассмотрим выражение траектории электрона, исходящего с внешней границы трубчатого пучка [1], которое в наших обозначениях имеет вид:

$$\frac{z}{b} = \sqrt{\frac{8\pi\epsilon_0\sqrt{2\eta}}{P}} \frac{b^2 - a^2}{b^2 - r_e^2} \int_0^{\sqrt{\ln \frac{r}{b}}} e^{u^2} du. \quad (25)$$

Здесь $b \leq r \leq R_2$.

Условием максимального первенца в этом случае является

$$\frac{r}{b} = \frac{R_2}{b} \quad \text{при} \quad \frac{z}{b} = \frac{l}{b}. \quad (26)$$

Подставляя значения универсальных постоянных в формулу (25), с учетом (2) и (26) получится следующий результат:

$$P_{\max} = 1,32 \cdot 10^{-4} \left(\frac{b}{l}\right)^2 \left[\frac{g\left(\sqrt{\ln \frac{R_2}{b}}\right)}{G\left(\frac{R_2}{R_1}, \frac{b}{a}, \frac{a}{R_1}\right)} \right]^2 \frac{a}{e^{3/2}}, \quad (27)$$

где

$$g(x) = \int_0^x e^{u^2} du, \quad (28)$$

а

$$G\left(\frac{R_2}{R_1}, \frac{b}{a}, \frac{a}{R_1}\right) = \sqrt{\frac{\ln \frac{a}{R_1} - \frac{1}{2} + \frac{\ln \frac{b}{a}}{1 - \left(\frac{a}{b}\right)^2}}{\ln \frac{R_2}{R_1}}}. \quad (29)$$

(Значения функции $g(x)$ могут быть найдены с помощью таблиц).

Аналогично, для максимальной длины системы получаем:

$$\left(\frac{l}{b}\right)_{\max} = \frac{1,15 \cdot 10^{-2}}{\sqrt{P}} \cdot \frac{g \left(\sqrt{\ln \frac{R_2}{b}} \right)}{G \left(\frac{R_2}{R_1}, \frac{b}{a}, \frac{a}{R_1} \right)}. \quad (30)$$

При решении конкретных задач необходимо, конечно, исследовать обе траектории по формулам (15) и (25). Максимальная величина первеанса определяется всегда той из формул (23) и (27), которая дает меньшее значение. Такое же правило имеет место и при определении максимальной длины системы на основании формул (24) и (30).

В качестве примера рассмотрен пучок с первеансом $P = 1,92 \cdot 10^{-6} a/\theta^{3/2}$, движущийся в системе, которая имеет следующие параметры: $\frac{a}{R_1} = 2$, $\frac{b}{R_1} = 3$ и $\frac{R_2}{R_1} = 4$. В этом случае по формуле (24) получается $\left(\frac{l}{R_1}\right)_{\max} = 19,38$, а по формуле (30) — $\left(\frac{l}{R_1}\right)_{\max} = 18,04$.

ЛИТЕРАТУРА

1. N. WAX, J. Appl. Phys., **20**, 242, 1949.
2. L. A. HARRIS, IRE Convention Record, part 3., p. 11—18, 1956.
3. K. K. N. CHANG, Proc. IRE, **45**, 1522, 1957.

CALCULATION OF THE TRAJECTORY OF AN ELECTRON MOVING BETWEEN COAXIAL TUBES IN THE PRESENCE OF A HOLLOW ELECTRON BEAM

By
M. SZILÁGYI

A b s t r a c t

The trajectory of an electron starting off the internal boundary of an axially symmetrical hollow dense electron beam moving between two coaxial long conductive cylinders is determined. The influence of different parameters of the system on the electron motion is investigated. Formulae are given for the determination of the maximum beam perveance and system length.

ПЕРИОДИЧЕСКАЯ ЭЛЕКТРОСТАТИЧЕСКАЯ ФОКУСИРОВКА ЛЕНТОЧНЫХ ЭЛЕКТРОННЫХ ПОТОКОВ

М. Силади

ИНСТИТУТ ТЕХНИЧЕСКОЙ ФИЗИКИ ВЕНГЕРСКОЙ АН, БУДАПЕШТ

(Представлено Г. Сигети. — Поступило 24. XI. 1964)

В работе исследуется периодическая электростатическая фокусировка ленточного электронного пучка. Фокусирующая система имеет плоскость симметрии, совпадающую со средней плоскостью пучка. Толщина потока может быть соизмеримой с периодом системы. Определены условия оптимальной фокусировки: величина фокусирующего потенциала, приближенная траектория электронов, первеанс пучка, а также необходимое распределение плотности тока по сечению пучка. Параксиальное приближение рассматривается как частный случай. Для этого случая приводится сравнение условий фокусировки ленточного потока с характеристиками фокусировки цилиндрического пучка. В заключении определена форма электродов для рассматриваемого вида поля, а также зависимость первеанса пучка от геометрических параметров. Найдено, что максимальная величина первеанса достигается вне параксиальной области.

Введение

Периодическая электростатическая фокусировка с успехом применяется для сохранения формы интенсивных электронных потоков. В настоящее время достаточно полно разработана теория периодической электростатической фокусировки цилиндрических пучков [1, 2, 9]. На практике, однако, в различных электронных приборах часто применяются также и ленточные пучки большой интенсивности. Для фокусировки таких пучков также используются различные периодические электростатические системы [3—5].

Теория периодической электростатической фокусировки ленточных пучков в параксиальном приближении дана в работах [5, 6]. Фокусировка ленточных пучков серией тонких линз рассматривалась в работе [7].

В настоящей работе исследуется фокусировка широкого ленточного электронного потока периодической электростатической системой, имеющей плоскость симметрии, которая совпадает со средней плоскостью пучка. Рассматриваемый случай существенно отличается от случая криволинейных ленточных потоков [10—13]. Период системы может быть соизмеримым с толщиной пучка, или быть намного больше этой величины. Рассматривается случай оптимальной фокусировки, которая определяется минимальной волнистостью пучка.

Результаты работы приближенно могут быть распространены также и на случай трубчатых пучков, если толщина пучка и период системы малы

по сравнению с диаметром пучка. (Мы получим соответствующую трубчатую систему, если сечение плоской системы повернем вокруг оси симметрии.)

Оптимальная фокусировка ленточного пучка

Рассмотрим длинный интенсивный ленточный электронный поток. Расположим прямоугольную систему координат x, y, z таким образом, чтобы

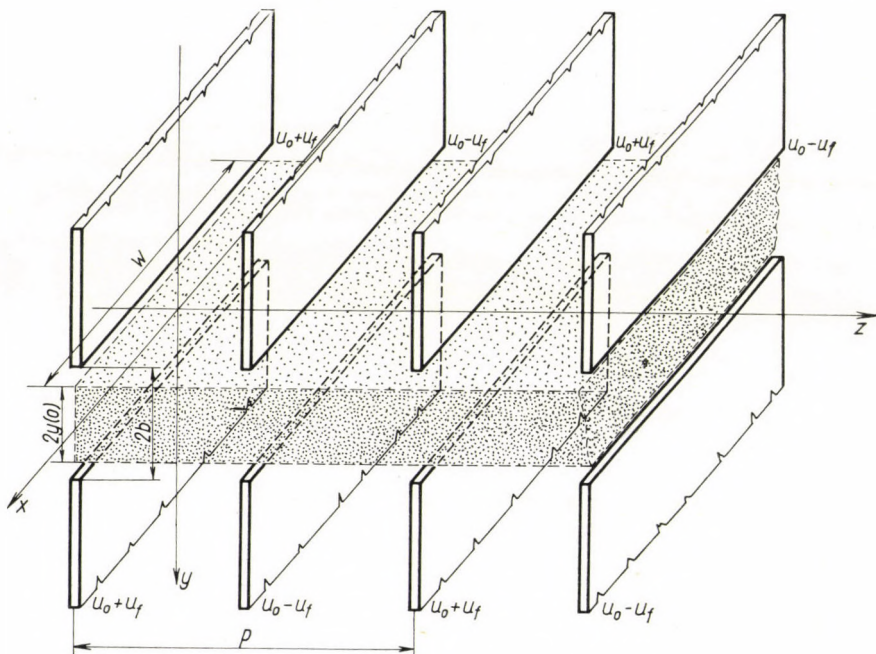


Рис. 1

направление движения пучка совпало с направлением оси z (рис. 1). Пусть ширина пучка W (по направлению оси x) намного больше его толщины (по направлению оси y), а в то же время длина пучка намного превышает его ширину. В этом случае можно считать, что силы пространственного заряда действуют только по направлению оси y . Эти силы компенсируются постоянным во времени электрическим полем электродной системы, расположенной с двух сторон вблизи пучка. Электроды сильно вытянуты по направлению оси x . На них прикладываются потенциалы, периодически меняющиеся по направлению оси z , таким образом, чтобы фокусирующая система, так же как и поток, были симметричными относительно плоскости xz (рис. 1.). Практически по направлению оси x силы не действуют, т. к. ширина пучка и длина электродов велики. По этой причине, если электроны входят в систему

в плоскости $z = 0$ параллельно оси z , они будут двигаться в плоскостях, параллельных плоскости yz . Поэтому все рассмотрение может быть проведено в этой плоскости, для системы, симметричной относительно оси z .

Примем также следующие допущения:

а) Поток считается ламинарным, электронные траектории не пересекаются. Таким образом, влиянием тепловых скоростей пренебрегаем. В этом приближении величина силы тока постоянна внутри любого слоя пучка, ограниченного электронными траекториями.

б) Компенсирующим влиянием положительных ионов, находящихся в потоке, пренебрегаем.

в) Ограничиваемся рассмотрением таких потоков, в которых скорости электронов очень малы по сравнению со скоростью света. Таким образом, релятивистские эффекты могут не учитываться. Это влечет за собой пренебрежение магнитными силами, возникающими между параллельно движущимися электронами.

В работе применяется практическая система единиц МКСА.

Распределение потенциала фокусирующей системы в средней плоскости задается следующим простым выражением:

$$\Phi(z) = U_0 + U_1 \cos \frac{2\pi}{p} z. \quad (1)$$

Здесь U_0 — средний потенциал по оси z , на который накладывается периодическая составляющая потенциала с амплитудой U_1 ; p — период фокусирующей системы. Если известно осевое распределение потенциала, то величина потенциала в произвольной точке пространства может быть найдена с помощью следующего соотношения [8]:

$$U(y, z) = \frac{1}{2} [\Phi(z + iy) + \Phi(z - iy)]. \quad (2)$$

Подставляя выражение (1) в (2), получим общее распределение потенциала, которое имеет вид:

$$U(y, z) = U_0 + U_1 \operatorname{ch} \frac{2\pi}{p} y \cos \frac{2\pi}{p} z. \quad (3)$$

Пусть на электроды фокусирующей системы попаременно приложены потенциалы $(U_0 + U_f)$ и $(U_0 - U_f)$, а величину расстояния между симметрично расположенными электродами обозначим через $2b$ (рис. 1). Тогда,

подставляя в (3) значения $U = U_0 \pm U_f$, $z = k \frac{p}{2}$ и $y = b$, мы получим

величину U_1 как функцию параметров фокусирующей системы (здесь k четное или нечетное целое число, в зависимости от потенциала электрода):

$$U_1 = \frac{U_f}{\operatorname{ch} \frac{2\pi}{p} b} . \quad (4)$$

Мы будем рассматривать случай, когда

$$\frac{U_f}{U_0} \ll 1 ,$$

то-есть ограничиваемся малыми значениями фокусирующего потенциала U_f .

Применим для нашего случая метод анализа, разработанный для аксиально-симметричных пучков [2]. Траекторию любого электрона пучка будем искать в виде

$$y(z) = y_0 + y_1(z) . \quad (5)$$

Если удалось осуществить оптимальную фокусировку, то y_1 является периодической функцией от z , амплитуда которой намного меньше, чем постоянная составляющая y_0 . В этом случае наклон траектории также является малой величиной. Таким образом,

$$2\pi \frac{y_1}{y_0} \ll 1 , \quad \frac{dy_1}{dz} \ll 1 .$$

Представим выражение (3) в виде ряда Тэйлора, с учетом (5). Получится следующий результат:

$$U(y, z) = U_0 + U_1 \left[\operatorname{ch} \frac{2\pi}{p} y_0 + y_1 \frac{2\pi}{p} \operatorname{sh} \frac{2\pi}{p} y_0 + \right. \\ \left. + \frac{y_1^2}{2} \left(\frac{2\pi}{p} \right)^2 \operatorname{ch} \frac{2\pi}{p} y_0 + \dots \right] \cos \frac{2\pi}{p} z . \quad (6)$$

Из малости величины $\frac{2\pi y_1}{y_0}$ следует, что и величина $\frac{2\pi y_1}{p}$ мала, если период системы намного больше y_0 или соизмерим с этой величиной (случай $\frac{p}{y_0} \ll 1$ является практически мало интересным). По этой причине члены ряда, содержащие $\frac{2\pi y_1}{p}$ в степени выше второй, могут быть опущены.

Величина y -вой составляющей электрического поля, созданного фокусирующей системой, может быть выражена с помощью (5) и (6). Получается

$$\begin{aligned} E(y, z) = - \frac{\partial U(y, z)}{\partial y} = - U_1 \left[\frac{2\pi}{p} \operatorname{sh} \frac{2\pi}{p} y_0 + \right. \\ \left. + y_1 \left(\frac{2\pi}{p} \right)^2 \operatorname{ch} \frac{2\pi}{p} y_0 + \frac{y_1^2}{2} \left(\frac{2\pi}{p} \right)^3 \operatorname{sh} \frac{2\pi}{p} y_0 \right] \cos \frac{2\pi}{p} z. \end{aligned} \quad (7)$$

Кроме этого, действует еще и поле пространственного заряда, причем также по направлению оси y . Предположим сначала, что плотность тока равномерно распределяется по сечению пучка. В этом случае величина напряженности поля пространственного заряда равна

$$E_\varrho(y, z) = - \frac{I(y)}{2\epsilon_0 W u(z)}, \quad (8)$$

где $I(y)$ — сила тока в слое пучка с толщиной $2y$, ограниченном поверхностями, определенными рассматриваемой и симметричной ей траекториями. Величина этой силы тока с учетом (5) связана с полным током пучка I_n следующим соотношением:

$$I(y) \approx I_n \frac{y_0}{y_{0 \max}} = I(y_0) = \text{const}. \quad (9)$$

Здесь $y_{0 \max}$ — средняя величина расстояния крайней траектории пучка от оси, $u(z)$ — средняя скорость электронов по сечению пучка, а ϵ_0 — величина диэлектрической проницаемости вакуума.

Уравнение движения рассматриваемого электрона имеет вид:

$$\frac{d^2 y}{dt^2} = -\eta(E + E_\varrho), \quad (10)$$

где $\eta = \frac{e}{m}$ — абсолютная величина отношения заряда электрона к его массе.

Перейдем в этом уравнении от производной по времени к производной по координате z , на основании соотношения

$$\frac{dz}{dt} = v_z(y, z), \quad (11)$$

где v_z — составляющая скорости v по направлению оси z , в точке с координатами (y, z) . Из (11) следует, что

$$\frac{d^2 y}{dt^2} = v_z^2 \frac{d^2 y}{dz^2} + v_z \frac{dv_z}{dz} \frac{dy}{dz}. \quad (12)$$

Теперь перепишем уравнение (10) с учетом (7), (8), (12), (5) и (9). Получается следующее дифференциальное уравнение второго порядка:

$$\begin{aligned} \frac{d^2 y_1}{dz^2} + \frac{1}{v_z} \frac{dv_z}{dz} \frac{dy_1}{dz} - \frac{\eta}{v_z^2} U_1 \left[\left(\frac{2\pi}{p} \right)^2 y_1 \operatorname{ch} \frac{2\pi}{p} y_0 + \right. \\ \left. + \left(\frac{2\pi}{p} \right)^3 \frac{y_1^2}{p} \operatorname{sh} \frac{2\pi}{p} y_0 \right] \cos \frac{2\pi}{p} z = \\ = \frac{\eta}{v_z^2} U_1 \frac{2\pi}{p} \operatorname{sh} \frac{2\pi}{p} y_0 \cos \frac{2\pi}{p} z + \frac{\eta I(y_0)}{2\varepsilon_0 W v_z^2 u(z)}. \end{aligned} \quad (13)$$

Так как в случае оптимальной фокусировки поперечная составляющая скорости электрона пренебрежимо мала по сравнению с z -вой составляющей, можно считать, что

$$v_z(y, z) \approx v(y, z) = \sqrt{2\eta U(y, z)}. \quad (14)$$

На основании соотношений (3) и (4), а также условий

$$\frac{U_f}{U_0} \ll 1, \quad \frac{2\pi y_1}{p} \ll 1, \quad \frac{dy_1}{dz} \ll 1 \quad (15)$$

можно написать:

$$\begin{aligned} v_z \approx \sqrt{2\eta U_0} \left\{ 1 + \frac{U_1}{2U_0} \cos \frac{2\pi}{p} z \left[\operatorname{ch} \frac{2\pi}{p} y_0 + \right. \right. \\ \left. \left. + y_1 \frac{2\pi}{p} \operatorname{sh} \frac{2\pi}{p} y_0 + \frac{y_1^2}{2} \left(\frac{2\pi}{p} \right)^2 \operatorname{ch} \frac{2\pi}{p} y_0 \right] - \right. \\ \left. - \frac{1}{8} \left(\frac{U_1}{U_0} \right)^2 \cos^2 \frac{2\pi}{p} z \left[\operatorname{ch}^2 \frac{2\pi}{p} y_0 + y_1 \frac{2\pi}{p} \operatorname{sh} \frac{4\pi}{p} y_0 \right] \right\}, \end{aligned} \quad (16)$$

$$\begin{aligned} \frac{dv_z}{dz} \approx \sqrt{2\eta U_0} \left\{ - \frac{U_1}{2U_0} \frac{2\pi}{p} \sin \frac{2\pi}{p} z \left[\operatorname{ch} \frac{2\pi}{p} y_0 + \right. \right. \\ \left. \left. + y_1 \frac{2\pi}{p} \operatorname{sh} \frac{2\pi}{p} y_0 \right] + \frac{U_1}{2U_0} \frac{2\pi}{p} \cos \frac{2\pi}{p} z \frac{dy_1}{dz} \operatorname{sh} \frac{2\pi}{p} y_0 + \right. \\ \left. + \frac{1}{8} \left(\frac{U_1}{U_0} \right)^2 \frac{2\pi}{p} \sin \frac{4\pi}{p} z \operatorname{ch}^2 \frac{2\pi}{p} y_0 \right\}, \end{aligned} \quad (17)$$

$$\frac{1}{v_z} \approx \frac{1}{\sqrt{2\eta U_0}} \left\{ 1 - \frac{U_1}{2U_0} \cos \frac{2\pi}{p} z \left[\operatorname{ch} \frac{2\pi}{p} y_0 + \right. \right. \\ \left. \left. + y_1 \frac{2\pi}{p} \operatorname{sh} \frac{2\pi}{p} y_0 \right] + \frac{3}{8} \left(\frac{U_1}{U_0} \right)^2 \cos^2 \frac{2\pi}{p} z \operatorname{ch}^2 \frac{2\pi}{p} y_0 \right\}, \quad (18)$$

$$\frac{1}{v_z^2} \approx \frac{1}{2\eta U_0} \left\{ 1 + \left(\frac{U_1}{U_0} \right)^2 \cos^2 \frac{2\pi}{p} z \operatorname{ch}^2 \frac{2\pi}{p} y_0 - \right. \\ \left. - \frac{U_1}{U_0} \cos \frac{2\pi}{p} z \left[\operatorname{ch} \frac{2\pi}{p} y_0 + y_1 \frac{2\pi}{p} \operatorname{sh} \frac{2\pi}{p} y_0 \right] \right\}. \quad (19)$$

Подставим эти выражения в уравнение (13). Если ограничиться членами второго порядка малости, то получим следующее линейное неоднородное дифференциальное уравнение второго порядка:

$$\frac{p}{2\pi} \frac{d^2 y_1}{dz^2} - \frac{U_1}{2U_0} \operatorname{ch} \frac{2\pi}{p} y_0 \sin \frac{2\pi}{p} z \frac{dy_1}{dz} - \\ - \frac{2\pi}{p} \frac{U_1}{2U_0} \operatorname{ch} \frac{2\pi}{p} y_0 \cos \frac{2\pi}{p} z \cdot y_1 = \frac{U_1}{2U_0} \operatorname{sh} \frac{2\pi}{p} y_0 \cos \frac{2\pi}{p} z - \\ - \frac{1}{4} \left(\frac{U_1}{U_0} \right)^2 \operatorname{sh} \frac{4\pi}{p} y_0 \cos^2 \frac{2\pi}{p} z + \frac{pI(y_0)}{8\pi\varepsilon_0 W \sqrt{2\eta} U_0^{3/2}}. \quad (20)$$

При выводе уравнения (20) было учтено, что его последний член имеет величину второго порядка малости [2]; поэтому в данном приближении средняя скорость электронов может быть задана выражением

$$u(z) = \sqrt{2\eta U_0} = \text{const.} \quad (21)$$

Для приближенного определения траектории электрона рассмотрим только те члены уравнения (20), которые имеют величины первого порядка малости, то есть следующее дифференциальное уравнение:

$$\frac{d^2 y_1}{dz^2} = \frac{2\pi}{p} \frac{U_1}{2U_0} \operatorname{sh} \frac{2\pi}{p} y_0 \cos \frac{2\pi}{p} z. \quad (22)$$

В это уравнение не входит член, характеризующий пространственный заряд пучка. Таким образом, пространственный заряд в периодическом фокусирующем поле в первом приближении не влияет на форму траектории.

Решение уравнения имеет вид:

$$y_1(z) = c_1 + c_2 z - \frac{p}{2\pi} \frac{U_1}{2U_0} \operatorname{sh} \frac{2\pi}{p} y_0 \cos \frac{2\pi}{p} z. \quad (23)$$

Произвольные постоянные c_1 и c_2 могут быть определены из начальных условий. Пусть электрон входит в систему параллельно оси z и его начальное расстояние от оси составляет

$$y(0) = y_0 - \frac{p}{2\pi} \frac{U_1}{2U_0} \operatorname{sh} \frac{2\pi}{p} y_0. \quad (24)$$

Тогда начальные условия имеют вид:

$$y_1(0) = -\frac{p}{2\pi} \frac{U_1}{2U_0} \operatorname{sh} \frac{2\pi}{p} y_0 \quad (25)$$

и

$$\left. \frac{dy_1}{dz} \right|_{z=0} = 0. \quad (26)$$

В этом случае $c_1 = c_2 = 0$ и окончательным решением, согласно (23), будет

$$y_1(z) = -\frac{p}{2\pi} \frac{U_1}{2U_0} \operatorname{sh} \frac{2\pi}{p} y_0 \cos \frac{2\pi}{p} z. \quad (27)$$

Теперь подставим величины y_1 и его производных, рассчитанных на основании выражения (27), обратно в уравнение (20) и выпишем постоянные члены полученного равенства. После простых преобразований получится следующий результат:

$$\left(\frac{U_1}{U_0} \right)^2 = \frac{pI(y_0)}{\pi \varepsilon_0 W \sqrt{2\eta} U_0^{3/2}} \cdot \frac{1}{\operatorname{sh} \frac{4\pi}{p} y_0}. \quad (28)$$

Это соотношение выражает необходимое условие оптимальной фокусировки: равновесие фокусирующих сил с силами пространственного заряда. (Конечно, речь идет о равновесии средних величин). Если подобрать параметры фокусирующей системы таким образом, чтобы имело место соотношение (28), то траектория электрона будет почти прямолинейной и на основании (5) и (27) она приближенно будет определяться выражением

$$y(z) = y_0 - \frac{p}{2\pi} \frac{U_1}{2U_0} \operatorname{sh} \frac{2\pi}{p} y_0 \cos \frac{2\pi}{p} z, \quad (29)$$

где необходимая величина $\frac{U_1}{U_0}$ рассчитывается по (28). В случае оптимальной фокусировки точного решения уравнения (20) не требуется, так как амплитуда волнистости траектории очень мала.

Соотношение (28) должно выполняться при всех значениях y внутри потока, иначе возникнут пертурбации. Так как фокусирующая сила быстро растет при удалении от оси, поэтому для выполнения этого требования необходимо, чтобы сила пространственного заряда также возрастала по такому же закону. Говоря языком оптики, по сути дела речь идет о том, что специально подобранное распределение плотности тока пучка $j(y)$ должно скомпенсировать сферическую aberrацию системы. Теперь рассчитаем это распределение.

Если плотность тока меняется по поперечному сечению пучка, то вместо (9) будет действительным следующее соотношение:

$$I(y) = 2W \int_0^y j(y) dy. \quad (30)$$

При произвольном значении y выражение (28) дает:

$$I(y) = \frac{\pi \varepsilon_0 W \sqrt{2\eta} U_0^{3/2}}{P} \left(\frac{U_1}{U_0} \right)^2 \operatorname{sh} \frac{4\pi}{P} y. \quad (31)$$

Искомое распределение плотности тока получится из (30) и (31):

$$j(y) = \frac{1}{2W} \frac{dI}{dy} = \frac{2\pi^2 \varepsilon_0 \sqrt{2\eta} U_0^{3/2}}{P^2} \left(\frac{U_1}{U_0} \right)^2 \operatorname{ch} \frac{4\pi}{P} y. \quad (32)$$

Следует отметить, что практическое осуществление такого распределения является сложной задачей.

Введем величину среднего первеанса пучка, которая — как обычно — выражается через

$$P = \frac{I_n}{U_0^{3/2}} \quad a/e^{3/2}. \quad (33)$$

Запишем соотношение (28) для крайней траектории пучка $y_0 = y_{0\max}$. Тогда с учетом (33) получим первеанс пучка, который может быть оптимально сфокусирован при заданном значении $\frac{U_1}{U_0}$:

$$P = \pi \varepsilon_0 \sqrt{2\eta} \frac{W}{P} \left(\frac{U_1}{U_0} \right)^2 \operatorname{sh} \frac{4\pi}{P} y_{0\max}. \quad (34)$$

Параксиальный случай

Если выполняется условие

$$\frac{4\pi}{p} y_0 \max \ll 1, \quad (35)$$

то может быть применено параксиальное приближение и задача упростится. В этом случае вместо соотношений (28) и (29) — с учетом (9) и (35) — можем пользоваться следующими выражениями:

$$\left(\frac{U_1}{U_0} \right)^2 = \frac{p^2 I_n}{4\pi^2 \varepsilon_0 W \sqrt{2\eta} U_0^{3/2} y_0 \max} \quad (36)$$

и

$$y(z) = y_0 \left(1 - \frac{1}{2} \frac{U_1}{U_0} \cos \frac{2\pi}{p} z \right). \quad (37)$$

Выражения (36) и (37) совпадают с формулами, полученными в работе [5] путем приближенного решения параксиального уравнения. В этом случае необходимая величина $\frac{U_1}{U_0}$ не зависит от величины y_0 , поэтому плотность тока равномерно распределяется по сечению пучка:

$$j = \frac{2\pi^2 \varepsilon_0 \sqrt{2\eta} U_0^{3/2}}{p^2} \left(\frac{U_1}{U_0} \right)^2 = \text{const.}, \quad (38)$$

согласно (32) и (35), так как в параксиальном случае сферической аберрации можно пренебречь.

Величина первенца пучка в этом случае может быть получена из выражений (33) и (36), или из (34) и (35):

$$P = 4\pi^2 \varepsilon_0 \sqrt{2\eta} \frac{W y_0 \max}{p^2} \left(\frac{U_1}{U_0} \right)^2. \quad (39)$$

Сравнение условий фокусировки цилиндрического и ленточного пучков

В параксиальном случае легко можно сравнить друг с другом условия оптимальной фокусировки ленточного и аксиально-симметричного цилиндрического пучков. С этой целью будем рассматривать пучки, имеющие оди-

наковые параметры и одинаковые средние поперечные сечения, которые обозначим через S_0 . Для ленточного пучка

$$S_0 = 2W_{y_0 \max}, \quad (40)$$

а для цилиндрического пучка

$$S_0 = \pi r_{0 \max}^2, \quad (41)$$

где $r_{0 \max}$ — средний радиус пучка. Обозначим параметр фокусировки $\frac{U_1}{U_0}$ в случае ленточного пучка через F_λ , а в случае цилиндрического пучка через F_μ . Аналогично, амплитуды волнистости траекторий, рассчитанных в первом приближении, будут соответственно выражены через δ_λ и δ_μ .

Из выражений (36), (37) и (40) следует, что

$$F_\lambda = \sqrt{\frac{p^2 I_n}{2\pi^2 \varepsilon_0 \sqrt{2\eta} U_0^{3/2} S_0}} \quad (42)$$

и

$$\delta_\lambda = \frac{1}{2} F_\lambda. \quad (43)$$

В случае цилиндрического пучка, на основании результатов работы [1], а также выражения (41), можно написать:

$$F_\mu = \sqrt{\frac{2p^2 I_n}{3\pi^2 \varepsilon_0 \sqrt{2\eta} U_0^{3/2} S_0}} \quad (44)$$

и

$$\delta_\mu = \frac{1}{4} F_\mu. \quad (45)$$

Эти формулы верны, если осевое распределение фокусирующего потенциала определяется выражением (1).

Из сравнения формул (42)–(45) получаем, что

$$\frac{F_\lambda}{F_\mu} = \frac{\sqrt{3}}{2} = 0,866 \quad (46)$$

и

$$\frac{\delta_\lambda}{\delta_\mu} = \sqrt{3} = 1,732. \quad (47)$$

Итак, если параметры обоих пучков одинаковы, то для фокусировки ленточного пучка требуется несколько меньшее поле, но волнистость потока будет больше, чем в аксиально-симметричном случае.

Наконец сравним между собой величины первеансов при оптимальной фокусировке, в случае $F_\lambda = F_\mu = F$. Величину первеанса цилиндрического пучка в параксиальном приближении получим из выражений (33), (41) и (44):

$$P_\mu = \frac{3}{2} \pi^3 \varepsilon_0 \sqrt{2\eta} \left(\frac{r_{0 \max}}{P} \right)^2 F^2. \quad (48)$$

Обозначим первеанс ленточного потока через P_λ . Тогда из (39) и (48) получаем, что

$$\frac{P_\lambda}{P_\mu} = \frac{8W y_{0 \max}}{3\pi r_{0 \max}^2}. \quad (49)$$

Из этого выражения видно, что при $r_{0 \max} \approx y_{0 \max}$ и прочих равных параметрах первеанс оптимально фокусируемого ленточного пучка может намного превышать первеанс цилиндрического пучка, так как $W \geq y_{0 \max}$ по определению.

Заключение

Выше были определены условия оптимальной фокусировки ленточных электронных потоков электростатическими полями при произвольной величине периода поля. Распределение потенциала на оси задавалось простым выражением (1), которое является характерным для применяемых на практике фокусирующих систем. Поэтому, полученные результаты качественно верны для любой плоско-симметричной электростатической периодической системы.* (Каждая конкретная система в первом приближении может быть охарактеризована своей величиной U_1). Тем не менее, представляет интерес фокусирующая система, для которой формула (1) является строгим выражением распределения поля.

Определим сначала форму электродов, создающих такое распределение. С этой целью подставим величины $U_0 \pm U_f$ в левую часть выражения (3), а величину U_1 , рассчитанную по формуле (4), — в правую часть этого выражения. Получается следующее уравнение:

$$\cos \frac{2\pi}{P} z = \pm \frac{\operatorname{ch} \frac{2\pi}{P} b}{\operatorname{ch} \frac{2\pi}{P} y}. \quad (50)$$

* В работе [4], например, рассматривалась специальная система. Первеанс пучка имел величину такого же порядка, как и в настоящей работе.

Здесь положительный знак относится к электродам с потенциалом $(U_0 + U_f)$, а отрицательный знак — к электродам с потенциалом $(U_0 - U_f)$. Форма электродов, рассчитанная по формуле (50) для случая $\frac{b}{p} = \frac{1}{4}$ показана на рис. 2. На рисунке указаны также эквипотенциальные линии U_0 , $(U_0 + U_1)$ и $(U_0 - U_1)$.

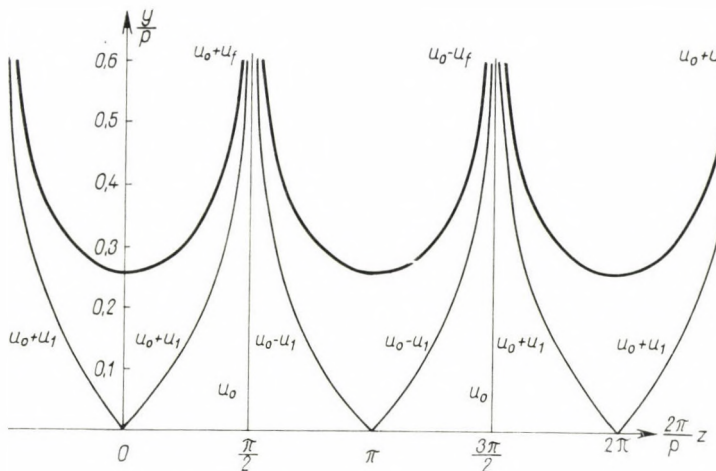


Рис. 2

Для этой системы выражение (4) является строгим соотношением. Представляя величину U_1 из (4) в формулы (28), (29), (32) и (34), мы получаем условия оптимальной фокусировки для данной системы:

$$\left(\frac{U_f}{U_0}\right)^2 = \frac{pI(y_0)}{\pi\varepsilon_0\sqrt{2\eta}WU_0^{3/2}} \frac{\operatorname{ch}^2 \frac{2\pi}{p} b}{\operatorname{sh} \frac{4\pi}{p} y_0}, \quad (51)$$

$$y(z) = y_0 - \frac{p}{4\pi} \frac{U_f}{U_0} \frac{\operatorname{sh} \frac{2\pi}{p} y_0}{\operatorname{ch} \frac{2\pi}{p} b} \cos \frac{2\pi}{p} z, \quad (52)$$

$$j(y) = \frac{2\pi^2 \varepsilon_0 \sqrt{2\eta} U_0^{3/2}}{p^2} \left(\frac{U_f}{U_0}\right)^2 \frac{\operatorname{ch} \frac{4\pi}{p} y}{\operatorname{ch}^2 \frac{2\pi}{p} b} \quad (53)$$

и

$$P = \pi \varepsilon_0 \sqrt{2\eta} \frac{W}{p} \left(\frac{U_f}{U_0} \right)^2 \frac{\operatorname{sh} \frac{4\pi}{p} y_{0 \max}}{\operatorname{ch}^2 \frac{2\pi}{p} b}. \quad (54)$$

Рассмотрим еще вопрос о том, как будет изменяться величина первеанса при фиксированном значении $\frac{U_f}{U_0}$, если менять величину отношения $\frac{y_{0 \max}}{p}$.

Пусть $\frac{W}{y_{0 \max}} = \text{const}$. Введем следующие обозначения:

$$\frac{y_{0 \max}}{b} = \gamma < 1 \quad (55)$$

и

$$2\pi \frac{y_{0 \max}}{p} = \xi. \quad (56)$$

Тогда на основании (54), (55) и (56), подставив значения универсальных постоянных, получим следующее выражение для первеанса:

$$P = 2,63 \cdot 10^{-6} \left(\frac{U_f}{U_0} \right)^2 \frac{W}{y_{0 \max}} f(\xi, \gamma) a/e^{3/2}, \quad (57)$$

где

$$f(\xi, \gamma) = \xi \frac{\operatorname{sh} 2\xi}{\operatorname{ch}^2 \frac{\xi}{\gamma}}. \quad (58)$$

Функция $f(\xi, \gamma)$ имеет следующие асимптоты:

а) При $\xi \ll 1$ (параксиальный случай):

$$f(\xi, \gamma) \approx 2\xi^2, \quad (59)$$

если γ не очень малая величина.

б) При $\xi \gg 1$

$$f(\xi, \gamma) \approx 2\xi \exp \left[-2\xi \frac{1-\gamma}{\gamma} \right]. \quad (60)$$

Таким образом, величина первеанса с ростом ξ сначала растет, а потом резко убывает. При некотором значении $\xi = \xi_{\text{opt}}$ первеанс достигает максимальной величины. Согласно (58), величина ξ_{opt} определяется следующим трансцендентным уравнением:

$$\left(\frac{1}{\gamma} \operatorname{th} \frac{\xi_{\text{opt.}}}{\gamma} - \frac{1}{2\xi_{\text{opt.}}} \right) \operatorname{th} 2\xi_{\text{opt.}} = 1. \quad (61)$$

Графики функции $f(\xi, \gamma)$ показаны на рис. 3. при трех разных значениях γ . На рисунке видно, что ростом γ величина первенца сильно растет и в то же время положение максимума смещается в сторону больших значений ξ . (См. таблицу 1.).

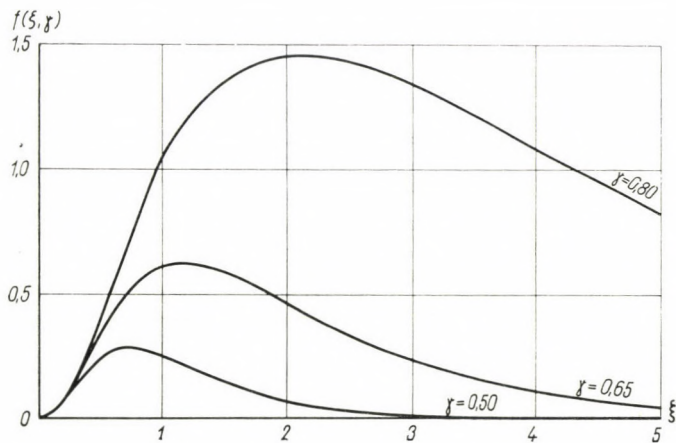


Рис. 3

Из таблицы видно, что при всех практически интересных значениях коэффициента заполнения γ максимальная величина первенца достигается вне параксиальной области. Практическая полезность настоящей работы состоит как раз в том, что с ее помощью становится возможным расчет фокусирующих систем для более интенсивных ленточных потоков, чем с помощью параксиальной теории. Сильно меняющиеся с расстоянием периодические поля ($p \approx y_{\max}$) имеют еще и то преимущество, что в них флуктуации пространственного заряда имеют меньшее влияние, вследствие чего увеличивается стабильность фокусировки.

Таблица 1

γ	$\xi_{\text{opt.}}$	f_{\max}
0,50	0,73	0,289
0,65	1,15	0,623
0,80	2,11	1,454

ЛИТЕРАТУРА

1. A. M. CLOGSTON and H. HEFFNER, J. Appl. Phys., **25**, 436, 1954.
2. P. K. TIEN, J. Appl. Phys., **25**, 1281, 1954.
3. R. ADLER, O. M. KROMHOUT and P. A. CLAVIER, Proc. IRE, **44**, 82, 1956.
4. C. C. JOHNSON, IRE Trans. El. Dev., ED-5, 233, 1958.
5. W. E. WATERS, J. Appl. Phys., **31**, 1814, 1960.
6. R. ADLER, O. M. KROMHOUT and P. A. CLAVIER, Proc. IRE, **43**, 339, 1955.
7. M. SZILÁGYI, Acta Phys. Hung., **18**, 87, 1965.
8. J. R. PIERCE, Theory and Design of Electron Beams, Chapter I, Van Nostrand, New York, 1954.
9. K. K. N. CHANG, Proc. IRE, **45**, 1522, 1957.
10. J. R. HECHTEL, The Microwave Journ., **3**, 41 and 81, 1960.
11. H. A. C. HOGG, Proc. IEE, **B-105**, 1016, 1958.
12. P. A. STURROCK, J. Electr. Control, **7**, 153, 1959.
13. F. J. NEWLAND, Microwaves (Proc. 4th Intern. Congr. on Microwave Tubes), K-17, p. 620–625, 1963.

PERIODIC ELECTROSTATIC FOCUSING OF SHEET ELECTRON BEAMS

By

M. SZILÁGYI

A b s t r a c t

An investigation of the periodic electrostatic focusing of sheet electron streams is given. The focusing system has a plane of symmetry, which coincides with the medium plane of the beam. The beam thickness may be comparable with the period of the system. The following optimal focusing conditions are determined: the value of the focusing potential, the approximate electron trajectories, the beam permeance and the required current density distribution in the beam cross section. The paraxial approximation is considered as a special case. In this case the focusing conditions for sheet beams are compared with those for the cylindrical ones. Finally the electrode shapes for the considered type of electric field are determined, and the beam permeance as a function of geometric parameters is given. It is found that the maximum value of the permeance is achieved out of the paraxial region.

THE MUON DECAY IN THE RENORMALIZABLE VECTOR BOSON THEORY

By

J. NYIRI and A. SEBESTYÉN

CENTRAL RESEARCH INSTITUTE OF PHYSICS OF THE HUNGARIAN ACADEMY OF SCIENCES, BUDAPEST

(Presented by L. Jánossy . — Received 26. XI. 1964)

The mechanism of the muon decay is investigated on the basis of a renormalizable vector boson (r. v. b.) theory. It is found, that the r. v. b. and Fermi theories lead essentially to the same results.

In a recent paper [1] A. FRENKEL and P. HRASKÓ have discussed in detail the effect of a renormalizable vector boson theory on some processes of weak interactions. In calculating transition matrix elements the presence of an intermediate boson was taken into account by including the following propagator:

$$\frac{i}{(2\pi)^4} \left(g_{\alpha\beta} - \frac{k_\alpha k_\beta}{k^2} \right) \frac{1}{m_w^2 - k^2}, \quad (1)$$

where m_w is the mass of the boson. Several authors also pointed out the possibility of using this propagator, which leads to a renormalizable theory.

In the case of $m_w \gg |k_\alpha|$ this propagator takes the form

$$\frac{i}{(2\pi)^4} \left(g_{\alpha\beta} - \frac{k_\alpha k_\beta}{k^2} \right) \frac{1}{m_w^2} \quad (2)$$

which indicates that, in contradiction to the vector boson theory generally used, this propagator may yield some deviations from a four-fermion interaction. Indeed, in [1] the authors show that the spectrum of unpolarised electrons of neutron-decay calculated on the basis of the propagator (1) differs from that of the Fermi theory, and fits the experimental data somewhat better. In the same work it is shown that the shape of the spectrum for the decay of the H^3 nucleus is reproduced by the r. v. b. theory as well as it is by the Fermi theory.

In the present work the decay of the muon is discussed by making use of the propagator (1). We have investigated the spectrum of unpolarized electrons, compared it with that of the Fermi theory, and the same was done for the angular correlation function. We remark that we considered everywhere pure $V - A$ coupling. The effect of Coulomb correction was neglected in the

calculation, as its handling is rather unclarified, and therefore we compared the results with the corresponding uncorrected expressions of the Fermi theory.

In the formulae natural units $\hbar = c = 1$ were used.

1. The spectrum of electrons

In the Fermi theory the spectrum of electrons of the muon-decay has the following form

$$W_{\text{Fermi}}(y) = \frac{2f^2}{(2\pi)^3} m_\mu^5 \left\{ \sqrt{y^2 - a} \left[-\frac{4}{3} y^2 + (a+1)y - \frac{2}{3} a \right] \right\}, \quad (3)$$

where $a = \left(\frac{m_e}{m_\mu}\right)^2$, and f , m_e and m_μ stand for the coupling constant, the electron and muon mass respectively; y is the total energy of the outgoing electron, measured in units of m_μ . Kinematics shows that y lies in the interval $\left[\sqrt{a}, \frac{a+1}{2}\right]$.

If the relativistic limit is taken in (3), one can identify the Michel parameter ϱ , and it is found that $\varrho = \frac{3}{4}$. This value is confirmed by experimental data [4, 5].

The corresponding expression of the r. v. b. theory is the following

$$\begin{aligned} W(y) &= \frac{g^4}{(2\pi)^3} \frac{m_\mu}{4\beta^2} \left\{ \sqrt{y^2 - a} \left[-\frac{4}{3\beta} y^3 + \frac{4}{3} \left(\frac{a}{\beta} + \frac{1}{\beta} - 1 \right) y^2 + \right. \right. \\ &\quad \left. \left. + \left(\frac{5a}{6\beta} + a + 1 \right) y - \frac{a}{6} \left(\frac{5a}{\beta} + \frac{5}{\beta} + 7 \right) \right] \right\} + \\ &+ \ln \frac{y - \sqrt{y^2 - a}}{y + \sqrt{y^2 + a}} \left[-ay + \frac{3}{8} a(a+1) + \frac{a}{4\beta} \right] = \frac{g^4}{(2\pi)^3} \frac{m_\mu}{4\beta^2} f_1(y). \end{aligned} \quad (4)$$

Here g denotes the coupling constant, and

$$\beta = \left(\frac{m_w}{m_\mu} \right)^2.$$

g is related to the Fermi coupling constant in the following way

$$f = \frac{1}{\sqrt{8}} \frac{g^2}{m_w^2}.$$

It is easily seen, that for large values of β the two spectra will coincide.

In Fig. 1 we have plotted the spectrum of electrons $f_1(y)$ (continuous line) for $m_w = 10m_\mu$.

As the difference between the Fermi and r. v. b. spectra is very small even at this value of the boson mass m_w , we have only indicated a few points of the Fermi spectrum by small circles.

In theories taking into account the effect of an intermediate boson, strong indications can be found that the mass of the boson must be even

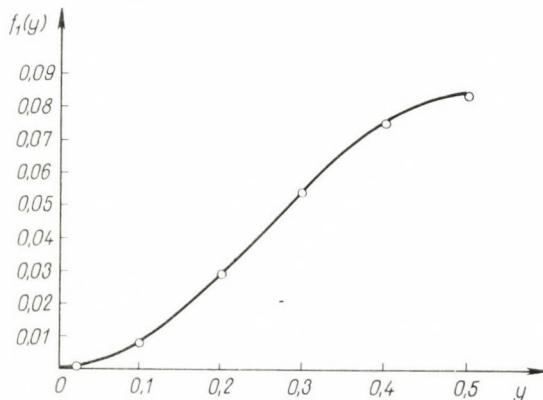


Fig. 1

greater than the value mentioned above [6]. In [1] the authors also hold the opinion that $m_w \sim 50$ GeV. The latest experiments seem to indicate [8] that if a vector boson exists at all, its mass must be greater than 1.8 GeV, which corresponds in our notation to $m_w = 17 m_\mu$.

2. The coupling constant

Following the well-known procedure of integrating the spectrum for the electron energy, we get the relation between the life-time of the muon τ and the coupling constant

$$\frac{1}{\tau} = \frac{m_\mu^5 c^4}{192 \pi^3 \hbar^7} \frac{1}{8} \frac{g^4}{m_w^4}.$$

If we put

$$f = \frac{1}{\sqrt{8}} \frac{g^2}{m_w^2},$$

we get back the formula of the Fermi theory. Wu shows [9] that using the experimental value of the life-time

$$\tau = 2,198 \cdot 10^{-6} \text{ sec},$$

we get

$$f = 1,435 \cdot 10^{-49} \text{ erg cm}^3$$

which corresponds to

$$\frac{g^2}{m_\nu^2} = 4,059 \cdot 10^{-49} \text{ erg cm}^3.$$

3. The angular correlation function

Calculating the angular correlation function on the basis of the $V-A$ theory, we get the following expression

$$\left[\frac{dN}{d(\cos \vartheta)} \right]_{\text{Fermi}} \sim \left\{ \sqrt{y^2 - a} \left[-\frac{4}{3} y^2 + (a+1)y - \frac{2}{3} a \right] - \left[\frac{4}{3} y^3 - \left(a + \frac{1}{3} \right) y^2 - \frac{4a}{3} y + a^2 + \frac{1}{3} a \right] \cos \vartheta \right\}, \quad (5)$$

where ϑ is the angle between the directions of the muon spin and of the electron momentum. The corresponding formula in the r. v. b. theory is given by

$$\begin{aligned} \frac{dN}{d(\cos \vartheta)} \sim & \left\{ \sqrt{y^2 - a} \left[-\frac{4}{3\beta} y^3 + \frac{4}{3} \left(\frac{a}{\beta} + \frac{1}{\beta} - 1 \right) y^2 + \left(\frac{5a}{6\beta} + a + 1 \right) y - \right. \right. \\ & - \frac{a}{6} \left(\frac{5a}{\beta} + \frac{5}{\beta} + 7 \right) \left. \right] + \ln \frac{y - \sqrt{y^2 - a}}{y + \sqrt{y^2 - a}} \left[-ay + \frac{3}{8} a(a+1) + \frac{a^2}{4\beta} \right] - \\ & - \left[\frac{4}{3\beta} y^4 - \frac{4}{3} y^3 \left(\frac{a}{\beta} - 1 \right) - y^2 \left(\frac{11a}{6\beta} + a + \frac{1}{3} \right) + y \frac{a}{3} \left(\frac{11a}{2\beta} + 2 \right) - \right. \quad (6) \\ & - \frac{a}{4} \left(a + \frac{5}{3} \right) + \frac{1}{\sqrt{y^2 - a}} \ln \frac{y - \sqrt{y^2 - a}}{y + \sqrt{y^2 - a}} \left[ay^2 - y \left(\frac{a}{8} (5a+3) + \frac{a^2}{4\beta} \right) + \right. \\ & \left. \left. + \frac{a^3}{4\beta} \right] \cos \vartheta \right\} = f_1(y) - f_2(y) \cos \vartheta, \end{aligned}$$

where $f_1(y)$ is the same as before. The definition of $f_2(y)$ can be read from formula (6), and it is essentially the spectrum of "forward-backward" difference. The omitted constants of proportionality contain the coupling constants, the mass of muon e. t. c., and their numerical values coincide for the Fermi and the r. v. b. formulae.

In Fig. 2 $f_2(y)$ is plotted (continuous line), and its agreement with the corresponding Fermi term is indicated in a manner similar to Fig. 1.

4. The helicity of the electron

The Fermi theory gives for the ratio of the probability of forward-backward polarization and the total probability the following formula

$$\left(\frac{\uparrow - \downarrow}{w} \right)_{\text{Fermi}} = \sqrt{y^2 - a} \frac{4y - a - 3}{-4y^2 + 3(a+1)y - 2a}. \quad (7)$$

The same expression in the r. v. b. theory takes the form

$$\begin{aligned} \frac{\uparrow - \downarrow}{w} = & \left\{ \frac{(y^2 - a)(4y - a - 3)}{3} + \frac{a(8y - 3a - 5)}{4} + \right. \\ & \left. + \frac{ay(8y - 3a - 5)}{8\sqrt{y^2 - a}} \ln \frac{y - \sqrt{y^2 - a}}{y + \sqrt{y^2 - a}} \right\} \times \\ & \times \left\{ \sqrt{y^2 - a} \left[-\frac{4}{3}y^2 + (a+1)y - \frac{7}{6}a \right] + \right. \\ & \left. + \left[-ay + \frac{3}{8}a(a+1) \right] \ln \frac{y - \sqrt{y^2 - a}}{y + \sqrt{y^2 - a}} \right\}^{-1}. \end{aligned} \quad (8)$$

The quantities occurring in these formulae are the same as before.

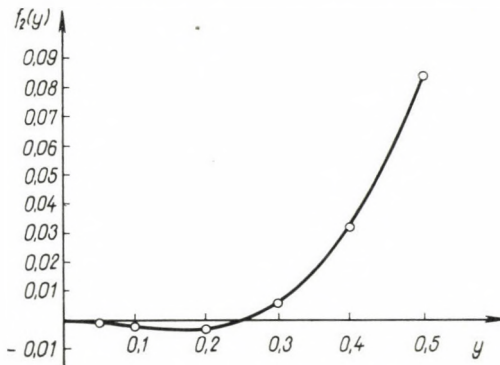


Fig. 2

At the lowest electron energy, i. e. $y = \sqrt{a}$, these two expressions give equally zero; at the highest energy $y = \frac{a+1}{2}$ the Fermi theory gives -1 , in contrast to the r. v. b. theory, which yields a value of $-1 + 6.08 \cdot 10^{-4}$. The difference between the two expressions is the greatest in the immediate neighbourhood of the lower limit, and practically disappears above 1 MeV. Experimental data are unfortunately absent at these low electron energies.

5. Conclusions

It may be seen from the formulae and the figures as well that for $m_w \gg 10m_\mu$ the agreement of the spectra and angular correlations for the Fermi and the r. v. b. theories is very pronounced. Therefore the shapes of the curves in the two theories are essentially the same. Present experimental data agree fairly well with these shapes of spectrum and angular correlation function. Measuring errors, however, put the choice between the two theories far beyond the reach of possibilities. As to the coupling constant, it differs from the value calculated in [1]. The reason for this deviation is not quite clear, nevertheless it is commonly accepted that the muon decay provides a better tool for the determination of the coupling constant than the nuclear β -decay.

In [1] the authors have supposed the universal feature of weak interactions. We must emphasize, however, that the different results concerning the coupling constant of nuclear β and muon decay might be understood by giving up this assumption. In this case we presume that the interaction Lagrangian of nuclear decay must take the following form

$$\begin{aligned} L_{\text{nuc1 ar}}(x) = & g_n : \bar{\psi}_n(x) (1 + i \lambda \gamma^5) \gamma^a \psi_p(x) B_a(x) : + H. c. + \\ & + g_e : \bar{\psi}_e(x) (1 + i \gamma^5) \gamma^a \psi_v(x) B_a(x) : + H. c. \end{aligned}$$

Similarly for muon decay

$$\begin{aligned} L_\mu(x) = & g_\mu : \bar{\psi}_\mu(x) (1 + i \gamma^5) \gamma^a \psi_v(x) B_a(x) : + H. c. + \\ & + g_e : \bar{\psi}_e(x) (1 + i \gamma^5) \gamma^a \psi_v(x) B_a(x) : + H. c., \end{aligned}$$

where H. c. means the Hermitian conjugate; ψ_n , ψ_p , ψ_e , ψ_v and ψ_μ stand for the neutron, proton, electron, neutrino and muon fields, respectively. $B_a(x)$ is the a -th component of the vector boson operator, and g_n , g_μ , g_e are the different coupling constants which, in this picture, are not equal. According to this assumption, instead of the result of [1] $\frac{g^2}{m_w^2} = 4,84 \cdot 10^{-49} \text{ erg cm}^3$

we have to write $\frac{g_e g_n}{m_w^2} = 4,84 \cdot 10^{-49} \text{ erg cm}^3$; similarly for the muon decay

$$\frac{g_e g_\mu}{m_w^2} = 4,059 \cdot 10^{-49} \text{ erg cm}^3 .$$

This way we can deduce the ratio

$$\frac{g_n}{g_\mu} = 1,192 .$$

By measuring a sufficient number of different processes, it is possible to determine the value of each coupling constant separately.

Finally we wish to express our sincere thanks to Mr. A. FRENKEL and Mr. P. HRASKÓ for the many valuable discussions.

REFERENCES

1. A. FRENKEL and P. HRASKÓ, *Acta Phys. Hung.*, **17**, 361, 1964.
2. J. BIAŁYNICKI-BIRULA, *Journal of Mathematical Physics*, **3**, 1094, 1962.
3. S. S. SCHWEBER: *An Introduction to Relativistic Quantum Field Theory*, p. 604, Row, Peterson & Co. New York, 1961.
4. R. PLANO, *Phys. Rev.*, **119**, 1400, 1960.
5. M. M. BLOCK et al., *Nuovo Cimento*, **23**, 1114, 1962.
6. Л. Б. Окунь: Слабое взаимодействие элементарных частиц, стр. 220, Физматгиз, Москва, 1963.
7. А. О. Вайсенберг: Мю-мезон, стр. 70, 78, Наука, Москва, 1963.
8. G. BERNARDINI, H. BIENLEIN et al., *International Conference on High-Energy Physics*, 1964.
9. C. S. WU, *Rev. Mod. Phys.*, **35**, 618, 1964.

РАСПАД МЮОНА В ПЕРЕНОРМИРУЕМОЙ ТЕОРИИ СЛАБЫХ ВЗАИМОДЕЙСТВИЙ

Ю. НИРИ и А. ШЕБЕШТЕН

Р е з ю м е

Рассматривается механизм распада мюона на основании перенормируемой теории с промежуточным векторным бозоном. Показано, что эта теория и теория Ферми приводят практически к одному и тому же результату.

EXTRAORDINARY ORBITALS IN THE UNITED ATOM MODEL

By

I. TAMÁSSY-LENTEI

INSTITUTE OF THEORETICAL PHYSICS, KOSSUTH LAJOS UNIVERSITY, DEBRECEN

(Presented by A. Kónya — Received 29. XII. 1964)

For a representation of the one-electron orbitals in the united atom model one can use, in addition to the usual hydrogen-like orbitals, also extraordinary functions, continuous in the electron coordinates but having only piecewise continuous derivatives. Computations are made for H_2^+ with a linear combination of middle point centred ordinary ψ_{1s} , $\psi_{1s'}$, ψ_{3dz} and extraordinary $|\psi_{2pz}|$ orbitals. The results obtained for the energy show a considerable improvement on introducing the extraordinary orbital $|\psi_{2pz}|$.

Owing to mathematical difficulties the wave function of molecules with several electrons can be determined only approximately, even in the simplest diatomic case. If the Hamiltonian operator is H , with the help of the variational method we can always approximate the energy of the system by minimizing the expression

$$E = \frac{\int \psi^* H \psi \, dv}{\int \psi^* \psi \, dv}$$

with respect to the trial function ψ .

If we want to overcome the difficulties of the many-centre integrals, one of the possibilities is to use the approximation method known as the united atom model (sometimes called as one-centre method). In this model the electron orbitals are constructed from one-electron functions centred on a single point. For molecules of type X_2 the middle point of the nuclei can be chosen for such centre.

As one-electron functions one often chooses hydrogenlike functions of the form

$$\psi_{nlm_l} = R_{nl}(r) Y_{lm_l}(\vartheta, \varphi),$$

where R_{nl} is the normalized radial wave function,

$$R_{nl}(r) = - \left\{ \frac{(n-l-1)!}{[(n+l)!]^3 2n} \right\}^{1/2} \left| \frac{2Z}{na_0} \right|^{3/2} e^{-\varrho/2} \varrho^l L_{n+l}^{2l+1}(\varrho)^*,$$
$$\varrho = \frac{2Zr}{na_0};$$

* We are going to use atomic units, i.e. we measure distance in a_0 units, and energy in e^2/a_0 units (e is the positive elementary charge, and a_0 the radius of the first Bohr-orbit in the hydrogen atom).

L_{n+l}^{2l+1} is the $(n+l)$ -th derivative of the $(2l+1)$ -th Laguerre polynomial. Moreover,

$$Ylm_l(\vartheta, \varphi) = \left[\frac{2l+1}{4\pi} \frac{(l-|m_l|)!}{(l+|m_l|)!} \right]^{1/2} P_l^{|m_l|}(\cos \vartheta) e^{im_l \varphi}$$

is the normalized spherical harmonic,

$$P_l^{|m_l|}(x) = \frac{1}{2^l l!} (1-x^2)^{|m_l|/2} \frac{d^{l+|m_l|}}{dx^{l+|m_l|}} (x^2 - 1)^l$$

the non-normalized associated Legendre polynomial and

$$x = \cos \vartheta.$$

The one-electron functions belonging to the ground state and to some of the low-lying excited states are of the form

$$\psi_{10} = \left(\frac{a_{10}^3}{\pi} \right)^{1/2} e^{-a_{10}r},$$

$$\psi_{2p_0} = \left(\frac{a_{21}^5}{32\pi} \right)^{1/2} r e^{-\frac{a_{21}r}{2}} \cos \vartheta,$$

$$\psi_{3d_0} = \frac{1}{81} \left(\frac{a_{32}^7}{6\pi} \right)^{1/2} r^2 e^{-\frac{a_{32}r}{3}} (3\cos^2 \vartheta - 1).$$

The parameters a_{nl} occurring in the functions are treated usually as variational parameters.

Any molecular orbital can be expressed in the form

$$\psi = \sum_i k_i \psi_i,$$

where the ψ_i constitute a complete system of functions. Since in practice only the first few terms of the series are retained, it is very important to assure rapid convergence by a suitable choice of the functions ψ_i (here it is not important any more that the functions chosen should be members of a complete system). Besides rapid convergence we require also that the computation of the integrals should be relatively easy. For this reason, also in the case of

the one-centre method, the choice $P_l^{m_l}(\cos \vartheta) e^{im_l\varphi}$ for angular dependence (advantageous because of the orthogonality) combined with a hydrogen-like radial part is often made. Experience shows that for molecules the convergence of these orbitals is less rapid than for atoms, but it is still satisfactory. Thus, with help of the complete system ψ_{nlm_l} the one-electron orbitals can be represented in the form

$$\psi = \sum_{nlm_l} k_{nlm_l} \psi_{nlm_l}.$$

If we restrict our attention to spherically symmetrical approximation, then we have only to consider the terms with $l = m_l = 0$, i.e. only the superposition of *s* states. In general, however, not even a linear combination of infinitely many *s* states will yield the characteristics of the molecule with the desired accuracy. In practice, when we can restrict ourselves to a finite number of terms of the series, it is advantageous to take into consideration besides the *s* states also states of *p*, *d*, *f*, ... character, i.e. states with higher angular momentum.

In the case of molecules of type X_2 , the centre is usually located at the middle point of the nuclei, and then, in case of a single electron, for reasons of symmetry the states with *l* odd cannot occur in the linear combination. Orbitals with lower value *l* give as a rule a more substantial contribution to the energy. Therefore, ordinary *p*-orbitals being not suited in our case, we might try a modified version of them.

In computing electron energies, SNYDER and PARR [1] have considered among the basic functions also extraordinary functions continuous in the electron coordinates but having only piecewise continuous derivatives. If we work with such a function having a non-continuous derivative, between the nodal planes atomic orbitals can be split into individual lobes, e.g.

$$\psi_{p_z} = \frac{1}{\sqrt{2}} (\psi_{p_z}^+ - \psi_{p_z}^-),$$

$$\psi_{p_z}^+ = \begin{cases} \sqrt{2} \psi_{p_z} & (z>0) \\ 0 & (z<0), \end{cases} \quad \psi_{p_z}^- = \begin{cases} 0 & (z>0) \\ -\sqrt{2} \psi_{p_z} & (z<0). \end{cases}$$

SNYDER and PARR have used this method for He, a two-electron system, in order to take into account correlation. According to their calculations, the electrons prefer being located in opposite lobes instead of the same lobe. But for He there was no great improvement in the energy in comparison with the usual basic functions.

The usual functions of types *s*, p_x , p_y and p_z were considered by SNYDER and PARR also in connection with the extraordinary functions $|p_x|$, $|p_y|$ and $|p_z|$.

In the case of molecular systems extraordinary functions have first been employed by DEWAR [2] and his group, in order to describe π electrons of conjugated unsaturated molecules; they located electrons with opposite spins in opposite lobes of the π -atomic orbitals. The "split-p-orbital" (SPO) method worked out by them in order to account for the vertical correlation of π electronic systems represents the wave function of molecules as a linear combination of lobes of the same type.

In the case of the one-centre model such extraordinary functions can also be taken into account instead of the functions with l odd. The effect of these extraordinary functions on the results will be exposed in detail in the following for the case of H_2^+ .

For the ground state of H_2^+ computations have already been made with the help of the united atom model, where the wave function was taken as a linear combination of a few ordinary hydrogen-like functions centred in the middle point [3], or upon an arbitrary point [4]. Let us now complete the wave function of this one-electron molecule also with an extraordinary function of type $|p_z|$ in addition to the usual hydrogen-like s, d functions so that

$$|\psi_{2p_z}| = \begin{cases} \psi_{2p_z}^+ = \psi_{2p_z} = \left(\frac{a_{2p}^5}{32\pi} \right)^{1/2} r e^{-\frac{a_{2p}r}{2}} \cos \vartheta, & (0 \leq \vartheta \leq \pi/2), \\ \psi_{2p_z}^- = -\psi_{2p_z} = -\left(\frac{a_{2p}^5}{32\pi} \right)^{1/2} r e^{-\frac{a_{2p}r}{2}} \cos \vartheta, & (\pi/2 < \vartheta \leq \pi). \end{cases}$$

Thus we choose the Z-axis as molecular axis. Let us therefore represent the wave function in the form of the following linear combination

$$\psi = \sum_i k_i \psi_i, \quad (i = 1s, 1s', (2p_z), 3d_z).$$

Here the non-orthogonality of the function $|\psi_{2p_z}|$ and s and d -type ones can be taken into account exactly. If the Hamiltonian operator is

$$H = -\frac{1}{2} \Delta_1 - \frac{1}{r_{a1}} - \frac{1}{r_{b1}} + \frac{1}{R},$$

the energy of the system can be determined from the secular equation

$$|| H_{ij} - ES_{ij} || = 0,$$

where

$$H_{ij} = \int \psi_i^* H \psi_j dv$$

and

$$S_{ij} = \int \psi_i^* \psi_j dv.$$

For the usual ordinary functions the energy terms of type

$$L_{ij}^u = \int \psi_i^*(1) \frac{1}{r_{u1}} \psi_j(1) dv_1, \quad (u = a, b)$$

due to the attraction between the electron and the nucleus, are easily determined, if we expand $1/r_{u1}$ in a series of Legendre polynomials. As is well known,

$$\frac{1}{r_{u1}} = \sum_{h=0}^{\infty} \sum_{m=-h}^h \frac{(h - |m|)!}{(h + |m|)!} \frac{r_{<}^h}{r_{>}^{h+1}} P_h^{|m|}(\cos \vartheta_u) P_h^{|m|}(\cos \vartheta_1) e^{im(\varphi_u - \varphi_1)}$$

and so

$$L_{ij}^u = \sum_n \left[\frac{(h - |m_l - m'_l|)!}{(h + |m_l - m'_l|)!} \right]^{1/2} c^h \cdot (lm_l, l' m'_l) \\ g^h(nl, n' l') P_h^{|m_l - m'_l|}(\cos \vartheta_u) e^{i(m_l - m'_l)\varphi_u}$$

with

$$g^h(nl, n' l') = \int_0^\infty R_{nl}^*(r) R_{n'l'}(r) \frac{r_{<}^h}{r_{>}^{h+1}} r^2 dr$$

and

$$c^h(lm_l, l'm_{l'}) = \left[\frac{(h - |m_l - m'_l|)!}{(h + |m_l - m'_l|)!} \frac{(2l+1)(l - |m_l|)!}{(l + |m_l|)!} \frac{(2l'+1)(l' - |m'_l|)!}{(l' + |m'_l|)!} \right]^{1/2} \times \\ \times \int_0^\pi P_l^{|m_l|}(\cos \vartheta) P_{l'}^{|m'_l|}(\cos \vartheta) P_h^{|m_l - m'_l|}(\cos \vartheta) \frac{\sin \vartheta}{2} d\vartheta.$$

The value of the coefficients c^h resulting from the integration with respect to the angle is to be found in the book of CONDON-SHORTLEY[5], e. g.

When extraordinary functions occur, it is expedient to use the above series of Legendre polynomials, and then

$$L_{ij}^u = \int \psi_i^*(1) \frac{1}{r_{u1}} \psi_j(1) dv_1 = \sum_h C^h(l0, l'0) g^h(nl, n'l')$$

($m_l = 0$ for all functions). If one of ψ_i and ψ_j is identical with $|\psi_{2p_z}|$ then it is advisable in calculating C^h to split the integration according to ϑ for the product of the Legendre polynomials into two domains one extending from 0 to $\pi/2$ (C_+^h) and the other from $\pi/2$ to π (C_-^h). Thus

$$C^h(l0, l'0) = C_+^h(l0, l'0) + C_-^h(l0, l'0).$$

Table I

h	$C_+^h(00, 10)$	$C_-^h(00, 10)$	$C_+^h(10, 20)$	$C_-^h(10, 20)$
0	$\sqrt{3}/4$	$\sqrt{3}/4$	$\sqrt{15}/16$	$\sqrt{15}/16$
1	$1/2\sqrt{3}$	$-1/2\sqrt{3}$	$-\sqrt{15}/15$	$-\sqrt{15}/15$
2	$\sqrt{3}/16$	$\sqrt{3}/16$	$\sqrt{15}/16$	$\sqrt{15}/16$
3	0	0	$3\sqrt{15}/70$	$3\sqrt{15}/70$
4	$-\sqrt{3}/96$	$-\sqrt{3}/96$	$13\sqrt{15}/768$	$13\sqrt{15}/768$
5	0	0	0	0
6	$\sqrt{3}/256$	$\sqrt{3}/256$	$-\sqrt{15}/320$	$-\sqrt{15}/320$
7	0	0	0	0
8	$-\sqrt{3}/512$	$-\sqrt{3}/512$	$13\sqrt{15}/10240$	$13\sqrt{15}/10240$
9	0	0	0	0
10	$7\sqrt{3}/6144$	$7\sqrt{3}/6144$	$-29\sqrt{15}/43008$	$-29\sqrt{15}/43008$

While in the ordinary case the series reduces to a few terms, because the c^h with higher indices vanish, such a simplification does not take place here. The coefficients C^h occurring in the course of the computations are given in Table I.

The series consists now of infinitely many terms, but it can be seen that the coefficients C^h rapidly decrease as h increases, and the situation is similar for the multiplicative factors $g^h(nl, n'l')$ too. Thus we can achieve satisfactory accuracy by retaining only a few terms of the series.

In Table II we survey the values obtained with the orbital containing also the extraordinary function, when taking into account the first ten members of the sum. The same Table contains also the values of the variational parameters yielding the minimum energy, and the total energy value for the experimental nuclear distance $R = 2$.

Table II

$\psi = \sum_i k_i \psi_i$	a_{10}	a'_{10}	a_{12p_z}	a_{sdz}	E
$i = 1s, 1s'$	1,5	1,6			-0,516149
$1s, 2p_z $	1		3		-0,514116
$1s, 3d_z$	0,9			6,4	-0,518411
$1s, 1s', 2p_z $	1,5	1,7	3		-0,54387
$1s, 2p_z , 3d_z$	1		3	6,6	-0,54919
$1s, 1s', 2p_z , 3d_z$	1,5	1,7	3	6,6	-0,58674

The exact value of the energy is $E = -0,60263$ [6]. (For H_2^+ this computed value of the energy is to be considered more accurate than the experimental one.) So the functions $|\psi_{2p_z}|$ with non-continuous derivatives complete advantageously the usual hydrogen-like functions and improve the energy considerably.

If necessary, the orbitals can be augmented in a similar way by further extraordinary orbitals with higher odd values of l .

REFERENCES

1. L. C. SNYDER and R. G. PARR, J. Chem. Phys., **28**, 1250, 1958; **34**, 1661, 1961; **37**, 2986, 1963.
2. M. J. S. DEWAR and C. E. WULFMAN, J. Chem. Phys., **29**, 158, 1958.
M. J. S. DEWAR and H. N. SCHMEISING, Tetrahedron, **5**, 166, 1959; **11**, 96, 1960.
3. M. J. S. DEWAR and N. L. HOJVAT, J. Chem. Phys., **34**, 1232, 1961. Proc. Roy. Soc. **A264**, 431, 1961.
M. J. S. DEWAR and N. S. SABELLI, J. Phys. Chim., **66**, 2310, 1962.
M. J. S. DEWAR and A. L. H. CHUNG, J. Chem. Phys., **39**, 1741, 1963.
4. I. TAMÁSSY-LENTEI and Á. BÁVA, Acta Phys. Hung., **7**, 151, 1957.
5. E. U. CONDON and G. H. SHORTLEY, The Theory of Atomic Spectra, Cambridge, At the University Press, 1951.
6. D. R. BATES, K. LEDSHAM and A. L. STEWART, Phil. Trans. Roy. Soc., **A246**, 215, 1953.

НЕОБЫКНОВЕННЫЕ ОРБИТЫ В СОЕДИНЕННОЙ АТОМНОЙ МОДЕЛИ

И. ТАМАШИ-ЛЕНТЕИ

Р е з и о м е

Для представления одноэлектронных орбит в соединённой атомной модели наряду с обычными водородоподобными орбиталями можно использовать также и необыкновенные функции, непрерывные в координате электрона, но имеющие только отрывочно непрерывные производные. Вычисления проведены для H_2^+ применением линейной комбинации среднеточечных центрированных орбит ψ_{1s} , $\psi_{1s'}$, ψ_{3dz} и необыкновенных орбит $|\psi_{2p_z}|$. Полученный результат для энергии показывает, что введением необыкновенных орбит $|\psi_{2p_z}|$ можно добиться значительного улучшения модели.

COMMUNICATIONES BREVES

ÜBER DIE GEGENSEITIGE BEZIEHUNG VON KONSTANTEN EINIGER THEORIEN ÜBER KONZENTRATIONSAUSLÖSCHUNG UND KONZENTRATIONSDEPOLARISATION DER PHOTOLUMINESZENZ VON LÖSUNGEN

Von

C. BOJARSKI

I. PHYSIKALISCHES INSTITUT, TECHNISCHE HOCHSCHULE GDAŃSK, GDAŃSK, POLEN

(Eingegangen 28. V. 1964)

In den gegenwärtig bestehenden Theorien über den Einfluss der Konzentration auf die Lumineszenz von Lösungen treten gewisse Konstanten auf, die durch Vergleich von Theorie und Versuchsergebnissen [1]—[5] bestimmt werden können. So tritt in der Theorie von FÖRSTER der kritische Abstand R_0 auf, während in der Theorie von JABŁOŃSKI der Radius R_J der sogenannten Wirkungssphäre auftritt. Die Frage der gegenseitigen Beziehung der Konstanten R_0 und R_J ist letztens in mehreren Abhandlungen diskutiert worden [6]—[13]. Im Falle der Photolumineszenzauslöschung durch Fremdstoffe erhielt JABŁOŃSKI [6]

$$R'_J = 1,327 R'_0, \quad (1)$$

im Falle von Konzentrationsdepolarisation dagegen nach KAWSKI [7]

$$R_J = 1,44 R_0. \quad (2)$$

In den Ausdrücken (1) und (2) $R'_0 = R_0$ gleichsetzend findet KAWSKI [13]

$$\frac{R_J}{R'_J} = 1,085 \quad (3)$$

und stellt fest, dass die Radien der Wirkungssphären für die Depolarisation und die Auslöschung durch absorbierende Fremdstoffe sich deutlich von einander unterscheiden. Abgesehen davon, dass die Beziehung (2) nicht einwandfrei ist, was in [14] erwiesen wird, muss die Grundlosigkeit der Annahme $R'_0 = R_0$ unterstrichen werden. Aus der Theorie von FÖRSTER [2] wissen wir nähmlich, dass der kritische Abstand zwischen den Molekülen von den individuellen Eigenschaften der einwirkenden Partner abhängig ist; er kann also im Falle der Konzentrationsdepolarisation nicht derselbe sein wie im Falle der Auslöschung durch absorbierende Fremdstoffe. Sofern nähmlich die erste

Erscheinung auf Grund der Übertragung von Anregungsenergie zwischen Molekülen derselben Art auftritt, so ist die zweite Erscheinung durch die Energieübertragung zwischen Molekülen verschiedener Art bedingt. Somit ist also die Behauptung KAWSKI's, dass R'_J und R_J sich deutlich unterscheiden, keineswegs der Fall. Dagegen glauben wir, die Beziehungen $\frac{R'_J}{R'_0}$ und $\frac{R_J}{R_0}$ vergleichen zu können. Der Vergleich scheint notwendig, da man für diese Beziehungen verschiedene Werte für den Fall des Auslöschen (1,327, [6]) und für den Fall der Depolarisation¹ (1,367, [8]; 1,44, [7]; 1,327, [10]) erhalten hat. Wir behaupten, dass die Werte dieser Beziehungen im Falle des Auslöschen wie im Falle der Depolarisation identisch sind, d. h.

$$\frac{R'_J}{R'_0} = \frac{R_J}{R_0} \quad (4)$$

ist. Um die Gleichung (4) zu beweisen, sei an die Definition des kritischen Abstandes und der Radien der Wirkungssphären für die Depolarisation und für das Auslöschen erinnert. Der Radius der Wirkungssphäre für die Depolarisation R_J wurde aus der Bedingung bestimmt, dass die relative Wahrscheinlichkeit der Energieübertragung für die Zentren mit zwei Molekülen 1/2 beträgt. Ähnlich bestimmte man den Radius der Wirkungssphäre für das Auslöschen R' aus der Bedingung, dass die relative Ausbeute der Zentren mit einem Löschenmolekül 1/2 beträgt. Der kritische Abstand R_0 wurde dagegen als derjenige Abstand zwischen zwei einwirkenden Molekülen definiert, bei dem die Wahrscheinlichkeit der Emission von Photolumineszenz und der strahlunglosen Übertragung von Anregungsenergie einander gleich sind. Bemerken wir, dass bei der Bestimmung der Radien der Wirkungssphären für die Depolarisation und das Auslöschen dieselben vereinfachenden Voraussetzungen angenommen wurden, denen zufolge die Wahrscheinlichkeit der Energieübertragung konstant und unabhängig von dem gegenseitigen Abstand R der einwirkenden Moleküle ist, die sich innerhalb der Wirkungssphäre befinden, dagegen ist sie gleich Null für Moleküle, die sich im Abstand $R > R_J$ beziehungsweise $R > R'_J$ befinden. Da die gegenseitigen Abstände zwischen einwirkenden Molekülen in verschiedenen Zentren, die zu derselben Gruppe von Zentren zugehören (z. B. mit einem Löschenmolekül), verschieden sein können, und die Wahrscheinlichkeit des Auslöschen eines angeregten Moleküls durch ein Löschenmolekül nach FÖRSTER [2] mit dem Abstand für die Dipol-Dipol-Wechselwirkung wie R^{-6} abnimmt, so ist $R'_J > R'_0$ mit der Beziehung (1) übereinstimmend, die aus der Bedingung, dass der mittlere Wert der relativen Ausbeute der Zentren mit einem Löschenmolekül gleich 1/2 ist, erhalten wurde.

¹ Die eingehende Diskussion der in den Abhandlungen [8] und [7] erhaltenen Werte ist in [11] und [14] angegeben worden.

Im Falle der Wirkungssphäre für die Depolarisation führt die Bedingung, dass der mittlere Wert der relativen Wahrscheinlichkeit der Übertragung von Energie für Zentren mit zwei lumineszierenden Molekülen $1/2$ beträgt, selbstverständlich zu demselben Wert der Beziehung $\frac{R_J}{R_0}$ wie im Falle der Auslöschung. Somit gilt also die Beziehung (1) nicht nur im Falle der Fremdlösung, sondern auch im Falle der Depolarisation. Genauere Berechnungen, die im Rahmen des sogenannten Schichtmodells des lumineszierenden Zentrums durchgeführt wurden, ergaben für die besprochene Beziehung den etwas geringeren Wert 1,279, der durch die auf Grund von Versuchen ermittelten Werte R_J und R_0 sehr gut bestätigt wird [11].

LITERATUR

1. S. I. WAWIŁOW, Mikrostruktur des Lichtes, Akademie-Verlag, Berlin, 1954.
2. TH. FÖRSTER, Ann. Physik, **2**, 55, 1948.
3. TH. FÖRSTER, Z. Naturforsch., **4a**, 321, 1949.
4. A. JABŁONSKI, Acta Phys. Polon., **13**, 175, 1954.
5. A. JABŁONSKI, Acta Phys. Polon., **14**, 295, 1955; **17**, 481, 1958.
6. A. JABŁONSKI, Bull. Acad. Polon. Sci. Cl. III, **6**, 663, 1958.
7. A. KAWSKI, Zesz. Nauk. WSP Gdańsk, Mat., Fiz., Chem., **1**, 17, 1961.
8. L. SZALAY und S. SÁRKÁNY, Acta Phys. et Chem. Szeged, **8**, 25, 1962.
9. A. BUDÓ und I. KETSKEMÉTY, Acta Phys. Hung., **14**, 167, 1962.
10. C. BOJARSKI, Ann. Phys. (Leipzig), **12**, 253, 1963.
11. C. BOJARSKI, Acta Phys. Polon., **25**, 179, 1964.
12. A. KAWSKI, Z. Naturforsch., **18a**, 961, 1963.
13. A. KAWSKI, Acta Phys. Hung., **16**, 293, 1963.
14. C. BOJARSKI, Acta Phys. Hung., (im Erscheinen).

UNIVERSAL POTENTIAL EIGENFUNCTIONS AND EIGENVALUES FOR THE SELENIUM ATOM

By

R. GÁSPÁR

RESEARCH GROUP FOR THEORETICAL PHYSICS OF THE HUNGARIAN ACADEMY OF SCIENCES,
BUDAPEST

(Received 8. XII. 1964)

This report completes a series of calculations for the elements in the VIIb column of the periodic table [1]. Se is extensively used as a semiconductor material and together with the other elements of the VIIb column it has a number of remarkable properties [2], the quantitative investigation of which is made possible by means of the eigenfunctions and potential values published here.

The radial Schrödinger equation

$$\frac{d^2 f}{dx^2} + \left[\varepsilon + \frac{\gamma}{x} \frac{e^{-\lambda_0 x}}{1 + A_0 x} - \xi \frac{e^{-ax}}{1 + Ax} - \frac{l(l+1)}{x^2} \right] f = 0, \quad (1)$$

where

$$\begin{aligned} \varepsilon &= 2E\mu^2 e^2 a_0^{-1}, \quad \gamma = 2Z\mu_0^{-1}, \quad \xi = \frac{8}{3} K_a C 0,8853^2 e^{-2} \\ x &= r\mu^{-1}, \quad \mu = 0,8853 a_0 Z^{-1/3}, \quad K_a = (3/4) (3/\pi)^{1/3} e^2 \end{aligned} \quad (2)$$

and

$$\lambda_0 = 0,1837, \quad A_0 = 1,05, \quad a = 0,04, \quad A = 9, \quad C = 3,1 a_0^{-1}$$

was solved with the boundary conditions

$$\begin{aligned} f(0) &= f'(0) = \dots = f^{(l-1)}(0) = 0 \\ f^{(l)} &= \text{const.}, \end{aligned}$$

and

$$\lim_{x \rightarrow \infty} f(x) = 0.$$

In (1) and (2) $Z = 34$ is the atomic number of selenium, E is the energy eigenvalue, f the radial eigenfunction of the electron, l the azimuthal quantum number and r the distance of the electron from the nucleus.

[3] gives details about the theoretical background of equation (1).

Table I

The radial eigenfunctions f of the electrons with quantum number $l = 0$ and total potential V in the Se atom. f and V are in atomic units of $1/a_0^{1/2}$ and e/a_0 , respectively, x is dimensionless (see text)

x	f				V
	1s	2s	3s	4s	
0,000	0,000	0,000	0,000	0,000	0,000
0,006	0,172	0,054	0,021	0,008	3078,86
0,012	0,325	0,102	0,040	0,015	1530,23
0,018	0,461	0,144	0,057	0,021	1014,00
0,024	0,582	0,181	0,071	0,026	755,853
0,030	0,687	0,213	0,084	0,031	600,968
0,036	0,780	0,241	0,095	0,035	497,714
0,042	0,861	0,264	0,104	0,038	423,966
0,048	0,931	0,284	0,112	0,041	368,662
0,054	0,990	0,300	0,118	0,043	325,657
0,060	1,041	0,312	0,123	0,045	291,261
0,066	1,083	0,321	0,126	0,046	263,129
0,072	1,118	0,328	0,128	0,047	239,694
0,078	1,146	0,331	0,129	0,047	219,875
0,084	1,167	0,332	0,130	0,047	202,895
0,090	1,183	0,331	0,129	0,047	188,188
0,108	1,202	0,315	0,121	0,044	153,917
0,126	1,188	0,284	0,108	0,039	129,500
0,144	1,150	0,242	0,090	0,033	111,243
0,162	1,096	0,191	0,069	0,025	97,0925
0,180	1,032	0,136	0,046	0,016	85,8161
0,198	0,962	0,077	0,021	0,007	76,6295
0,216	0,890	0,016	-0,004	-0,002	69,0095
0,234	0,818	-0,045	-0,029	-0,011	62,5938
0,252	0,747	-0,106	-0,053	-0,020	57,1232
0,270	0,679	-0,165	-0,077	-0,029	52,4081
0,288	0,614	-0,221	-0,099	-0,037	48,3057
0,324	0,498	-0,325	-0,139	-0,051	41,5285
0,360	0,398	-0,415	-0,171	-0,063	36,1743
0,396	0,316	-0,491	-0,196	-0,072	31,8509
0,432	0,248	-0,552	-0,213	-0,078	28,2968
0,468	0,194	-0,599	-0,223	-0,081	25,3315
0,504	0,150	-0,633	-0,225	-0,081	22,8260

Table I (continued)

<i>x</i>	<i>f</i>				<i>V</i>
	1s	2s	3s	4s	
0,540	0,115	-0,655	-0,222	-0,079	20,6859
0,576	0,088	-0,668	-0,213	-0,075	18,8409
0,612	0,066	-0,671	-0,199	-0,069	17,2371
0,648	0,049	-0,667	-0,181	-0,061	15,8328
0,684	0,035	-0,657	-0,159	-0,053	14,5954
0,720	0,024	-0,642	-0,135	-0,043	13,4984
0,756	0,014	-0,623	-0,108	-0,033	12,5210
0,792	0,005	-0,601	-0,080	-0,022	11,6460
0,828		-0,576	-0,051	-0,010	10,8591
0,864		-0,550	-0,021	+0,001	10,1488
0,900		-0,523	+0,009	0,012	9,50524
0,936		-0,495	0,038	0,024	8,92010
1,008		-0,440	0,097	0,045	7,89848
1,080		-0,386	0,152	0,065	7,03942
1,152		-0,335	0,203	0,083	6,30994
1,224		-0,289	0,248	0,098	5,68502
1,296		-0,246	0,287	0,110	5,14561
1,368		-0,209	0,321	0,119	4,67678
1,440		-0,176	0,349	0,125	4,26675
1,512		-0,147	0,372	0,129	3,90611
1,584		-0,121	0,390	0,130	3,58732
1,656		-0,099	0,403	0,129	3,30414
1,728		-0,079	0,411	0,126	3,05155
1,800		-0,062	0,416	0,120	2,82534
1,872		-0,047	0,417	0,114	2,62202
1,944		-0,033	0,416	0,105	2,43861
2,016		-0,020	0,412	0,096	2,27267
2,088		-0,008	0,405	0,085	2,12208
2,160			0,397	0,073	1,98504
2,304			0,377	0,048	1,74563
2,448			0,352	0,021	1,54444
2,592			0,326	-0,006	1,37394
2,736			0,298	-0,034	1,22833
2,880			0,271	-0,060	1,10311
3,024			0,245	-0,085	0,994765
3,168			0,219	-0,109	0,900475
3,312			0,196	-0,131	0,817989

Table I (continued)

<i>x</i>	<i>f</i>				<i>V</i>
	1 <i>s</i>	2 <i>s</i>	3 <i>s</i>	4 <i>s</i>	
3,456			0,174	-0,151	0,745483
3,600			0,154	-0,169	0,681463
3,744			0,136	-0,185	0,624711
3,888			0,120	-0,200	0,574200
4,032			0,105	-0,212	0,529092
4,176			0,092	-0,222	0,488668
4,320			0,080	-0,231	0,452333
4,608			0,061	-0,244	0,389968
4,896			0,046	-0,251	0,338747
5,184			0,034	-0,253	0,296276
5,472			0,025	-0,252	0,260755
5,760			0,019	-0,248	0,230815
6,048			0,013	-0,241	0,205397
6,336			0,009	-0,232	0,183680
6,624			0,006	-0,222	0,165013
6,912			0,004	-0,212	0,148878
7,200			0,001	-0,200	0,134859
7,488				-0,188	0,122622
7,776				-0,176	0,111891
8,064				-0,165	0,102442
8,640				-0,141	0,086675
9,216				-0,120	0,074174
9,792				-0,099	0,064131
10,368				-0,081	0,055965
10,944				-0,064	0,049251
11,520				-0,048	0,043677
12,096				-0,034	0,039003
12,672				-0,020	0,035051
13,248				-0,007	0,031681
13,824					0,028786
14,400					0,026280
14,976					0,024098
16,128					0,020497
17,280					0,017666
18,432					0,015395
19,584					0,013539
20,736					0,012000
21,888					0,010705
23,040					0,009603
24,192					0,008655
25,344					0,007832
26,496					0,007112

Table II

The radial eigenfunctions f of the electrons with quantum number $l = 1, 2$ and the total radial charge density D in the Se atom. f and D are in atomic units of $1/a_0^{1/2}$ and $1/a_0$, respectively. x is in dimensionless units (see text)

x	f				D
	$2p$	$3p$	$4p$	$3d$	
0,006	0,001	0,000	0,001	0,000	0,0659
0,012	0,003	0,001	0,004	0,000	0,2357
0,018	0,007	0,003	0,008	0,000	0,4744
0,024	0,012	0,005	0,015	0,000	0,7546
0,030	0,019	0,007	0,022	0,000	1,0548
0,036	0,026	0,010	0,031	0,000	1,3591
0,042	0,035	0,014	0,041	0,000	1,6556
0,048	0,044	0,017	0,052	0,000	1,9358
0,054	0,054	0,021	0,064	0,000	2,1936
0,060	0,065	0,026	0,077	0,001	2,4257
0,066	0,076	0,030	0,091	0,001	2,6300
0,072	0,089	0,035	0,105	0,001	2,8059
0,078	0,101	0,040	0,120	0,001	2,9535
0,084	0,114	0,045	0,135	0,002	3,0740
0,090	0,127	0,050	0,150	0,002	3,1691
0,108	0,169	0,066	0,199	0,003	3,3216
0,126	0,212	0,083	0,249	0,005	3,3240
0,144	0,256	0,100	0,298	0,007	3,2103
0,162	0,299	0,116	0,346	0,009	3,1083
0,180	0,340	0,131	0,392	0,012	2,9776
0,198	0,380	0,146	0,435	0,015	2,8686
0,216	0,418	0,159	0,474	0,019	2,7959
0,234	0,453	0,171	0,509	0,023	2,7646
0,252	0,485	0,181	0,540	0,027	2,7748
0,270	0,515	0,191	0,566	0,032	2,8224
0,288	0,542	0,198	0,588	0,037	2,9009
0,324	0,587	0,209	0,618	0,047	3,1202
0,360	0,622	0,214	0,630	0,059	3,3727
0,396	0,645	0,214	0,625	0,071	3,6086
0,432	0,660	0,208	0,605	0,085	3,7943
0,468	0,666	0,198	0,571	0,098	3,9118
0,504	0,665	0,184	0,525	0,112	3,9556
0,540	0,658	0,167	0,469	0,126	3,9300
0,576	0,646	0,147	0,404	0,140	3,8446
0,612	0,630	0,125	0,333	0,154	3,7122

Table II (continued)

<i>x</i>	<i>f</i>				<i>D</i>
	<i>2p</i>	<i>3p</i>	<i>4p</i>	<i>3d</i>	
0,648	0,610	0,101	0,257	0,168	3,5467
0,684	0,588	0,075	0,177	0,182	3,3615
0,720	0,564	0,049	0,094	0,195	3,1686
0,756	0,539	0,022	0,011	0,208	2,9781
0,792	0,512	-0,005	-0,073	0,221	2,7980
0,828	0,486	-0,032	-0,156	0,233	2,6343
0,864	0,459	-0,059	-0,237	0,244	2,4910
0,900	0,433	-0,085	-0,316	0,255	2,3704
0,936	0,407	-0,110	-0,392	0,265	2,2736
1,008	0,358	-0,159	-0,534	0,284	2,1498
1,080	0,312	-0,204	-0,660	0,301	2,1089
1,152	0,270	-0,244	-0,767	0,316	2,1329
1,224	0,232	-0,279	-0,856	0,328	2,2014
1,296	0,199	-0,309	-0,926	0,338	2,2951
1,368	0,170	-0,334	-0,977	0,345	2,3972
1,440	0,144	-0,355	-1,011	0,351	2,4947
1,512	0,122	-0,372	-1,027	0,355	2,5778
1,584	0,103	-0,384	-1,027	0,358	2,6406
1,656	0,087	-0,393	-1,013	0,359	2,6795
1,728	0,073	-0,399	-0,986	0,359	2,6935
1,800	0,061	-0,401	-0,946	0,357	2,6830
1,872	0,051	-0,401	-0,896	0,355	2,6499
1,944	0,043	-0,399	-0,837	0,351	2,5966
2,016	0,036	-0,395	-0,770	0,347	2,5261
2,088	0,030	-0,389	-0,696	0,342	2,4415
2,160	0,025	-0,381	-0,616	0,336	2,3460
2,304	0,017	-0,363	-0,442	0,323	2,1328
2,448	0,012	-0,342	-0,257	0,309	1,9065
2,592	0,008	-0,319	-0,065	0,293	1,6828
2,736	0,005	-0,295	+0,129	0,277	1,4724
2,880	0,004	-0,271	0,319	0,261	1,2817
3,024	0,002	-0,247	0,505	0,245	1,1139
3,168	0,001	-0,225	0,683	0,230	0,9698
3,312	0,001	-0,203	0,852	0,214	0,8484
3,456		-0,183	1,011	0,200	0,7481
3,600		-0,165	1,159	0,186	0,6663
3,744		-0,147	1,295	0,172	0,6005

Table II (continued)

<i>x</i>	<i>f</i>				<i>D</i>
	2 <i>p</i>	3 <i>p</i>	4 <i>p</i>	3 <i>d</i>	
3,888		-0,132	1,420	0,160	0,5481
4,032		-0,117	1,534	0,148	0,5069
4,176		-0,104	1,636	0,137	0,4745
4,320		-0,092	1,727	0,126	0,4492
4,608		-0,072	1,879	0,107	0,4135
4,896		-0,056	1,993	0,091	0,3902
5,184		-0,043	2,074	0,077	0,3727
5,472		-0,033	2,126	0,065	0,3573
5,760		-0,025	2,153	0,054	0,3419
6,048		-0,018	2,159	0,046	0,3256
6,336		-0,013	2,147	0,038	0,3081
6,624		-0,008	2,121	0,032	0,2897
6,912		-0,004	2,084	0,027	0,2705
7,200			2,037	0,022	0,2511
7,488			1,983	0,019	0,2317
7,776			1,923	0,016	0,2126
8,064			1,859	0,013	0,1942
8,640			1,724	0,009	0,1598
9,216			1,585	0,006	0,1295
9,792			1,447	0,004	0,1038
10,368			1,314	0,003	0,0823
10,944			1,188	0,002	0,0647
11,520			1,070	0,001	0,0505
12,096			0,961	0,001	0,0392
12,672			0,860		0,0304
13,248			0,768		0,0237
13,824			0,685		0,0188
14,400			0,610		0,0149
14,976			0,542		0,0117
16,128			0,426		0,0072
17,280			0,333		0,0044
18,432			0,258		0,0027
19,584			0,199		0,0016
20,736			0,151		0,0009
21,888			0,113		0,0005
23,040			0,081		0,0003
24,192			0,055		0,0001
25,341			0,033		0,00004
26,496			0,012		0,00001

The configuration of electrons in the Se atom is

$$(1s)^2 (2s)^2 (2p)^6 (3s)^2 (3p)^6 (3d)^10 (4s)^2 (4p)^4.$$

The radial eigenfunctions and the energy eigenvalues of the electrons are given in the Tables I, II and III together with the radial particle density

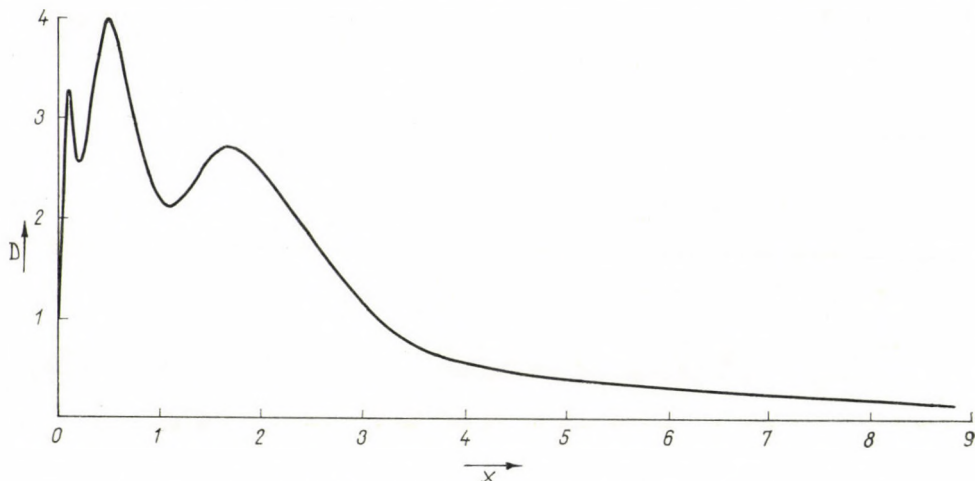


Fig. 1. The radial particle density $D = 4\pi r^2 \rho$ in the Se atom

Table III

The energy eigenvalues of the universal potential for the electrons in the Se atom and the X-ray term values in atomic units of e^2/a_0

	1s	2s	3s	4s
Universal potential	460,51	58,237	8,3936	0,7700
LANDOLT—BÖRNSTEIN*	466,26	60,93	8,605	
	2p	3p	4p	
Universal potential	52,762	6,39	0,3568	
LANDOLT—BÖRNSTEIN*	53,734	6,09	0,34	
	3d			
Universal potential	2,6499			
LANDOLT—BÖRNSTEIN*	2,446			

* LANDOLT—BÖRNSTEIN, Zahlenwerte und Funktionen, Atom und Molekularphysik, 1. Teil, Atome und Ionen, Springer-Vlg, Berlin, 1954, p. 226—228.

and the total potential in the Se atom. The energy eigenvalues are compared with the average X-ray doublet term values corrected by the work function of selenium, 4,87 eV. In Fig. 1 the radial particle density of the Se atom is displayed, where the formation of the various electron groups is clearly visible.

Help with the numerical calculations is acknowledged to Mrs. J. Kocsis.

REFERENCES

1. See for references e.g. R. GÁSPÁR, Acta Phys. Hung., **15**, 257, 1963.
2. R. GÁSPÁR, Acta Phys. Hung., **7**, 289, 1957, ibid. **7**, 313, 1957.
3. R. GÁSPÁR, Acta Phys. Hung., **3**, 263, 1954.
4. LANDOLT-BÖRNSTEIN, Zahlenwerte und Funktionen, Atom und Molekularphysik, 1. Teil, Kristalle. Springer-Vlg, Berlin, Göttingen, Heidelberg, 1956, p. 259.

A SIMPLE METHOD FOR THE CALCULATION OF COULOMB AND HYBRID INTEGRALS

By

T. SZONDY

RESEARCH GROUP FOR THEORETICAL PHYSICS OF THE HUNGARIAN ACADEMY OF SCIENCES,
BUDAPEST

(Received 4. II. 1965)

This paper deals with a simple method for reducing the calculation of Coulomb and hybrid integrals (3) to the calculation of overlap integrals (2). The present method may have advantages over the customary ones if the basic charge distributions (1) have large azimuthal and/or principal quantum numbers.

Let us introduce the notation

$$\varrho_{n,l,m}(\mathbf{r}; \zeta) = r^n e^{-\zeta r} S_{l,m}(\theta, \phi); \quad (n \geq l \geq 0; \quad l \text{ integer}), \quad (1)$$

where r , θ and ϕ denote spherical polar co-ordinates and $S_{l,m}(\theta, \phi)$ denotes a normalized real spherical harmonic [1]. We shall consider overlap integrals defined by

$$O_{n,l,m}(\zeta) = \int d\tau \sigma(\mathbf{r}) \varrho_{n,l,m}(\mathbf{r}; \zeta), \quad (2)$$

and Coulomb or hybrid integrals defined by

$$C_{n,l,m}(\zeta) = \iint d\tau_1 d\tau_2 \sigma(\mathbf{r}_1) r_{12}^{-1} \varrho_{n,l,m}(\mathbf{r}_2; \zeta), \quad (3)$$

where the subscripts 1 and 2 refer to the electrons and $\sigma(\mathbf{r})$ denotes any charge distribution satisfying the usual continuity and normalizability conditions.

By virtue of the relation [2]

$$-\frac{1}{4\pi} \mathcal{A}_2 r_{12}^{-1} = \delta^{(3)}(\mathbf{r}_{12}), \quad (4)$$

where \mathcal{A}_2 denotes the Laplace operator acting on the co-ordinates of electron 2, we obtain from (2)

$$O_{n,l,m}(\zeta) = -\frac{1}{4\pi} \iint d\tau_1 d\tau_2 \sigma(\mathbf{r}_1) [\mathcal{A}_2 r_{12}^{-1}] \varrho_{n,l,m}(\mathbf{r}_2; \zeta). \quad (5)$$

Considering only cases when $n \geq l + 2$, integrating by parts and taking into account that

$$\Delta_2 \varrho_{n,l,m}(\mathbf{r}_2; \zeta) = r_2^{-1} \frac{d^2}{dr_2^2} r_2 \varrho_{n,l,m}(\mathbf{r}_2; \zeta) - l(l+1) r_2^{-2} \varrho_{n,l,m}(\mathbf{r}_2; \zeta) \quad (6)$$

the result

$$\begin{aligned} C_{n,l,m}(\zeta) = & -\frac{4\pi}{\zeta^2} \partial_{n,l,m}(\zeta) + \frac{2(n+1)}{\zeta} C_{n-1,l,m}(\zeta) - \\ & - \frac{n(n+1)-l(l+1)}{\zeta^2} C_{n-2,l,m}(\zeta) \end{aligned} \quad (7)$$

follows in a straightforward manner. The recurrence relation (7) makes possible a systematic raising (or after recasting a systematic lowering) of the subscript n and its use requires only the calculation of overlap integrals of the type (2).

In order to make use of the recurrence relation (7) we have to calculate the starting terms. This can be done within the framework of the present program in the following way.

By making use of the expansion [3]

$$r_{12}^{-1} = \begin{cases} \sum_{l=0}^{\infty} \sum_{m=-l}^l \frac{4\pi}{2l+1} r_1^{-l-1} r_2^l S_{l,m}(\Theta_1, \Phi_1) S_{l,m}(\Theta_2, \Phi_2) & \text{if } r_1 > r_2 \\ \sum_{l=0}^{\infty} \sum_{m=-l}^l \frac{4\pi}{2l+1} r_1^l r_2^{-l-1} S_{l,m}(\Theta_1, \Phi_1) S_{l,m}(\Theta_2, \Phi_2) & \text{if } r_1 < r_2 \end{cases} \quad (8)$$

and of the orthogonality relations

$$\int_0^{\pi} d\Theta \sin \Theta \int_0^{2\pi} d\Phi S_{l,m}(\Theta, \Phi) S_{l',m'}(\Theta, \Phi) = \delta_{l,l'} \delta_{m,m'} \quad (9)$$

the well known relation

$$\begin{aligned} C_{n,l,m}(\zeta) = & \frac{4\pi}{2l+1} \int d\tau \sigma(\mathbf{r}) \left[r^{-l-1} S_{l,m}(\Theta, \Phi) \int_0^r ds s^{n+l+2} e^{-\zeta s} + \right. \\ & \left. + r^l S_{l,m}(\Theta, \Phi) \int_r^{\infty} ds s^{n-l+1} e^{-\zeta s} \right] \end{aligned} \quad (10)$$

follows immediately. Let us define now the function

$$\begin{aligned} C_{n,l,m}(\zeta; a) = & \frac{4\pi}{2l+1} \int d\tau \sigma(\mathbf{r}) \left[r^{-l-1} S_{l,m}(\Theta, \Phi) \int_0^{ar} ds s^{n+l+2} e^{-\zeta s} + \right. \\ & \left. + r^l S_{l,m}(\Theta, \Phi) \int_{ar}^{\infty} ds s^{n-l+1} e^{-\zeta s} \right]. \end{aligned} \quad (11)$$

Evidently

$$C_{n,l,m}(\zeta) = C_{n,l,m}(\zeta; 1) = C_{n,l,m}(\zeta; 0) + \int_0^1 da \frac{\partial C_{n,l,m}(\zeta; a)}{\partial a}. \quad (12)$$

From (11) it follows that

$$C_{n,l,m}(\zeta; 0) = \frac{4\pi}{2l+1} \frac{(n-l+1)!}{\zeta^{n-l+2}} O_{l,l,m}(0) \quad (13)$$

and

$$\frac{\partial C_{n,l,m}(\zeta; a)}{\partial a} = \frac{4\pi}{2l+1} (\alpha^{n+l+2} - \alpha^{n-l+1}) O_{n+2,l,m}(\alpha\zeta), \quad (14)$$

i.e.

$$\begin{aligned} C_{n,l,m}(\zeta) &= \frac{4\pi}{2l+1} \left[\frac{(n-l+1)!}{\zeta^{n-l+2}} O_{l,l,m}(0) + \right. \\ &\quad \left. + \int_0^1 da (\alpha^{n+l+2} - \alpha^{n-l+1}) O_{n+2,l,m}(\alpha\zeta) \right]. \end{aligned} \quad (15)$$

It can be expected that the integrand on the right hand side of (15) is generally a very smooth function of a and thus the integral is very well suited for numerical evaluation. In this case, however, the calculation of $C_{n,l,m}(\zeta)$ requires only the calculation of a few overlap integrals of the type (2).

The method discussed here can be applied also to Coulomb and hybrid integrals in which the Slater-type charge distribution (1) is replaced by a Gaussian one. Similar tricks can, in principle, be applied also to other types of, integrals (e.g. exchange integrals) but the results could not, so far, be brought to a form which appears practically useful.

Somewhat similar techniques have been used in a paper by D. M. SCHRADER [4] for the evaluation of other integrals. This paper contains also a few references interesting in this connection. Compare also with a paper of J. S. WANG [5].

REFERENCES

1. The definition of the $S_{l,m}(\theta, \phi)$'s can be found e.g. in the paper by C. C. J. ROOTHAAN in J. Chem. Phys., **19**, 1445, 1951.
2. See e.g. H. A. BETHE, E. E. SALPETER, Encyclopaedia of Physics, Vol. XXXV., p. 266. (Springer, Berlin—Göttingen—Heidelberg, 1957.)
3. Cf. e.g. L. I. SCHIFF, Quantum Mechanics, p. 173. (McGraw-Hill, New York—Toronto—London, 1949.) and ref. [1].
4. D. M. SCHRADER, J. Chem. Phys., **41**, 3266, 1964.
5. J. S. WANG, Chinese J. Phys., **3**, 67, 1939.

RECENSIONES

TARNÓCZY TAMÁS

Akusztika, Fizikai akusztika

(Acoustics. Physical Acoustics). In Hungarian. Akadémiai Kiadó, Budapest 1963, 550 pages

The title "Physical Acoustics" indicates the subject and purpose of this book, which deals with a wide range of acoustical phenomena, the discussion not being restricted to special fields of certain research methods or applications. The book discusses several technical problems which lie outside the scope of the title.

The style of the book is not quite homogeneous. Occasionally, it gives a theoretical analysis of the problems in experimental physics, while in many cases only the results are given. The bibliographic material treated is very large; it includes many references to "classical" sources as well as to modern publications. In addition to references in foreign languages, many Hungarian publications are given in the bibliography. These pages illustrate the wide range of the author's publications also. Unfortunately, the short references (name, date) scattered throughout the text are not precise enough to facilitate further checking, but in spite of this the exact bibliography at the end of the chapters can be used for extensive studies.

The book consists of eight chapters.

Chapter 1 begins with the survey of simple laboratory equipment used for detecting and recording vibrations. This is followed by the now classical discussion of free and forced vibrations of a simple, single degree-of-freedom vibrating system. The discussion is completed by a description of self-sustained vibrations, and non-linear systems.

Chapter 2 deals with vibration superpositions and their theory. After discussing Fourier series, graphical Fourier analysis and mechanical analyzers, the chapter ends with correlation analysis.

Chapter 3 mainly deals with one- and two-dimensional vibrating bodies, which are large compared with the wavelength. As a possible application it discusses the musical instruments and this is followed by a survey of human voice generation and mechanical sound sources (pipes, sirens). A schematic summing up of thermo and electromechanical transducers ends the Chapter.

Chapter 4 discusses the sound-wave equation, plane and spherical waves and sound radiation. Several methods are treated, by which it becomes possible to make sound waves visible by means of mechanical and optical devices. Non-linear phenomena and radiation pressure are considered.

In Chapter 5 several characteristics of sound propagation (Doppler effect, dispersion, absorption, diffraction, reflection, refraction) are dealt with and many numerical values are given. The discussion of some applications and special phenomena completes this Chapter.

Chapter 6 deals with the technical applications of the information given in the previous chapters: matching problems on the interface of different media, acoustic lenses, mirrors and wave guides, Helmholtz resonators, sound absorbers and acoustic filters.

In Chapter 7, after dealing with the basic concepts of statistical room-acoustics, the principles of standing waves in an enclosure are discussed, definitions of diffusion and clarity are given. Methods of sound amplification are also dealt with.

Chapter 8 is concerned with the schematic discussion of microphones, the measurements of frequency, wavelength, velocity, power, etc., as well as the methods of sound recording.

Thus, the book covers an extremely wide field of science and this seems to be the reason for some of the unfortunate mistakes found in the text. For example the method of defining the constant k by measurements in equ. 1.6; the doubtful method of solving the differential equ. 1.10; the numerical example given on pages 238—239; the wrong sign in the differential equ. 8.13 and the presence of capacity C ; and finally the errors in the dimensions and the numerical factors of equs. 4.121, 8.27, 8.30, 8.31.

Special attention should be drawn to the careful selection of the contents of the book and to the remarkably good figures. Owing to the several references of historical, artistic or technical nature, the text of the book is interesting.

Owing to language difficulties this beautifully printed book will be accessible to a limited number of readers only, however, in the Hungarian literature of acoustics it will certainly satisfy a long-felt need.

Z. BARÁT

R. RITSCHL und G. HOLDT

Emissionspektroskopie

Akademie-Verlag, Berlin, 1964, 411 pp.

The Physical Society of the German Democratic Republic and the German Academy of Sciences in Berlin held a conference on emission spectroscopy on October 9–12, 1962 with a number of participants from abroad. The book reviewed here contains the lectures delivered at the conference. 253 figures and 70 tables add to the value of this well produced book in an attractive cloth binding.

Through the publication of the forty-three lectures delivered, the book affords a good outline of the present European level of emission spectroscopy. Side by side with the theoretical lectures problems occurring in practice have also been considered. Some of the more important lectures have been dealt with in full, while the rest have been summarized according to subject-matter.

In his lecture V. VUKANOVIC deals with processes taking place in the arc which are important in tracer element investigations. The processes are treated with mathematical exactitude. The experiments were carried out in connection with gallium contamination. He concludes that the changes in three parameters (arc temperature, electron pressure and transport velocity) must be taken into consideration.

G. EHRLICH lectured on the developmental trends of the spectroscopical investigation of substances of high purity emphasizing that the detection-limit is as low as 0,01 ppm at best. In his lecture he dwelt at length upon the direction of development, and suggested a few possibilities that may increase the efficiency of the methods employed.

K. ZIMMER outlined the present state of density transformations with a critical approach to the various transformation processes.

G. HOLDT deals with the application of dispersion diagrams. He discusses in detail the dispersion curves formed by the value pairs of Y from the inter-related analysis — and standard lines. A number of examples are displayed for the examination of dispersion diagrams.

T. TÖRÖK deals with the theory of L -transformation by which the basic features of the L -transformation may well be interpreted.

J. RUBESKA dealt in two lectures with the measurement of the width of spectral lines, and with one of the methods of concentration determination and the problems of principles arising therefrom; in the second lecture he introduced some practical examples of this method.

K. LENZ reports on his investigations with ruby lasers. A detailed account was given of his results concerning the investigation of the optimal chromium content of the ruby crystal.

The rest of the lectures will be discussed under various subject headings.

A number of accounts were given on the construction of various spectroscopical apparatus and component parts as well as on their favourable applications.

G. SCHEIBER dealt with photographic problems of spectra, J. WITTING discussed the Raman-spectroscopical application of low-pressure mercury vapour lamps, R. RITSCHL and CH. RÖSELER examined the fine structure of mercury lines in low-pressure discharges, E. KRAZD discussed the construction and peculiarities of a plasma burner free from contamination, M. RIEMANN reported on the stabilized arc necessary for analysis in solution, E. SCHELLER spoke of the addition of a 70 cm camera lens to a three-prism glass spectrograph, P. KRÖPLIN introduced the pre-resolving-apparatus of a PGS 2 plane-grating spectrograph. W. GUTTMANN discussed the application of a duplo-meter, while M. FRANK gave an account of his investigations with the A. R. L. quantometer. J. GAUDNIK also lectured on investigations executed with a direct-measuring apparatus. K. GAULRAPP and

G. SCHMUTZLER spoke of their researches carried out by a heavy-duty three-meter grating-polychromator and a vacuum polychromator.

A number of lectures covered the investigations of spectra resolved in time. A vibrating mirror was employed by B. VORSATZ, and the apparatus employed by him was improved by M. ZEISE. A valuable lecture in this field was delivered by E. PLSKO.

Many lectures were given covering the field of spectrochemical analysis. In accordance with the treatment of the material employed so far, these, too, will be reviewed in the order adopted by the book. V. SVOBODA dealt with the spectrographic examination of radioactive substances, R. GERBATSCHEV employed atomic absorption flame photometry in the examination of substances of high purity, R. SCHINDLER and H. FUCHS discussed the application of X-ray fluorescence spectral analysis in geology. J. CZAKOW and R. GRZELAK determined the contaminating elements of lead by means of a specially constructed electrode. V. S. BURAKOV and A. A. JANKOVSKII dealt with the possibilities of reducing the effects of the third element, G. J. KIBISOV, L. N. ANTROPOV, N. B. KUBASOVA, and V. E. KOLOBKOVAYA gave an account of a spectrographic quantitative method of universal application. L. PÉTER determined the magnesium content of alumina alloys by means of a new method. E. GEGUS introduced a new spectrochemical process for the analysis of the inclusions of steels. H. HENNIGER and H. SCHELLER detected carbon content in steels of low and high alloyage by means of the PGS 2 plane grating spectrograph. K. DOERFFEL and R. WAGNER gave information on a method developed for the quantitative analysis of ancient archeological bronze findings. F. MACHER carried out a spectrochemical analysis of furnace aluminum by means of spark excitation, and L. PAKSY gave news of a model experiment concerning contamination. CH. KERÉKES determined thorium in wolfram confirming his experimental results theoretically as well, L. MOENKE-BLANKENBURG carried out geochemical examinations by employing a grating spectrograph. B. BERNOLÁK and K. Soós reported on the spectrographical analysis of ferrites and their bases, G. DÜMACKE gave an account of his spectrochemical process for analyzing silicates. A. SPACKOVA and L. BOUBEROVA detected scandium in minerals, O. SZAKÁCS dealt with the solution analysis of trace contaminations. A. PETHŐ spoke about the direct determination of the vanadium and nickel content of mineral-oils, and, similarly, petrochemical spectroscopical examination was discussed by P. BUNCÁK.

Briefly it is certain that the material of this valuable conference at the highest level has appeared as a useful referencebook — owing to the painstaking work of editorship and typography — for which our congratulations must be expressed to the editors, R. RITSCHL and G. HOLDT.

I. Kovács*

G. YA. LYUBARSKII

The Application of Group Theory in Physics

Pergamon Press, Oxford, 1960.

In recent years the applications of group theory in modern theoretical physics have expanded remarkably. Without a knowledge of group theory it is hardly possible to study the physics of elementary particles theoretically. This is why physicists are especially interested in books on group theory concerned with problems related to physics or the applications of group theory in physics. LYUBARSKII's book completely satisfies the requirements of physicists in this respect. In the Introduction we read that the author had three aims in writing the book: "... to present in detail, consistently and as concisely as possible those parts of the theory of representations of finite and continuous groups that are most important in application; to consider groups of interest in theoretical physics; and, finally, to demonstrate the principles according to which the abstract concepts and the theorems of representation theory are applied in theoretical physics."

Chapters I and II deal with the elements of group theory and the general mathematical characterization of some specific (perturbation, rotation, full orthogonal, Euclidean, point) groups. The next three Chapters comprising about sixty pages treat of the theory of group representations. This general part is followed by ample physical applications in Chapters VI,

* Department of Atomic Physics, Polytechnical University, Budapest.

VII and VIII, including, in particular, the small oscillations of symmetrical systems, the problems of second order phase transitions and the group theory of the physical properties of crystals. Chapter IX is concerned with infinite groups in general and in particular with the Lie group. In Chapter X the representations of the rotation group in two or three dimensions are considered. This Chapter also deals with spinor and tensor algebra, as well as the representation theory of the full orthogonal group. Then follows the description of the properties and calculation of Clebsch-Gordan and Racah coefficients.

Chapter XII entitled "The Schrödinger Equation" deals with conservations laws and the classification of quantum states. A separate Chapter is devoted to the problems of absorption and the Raman scattering of light. The main emphasis is laid on the group-theoretical treatment of selection rules concerning the scattering of light on atoms and molecules and absorption.

The representations of the Lorentz group, so important in physics, are considered in detail. In addition to the general characteristics of the Lorentz group the infinitesimal operators of the Lorentz group, the classification of irreducible representations, the product of the irreducible representations of the Lorentz group, complex-conjugated representations, spinor and tensor algebra are described. The Chapter ends with the representation of the full Lorentz group.

In the Chapters concerned with relativistically invariant equations the group-theoretical treatment of problems relating to the Dirac equation, the spin and the relativistically invariant operation of time-inversion are given.

The last Chapter contains applications in nuclear physics (scattering matrix, angular distribution in nuclear reactions).

At the end of the book an Appendix consisting of five Paragraphs and a detailed bibliography are attached. The Appendix includes exact Tables for the irreducible representations of the perturbation group, the irreducible representations of point groups and Racah coefficients.

It can be regarded as a particular merit of G. YA. LYUBARSKII's book that, in addition to a rigorous mathematical exactitude, it never fails to observe the physicist's viewpoint. This is why it has become a handbook much used by theoretical physicists.

K. NAGY

Printed in Hungary

The *Acta Physica* publish papers on physics, in English, German, French and Russian.
The *Acta Physica* appear in parts of varying size, making up volumes.
Manuscripts should be addressed to:

Acta Physica, Budapest 502, Postafiók 24.

Correspondence with the editors and publishers should be sent to the same address.
The rate of subscription to the *Acta Physica* is 110 forints a volume. Orders may be placed with "Kultúra" Foreign Trade Company for Books and Newspapers (Budapest I., Fő u. 32. Account No. 43-790-057-181) or with representatives abroad.

Les *Acta Physica* paraissent en français, allemand, anglais et russe et publient de travaux du domaine de la physique.

Les *Acta Physica* sont publiés sous forme de fascicules qui seront réunis en volumes.
On est prié d'envoyer les manuscrits destinés à la rédaction à l'adresse suivante:

Acta Physica, Budapest 502, Postafiók 24.

Toute correspondance doit être envoyée à cette même adresse.

Le prix de l'abonnement est de 110 forints par volume.

On peut s'abonner à l'Entreprise du Commerce Extérieur de Livres et Journaux «Kultúra» (Budapest I., Fő u. 32. — Compte-courant No. 43-790-057-181) ou à l'étranger chez tous les représentants ou dépositaires.

«*Acta Physica*» публикуют трактаты из области физических наук на русском, немецком, английском и французском языках.

«*Acta Physica*» выходят отдельными выпусками разного объема. Несколько выпусков составляют один том.

Предназначенные для публикации рукописи следует направлять по адресу:

Acta Physica, Budapest 502, Postafiók 24.

По этому же адресу направлять всякую корреспонденцию для редакции и администрации.

Подписная цена «*Acta Physica*» — 110 форинтов за том. Заказы принимает предприятие по внешней торговле книг и газет «Kultúra» (Budapest I., Fő u. 32. Текущий счет: № 43-790-057-181) или его заграничные представительства и уполномоченные:

INDEX

<i>Gy. Fáy:</i> Notes on the Quantum-mechanical Discussion of the Gibbs Paradox. — <i>Д. Фай:</i> Замечания к квантовомеханическому рассмотрению парадокса Гиббса	273
<i>L. Kohlmann and T. Vörös:</i> New Alpha-Decay Barrier Penetrabilities with Igo Potential: Even- and Odd-Mass Nuclei. — <i>Л. Кольманн и Т. Вереш:</i> Новая проходимость через потенциальный барьер с потенциалом Иго при α -распаде: четные и нечетные ядра	285
<i>J. Bacso, J. Csikai and A. Pázsit:</i> Investigation of $\text{Mo}^{92}(n, 2n) \text{Mo}^{91+91m}$ Reaction. — <i>Й. Бачо, Й. Чикаи и А. Пажсит:</i> Исследование реакции $\text{Mo}^{92}(n, 2n) \text{Mo}^{91+91m}$	295
<i>Г. Нергеш, М. Ш. Силади и Б. Визкеleti:</i> Исследование диффузионного процесса в германии. — <i>G. Nyerges, M. S. Szilágyi and B. Vizkeleti:</i> Investigation of the Diffusion Process in Germanium	299
<i>F. Berencz:</i> Die Berechnungen der $1sns^1S$ -Zustände des Wasserstoffmoleküls auf Grund der Methode der Molekülbahnen II. — <i>Ф. Беренц:</i> Определение состояния $1sns^1S$ молекулы водорода методом молекулярных орбит II.	307
<i>M. Tisza:</i> Calculation of Nuclear Quadrupole Moments. — <i>M. Tuca:</i> Вычисление ядерного квадрупольного момента	321
<i>M. Силади:</i> Расчет траектории электрона, движущегося между коаксиальными трубами, в присутствии полого электронного пучка. — <i>M. Szilágyi:</i> Calculation of the Trajectory of an Electron Moving between Coaxial Tubes in the Presence of a Hollow Electron Beam	325
<i>M. Силади:</i> Периодическая электростатическая фокусировка ленточных электронных потоков — <i>M. Szilágyi:</i> Periodic Electrostatic Focusing of Sheet Electron Beams	335
<i>J. Nyiri and A. Sebestyén:</i> The Muon Decay in the Renormalizable Vector Boson Theory. — <i>Ю. Нир и А. Шебештен:</i> Распад мюона в перенормируемой теории слабых взаимодействий	351
<i>I. Tamásy-Lentei:</i> Extraordinary Orbitals in the United Atom Model. — <i>И. Тамаш-Лентей:</i> Необыкновенные орбиты в соединенной атомной модели	359

COMMUNICATIONES BREVES

<i>C. Bojarski:</i> Über die gegenseitige Beziehung von Konstanten einiger Theorien über Konzentrationsauslöschung und Konzentrationspolarisation der Photolumineszenz von Lösungen	367
<i>R. Gáspár:</i> Universal Potential Eigenfunctions and Eigenvalues for the Selenium Atom	371
<i>T. Szondy:</i> A Simple Method for the Calculation of Coulomb and Hybrid Integrals	381

RECENSIONES

<i>Z. Barát:</i> Tarnóczy Tamás, Akusztika, Fizikai akusztika	385
<i>I. Kovács:</i> R. Ritschl und G. Holdt, Emissionsspektroskopie	386
<i>K. Nagy:</i> G. Ya. Lyubarskii, The Application of Group Theory in Physics	387

Acta Phys. Hung. Tom. XVIII. Fasc. 4. Budapest, 31. V. 1965